frontiers | Research Topics

Nutrients, neurotransmitters and brain energetics, volume II

Edited by
Rubem C. A. Guedes, Adriana Ximenes-da-Silva and Daniel C. Anthony

Published in
Frontiers in Neuroscience
Frontiers in Nutrition

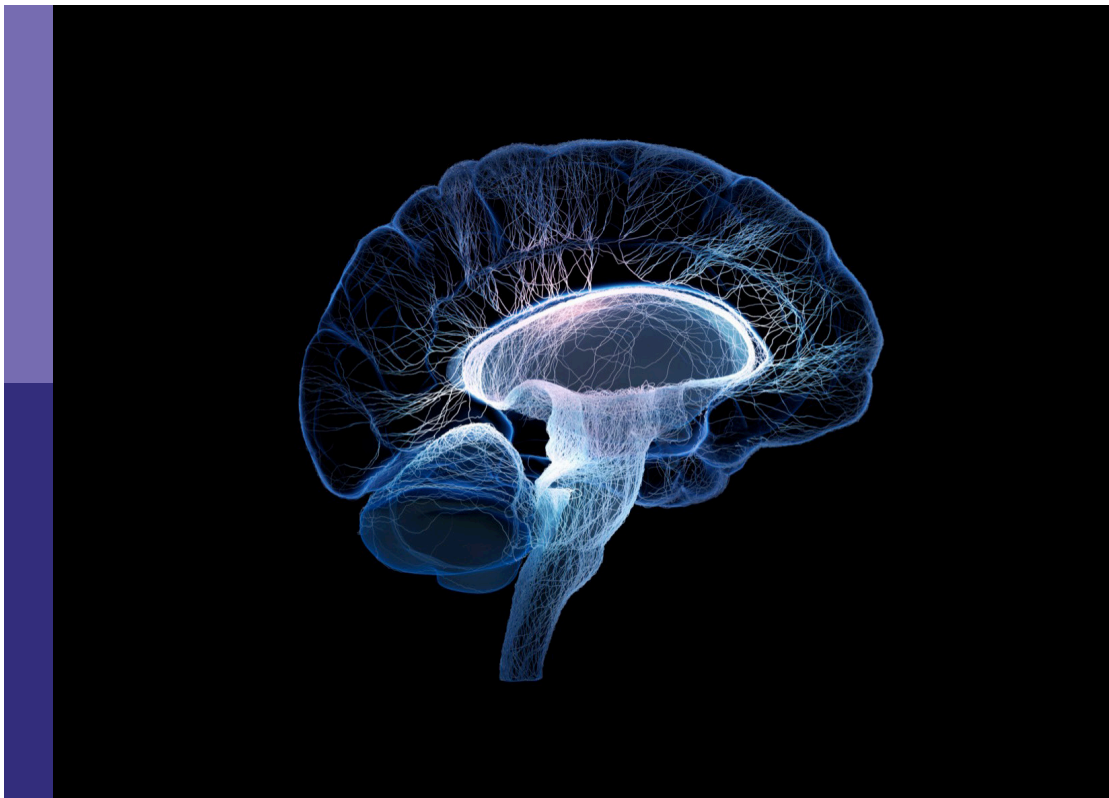

ISSN 1664-8714
ISBN 978-2-8325-6489-9
DOI 10.3389/978-2-8325-6489-9

Generative AI statement
Any alternative text (Alt text) provided alongside figures in the articles in this ebook has been generated by Frontiers with the support of artificial intelligence and reasonable efforts have been made to ensure accuracy, including review by the authors wherever possible. If you identify any issues, please contact us.

About Frontiers

Frontiers is more than just an open access publisher of scholarly articles: it is a pioneering approach to the world of academia, radically improving the way scholarly research is managed. The grand vision of Frontiers is a world where all people have an equal opportunity to seek, share and generate knowledge. Frontiers provides immediate and permanent online open access to all its publications, but this alone is not enough to realize our grand goals.

Frontiers journal series

The Frontiers journal series is a multi-tier and interdisciplinary set of open-access, online journals, promising a paradigm shift from the current review, selection and dissemination processes in academic publishing. All Frontiers journals are driven by researchers for researchers; therefore, they constitute a service to the scholarly community. At the same time, the *Frontiers journal series* operates on a revolutionary invention, the tiered publishing system, initially addressing specific communities of scholars, and gradually climbing up to broader public understanding, thus serving the interests of the lay society, too.

Dedication to quality

Each Frontiers article is a landmark of the highest quality, thanks to genuinely collaborative interactions between authors and review editors, who include some of the world's best academicians. Research must be certified by peers before entering a stream of knowledge that may eventually reach the public - and shape society; therefore, Frontiers only applies the most rigorous and unbiased reviews. Frontiers revolutionizes research publishing by freely delivering the most outstanding research, evaluated with no bias from both the academic and social point of view. By applying the most advanced information technologies, Frontiers is catapulting scholarly publishing into a new generation.

What are Frontiers Research Topics?

Frontiers Research Topics are very popular trademarks of the *Frontiers journals series*: they are collections of at least ten articles, all centered on a particular subject. With their unique mix of varied contributions from Original Research to Review Articles, Frontiers Research Topics unify the most influential researchers, the latest key findings and historical advances in a hot research area.

Find out more on how to host your own Frontiers Research Topic or contribute to one as an author by contacting the Frontiers editorial office: frontiersin.org/about/contact

Nutrients, neurotransmitters and brain energetics, volume II

Topic editors

Rubem C. A. Guedes — Federal University of Pernambuco, Brazil

Adriana Ximenes-da-Silva — Federal University of Alagoas, Brazil

Daniel C. Anthony — University of Oxford, United Kingdom

Citation

Guedes, R. C. A., Ximenes-da-Silva, A., Anthony, D. C., eds. (2025). *Nutrients, neurotransmitters and brain energetics, volume II*. Lausanne: Frontiers Media SA. doi: 10.3389/978-2-8325-6489-9

Table of contents

frontiers | Frontiers in Neuroscience

TYPE Editorial
PUBLISHED 10 June 2025
DOI 10.3389/fnins.2025.1621811

OPEN ACCESS

EDITED AND REVIEWED BY
Matthias Tasso Wyss,
University of Zurich, Switzerland

*CORRESPONDENCE
Rubem Carlos Araújo Guedes
✉ guedes.rca@gmail.com

RECEIVED 01 May 2025
ACCEPTED 28 May 2025
PUBLISHED 10 June 2025

CITATION
Guedes RCA, Ximenes-da-Silva A and Anthony DC (2025) Editorial: Nutrients, neurotransmitters and brain energetics, volume II. *Front. Neurosci.* 19:1621811. doi: 10.3389/fnins.2025.1621811

Editorial: Nutrients, neurotransmitters and brain energetics, volume II

Rubem Carlos Araújo Guedes[1]*, Adriana Ximenes-da-Silva[2] and Daniel C. Anthony[3]

[1]Department of Nutrition, Federal University of Pernambuco, Recife, Brazil, [2]Department of Physiology, Federal University of Alagoas, Maceió, Brazil, [3]Department of Pharmacology, University of Oxford, Oxford, United Kingdom

KEYWORDS

nutrient, redox imbalance, neurotransmitter receptor, behavior, brain electrophysiology, brain metabolism

Editorial on the Research Topic
Nutrients, neurotransmitters and brain energetics, volume II

1 Introduction

The extraordinary energy demands of the brain make it uniquely sensitive to nutritional and metabolic influences. From early development through to late-life neurodegeneration, nutrient availability and metabolic state profoundly shape neuronal excitability, synaptic plasticity, and the integrity of brain networks. It is increasingly evident that these relationships are bidirectional: neurotransmitter systems and cellular energetics are not only regulated by dietary factors but also actively modulate how the brain responds to physiological and environmental challenges. Yet, despite a growing body of evidence linking diet and metabolism to brain function, the underlying mechanisms remain incompletely defined, particularly in relation to neurodegenerative and neuropsychiatric conditions.

This Research Topic brings together a multidisciplinary collection of articles examining the intersections between nutrition, neurotransmission, and brain energetics. The contributions span animal models, human studies, and bioinformatic analyses, and together offer insight into how specific dietary components, neuromodulatory pathways, and metabolic regulators influence brain health. Although diverse in scope, the studies share a central theme: that metabolism is not simply a background process but a dynamic determinant of brain function and dysfunction.

The issue is organized around three interconnected themes. Firstly, studies on nutrition explore the roles of vitamins, fatty acid profiles, caloric restriction, and ketogenic diets in shaping cognitive outcomes, emotional regulation, and neuroprotection. Secondly, the interface between nutrition and neurotransmission is examined through investigations into melatonin signaling, yoga-based neuromodulation, and acupuncture-induced molecular cascades. Thirdly, a set of studies focused on brain energetics highlights how mitochondrial metabolism, redox balance, and network-level connectivity are influenced by dietary and metabolic interventions.

Together, these studies illustrate the breadth of current approaches to understanding how food, metabolism, and signaling converge in the brain. They underscore the need for

integrated models that span molecular, cellular, and systems-level domains — and they point toward promising avenues for developing personalized nutritional and metabolic strategies to support cognitive resilience and prevent neurological disease.

2 Studies on the subtopic "Nutrition"

A number of studies in this Research Topic underscore the importance of dietary components in shaping cognitive function and vulnerability to neurological disease. The association between vitamin status and brain health is particularly well-illustrated by two large-scale epidemiological studies. Zhang et al. (also see Section 4) report that higher dietary intake of niacin—a precursor of the essential redox coenzyme NAD^+—was associated with a significantly lower risk of Parkinson's disease in US adults, with each 10 mg increase in niacin intake linked to a 23% risk reduction. Similarly, Pan et al. demonstrate a robust inverse association between serum 25-hydroxyvitamin D levels and cognitive frailty in older adults, with a 12% reduction in frailty risk per unit increase in 25-(OH)D. Together, these findings suggest that even modest differences in micronutrient intake or status may confer meaningful protection against neurodegeneration and age-related cognitive decline.

In contrast to these beneficial effects, Wang et al. highlight a potentially adverse nutritional signal: elevated levels of plasma polyunsaturated fatty acids (PUFAs), and in particular a high arachidonic acid to docosahexaenoic acid (AA/DHA) ratio, were associated with increased depressive symptoms in US adults. These data support the idea that the balance—not just the quantity—of dietary fats may be critical for maintaining mental health and further suggest that dietary lipid profiles could serve as modifiable risk factors in mood disorders.

Experimental studies in rodents provided mechanistic insights into how nutrition influences brain function at both cellular and systems levels. van Rooij et al. (also see Section 4) investigated the effects of caloric restriction (CR) and resveratrol supplementation—a proposed CR mimetic—on resting-state functional connectivity using fMRI in male and female rats. Both interventions altered large-scale brain network activity, with a striking sex-specific effect: reduced functional connectivity between key subcortical and cortical regions was observed predominantly in females. These findings raise important questions about sex differences in metabolic responses and their downstream effects on brain architecture and function.

Finally, the neuroprotective potential of dietary interventions in pathological states was explored by Granados-Rojas et al. (also see Section 4), who examined the impact of a ketogenic diet (KD) in a rodent model of epilepsy. KD feeding preserved expression of the chloride transporter KCC2 in hippocampal subregions, counteracting the reduction induced by seizure activity and shortening after-discharge durations. This suggests that diet-induced shifts in brain energy substrates may not only enhance mitochondrial efficiency but also modulate key ion transport mechanisms critical to neural excitability.

Together, these studies provide compelling evidence that dietary patterns and nutrient composition have profound effects on brain function—from modulating network connectivity in healthy individuals to altering cellular mechanisms in disease. They collectively reinforce the view that targeted nutritional strategies may offer accessible, low-risk interventions to support brain health across the lifespan.

3 Studies on the interface "Nutrition and Neurotransmitters"

Cell excitability and transmitter actions were examined through multidisciplinary approaches to evaluate the potential therapeutic effects of melatonin administration, yoga practice and acupuncture stimulation, on behavioral, electrophysiological, and biochemical parameters.

Melatonin is a neurohormone that plays a crucial role in regulating sleep and the circadian rhythm. Additionally, it exhibits a wide range of effects, including blood pressure regulation, antioxidant and anti-inflammatory properties, alongside neuroprotective effects.

Araújo et al. examined in rats the effects of administering two different doses of melatonin on behavioral and electrophysiological parameters of cortical spreading depression (CSD), and redox balance status during brain development.

Animal groups that received a low dose of melatonin (10 mg/kg) exhibited reduced anxiety levels, as measured by the open field and elevated plus maze tests. Both melatonin doses (10 and 40 mg/kg, respectively) influenced brain electrophysiological parameters, with the lower dose significantly decelerating and the higher dose accelerating CSD propagation velocity. Lower malondialdehyde levels and higher superoxide dismutase levels were observed in the cerebral cortex of the group that received the low dose of melatonin. This study highlighted the importance of melatonin's dose-dependent effects on behavior, brain excitability, and redox balance throughout development, and corroborates with the findings from studies with different doses of other antioxidant molecules (Mendes-da-Silva et al., 2014).

Reduced anxiety levels are commonly associated with yoga practice. In this Research Topic, Li et al. investigated in humans the potential effects of yoga practice on reducing anxiety levels through a study assessing the impact of breathing exercises, postures, and mindfulness meditation on brain activity in the prefrontal cortex (PFC).

The study revealed distinct differences in PFC activation between long-term yoga practitioners (>3 times/week for 6.05 years) and short-term practitioners (>3 times/week for 0.91 years). Long-term practitioners exhibited increased oxygenated hemoglobin concentration in the dorsolateral prefrontal cortex, along with enhanced cognitive and emotional regulation. These findings highlight the potential benefits of long-term yoga practice in promoting cognitive improvement and reducing anxiety.

In recent years, several studies have focused on elucidating the cellular mechanisms underlying the physiological effects induced by acupuncture stimulation. Acupoint catgut embedding (ACE) therapy is based on traditional acupuncture techniques and involves the application of absorbable catgut at acupoints. This technique provides prolonged stimulation of acupoints compared to traditional methods, which can be especially beneficial in the treatment of chronic conditions.

Hou et al. investigated in rats the role of mechanically sensitive transient receptor potential vanilloid (TRPV) channels, including TRPV2 and TRPV4, in the regulatory pathways of ACE therapy. Their findings revealed stimulation effects resulting in a physico-chemical-immune response mediated by TRPV channels, calcium influx, and the activation of macrophage CD68 and mast cell tryptase, providing valuable insights into the cellular mechanisms underlying ACE therapy.

4 Studies on the interface "Nutrition and Brain Energetics"

Energy metabolism is fundamental to brain function, underpinning processes from ion homeostasis and neurotransmission to large-scale network activity. While not always explicitly framed in terms of energetics, several of the contributions to this Research Topic shed important light on how metabolic interventions and nutritional factors shape neural activity and resilience. A particularly clear mechanistic insight came from the work of Granados-Rojas et al., who examined the effects of a ketogenic diet (KD) in a well-established rodent model of epilepsy. Beyond its recognized role in reducing seizure frequency, KD selectively preserved expression of the chloride transporter KCC2 and shortened after-discharges in hippocampal regions, counteracting the downregulation induced by amygdala kindling. Higher KCC2 levels are linked to shorter generalized seizures, explaining the KD's beneficial effect on epilepsy. Since KCC2 is essential for maintaining inhibitory synaptic transmission, its preservation likely reflects improved cellular energetics and ionic homeostasis under ketotic conditions. Notably, KCC2 levels correlated inversely with after-discharge duration, suggesting that diet-driven shifts in brain metabolism can have direct functional consequences for excitability.

At the level of brain networks, van Rooij et al. demonstrated that both caloric restriction (CR) and the CR-mimetic resveratrol modulated resting-state functional connectivity (FC) in rats, with pronounced and sex-specific effects. In females, both interventions reduced connectivity between key subcortical and cortical regions, including the hippocampus. These findings raise intriguing questions about the relationship between systemic metabolic state, neurovascular coupling, and network dynamics. The authors discuss the possibility of the vascular contribution to the BOLD signal in the context of their interventions, which seemed very interesting to us. This study's insight could be considered a functional connectivity reference for further investigation. Given the energy demands of maintaining synchronized neural activity, interventions that reshape connectivity may ultimately act, at least in part, via modulation of brain energetics.

Perhaps unsurprisingly, mitochondrial metabolism emerged as a recurring theme. Qin et al., using a bioinformatics approach, identified key genes involved in acetyl-CoA synthesis, mitochondrial respiration and pyruvate metabolism that may serve as biomarkers of cuproptosis in cerebral ischemia. These processes are central to cellular energy metabolism, linking nutrient oxidation to ATP generation. Their findings further underscore the critical role of mitochondrial integrity in brain injury and repair.

Finally, dietary micronutrients with recognized roles in redox and energy metabolism were linked to neurodegenerative disease risk. Zhang et al. found that higher dietary niacin intake—a precursor of NAD+, a vital coenzyme in mitochondrial metabolism—was inversely associated with Parkinson's disease prevalence in a large US cohort, with a 23% reduction in risk for each 10 mg increase in niacin intake This raises the possibility that even subtle nutritional deficits may impair brain energetics over the lifespan, contributing to neurodegeneration.

These findings align with our own previous observations that systemic metabolic state and peripheral inflammation can influence brain metabolism, including in the context of neurodegenerative and neuropsychiatric conditions (Dunstan et al., 2024; Aziz et al., 2025). In particular, our work has highlighted the interaction between metabolic substrates, inflammatory mediators, and astrocyte-neuron coupling (Radford-Smith et al., 2024) as a critical determinant of brain energy homeostasis—a theme echoed in several of the contributions to this Research Topic.

Together, the studies reviewed here highlight the rich interplay between diet, metabolism, and brain energetics. While mechanisms range from the cellular to the network level, all emphasize the potential of nutritional and metabolic interventions to modulate brain function and potentially ameliorate disease processes.

5 Concluding remarks

In conclusion, the studies published in this Research Topic represent an important contribution to our evolving understanding of how nutrition, neurotransmitters and brain energetics interact to shape brain function across the lifespan. Although diverse in approach and focus, together they highlight the intricate ways in which metabolic and nutritional factors can influence neuronal excitability, network connectivity, and ultimately, behavior and cognition.

In the nutrition theme, several of the studies underscored the protective or deleterious roles of dietary components on brain health. While higher intake of vitamins such as niacin and vitamin D was associated with reduced risk of Parkinson's disease and cognitive frailty, respectively, other findings highlighted potential risks of imbalanced dietary fat composition. The study of polyunsaturated fatty acids revealed that an elevated AA/DHA ratio may increase susceptibility to depression, illustrating how nutritional imbalances may perturb brain function and mental health.

In the neurotransmitters and neuromodulation section, multidisciplinary approaches revealed that targeted interventions such as melatonin supplementation, yoga, and acupuncture can modulate anxiety, excitability and redox status. These findings point to a key role for neuromodulatory systems in mediating the effects of lifestyle and therapeutic interventions on brain activity. Of particular interest is the evidence that both low-dose melatonin and long-term yoga practice exert anxiolytic and cognitive benefits, mediated through alterations in cortical excitability and prefrontal cortex function.

Under the Brain Energetics theme of volume II, while not all contributions addressed this subtopic explicitly, many provided critical insights. Studies demonstrated that metabolic

interventions—from ketogenic diets and caloric restriction to micronutrient supplementation—can reshape brain function through mechanisms ranging from mitochondrial modulation and cuproptosis-related pathways to altered functional connectivity. Dietary modulation of substrates and redox cofactors, as seen with niacin intake and KCC2 regulation, further supports the view that brain energetics is a crucial integrative axis linking nutrition and neuronal physiology. These observations are in keeping with emerging work suggesting that systemic metabolic state, peripheral inflammation and astrocyte-neuron metabolic coupling together determine energetic resilience in the brain.

Taken together, the contributions in this Research Topic reflect a growing recognition of the importance of integrating molecular, cellular, and systems-level perspectives in the study of brain energetics and its nutritional and neurochemical determinants. The multidisciplinary approaches presented here—ranging from human cohort studies to animal models and bioinformatics—provide valuable platforms for future research aimed at developing novel metabolic and nutritional strategies to promote brain health and prevent or mitigate neurodegenerative and neuropsychiatric disorders.

Author contributions

RG: Writing – original draft, Writing – review & editing. AX-d-S Writing – original draft, Writing – review & editing. DA: Writing – original draft, Writing – review & editing.

Funding

The author(s) declare that financial support was received for the research and/or publication of this article. This research was supported in part by the following Agencies: (1, to RG) = National Council for Scientific and Technological Development (CNPq), [grant nos 406495/2018-1 and 305998/2018-8], Coordination for the Improvement of Higher Level -or Education Personnel (CAPES), [grant no Capes BEX 2036/ 15-0. Finance Code 001]. (2, to DA) = the Aqua-Synapse EU framework (2022-2026), funded by the European Union's Horizon 2020 Research and Innovation programme under the Marie Sklodowska-Curie Grant Agreement No. 101086453. The authors are solely responsible for the content of this publication, which does not necessarily represent the official views of the European Union or the European Research Executive Agency.

Conflict of interest

The authors declare that the research was conducted in the absence of any commercial or financial relationships that could be construed as a potential conflict of interest.

The author(s) declared that they were an editorial board member of Frontiers, at the time of submission. This had no impact on the peer review process and the final decision.

Publisher's note

References

Aziz, A., Alves-Costa, C. F. F., Zhao, E., Radford-Smith, D., Probert, F., Anthony, D. C., et al. (2025). Repeated administration of L-alanine to mice reduces behavioural despair and increases hippocampal mammalian target of rapamycin signalling: analysis of gender and metabolic effects. *J. Psychopharmacol.* 1–12. doi: 10.1177/02698811251332838

Dunstan, I. K., McLeod, R., Radford-Smith, D. E., Xiong, W., Pate, T., Probert, F., et al. (2024). Unique pathways downstream of TLR-4 and TLR-7 activation: sex-dependent behavioural, cytokine, and metabolic consequences. *Front. Cell. Neurosci.* 18:1345441. doi: 10.3389/fncel.2024.1345441

Mendes-da-Silva, R. F., Cunha-Lopes, A. A., Bandim-da-Silva, M. E., Cavalcanti, G. A., Rodrigues, A. R. O., Andrade-da-Costa, B. L. S., et al. (2014). Prooxidant versus antioxidant brain action of ascorbic acid in well-nourished and malnourished rats as a function of dose: a cortical spreading depression and malondialdehyde analysis. *Neuropharmacology* 86, 155–160. doi: 10.1016/j.neuropharm.2014.06.027

Radford-Smith, D., Ng, T. T., Yates, A. G., Dunstan, I., Claridge, T. D. W., Anthony, D. C., et al. (2024). *Ex-vivo* 13C NMR spectroscopy of rodent brain: TNF restricts neuronal utilization of astrocyte-derived metabolites. *J. Proteome Res.* 2024, 23, 3383–3392. doi: 10.1021/acs.jproteome.4c00035

frontiers | Frontiers in Neuroscience

TYPE Original Research
PUBLISHED 12 October 2023
DOI 10.3389/fnins.2023.1269609

OPEN ACCESS

EDITED BY
Fengchun Wu,
The Affiliated Brain Hospital of Guangzhou Medical University, China

REVIEWED BY
Veronica Folakemi Salau,
University of the Free State, South Africa
Huan Gao,
Zhejiang University, China

*CORRESPONDENCE
Rubem Carlos Araújo Guedes
✉ guedes.rca@gmail.com;
✉ rubem.guedes@ufpe.br

RECEIVED 30 July 2023
ACCEPTED 18 September 2023
PUBLISHED 12 October 2023

CITATION
Araújo AdO, Figueira-de-Oliveira ML, Noya AGAFdC, Oliveira e Silva VP, Carvalho JMd, Vieira Filho LD and Guedes RCA (2023) Effect of neonatal melatonin administration on behavioral and brain electrophysiological and redox imbalance in rats.
Front. Neurosci. 17:1269609.
doi: 10.3389/fnins.2023.1269609

Effect of neonatal melatonin administration on behavioral and brain electrophysiological and redox imbalance in rats

Amanda de Oliveira Araújo[1], Maria Luísa Figueira-de-Oliveira[1], Arthur Gabriel Alves Furtado de Carvalho Noya[2], Vitor Palmares Oliveira e Silva[2], Jennyfer Martins de Carvalho[1], Leucio Duarte Vieira Filho[1] and Rubem Carlos Araújo Guedes[2]*

[1]Department of Physiology and Pharmacology, Universidade Federal de Pernambuco, Recife, Pernambuco, Brazil, [2]Department of Nutrition, Universidade Federal de Pernambuco, Recife, Pernambuco, Brazil

Introduction: Melatonin (MLT) reportedly has beneficial effects in neurological disorders involving brain excitability (e.g., Epilepsy and Migraine) and behavioral patterns (e.g., Anxiety and Depression). This study was performed to investigate, in the developing rat brain, the effect of early-in-life administration of two different doses of exogenous MLT on behavioral (anxiety and memory) and electrophysiological (CSD analysis) aspects of brain function. Additionally, brain levels of malondialdehyde (MDA) and superoxide dismutase (SOD), both cellular indicators of redox balance status, were evaluated. We hypothesize that MLT differentially affects the behavioral and CSD parameters as a function of the MLT dose.

Materials and methods: Male Wistar rats received, from the 7th to the 27th postnatal day (PND), on alternate days, vehicle solution, or 10 mg/kg/or 40 mg/kg MLT (MLT-10 and MLT-40 groups), or no treatment (intact group). To perform behavioral and cognition analysis, from PND30 to PND32, they were tested in the open field apparatus, first for anxiety (PND30) and then for object recognition memory tasks: spatial position recognition (PND31) and shape recognition (PND32). On PND34, they were tested in the elevated plus maze. From PND36 to 42, the excitability-related phenomenon known as cortical spreading depression (CSD) was recorded, and its features were analyzed.

Results: Treatment with MLT did not change the animals' body weight or blood glucose levels. The MLT-10 treatment, but not the MLT-40 treatment, was associated with behaviors that suggest less anxiety and improved memory. MLT-10 and MLT-40 treatments, respectively, decelerated and accelerated CSD propagation (speed of 2.86 $\pm$ 0.14 mm/min and 3.96 $\pm$ 0.16 mm/min), compared with the control groups (3.3 $\pm$ 0.10 mm/min and 3.25 $\pm$ 0.11 mm/min, for the intact and vehicle groups, respectively; $p < 0.01$). Cerebral cortex levels of malondialdehyde and superoxide dismutase were, respectively, lower and higher in the MLT-10 group but not in the MLT40 group.

Conclusion: Our findings suggest that MLT intraperitoneal administration during brain development may differentially act as an antioxidant agent when administered at a low dose but not at a high dose, according to behavioral, electrophysiological, and biochemical parameters.

KEYWORDS

melatonin, brain development, anxiety, memory, spreading depression, redox imbalance

1. Introduction

Melatonin (MLT) is an antioxidant hormone (Poeggeler et al., 1993; Boutin et al., 2023) that, when used in physiological doses, could benefit patients suffering from several diseases (Arendt, 2005), including excitability-related disorders, such as epilepsy (Gunata et al., 2020) and neonatal hypoxia-ischemia (Flinn et al., 2020; for a review, see Cardinali, 2019). The amphipathic nature of MLT facilitates its passage through the blood–brain barrier and enables its effect on the nervous system, either independent of or mediated by MLT receptors. MLT is a powerful antioxidant, free radical scavenger, and immune system regulator with an anti-inflammatory and circadian rhythm regulator role (Gunata et al., 2020). This hormone neutralizes reactive oxygen species (ROS) and enzymatically converts them into less harmful species (Reiter et al., 2017, 2018). MLT receptors have been classified into three types (MT1, MT2, and MT3). In the mammalian brain, MT1 receptors are mainly found in the suprachiasmatic nucleus, hippocampus, habenula, pituitary gland, raphe nucleus, substantia nigra and superior colliculus; MT2 receptors are located in the retina, hypothalamus, hippocampus, periaqueductal gray, thalamic and supraoptic nuclei, substantia nigra and inferior colliculus (Dubocovich et al., 1998; Lacoste et al., 2015). These two types of receptors are substantially involved in circadian rhythm regulation. The MT3 receptors are the co-substrate of the enzyme quinone reductase-2, with a putative involvement in the brain redox balance (Nosjean et al., 2001; Tan et al., 2007; Wang et al., 2019a). Furthermore, MLT levels are low in patients with neurological diseases, such as epilepsy, a brain excitability disorder that mainly affects age extremes: childhood and elderly (Sanchez-Barcelo et al., 2017). Children with drug-resistant epilepsy have more sleep disorders than healthy children (Proost et al., 2022). Besides, MLT may protect epilepsy through its antioxidant, anti-excitotoxic, and central nervous system free radical scavenging properties (Akyuz et al., 2021).

In addition to its fundamental role in circadian rhythm regulation and scavenging free radicals, MLT can improve neurobehavioral deficits (Rodriguez et al., 2004). MLT can interact with other physiological systems to control anxiety and depression (Bouslama et al., 2007; Lamtai et al., 2021). Another benefit of MLT is its influence on memory formation in the hippocampus (El-Sherif et al., 2003; Iwashita et al., 2021). MLT has also been shown to be protective against neuronal damage in the hippocampus, resulting in improved learning and memory due to its potent antioxidant properties (Soleimani et al., 2017). However, it is not yet known whether its administration in high doses would have the opposite (prooxidant) effect on behavioral and electrophysiological aspects of brain function, as demonstrated in the rat brain for other antioxidant molecules, including ascorbic acid (Mendes-da-Silva et al., 2014) and pyridoxine (Gondim-Silva et al., 2021) in an electrophysiological phenomenon known as cortical spreading depression (CSD).

CSD is a fully reversible, depolarizing "wave" of reduction of the amplitude of the electrocorticographic activity (ECoG depression), which is elicited in response to the stimulation of a point of the cortical tissue (Leão, 1944). During the ECoG depression, a direct current (DC) slow potential shift appears (Leão, 1947). This DC signal has all-or-none features, is the CSD hallmark, and is very useful in calculating the CSD velocity of propagation. Regarding the human species, CSD appears to be involved in several neurological diseases, such as migraine, epilepsy, subarachnoid hemorrhage, and traumatic brain injury (for an overview, see Lauritzen and Strong, 2017; Guedes and Abadie-Guedes, 2019). The evidence suggests that analysis of CSD propagation velocity represents a valuable index to understanding excitability-dependent aspects of brain functioning (Guedes et al., 2017). CSD has been employed in our laboratory over a few decades, and it has been largely and compellingly demonstrated that factors that affect CSD can also affect other aspects of brain function, including behavior and redox balance (for an overview, see Guedes, 2011; Guedes and Abadie-Guedes, 2019).

From the above, the present study was performed to investigate, in the developing rat brain, the effect of early-in-life administration of two different doses of exogenous MLT on behavioral (anxiety and memory) and electrophysiological (CSD analysis) aspects of brain function, as will be described below. Additionally, brain levels of malondialdehyde (MDA) and superoxide dismutase (SOD), both cellular indicators of redox balance status, were evaluated. We hypothesize that MLT differentially affects the behavioral and CSD parameters as a function of the MLT dose.

2. Materials and methods

2.1. Animals

All experimental procedures were approved by our University's Animal Research Ethics Committee (approval protocol no. 0006/2020), whose standards comply with those established by the National Institutes of Health Guide for Care and Use of Laboratory Animals (Bethesda, MD, United States). Newborn male and female Wistar rats were suckled in a litter with eight pups. After weaning, pups were separated by sex and housed in polypropylene cages (51 cm × 35.5 cm × 18.5 cm) under controlled temperature (23°C ± 1°C) with a 12–12-h light–dark cycle (lights on at 7 p.m.). Only male pups ($n = 40$; 10 rats per group) were used in this study. Each group was formed with pups from 3 to 5 distinct litters.

2.2. Treatment with MLT

MLT (purchased from Sigma Aldrich, St Louis, United States) was administered every other day, from PND7 to PND27, at 2 p.m. (11 days of MLT administration). Two groups of rats ($n = 10$ per group) received intraperitoneal injections of 10 or 40 mg/kg MLT (MLT10 and MLT40 groups, respectively). MLT was dissolved in 0.1 mL of saline solution containing 5% ethanol. These experimental groups were compared with two control groups, treated with the vehicle used to dissolve MLT (vehicle group; $n = 10$) or not treated (intact group; $n = 10$).

2.3. Body weight

Body weight was measured using a precision digital scale (Marte, São Paulo) on PND7, PND14, PND21, and PND28.

2.4. Glycemia analysis

At two time points on PND27 (4 h before and 4 h after the administration of MLT), plasma glucose concentrations were determined in one-drop blood samples from the animal's tail, using a glucometer (Accu-Chek Active, Roche, São Paulo, Brazil).

2.5. Behavioral tests

All behavioral tests were performed between PND30 and PND34 in the following temporal sequence: first, on PND30-32, the animals were tested in the open field apparatus (OF) for anxiety (PND30) and for two recognition memory tasks: spatial position recognition (PR; PND31) and shape recognition (SR; PND32). Second, after 48 h, the animals were tested on PND34 in the elevated plus-maze (EPM). A video camera recorded the animal's behavioral activity in all tests, which was further analyzed with ANYmaze™ software version 4.99 m (Stoelting Co., Wood Dale, IL, United States). After each test, the device was cleaned with a 70:30 ethanol:water solution. The animals were randomly tested between 8 a.m. and 1 p.m.

The tests were conducted in a room with sound attenuation and low light intensity (red light). Before each test, the animal was introduced to the test room for 20 min to adapt to the environment (adaptation period). Each anxiety behavior test (OF and EPM) consisted of one 5-min session. In comparison, each recognition memory test (PR and SR) consisted of two 5-min sessions (the training session and test session), separated by a 40-min interval.

2.5.1. Behavior indicative of anxiety: tests in the OF and EPM

The OF and EPM aim to assess the ability of the animal to recognize anxiogenic sites (the central part of the OF and the open arms in the EPM), where less time is usually spent during the test (Calza et al., 2010). The OF consisted of a circular arena made of varnished wood, with a diameter of 89 cm, surrounded by a wall, also made of wood, 52 cm high. For the OF test (PND30), the animal's behavior was evaluated for 5 min after the adaptation period. The center of the OF was defined as an area with a diameter of 62 cm. The following four parameters were measured on the OF: (1) number of entries into the central area, (2) time spent in the central area, (3) distance traveled, and (4) immobility time. The animal's entrance to the center was considered when its four paws were in the center. Then, memory tests of recognition of a new spatial position (PND31) and a new shape (PND32) of objects placed in the OF were performed (see Part 4.5.2 below). After 48 h, the animals were tested in the EPM (PND34).

The EPM (raised 55 cm from the floor) was made of varnished wood, consisting of two open and two closed arms perpendicular to the open arms (each measuring 49 cm × 10 cm) and connected by a 10 cm-long central square. After the adaptation period, the animal was placed in the central square facing an open arm. The following four parameters were evaluated in the EPM: (1) number of entries into the open arms, (2) time spent in the open arms, (3) distance traveled, and (4) immobility time. The animal's entrance to one arm was considered when its four paws were in that arm.

2.5.2. Behavior indicative of memory: object recognition tests

These tests assessed the animal's ability to recognize a specific object's novel shape or spatial position. It is based on the animal's natural tendency to spend more time exploring a new object or a novel spatial position of a familiar object that has been previously explored (Francisco and Guedes, 2015). Ennaceur and Delacour (1988) and Dere et al. (2005) described these methods for object recognition tests, which are briefly summarized below:

(1) For the PR task, the two chosen objects were identical, made of the same material (glass), with similar interaction possibilities. Initially, the two identical objects (A and B) were placed in the OF, and the animal explored them for 5 min. After a 40-min intermission, the animal returned to the OF (second session) in the presence of the same objects (A and B); however, in this second moment, object B was located at a novel spatial position. When the animal identified the novel position, it explored the object more in the novel placement point.

(2) For shape recognition, objects had distinct geometries and different shapes, heights, and colors, which the animal could quickly identify. This condition is believed to minimize the influence of natural preferences (Viana et al., 2013). Two identical objects (A and B) were initially positioned in the arena for a 5-min exploration. After a 40-min interval, the animals returned to the arena. For this second 5-min session, the spatial position of the objects remained the same as in the first session, but object B was replaced by a novel object (C) with a different shape. The animal demonstrated that it could differentiate the shapes when it dedicated more time to exploring the novel object in this second session. To better evaluate the memory effects, the discrimination index (DI; Viana et al., 2013) was calculated using the formula $DI = (TN - TF)/(TN + TF)$, where TN and TF represent the exploration time of the object with a novel and familiar characteristic, respectively (either by shape or spatial position). The criterion for defining exploration was based on 'active operation,' when the animal touched objects at least with its nose.

2.6. Recording of cortical spreading depression

On PND36-42, the animals were anesthetized with an intraperitoneal injection of a mixture of urethane and chloralose (1 g/kg and 40 mg/kg, respectively). Three trephine holes were drilled on the right side of the skull, aligned in the frontal-occipital direction and parallel to the midline. One hole (2–3 mm in diameter) was positioned on the frontal bone and was used to apply the cortical spreading depression (CSD)-eliciting stimulus (KCl solution). The parietal bone's other two holes (3–4 mm in diameter) were used to record the propagated CSD wave. During surgery and recording, the animals breathed spontaneously, and their rectal temperature was monitored and kept at 37 ± 1°C. As a rule, topical application of 2% KCl (approximately 270 mM) for 1 min at a point on the exposed frontal cortical surface elicited a single episode of CSD. KCl application was repeated every 20 min during the 4-h recording session. The depression of the ECoG waves and the slow potential shift of the CSD were recorded using two Ag-AgCl-Agar-Ringer electrodes located at the parietal region on the stimulated hemisphere. A third electrode of the same type was placed on the nasal bones and was a standard reference for the other two recording electrodes. The CSD propagation velocity was calculated from the time required for a CSD wave to cross the distance between the two cortical recording points. The starting point of each ascending phase of the negative component of the slow potential shift of CSD was used as a reference point to calculate the propagation velocities of the phenomenon. Additionally, the amplitude and duration of the negative component of CSD were calculated, as previously reported (Mendes-da-Silva et al., 2014). Figure 1 shows the time points of melatonin treatment (postnatal days 7 to 27), behavioral tests (PND 30–34), and CSD electrophysiological recordings (PND 36–42).

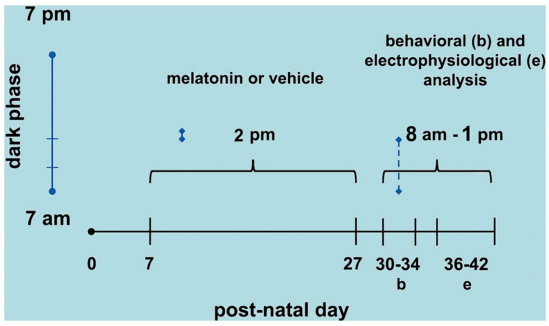

FIGURE 1
Schematic diagram showing the time points of melatonin treatment (postnatal day 7 to 27), behavioral tests (PND 30–34), and CSD electrophysiological recordings (PND 36–42).

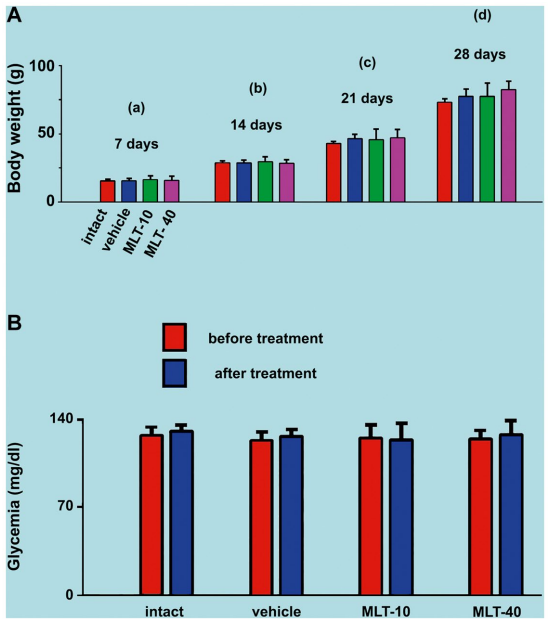

FIGURE 2
(A) Mean body weights of the two control groups (intact and vehicle) and those treated with MLT (10 and 40mg/kg/day; MLT-10 and MLT-40 groups, respectively). Animals were weighed on Days 7 (a), 14 (b), 21 (c), and 28 (d) of postnatal life. MLT treatment did not influence weight gain. The two-way ANOVA for repeated measures and one-way ANOVA confirmed that, at an older age, animals from the same group were significantly heavier than at a younger age, and the absence of intergroup differences indicated a similar weight gain for all groups. **(B)** Blood glucose levels of the four groups in this study. Blood glucose was measured twice at PND28, 4h before and 4h after MLT administration; under these conditions, the treatment with MLT did not influence the glycemia of the animals (intragroup comparison: $p>0.05$; paired *t*-test). The comparison between MLT-treated and non-treated groups revealed no intergroup difference [one-way ANOVA; $F(3, 36)=0.216$; $p=0.885$]. Data are expressed as the mean±standard deviation. The n is 10 for each group, as stated in the methods.

2.7. Analyses of brain MDA and SOD

In the four experimental groups, malondialdehyde (MDA) and superoxide dismutase (SOD) levels were measured in 20 rats (5 animals from each group). After the CSD recording session, these 20 animals were decapitated, and the entire cortex of the right hemisphere was dissected and individually homogenated. We measured MDA levels using a thiobarbituric acid-reactive substances-based method as a way to estimate the levels of lipid peroxidation in the brain (Ohkawa et al., 1979; Mendes-da-Silva et al., 2014). Initially, 40 µL of 8.1% sodium dodecyl sulfate, 300 µL of 20% acetic acid (pH 3.5), and 300 µL of 0.8% thiobarbituric acid solutions were added to a 100-µL homogenate aliquot in a boiling water bath for 30 min. Then, the tubes were cooled with tap water, and 300 µL of n-butanol was added to the sample. After centrifuging the tubes at 2,500 ×g for 10 min, the organic phase was read at 532 nm using a plate reader. MDA values were expressed as nmol/mg of protein in the homogenate.

The levels of SOD were assessed as described elsewhere (Misra and Fridovich, 1972), based upon the brain tissue's ability to reduce the formation of the pink chromophore, adrenochrome, from the oxidation of epinephrine. Briefly, brain homogenates were prepared at 10 mg of protein/mL dilution and added to a 96-well plate to determine enzymatic activity. Then, the solution was supplemented with 1.5 mM epinephrine. The rate of adrenochrome formation was estimated by measuring absorbance at 15-s intervals for 2 min. SOD values were expressed as U SOD.min^{-1}/mg of protein, where one unit of SOD is defined as the amount of enzyme required to halve the spontaneous rate of adrenochrome formation.

The total protein concentrations in the homogenates were determined with the BCA Protein Assay Kit (Pierce, Rockford, IL, United States). Measurements were carried out in triplicate.

2.8. Statistics

The results are expressed as the means ± standard deviations. The four treatment groups' ponderal, behavioral, CSD, and biochemical parameters were compared using one-way ANOVA, followed by a *post hoc* test (Holm–Sidak), where indicated. Weight differences over distinct ages were analyzed with ANOVA for repeated measures. The same animal's blood glucose levels before and after MLT were compared using the paired *t*-test. Intergroup glucose levels were analyzed with one-way ANOVA. A value of $p < 0.05$ was considered significant.

3. Results

3.1. Body weights

As illustrated in Figure 2A, ANOVA showed no significant intergroup difference in body weight at 7 days of age [$F(3, 36)=0.199$; $p=0.896$], at 14 days [$F(3, 36)=0.352$; $p=0.788$], at 21 days [$F(3, 36)=0.762$; $p=0.525$], and 28 days [$F(3, 36)=1.939$; $p=0.151$]. The administration of the two different doses of MLT did not change the weight gain of the animals.

3.2. Glycemia

ANOVA revealed no intergroup difference in the blood glucose levels [$F(3, 36)=0.216$; $p=0.885$], i.e., at PND28 (end of MLT treatment), control groups and MLT-treated groups displayed similar blood glucose levels. MLT also had no acute effect when comparing, in the same animal, blood glucose before and after MLT administration

in the two treated groups ($p > 0.05$; paired t-test). Data on glycemia are shown in Figure 2B.

3.3. Behavioral reactions

3.3.1. Behavior suggestive of anxiety

The effect of MLT administration on behavioral activity in the OF test is shown in Figure 3, left part. ANOVA indicated intergroup differences for the number of entries into the central area [$F(3, 36) = 8.706$; $p < 0.001$] and time in the central area [$F(3, 36) = 5.993$; $p = 0.003$]. The *post hoc* test indicated that the animals from the MLT-10 group entered the central area more often and remained there longer than the other three groups. There were no intergroup differences regarding the distance traveled [$F(3, 36) = 0.456$; $p = 0.600$] or immobility time [$F(3, 36) = 0.194$; $p = 0.899$].

The EPM test outcome is shown in Figure 3, right part. ANOVA indicated intergroup differences for the entries into the open arms [$F(3, 35) = 4.200$; $p = 0.015$] and time spent in the open arms [$F(3, 35) = 10.036$; $p < 0.001$]. The *post hoc* test (Holm–Sidak test) indicated that the MLT-10 group entered the open arms more frequently and stayed longer in the open arms than the control groups (intact and vehicle). There was no intergroup difference regarding the traveled distance [$F(3, 35) = 0.631$; $p = 0.600$] or immobility time [$F(3, 35) = 0.852$; $p = 0.475$].

3.3.2. Behavior in the object recognition memory test

The outcome of the object recognition memory tests (performed on PND31 and PND32) is shown in Figure 4. The upper graph refers to the discrimination indices that indicate the recognition of a novel spatial position of a familiar object. The lower graph corresponds to the discrimination indices for recognizing an object with a novel shape different from a familiar object's. ANOVA revealed intergroup differences in spatial recognition [$F(3, 36) = 7.813$; $p < 0.001$] but not in shape recognition [$F(3, 35) = 2.025$; $p = 0.136$]. The *post hoc* (Holm–Sidak) test revealed that the MLT-10 group performed significantly better ($p < 0.05$) than the other three groups.

3.4. Cortical spreading depression features

Application of a cotton ball (1–2 mm in diameter) soaked in 2% KCl solution (approximately 270 mM) for 1 min, at 20 min intervals, to a point in the frontal cortex, usually elicited a single wave of CSD (Figure 5A). The propagating CSD wave was recorded by the two more posterior electrodes on the stimulated hemisphere (see recording points 1 and 2 in the skull diagram in Figure 5A).

Regarding the propagation velocity of CSD (Figure 5B), ANOVA indicated intergroup differences [$F(3, 36) = 85.130$; $p < 0.001$]. *Post hoc* (Holm–Sidak) test comparisons showed that the low and the high doses of MLT (10 and 40 mg/kg, respectively) significantly decelerated and accelerated CSD (2.86 ± 0.14 mm/min and 3.96 ± 0.16 mm/min, respectively; $p < 0.01$), compared to the control groups (3.31 ± 0.10 mm/min for the intact control and 3.25 ± 0.11 mm/min for the vehicle-treated groups).

The amplitude and duration of the negative component of the slow potential change, which is the hallmark of CSD, are shown in Figures 5C,D, respectively. ANOVA indicated a main effect of treatment for amplitude [$F(3, 36) = 9.520$; $p < 0.001$] and duration [$F(3, 36) = 29.767$; $p < 0.001$]. The mean amplitudes in the two control groups were 8.9 ± 2.4 mV and 9.0 ± 1.7 mV, respectively, for the intact and vehicle-treated groups. For the groups treated with MLT (MLT-10 and MLT-40), the amplitude was 6.8 ± 1.2 mV and 13.2 ± 2.3 mV, respectively, indicating that the treatment with the low and high doses of MLT was associated with a significantly lower and higher amplitude

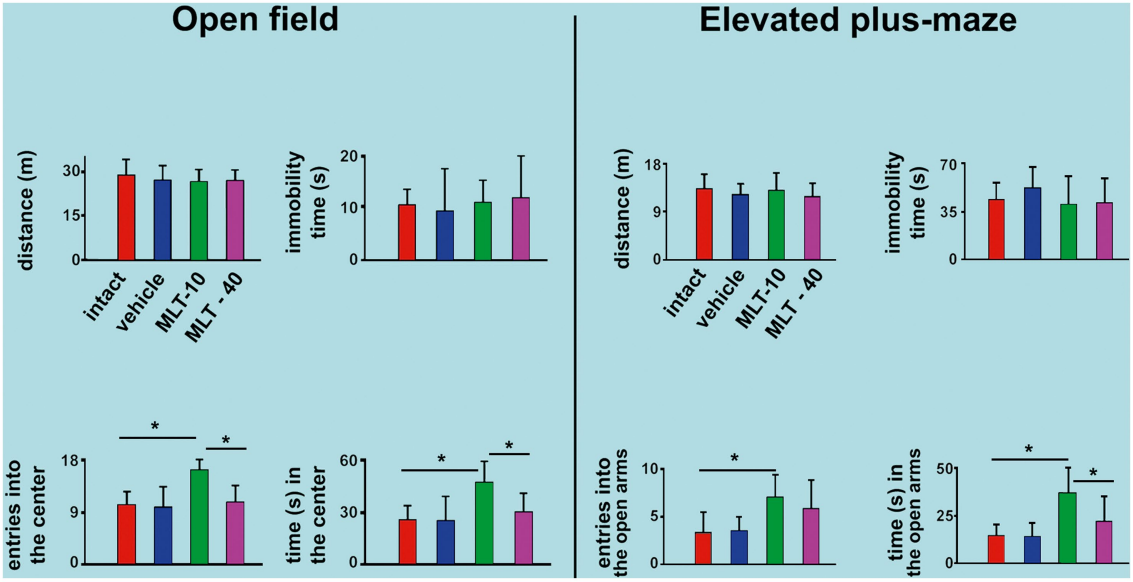

FIGURE 3
Behavioral parameters were evaluated in the open-field (OF) apparatus and the elevated plus maze (EPM) task in 30-and 34-day-old rats. In both tests, data are presented as the mean ± standard deviation. The n is 10 for each group, as stated in the methods. *$p < 0.05$ (ANOVA plus Holm–Sidak test).

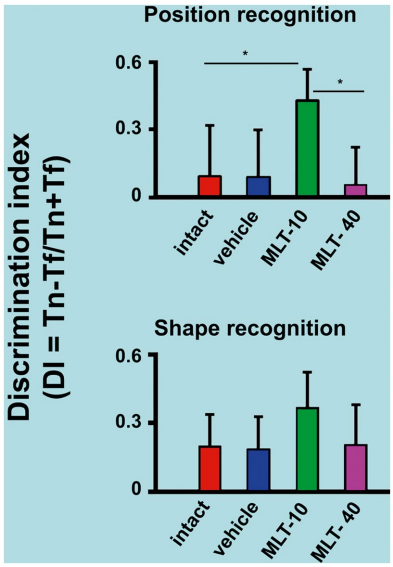

FIGURE 4
Discrimination indices of rats that were subjected to the object recognition memory test. The upper graph of this figure refers to the recognition of a new spatial position (PND31) of an already known (or familiar) object. The bottom graph represents the recognition of an object with a new shape (PND32) but in a familiar spatial position. *$p < 0.05$ (ANOVA followed by the Holm–Sidak test). The n is 10 for each group, as stated in the methods.

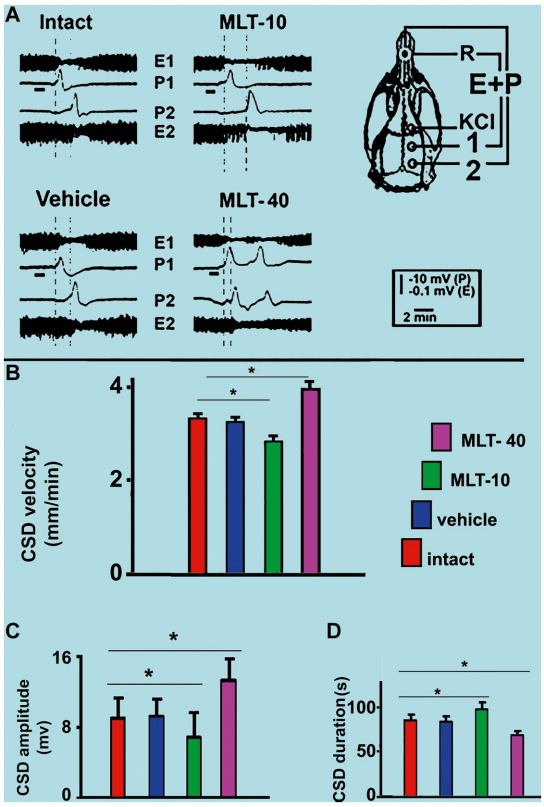

FIGURE 5
(A) Representative traces illustrating the typical ECoG depression (E) and the slow potential change (P) of cortical spreading depression (CSD). These traces were recorded at two cortical points (1 and 2) in two control (intact and vehicle) and two MLT-treated, 36–42-day-old male rats. The skull diagram shows the first and second recording positions (1 and 2), from which the traces marked with the same numbers were obtained. The position of the standard reference electrode (R) on the nasal bones and the application point of the CSD-eliciting stimulus on the frontal cortex is also shown. CSD was elicited in the frontal cortex by chemical stimulation (a 1–2 mm diameter cotton ball soaked with 2% KCl) applied for 1 min on the intact dura mater, as indicated by the horizontal bars under the traces at point 1. The vertical dashed lines indicate the latency for a CSD wave to cross the interelectrode distance. Longer and shorter latencies were observed in the MLT-10 and MLT-40 groups, respectively. Panels **(B–D)** show the CSD propagation velocity, amplitude, and duration, respectively. Data are the mean values of 10–12 CSD episodes per rat from 20 controls (10 intact and 10 saline-treated rats) and 20 MLT-treated rats (10 MLT-10 and 10 MLT-40 animals) recorded over a 4-h recording session. *$p < 0.005$ (ANOVA followed by the Holm–Sidak test).

in comparison to the control groups. The Holm–Sidak test indicated that the two groups that were treated with 10 and 40 mg/kg MLT had longer and shorter CSD durations, respectively (96.5 ± 9.1 s and 70.7 ± 4.0 s, respectively), than the two control groups (83.9 ± 5.4 s and 82.1 ± 4.0 s for the intact and vehicle groups, respectively).

3.5. MDA and SOD levels in the cerebral cortex

Table 1 presents the levels of MDA and SOD in the cerebral cortex of control-and MLT-treated rats. ANOVA indicated intergroup differences [$F(3, 16) = 6.152$; $p = 0.006$ for MDA, and 12.293; $p = 0.001$ for SOD]. The *post hoc* test indicated that the MLT-10 group, but not the MLT-40 group, presented with lower levels of MDA (3.34 ± 1.24 nMol/mg protein) and higher levels of SOD (19.49 ± 4.57 AU/min/mg protein), as compared to the intact (MDA, 6.21 ± 0.58 nMol/mg protein; SOD, 7.39 ± 3.88 AU/min/mg protein) and vehicle controls (MDA, 6.93 ± 2.53 nMol/mg protein; SOD, 7.59 ± 3.71 AU/min/mg protein) [Holm–Sidak *post hoc* test; $p < 0.01$].

4. Discussion

For the first time, we have documented, in the brains of developing rats, the differential, dose-dependent effects of MLT treatment on behavioral (anxiety and memory) and electrophysiological (spreading depression) aspects of brain function. Our data from the anxiety and memory tasks suggest an anxiolytic effect of the lower dose but not the higher dose of MLT (see Figures 3, 4). In addition, our CSD findings indicate that MLT may act differentially in the brain at low and high doses, decelerating and accelerating CSD propagation, respectively (see Figure 5).

The introduction mentions that MLT1 and MLT2 receptors are predominantly found in subcortical brain regions (Dubocovich et al., 1998; Lacoste et al., 2015). Therefore, these receptors are unlikely to directly mediate the MLT action on a cortically-based phenomenon like CSD. However, we cannot exclude the role of MLT receptors in processes such as anxiety and memory. On the other hand, MLT at physiological concentrations protects mitochondria from oxidative damage (Zhang and Zhang, 2014). *In vitro* evidence suggests that, depending on the concentration, MLT can generate functionally

TABLE 1 MDA and SOD levels in the cerebral cortex of 36–42-day-old rats ($n = 20$) previously treated (5 rats per group) every other day, from postnatal day 7 to 27, with 10 or 40 mg/kg/d melatonin (groups MLT-10 and MLT-40, respectively), or vehicle, or not treated at all (intact group).

Treatment group ($n = 5$ per group)	MDA level (nMol/mg protein)	SOD (AU/min/mg prot.)
Intact	6.21 ± 0.58	7.39 ± 3.88
Vehicle	6.93 ± 2.53	7.59 ± 3.71
MLT-10	3.34 ± 1.24*	19.49 ± 4.57**
MLT-40	4.32 ± 0.82	11.00 ± 3.33

Data are expressed as mean ± standard deviation. *Significantly different from the intact and vehicle groups **Significantly different from the other three groups ($p < 0.01$; ANOVA followed by the Holm–Sidak test).

significant amounts of ROS (Zhang H. et al., 2011; Zhang H. M. et al., 2011; Martinis et al., 2012; Zhang and Zhang, 2014). As in other organs, the biochemical and morphological organization of the brain can be altered by oxidative stress after the imbalance represented by the increase in ROS production; on the other hand, the decrease in the effectiveness of antioxidant systems can also alter the redox imbalance (Guedes et al., 2012; Mendes-da-Silva et al., 2014). When this imbalance occurs early in life, the deleterious consequences for brain functioning may be more severe than in the adult brain (Grantham-Mcgregor, 1995; Guedes et al., 2012; Colella et al., 2016).

The absence of a weight gain difference after the administration of MLT (Figure 2A) is in line with the fact that the animals in the four groups of this study were subjected to the same conditions of food ingestion (free access to food) and caloric expenditure. Food intake and caloric expenditure were not presently calculated; notwithstanding that, the similar weight gain in all groups suggests no relevant effect of MLT on those parameters under the experimental conditions and age range of the animals in our experiment. The young animals from this study were clinically healthy; no significant difference in blood glucose levels was found between the MLT-treated and control groups (Figure 2B). Our speculations in this regard are limited, as we did not measure insulin and lipid levels that could prove any relationship with MLT. However, some studies reported a greater insulin secretion after MLT administration, linking oscillations in the circadian rhythm to diabetes development [see the recent study by Xia et al. (2023)].

The interpretation of the parameters provided by the behavioral tests with rodents is based on established behavioral neuroscience literature (see Améndola et al., 2022). The present results revealed that MLT had an anxiolytic action (Figure 3) and positively impacted object recognition memory tests (Figure 4). In the OF task, the number of entries into the center and the time spent in this area represent a "risky activity" for the animal. Therefore, the MLT-10 group exhibited anxiolytic-like behavior compared to all other groups. In the EPM task, the "risky activity" is represented by the number of entries into the open arms and the time spent in these areas (Pellow et al., 1985). The animals that received the lower dose of MLT (10 mg/kg) entered more frequently and remained longer in the aversive region (open arms). Therefore, the MLT-10 group, but not the MLT-40 group, showed an anxiolytic-like behavior compared to the Control and Intact groups.

In the PR and SR tasks, the discrimination index calculates cognitive performance—represented by sensory-spatial ability—(see section 2). The higher the index, the better the animal's cognitive performance. Therefore, the MLT-10 group showed better cognitive activity in the spatial recognition task than all other groups. The results of OF and EPM indicate that the MLT-treated rats presented less anxiety behavior and improved memory, and surprisingly, these effects were significant at the low MLT dose. We suggest this is related to the dose-associated redox imbalance, as our brain MDA and SOD measurements indicated (Table 1). Indeed, the decreased levels of MDA and increased levels of SOD in the MLT-10 group suggest that melatonin at this dose had an antioxidant effect in the developing brain. A recent study (Al Gburi et al., 2023) came to the same suggestion.

Childhood and adolescence are crucial for developing learning, memory, and emotional responses (Sun et al., 2021). MLT has anti-inflammatory, anti-amyloidogenic, and antioxidant properties that underlie its potential to reduce brain damage resulting from inflammatory, amyloidogenic, and oxidant processes and improve learning and memory deficits with long-term treatment (Zakaria et al., 2016; Iwashita et al., 2021). A single administration of MLT facilitates cognitive performance in humans (Foster et al., 2014).

This study used electrophysiological analysis of CSD parameters to identify MLT's possible antioxidant (CSD deceleration) and prooxidant (CSD acceleration) actions. Some exogenous and endogenous antioxidant compounds can, under certain circumstances, exert prooxidant activities. That is the case for tocopherol (Gogvadze et al., 2010) and ascorbate (Otero et al., 1997; Podmore et al., 1998; Doseděl et al., 2021). Our group has demonstrated that rats treated with increasing doses of ascorbic acid displayed a biphasic effect of this treatment on the propagation of CSD, with a deceleration of the phenomenon at a lower dose and an acceleration of CSD with higher doses. The CSD decelerating effect of low doses of ascorbic acid was associated with decreased malondialdehyde levels in the brain, compared with those in the corresponding saline and intact groups (Mendes-da-Silva et al., 2014).

The mechanisms by which high concentrations of MLT could stimulate the production of ROS have yet to be determined. Zhang and Zhang (2014) suggested that the weak interaction between calmodulin and MLT might be involved in the stimulation of ROS production. One possible speculation is that different concentrations of MLT may differentially modulate the subcellular localization of calmodulin, thus dictating its involvement in prooxidant vs. antioxidant activities. Calmodulin is a protein that binds with low affinity to MLT and appears to mediate MLT prooxidant action. Furthermore, MLT can interact with mitochondria to promote the generation of ROS. Notably, applying a high concentration of KCl to the rat cortex (a procedure that indeed triggers CSD) influences the expression of calmodulin (Torrão et al., 2002).

In vivo evidence indicates that MLT is a potent antioxidant at typical pharmacological concentrations but may have a prooxidant action in the presence of copper ions (Wang et al., 2019b). We do not know whether brain copper levels were altered in our animals; probably not. However, it is worth mentioning that, under this curious

condition, melatonin can act as a prooxidant molecule (Wang et al., 2019a,b). In *in vitro* experiments, the prooxidant action of MLT promotes inflammatory responses and apoptosis (Wolfler et al., 2001; Radogna et al., 2010). Interestingly, the extracellular increase in ROS facilitates CSD elicitation and propagation, both *in vitro* (Netto and Martins-Ferreira, 1989) and *in vivo* (El-Bachá et al., 1998). CSD is modulated by changes in brain excitability (Koroleva and Bures, 1980; Guedes and Abadie-Guedes, 2019) and is influenced by the production of ROS-like superoxide anions in brain tissue (El-Bachá et al., 1998; Sousa et al., 2021). Although we did not measure ROS directly, we measured MDA and SOD levels in the cerebral cortex. These molecules are cellular markers of redox imbalance because they change proportionally to the amount of ROS. MLT can also exert anti-excitotoxic effects through its neuroprotective action involving gamma-aminobutyric acid (GABA) as a mediator (Pandi-Perumal et al., 2013). This possibility is supported by studies indicating that MLT protects neurons from the toxicity of beta-amyloid peptide (the main neurotoxin involved in Alzheimer's disease) by activating GABAergic receptors (Louzada et al., 2004). After hypoxia injury in rats, MLT administration reduced glutamate levels and hypoxia-induced structural damage to neurons, axons, and dendrites in the brainstem, suggesting that it can ameliorate excitotoxic injury (Kaur et al., 2011). Notably, gamma-aminobutyric acid and glutamate neurotransmitters are causally related to the neuroexcitability influences on CSD (Lima et al., 2009; Barhorst et al., 2022).

The findings of this study cannot be attributed to the use of negligible amounts of ethanol to dissolve MLT or to the stress related to intraperitoneal injection, as the two control groups (vehicle and intact animals) showed similar behavioral reactions and CSD features. The oral route of administration is clinically the most used in the case of MLT. When ingested orally, only 15% of the MLT dose reaches the systemic circulation; the remaining 85% may undergo significant first-pass metabolism (Demuro et al., 2000). In addition, MLT does not appear to produce physiological or psychological dependence (Andersen et al., 2016).

5. Limitations of this study

5.1. Animal's sex

Although we recognize sex as an essential biological variable on the effects of endogenous melatonin (Kawabata-Sakata et al., 2020), our study included only male rats. This limitation occurred because the hormonal oscillations of the female rat due to the estrous cycle are fast and complex and can alter the parameters that we addressed currently, including CSD (Accioly and Guedes, 2020). The need to use males only becomes even more evident when we use rats in the age of sexual maturation (i.e., from PND 35; Sengupta, 2013). Therefore, in various study groups in fundamental neuroscience, it is common to invest an initial effort in male rats and only then, with a well-established database, apply the same methodologies in female rats.

5.2. Endogenous MLT

Even though we evaluated the administration of exogenous MLT at two concentrations (10 and 40 mg/kg), we did not measure the impact of endogenous MLT—and its physiological oscillations—on electrophysiological parameters, for example. In this study, all experiments were performed during the dark phase of the circadian cycle, when the concentration of endogenous MLT is known to be higher (Govindarajulu et al., 2022). However, it would be interesting to study a control group in which the experiments were carried out in the rat's light phase.

5.3. Routes of exogenous MLT administration

According to Yeleswaram et al. (1997), after intraperitoneal administration of 10 mg/kg Melatonin in rats, only 74% of this initial amount is bioavailable in the plasma due to the hepatic first-pass metabolism. Such pharmacokinetic effect is also observed in the oral route (Demuro et al., 2000). So, to evaluate the importance of the initial metabolism of the drug, it would be interesting to compare it with another parenteral route (e.g., intradermal, intravenous, or intracerebroventricular).

5.4. MLT-receptor dependent vs. independent action

Although we evaluated some of the receptor-independent effects of MLT—e.g., oxidative stress markers—we did not analyze in-depth MLT receptor expression or their downstream impacts. As stated in the Discussion, it is unlikely that these receptors mediate the MLT action on a cortically-based phenomenon like CSD, but we cannot exclude the role of MLT receptors in processes such as anxiety and memory (Dubocovich et al., 1998; Lacoste et al., 2015). Therefore, we encourage future work on this topic.

In conclusion, our findings demonstrate that the behavioral and electrophysiological effects of MLT treatment early in life differentially change as a function of the MLT dose. In behavioral parameters suggestive of anxiety and memory, MLT diminished anxiety and improved object recognition memory at the low dose but not at the high dose. Accordingly, MLT decelerated CSD propagation at the low dose (10 mg/kg) and accelerated CSD at the high dose (40 mg/kg) on the developing rat cortex. In this study, MLT at the low dose (but not at the high dose) was associated with significantly lower MDA and higher SOD cortical levels than the control groups. Based on these behavioral, electrophysiological, and biochemical pieces of evidence, we suggest that, in addition to the receptor-mediated MLT actions (Dubocovich et al., 1998; Lacoste et al., 2015), MLT acts as an antioxidant when given in low doses and may act as a prooxidant when given in high doses, as occurred with CSD under treatment with ascorbic acid (Mendes-da-Silva et al., 2014). However, confirming this suggestion requires a more detailed evaluation of the redox imbalance in the brain.

It is still uncertain whether this new effect of MLT can be extrapolated from the rat to the developing human brain (Vine et al., 2022; Reiter et al., 2023). However, the clinical evidence suggests that melatonin may improve sleep disorders, cognitive functioning (Sumsuzzman et al., 2021), and neonatal hypoxic–ischemic brain lesions (Cardinali, 2019). In addition, melatonin may benefit classical migraine patients (Ebert et al., 1999) and improve blood glucose levels

in diabetes (Delpino et al., 2021). Interestingly, melatonin levels are reduced in some metabolic, cardiovascular, and neurological diseases (Cardinali, 2020). This evidence suggests a possible relevant implication of our novel findings in the developing rat brain.

Data availability statement

The raw data supporting the conclusions of this article will be made available by the authors, without undue reservation.

Ethics statement

The animal study was approved by CEUA—Comitte de Etica e Uso de Animais da UFPE (approval protocol no. 0006/2020). The study was conducted in accordance with the local legislation and institutional requirements.

Author contributions

AA: Data curation, Formal analysis, Investigation, Methodology, Project administration, Visualization, Writing – original draft. MF-d-O: Conceptualization, Formal analysis, Investigation, Validation, Writing – review & editing. AN: Conceptualization, Formal analysis, Methodology, Writing – review & editing. VO: Data curation, Methodology, Writing – review & editing. JC: Conceptualization, Formal analysis, Investigation, Methodology, Writing – original draft. LV: Conceptualization, Formal analysis, Methodology, Writing – review & editing. RG: Conceptualization, Formal analysis, Funding acquisition, Supervision, Writing – review & editing.

Funding

The author(s) declare financial support was received for the research, authorship, and/or publication of this article. This work was supported by the Conselho Nacional de Desenvolvimento Científico e Tecnológico (CNPq no. 40.6495/2018-1), Instituto Nacional de Ciência e Tecnologia (projeto: "Doenças cerebrais, excitotoxicidade e neuroproteção"—Edital INCT/MCT/CNPq), Universidade Federal de Pernambuco; grant number 054179/2022-85, the Pernambuco State Funding Institution for Scientific and Technological Development (Fundação de Amparo à Ciência e Tecnologia de Pernambuco, FACEPE; grant numbers IBPG-0469-2.08/20, APQ-1072-2.07/15, and APQ-0409-2.07/14). RG is a research fellow from CNPq (no. 30.5998/2018-8).

Acknowledgments

The authors thank Dayane Aparecida Gomes for providing access to the apparatus located in her lab (Multiuser Platform in Cellular and Molecular Biology—FACEPE 16/2012; no 1133-2.07/2012). We thank Melissa Mesquita, Claudia Oliveira, Thais Almeida, Filipe Barbosa, and Marcelo da Rocha for their technical support.

Conflict of interest

The authors declare that the research was conducted in the absence of any commercial or financial relationships that could be construed as a potential conflict of interest.

The author(s) declared that they were an editorial board member of Frontiers, at the time of submission. This had no impact on the peer review process and the final decision.

Publisher's note

References

Accioly, N. E., and Guedes, R. C. A. (2020). Topical cortical application of ovarian hormones and modulation of brain electrical activity: analysis of spreading depression in well-nourished and malnourished female rats. *Nutr. Neurosci.* 23, 887–895. doi: 10.1080/1028415X.2019.1575574

Akyuz, E., Polat, A. K., Eroglu, E., Kullu, I., Angelopoulou, E., and Paudel, Y. N. (2021). Revisiting the role of neurotransmitters in epilepsy: an updated review. *Life Sci.* 265:118826. doi: 10.1016/j.lfs.2020.118826

Al Gburi, M. R. A., Altinoz, E., Elbe Onal, M. O., Yilmaz, U., Yilmaz, N., Karayakali, M., et al. (2023). Pinealectomy and melatonin administration in rats: their effects on pulmonary edema induced by α-naphthylthiourea. *Drug Chem. Toxicol.* 46, 1024–1034. doi: 10.1080/01480545.2022.2119994

Améndola, L., Weary, D., and Zobel, G. (2022). Effects of personality on assessments of anxiety and cognition. *Neurosci. Biobehav. Rev.* 141:104827. doi: 10.1016/j.neubiorev.2022.104827

Andersen, L. P., Gögenur, I., Rosenberg, J., and Reiter, R. J. (2016). The safety of melatonin in humans. *Clin. Drug Investig.* 36, 169–175. doi: 10.1007/s40261-015-0368-5

Arendt, J. (2005). Melatonin: characteristics, concerns, and prospects. *J. Biol. Rhythms* 20, 291–303. doi: 10.1177/0748730405277492

Barhorst, K. A., Alfawares, Y., McGuire, J. L., Danzer, S. C., Hartings, J. A., and Ngwenya, L. B. (2022). Remote and persistent alterations in glutamate receptor subunit composition induced by spreading depolarizations in rat brain. *Cell. Mol. Neurobiol.* 42, 1253–1260. doi: 10.1007/s10571-020-01000-3

Bouslama, M., Renaud, J., Olivier, P., Fontaine, R. H., Matrot, B., Gressens, P., et al. (2007). Melatonin prevents learning disorders in brain-lesioned newborn mice. *Neuroscience* 150, 712–719. doi: 10.1016/j.neuroscience.2007.09.030

Boutin, J. A., Kennaway, D. J., and Jockers, R. (2023). Melatonin: facts, Extrapolations and Clinical Trials. *Biomolecules* 13:943. doi: 10.3390/biom13060943

Calza, A., Sogliano, C., Santoru, F., Marra, C., Angioni, M. M., Mostallino, M. C., et al. (2010). Neonatal exposure to estradiol in rats influences neuroactive steroid concentrations, GABAA receptor expression, and behavioral sensitivity to anxiolytic drugs. *J. Neurochem.* 113, 1285–1295. doi: 10.1111/j.1471-4159.2010.06696.x

Cardinali, D. P. (2019). An assessment of Melatonin's therapeutic value in the hypoxic-ischemic encephalopathy of the newborn. *Front Synap Neurosci.* 11:34. doi: 10.3389/fnsyn.2019.00034

Cardinali, D. P. (2020). Melatonin and healthy aging. *Vitam. Horm.* 115, 67–88. doi: 10.1016/bs.vh.2020.12.004

Colella, M., Biran, V., and Baud, O. (2016). Melatonin and the newborn brain. *Early Hum. Dev.* 102, 1–3. doi: 10.1016/j.earlhumdev.2016.09.001

Delpino, F. M., Figueiredo, L. M., and Nunes, B. P. (2021). Effects of melatonin supplementation on diabetes: a systematic review and meta-analysis of randomized clinical trials. *Clin. Nutr.* 40, 4595–4605. doi: 10.1016/j.clnu.2021.06.007

DeMuro, R. L., Nafziger, A. N., Blask, D. E., Menhinick, A. M., and Bertino, J. S. Jr. (2000). The absolute bioavailability of oral melatonin. *J. Clin. Pharmacol.* 40, 781–784. doi: 10.1177/00912700022009422

Dere, E., Huston, J. P., and De Souza Silva, M. A. (2005). Integrated memory for objects, places, and temporal order: evidence for episodic-like memory in mice. *Neurobiol. Learn. Mem.* 84, 214–221. doi: 10.1016/j.nlm.2005.07.002

Doseděl, M., Jirkovský, E., Macáková, K., Krčmová, L. K., Javorská, L., Pourová, J., et al. (2021). Vitamin C-sources, physiological role, kinetics, deficiency, use, toxicity, and determination. *Nutrients* 13:615. doi: 10.3390/nu13020615

Dubocovich, M. L., Yun, K., Wm, A.-G., Benloucif, S., and Masana, M. I. (1998). Selective MT2 melatonin receptor antagonists block melatonin-mediated phase advances of circadian rhythms. *FASEB J.* 12, 1211–1220. doi: 10.1096/fasebj.12.12.1211

Ebert, E., Hanke, W., Wiedemann, M., and Fernandes de Lima, V. M. (1999). Biphasic effects of melatonin on the propagation of excitation waves in the chicken retina. *Neurosci. Lett.* 268, 37–40. doi: 10.1016/s0304-3940(99)00376-6

El-Bachá, R. S., De-Lima-Filho, J. L., and Guedes, R. C. (1998). Dietary antioxidant deficiency facilitates cortical spreading depression induced by photo-activated riboflavin. *Nutr. Neurosci.* 1, 205–212. doi: 10.1080/1028415X.1998.11747230

El-Sherif, Y., Tesoriero, J., Hogan, M. V., and Wieraszko, A. (2003). Melatonin regulates neuronal plasticity in the hippocampus. *J. Neurosci. Res.* 72, 454–460. doi: 10.1002/jnr.10605

Ennaceur, A., and Delacour, J. (1988). A new one-trial test for neurobiological studies of memory in rats. 1: behavioral data. *Behav. Brain Res.* 31, 47–59. doi: 10.1016/0166-4328(88)90157-x

Flinn, T., McCarthy, N. L., Swinbourne, A. M., Gatford, K. L., Weaver, A. C., McGrice, H. A., et al. (2020). Supplementing merino ewes with melatonin during the last half of pregnancy improves tolerance of prolonged parturition and survival of second-born twin lambs. *J. Anim. Sci.* 98, 1–10. doi: 10.1093/jas/skaa372

Foster, P. S., Campbell, R. W., Williams, M. R., Branch, K. K., Roosa, K. M., Orman, C., et al. (2014). Administration of exogenous melatonin increases spreading activation in lexical memory networks. *Hum. Psychopharmacol.* 29, 397–404. doi: 10.1002/hup.2416

Francisco, E. S., and Guedes, R. C. A. (2015). Neonatal taurine and alanine modulate anxiety-like behavior and decelerate cortical spreading depression in rats previously suckled under different litter sizes. *Amino Acids* 47, 2437–2445. doi: 10.1007/s00726-015-2036-8

Gogvadze, V., Norberg, E., Orrenius, S., and Zhivotovsky, B. (2010). Involvement of ca(2+) and ROS in alpha-tocopheryl succinate-induced mitochondrial permeabilization. *Int. J. Cancer* 127, 1823–1832. doi: 10.1002/ijc.25204

Gondim-Silva, K. R., da Silva, J. M., LAV, S., and RCA, G. (2021). Neonatal pyridoxine administration long lastingly accelerates cortical spreading depression in male rats, without affecting anxiety-like behavior. *Nutr. Neurosci.* 24, 363–370. doi: 10.1080/1028415X.2019.1632570

Govindarajulu, M., Patel, M. Y., Wilder, D. M., Long, J. B., and Arun, P. (2022). Blast exposure dysregulates nighttime melatonin synthesis and signaling in the pineal gland: a potential mechanism of blast-induced sleep disruptions. *Brain Sci.* 12:1340. doi: 10.3390/brainsci12101340

Grantham-Mcgregor, S. (1995). A review of studies of the effect of severe malnutrition on mental development. *J. Nutr.* 125, 2233S–2238S. doi: 10.1093/jn/125.suppl_8.2233S

Guedes, R. C. A. (2011). "Cortical spreading depression: a model for studying brain consequences of malnutrition" in *Handbook of Behavior, Food and Nutrition*. eds. V. R. Preedy, R. R. Watson and C. R. Martin (London: Springer), 2343–2355.

Guedes, R. C. A., and Abadie-Guedes, R. (2019). Brain aging and electrophysiological signaling: revisiting the spreading depression model. *Front. Aging Neurosci.* 11:136. doi: 10.3389/fnagi.2019.00136

Guedes, R. C., Abadie-Guedes, R., and Bezerra, R. S. (2012). The use of cortical spreading depression for studying the brain actions of antioxidants. *Nutr. Neurosci.* 15, 111–119. doi: 10.1179/1476830511Y.0000000024

Guedes, R. C. A., Araújo, M. G. R., Verçosa, T. C., Bion, F. M., de Sá, A. L., Pereira, A. Jr., et al. (2017). Evidence of an inverse correlation between serotonergic activity and spreading depression propagation in the rat cortex. *Brain Res.* 1672, 29–34. doi: 10.1016/j.brainres.2017.07.011

Gunata, M., Parlakpinar, H., and Acet, H. A. (2020). Melatonin: a review of its potential functions and effects on neurological diseases. *Rev. Neurol.* 176, 148–165. doi: 10.1016/j.neurol.2019.07.025

Iwashita, H., Matsumoto, Y., Maruyama, Y., Watanabe, K., Chiba, A., and Hattori, A. (2021). The melatonin metabolite N1-acetyl-5-methoxykynuramine facilitates long-term object memory in young and aging mice. *J. Pineal Res.* 70:e12703. doi: 10.1111/jpi.12703

Kaur, C., Viswanathan, S., and Ling, E. A. (2011). Hypoxia-induced cellular and vascular changes in the nucleus tractus solitarius and ventrolateral medulla. *J. Neuropathol. Exp. Neurol.* 70, 201–217. doi: 10.1097/nen.0b013e31820d8f92

Kawabata-Sakata, Y., Nishiike, Y., Fleming, T., Kikuchi, Y., and Okubo, K. (2020). Androgen-dependent sexual dimorphism in pituitary tryptophan hydroxylase expression: relevance to sex differences in pituitary hormones. *Proc. R. Soc.* 287:20200713. doi: 10.1098/rspb.2020.0713

Koroleva, V. I., and Bures, J. (1980). Blockade of cortical spreading depression in electrically and chemically stimulated areas of cerebral cortex in rats. *Electroencephalogr. Clin. Neurophysiol.* 48, 1–15. doi: 10.1016/0013-4694(80)90038-3

Lacoste, B., Angeloni, D., Dominguez-Lopez, S., Calderoni, S., Mauro, A., Fraschini, F., et al. (2015). Anatomical and cellular localization of melatonin MT1 and MT2 receptors in the adult rat brain. *J. Pineal Res.* 58, 397–417. doi: 10.1111/jpi.12224

Lamtai, M., Azirar, S., Zghari, O., Ouakki, S., El Hessni, A., Mesfioui, A., et al. (2021). Melatonin ameliorates cadmium-induced affective and cognitive impairments and hippocampal oxidative stress in rat. *Biol. Trace Elem. Res.* 199, 1445–1455. doi: 10.1007/s12011-020-02247-z

Lauritzen, M., and Strong, A. J. (2017). 'Spreading depression of Leão' and its emerging relevance to acute brain injury in humans. *J. Cereb. Blood Flow Metab.* 37, 1553–1570. doi: 10.1177/0271678X16657092

Leão, A. A. (1944). Spreading depression of activity in the cerebral cortex. *J. Neurophysiol.* 7, 359–390. doi: 10.1152/jn.1944.7.6.359

Leão, A. A. (1947). Further observations on the spreading depression of activity in the cerebral cortex. *J. Neurophysiol.* 10, 409–414. doi: 10.1152/jn.1947.10.6.409

Lima, D. S., Maia, L. M., Barboza Ede, A., Duarte, R. A., de Souza, L. S., and Guedes, R. C. A. (2009). L-glutamine supplementation during the lactation period facilitates cortical spreading depression in well-nourished and early-malnourished rats. *Life Sci.* 85, 241–247. doi: 10.1016/j.lfs.2009.05.017

Louzada, P. R., Paula Lima, A. C., Mendonça-Silva, D. L., Noël, F., De Mello, F. G., and Ferreira, S. T. (2004). Taurine prevents the neurotoxicity of beta-amyloid and glutamate receptor agonists: activation of GABA receptors and possible implications for Alzheimer's disease and other neurological disorders. *FASEB J.* 18, 511–518. doi: 10.1096/fj.03-0739com

Martinis, P., Zago, L., Maritati, M., Battaglia, V., Grancara, S., Rizzoli, V., et al. (2012). Interactions of melatonin with mammalian mitochondria. Reducer of energy capacity and amplifier of permeability transition. *Amino Acids* 42, 1827–1837. doi: 10.1007/s00726-011-0903-5

Mendes-Da-Silva, R. F., Cunha-Lopes, A. A., Bandim-da-Silva, M. E., Cavalcanti, G. A., Rodrigues, A. R. O., Andrade-da-Costa, B. L. S., et al. (2014). Prooxidant versus antioxidant brain action of ascorbic acid in well-nourished and malnourished rats as a function of dose: a cortical spreading depression and malondialdehyde analysis. *Neuropharmacology* 86, 155–160. doi: 10.1016/j.neuropharm.2014.06.027

Misra, H. P., and Fridovich, I. (1972). The role of superoxide anion in the autoxidation of epinephrine and a simple assay for superoxide dismutase. *J. Biol. Chem.* 247, 3170–3175.

Netto, M., and Martins-Ferreira, H. (1989). Elicitation of spreading depression by rose Bengal photodynamic action. *Photochem. Photobiol.* 50, 229–234. doi: 10.1111/j.1751-1097.1989.tb04153.x

Nosjean, O., Nicolas, J. P., Klupsch, F., Delagrange, P., Canet, E., Jean, A., et al. (2001). Comparative pharmacological studies of melatonin receptors: MT1, MT2 and MT3/QR2. Tissue distribution of MT3/QR2. *Biochem. Pharmacol.* 61, 1369–1379. doi: 10.1016/S0006-2952(01)00615-3

Ohkawa, H., Ohishi, N., and Yagi, K. (1979). Assay for lipid peroxides in animal tissues by thiobarbituric acid reaction. *Anal. Biochem.* 95, 351–358. doi: 10.1016/0003-2697(79)90738-3

Otero, P., Viana, M., Herrera, E., and Bonet, B. (1997). Antioxidant and prooxidant effects of ascorbic acid, dehydroascorbic acid and flavonoids on LDL submitted to different degrees of oxidation. *Free Radic. Res.* 27, 619–626. doi: 10.3109/10715769709097865

Pandi-Perumal, S. R., BaHammam, A. S., Brown, G. M., Spence, D. W., Bharti, V. K., Kaur, C., et al. (2013). Melatonin antioxidative defense: therapeutical implications for aging and neurodegenerative processes. *Neurotox. Res.* 23, 267–300. doi: 10.1007/s12640-012-9337-4

Pellow, S., Chopin, P., File, S. E., and Briley, M. (1985). Validation of open:closed arm entries in an elevated plus-maze as a measure of anxiety in the rat. *J. Neurosci. Methods* 14, 149–167. doi: 10.1016/0165-0270(85)90031-7

Podmore, I. D., Griffiths, H. R., Herbert, K. E., Mistry, N., Mistry, P., and Lunec, J. (1998). Vitamin C exhibits prooxidant properties. *Nature* 392:559. doi: 10.1038/33308

Poeggeler, B., Reiter, R. J., Tan, D.-X., Chen, L.-D., and Manchester, L. C. (1993). Melatonin, hydroxyl radical-mediated oxidative damage, and aging: a hypothesis. *J. Pineal Res.* 14, 151–168. doi: 10.1111/j.1600-079x.1993.tb00498.x

Proost, R., Lagae, L., Van Paesschen, W., and Jansen, K. (2022). Sleep in children with refractory epilepsy and epileptic encephalopathies: a systematic review of literature. *Eur. J. Paediatr. Neurol.* 38, 53–61. doi: 10.1016/j.ejpn.2022.03.010

Radogna, F., Diederich, M., and Ghibelli, L. (2010). Melatonin: a pleiotropic molecule regulating inflammation. *Biochem. Pharmacol.* 80, 1844–1852. doi: 10.1016/j.bcp.2010.07.041

Reiter, R. J., Rosales-Corral, S., Tan, D. X., Jou, M. J., Galano, A., and Xu, B. (2017). Melatonin as a mitochondria-targeted antioxidant: one of evolution's best ideas. *Cell. Mol. Life Sci.* 74, 3863–3881. doi: 10.1007/s00018-017-2609-7

Reiter, R. J., Sharma, R., Cucielo, M. S., Tan, D. X., Rosales-Corral, S., Gancitano, G., et al. (2023). Brain washing and neural health: role of age, sleep, and the cerebrospinal fluid melatonin rhythm. *Cell. Mol. Life Sci.* 80:88. doi: 10.1007/s00018-023-04736-5

Reiter, R., Tan, D. X., Rosales-Corral, S., Galano, A., Zhou, X. J., and Xu, B. (2018). Mitochondria: central organelles for melatonin's antioxidant and anti-aging actions. *Molecules* 23:509. doi: 10.3390/molecules23020509

Rodriguez, C., Mayo, J. C., Sainz, R. M., Antolín, I., Herrera, F., Martín, V., et al. (2004). Regulation of antioxidant enzymes: a significant role for melatonin. *J. Pineal Res.* 36, 1–9. doi: 10.1046/j.1600-079x.2003.00092.x

Sanchez-Barcelo, E. J., Rueda, N., Mediavilla, M. D., Martinez-Cue, C., and Reiter, R. J. (2017). Clinical uses of melatonin in neurological diseases and mental and behavioural disorders. *Curr. Med. Chem.* 24, 3851–3878. doi: 10.2174/0929867324666170718105557

Sengupta, P. (2013). The laboratory rat: relating its age with Human's. *Int. J. Prev. Med.* 4, 866–875.

Soleimani, E., Goudarzi, I., Abrari, K., and Lashkarbolouki, T. (2017). Maternal administration of melatonin prevents spatial learning and memory deficits induced by developmental ethanol and lead co-exposure. *Physiol. Behav.* 173, 200–208. doi: 10.1016/j.physbeh.2017.02.012

Sousa, M. S. B., Alves, D. V. S., Monteiro, H. M. C., Gomes, D. A., Lira, E. C., and Amancio-Dos-Santos, A. (2021). Sepsis impairs the propagation of cortical spreading depression in rats and this effect is prevented by antioxidant extract. *Nutr. Neurosci.* 24, 130–139. doi: 10.1080/1028415X.2019.1602987

Sumsuzzman, D. M., Choi, J., Jin, Y., and Hong, Y. (2021). Neurocognitive effects of melatonin treatment in healthy adults and individuals with Alzheimer's disease and insomnia: a systematic review and meta-analysis of randomized controlled trials. *Neurosci. Biobehav. Rev.* 127, 459–473. doi: 10.1016/j.neubiorev.2021.04.034

Sun, Y., Ma, L., Jin, M., Zheng, Y., Wang, D., and Ni, H. (2021). Effects of melatonin on Neurobehavior and cognition in a cerebral palsy model of plppr5−/− mice. *Front. Endocrinol.* 12:598788. doi: 10.3389/fendo.2021.598788

Tan, D.-X., Manchester, L. C., Terron, M. P., Flores, L. J., Tamura, H., and Reiter, R. J. (2007). Melatonin as a naturally occurring co-substrate of quinone reductase-2, the putative MT3 melatonin membrane receptor: hypothesis and significance. *J. Pineal Res.* 43, 317–320. doi: 10.1111/j.1600-079X.2007.00513.x

Torrão, A. S., Gobersztejn, F., Guedes, R. C. A., and Britto, L. R. G. (2002). Application of potassium chloride to the surface of the rat visual cortex differentially affects the expression of presumptive neuroprotective molecules. *J. Neurocytol.* 31, 49–55. doi: 10.1023/a:1022575716111

Viana, L. C., Lima, C. M., Oliveira, M. A., Borges, R. P., Cardoso, T. T., Almeida, I. N. F., et al. (2013). Litter size, age-related memory impairments, and microglial changes in rat dentate gyrus: stereological analysis and three dimensional morphometry. *Neuroscience* 238, 280–296. doi: 10.1016/j.neuroscience.2013.02.019

Vine, T., Brown, G. M., and Frey, B. N. (2022). Melatonin use during pregnancy and lactation: a scoping review of human studies. *Braz J Psychiatry.* 44, 342–348. doi: 10.1590/1516-4446-2021-2156

Wang, J., Jiang, C., Zhang, K., Lan, X., Chen, X., Zang, W., et al. (2019b). Melatonin receptor activation provides cerebral protection after traumatic brain injury by mitigating oxidative stress and inflammation via the Nrf2 signaling pathway. *Free Radic. Biol. Med.* 131, 345–355. doi: 10.1016/j.freeradbiomed.2018.12.014

Wang, J., Wang, X., He, Y., Jia, L., Yang, C. S., Reiter RJ, R. J., et al. (2019a). Antioxidant and Prooxidant activities of melatonin in the presence of copper and polyphenols in vitro and in vivo. *Cells* 8:903. doi: 10.3390/cells8080903

Wolfler, A., Caluba, H. C., Abuja, P. M., Dohr, G., Schauenstein, K., and Liebmann, P. M. (2001). Prooxidant activity of melatonin promotes fas-induced cell death in human leukemic Jurkat cells. *FEBS Lett.* 502, 127–131. doi: 10.1016/s0014-5793(01)02680-1

Xia, A.-Y., Zhu, H., Zhao, Z.-J., Liu, H.-Y., Wang, P.-H., Ji, L.-D., et al. (2023). Molecular Mechanisms of the Melatonin Receptor Pathway Linking Circadian Rhythm to Type 2 Diabetes Mellitus. *Nutrients* 15:1406. doi: 10.3390/nu15061406

Yeleswaram, K., McLaughlin, L. G., Knipe, J. O., and Schabdach, D. (1997). Pharmacokinetics and oral bioavailability of exogenous melatonin in preclinical animal models and clinical implications. *J. Pineal Res.* 22, 45–51. doi: 10.1111/j.1600-079x.1997.tb00302.x

Zakaria, R., Ahmad, A. H., and Othman, Z. (2016). The potential role of melatonin on memory function: lessons from rodent studies. *Folia Biol.* 62, 181–187.

Zhang, H. M., and Zhang, Y. (2014). Melatonin: a well-documented antioxidant with conditional prooxidant actions. *J. Pineal Res.* 57, 131–146. doi: 10.1111/jpi.12162

Zhang, H., Zhang, H. M., Wu, L. P., Tan, D. X., Kamat, A., Li, Y. Q., et al. (2011). Impaired mitochondrial complex III and melatonin responsive reactive oxygen species generation in kidney mitochondria of db/db mice. *J. Pineal Res.* 51, 338–344. doi: 10.1111/j.1600-079X.2011.00894.x

Zhang, H. M., Zhang, Y., and Zhang, B. X. (2011). The role of mitochondrial complex III in melatonin-induced ROS production in cultured mesangial cells. *J. Pineal Res.* 50, 78–82. doi: 10.1111/j.1600-079X.2010.00815.x

frontiers | Frontiers in Neuroscience

TYPE Original Research
PUBLISHED 27 February 2024
DOI 10.3389/fnins.2024.1349421

OPEN ACCESS

EDITED BY
Fahmeed Hyder,
Yale University, United States

REVIEWED BY
Ana-Maria Oros-Peusquens,
Helmholtz Association of German Research Centres (HZ), Germany
Charles Springer,
Oregon Health and Science University, United States

*CORRESPONDENCE
Adriana Ximenes-da-Silva
✉ aximenes@ccbi.ufal.br

RECEIVED 04 December 2023
ACCEPTED 07 February 2024
PUBLISHED 27 February 2024

CITATION
Mendes CB, da Rocha LS, de Carvalho Frag CA and Ximenes-da-Silva A (2024) Homeostatic status of thyroid hormones and brain water movement as determinant factors in biology of cerebral gliomas: a pilot study using a bioinformatics approach. *Front. Neurosci.* 18:1349421. doi: 10.3389/fnins.2024.1349421

Homeostatic status of thyroid hormones and brain water movement as determinant factors in biology of cerebral gliomas: a pilot study using a bioinformatics approach

Carmelita Bastos Mendes[1], Lanni Sarmento da Rocha[1], Carlos Alberto de Carvalho Fraga[2] and Adriana Ximenes-da-Silva[1]*

[1]Laboratório de Eletrofisiologia e Metabolismo Cerebral, Instituto de Ciências Biológicas e da Saúde, Universidade Federal de Alagoas, Maceió, Brazil, [2]Faculdade de Medicina, Universidade Federal de Alagoas, Arapiraca, Brazil

Introduction: The expression and localization of the water channel transporters, aquaporins (AQPs), in the brain are substantially modified in gliomas during tumorigenesis, cell migration, edema formation, and resolution. We hypothesized that the molecular changes associated with AQP1 and AQP4 in the brain may potentially be anticancer therapeutic targets. To test this hypothesis, a bioinformatics analysis of publicly available data from international consortia was performed.

Methods: We used RNA-seq as an experimental strategy and identified the number of differential *AQP1* and *AQP4* transcript expressions in glioma tissue compared to normal brain tissue.

Results: AQPs genes are overexpressed in patients with glioma. Among the glioma subtypes, AQP1 and AQP4 were overexpressed in astrocytoma (low-grade glioma) and classical (high-grade glioma). Overall survival analysis demonstrated that both AQP genes can be used as prognostic factors for patients with low-grade glioma. Additionally, we observed a correlation between the expression of genes involved in the tyrosine and thyroid hormone pathways and AQPs, namely: *PNMT, ALDH1A3, AOC2, HGDATP1B1, ADCY5, PLCB4, ITPR1, ATP1A3, LRP2, HDAC1, MED24, MTOR,* and *ACTB1* (Spearman's coefficient = *geq* 0.20 and p-value = $\leq$ 0.05).

Conclusion: Our findings indicate that the thyroid hormone pathways and AQPs 1 and 4 are potential targets for new anti-tumor drugs and therapeutic biomarkers for malignant gliomas.

KEYWORDS

gliomas, AQPs, water movement, biomarkers, gene expression, thyroid hormones, correlation analysis

1 Introduction

Gliomas are the most common central nervous system tumor type accounting for approximately 80% of all malignant intracranial tumors with high episodes of recurrence (Ostrom et al., 2014).

Depending on the cell type of origin, they can be classified or subdivided into astrocytomas, ependymomas, oligodendrogliomas, oligoastrocytomas, and glioblastoma multiforme (GBM) (Ostrom et al., 2014).

Glioblastoma is the most aggressive brain tumor owing to its high invasiveness. Despite advances in therapeutic modalities (tumor resection combined with chemotherapy and radiotherapy), the overall patient survival rate is 12–15 months from the initial diagnosis, with only 5% of patients reaching a 5-year survival rate (Fedele et al., 2019).

Likewise, temozolomide (TMZ), a DNA alkylating agent, is the standard first-line treatment for GBM, has a significant tumor recurrence rate and confers drug resistance (Strobel et al., 2019) due to its low specificity and limitations in crossing the blood-brain barrier (BBB).

Persistent headaches, neurological and behavioral deficits, seizures, cognitive deficits, drowsiness, dysphagia, confusion, aphasia, motor deficits, fatigue, dyspnea, and mood changes are common symptoms in patients diagnosed with glioblastoma (Maugeri et al., 2016; IJzerman-Korevaar et al., 2018). Usually, its localization, size, and grade make it inoperable and difficult to treat, drastically decreasing the quality of life of patients with glioma (Fedele et al., 2019).

Many symptoms are derived from neurological findings such as increased intracranial pressure and brain herniation. Edema around the tumor causes hypoxia (lack of oxygen supply) (Solar et al., 2022), resulting in long-term disability, psychiatric disorders, substance abuse, or self-harm (Huang et al., 2021).

A clinical study carried out by Wu et al. (2015) showed that within the identification of peritumoral edema during the preoperative period in patients with glioblastoma, factors such as necrosis and edema extent were independent factors for poor outcome and overall survival (OS).

Aquaporins (AQPs), a family of transmembrane water channel proteins, play a critical role in responding to changes in the osmotic environment. Eight members of the water channel family are expressed in the central nervous system (Saadoun et al., 2002; Maugeri et al., 2016). AQP1 and AQP4 are the major water channels in the brain and play a pivotal role in water homeostasis and the maintenance of BBB integrity (Galán-Cobo et al., 2016).

Abbreviations: ANOVA, analysis of variance; AQP, aquaporin; BBB, blood-brain barrier; CI, confidence interval; CNS, central nervous system; CSF, cerebrospinal fluid; DEG, differentially expressed gene; GBM, glioblastoma; GTEx, the genotype-tissue expression; GEPIA, gene expression profiling interactive analysis; HR, hazard ratio; IDH, isocitrate dehydrogenase; KEGG, Kyoto Encyclopedia of Genes and Genomes; LGG, low-grade glioma; MGMT, O-6-methylguanine-DNA methyltransferase; NCBI, national center for biotechnology information; NTIS, Non-thyroidal illness syndrome; OS, overall survival; RNA-seq, *Ribonucleic Acid sequencing*; TCGA, the cancer genome atlas; TMZ, temozolomide; TIMER, tumor IMmune estimation resource; TPM, transcript per million; TSH, thyroid-stimulating hormone; WHO, World Health Organization.

Brain AQPs are distributed primarily in astroglial membranes, especially in perivascular astrocyte foot processes and glia limitans, near the brain fluid compartments (Hubbard et al., 2018; Li et al., 2019) and ependymal cells, providing an efficient system to promote water and solute transport between the perivascular space and glial cells, and to support brain parenchymal clearance through the glymphatic system (Smith et al., 2017; Mestre et al., 2018; Lohela et al., 2022).

AQP4, an orthodox AQP type, is upregulated in gliomas and is involved in the tumorigenesis process, that is, cell migration, invasion, and functional changes in the surrounding tissue. AQP4 distribution has been hypothesized to underlie mechanisms related to the degree of malignancy (Lan et al., 2017), edema formation in the peritumoral region, increased intracranial pressure, and seizure episodes (Dubois et al., 2014; Maugeri et al., 2016).

Tumor cell migration is a complex mechanism not well understood. However, angiogenesis is a critical feature differentiating high-grade and low-grade glioma. Glioblastoma as the most aggressive brain tumor shows morphological and vascular changes characterized by a high invasiveness and migration, which are associated with the expression of AQP1 and AQP4 and mesenchymal transformation as previously described (Hardee and Zagzag, 2012; Brennan et al., 2013).

Aquaporins have been described to have a vital role in enhanced invasion and tumor cell migration as reviewed by De Ieso and Yool (2018) and Moon et al. (2022). Of special importance is the role of AQP1 and -4 in the proposed mechanism of invasiveness and migration of glioma cells. During tumor cells metastasis modifications of blood supply, cytoskeleton and extracellular matrix structure are needed to promote angiogenesis for tissue demands of oxygen and nutrient delivery. AQP1 was found to boost endothelial cell migration and, in association with overexpression of AQP4 to regulate water influx and extracellular matrix interaction leading to tumor cell membrane filopodia formation, mechanisms linked to metastasis progression.

Several *in vitro* and *in vivo* studies have reported reduced invasive capacity and migration in tumors after AQP4 depletion or downregulation (Ding et al., 2010, 2011; Cheng et al., 2017) by decreasing water permeability, which in turn upregulates transmembrane water fluxes during tumor or healthy astroglial cell movement (Huang et al., 2021).

In contrast, AQP1 (also considered a classic aquaporin) is predominantly expressed in the circumventricular brain and areas associated with cerebrospinal fluid production. Its expression is altered in the human brain under pathological conditions (Lima et al., 2012) such as cancer. In brain tumors, AQP1 and AQP4 expression is upregulated with the malignancy grade (Saadoun et al., 2002).

Inhibition of tumor growth and suppression of vasculogenic mimicry formation were observed following *AQP1* silencing *in vivo*, which could be related to reduced tumor aggressiveness, malignancy, and metastasis (Perry and Wesseling, 2016).

More recently, the newly updated World Health Organization (WHO) Classification of Tumors of the Central Nervous System classifies brain tumors based on their histological appearance and molecular markers (genotypic classifications). Namely: isocitrate dehydrogenase (IDH) mutation, 1p/19q codeletion, and O-6-methylguanine-DNA methyltransferase (MGMT) methylation, avoiding imprecise

diagnosis, thereby significantly influencing in the selection of treatment options for patients (Martinez-Lage and Sahm, 2018; Huang et al., 2020).

Owing to the role of molecular markers in the early diagnosis of gliomas, we hypothesized that AQP1 and AQP4, as homeostatic brain proteins, could act as potential anticancer therapeutic targets.

In this study, we aimed to characterize the expression patterns of genes encoding AQP1 and AQP4 proteins and to identify the genes present in the cancerous microenvironment that potentially regulate or correlate with their expression in human gliomas. Our findings, from a bioinformatic approach, allowed us to conduct a wide and diversified scale analysis and provided evidence for the role of these proteins and other related genes, thus paving the way for the development of potential biomarker candidates for the diagnosis and therapeutic targets of glioma for future research.

2 Materials and methods

2.1 Experimental design

This study was executed using publicly available data from international consortia. In this study, RNA-seq was used as the search strategy. Differential expression analysis was performed using Bioconductor statistical packages with R software (version 4.1). Genomic data on human cancer samples originated from The Cancer Genome Atlas (TCGA) and healthy tissue of the Genotype-Tissue Expression (GTEx) project.

We used web tools to assess the variables beyond differential expression. Correlation analysis was performed using Gene Expression Profiling Interactive Analysis (GEPIA2) (Tang et al., 2019),[1] survival analysis, and Tumor IMmune Estimation Resource (TIMER) (Li et al., 2020).[2] In addition, we used the Atlas of Human Pathology[3] to visualize the distribution pattern of AQP1 and AQP4 proteins in healthy brain and cancer tissues.

The database annotation, visualization, and integrated discovery (DAVID) web server (Sherman et al., 2022)[4] was used to identify a network of related genes in altered pathways in the tumor microenvironment (functional enrichment analysis). The same analysis was performed using PathfindR package (Ulgen et al., 2019).

In a short time, the genes involved in the pathways of our choice were evaluated by the degree of correlation with *AQP1* and *AQP4* expression in glioma tissues, both low-grade glioma (LGG) and GBM, to find similarities in expression profiles and suggest some degree of co-regulation.

Clinical data from patients regarding brain tumor location were not accessed and were not included in this study.

1 http://gepia2.cancer-pku.cn

2 http://timer.cistrome.org/

3 https://www.proteinatlas.org/

4 https://david.ncifcrf.gov/

2.2 Transcriptional expression of *AQP1* and *AQP4*

Genetic profiles of normal and solid primary tumor tissues for the two types of cancer were downloaded from TCGA[5] using TCGAbiolinks R package version 2.12.6.

A dataset composed of 2,080 RNA-seq of both tumor stages (LGG and GBM, $N = 671$) and healthy patient samples ($N = 1{,}409$) from TCGA and GTEx projects was used. Data were derived from the Illumina HiSeq RNA-Seq platform. The transcript levels of orthodox AQPs (*AQP1* and *AQP4*) in tumor and non-tumor tissues were evaluated. All data were processed and standardized using R software version 4.1.0.

The GEPIA2 web-based tool was used to build graphs to better visualize the results. One-way analysis of variance (ANOVA) was used for the assessment of the disease state: tumor, $N = 518$ (LGG) and $N = 163$ (GBM), or normal brain cortex, $N = 207$, as the variable for calculating the differential expression. The expression data were first transformed using the formula log2 (TPM + 1).

The fold change (log2FC) was defined as the difference in the median value between the normal and tumor samples. Genes with $P \leq 0.05$ and $|\log2\text{fold change (FC)}| \geq 1.0$ were considered differentially expressed genes (DEGs). The same analysis was performed for glioma subtypes. All the results are presented in table and box plot forms.

The values were calculated using the corresponding formula:

$$log2FC = log2(B) - log2(A)$$

Where B and A are representative of the median values of the genes expressed in the tumor and median values of the expressed genes in normal tissue, respectively.

2.3 Survival analysis

We sought to assess whether our search goal genes in this study may have survival advantages and, thus, establish possible prognostic markers, confirming their clinical significance.

Patients with glioma were divided into high- or low-level groups based on the median value of genes, and OS rates were evaluated using Kaplan–Meier analysis. The TIMER tool used the log-rank test (Mantel-Cox test) for the hypothesis evaluation. The Cox proportional hazard ratio (HR) and 95% confidence interval (CI) were used as parameters in the Kaplan–Meier survival analysis. Statistical significance was set at $P < 0.05$.

2.4 Functional enrichment analysis

Kyoto Encyclopedia of Genes and Genomes (KEGG) is an integrated database resource for biological interpretation of genome sequences and other high-throughput data. KEGG analyses are available in the DAVID database (see text footnote 4), a data resource composed of an integrated biology knowledge base and analysis tools to extract meaningful biological information

5 https://portal.gdc.cancer.gov/

TABLE 1 AQP's differential expression in gliomas samples from TCGA and GTEx dataset.

GENE ID	LogFC	*P*-Value	Adjusted *P*-value
AQP1	1.42	1.66E−40	3.15E−40
AQP4	1.02	8.82E−26	1.48E−25
AQP5	−2.18	1.15E−100	3.51E−100
AQP7	−3.11	1.1E−114	3.76E−114
AQP8	−2.19	7.71E−124	2.83E−123

*Orthodox aquaporins: functional division of AQPS. This group is permeable to water, but not to small neutral solutes. Other members of the family of these proteins are aquaglyceroporins (Yasui et al., 1999; Soveral et al., 2010).

from large quantities of gene and protein collections. Dysregulated pathway identification analysis was performed on differentially expressed genes using the DAVID web tool. The DEG analysis showed 4,820 genes in glioma samples (see **Supplementary material**) that were divided into two groups of lists: upregulated and downregulated genes (logFC > 1 and logFC < 0). Subsequently, these lists were submitted separately to DAVID and the results were generated.

2.5 Correlation analysis using the GEPIA2 tool

A pairwise gene Spearman correlation analysis between AQP*1 or AQP4* and the expression of other preselected genes was performed using GEPIA2.

GEPIA data are presented as a log-scale axis and a non-log scale was used for calculation; the strength of the correlation was determined using the following guide for the absolute value: ≤0.2 (weak), 0.21–0.50 (moderate), 0.51–0.80 (strong), and 0.81–1.0 (very strong). Spearman's coefficients >0 indicate a positive correlation, and coefficients less than zero indicates a negative correlation. Spearman's coefficient ≥0.20 and *p*-values ≤0.05 were considered significant in the current study.

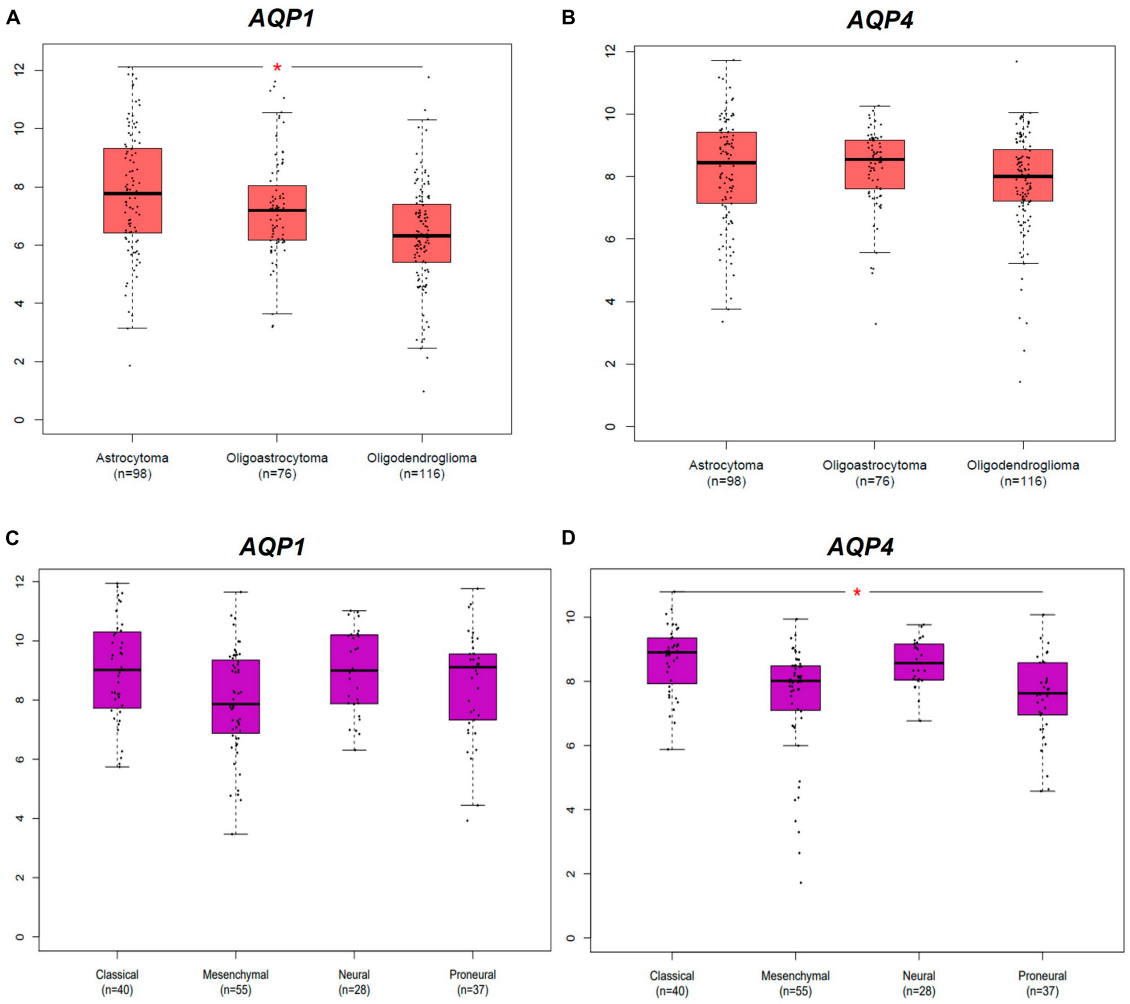

FIGURE 1
Differential expression AQPs mRNAs from gliomas samples from TCGA and GTEx dataset. AQP1 and AQP4 genes. Tumor samples are divided into LGG and GBM subtypes groups. **(A,B)** Represents both AQP1 and AQP4 profiles of expression in LGG subtypes. **(C,D)** Represents both AQP1 and AQP4 profiles of expression in GBM subtypes. LGG, low-grade glioma; GBM: glioblastoma multiforme. *$p < 0.05$. All graphs were derived by the GEPIA2 webserver in January 2021.

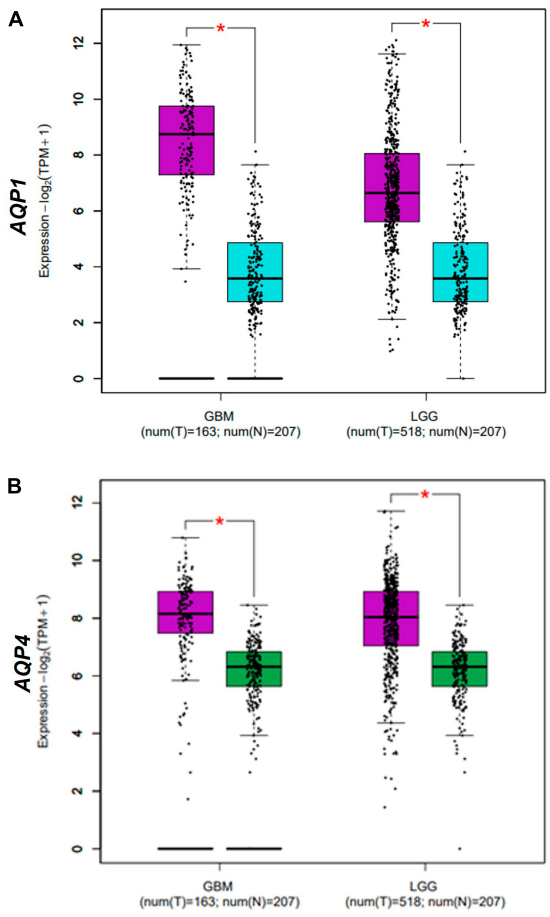

FIGURE 2
Differential expression AQPs mRNAs from gliomas samples from TCGA and GTEx dataset. *AQP1* **(A)** and *AQP4* **(B)** genes in normal (*N* = 163; blue box for AQP1 data and green box for AQP4 data) and tumor (*N* = 207; purple box) samples. Tumor samples are divided into LGG and GBM groups (*X*-axis of both graphs). TPM, transcripts per kilobase million; LGG, low-grade glioma; GBM, glioblastoma multiforme. *$p < 0.05$. Graphs **(A,B)** were derived by the GEPIA2 webserver in January 2021.

3 Results

3.1 *AQP1* and *AQP4* genes are overexpressed in gliomas compared to normal brain samples

To characterize gene expression, differential expression analysis from TCGA and GTEx datasets was performed using the R software. This analysis revealed a list of 4,819 genes. Among these, five *AQPs* family members were identified: *AQP1*, *AQP4*, *AQP5*, *AQP7*, and *AQP8*.

As expected, both *AQP1* and *AQP4* mRNAs were overexpressed in glioma samples (logFC = 1.42 x 10+14 and 1.02 x 10+14; *P*-value = 1.66E-40 and 8.82E-26, respectively) compared with the healthy brain samples (Table 1 and Figures 1A, B, 2).

Histological samples of tumor and normal brain tissues from the Human Protein Atlas database show the distribution of AQP1 and AQP4 proteins. The staining intensity of both proteins increased with the degree of tumor malignancy. Figures 3A–C show AQP1 staining, while Figures 3D–F show AQP4 staining.

In addition, both AQP1 and AQP4 showed a significant difference in expression pattern upon comparison with tumor markers/antigens in gliomas that are consensually used in clinical practice to establish degrees of malignancy and prognosis (Soldatelli et al., 2022). For instance: TP53, ATRX, TERT, IDH1, EGFR, and GFAP (Figure 4).

These results revealed a pivotal role of the above-mentioned genes in the gliomagenesis process.

3.2 *AQP1* and *AQP4* seem to play substantial roles in the molecular glioma subtype

In a complementary manner, Figure 2 shows the differential expression of AQP1 and AQP4 in glioma subtypes. A and B represent the expression patterns in the LGG subtypes (astrocytoma, oligoastrocytoma, and oligodendroglioma). In this case, AQP1 showed an increased number of transcripts in astrocytomas compared than in oligodendroglioma tumors (*$p \leq 0.05$) (Figure 2A). AQP4 mRNAs levels were not significant in these LGG samples (Figure 2B).

Regarding the GBM subtypes (classical, mesenchymal, neural, and proneural), only AQP4 presented considerable variation in its expression between classical and proneural subtypes, being more expressed in the classical case (*$p \leq 0.05$) (Figure 2D). AQP1 mRNAs levels were not significant in these GBM samples (Figure 2C).

These results indicate that the aquaporins in question most likely have an oncogenic role only in cells of astrocytic origin.

3.3 *AQP1* and *AQP4* could be potential risk factors and prognostic indicators for patients with low-grade glioma

One of the factors in assigning clinical importance to a therapeutic target is the probability of increasing the chances of patient survival. Kaplan–Meier analysis revealed that OS was lower in patients with LGG who had high *AQP1* (HR = 1.458; log-rank = 0) and *AQP4* (HR:1.191; log-rank = 0.003) expression (Figures 5B, D). In the GBM patient groups, there was no difference between the high and low expression groups of these selected genes (Figures 5A, C).

Our findings suggest that high expression of *AQP1* and *AQP4* may be a risk factor for poor prognosis in patients with LGG because they are significantly associated with reduced survival.

3.4 Functional enrichment analysis

Understanding the disease functioning from different levels of information is a crucial step in this line of work, as we look for potential regulators of AQPs only in gliomas.

The DAVID tool analysis generated two lists of dysregulated pathways from upregulated and downregulated genes in the glioma

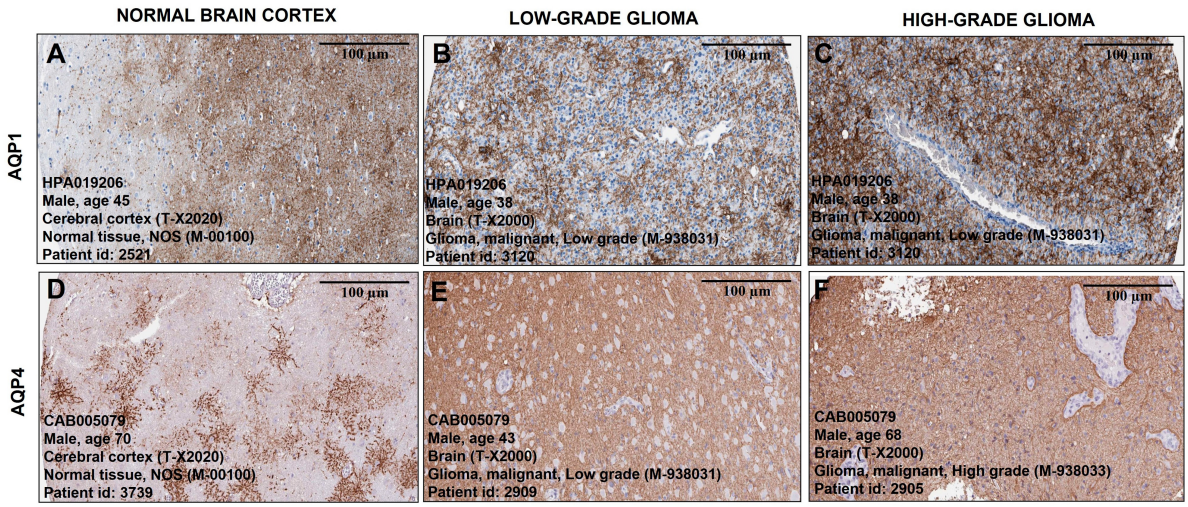

FIGURE 3
Representative immunohistochemical staining distribution of AQP1 and AQP4 expressions in normal and glioma patient samples. Plates **(A–F)** are captured in 100 µm. It is important to highlight that the staining (brownish) of the antibody for both proteins becomes more pronounced and denser as the degree of tumor malignancy increases compared to representative images of healthy brain tissue **(A,D)**. All data were extracted from the Human Protein Atlas (https://www.proteinatlas.org/).

microenvironment. A list of genes with LogFC $\geq$ 1.0 revealed 64 altered pathways (Supplementary Table 1). Among them, 31 presented statistical significance ($p < 0.05$). Sixty-six pathways were identified in genes with negative LogFC values (Table 2). Among them, 30 were statistically significant.

PathfindR analysis showed 113 pathways over-represented according to glioma differential expression (Supplementary Table 3).

Based on our previous study (Costa et al., 2019), where AQP4 was overexpressed both during central nervous system development and in human glioma cells and triiodothyronine (T3) played a negative role in this expression pattern, we chose tree-specific pathways in the downregulated list of the functional enrichment analysis: hsa00350 (Tyrosine metabolism [9 genes]); hsa04918 (Thyroid hormone synthesis [15 genes]); and hsa04919 (Thyroid hormone signaling pathway [7 genes]) (Supplementary Table 3). It is worth noting that choosing the genes from downregulated pathways was timely to antagonize the overexpression of AQPs as well as in our experimental previous study (*in vivo* and *in vitro*). In total, we identified 31 genes from the cellular pathways identified in the enrichment analysis.

3.5 Spearman's correlation

We hypothesized that the expression of both AQP1 and AQP4 could be modulated by genes involved in thyroid function. Although still controversial, accumulated evidence suggests that thyroid function plays an important role in several pathological and non-pathological processes of the central nervous system, including gliomagenesis, cell migration and cerebral edema resolution (Schiera et al., 2021) having AQP4 as one of its action targets, as shown in two experimental circumstances, mentioned above, evidenced by our research group (Costa et al., 2019). Tyrosine, in turn, is the precursor amino acid of thyroid hormones by the iodination of tyrosine residues in thyroglobulin and has their levels altered in some disease status (Khaliq et al., 2015). Here, we attempted to identify potential regulators that could interfere with some degree of regulation of the disposition and function of AQP1 and AQP4 in tumor cells (Tables 2–4).

Within the tyrosine metabolism pathway, five genes were correlated with AQP1 and AQP4, although only four met the statistical requirements already established: *PNMT*, *ALDH1A3*, *AOC2*, and *HGD* (Table 2).

In the thyroid hormone synthesis pathway, six genes were statistically significant (Table 3): *ATP1B1*, *ADCY5*, *PLCB4*, *ITPR1*, *ATP1A3*, and *LRP2*. Only four genes involved in the thyroid hormone signaling pathway (Table 4) were within the statistical inclusion criteria described in Subsection 2.5: *HDAC1*, *MED24*, *MTOR*, and *ACTB1*. All these genes are also listed and have potential actions on AQPs, as summarized in Table 5. Our data refer to the number of transcripts using Spearman's correlation analysis (AQP1 and AQP4 vs. genes selected from the functional enrichment analysis). Thus, we can consider them regulators at the translational level.

4 Discussion

In this study, we aimed to identify the expression pattern of *AQP1* and *AQP4* genes in human gliomas, as well as to highlight their regulatory potential within the cancer microenvironment.

We used RNA-seq as a search strategy to identify the differential expression of AQP1 and AQP4 transcripts in glioma tissues data compared to normal brain tissues data. Indeed, AQPs genes are overexpressed in patients with glioma. Among the glioma subtypes, *AQP1* and *AQP4* are overexpressed in astrocytoma (LGG) and classical glioma (GBM). OS analysis showed that both AQP genes can be used as prognostic factors for patients with LGG, confirming the results of previous studies and reinforcing their clinical value.

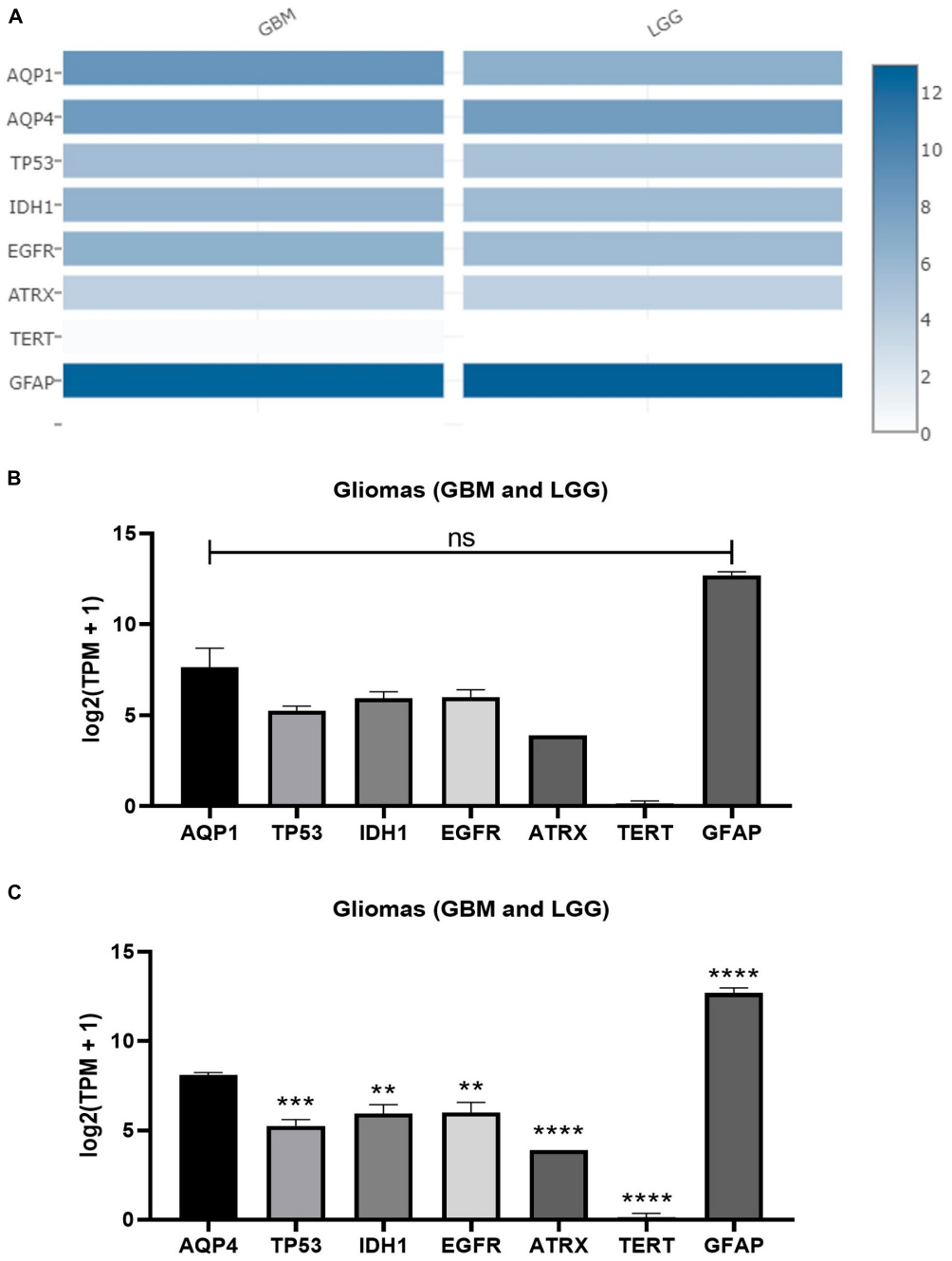

FIGURE 4
Expression matrix graphs based on a list of genes considered biomarkers of glioma and AQP1 and AQP4. **(A)** Heat Map derived from GEPIA2. The color density in each block represents the median value of gene expression in tumor tissue (GBM and LGG, separately) normalized by the maximum median value of the expression in all blocks. These data were transformed for plotting [linear to log2(TPM + 1)]. Graphs **(B,C)** were created from the values provided by the heap map for each gene with a subsequent comparison with both AQP1 and AQP4, respectively. For this, one-way ANOVA was performed followed by Tukey's multiple comparisons tests using GraphPad Prism version 8.0. $^{**}p < 0.01$, $^{***}p < 0.001$, $^{****}p < 0.0001$. TP53, tumor protein P53; IDH1, isocitrate dehydrogenase [NADP(+)] 1; EGFR, epidermal growth factor receptor; ATRX, ATRX chromatin remodeler; TERT, telomerase reverse transcriptase; TPM, transcripts per kilobase million; GFAP, glial fibrillary acidic protein.

We also observed a correlation between the expression of genes involved in the tyrosine and thyroid hormone pathways and AQPs.

Emerging evidence suggests a positive relationship between AQP1 and AQP4 expression and histological tumor grade and brain edema volume. Poor neurological prognosis has also been reported (Suzuki et al., 2018; Chow et al., 2020). Our results are supported by these findings, as aquaporin expression patterns increased when compared between molecular subtypes of gliomas: AQP1 is increased in other subtypes of LGG classification (astrocytoma); in contrast, AQP4 is increased in only the classical subtype GBM.

Some current studies have highlighted the regulatory function of AQPs on brain volume in many other neurological diseases besides tumors (Sun et al., 2022; Ohmura et al., 2023). In

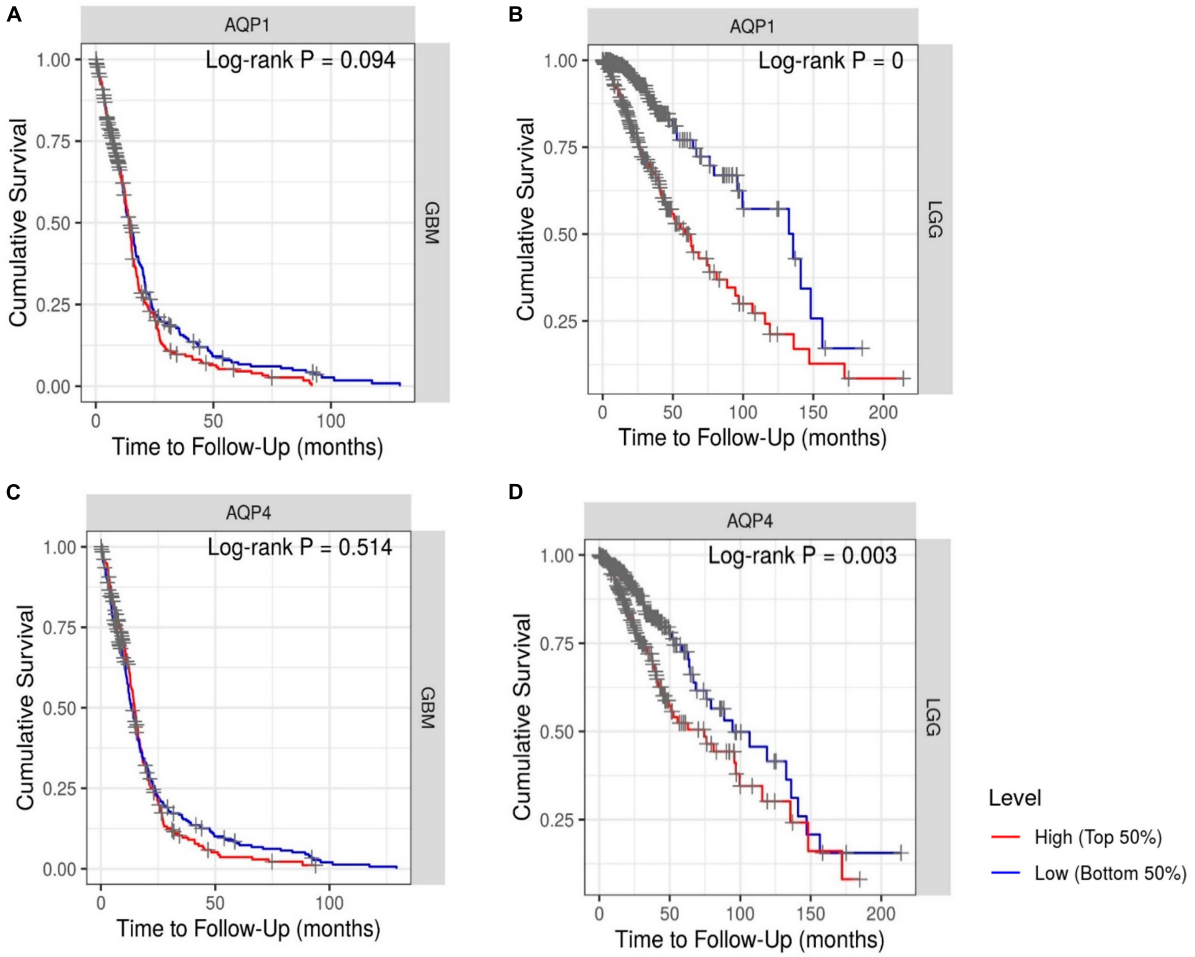

FIGURE 5
Kaplan–Meier survival analysis. **(A,C)** Patients with GBM and **(B,D)** patients with LGG. The Cox proportional hazard ratio (HR) and the 95% confidence interval were used in the Kaplan–Meier survival analysis. Red and blue curves represent high and low expression profiles, respectively. GBM, *N* = 523 patients with 448 dying. LGG, *N* = 514 patients with 125 dying. Log-rank *P*-values ≤0.05 were considered statistically significant. All graphs were derived by the TIMER database in September 2021.

gliomas, both AQP1 and AQP4, when suppressed, offer a better prognosis for patients affected by these types of tumors by edema reduction (Faraj et al., 2022; Ohmura et al., 2023), facilitating the management of neurological deficits in the pre- and postoperative periods, with peritumoral edema being more relevant, in terms of concerns the aggressiveness of this cancer, rather than its extent, *per se* (Faraj et al., 2022). AQP1, for example, is upregulated in the peritumoral area, especially in the vessels surrounding reactive astrocytes in high-grade gliomas. In LGG, it showed an intense pattern of intratumoral expression (Zoccarato et al., 2021). The discovery of the glymphatic system was also important for the consolidation of AQPs as targets therapeutic in brain edema regulation (Ding et al., 2023).

From these findings it is possible to suggest that *AQPs* are perhaps more relevant in the tumor progression process, that is, the transformation of LGG into GBM through the formation of expansive edema, facilitating the invasion of tumor cells into healthy tissue. The determining factors in the survival rate of patients with GBM, in turn, are other and more diversified, in addition to the expression pattern of *AQPs* (Deb et al., 2012; Saito et al., 2022), which would explain our results from the survival analysis, where *AQP* genes only functioned as a risk factor for survival in low-grade gliomas.

AQP4 isoforms, known as M1 and M23, have been shown to change the aggregation/disaggregation state into orthogonal arrangements of particles (OAPs) and glioma cell survival. One study revealed that the isoform M23 reduced the invasion and proliferation of glioma cells to promote their apoptosis (Simone et al., 2019).

Some endogenous factors such as hormonal and metabolic changes also modulate AQP4 expression in human gliomas (Lan et al., 2017). Likewise, an increase in *AQP1* expression was observed during central necrosis and hypoxia, which are characteristics of GBM tumors (Hayashi et al., 2007; Honasoge and Sontheimer, 2013).

Gene expression is orchestrated by several endogenous and exogenous factors, such as DNA-binding transcription factors, regulatory proteins, and profile hormones (Bhat et al., 2021).

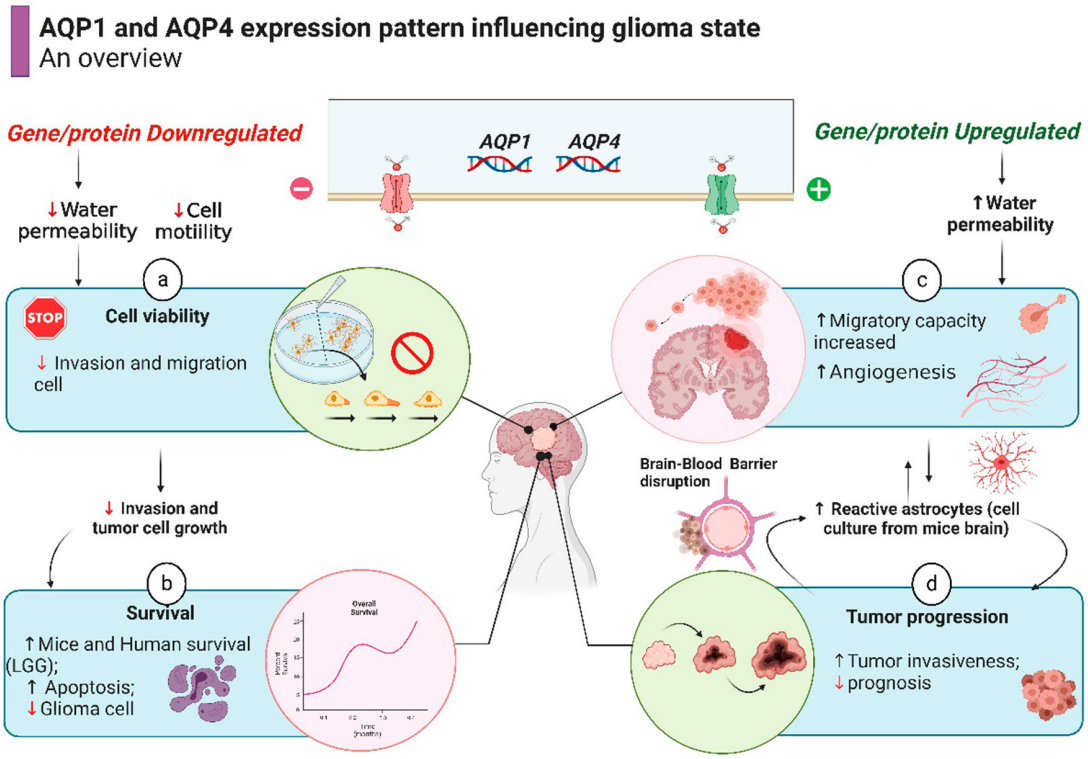

FIGURE 6
Schematic representation of cell processes involving AQPs activity in glioma state (already demonstrated by prior studies), resulting in better or worse outcome for a patient. The overall survival in human patient with LGG is shown in Figure 5. **Source: Subscription:** Individual, **Agreement number:** XZ26G6XU1D, **Journal name:** Frontiers in Neuroscience.

A study conducted by Nauman et al. (2004) evaluated the cellular concentrations of thyroxine (T4) and triiodothyronine (T3) in non-thyroidal illness syndrome (NTIS) patients with gliomas, where the thyroid stimulating hormone (TSH) serum concentration was within the normal range and T4/T3 levels were lower than normal (Nauman et al., 2004). They demonstrated that thyroid hormone levels were significantly lower in glioma tissues than in healthy tissues. In addition, both iodothyronine deiodinases (types 2 and 3) were higher in tumor tissues than in non-glioma tissues.

Some studies have shown that hypothyroidism is an important factor in the prognosis and progression of metastatic cancer in patients with brain cancer. For example, a cohort study (Berghoff et al., 2020) identified a beneficial role of this clinical condition in overall survival in patients with brain metastases, almost doubling life expectancy from the diagnosis of primary and metastatic cancer. Furthermore, the results of a clinical survey showed that almost 40% of patients with brain tumors evaluated had overt or subclinical hypothyroidism and 31% required hormone replacement (Faghih-Jouybari et al., 2018).

In pediatric patients, an important probability of developing thyroid dysfunction was found post-treatment with surgery, chemotherapy, and radiotherapy (Jin et al., 2018; Cosnarovici et al., 2020); moreover, abnormalities in thyroid function were found in patients with AQP4 antibody–seropositive optic neuritis (Zhao et al., 2017).

TABLE 2 Correlation analysis between genes involved in the tyrosine metabolism pathway and AQP's genes.

	AQP1		*AQP4*	
Gene ID	Coeffici-ent	*P*-Value	Coeffici-ent	*P*-Value
Gliomas (LGG and GBM)				
PNMT	0.25	4.5e−17	0.31	4.5e−17
ALDH1A3	0.31	5.3e−17	0.17	5.3e−17
TPO	0.056	0.14	0.0062	0.87
AOC2	−0.21	3.7e−08	−0.15	3.7e−08
GOT1	−0.076	0.046	0.055	0.15
HGD	0.41	6.5e−29	0.14	6.5e−29
ADH1B	−0.063	0.1	0.079	0.039
TYRP1	0.12	0.0017	0.17	1.2e−05
TH	−0.01	0.79	−0.033	0.39

We previously identified a negative modulator of AQP4 protein and demonstrated that triiodothyronine (T3) treatment of GBM-95-line cells resulted in a slight reduction in cell migration (Costa et al., 2019); other studies have also evaluated the modulatory action of this hormone on the expression of AQP4 in stroke animal models (Sadana et al., 2015).

TABLE 3 Correlation analysis between genes involved in the thyroid hormones synthesis pathway and AQP's genes.

	AQP1		*AQP4*	
Gene ID	Coeffici-ent	*P*-Value	Coeffici-ent	*P*-Value
Gliomas (LGG and GBM)				
PRKCG	−0.075	0.049	0.17	4.8e−06
ADCY1	0.12	0.0023	0.18	1.2e−06
ATP1B1	0.23	1.2e−09	0.35	5.9e−21
ADCY5	−0.32	2.9e−17	0.0065	0.86
TPO	0.056	0.14	0.0062	0.87
PLCB4	−0.3	8.9e−16	−0.096	0.012
TG	0.18	4.3e−06	0.16	3.2e−05
CREB3L3	−0.082	0.033	0.1	0.0076
IYD	0.048	0.21	0.056	0.14
GPX2	−0.065	0.088	0.045	0.24
PRKCB	−0.18	1.3e−06	0.11	1.3e−06
ADCY4	0.068	0.076	−0.037	0.33
ITPR1	0.23	2.6e−09	0.26	2.6e−09
ATP1A3	−0.31	1.2e−16	−0.12	1.2e−16
LRP2	0.16	3.4e−05	0.22	3.4e−05

TABLE 4 Correlation analysis between genes involved in the thyroid hormones signaling pathway and AQP's genes.

	AQP1		*AQP4*	
Gene ID	Coeffici-ent	*P*-Value	Coeffici-ent	*P*-Value
Gliomas (LGG and GBM)				
SIN3A	−0.14	0.00041	0.14	0.00024
HDAC1	0.44	3.6e−34	0.15	7.6e−05
MED24	−0.24	2.1e−10	−0.22	5e−09
ATP2A2	−0.15	0.00013	0.16	3.5e−05
MTOR	0.27	3.3e−13	0.26	8e−12
ACTG1	0.096	0.012	0.029	0.45
ACTB	0.35	1e−20	0.038	0.32

TABLE 5 Genes involved in the thyroid hormone and tyrosine pathways.

Official symbol	Official full name
PRKCG	Protein kinase C gamma
ADCY1	Adenylate cyclase 1
ATP1B1	Atpase Na+/k+ transporting subunit beta 1
ADCY5	Adenylate cyclase 5
TPO	Thyroid peroxidase
PLCB4	Phospholipase C beta 4
TG	Thyroglobulin
CREB3L3	Camp responsive element binding protein 3 like 3
IYD	Iodotyrosine deiodinase
GPX2	Glutathione peroxidase 2
PRKCB	Protein kinase C beta type
ADCY4	Adenylate cyclase 4
ITPR1	Inositol 1,4,5—triphosphate receptor type 1
ATP1A3	Atpase Na+/k+ transporting subunit alfa 3
LRP2	LDL receptor related protein 2
SIN3A	Transcription regulator Family member A
HDAC1	Histone deacetylase 1
MED24	Mediator complex subunit 24
ATP2A2	Atpase Na+/k+ transporting subunit alfa 2
MTOR	Mechanistic Target of Rapamycin kinase
ACTG1	Actin gamma 1
ACTB	Actin beta
PNMT	Phenylethanolamine *N*-methyltransferase
ALDH1A3	Aldehyde dehydrogenase 1 family member A3
AOC2	Amine Oxidase Copper Containing 2
HGD	Homogentisate 1,2–dioxygenase
ADH1B	Alcohol dehydrogenase 1B
TYRP1	Tyrosinase-related protein 1
TH	Tyrosine Hydroxylase

All information was derived from the National Center for Biotechnology Information (NCBI) database. Available in: https://www.ncbi.nlm.nih.gov/guide/genes-expression/.

In recent years, a specific AQP4 inhibitor has been tested in rodents and human brain glioma to directly measure water efflux rate during tumorigeneses (Harrison et al., 2020; Rosu et al., 2020). A promising study conducted by Jia et al. (2023) found a correlation with water efflux in glioma cell cultures, rat and human glioma and cell proliferation as measured by magnetic resonance imaging. This discovery is in agreement with our results showing overexpression of AQP4 genes in gliomas, placing aquaporin 4 as an important biomarker to be used both in bioinformatics analyzes and in brain imaging as a potential therapeutic treatment of gliomas. A summary of what is hypothesized/proven about the modulation of the expression of AQPs 1 and 4 in gliomas is briefly outlined in Figure 6.

Therefore, according to our results, we suggest two new hypotheses: (1) As all patient data are post-mortem (including data other than this one), it is possible that standard cancer treatment led to hypothyroidism and subsequently downregulated the thyroid hormone pathways. This could result in the overexpression of AQP1 and AQP4 in the more aggressive glioma subtypes [astrocytoma (LGG) and classical, (GBM)], as we present in the differential expression results, (2) hypothyroidism would already be a clinical risk condition for the development of glioma; patients diagnosed early with the tumor would present a sub-clinical pattern of thyroid gland dysfunction. This condition would be accentuated by the anticancer therapeutic approach, and these patients would have the same outcome and genetic, and molecular profiles as mentioned in hypothesis 1.

Additional studies to clarify the specific inhibitors or promoters of these pathways, as well as transcription factors and post-transcription/translation modification methods, will help to identify the most appropriate therapeutic targets for AQP1 and

AQP4 modulation, relationships between genes, and signaling pathways in gliomas.

To the best of our knowledge, this is the first study to suggest a modulatory interaction between the gene encoding AQP1 and pathways related to thyroid hormones.

5 Limitations

The brain tissue is substantially plastic and heterogeneous. Factors such as age and sex can influence their genetic constitution. Glial tumor characteristics may also change depending on the topographic region of the brain where the tumor occurs. The non-separation of categorical patient groups based on the aforementioned factors is a limitation of this study. Single-cell analysis from different glioma patient groups would help us to confirm the oncogenic role of the AQPs studied here, as well as their modulation by thyroid hormones.

6 Conclusion

To the best of our knowledge this study is the first to show a strong potential functional relationship between AQP1 and thyroid hormone pathways in brain tumors. The expression of AQP1 and AQP4 is significantly associated with a worse prognosis in patients with LGG. The molecular pathways and AQP1 and AQP4 genes identified here may be useful for the molecular diagnosis of gliomas and for screening new anti-tumor drugs for these malignant tumors.

Data availability statement

The datasets presented in this study can be found in online repositories. The names of the repository/repositories and accession number(s) can be found in the article/ **Supplementary material**.

Author contributions

CM: Conceptualization, Formal Analysis, Investigation, Writing – original draft, Writing – review and editing. LR: Writing – review and editing. CC: Data curation, Writing – original draft. AX: Conceptualization, Data curation, Project administration, Supervision, Writing – original draft, Writing – review and editing.

Funding

The author(s) declare financial support was received for the research, authorship, and/or publication of this article. CM was recipient of a Master fellowship from Brazilian Federal Agency for Support and Evaluation of Graduate Education (Capes).

Acknowledgments

To the Coordination for the Improvement of Higher Education Personnel (CAPES) for granting a master's scholarship (CBM). The results shown here are in part based on data generated by TCGA Research Network: https://www.cancer.gov/tcga. The Genotype-Tissue Expression (GTEx) Project was supported by the Common Fund of the Office of the Director of the National Institutes of Health and by NCI, NHGRI, NHLBI, NIDA, NIMH, and NINDS. The data used for the analyses described in this manuscript were obtained from the GTEx Portal on 08/12/2022.

Conflict of interest

The authors declare that the research was conducted in the absence of any commercial or financial relationships that could be construed as a potential conflict of interest.

Publisher's note

Supplementary material

The Supplementary Material for this article can be found online at: https://www.frontiersin.org/articles/10.3389/fnins.2024.1349421/full#supplementary-material

References

Berghoff, A., Wippel, C., Starzer, A., Ballarini, N., Wolpert, F., and Bergen, E. (2020). Hypothyroidism correlates with favourable survival prognosis in patients with brain metastatic cancer. *Eur. J. Cancer* 135, 150–158. doi: 10.1016/j.ejca.2020.05.011

Bhat, P., Honson, D., and Guttman, M. (2021). Nuclear compartmentalization as a mechanism of quantitative control of gene expression. *Nat. Rev. Mol. Cell Biol.* 22, 653–670.

Brennan, C., Verhaak, R., McKenna, A., Campos, B., Noushmehr, H., Salama, S., et al. (2013). The somatic genomic landscape of glioblastoma. *Cell* 155, 462–477.

Cheng, Y., Gao, F., Jiang, R., Lui, H., Hou, J., Yi, Y., et al. (2017). Down-regulation of AQP4 expression via p38 MAPK signaling in temozolomide-induced glioma cells growth inhibition and invasion impairment. *J. Cell Biochem.* 118, 4905–4913.

Chow, P., Bowen, J., and Yool, A. (2020). Combined systematic review and transcriptomic analyses of mammalian aquaporin classes 1 to 10 as biomarkers and prognostic indicators in diverse cancers. *Cancers* 12:1911.

Cosnarovici, M., Piciu, A., Bonci, E., Bădan, M., Bădulescu, C., and Stefan, A. (2020). Post-treatment thyroid diseases in children with brain tumors: a single-center experience at "Prof. Dr. Ion Chiricuţă" institute of oncology, Cluj-Napoca. *Diagnostics* 10:142.

Costa, L., Clementino-Neto, J., Mendes, C., Franzon, N., Costa, E., Moura-Neto, V., et al. (2019). Evidence of aquaporin 4 regulation by thyroid hormone during mouse brain development and in cultured human glioblastoma multiforme cells. *Front. Neurosci.* 13:137. doi: 10.3389/fnins.2019.00317

De Ieso, M., and Yool, A. (2018). Mechanisms of aquaporin-facilitated cancer invasion and metastasis. *Front. Chem.* 6:135. doi: 10.3389/fchem.2018.00135

Deb, P., Pal, S., Dutta, V., Boruah, D., Chandran, V. M., and Bhatoe, H. S. (2012). Correlation of expression pattern of aquaporin-1 in primary central nervous system tumors with tumor type, grade, proliferation, microvessel density, contrast-enhancement and perilesional edema. *J. Cancer Res. Therapeutics* 8, 571–577.

Ding, T., Gu, F., Fu, L., and Ma, Y. (2010). Aquaporin-4 in glioma invasion and an analysis of molecular mechanisms. *J. Clin. Neurosci.* 17, 1359–1361.

Ding, T., Ma, Y., Li, W., Liu, X., Ying, G., Fu, L., et al. (2011). Role of aquaporin-4 in the regulation of migration and invasion of human glioma cells. *Int. J. Oncol.* 38, 1521–1531.

Ding, Z., Fan, X., Zhang, Y., Yao, M., Wang, G., Dong, Y., et al. (2023). The glymphatic system: a new perspective on brain diseases. *Front. Aging Neurosci.* 15:1179988. doi: 10.3389/fnagi.2023.1179988

Dubois, L., Campanati, L., Righy, C., D'Andrea-Meira, I., Spohr, T., Porto-Carreiro, I., et al. (2014). Gliomas and the vascular fragility of the blood brain barrier. *Front. Cell Neurosci.* 8:418. doi: 10.3389/fncel.2014.00418

Faghih-Jouybari, M., Naderi, S., Mashayekhi, S., Padeganeh, T., and Abdollahzade, S. (2018). Hypothyroidism among patients with glioblastoma multiforme. *Iran J. Neurol.* 17, 149–151.

Faraj, C. A., Snyder, R. I., and McCutcheon, I. E. (2022). Intracranial emergencies in neurosurgical oncology: pathophysiology and clinical management. *Emerg. Cancer Care* 1:13.

Fedele, M., Cerchia, L., Pegoraro, S., Sgarra, R., and Manfioletti, G. (2019). Proneural-mesenchymal transition: phenotypic plasticity to acquire multitherapy resistance in glioblastoma. *Int. J. Mol. Sci.* 20:2746.

Galán-Cobo, A., Ramírez-Lorca, R., and Echevarría, M. (2016). Role of aquaporins in cell proliferation: what else beyond water permeability? *Channels* 10, 185–201.

Hardee, M., and Zagzag, D. (2012). Mechanisms of glioma-associated neovascularization. *Am. J. Pathol.* 181, 1126–1141.

Harrison, I., Ismail, O., Machhada, A., Colgan, N., Ohene, Y., Nahavandi, P., et al. (2020). Impaired glymphatic function and clearance of tau in an Alzheimer's disease model. *Brain* 143, 2576–2593.

Hayashi, Y., Edwards, N., Proescholdt, M., Oldfield, E., and Merrill, M. (2007). Regulation and function of aquaporin-1 in glioma cells. *Neoplasia* 9, 777–787.

Honasoge, A., and Sontheimer, H. (2013). Involvement of tumor acidification in brain cancer pathophysiology. *Front Physiol.* 4:316. doi: 10.3389/fphys.2013.00316

Huang, S., Jiang, H., Hu, H., and Lv, D. (2021). Targeting AQP4 localization as a novel therapeutic target in CNS edema. *Acta Biochim. Biophys. Sin.* 53, 269–272.

Huang, Z., Wong, L., Su, Y., Huang, X., Wang, N., Chen, H., et al. (2020). Blood-brain barrier integrity in the pathogenesis of Alzheimer's disease. *Front. Neuroendocrinol.* 59:100857. doi: 10.1016/j.yfrne.2020.100857

Hubbard, J., Szu, J., and Binder, D. (2018). The role of aquaporin-4 in synaptic plasticity, memory and disease. *Brain Res. Bull.* 136, 118–129.

IJzerman-Korevaar, M., Snijders, T., de Graeff, A., Teunissen, S., and de Vos, F. (2018). Prevalence of symptoms in glioma patients throughout the disease trajectory: a systematic review. *J. Neurooncol.* 140, 485–496.

Jia, Y., Xu, S., Han, G., Wang, B., Wang, Z., and Lan, C. (2023). Transmembrane water-efflux rate measured by magnetic resonance imaging as a biomarker of the expression of aquaporin-4 in gliomas. *Nat. Biomed. Eng.* 7, 236–252.

Jin, S., Choi, J., Park, K., Kang, H., Shin, H., and Phi, J. (2018). Thyroid dysfunction in patients with childhood-onset medulloblastoma or primitive neuroectodermal tumor. *Ann. Pediatr. Endocrinol. Metab.* 23, 88–93.

Khaliq, W., Andreis, D., Kleyman, A., Gräler, M., and Singer, M. (2015). Reductions in tyrosine levels are associated with thyroid hormone and catecholamine disturbances in sepsis. *Intensive Care Med Exp.* 3(Suppl. 1), A686.

Lan, Y., Wang, X., Lou, J., Ma, X., and Zhang, B. (2017). The potential roles of aquaporin 4 in malignant gliomas. *Oncotarget* 8, 32345–32355.

Li, B., Li, T., Liu, J., and Liu, X. (2020). Computational deconvolution of tumor-infiltrating immune components with bulk tumor gene expression data. *Methods Mol. Biol.* 2120, 249–262.

Li, J., Jia, M., Chen, G., Nie, S., Zheng, C., and Zeng, W. (2019). Involvement of p38 mitogen-activated protein kinase in altered expressions of AQP1 and AQP4 after carbon monoxide poisoning in rat astrocytes. *Basic Clin. Pharmacol. Toxicol.* 125, 394–404.

Lima, F., Kahn, S., Soletti, R., Biasoli, D., Alves, T., da Fonseca, A., et al. (2012). Glioblastoma: therapeutic challenges, what lies ahead. *Biochim. Biophys. Acta Rev. Cancer* 2, 338–349.

Lohela, T., Lilius, T., and Nedergaard, M. (2022). The glymphatic system: implications for drugs for central nervous system diseases. *Nat. Rev. Drug Discov.* Epub ahead of print. doi: 10.1038/s41573-022-00500-9

Martinez-Lage, M., and Sahm, F. (2018). Practical implications of the updated WHO classification of brain tumors. *Semin. Neurol.* 38, 11–18.

Maugeri, R., Schiera, G., Di Liegro, C., Fricano, A., Iacopino, D., and Di Liegro, I. (2016). Aquaporins and brain tumors. *Int. J. Mol. Sci.* 17:1029.

Mestre, H., Tithof, J., Du, T., Song, W., Peng, W., Sweeney, A., et al. (2018). Flow of cerebrospinal fluid is driven by arterial pulsations and is reduced in hypertension. *Nat. Commun.* 9:4878.

Moon, C., Moon, D., and Kang, S. (2022). Aquaporins in cancer biology. *Front. Oncol.* 12:782829. doi: 10.3389/fonc.2022.782829

Nauman, P., Bonicki, W., Michalik, R., Warzecha, A., and Czernicki, Z. (2004). The concentration of thyroid hormones and activities of iodothyronine deiodinases are altered in human brain gliomas. *Folia Neuropathol.* 42, 67–73.

Ohmura, K., Tomita, H., and Hara, A. (2023). Peritumoral edema in gliomas: a review of mechanisms and management. *Biomedicines* 11: 2731.

Ostrom, Q., Bauchet, L., Davis, F., Deltour, I., Fisher, J., Langer, C., et al. (2014). The epidemiology of glioma in adults: a state of the science review. *Neuro Oncol.* 16, 896–913.

Perry, A., and Wesseling, P. (2016). "Histologic classification of gliomas," in *Handbook of Clinical Neurology*, ed. Elsevier (Cambridge, MA: Academic Press).

Rosu, G., Catalin, B., Balseanu, T., Laurentiu, M., Claudiu, M., Kumar-Singh, S., et al. (2020). Inhibition of Aquaporin 4 Decreases Amyloid Abeta40 Drainage Around Cerebral Vessels. *Mol. Neurobiol.* 57, 4720–4734.

Saadoun, S., Papadopoulos, M., Davies, D., Krishna, S., and Bell, B. (2002). Aquaporin-4 expression is increased in oedematous human brain tumours. *J. Neurol. Neurosurg. Psychiatry* 72, 262–265.

Sadana, P., Coughlin, L., Burke, J., Woods, R., and Mdzinarishvili, A. (2015). Anti-edema action of thyroid hormone in MCAO model of ischemic brain stroke: possible association with AQP4 modulation. *J. Neurol. Sci.* 354, 37–45.

Saito, T., Mizumoto, M., Liang, H., Nakai, K., Sumiya, T., and Iizumi, T. (2022). Factors involved in preoperative edema in high-grade gliomas. *Cureus* 14: e31379.

Schiera, G., Di Liegro, C., and Di Liegro, I. (2021). Involvement of thyroid hormones in brain development and cancer. *Cancers* 13:2693.

Sherman, B., Hao, M., Qiu, J., Jiao, X., Baseler, M., Lane, H., et al. (2022). DAVID: a web server for functional enrichment analysis and functional annotation of gene lists (2021 update). *Nucleic Acids Res.* 50, W216–W221.

Simone, L., Pisani, F., Mola, M., De Bellis, M., Merla, G., Micale, L., et al. (2019). AQP4 aggregation state is a determinant for glioma cell fate. *Cancer Res.* 79, 2182–2194.

Smith, A., Yao, X., Dix, J., Jin, B., and Verkman, A. (2017). Test of the 'glymphatic' hypothesis demonstrates diffusive and aquaporin-4-independent solute transport in rodent brain parenchyma. *eLife* 6:e27679.

Solar, P., Hendrych, M., Barak, M., Valekova, H., Hermanova, M., and Jancalek, R. (2022). Blood-brain barrier alterations and edema formation in different brain mass lesions. *Front. Cell Neurosci.* 16:922181. doi: 10.3389/fncel.2022.922181

Soldatelli, J., Oliveira, I., Kneubil, M., and Henriques, J. (2022). Gliomas molecular markers: importance in treatment, prognosis and applicability in brazilian health system. *Acad. Bras. Cienc.* 94:e20211075.

Soveral, G., Prista, C., Moura, T. F., and Loureiro-Dias, M. C. (2010). Yeast water channels: One overview of orthodox aquaporins. *Cell Biol.* 103, 35–54. doi: 10.1042/BC20100102

Strobel, H., Baisch, T., Fitzel, R., Schilberg, K., Siegelin, M., Karpel-Massler, G., et al. (2019). Temozolomide and other alkylating agents in glioblastoma therapy. *Biomedicines* 7:69.

Sun, C., Lin, L., Yin, L., Hao, X., Tian, J., Zhang, X., et al. (2022). Acutely inhibiting AQP4 With TGN-020 improves functional outcome by attenuating edema and peri-infarct astrogliosis after cerebral ischemia. *Front. Immunol.* 13:870029. doi: 10.3389/fimmu.2022.870029

Suzuki, Y., Nakamura, Y., Yamada, K., Kurabe, S., Okamoto, K., and Aoki, H. (2018). Aquaporin positron emission tomography differentiates between grade III and IV human astrocytoma. *Neurosurgery* 82, 842–846.

Tang, Z., Kang, B., Li, C., Chen, T., and Zhang, Z. (2019). GEPIA2: an enhanced web server for large-scale expression profiling and interactive analysis. *Nucleic Acids Res.* 47, W556–W560.

Ulgen, E., Ozisik, O., and Sezerman, O. (2019). pathfindR: an r package for comprehensive identification of enriched pathways in omics data through active subnetworks. *Front. Genet.* 10:858. doi: 10.3389/fgene.2019.00858

Wu, C., Lin, G., Lin, Z., Zhang, J., Liu, S., and Zhou, C. (2015). Peritumoral edema shown by MRI predicts poor clinical outcome in glioblastoma. *World J. Surg. Oncol.* 13:97.

Yasui, M., Hazama, A., Kwon, T. H., Nielsen, S., Guggino, W. B., Agre, P. (1999). Rapid gating and anion permeability of an intracellular aquaporin. *Nature* 402, 184–187. doi: 10.1038/46045

Zhao, S., Zhou, H., Peng, X., Tan, S., Liu, Z., Chen, T., et al. (2017). Detection of thyroid abnormalities in Aquaporin-4 antibody-seropositive optic neuritis patients. *J. Neuroophthalmol.* 37, 24–29.

Zoccarato, M., Nardetto, L., Basile, A., Giometto, B., Zagonel, V., and Lombardi, G. (2021). Seizures, edema, thrombosis, and hemorrhages: an update review on the medical management of gliomas. *Front Oncol.* 11:617966. doi: 10.3389/fonc.2021.617966

frontiers | Frontiers in Nutrition

TYPE Original Research
PUBLISHED 13 March 2024
DOI 10.3389/fnut.2024.1342304

OPEN ACCESS

EDITED BY
Adriana Ximenes-da-Silva,
Federal University of Alagoas, Brazil

REVIEWED BY
Xuping Gao,
Peking University Sixth Hospital, China
Marija Takic,
University of Belgrade, Serbia

*CORRESPONDENCE
Wenhan Yang
✉ wenhan-yang@gdpu.edu.cn
Juan Gan
✉ 1198531895@qq.com

RECEIVED 21 November 2023
ACCEPTED 28 February 2024
PUBLISHED 13 March 2024

CITATION
Wang M, Yan X, Li Y, Li Q, Xu Y, Huang J, Gan J and Yang W (2024) Association between plasma polyunsaturated fatty acids and depressive among US adults.
Front. Nutr. 11:1342304.
doi: 10.3389/fnut.2024.1342304

Association between plasma polyunsaturated fatty acids and depressive among US adults

Man Wang[1], Xiaofang Yan[2], Yanmei Li[2], Qian Li[2], Yingxia Xu[2], Jitian Huang[2], Juan Gan[3]* and Wenhan Yang[1,2]*

[1]Department of Nutrition and Food Health, School of Public Health, Guangdong Pharmaceutical University, Guangzhou, Guangdong Province, China, [2]Department of Child and Adolescent Health, School of Public Health, Guangdong Pharmaceutical University, Guangzhou, Guangdong Province, China, [3]Guangzhou Baiyun District Maternal and Childcare Hospital, Guangzhou, Guangdong Province, China

Background: Depression is associated with greater functional impairment and high societal costs than many other mental disorders. Research on the association between plasma polyunsaturated fatty acids (PUFAs) levels and depression have yielded inconsistent results.

Objective: To evaluate whether plasma n-3 and n-6 PUFAs levels are associated with depression in American adults.

Methods: A cross-sectional study included 2053 adults (aged ≥20 y) in the National Health and Nutrition Examination Survey (NHANES), 2011–2012. The level of plasma n-3 and n-6 PUFAs were obtained for analysis. Self-reported Patient Health Questionnaire-9 (PHQ-9) was used to identify the depression status. Binary logistic regression analysis was performed to evaluate the association between quartiles of plasma n-3 and n-6 PUFAs and depression after adjustments for confounders.

Results: The study of 2053 respondents over 20 years of age with a weighted depression prevalence of 7.29% comprised 1,043 men (weighted proportion, 49.13%) and 1,010 women (weighted, 50.87%), with a weighted mean (SE) age of 47.58 (0.67) years. Significantly increased risks of depression over non-depression were observed in the third quartiles (OR = 1.65, 95% CI = 1.05–2.62) for arachidonic acid (AA; 20:4n-6); the third quartiles (OR = 2.20, 95% CI = 1.20–4.05) for docosatetraenoic acid (DTA; 22:4n-6); the third (OR = 2.33, 95% CI = 1.34–4.07), and highest quartiles (OR = 1.83, 95% CI = 1.03–3.26) for docosapentaenoic acid (DPAn-6; 22:5n-6); and the third (OR = 2.18, 95% CI = 1.18–4.03) and highest quartiles (OR = 2.47, 95% CI = 1.31–4.68) for docosapentaenoic acid (DPAn-3; 22:5n-3); the second (OR = 2.13, 95% CI = 1.24–3.66), third (OR = 2.40, 95% CI = 1.28–4.50), and highest quartiles (OR = 2.24, 95% CI = 1.08–4.69) for AA/docosahexaenoic acid (DHA; 22:6n-3) ratio compared with the lowest quartile after adjusting for confounding factors.

Conclusion: Higher plasma levels of AA, DTA, DPAn-6, DPAn-3 PUFAs, and AA/DHA ratio may be potential risk factors for depression in US adults.

KEYWORDS

n-3, n-6, polyunsaturated fatty acids, depression, NHANES, PHQ-9, American, adult

1 Introduction

Depression is a common and serious mental disorder and affects more than 280 million people globally (1). In fact, the World Health Organization ranked severe depression as the third cause of burden of disease worldwide as early as 2008 and projected that the disease will be the leading cause of disease burden worldwide by the year 2030 (2). In recent years, many studies have reported understanding the role of different influence factors, such as neurotransmitter, inflammatory markers and nutritional factors, to elucidate the underlying pathophysiology of depression in adults (3–5). Polyunsaturated fatty acids (PUFAs), as important nutrients, exhibit significant effects on the composition of the intestinal microflora as well as the function of the brain (6), and participate in numerous biological processes such as oxidation, neurotransmission, and inflammation (7, 8). Notably, PUFAs may play an important role in depression and its symptoms. Increasing evidence suggests that PUFAs could be associated with the pathophysiology of depression, as well as with the mechanisms underlying the therapeutic actions of antidepressants (9–11).

PUFAs are a class of fatty acids with two or more carbon–carbon double bonds (10). In human health, some PUFAs are considered essential nutrients, mainly including n-3 (primarily from fish, walnuts, wheat germ, and flaxseed) and n-6 PUFAs (primarily from refined vegetable oils such as corn, sunflower, and soybean), which cannot be synthesized in the body and must be obtained from dietary sources (8, 9). Various mental disorders such as Alzheimer disease (AD), dementia, attention-deficit/hyperactivity disorder (ADHD), autism spectrum disorder (ASD), schizophrenia, Bipolar disorders (BD) and depression have been suggested to be associated with altered levels and functions of PUFAs (6, 12–14). However, inconsistent conclusions remain, especially in the studies on depression.

The association between n-3 PUFAs and depression has been extensively investigated. Many studies showed that higher levels of n-3 PUFAs, mainly eicosapentaenoic acid (EPA; 20:5n-3) and DHA, were associated with a lower risk of depression (15–22). However, a few studies observed no apparent association with n-3 PUFAs (23–27), and, in particular, a recent longitudinal study did not support a protective effect of n-3 PUFAs on depression risk (28). In contrast to the cumulative evidence indicating the association of n-3 PUFAs with depression, the relationship between n-6 PUFAs and depression have received much less attention. Some studies found higher levels of n-6 PUFAs related to higher severity of depression, although the results of the relevant studies have been inconsistent (27, 29–32). Okubo's study performed among Japanese breast cancer survivors indicated that a higher blood levels of n-6 PUFAs may increase the risk of depression, while the Avon Longitudinal Study (31) and Thesing's study (33) reported no association in British and Dutch populations. Moreover, studies on the association of n-6/n-3 ratio and depression are also controversial. Some cross-sectional or longitudinal studies suggested a positive association (18, 34–36), whereas several other studies reported a negative association (37) or no association (25, 38).

Therefore, we comprehensively estimated the association of plasma n-3 and n-6 PUFAs and depression in a nationally representative sample of US adults aged 20 years and older. In order to provide a reference for elucidating the role of PUFAs on depression and a safer and more effective strategy to prevent or mitigate depressive symptoms in US adults.

2 Methods

2.1 Study design and sample

This is a cross-sectional study, done using the 2011–2012 cycle of The National Health and Nutrition Examination Survey (NHANES) data (39). NHANES is a stratified multistage probability sampling design to represent the noninstitutionalized civilian US population. Participants completed the survey through a computer-assisted personal interview and a medical examination at a mobile examination center (MEC). More detailed information regarding the survey design and data collection procedure are available elsewhere (40). The study protocol was approved by the National Center for Health Statistics research ethics review board. Written informed consent was obtained for all participants. The 2011–2012 cycle was utilized since all the main independent and dependent variables of interest were available only in this dataset (especially plasma PUFA). Since depression is more common in adult group ($\geq$ 20 years), participants who were < 20 years were excluded for this study. Participants who did not fully respond to the depression screener questionnaire (PHQ-9) were excluded from the study (41). A total of 2053 adults from the United States were included in this study.

2.2 Determination and classification of depression status

Depression status were determined based on participant's responses to the PHQ-9 questionnaire in the mental health-depression screener of questionnaire data of NHANES 2011–2012 cycle. PHQ-9 is the 9-item self-report depression scale that asks questions about the frequency of symptoms of depression over the past 2 weeks. Each item can be scored from 0 (not at all) to 3 (nearly every day) (42). The PHQ-9 score ranges from 0 to 27 and thus, classified in two categories. The individuals with PHQ-score < 9 were classified as "no or mild depression" and those with PHQ-score of 10 or more, were classified as "moderate to severe depression" (43, 44).

2.3 Assessment of plasma n-3 and n-6 PUFAs

Thirty fatty acids analyzed by means of gas chromatography–mass spectrometry and expressed in μmol/L were measured in serum with the goal of obtaining US reference ranges for most circulating fatty acids in a fasting subsample of participants. Briefly, total fatty acids were hexane-extracted from the matrix (100uL serum or plasma) along with an internal standard solution for fatty acid recovery. The extract was derivatized with pentafluorobenzyl bromide to form pentafluorobenzyl esters. The reaction mixture is injected onto a capillary gas chromatograph column (45). More details about plasma fatty acids profile analysis are available in the NHANES manual (40).

We chose all types of plasma n-3 and n-6 PUFAs tested in NHANES for our analysis. Moreover, we selected the most representative AA in n-6 PUFAs and the most representative DHA and EPA in n-3 PUFAs, and analyzed their ratios to reflect the different

roles of n-3 and n-6 PUFAs in depression. Seventeen variables, total n-3 PUFAs, ALA, stearidonic acid (SDA; 18:4n-3), EPA, DHA, DPAn-3, total n-6 PUFAs, linoleic acid (LA; 18:2n-6), gamma-Linolenic acid (GLA; 18:3n-6), homo-gamma-Linolenic acid (DGLA; 20:3n-6), eicosadienoic acid (EDA; 20:2n-6), AA, DTA, DPAn-6, total n-6/n-3 ratio, AA/EPA ratio, and AA/DHA ratio, were evaluated in the present study.

2.4 Assessment of life's essential 8

LE8 scoring algorithm consists of 4 health behaviors (diet, physical activity, nicotine exposure, and sleep health) and 4 health factors (body mass index [BMI], blood pressure, glucose, lipids) (46). This study selected 5 individual LE8 metrics (i.e., blood pressure, lipids, glucose, BMI and nicotine exposure) that were more relevant to the study variables (Table 1). LE8 has great potential to assess and promote cardiovascular health (CVH) across life course. CVH is associated with cardiovascular disease (CVD), as well as non-CVD outcomes such as cognitive impairment and depression (47). CVH-related factors routinely collected (i.e., BMI, smoking, hypertension, hypercholesterolemia, and diabetes) were more relevant to our study variables and could be used to accurately estimate individuals' overall CVH across time even when LE8 metrics are incomplete (48).

TABLE 1 Scoring criteria of CVH-related factors metrics based on life's essential 8.

Metric	Points and criteria
Blood pressure	100: SBP < 115 mmHg and DBP < 75 mmHg 75: SBP 115-124 mmHg and DBP < 75 mmHg 50: SBP 125-134 mmHg or DBP: 75-84 mmHg 25: SBP 135-154 mmHg or DBP 85-94 mmHg 0: SBP ≥ 155 mmHg or DBP ≥ 95 mmHg (Subtract 20 points if treated level)
HbA1c	100: No history of diabetes and HbA1c < 5.7% 60: No diabetes and HbA1c 5.7–6.4% 40: Diabetes with HbA1c < 7.0% 30: Diabetes with HbA1c 7.0–7.9% 20: Diabetes with HbA1c 8.0–8.9% 10: Diabetes with HbA1c 9.0–9.9% 0: Diabetes with HbA1c ≥ 10.0%
Blood lipids	100: Non-HDL cholesterol <130 mg/dL 60: Non-HDL cholesterol 130–159 mg/dL 40: Non-HDL cholesterol 160–189 mg/dL 20: Non-HDL cholesterol 190–219 mg/dL 0: Non-HDL cholesterol ≥220 mg/dL (Subtract 20 points if treated level)
Nicotine exposure	100: Never smoker 75: Former smoker, quit ≥5 year 50: Former smoker, quit 1–5 year 25: Former smoker, quit <1 year 0: Current smoker (Subtract 20 points if living with active indoor smoker in home)
BMI	100: < 25 kg/m2 70: 25.0–29.9 kg/m2 30: 30.0–34.9 kg/m2 15: 35.0–39.9 kg/m2 0: ≥ 40.0 kg/m2

BMI, body mass index; CVH, cardiovascular health; DBP, diastolic blood pressure; HbA1c, glycohemoglobin; HDL, high-density lipoprotein; SBP, systolic blood pressure.

2.5 Other covariates

Based on existing literatures on PUFAs and depression, age, sex, race/ethnicity (Non-Hispanic White, Non-Hispanic Black, Mexican American, Other Hispanic and Other race), educational level and poverty income ratio (PIR) were included in this study as other potential confounders (28, 31, 49). Highest educational level was categorized into 3 levels: (1) Less than high school/general education development (GED), (2) High school graduate/GED or equivalent and (3) higher than high school graduate/GED. PIR represent the ratio of family or unrelated individual income to their appropriate poverty threshold (50). It was categorized into three groups: (1) low: ≤ 1.3, (2) medium: 1.3–3.5, (3) high: > 3.5 (51).

2.6 Statistical analysis

Following the NHANES analytic guidelines, all analyses in this study accounted for sample weights, clustering, and stratification to generate nationally representative estimates (39).

Means and percentages of baseline characteristics were compared using t-tests for continuous variables and χ^2 test for categorical variables. PUFAs were grouped into quartiles and analyzed for the inter-quartile group trend. The lowest quartile (first quartile) was defined as the reference group in each model. Binary logistic regression analysis was used to assess the relation between quartiles of plasma PUFAs level and depression. These regression analyses employed 4 sets of covariates: model 1 was crude model; model 2 adjusted for age, sex and race/ethnicity; Model 3 adjusted the ratio of family income to poverty and personal highest education level on the basis of Model 2; and Model 4 additionally adjusted cardiovascular health on the basis of Model 3.

All statistical analyses were performed using SAS software, version 9.4 (SAS Institute, Cary, NC, United States). Statistical significance was set at 2-sided $p < 0.05$.

This analysis was conducted using publicly available, deidentified data and was not subject to review by the Guangdong Pharmaceutical University's institutional review board.

3 Results

3.1 Demographic characteristics of study population

A total of 2053 US adults aged 20–80 who participated in NHANES 2011–2012 enrolled into the study (Table 2). 7.29% (weighted) subjects had a PHQ-9 score ≥ 10 and were categorized as depressed (moderate to severe depression), and 92.71% (weighted) subjects with PHQ-9 score < 10 were categorized as not depressed. The

TABLE 2 Descriptive characteristics of all Participants for total sample and by depression level groups among US adults in NANES, 2011–2012.

Characteristics	Total	Without depression	Depression	χ^2/ t	*p* value
No. of participants (%)	2053(100)	1890(92.71)	163(7.29)	–	–
Age, y [mean(SE)]	47.58(0.67)	47.70(0.72)	46.03(0.93)	−1.41	0.18
Sex, N (%)					
Male	1,043(49.13)	983(49.99)	60(38.24)	3.59	0.06
Female	1,010(50.87)	907(50.01)	103(61.76)		
Race/ethnicity, N (%)					
Mexican American	213(7.42)	198(7.55)	15(5.86)	0.73	0.57
Other Hispanic	209(5.89)	187(5.66)	22(8.78)		
Non-Hispanic White	821(68.10)	746(68.08)	75(68.34)		
Non-Hispanic Black	477(11.21)	443(11.36)	34(9.33)		
Others	333(7.37)	316(7.35)	17(7.70)		
Education level, N (%)					
< High school	457(16.39)	402(15.82)	55(23.68)	2.51	0.08
High school	433(20.04)	389(19.48)	44(27.24)		
> High school	1,162(63.55)	1,098(64.69)	64(49.08)		
Missing	1(0.01)	1(0.01)	0(0)		
Ratio of family income to poverty, N (%)					
≤ 1.3	655(22.40)	557(20.60)	98(45.36)	13.78	< 0.001*
1.3–3.5	659(33.66)	617(33.54)	42(35.29)		
> 3.5	573(37.89)	560(39.79)	13(13.62)		
Missing	166(6.05)	156(6.07)	10(5.73)		
Total CVH-related factors score, [mean(SE)]					
Body mass index score	61.16(1.56)	61.48(1.63)	57.03(3.34)	−1.15	0.26
Nicotine exposure score	73.15(1.40)	74.85(1.34)	51.54(4.56)	−5.19	< 0.001*
Blood lipids score	64.28(1.14)	64.90(1.21)	56.48(2.70)	−2.62	0.02*
HbA1c score	84.77(0.97)	84.99(1.01)	81.98(2.39)	−1.23	0.23
Blood pressure score	66.71(1.20)	66.84(1.21)	65.10(2.49)	−0.73	0.48
Total score	70.54(0.82)	71.17(0.83)	62.60(1.38)	−4.47	0.003*
Cardiovascular health[a], N (%)					
Low	450(17.62)	390(16.98)	60(25.75)	4.44	0.01*
Moderate	1,041(52.20)	967(51.94)	74(55.62)		
High	562(30.18)	533(31.08)	29(18.64)		

*$p < 0.05$.
[a]Low CVH was defined as a CVH-related factors score of 0 to 49, moderate CVH of 50–79, and high CVH of 80–100.

weighted mean (standard error, SE) age of the study participants was 47.58 (0.67) years, and male and female participants were almost equally distributed gender wise. Among the participants, 821 (68.10%) were non-Hispanic white, 477 (11.21%) were non-Hispanic black, 213 (7.42%) were Mexican-American, 209 (5.89%) were Other Hispanic, and 333 (7.37%) were other race/ethnicity. About 83.59% of respondent had completed at least high school/GED. Among adults, 22.40% had low income (PIR ≤ 1.3), 33.66% had medium income (1.3 < PIR ≤ 3.5) and 37.89% high income (3.5 < PIR). Average CVH score was 70.54 (0.82) and the percentages of low, moderate, and high CVH were17.62, 52.20, and 30.18%, respectively. Significantly participants with lower PIR and CVH level were more likely to have depression.

3.2 The association between PUFAs and depression: univariate analyses

The univariate analyses of PUFAs as continuous variables indicated that there was an association between part of plasma PUFAs levels and depression among US adults ($p < 0.05$). The weighted mean (SE) of those plasma PUFAs for GLA, DGLA, EDA, EPA, DTA, DHA, DPAn-6, DPAn-3 and AA/DHA ratio were 64.67 (1.46), 167.35 (2.85), 23.92 (0.47), 70.96 (1.99), 27.36 (0.58), 162.61 (4.74), 20.78 (0.43), 53.69 (0.78), and 6.33 (0.16) respectively (Table 3); PUFAs as categorical variables indicated that there were a difference in quartiles of plasma PUFAs levels of DTA, DHA, DPAn-6, total n-6/n-3 ratio and AA/DHA ratio among US adults with depression and non-depression ($p < 0.05$; Table 4).

TABLE 3 Univariate analyses results of the relationship between continuous plasma n-3 and n-6 polyunsaturated fatty acids and depression in American adults: NHANES, 2011–2012.

PUFA, μmol/L, [mean(SE)]	Total	Without depression	Depression	t	*p* value
LA(18:2n-6)	3848.96(48.05)	3837.00(48.93)	3999.65(112.63)	1.42	0.17
GLA(18:3n-6)	64.67(1.46)	64.09(1.38)	72.00(3.31)	3.28	0.004*
ALA(18:3n-3)	93.42(2.02)	93.09(1.98)	97.64(4.25)	1.41	0.18
SDA(C18:4n-3)	4.26(0.16)	4.19(0.16)	5.11(0.56)	1.99	0.06
DGLA(20:3n-6)	167.35(2.85)	166.10(2.95)	184.48(7.61)	2.30	0.03*
EDA(20:2n-6)	23.92(0.47)	23.77(0.44)	25.91(1.34)	2.46	0.03*
AA(20:4n-6)	891.57(10.22)	888.89(9.83)	925.38(22.32)	1.96	0.07
EPA(20:5n-3)	70.96(1.99)	71.83(2.03)	59.95(4.01)	−2.21	0.04*
DTA(22:4n-6)	27.36(0.58)	27.08(0.54)	31.05(1.35)	4.90	< 0.001*
DHA(22:6n-3)	162.61(4.74)	162.61(4.74)	146.53(5.40)	−3.07	0.007*
DPA6(22:5n-6)	20.78(0.43)	20.56(0.41)	23.57(0.95)	4.95	< 0.001*
DPA3 (22:5n-3)	53.69(0.78)	53.44(0.76)	56.92(1.82)	2.33	0.03*
Total n-3	386.21(6.28)	387.54(6.60)	369.43(11.55)	−1.21	0.24
Total n-6	5049.47(64.66)	5033.69(66.24)	5268.74(142.14)	1.60	0.13
n-6/n-3 ratio	14.49(0.31)	14.46(0.32)	14.95(0.32)	1.49	0.15
AA/EPA	18.05(0.50)	17.90(0.46)	19.92(1.41)	1.87	0.08
AA/DHA	6.33(0.16)	6.29(0.16)	6.86(0.20)	3.33	0.004*

*$p < 0.05$.

3.3 The association between PUFAs and depression: multiple regression analysis

Table 5 present the OR and 95% CI of depression for quartiles of PUFAs concentrations, using the lowest quartile category as the reference. After controlling for age, sex, race/ethnicity, ratio of family income to poverty, personal highest education level and CVH in the fully adjusted model (model 4), there was a positive relationship between depression and PUFAs in the third quartiles (OR = 1.65, 95% CI = 1.05–2.62) for AA; the third quartiles (OR = 2.20, 95% CI = 1.20–4.05) for DTA; the third (OR = 2.33, 95% CI = 1.34–4.07), and highest quartiles (OR = 1.83, 95% CI = 1.03–3.26) for DPAn-6; and the third (OR = 2.18, 95% CI = 1.18–4.03) and highest quartiles (OR = 2.47, 95% CI = 1.31–4.68) for DPAn-3; 22:5n-3; the second (OR = 2.13, 95% CI = 1.24–3.66), third (OR = 2.40, 95% CI = 1.28–4.50), and highest quartiles (OR = 2.24, 95% CI = 1.08–4.69) for AA/DHA ratio (Table 5).

3.4 The association between PUFAs and depression: stratified analyses

Adjusted model was performed to observe the association between the PUFAs and depression by keeping all other study variables constant (Table 6). With increased plasma levels of AA, DPAn-3 and AA/DHA ratio as well as decreased plasma levels of DHA, women have an increased risk of depression. The risk of depression increases with increased plasma levels of AA and DPAn-6 among ≥60 years age group. Participants aged between 40 and 59 years old were more likely to develop depression due to elevated plasma DPAn-3 levels. Furthermore, elevated plasma AA/DHA levels in the 20–39 years age group may be a risk factor for depression.

4 Discussion

Our findings suggest that there was a significant association between plasma PUFAs with moderate or severe level of depression in American adults after controlling all potential confounders. There were higher odds of developing depression among people who have higher plasma levels of n-6 PUFAs (AA, DTA, and DPAn-6), n-3 PUFAs (DPAn-3) and AA/DHA ratio. Our analysis consolidated the risk role of higher plasma levels of AA and AA/DHA ratio in depression, and was the first to report a positive association between higher plasma DTA, DPAn-6, and DPAn-3 levels and depression in America adult.

The weighted prevalence of depression among subjects was 7.29% in our study. A report from NHANES, 2009–2012 data set has indicated that 7.6% of Americans aged 12 and over had depression (52). The incidence rate is approximately the same as our study. We assessed the participants' blood lipid levels by LE8, and the blood lipids score was 64.28 (1.14). In Lili Wang's research on the associations between LE8 and non-alcoholic fatty liver disease among US adults, the blood lipids score was 67.0 (2.7) which is also roughly in the same way as in our study (53). Overall, our findings suggest that the prevalence of depression and blood lipid levels in our study are roughly in line with the other relevant studies.

Our data provided evidence for existence of associations of depression with higher plasma levels of AA and AA/DHA ratio in American adult sample, which is consistent with some earlier research (54–56). This may reflect the opposing effects of AA and DHA on depression, although the association between plasma DHA and depression did not persist after controlling for all the potential confounding factors. AA, is an abundant n-6 PUFA in the membrane phospholipids, where it is stored in the sn-2 position of phospholipids

10.3389/fnut.2024.1342304

TABLE 4 Univariate analyses results of the relationship between quartiles of plasma n-3 and n-6 polyunsaturated fatty acids and depression in American adults: NHANES, 2011–2012.

PUFA, μmol/L, N (%)	Total	Without depression	Depression	χ^2	*p* value
LA(18:2n-6)	1,593(100)	1,467(92.52)	126(7.48)		
[1430.00, 2989.84]	373(24.61)	341(24.57)	32(25.06)	0.23	0.88
[2989.84, 3451.86]	391(25.28)	365(25.51)	26(22.52)		
[3451.86, 4026.28]	413(25.00)	383(25.10)	30(23.72)		
[4026.28, 15900.00]	416(25.11)	378(24.82)	38(28.70)		
GLA(18:3n-6)	1,549(100)	1,428(92.80)	121(7.20)		
[6.61, 30.22]	371(24.99)	341(25.22)	30(21.93)	0.37	0.77
[30.22, 42.89]	368(24.72)	343(24.73)	25(24.55)		
[42.89, 64.91]	411(25.29)	381(25.41)	30(23.70)		
[64.91, 391.00]	399(25.01)	363(24.63)	36(29.82)		
ALA(18:3n-3)	1,592(100)	1,466(92.52)	126(7.48)		
[16.80, 50.91]	379(24.98)	346(24.84)	33(26.69)	0.36	079
[50.91, 68.27]	384(24.89)	359(25.22)	25(20.89)		
[68.27, 96.45]	414(25.08)	384(25.19)	30(23.72)		
[96.45, 803.00]	415(25.05)	377(24.75)	38(28.70)		
SDA(C18:4n-3)	1798(100)	1,648(92.48)	150(7.52)		
[0.17, 2.05]	500(24.74)	463(25.11)	37(20.28)	1.98	0.11
[2.05, 3.18]	475(25.22)	438(25.53)	37(21.48)		
[3.18, 5.13]	408(24.89)	376(25.06)	32(22.89)		
[5.13, 104.00]	415(25.13)	371(24.30)	44(35.35)		
DGLA(20:3n-6)	1934(100)	1787(93.16)	147(6.84)		
[29.00, 122.75]	560(24.02)	529(24.33)	31(19.83)	2.20	0.09
[122.75, 161.13]	527(25.91)	492(26.49)	35(18.02)		
[161.13, 197.92]	393(24.29)	358(24.08)	35(27.22)		
[197.92, 465.00]	454(25.77)	408(25.10)	46(34.92)		
EDA(20:2n-6)	1826(100)	1,679(92.70)	147(7.30)		
[8.75, 18.09]	439(24.32)	410(22.58)	29(23.86)	0.76	0.52
[18.09, 22.18]	444(24.74)	411(23.35)	33(19.05)		
[22.18, 27.71]	468(25.86)	432(24.11)	36(23.99)		
[27.71, 134.00]	475(25.07)	426(22.66)	49(33.09)		
AA(20:4n-6)	2041(100)	1878(92.66)	163(7.34)		
[187.00, 713.84]	533(24.96)	500(25.51)	33(18.09)	1.81	0.14
[713.84, 868.54]	515(24.97)	476(24.83)	39(26.75)		
[868.54, 1040.25]	492(25.05)	450(24.60)	42(30.71)		
[1040.25, 2570.00]	501(25.02)	452(25.07)	49(24.44)		
EPA(20:5n-3)	2041(100)	1878(92.66)	163(7.34)		
[8.76, 35.96]	551(24.89)	508(24.84)	43(25.55)	1.24	0.29
[35.96, 53.19]	492(24.87)	450(24.72)	42(26.76)		
[53.19, 82.38]	512(25.14)	465(24.64)	47(31.44)		
[82.38, 1090.00]	486(25.10)	455(25.80)	31(16.25)		
DTA(22:4n-6)	1975(100)	1822(92.96)	153(7.26)		
[1.71, 20.23]	543(24.87)	522(25.82)	21(12.76)	4.32	0.005*
[20.23, 25.63]	489(24.97)	485(25.49)	31(18.42)		
[25.63, 32.48]	461(24.71)	412(23.94)	49(34.66)		

(Continued)

TABLE 4 (Continued)

PUFA, μmol/L, N (%)	Total	Without depression	Depression	χ^2	*p* value
[32.48, 204.00]	482(25.44)	430(24.76)	52(34.16)		
DHA(22:6n-3)	2032(100)	1870(92.68)	162(7.32)		
[25.70, 107.61]	449(24.80)	245(25.10)	32(23.58)	3.76	0.01*
[107.61, 144.05]	480(25.17)	247(23.14)	55(44.07)		
[144.05, 195.42]	519(24.82)	289(25.38)	32(14.75)		
[195.42, 918.00]	584(25.22)	326(26.38)	43(17.61)		
DPA6(22:5n-6)	1982(100)	1828(92.72)	154(7.28)		
[2.18, 14.56]	485(24.89)	466(25.78)	19(13.51)	9.34	< 0.001*
[14.56, 19.22]	489(24.94)	461(25.85)	28(13.33)		
[19.22, 25.15]	492(24.91)	444(23.87)	48(38.03)		
[25.15, 126.00]	516(25.27)	457(24.49)	59(35.12)		
DPA3 (22:5n-3)	1998(100)	1844(92.82)	154(7.18)		
[12.60, 40.17]	562(24.77)	534(25.55)	28(14.67)	2.11	0.10
[40.17, 49.70]	497(25.21)	460(25.22)	37(25.10)		
[49.70, 62.06]	451(24.85)	412(24.63)	39(27.80)		
[62.06, 229.00]	488(25.16)	438(24.60)	50(32.43)		
Total n-3	1,369(100)	1,260(92.56)	368(25.03)		
[91.58, 268.26]	310(24.82)	284(25.26)	26(19.34)	1.35	0.26
[268.26, 344.47]	355(25.08)	330(24.49)	25(32.39)		
[344.47, 441.24]	336(25.07)	303(24.49)	33(32.35)		
[441.24, 1917.50]	368(25.03)	343(25.76)	25(15.93)		
Total n-6	1,323(100)	1,226(93.55)	97(6.45)		
[2913.92, 4193.90]	321(24.89)	300(25.47)	21(16,54)	0.84	0.47
[4193.90, 4662.68]	328(25.09)	307(25.22)	21(23.24)		
[4662.68, 5296.08]	332(25.00)	308(24.59)	24(30.94)		
[5296.08, 17189.00]	342(25.01)	311(24.72)	31(29.28)		
n-6/n-3 ratio	1,198(100)	1,107(93.52)	91(6.48)		
[2.25, 11.38]	311(24.88)	290(25.05)	21(22.30)	2.85	0.04*
[11.38, 14.17]	312(25.10)	287(25.12)	25(24.84)		
[14.17, 16.75]	296(25.02)	269(24.12)	27(37.95)		
[16.75, 28.60]	279(25.01)	261(25.71)	18(14.91)		
AA/EPA	2040(100)	1877(92.65)	163(7.35)		
[0.36, 11.19]	494(24.79)	468(25.62)	26(14.30)	2.35	0.07
[11.19, 16.85]	500(25.14)	450(24.45)	50(33.87)		
[16.85, 23.24]	468(25.04)	435(25.22)	33(22.71)		
[23.24, 73.13]	578(25.03)	524(24.71)	54(29.12)		
AA/DHA	2032(100)	1870(92.68)	162(7.32)		
[0.77, 4.47]	575(25.00)	545(26.11)	30(10.88)	7.44	< 0.001*
[4.47, 6.15]	532(24.96)	489(24.88)	43(26.08)		
[6.15, 7.73]	487(24.88)	437(24.31)	50(32.16)		
[7.73, 18.91]	438(25.16)	399(24.71)	39(30.88)		

*$p < 0.05$.

(57). AA-derived eicosanoids from cyclooxygenase (COX) pathways or lipoxygenase (LOX) pathways are important lipid mediators involved in a number of physiological and pathophysiological processes ranging from inflammation, allergic responses, blood lipid regulation, to cell metabolism (58). Cyclooxygenases participate in the production of pro-inflammatory eicosanoids, such as

10.3389/fnut.2024.1342304

TABLE 5 Association of plasma n-3 and n-6 polyunsaturated fatty acids levels with depression in American adults: NHANES, 2011–2012[a].

PUFA, μmol/L, N	Model 1	Model 2	Model 3	Model 4	*p* trend[b]
	OR (95% CI)	OR (95% CI)	OR (95% CI)	OR (95% CI)	
AA(20:4n-6)					
[187.00, 713.84](*n* = 533)	Ref	Ref	Ref	Ref	0.86
[713.84, 868.54](*n* = 515)	1.52(0.79, 2.94)	1.60(0.85, 3.02)	1.58(0.82, 3.03)	1.46(0.76, 2.80)	
[868.54, 1040.25](*n* = 492)	1.76(1.09, 2.86)	1.88(1.16, 3.05)	1.93(1.25, 3.00)	1.65(1.05, 2.62)	
[1040.25, 2570.00](*n* = 501)	1.38(0.88, 2.15)	1.51(0.91, 2.50)	1.41(0.77, 2.58)	1.15(0.66, 2.02)	
DTA(22:4n-6)					
[1.71, 20.23](*n* = 543)	Ref	Ref	Ref	Ref	0.15
[20.23, 25.63](*n* = 489)	1.46(0.55, 3.91)	1.54(0.59, 4.01)	1.40(0.50, 3.95)	1.25(0.44, 3.57)	
[25.63, 32.48](*n* = 461)	2.93(1.65, 5.21)	3.19(1.84, 5.55)	2.63(1.50, 4.61)	2.20(1.20, 4.05)	
[32.48, 204.00](*n* = 482)	2.79(1.44, 5.42)	3.18(1.72, 5.87)	2.63(1.22, 5.70)	2.13(0.96, 4.70)	
DPA6(22:5n-6)					
[2.18, 14.56](*n* = 485)	Ref	Ref	Ref	Ref	0.06
[14.56, 19.22](*n* = 489)	0.98(0.62, 1.57)	0.95(0.59, 1.53)	0.85(0.48, 1.52)	0.75(0.40, 1.41)	
[19.22, 25.15](*n* = 492)	3.04(1.73, 5.35)	3.02(1.71, 5.33)	2.68(1.57, 4.57)	2.33(1.34, 4.07)	
[25.15, 126.00](*n* = 516)	2.74(1.82, 4.12)	2.71(1.79, 4.11)	2.26(1.30, 3.91)	1.83(1.03, 3.26)	
DPA3 (22:5n-3)					
[12.60, 40.17](*n* = 562)	Ref	Ref	Ref	Ref	0.08
[40.17, 49.70](*n* = 497)	1.73(0.85, 3.55)	1.99(0.97, 4.11)	2.18(1.09, 4.36)	1.95(0.96, 3.95)	
[49.70, 62.06](*n* = 451)	1.97(1.02, 3.81)	2.39(1.19, 4.79)	2.46(1.37, 4.42)	2.18(1.18, 4.03)	
[62.06, 229.00](*n* = 488)	2.30(1.35, 3.92)	2.84(1.71, 4.73)	2.95(1.62, 5.39)	2.47(1.31, 4.68)	
AA/DHA ratio					
[0.77, 4.47](*n* = 575)	Ref	Ref	Ref	Ref	0.12
[4.47, 6.15](*n* = 532)	2.52(1.52, 4.17)	2.58(1.55, 4.29)	2.24(1.31, 3.85)	2.13(1.24, 3.66)	
[6.15, 7.73](*n* = 487)	3.18(1.89, 5.35)	3.42(1.97, 5.93)	2.54(1.35, 4.80)	2.40(1.28, 4.50)	
[7.73, 18.91](*n* = 438)	3.00(1.68, 5.36)	3.42(1.74, 6.74)	2.40(1.13, 5.10)	2.24(1.08, 4.69)	

Model 1: crude model. Model 2: adjusted for age, sex and race/ethnicity. Model 3: Model 2 plus ratio of family income to poverty, personal highest education level. Model 4: Model 3 plus CVH.
[a]Only the statistically significant results were shown after controlling all potential confounders.
[b]Test for trend based on the variable containing a median value for each quartile.

prostaglandins and thromboxanes. On the other hand, lipoxygenases generate both leukotrienes and anti-inflammatory eicosanoids like lipoxins. Consequently, an imbalance between these AA-derived eicosanoids has been suggested as a contributing factor to inflammatory effects. Inflammatory processes within the central nervous system (CNS) are essential for the development of brain pathologies, including depression (59). Increased levels of inflammatory cytokines have been reported in depressed patients (60), and found to promote abnormalities in neurotransmitter metabolism and neuroendocrine function, which are related to the pathophysiology of depression (61). Whereas DHA, an n-3 PUFA, has a certain anti-inflammatory effect through competition with AA. Furthermore, DHA also has a neuroprotective effect against decreased neurogenesis and increased neuronal apoptosis (22). Increased plasma levels of AA and/or decreased DHA may cause a disproportionate ratio of n-6 to n-3 and lead to depression through increased inflammatory processes.

This study also found elevated plasma level of other n-6 PUFAs such as DTA and DPAn-6 in patients with moderate to severe depression. DTA, a 2-carbon elongation product of AA, can be desaturated to generate DPAn-6 (62). Previous studies have shown that DTA can impair neurobehavioral development by increasing reactive oxidative species production in Caenorhabditis elegans (63), and higher DPAn-6 status also showed an association with worse mental health in older adults with mild cognitive impairment (64) and children and adolescents with bipolar disorder (65). The Western diet, which is high in processed foods with fat and sugar, is increasing the risk of depression (66). In addition, reactive oxygen species and inflammatory cytokines that could be induced by unreasonable intake of PUFAs have the importance in the progression of depression (67). Previous studies have shown that some n-6 PUFAs are able to activate inflammatory responses and lead to the accumulation of reactive oxygen species and pro-inflammatory factors (68, 69). These alterations might affect the integrity of the cell membrane, leading to alteration of intestinal flora, systemic inflammation and abnormal neurotransmitter transport in the brain (6, 70). In summary, abnormalities in plasma n-6 PUFAs metabolism may be involved in the progress of depression.

TABLE 6 Stratified analyses of the association of plasma n-3 and n-6 polyunsaturated fatty acids levels with depression in American adults: NHANES, 2011–2012.[a]

PUFA, μmol/L, N	Male	OR (95% CI)	*p* trend[b]	Female	OR (95% CI)	*p* trend[b]
AA(20:4n-6)	*n* = 1,039			*n* = 1,002		
	[187.00, 711.80](*n* = 290)	Ref	0.68	[295.00, 718.63](*n* = 243)	Ref	0.99
	[711.80, 856.29](*n* = 273)	0.92(0.37, 2.29)		[718.63, 878.13](*n* = 242)	1.99(1.00, 3.93)	
	[856.29, 1033.88](*n* = 242)	1.26(0.48, 3.26)		[878.13, 1053.00](*n* = 250)	2.44(1.36, 4.39)	
	[1033.88, 2570.00](*n* = 234)	0.84(0.34, 2.09)		[1053.00, 2560.00](*n* = 267)	1.41(0.65, 3.05)	
DHA(22:6n-3)	*n* = 1,033			*n* = 999		
	[34.30, 99.89](*n* = 273)	Ref	0.30	[25.70, 116.76](*n* = 176)	Ref	0.005*
	[99.89, 136.00](*n* = 253)	2.06(0.53, 8.08)		[116.76, 152.40](*n* = 227)	2.24(0.86, 5.88)	
	[136.00, 187.07](*n* = 258)	1.11(0.25, 4.90)		[152.40, 205.87](*n* = 261)	0.50(0.28, 0.87)	
	[187.07, 918.00](*n* = 249)	1.96(0.91, 4.22)		[205.87, 799.00](*n* = 335)	0.49(0.25, 0.96)	
DPA3 (22:5n-3)	*n* = 1,014			*n* = 984		
	[12.6 40.79](*n* = 271)	Ref	0.15	[15.10, 39.97](*n* = 291)	Ref	0.13
	[40.79, 49.90](*n* = 259)	1.66(0.49, 5.62)		[39.97, 49.39](*n* = 238)	2.06(1.00, 4.25)	
	[49.90, 61.18](*n* = 240)	2.32(0.78, 6.86)		[49.39, 62.65](*n* = 211)	2.08(0.96, 4.51)	
	[61.18, 229.00](*n* = 244)	2.40(0.78, 7.42)		[62.65, 198.00](*n* = 244)	2.39(1.28, 4.47)	
AA/DHA	*n* = 1,033			*n* = 999		
	[0.92, 4.82](*n* = 266)	Ref	0.17	[0.77, 4.36](*n* = 309)	Ref	0.004*
	[4.82, 6.52](*n* = 254)	2.38(0.81, 7.00)		[4.36, 5.98](*n* = 278)	1.94(0.77, 4.88)	
	[6.52, 8.12](*n* = 244)	2.07(0.73, 5.84)		[5.98, 7.28](*n* = 243)	2.32(1.12, 4.81)	
	[8.12, 18.91](*n* = 269)	0.89(0.19, 4.19)		[7.28, 17.40](*n* = 169)	4.09(2.14, 7.84)	

PUFA, μmol/L, N	Aged 20–39 years	OR (95% CI)	*p* trend[b]	Aged 40–59 years	OR (95% CI)	Aged ≥ 60 years	OR (95% CI)	*p* trend[b]
AA(20:4n-6)	*n* = 730			*n* = 651		*n* = 660		
	[187.00, 652.27](*n* = 276)	Ref	0.38	[341.00, 764.41](*n* = 124)	Ref	[217.00, 753.56](*n* = 133)	Ref	0.41
	[652.27, 786.73](*n* = 201)	0.97(0.39, 2.39)		[764.41, 915.79](*n* = 144)	1.50(0.48, 4.74)	[753.56, 905.57](*n* = 170)	2.96(0.81, 10.83)	
	[786.73, 930.49](*n* = 152)	0.95(0.38, 2.39)		[915.79, 1107.05](*n* = 178)	1.22(0.66, 2.24)	[905.57, 1079.37](*n* = 162)	7.70(1.73, 34.33)	
	[930.49, 2300.00](*n* = 101)	0.71(0.30, 1.68)		[1107.05, 2570.00](*n* = 205)	0.77(0.28, 2.13)	[1079.37, 1880.00](*n* = 195)	3.30(0.98, 11.12)	
DPA6(22:5n-6)	*n* = 712			*n* = 633		*n* = 637		
	[3.72, 14.52](*n* = 188)	Ref	0.41	[4.32, 15.26](*n* = 135)	Ref	[2.18, 13.62](*n* = 162)	Ref	0.001*
	[14.52, 18.50](*n* = 208)	1.16(0.32, 4.25)		[15.26, 20.59](*n* = 134)	0.43(0.17, 1.11)	[13.62, 18.57](*n* = 147)	0.52(0.04, 7.53)	
	[18.50, 24.02](*n* = 161)	2.26(0.67, 7.61)		[20.59, 26.72](*n* = 178)	1.53(0.62, 3.78)	[18.57, 24.89](*n* = 153)	2.93(0.52, 16.72)	
	[24.02, 68.60](*n* = 155)	0.85(0.23, 3.14)		[26.72, 126.00](*n* = 186)	1.40(0.49, 3.97)	[24.89, 69.30](*n* = 175)	2.84(1.12, 7.19)	

(Continued)

10.3389/fnut.2024.1342304

TABLE 6 (Continued)

PUFA, μmol/L, N	Aged 20–39 years	OR (95% CI)	*p* trend[b]	Aged 40–59 years	OR (95% CI)	Aged ≥ 60 years	OR (95% CI)	*p* trend[b]
DPA3 (22:5n-3)	*n* = 715			*n* = 638		*n* = 645		
	[12.60, 35.09](*n* = 296)	Ref	0.11	[15.10, 44.29](*n* = 137)	Ref	[21.00, 44.44](*n* = 129)	Ref	0.83
	[35.09, 43.35](*n* = 185)	0.89(0.32, 2.48)		[44.29, 53.08](*n* = 156)	2.76(1.10, 6.91)	[44.44, 54.84](*n* = 156)	1.46(0.33, 6.47)	
	[43.35, 52.92](*n* = 136)	2.26(0.87, 5.85)		[53.08, 67.87](*n* = 158)	1.52(0.72, 3.23)	[54.84, 66.95](*n* = 157)	2.91(0.57, 14.94)	
	[52.92, 192.00](*n* = 98)	1.02(0.43, 2.42)		[67.87, 229.00](*n* = 187)	3.17(1.53, 6.59)	[66.95, 177.00](*n* = 203)	1.60(0.30, 8.48)	
AA/DHA	*n* = 726			*n* = 650		*n* = 656		
	[1.00, 4.85](*n* = 172)	Ref	0.16	[0.77, 4.84](*n* = 169)	Ref	[0.98, 3.95](*n* = 234)	Ref	0.12
	[4.85, 6.34](*n* = 192)	10.28(1.24, 84.89)		[4.84, 6.52](*n* = 165)	2.41(0.60, 9.70)	[3.95, 5.51](*n* = 175)	1.10(0.52, 2.32)	
	[6.34, 7.76](*n* = 190)	11.37(1.34, 96.29)		[6.52, 7.91](*n* = 158)	2.06(0.59, 7.19)	[5.51, 7.30](*n* = 139)	1.42(0.27, 7.43)	
	[7.76, 18.21](*n* = 172)	7.53(0.68, 83.86)		[7.91, 18.91](*n* = 158)	2.05(0.58, 7.23)	[7.30, 17.00](*n* = 108)	1.96(0.52, 7.42)	

*$p < 0.05$.

[a]Analyses were adjusted for age, sex, education, race/ethnicity, ratio of family income to poverty and CVH except the stratification variable, and only the statistically significant results were shown after controlling all potential confounders.

[b]Test for trend based on the variable containing a median value for each quartile.

The DPAn-3 is less studied as a new player in the n-3 PUFAs family, compared to its counterparts EPA and DHA. The literature on DPAn-3 is limited, however most of the available data suggests it has beneficial health effects which is contrary to our found that higher DPAn-3 was associated with depression. Our result agrees with a minority of reports concerning DPAn-3 (71). More research remains to be done to further investigate the biological effects of this DPAn-3.

There were also some studies that did not observe an association between plasma PUFAs levels and depression (31, 33, 49, 72, 73). But most of these studies have focused only on the total n-3 PUFAs and/or the total n-6 PUFAs, or the canonical fatty acids among them. A longitudinal study in middle-aged Finnish men did not find evidence that serum polyunsaturated fatty acids would be associated with risk of depression (38). The composition ratio of sex may partially influence results. According to previous studies of dietary intervention in Western countries, the association appears to be observed more in women than in men (21, 74). We also observed a significant association for AA, DHA, DPAn-3, and AA/DHA ratio in women through a sub-analysis stratified by sex. However, this finding should be interpreted with caution in light of the source of PUFAs.

One of the strengths of this study is the use of data from a nationally representative survey with a large sample size from a multiracial/multiethnic population. Even a large number of analyses have been conducted to assess the role of PUFAs in depression from multiple perspectives, especially at the supplement and diet levels, but only a few studies with small sample sizes have examined the association between depression and plasma PUFAs. To our knowledge, our study is the first observational study to examine the association between plasma PUFAs and depression among American adult using part of the LE8 indicators as the primary covariate.

Another strength of this study is that we used plasma PUFAs, which better reflects tissue levels of PUFAs than the more subjective measures of the Food Frequency Questionnaires (FFQ) and food records. Several limitations also need to be acknowledged. A major limitation is that this study is only a cross-sectional exploratory investigation, so a causal relationship cannot be concluded. Additionally, the PHQ-9 items measure only a subset of the symptoms of depression. Apart from the nine symptoms of the PHQ, other depressive symptoms were not included in this study which may be counted as a limitation.

5 Conclusion

In conclusion, this population-based cross-sectional study examining the association between plasma PUFAs and depression risk in American adults revealed an association between higher plasma levels of AA, DTA, DPAn-6, DPAn-3 and AA/DHA ratio and increased risk of depression. The complexity of PUFAs metabolism, interactions and competition between n-3 PUFAs and n-6 PUFAs and the mechanism by which these may influence depression requires continued study.

Data availability statement

Publicly available datasets were analyzed in this study. This data can be found here: https://www.cdc.gov/.

Ethics statement

The studies involving humans were approved by National Center for Health Statistics research ethics review board. The studies were conducted in accordance with the local legislation and institutional requirements. The participants provided their written informed consent to participate in this study.

Author contributions

MW: Conceptualization, Data curation, Formal analysis, Investigation, Methodology, Software, Writing – original draft, Writing – review & editing. XY: Data curation, Formal analysis, Software, Writing – review & editing. YL: Data curation, Methodology, Writing – review & editing. QL: Software, Supervision, Writing – review & editing. YX: Data curation, Project administration, Writing – review & editing. JH: Data curation, Methodology, Writing – review & editing. JG: Funding acquisition, Project administration, Resources, Validation, Visualization, Writing – review & editing. WY: Conceptualization, Formal analysis, Funding acquisition, Project administration, Resources, Validation, Visualization, Writing – review & editing.

Funding

The author(s) declare financial support was received for the research, authorship, and/or publication of this article. WY, male, Doctor of Medicine, member of the Health Professional Committee of Children and Adolescent of Guangdong Provincial, member of the Children 's Mental Health Promotion Professional Committee of Guangdong Provincial Clinical Medical Association, has been committed to the study of children's health. He has presided over 13 scientific research projects at all levels such as the general project of the National Natural Science Foundation of China, and participated in the compilation of 2 college planning textbooks. Published more than 30 SCI papers, including 4 Top journal articles by MW and WY, and participated in the review of Nature Communications, Epidemiology and Psychiatric Sciences, and Journal of Pediatrics, etc. National Natural Science Foundation of China (Gant no. 81973063) and Natural Science Foundation of Guangdong, China (Grant no. 2018A030313723).

Acknowledgments

The authors would like to acknowledge the support from all the team members and all staff of the National Center for Health Statistics of the US Centers for Disease Control and Prevention.

Conflict of interest

The authors declare that the research was conducted in the absence of any commercial or financial relationships that could be construed as a potential conflict of interest.

Publisher's note

All claims expressed in this article are solely those of the authors and do not necessarily represent those of their affiliated organizations, or those of the publisher, the editors and the reviewers. Any product that may be evaluated in this article, or claim that may be made by its manufacturer, is not guaranteed or endorsed by the publisher.

References

1. World Health Organization. Depressive disorder (depression). Available online at: https://www.who.int/zh/news-room/fact-sheets/detail/depression (Accessed May 5, 2023).

2. World Health Organization. *Global burden of mental disorders and the need for a comprehensive, coordinated response from health and social sectors at the country level: report by the secretariat* World Health Organization (2012).

3. Malhi GS, Mann JJ. Depression. *Lancet* (2018) 392:2299–312. doi: 10.1016/s0140-6736(18)31948-2

4. Beurel E, Toups M, Nemeroff CB. The bidirectional relationship of depression and inflammation: double trouble. *Neuron* (2020) 107:234–56. doi: 10.1016/j.neuron.2020.06.002

5. Kunugi H. Depression and lifestyle: focusing on nutrition, exercise, and their possible relevance to molecular mechanisms. *Psychiatry Clin Neurosci* (2023) 77:420–33. doi: 10.1111/pcn.13551

6. Ortega MA, Álvarez-Mon MA, García-Montero C. Microbiota-gut-brain axis mechanisms in the complex network of bipolar disorders: potential clinical implications and translational opportunities. *Mol Psychiatry* (2023) 28:2645–73. doi: 10.1038/s41380-023-01964-w

7. Melo HM, Santos LE, Ferreira ST. Diet-derived fatty acids, brain inflammation, and mental health. *Front Neurosci* (2019) 13:265. doi: 10.3389/fnins.2019.00265

8. Custers EEM, Kiliaan AJ. Dietary lipids from body to brain. *Prog Lipid Res* (2022) 85:101144. doi: 10.1016/j.plipres.2021.101144

9. Decandia D, Landolfo E, Sacchetti S, Gelfo F, Petrosini L, Cutuli D. N-3 PUFA improve emotion and cognition during menopause: a systematic review. *Nutrients* (2022) 14:1982. doi: 10.3390/nu14091982

10. Liu X, Hao J, Yao E, Cao J, Zheng X, Yao D, et al. Polyunsaturated fatty acid supplement alleviates depression-incident cognitive dysfunction by protecting the cerebrovascular and glymphatic systems. *Brain Behav Immun* (2020) 89:357–70. doi: 10.1016/j.bbi.2020.07.022

11. Zeng L, Lv H, Wang X, Xue R, Zhou C, Liu X, et al. Causal effects of fatty acids on depression: Mendelian randomization study. *Front Nutr* (2022) 9:1010476. doi: 10.3389/fnut.2022.1010476

12. Mazahery H, Stonehouse W, Delshad M, Kruger M, Conlon C, Beck K, et al. Relationship between long chain n-3 polyunsaturated fatty acids and autism Spectrum disorder: systematic review and Meta-analysis of case-control and randomised controlled trials. *Nutrients* (2017) 9:155. doi: 10.3390/nu9020155

13. McNamara RK, Welge JA. Meta-analysis of erythrocyte polyunsaturated fatty acid biostatus in bipolar disorder. *Bipolar Disord* (2016) 18:300–6. doi: 10.1111/bdi.12386

14. Zhang Y, Chen J, Qiu J, Li Y, Wang J, Jiao J. Intakes of fish and polyunsaturated fatty acids and mild-to-severe cognitive impairment risks: a dose-response meta-analysis of 21 cohort studies. *Am J Clin Nutr* (2016) 103:330–40. doi: 10.3945/ajcn.115.124081

15. Lin PY, Huang SY, Su KP. A meta-analytic review of polyunsaturated fatty acid compositions in patients with depression. *Biol Psychiatry* (2010) 68:140–7. doi: 10.1016/j.biopsych.2010.03.018

16. Ganança L, Galfalvy HC, Cisneros-Trujillo S, Basseda Z, Cooper TB, Ren X, et al. Relationships between inflammatory markers and suicide risk status in major depression. *J Psychiatr Res* (2021) 134:192–9. doi: 10.1016/j.jpsychires.2020.12.029

17. Horikawa C, Otsuka R, Kato Y, Nishita Y, Tange C, Kakutani S, et al. Cross-sectional association between serum concentrations of n-3 long-chain PUFA and depressive symptoms: results in Japanese community dwellers. *Br J Nutr* (2016) 115:672–80. doi: 10.1017/s0007114515004754

18. Davyson E, Shen X, Gadd DA, Bernabeu E, Hillary RF, McCartney DL, et al. Metabolomic investigation of major depressive disorder identifies a potentially causal

association with polyunsaturated fatty acids. *Biol Psychiatry* (2023) 94:630–9. doi: 10.1016/j.biopsych.2023.01.027

19. Féart C, Peuchant E, Letenneur L, Samieri C, Montagnier D, Fourrier-Reglat A, et al. Plasma eicosapentaenoic acid is inversely associated with severity of depressive symptomatology in the elderly: data from the Bordeaux sample of the Three-City study. *Am J Clin Nutr* (2008) 87:1156–62. doi: 10.1093/ajcn/87.5.1156

20. Matsuoka YJ, Sawada N, Mimura M, Shikimoto R, Nozaki S, Hamazaki K, et al. Dietary fish, n-3 polyunsaturated fatty acid consumption, and depression risk in Japan: a population-based prospective cohort study. Transl. *Psychiatry* (2017) 7:e 1242. doi: 10.1038/tp.2017.206

21. Beydoun MA, Fanelli Kuczmarski MT, Beydoun HA, Hibbeln JR, Evans MK, Zonderman AB. ω-3 fatty acid intakes are inversely related to elevated depressive symptoms among United States women. *J Nutr* (2013) 143:1743–52. doi: 10.3945/jn.113.179119

22. Borsini A, Nicolaou A, Camacho-Muñoz D, Kendall AC, di Benedetto MG, Giacobbe J, et al. Omega-3 polyunsaturated fatty acids protect against inflammation through production of LOX and CYP450 lipid mediators: relevance for major depression and for human hippocampal neurogenesis. *Mol Psychiatry* (2021) 26:6773–88. doi: 10.1038/s41380-021-01160-8

23. Hamazaki K, Matsuoka YJ, Yamaji T, Sawada N, Mimura M, Nozaki S, et al. Plasma phospholipid n-3 polyunsaturated fatty acids and major depressive disorder in Japanese elderly: the Japan public health center-based prospective study. *Sci Rep* (2021) 11:4003. doi: 10.1038/s41598-021-83478-5

24. Patra BN, Khandelwal SK, Chadda RK, Lakshmy R, Abraham RA. A controlled study of plasma fatty acids in Indian patients with depressive episode. *Asian J Psychiatr* (2018) 31:152–6. doi: 10.1016/j.ajp.2017.12.006

25. Rubí Vargas M, Terrazas-Medina EA, Leyva-López AG, Peralta-Peña SL, Cupul-Uicab LA. Depressive symptoms and serum levels of polyunsaturated fatty acids omega-3 and omega-6 among college students from northern Mexico. *Nutr Hosp* (2017) 35:148–52. doi: 10.20960/nh.1311

26. Tsai AC, Lucas M, Okereke OI, O'Reilly EJ, Mirzaei F, Kawachi I, et al. Suicide mortality in relation to dietary intake of n-3 and n-6 polyunsaturated fatty acids and fish: equivocal findings from 3 large US cohort studies. *Am J Epidemiol* (2014) 179:1458–66. doi: 10.1093/aje/kwu086

27. Lucas M, Mirzaei F, O'Reilly EJ. Dietary intake of n-3 and n-6 fatty acids and the risk of clinical depression in women: a 10-y prospective follow-up study. *Am J Clin Nutr* (2011) 93:1337–43. doi: 10.3945/ajcn.111.011817

28. Thesing CS, Bot M, Milaneschi Y, Giltay EJ, Penninx BWJH. Bidirectional longitudinal associations of omega-3 polyunsaturated fatty acid plasma levels with depressive disorders. *J Psychiatr Res* (2020) 124:1–8. doi: 10.1016/j.jpsychires.2020.02.011

29. Zhang R, Sun J, Li Y, Zhang D. Associations of n-3, n-6 fatty acids intakes and n-6: n-3 ratio with the risk of depressive symptoms: NHANES 2009-2016. *Nutrients* (2020) 12:240. doi: 10.3390/nu12010240

30. Currenti W, Godos J, Alanazi AM, Lanza G, Ferri R, Caraci F, et al. Dietary fats and depressive symptoms in Italian adults. *Nutrients* (2023) 15:675. doi: 10.3390/nu15030675

31. Mongan D, Healy C, Jones HJ, Zammit S, Cannon M, Cotter DR. Plasma polyunsaturated fatty acids and mental disorders in adolescence and early adulthood: cross-sectional and longitudinal associations in a general population cohort. *Transl Psychiatry* (2021) 11:321. doi: 10.1038/s41398-021-01425-4

32. Okubo R, Noguchi H, Hamazaki K, Sekiguchi M, Kinoshita T, Katsumata N, et al. Association between blood polyunsaturated fatty acid levels and depressive symptoms in breast cancer survivors. *Prostaglandins Leukot Essent Fatty Acids* (2018) 139:9–13. doi: 10.1016/j.plefa.2018.11.002

33. Thesing CS, Lok A, Milaneschi Y, Assies J, Bockting CLH, Figueroa CA, et al. Fatty acids and recurrence of major depressive disorder: combined analysis of two Dutch clinical cohorts. *Acta Psychiatr Scand* (2020) 141:362–73. doi: 10.1111/acps.13136

34. Shibata M, Ohara T, Yoshida D, Hata J, Mukai N, Kawano H, et al. Association between the ratio of serum arachidonic acid to eicosapentaenoic acid and the presence of depressive symptoms in a general Japanese population: the Hisayama study. *J Affect Disord* (2018) 237:73–9. doi: 10.1016/j.jad.2018.05.004

35. Berger ME, Smesny S, Kim SW, Davey CG, Rice S, Sarnyai Z, et al. Omega-6 to omega-3 polyunsaturated fatty acid ratio and subsequent mood disorders in young people with at-risk mental states: a 7-year longitudinal study. Transl. *Psychiatry* (2017) 7:e 1220. doi: 10.1038/tp.2017.190

36. Hoge A, Tabar V, Donneau AF, Dardenne N, Degée S, Timmermans M, et al. Imbalance between Omega-6 and Omega-3 polyunsaturated fatty acids in early pregnancy is predictive of postpartum depression in a Belgian cohort. *Nutrients* (2019) 11:876. doi: 10.3390/nu11040876

37. Beydoun MA, Fanelli Kuczmarski MT, Beydoun HA, Rostant OS, Evans MK, Zonderman AB. Associations of the ratios of n-3 to n-6 dietary fatty acids with longitudinal changes in depressive symptoms among US women. *Am J Epidemiol* (2015) 181:691–705. doi: 10.1093/aje/kwu334

38. Ruusunen A, Virtanen JK, Lehto SM, Tolmunen T, Kauhanen J, Voutilainen S. Serum polyunsaturated fatty acids are not associated with the risk of severe depression in middle-aged Finnish men: Kuopio Ischaemic heart disease risk factor (KIHD) study. *Eur J Nutr* (2011) 50:89–96. doi: 10.1007/s00394-010-0118-7

39. US Centers for Disease Control and Prevention. National Health and nutrition examination survey, (2011-2012). Available at: https://wwwn.cdc.gov/nchs/nhanes/continuousnhanes/default.aspx?BeginYear=2011

40. US Centers for Disease Control and Prevention. National Health and nutrition examination survey. Available at: https://wwwn.cdc.gov/nchs/nhanes/Default.aspx (Accessed January 2, 2023)

41. Scinicariello F, Przybyla J, Carroll Y, Eichwald J, Decker J, Breysse PN. Age and sex differences in hearing loss association with depressive symptoms: analyses of NHANES 2011-2012. *Psychol Med* (2019) 49:962–8. doi: 10.1017/s0033291718001617

42. Kroenke K, Spitzer RL, Williams JB. The PHQ-9: validity of a brief depression severity measure. *J Gen Intern Med* (2001) 16:606–13. doi: 10.1046/j.1525-1497.2001.016009606.x

43. Wittayanukorn S, Qian J, Hansen RA. Prevalence of depressive symptoms and predictors of treatment among U.S. adults from 2005 to 2010. *Gen Hosp Psychiatry* (2014) 36:330–6. doi: 10.1016/j.genhosppsych.2013.12.009

44. Rethorst CD, Bernstein I, Trivedi MH. Inflammation, obesity, and metabolic syndrome in depression: analysis of the 2009-2010 National Health and nutrition examination survey (NHANES). *J Clin Psychiatry* (2014) 75:e1428–32. doi: 10.4088/JCP.14m09009

45. US Centers for Disease Control and Prevention. NHANES, (2011-2012). Data documentation, codebook, and frequencies: Fatty acids- serum (FAS_G). Available at: https://wwwn.cdc.gov/Nchs/Nhanes/2011-2012/FAS_G.htm

46. Lloyd-Jones DM, Allen NB, Anderson CAM, Black T, Brewer LC, Foraker RE, et al. Life's essential 8: updating and enhancing the American Heart Association's construct of cardiovascular health: a presidential advisory from the American Heart Association. *Circulation* (2022) 146:e18–43. doi: 10.1161/cir.0000000000001078

47. Tibuakuu M, Okunrintemi V, Savji N, Stone NJ, Virani SS, Blankstein R, et al. Nondietary cardiovascular health metrics with patient experience and loss of productivity among US adults without cardiovascular disease: the medical expenditure panel survey 2006 to 2015. *J Am Heart Assoc* (2020) 9:e016744. doi: 10.1161/jaha.120.016744

48. Zheng Y, Huang T, Guasch-Ferre M, Hart J, Laden F, Chavarro J, et al. Estimation of life's essential 8 score with incomplete data of individual metrics. *Front Cardiovasc Med* (2023) 10:1216693. doi: 10.3389/fcvm.2023.1216693

49. Thesing CS, Bot M, Milaneschi Y, Giltay EJ, Penninx BWJH. Omega-3 and omega-6 fatty acid levels in depressive and anxiety disorders. *Psychoneuroendocrinology* (2018) 87:53–62. doi: 10.1016/j.psyneuen.2017.10.005

50. Madhav KC, Sherchand SP, Sherchan S. Association between screen time and depression among US adults. *Prev Med Rep* (2017) 8:67–71. doi: 10.1016/j.pmedr.2017.08.005

51. Petersen KS, Sullivan VK, Fulgoni VL. Circulating concentrations of essential fatty acids, linoleic and α-linolenic acid, in US adults in 2003-2004 and 2011-2012 and the relation with risk factors for Cardiometabolic disease: an NHANES analysis. *Curr Dev Nutr* (2020) 4:nzaa149. doi: 10.1093/cdn/nzaa149

52. Pratt LA, Brody DJ. Depression in the U.S. household population, 2009-2012. *NCHS Data Brief* (2014) 172:1–8.

53. Wang L, Yi J, Guo X, Ren X. Associations between life's essential 8 and non-alcoholic fatty liver disease among US adults. *J Transl Med* (2022) 20:616. doi: 10.1186/s12967-022-03839-0

54. Gopaldas M, Zanderigo F, Zhan S, Ogden RT, Miller JM, Rubin-Falcone H, et al. Brain serotonin transporter binding, plasma arachidonic acid and depression severity: a positron emission tomography study of major depression. *J Affect Disord* (2019) 257:495–503. doi: 10.1016/j.jad.2019.07.035

55. Conklin SM, Manuck SB, Yao JK, Flory JD, Hibbeln JR, Muldoon MF. High omega-6 and low omega-3 fatty acids are associated with depressive symptoms and neuroticism. *Psychosom Med* (2007) 69:932–4. doi: 10.1097/PSY.0b013e31815aaa42

56. Samieri C, Féart C, Letenneur L, Dartigues JF, Pérès K, Auriacombe S, et al. Low plasma eicosapentaenoic acid and depressive symptomatology are independent predictors of dementia risk. *Am J Clin Nutr* (2008) 88:714–21. doi: 10.1093/ajcn/88.3.714

57. Yui K, Imataka G, Nakamura H, Ohara N, Naito Y. Eicosanoids derived from arachidonic acid and their family prostaglandins and cyclooxygenase in psychiatric disorders. *Curr Neuropharmacol* (2015) 13:776–85. doi: 10.2174/1570159x13666151102103305

58. Yin H, Zhou Y, Zhu M, Hou S, Li Z, Zhong H, et al. Role of mitochondria in programmed cell death mediated by arachidonic acid-derived eicosanoids. *Mitochondrion* (2013) 13:209–24. doi: 10.1016/j.mito.2012.10.003

59. Regulska M, Szuster-Głuszczak M, Trojan E, Leśkiewicz M, Basta-Kaim A. The emerging role of the double-edged impact of arachidonic acid-derived eicosanoids in the Neuroinflammatory background of depression. *Curr Neuropharmacol* (2021) 19:278–93. doi: 10.2174/1570159X18666200807144530

60. Jia Y, Liu L, Sheng C, Cheng Z, Cui L, Li M, et al. Increased serum levels of cortisol and inflammatory cytokines in people with depression. *J Nerv Ment Dis* (2019) 207:271–6. doi: 10.1097/nmd.0000000000000957

61. Felger JC, Lotrich FE. Inflammatory cytokines in depression: neurobiological mechanisms and therapeutic implications. *Neuroscience* (2013) 246:199–229. doi: 10.1016/j.neuroscience.2013.04.060

62. Weylandt KH. Docosapentaenoic acid derived metabolites and mediators - the new world of lipid mediator medicine in a nutshell. *Eur J Pharmacol* (2016) 785:108–15. doi: 10.1016/j.ejphar.2015.11.002

63. Wu CH, Hsu WL, Tsai CC, Chao HR, Wu CY, Chen YH, et al. 7, 10, 13,16-Docosatetraenoic acid impairs neurobehavioral development by increasing reactive oxidative species production in Caenorhabditis elegans. *Life Sci* (2023) 319:121500. doi: 10.1016/j.lfs.2023.121500

64. Milte CM, Sinn N, Street SJ, Buckley JD, Coates AM, Howe PRC. Erythrocyte polyunsaturated fatty acid status, memory, cognition and mood in older adults with mild cognitive impairment and healthy controls. *Prostaglandins Leukot Essent Fatty Acids* (2011) 84:153–61. doi: 10.1016/j.plefa.2011.02.002

65. Gracious BL, Chirieac MC, Costescu S, Finucane TL, Youngstrom EA, Hibbeln JR. Randomized, placebo-controlled trial of flax oil in pediatric bipolar disorder. *Bipolar Disord* (2010) 12:142–54. doi: 10.1111/j.1399-5618.2010.00799.x

66. Firth J, Stubbs B, Teasdale SB, Ward PB, Veronese N, Shivappa N, et al. Diet as a hot topic in psychiatry: a population-scale study of nutritional intake and inflammatory potential in severe mental illness. *World Psychiatry* (2018) 17:365–7. doi: 10.1002/wps.20571

67. Reemst K, Broos JY, Abbink MR, Cimetti C, Giera M, Kooij G, et al. Early-life stress and dietary fatty acids impact the brain lipid/oxylipin profile into adulthood, basally and in response to LPS. *Front Immunol* (2022) 13:967437. doi: 10.3389/fimmu.2022.967437

68. Stachowicz K. Application potential of modulation of cyclooxygenase-2 activity: a cognitive approach. *Postępy Higieny i Medycyny Doświadczalnej* (2021) 75:837–46. doi: 10.2478/ahem-2021-0022

69. Stachowicz K. The role of polyunsaturated fatty acids in neuronal signaling in depression and cognitive processes. *Arch Biochem Biophys* (2023) 737:109555. doi: 10.1016/j.abb.2023.109555

70. Pascoe MC, Crewther SG, Carey LM, et al. What you eat is what you are -- a role for polyunsaturated fatty acids in neuroinflammation induced depression? *Clin Nutr* (2011) 30:407–15. doi: 10.1016/j.clnu.2011.03.013

71. Liu T, Wang L, Guo J, Zhao T, Tang H, Dong F, et al. Erythrocyte membrane fatty acid composition as a potential biomarker for depression. *Int J Neuropsychopharmacol* (2023) 26:385–95. doi: 10.1093/ijnp/pyad021

72. Ma J, Peng L, Li S. Mendelian randomization of the causal relationship between ω-3 polyunsaturated fatty acids and major depression. *Wei Sheng Yan Jiu* (2023) 52:793–800. doi: 10.19813/j.cnki.weishengyanjiu.2023.05.018

73. Liu JJ, Galfalvy HC, Cooper TB, Oquendo MA, Grunebaum MF, Mann JJ, et al. Omega-3 polyunsaturated fatty acid (PUFA) status in major depressive disorder with comorbid anxiety disorders. *J Clin Psychiatry* (2013) 74:732–8. doi: 10.4088/JCP.12m07970

74. Colangelo LA, He K, Whooley MA, Daviglus ML, Liu K. Higher dietary intake of long-chain omega-3 polyunsaturated fatty acids is inversely associated with depressive symptoms in women. *Nutrition* (2009) 25:1011–9. doi: 10.1016/j.nut.2008.12.008

frontiers | Frontiers in Neuroscience

TYPE Original Research
PUBLISHED 21 March 2024
DOI 10.3389/fnins.2024.1322071

OPEN ACCESS

EDITED BY
Rubem C. A. Guedes,
Federal University of Pernambuco, Brazil

REVIEWED BY
Jaclyn Anne Stephens,
Colorado State University, United States
Andrea Zaccaro,
University of Studies G. d'Annunzio Chieti and Pescara, Italy

*CORRESPONDENCE
Xiaochun Wang
✉ wangxiaochun@sus.edu.cn

RECEIVED 15 October 2023
ACCEPTED 26 February 2024
PUBLISHED 21 March 2024

CITATION
Li X, Zhou Y, Zhang C, Wang H and Wang X (2024) Neural correlates of breath work, mental imagery of yoga postures, and meditation in yoga practitioners: a functional near-infrared spectroscopy study. *Front. Neurosci.* 18:1322071. doi: 10.3389/fnins.2024.1322071

Neural correlates of breath work, mental imagery of yoga postures, and meditation in yoga practitioners: a functional near-infrared spectroscopy study

Xiawen Li[1], Yu Zhou[2], Chenping Zhang[1], Hongbiao Wang[1] and Xiaochun Wang[2]*

[1]Shanghai University of Medicine and Health Sciences, Shanghai, China, [2]Shanghai University of Sport, Shanghai, China

Objective: Previous research has shown numerous health benefits of yoga, a multicomponent physical and mental activity. The three important aspects of both traditional and modern yoga are breath work, postures, and meditation. However, the neural mechanisms associated with these three aspects of yoga remain largely unknown. The present study investigated the neural underpinnings associated with each of these three yoga components in long- and short-term yoga practitioners to clarify the neural advantages of yoga experience, aiming to provide a more comprehensive understanding of yoga's health-promoting effects.

Methods: Participants were 40 Chinese women, 20 with a long-term yoga practice and 20 with a short-term yoga practice. Functional near-infrared spectroscopy was conducted while participants performed abdominal breathing, mental imagery of yoga postures, and mindfulness meditation. The oxygenated hemoglobin concentrations activated in the brain during these three tasks were used to assess the neural responses to the different aspects of yoga practice. The self-reported mastery of each yoga posture was used to assess the advantages of practicing yoga postures.

Results: Blood oxygen levels in the dorsolateral prefrontal cortex during breath work were significantly higher in long-term yoga practitioners than in short-term yoga practitioners. In the mental imagery of yoga postures task, self-reported data showed that long-term yoga practitioners had better mastery than short-term practitioners. Long-term yoga practitioners demonstrated lower activation in the ventrolateral prefrontal cortex, with lower blood oxygen levels associated with performing this task, than short-term yoga practitioners. In the mindfulness meditation task, blood oxygen levels in the orbitofrontal cortex and the ventrolateral prefrontal cortex were significantly higher in long-term yoga practitioners than in short-term yoga practitioners.

Conclusion: The three core yoga components, namely, yogic breathing, postures, and meditation, showed differences and similarities in the activation levels of the prefrontal cortex. Long-term practice of each component led to the neural benefits of efficient activation in the prefrontal cortex, especially in the dorsolateral prefrontal cortex, orbitofrontal cortex, and ventrolateral prefrontal cortex.

KEYWORDS
yoga, breath, meditation, posture, fNIRS

Introduction

Yoga, a multicomponent physical and mental activity, is increasingly favored by the public as a healthy practice. Practicing yoga can not only improve physical fitness but also help the practitioner achieve a state of mental balance, a sense of inner peace, and more harmonious interactions with the external environment (Brinsley et al., 2022; Joshanloo, 2022; Cagas et al., 2023). There are many varieties of yoga styles practiced worldwide. Although each yoga style has its own characteristics, evidence has shown that breath work, postures, and meditation are the three core components of almost all yoga classes (Mandlik et al., 2023). Currently, there is substantial evidence indicating that the behavioral effects of these three yoga components are not exactly the same, and each possesses its distinct set of benefits (Prado et al., 2014; Domingues, 2018; Vonderlin et al., 2020; Das et al., 2021; Maleki et al., 2022). However, the neural underpinnings of the three yoga components remain largely unknown. Thus, the present study aimed to examine the specific neural correlates associated with each of the three components within a single study.

Although little is known about the underlying neural characteristics of the yoga components, many researchers have compared the explicit effects of the separate yoga components. Semich (2012) explored how performing various postures only or a having a combined yoga practice of breath work, postures, and meditation affected perceived stress levels among the participants. They found that multi-component yoga was more effective than performing yoga postures alone to lower perceived stress levels (Semich, 2012). Wheeler et al. (2019) examined the individual effects of postures, breath work, and meditation on stress responses and found that these three yoga aspects reduced state anxiety with no difference between the three components. Studies associated with breath work have found that breath training can enhance lung function and reduce anxiety (Kupershmidt and Barnable, 2019; Maleki et al., 2022). Yoga posture training has been shown to correct poor body posture (Jorrakate et al., 2015), increase body balance (Prado et al., 2014), and decrease anxiety (Domingues, 2018). Studies associated with meditation show that meditation effectively relieves emotional problems and improves well-being (Vonderlin et al., 2020). Thus, these study results indicated that all three components not only have similar benefits, such as reducing emotional distress, but also have their own unique advantages.

Changes in explicit performance are often a result of corresponding changes in neural activity. Revealing how changes at the neural level are elicited by practicing specific yoga aspects can facilitate the development of yoga interventions in both healthy and clinical populations. In recent years, a few studies have used functional near-infrared spectroscopy (fNIRS) technology to explore the neural correlates of each of the three yoga components separately. In research on yogic breathing, Bhargav et al. (2014) observed significant changes in prefrontal cortex (PFC) activity after high frequency yogic breathing in healthy people. Singh et al. (2016) measured the effect of uninostril yogic breathing on PFC hemodynamics. They observed that right nostril yogic breathing increased activity in the left PFC more than left nostril yogic breathing (Singh et al., 2016). However, the neural underpinnings, as assessed by fNIRS, associated with yogic abdominal breathing remain largely unknow. The present study aimed to address this gap. Yogic breathing consists of a variety of styles in which slow and deep abdominal breathing is a basic and core technique. Yildiz et al. (2022) examined the impact of four yogic breath styles on brain health using a 3 T magnetic resonance imaging system. They found that the assessed meditator of brain health changes greatest during abdominal breathing (Yildiz et al., 2022). Burt et al. (2023) used fNIRS to find that activity in the PFC increases with increased breathing effort. Since abdominal breathing requires more effort in abdominal muscular recruitment than natural breathing (Bahensky et al., 2021), we hypothesized that the PFC hemodynamics during abdominal breathing would increase.

Other studies have focused on posture-based yoga. Chen et al. (2021) used fNIRS to find that yoga posture training, such as practicing the tree pose, activates the supplementary motor area, improving balance on one leg, which can be used as an exercise therapy for people with impaired balance (Chen et al., 2021). Dybvik and Steinert (2021) used fNIRS to investigate brain activity during yoga posture practice. They found differences in prefrontal activation when comparing simple postures to complex postures, differences that represented different cognitive loads (Dybvik and Steinert, 2021). The postures used in these studies are relatively simple; a novice with no practice experience could also complete these postures with guidance. Long-term yoga practitioners can perform many difficult postures with increased posture practice over time that short-term practitioners cannot. Since long-term exercise facilitates neuroplasticity of certain brain functions (Hötting and Röder, 2013), how different brain activities are evoked by these more difficult postures between long-term and short-term yoga practitioners may provide better understanding of the neural characteristics associated with yoga posture practice. Thus, the present study used mental imagery of yoga postures to assess whether neural activity differed between difficult vs. simple yoga postures in long-and short-term yoga practitioners.

Numerous clinical studies using fNIRS have shown that mindfulness meditation interventions can relieve emotion problems (Gundel et al., 2018) and improve attention and cognitive control performances (Gao and Zhang, 2023). Choo et al. (2019) highlighted the role of PFC activity during mindfulness meditation. Gao and Zhang (2023) observed a stronger activation of the dorsolateral PFC (DLPDC) during mindfulness meditation. But few studies have explored the neural responses to yogic mindfulness meditation. Jiang et al. (2021) found that brain activity in the PFC increased during an inhibitory control task after a yogic mindfulness meditation intervention. At present, there is limited research examining how PFC hemodynamics change during yogic mindfulness meditation. The effect of yogic mindfulness meditation practice experience on PFC activity also remains unclear.

Thus, the present study compared neural changes during abdominal breathing, mental imagery of postures, and mindfulness

meditation between long-and short-term yoga practitioners to further explore the separate neural responses to each yoga component. The study analyzed concentration changes in oxyhemoglobin caused by neural activation in the DLPFC, ventrolateral PFC (VLPFC), and orbitofrontal cortex. The DLPFC is important for regulating attention and is closely related to cognitive function (Mooneyham et al., 2016). The orbitofrontal cortex (OFC) has a wide connection with the emotional center and is closely related to emotion regulation (Kral, 2020). The VLPFC participates in self-related processing (Joshanloo, 2022) and motor activity (Selleck et al., 2018). As previously stated, the results of the aforementioned studies indicate that the three yoga components are associated with decreases in negative emotion and increases in attention focus and cognitive and motor control performances. Each of these functions is controlled largely by the various subdivisions of the PFC. Thus, we hypothesized that experienced yoga practitioners would show similar but also unique neural activities in the various subdivisions of the PFC during breath work, mental imagery of yoga postures, and mindfulness meditation. We also hypothesized that practice experience in the three yoga components would enhance neural activity in the corresponding PFC area.

Materials and methods

Participants

A total of 40 women were recruited from yoga studios in China: 20 long-term yoga practitioners and 20 short-term yoga practitioners. All participants were native Chinese women between 18 and 40 years of age. Long-term yoga practitioners practiced yoga more than 3 times a week for a mean (SD) of 6.05 (1.39) years, whereas short-term yoga practitioners practiced yoga more than 3 times a week for a mean (SD) of 0.91 (0.38) years. Table 1 summarizes the demographic characteristics of the participants. This study was approved by the Shanghai University of Sport Ethics Committee and was performed in accordance with the ethical standards laid down in the 1964 Declaration of Helsinki and its later amendments. All participants provided written informed consent prior to the study.

Stimuli

The present study selected 30 yoga posture images. Of them, 15 were simple postures and 15 were difficult postures. Each difficult posture was an advanced version of the corresponding simple posture, and there were some similarities in the activation of the muscles between the simple and difficult postures. All images were consistent in size and luminance. Table 2 gives the names of the postures that were used.

Procedure

The experiment consisted of three tasks: abdominal breathing (task 1), mental imagery of yoga posture (task 2), and mindfulness meditation (task 3). After the participants had been introduced to the experiment, the fNIRS instrumentation (NIRSport2, NIRx, Germany) was placed on them. Participants performed these three tasks while fNIRS data were recorded. The three tasks were compiled and run using E-Prime 3.0 software (Psychology software tools, INC, America). The three tasks were presented in a random order.

Task 1 began with a 10-s fixation screen appearing on a monitor, followed by a black blank screen for 3 min. During those 3 min, participants were instructed to practice abdominal breathing with their eyes closed, keeping the breath slow and deep and coming from the abdomen. They were further instructed that as they reached the end of each inhalation to begin exhaling without holding their breath (see Figure 1).

Task 2 began with a 20-s fixation screen, followed by the presentation of images of 15 different postures, each of which was presented for 3 s. Participants were instructed to view each image and imagine the activation of their body muscles as though they were performing each posture themselves. The experiment consisted of two groups of posture images: one group of 15 simple postures and one group of 15 difficult postures (Table 2). The order in which these two groups of images was presented was random, and each image in each group appeared twice. Participants were then asked to view these images again and to self-rate their mastery of each posture using the following scale: 1 represented not at all; 2, occasionally; 3, relatively easy; and 4, very easy. We did not conduct fNIRS while the participants self-reported their mastery of each posture (see Figure 1).

Task 3 began with a 10-s fixation screen, followed by a black blank screen for 3 min. During those 3 min, participants were asked to practice open monitoring mindfulness meditation. The participants were instructed to close their eyes while attempting to focus attention and stay aware of the present moment, thoughts, feelings without any judgement, that is, maintaining an open and receptive attitude to the moment (Kabat-Zinn, 2021) (see Figure 1).

Data acquisition and analyses

The fNIRS data were collected with the NIRSport2 system (NIRx, Germany). We acquired 760 and 850 nm dual-wavelength near-infrared light to measure the relative concentration changes of oxyhemoglobin and deoxyhemoglobin (Yamashita et al., 1996)

TABLE 1 Demographic and yoga training characteristics of participants.

Characteristic (years)	Long-term practitioners		Short-term practitioners		*t*-test scores
	Mean	SD	Mean	SD	
Age	31.95	7.13	28.50	6.99	0.13
Educational level	14.55	1.87	15.30	1.78	0.20
Yoga training	6.05	1.39	0.91	0.38	<0.01

TABLE 2 Postures used for performing mental imagery of yoga postures.

Simple postures	Difficult postures
Mountain pose with arms up	Handstand pose
Downward facing dog pose	Headstand pose
Plant pose	Crane pose
Locust pose	Full locust
Cat pose	Scorpion pose
Tree pose	Standing sun dial pose
Cobra pose	Snake king pose
Wide legged forward bend	Tortoise pose
Imaginary chair pose	Upsidedown chair
Forearm plank pose	Forearm balance
Pigeon pose	Hanuman pose
Triangle pose	Extend hand to big toe pose
dancer pose	Lord of the dance pose
bridge pose	Wheel pose
Skyscraper pose	Tiptoe pose

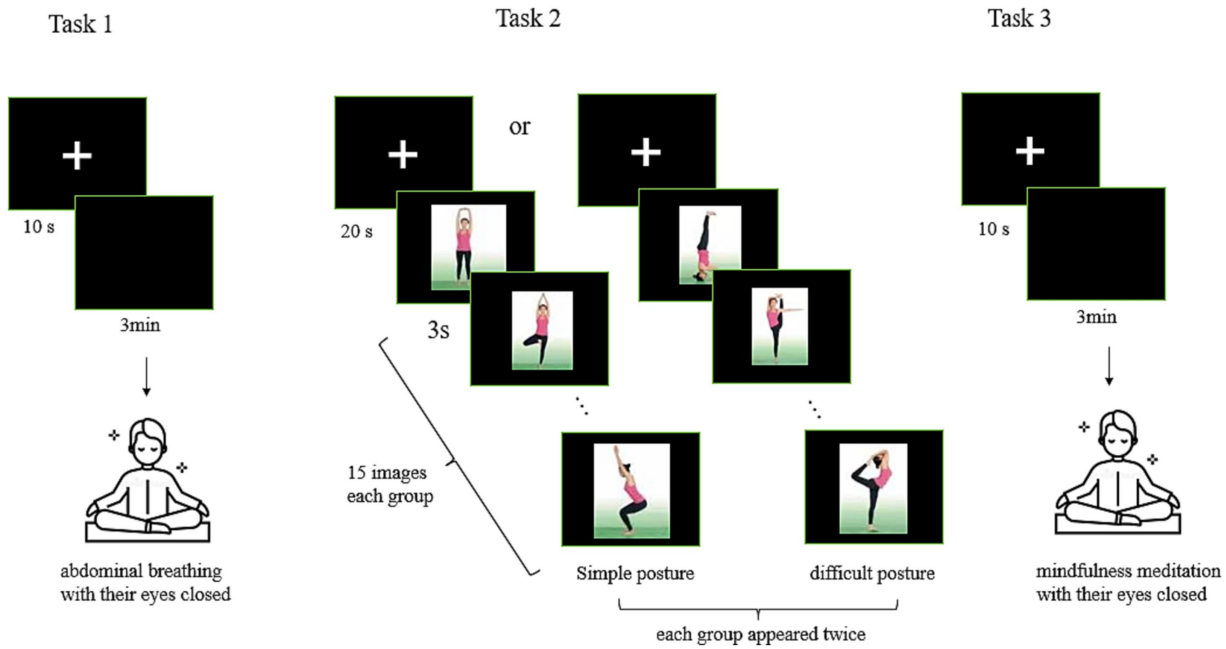

FIGURE 1
Procedures for the three yoga component tasks.

based on the modified Beer–Lambert law (Cope et al., 1988) with a sampling frequency of 10 Hz. For the fNIRS experiment, eight sources and seven detectors (yielding 20 channels) were placed over the PFC region. The distance between the source and the detector was 3 cm. Sensors were located by aligning the bottom row of electrodes with the International 10–20 AF7-Fp1-Fpz-Fp2-AF8 line (Jurcak et al., 2007). Researchers have identified a correspondence between the location of fNIRS channels and specific brain regions (Okamoto et al., 2004; Tsuzuki et al., 2007). In the present study, the ventrolateral prefrontal cortex (VLPFC) was represented by channels 1, 3, 18, and 20; the DLPFC, by channels 2, 5, 8, 9, 10, 15, and 17; the OFC, by channels 4, 11, 13, and 19; and the frontopolar prefrontal cortex (FPA), by channels 6, 7, 12, 14, and 16 (see Figure 2).

The fNIRS data were evaluated with Homer2 software (MGH-Martinos Center for Biomedical Imaging, Boston, MA, United States) using MATLAB (MathWorks, Natick, MA, United States). Motion artifacts were detected as signal changes more by than10% of the standard deviation of the signal within 0.5 s and were removed by wavelet filtering (Molavi and Dumont, 2012).

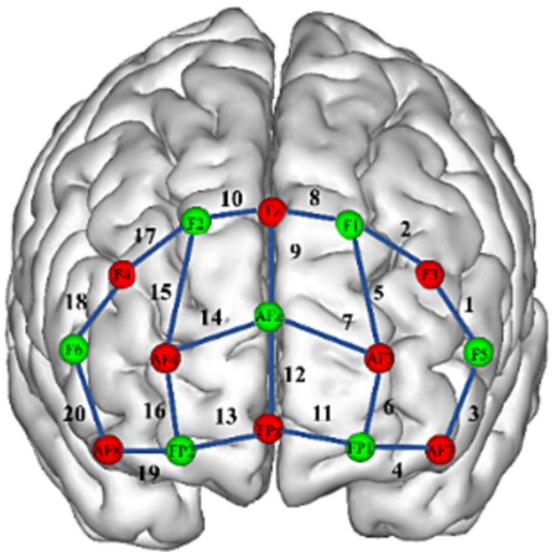

FIGURE 2
Each channel corresponds to an area within the prefrontal cortex.

Baseline drift was removed using a high-pass filter with a cutoff frequency of 0.01 Hz, and a low-pass filter with a frequency of 0.1 Hz was used to reduce the impact of the heartbeat, respiration, blood pressure, and skin blood flow signals. The changes in the oxygenated hemoglobin (HbO) concentration were calculated using the modified Beer–Lambert law. The average response of each participant in the three tasks at 20 channels was obtained by using the block average (Strangman et al., 2002).

Statistical analysis

Statistical analyses were performed in SPSS, version 22.0 (IBM Inc.). The independent samples t-test was used to determine the difference between two groups in the HbO concentration at 20 channels in the PFC during breath work and meditation. The self-reported mastery of each yoga posture and the HbO concentration activated in the PFC while processing that yoga posture were analyzed by two-way repeated-measures analyses of variance (ANOVAs), with main effects of group (long-term vs. short term yoga practitioners) and posture difficulty level (simple vs. difficult). The Benjamini-Hochberg false discovery rate procedure was used for the fNIRS data (Benjamini and Hochberg, 1995). Values are presented as means ± SDs. Differences with 2-sided p-values <0.05 were considered statistically significant.

Results

Task 1: breath work

The results of independent samples t-tests showed that the HbO concentration in the DLPFC (channel 9) of long-term yoga practitioners was significantly higher than that of short-term yoga practitioners ($p = 0.014$) during abdominal breathing. The increased activation in the DLPFC during breath work in long-term yoga practitioners may suggest a benefit of yogic breathing on DLPFC function (see Table 3).

Task 2: mental imagery of yoga postures

Repeated-measures ANOVA results for the self-reported mastery of yoga postures revealed a significant main effect of group ($F_{(1, 19)} = 30.276$, $p < 0.001$, $\eta_p^2 = 0.614$) and of posture difficulty level ($F_{(1, 19)} = 468.058$, $p < 0.001$, $\eta_p^2 = 0.961$), and a significant interaction between group and posture difficulty level ($F_{(1, 19)} = 25.831$, $p < 0.001$, $\eta_p^2 = 0.576$). Long-term yoga practitioners reported better mastery than short-term yoga practitioners of both simple ($p = 0.007$) and difficult ($p < 0.001$) yoga postures (see Figure 3).

Repeated-measures ANOVA results for the HbO concentration in the PFC during mental imagery of yoga postures revealed significant main effects or interactions between group and posture difficulty level in 3 (1, 3, and 20) of 20 channels. These channels were located over the VLPFC (see Table 4). After using *post hoc* tests and controlling for multiple comparisons using the Benjamini-Hochberg false discovery rate procedure, we found that the data from channel 3 remained significant (see Figure 4; Table 5) (Benjamini and Hochberg, 1995). There was a significant main effect of group ($F_{(1, 19)} = 9.035$, $p = 0.007$, $\eta_p^2 = 0.322$) and of posture difficulty level ($F_{(1, 19)} = 9.873$, $p = 0.005$, $\eta_p^2 = 0.342$). Long-term practitioners showed significantly lower activation than short-term practitioners in the VLPFC associated with the mental imagery of yoga postures. In addition, VLPFC activity elicited by mental imagery of the difficult postures was significantly lower than that elicited by the simple postures. There was also a significant interaction between group and posture difficulty level ($F_{(1, 19)} = 5.987$, $p = 0.024$, $\eta_p^2 = 0.240$). The HbO concentration in the VLPFC of long-term practitioners elicited by difficult postures was significantly lower than that of short-term practitioners ($p = 0.008$). By contrast, there was no significant difference in the VLPFC HbO concentration between these two groups during the mental imagery of simple postures (see Figure 4).

Task 3: mindfulness meditation

The independent samples t-test results showed that the HbO concentration in the OFC of long-term yoga practitioners during mindfulness meditation was significantly higher than that of short-term yoga practitioners for channel 4 ($p = 0.013$) and channel 11 ($p = 0.011$). The HbO concentration in the VLPFC cortex of long-term yoga practitioners was significantly higher than that of short-term yoga practitioners ($p = 0.032$) (see Table 6).

Discussion

The aim of this study was to characterize neural responses to three yoga-specific components: breath work, yoga postures, and mindfulness mediation. Participants with long-and short-term yoga practice experience completed abdominal breathing, mental imagery of yoga postures, and mindfulness meditation while fNIRS data were recorded. The results supported one of our hypotheses,

TABLE 3 Mean changes in HbO concentration assessed in four prefrontal cortical areas through 20 fNIRS channels during abdominal breathing between long-and short-term yoga practitioners.

		Long-term practitioners		Short-term practitioners					
Area	Channel	Mean/μm	SD	Mean/μm	SD	*t*	*p*-value	Corrected-p	Cohen's d
OFC									
	4	0.0063	0.0204	−0.0020	0.0194	1.308	0.199	0.796	0.417
	11	0.0051	0.0164	0.0018	0.0123	0.715	0.479	0.932	0.228
	13	0.0004	0.0109	0.0014	0.0155	−0.235	0.815	0.932	0.075
	19	0.0006	0.0114	0.0002	0.0116	0.086	0.932	0.932	0.035
VLPFC									
	1	0.0089	0.0402	−0.0013	0.0247	0.945	0.351	0.468	0.306
	3	0.0066	0.0172	0.0024	0.0287	0.561	0.578	0.578	0.178
	18	0.0522	0.2253	−0.0024	0.0150	1.054	0.299	0.468	0.342
	20	0.0049	0.0108	0.0011	0.0121	1.038	0.306	0.468	0.331
DLPFC									
	2	−0.0048	0.0400	−0.0059	0.0281	0.097	0.923	0.961	0.032
	5	0.0137	0.0328	0.0029	0.0246	1.160	0.253	0.455	0.373
	8	−0.0004	0.0122	−0.0006	0.0192	0.050	0.961	0.961	0.012
	9	0.0281	0.0453	−0.0165	0.0368	3.364	0.002 *	0.014*	1.081
	10	0.0000	0.0152	−0.0053	0.0168	1.045	0.303	0.455	0.331
	15	0.0259	0.1052	−0.0026	0.0299	1.138	0.263	0.455	0.369
	17	0.0062	0.0293	−0.0014	0.0158	0.998	0.325	0.455	0.323
FPA									
	6	0.0036	0.0131	0.0025	0.0179	0.220	0.827	0.827	0.070
	7	0.0052	0.0095	0.0042	0.0157	0.240	0.812	0.827	0.077
	12	0.0046	0.0160	−0.0018	0.0211	1.082	0.286	0.715	0.342
	14	0.0084	0.0191	−0.0010	0.0127	1.801	0.080	0.400	0.580
	16	0.0043	0.0163	0.0005	0.0148	0.774	0.444	0.740	0.244

p-values were corrected for multiple comparisons using the Benjamini-Hochberg false discovery rate procedure. OFC, orbitofrontal cortex; VLPFC, ventrolateral prefrontal cortex; DLPFC, dorsolateral prefrontal cortex; FPA, frontopolar cortex; fNIRS, functional near-infrared spectroscopy; HbO, oxygenated hemoglobin; SD, standard deviation; *$p < 0.05$.

namely, that experienced yoga practitioners showed similar but also unique neural activities in the various subdivisions of the PFC during the three yoga tasks. Hemodynamic changes in the DLPFC improved only during abdominal breathing, and OFC activity increased only during mindfulness meditation. The activity in the VLPFC changed during both mental imagery of postures and mindfulness meditation. To the best of our knowledge, this is the first demonstration of fNIRS comparing the neural characteristics of different yoga components. Consistent with our results, Desai et al. (2015) reviewed 15 studies using electroencephalography and found that breathing, meditation, and posture practice elicited similar but unique enhancements of brain wave activity. Alpha waves improved in amplitude and frequency during all three yoga components; the amplitude and frequency of beta waves increased only during breathing, and theta wave activity improved after both posture practice and breathing (Desai et al., 2015). Our hypothesis that the three components of yoga training would enhance activity in the corresponding PFC area was not fully accurate. During abdominal breathing and mindfulness meditation, we observed higher PFC activity in long-term yoga practitioners than in short-term yoga practitioners. However, long-term yoga practitioners showed much lower activity in the VLPFC compared with short-term yoga practitioners. Below, we discuss this finding further.

Breath work

Our fNIRS data showed that the HbO concentration in the DLPFC of long-term yoga practitioners was significantly higher than that of short-term yoga practitioners during abdominal breathing. The increased HbO concentration may be due to better slow breath control that led to better perfusion and oxygenation in long-term yoga practitioners. This may be a mechanistic underpinning of the deep abdominal breathing control benefits from long-term yoga experience. An enhanced ability to control breathing has been related to physical and mental health in daily life (Stutz and Schreiber, 2017). Zaccaro et al. (2022) compared the aftereffects of slow nasal breathing with a session of mouth breathing at the same respiratory rate. They showed that slow breathing modulates brain activity and hence the

10.3389/fnins.2024.1322071

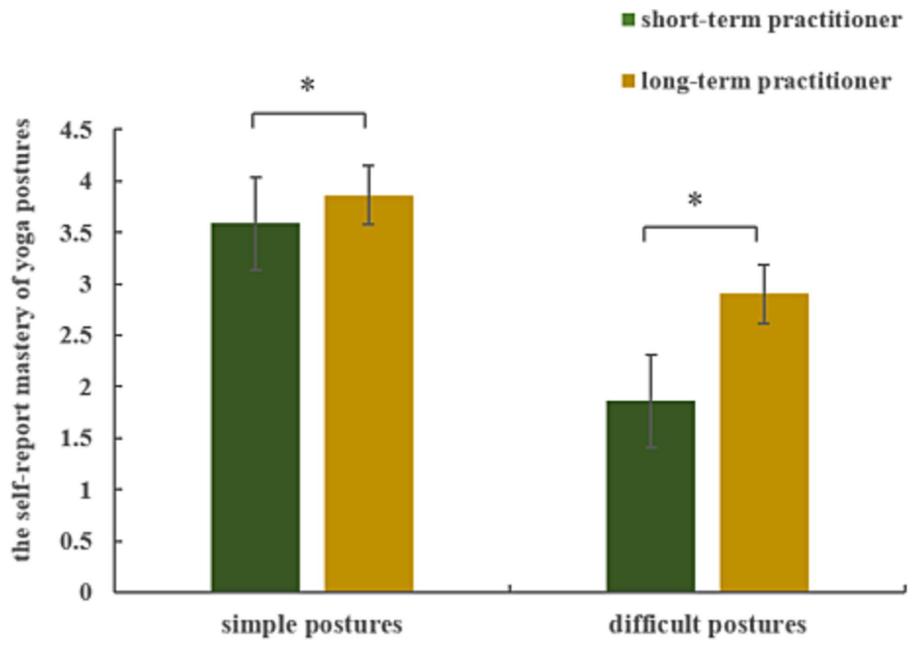

FIGURE 3
Self-reported mastery of yoga postures.

TABLE 4 Main effects and interactions during mental imagery of simple and difficult yoga postures for VLPFC activity (as assessed by HbO concentration) between long-and short-term yoga practitioners.

		Long-term practitioners		Short-term practitioners				
Area	Channel	Mean	SD	Mean	SD	Practice effect	Posture difficulty effect	Practice × posture difficulty
VLPFC								
	1							
	simple postures	−0.0432	0.0378	−0.0791	0.6531	$F_{(1, 19)} = 10.283$	$F_{(1, 19)} = 0.910$	$F_{(1, 19)} = 1.208$
	difficult postures	−0.0584	0.3940	0.3224	0.9905	$p = 0.005, \eta_p^2 = 0.351$	$p = 0.352, \eta_p^2 = 0.046$	$p = 0.285, \eta_p^2 = 0.060$
	3							
	simple postures	0.2007	0.1829	0.1857	0.3011	$F_{(1, 19)} = 9.035$	$F_{(1, 19)} = 9.873$	$F_{(1, 19)} = 5.987$
	difficult postures	−0.2301	0.3297	0.0577	0.3007	$p = 0.007, \eta_p^2 = 0.322$	$p = 0.005, \eta_p^2 = 0.342$	$p = 0.024, \eta_p^2 = 0.240$
	18							
	simple postures	−0.1177	0.3339	0.0330	0.3528	$F_{(1, 19)} = 0.085$	$F_{(1, 19)} = 0.149$	$F_{(1, 19)} = 0.243$
	difficult postures	0.0430	1.2800	−0.0206	0.5158	$p = 0.774, \eta_p^2 = 0.004$	$p = 0.704, \eta_p^2 = 0.008$	$p = 0.628, \eta_p^2 = 0.013$
	20							
	simple postures	0.2089	0.1948	0.1234	0.1928	$F_{(1, 19)} = 1.251$	$F_{(1, 19)} = 15.536$	$F_{(1, 19)} = 7.181$
	difficult postures	−0.1760	0.2414	0.0226	0.3161	$p = 0.277, \eta_p^2 = 0.062$	$p = 0.001, \eta_p^2 = 0.450$	$p = 0.015, \eta_p^2 = 0.274$

HbO, oxygenated hemoglobin; VLPFC, ventrolateral prefrontal cortex; SD, standard deviation; $*p < 0.05$.

subjective experience to the point of inducing a non-ordinary state of consciousness (Zaccaro et al., 2022). The increased HbO concentration in the DLPFC may also represent a benefit of long-term yogic breathing experience on DLPFC function. DLPFC is a cognition area responsible for planning, organizing, and regulating and is closely related to functions such as attention,

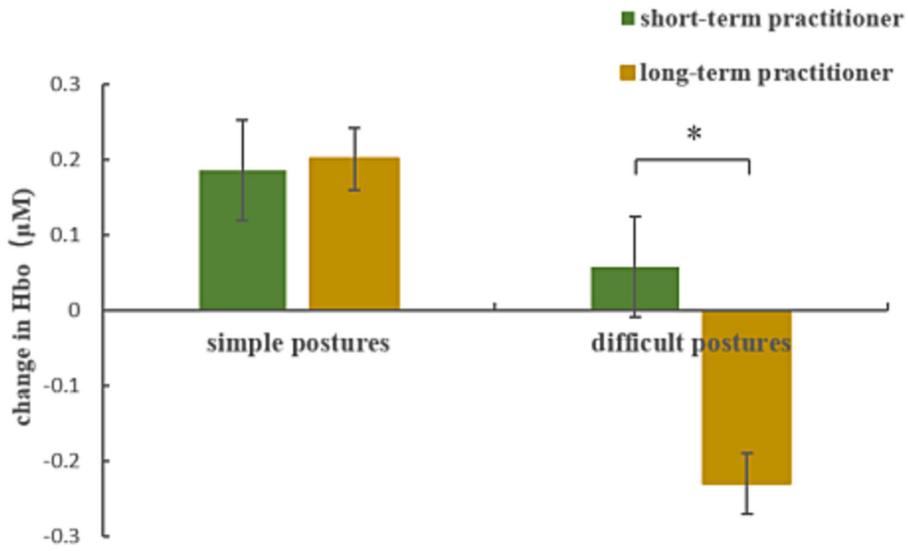

FIGURE 4
HbO concentration changes in the VLPFC (channel 3) between long-and short-term yoga practitioners during mental imagery of simple and difficult yoga postures.

TABLE 5 Mean changes in HbO concentrations in the VLPFC between long-and short-term yoga practitioners during mental imagery of difficult postures.

		Long-term practitioners		Short-term practitioners			
Area	Channel	Mean	SD	Mean	SD	*p*-value	Corrected-*p*
VLPFC							
	1	−0.0584	0.3940	0.3224	0.9905	0.095	0.127
	3	−0.2301	0.3297	0.0577	0.3007	0.002*	0.008*
	18	0.0430	1.2800	−0.0206	0.5158	0.860	0.860
	20	−0.1760	0.2414	0.0226	0.3161	0.026	0.052

p-values were corrected for multiple comparisons using the Benjamini-Hochberg false discovery rate procedure. HbO, oxygenated hemoglobin; VLPFC, ventrolateral prefrontal cortex; SD, standard deviation; *$p < 0.05$.

memory, and emotional control (Hertrich et al., 2021; Wischnewski et al., 2021). Studies have provided strong evidence for the advantages of regular yogic breathing on cognition. Yogic breathing has shown benefits for verbal and spatial cognition, memory, sustained attention and emotional regulation (Marshall et al., 2014; Ma et al., 2017). The current study provides new neural evidence for the cognitive benefits of yogic breathing.

Mental imagery of yoga postures

The self-assessment scores of yoga posture mastery indicated that the mastery levels of long-term yoga practitioners on both simple and difficult postures were higher than those of short-term yoga practitioners. Consistent with the present result, a previous study also observed a posture control advantage suggesting possible benefits in supraspinal feed-forward motor adaptations associated with yoga training (Pinto et al., 2022).

Inconsistent with our hypotheses, the present fNIRS data showed that the activation level of the VLPFC was significantly lower in the long-term yoga practitioners than in the short-term yoga practitioners during mental imagery of difficult yoga postures. The postures we selected for the mental imagery task may have impacted the neural results. Dybvik and Steinert (2021) used fNIRS to explore brain activity when participants actually practiced yoga postures and found that brain activation was significantly higher in difficult postures compared with simple postures. The inconsistency across studies for these results may be due to the different neural underpinnings associated with the two experimental paradigms. It is likely that using imagery for performing the postures in our study versus actually performing the postures as in the study by Dybvik et al. involve different neural correlates. Our findings suggest that long-term experienced practitioners required less neural activity to image more difficult postures than short-term yoga practitioners, which may have largely benefited from long-term posture training experience. Another previous study found that long-term exercise facilitated neuroplasticity associated with brain functions (Hötting and Röder, 2013). The VLPFC is part of a default mode network involved in self-awareness. Evidence indicates that activation of the default mode network is stronger during a resting state and is significantly decreased during target tasks (Sheline et al., 2009).

TABLE 6 Mean changes in HbO concentrations between long-and short-term yoga practitioners during mindfulness meditation as assessed in 20 prefrontal fNIRS channels over four cortical areas.

		Long-term practitioners		Short-term practitioners					
Area	Channel	Mean/ μm	SD	Mean/ μm	SD	*t*	*p*-value	Corrected-p	Cohen's d
OFC									
	4	0.0046	0.0130	−0.0113	0.0209	2.881	0.006*	0.013*	0.914
	11	0.0102	0.0270	−0.0129	0.0177	3.210	0.003*	0.011*	1.012
	13	−0.0025	0.0132	−0.0109	0.0197	1.579	0.123	0.164	0.501
	19	0.0013	0.0119	−0.0042	0.0146	1.326	0.193	0.193	0.413
VLPFC									
	1	0.0007	0.0106	−0.0038	0.0067	1.548	0.131	0.174	0.507
	3	0.0022	0.0133	−0.0087	0.0202	1.960	0.058	0.116	0.637
	18	0.0017	0.0194	−0.0032	0.0110	0.924	0.362	0.362	0.311
	20	0.0037	0.0126	−0.0059	0.0095	2.741	0.010*	0.032*	0.86
DLPFC									
	2	0.0011	0.0077	0.0000	0.0227	0.188	0.852	0.852	0.065
	5	0.0080	0.0134	−0.0014	0.0134	1.752	0.093	0.608	0.701
	8	−0.0027	0.0131	−0.0055	0.0134	0.667	0.509	0.852	0.211
	9	−0.0061	0.0159	0.0158	0.0504	−1.172	0.261	0.608	0.586
	10	0.0028	0.0172	0.0051	0.0318	−0.268	0.790	0.852	0.090
	15	−0.0019	0.0215	−0.0051	0.0151	0.441	0.663	0.852	0.172
	17	0.0075	0.0294	−0.0030	0.0140	1.383	0.175	0.608	0.456
FPA									
	6	−0.0024	0.0297	−0.0063	0.0111	0.539	0.593	0.593	0.174
	7	−0.0009	0.0213	−0.0052	0.0100	0.773	0.445	0.556	0.258
	12	0.0032	0.0160	−0.0029	0.0131	1.325	0.193	0.322	0.417
	14	0.0009	0.0169	−0.0062	0.0120	1.460	0.153	0.322	0.484
	16	0.0027	0.0120	−0.0032	0.0139	1.444	0.157	0.322	0.454

p-value was corrected for multiple comparisons using the Benjamini-Hochberg false discovery rate procedure. OFC, orbitofrontal cortex; VLPFC, ventrolateral prefrontal cortex; DLPFC, dorsolateral prefrontal cortex; FPA, frontopolar cortex; fNIRS: functional near-infrared spectroscopy; HbO, oxygenated hemoglobin; SD, standard deviation; *$p < 0.05$.

Consistent with these observations, the lower activation in the VLPFC observed during mental imagery of yoga postures in the present study may indicate more efficient neural recruitment. Findings in a study by Hertrich et al. (2021) suggested that the cognitive load associated with difficult postures is greater than that for simple postures during the actual performance. The more difficult the posture, the greater the cognitive load and the stronger the corresponding PFC activation. Cecchini et al. (2016) found that motor imagery is developed linked to the development of motor skills. Therefore, enhanced activation in the PFC during actual performance of postures may be a reasonable interpretation for efficient neural recruitment during the mental imagery of postures.

Mindfulness meditation

The HbO concentration in the OFC and VLPFC of long-term yoga practitioners during mindfulness mediation was significantly higher than that of short-term yoga practitioners. The results confirmed our hypotheses that yogic meditation training experience would amplify activities in the corresponding PFC area. Consistent with our results, Nascimento et al. (2018) reported increased activation of the PFC, especially in the OFC and VLPFC, during meditation. Other studies have also found a close neural association between meditation and these two brain areas. Kong et al. (2016) found that mindfulness was positively associated with OFC activation. Kurth et al. (2023) observed a negative relationship between age and OFC, and surprisingly, age-related declines in the OFC is diminished in meditation practitioners. Mooneyham et al. (2016) reported that mindfulness meditation was associated with the VLPFC. Meditation practice also enhanced the functional connectivity of the VLPFC to other brain regions (Barrós-Loscertales et al., 2021). Taken together, these studies indicate the neural benefits associated with yogic mindfulness meditation practice experience. Our findings provide additional neural evidence for the many behavioral studies showing the advantages of mindfulness meditation. Numerous

studies have found that mindfulness meditation benefits mental refreshment, attention, emotional control, and self-awareness, which are associated with the OFC and VLPFC (Shen et al., 2020; Miyashiro et al., 2021; Shen et al., 2023).

Limitations

The present study has some limitations. First, the present study lacks scientific behavioral assessments. Thus, it was not possible to connect the neural advantages of each yoga component with the corresponding behavioral advantage, reducing the significance of this study for practical application. Future research exploring the benefits of yoga should combine accurate behavioral measurements for breathing, posture imagery, and mindfulness meditation with neural indicators. Second, although we balanced the two groups for age and educational level, differences between the two groups beyond yoga training may still have confounded the results. Future research should recruit participants with no yoga experience and conduct long-term yoga interventions to more accurately explore the neurobehavioral benefits of yoga. Third, each of the three yoga components can be further subdivided into several categories, the benefits of which should be further explored in future research.

Conclusion

PFC activation, as assessed using HbO concentrations during fNIRS, showed some similarities as well as differences during the performance of the three core components of yoga practice, namely, yogic breathing, posture imagery, and mindfulness meditation. Long-term yoga practice experience was associated with the neural benefit of efficient activation in the PFC. Long-term mindfulness mediation experience improved brain activity in both the OFC and VLPFC, whereas long-term yogic breathing improved brain activity in the DLPFC. Long-term yoga posture practice experience was associated with efficient neural recruitment in the VLPFC, as reflected by lower activation during mental imagery of yoga postures.

Data availability statement

The original contributions presented in the study are included in the article/supplementary material, further inquiries can be directed to the corresponding author.

Ethics statement

The studies involving humans were approved by the Shanghai University of Sport Ethics Committee and was performed in accordance with the ethical standards laid down in the 1964 Declaration of Helsinki and its later amendments. The studies were conducted in accordance with the local legislation and institutional requirements. A total of 40 women were recruited from yoga studios in shanghai China. Written informed consent for participation was not required from the participants or the participants' legal guardians/next of kin in accordance with the national legislation and institutional requirements.

Author contributions

XL: Conceptualization, Funding acquisition, Methodology, Writing – original draft, Investigation, Supervision. YZ: Formal analysis, Investigation, Writing – review & editing. CZ: Conceptualization, Investigation, Methodology, Writing – review & editing. HW: Methodology, Resources, Writing – review & editing. XW: Conceptualization, Funding acquisition, Methodology, Supervision, Validation, Writing – review & editing.

Funding

The author(s) declare that financial support was received for the research, authorship, and/or publication of this article. This study was supported by Shanghai Science and Technology Planning Project (grant number 20080502800) and a grant from the funding of Education and Scientific Research Project of Shanghai (C2023115).

Conflict of interest

The authors declare that the research was conducted in the absence of any commercial or financial relationships that could be construed as a potential conflict of interest.

Publisher's note

References

Bahensky, P., Bunc, V., Malátová, R., Marko, D., Grosicki, G. J., and Schuster, J. (2021). Impact of a breathing intervention on engagement of abdominal, thoracic, and subclavian musculature during exercise, a randomized trial. *J. Clin. Med.* 10:3514. doi: 10.3390/jcm10163514

Barrós-Loscertales, A., Hernández, S. E., Xiao, Y., González-Mora, J. L., and Rubia, K. (2021). Resting state functional connectivity associated with Sahaja yoga meditation. *Front. Hum. Neurosci.* 15:614882. doi: 10.3389/fnhum.2021.614882

Benjamini, Y., and Hochberg, Y. (1995). Controlling the false discovery rate: a practical and powerful approach to multiple testing. *J. Royal Stat. Soc. Series B* 57, 289–300.

Bhargav, H., Nagendra, H. R., Gangadhar, B. N., and Nagarathna, R. (2014). Frontal hemodynamic responses to high frequency yoga breathing in schizophrenia: a functional near-infrared spectroscopy study. *Front. Psych.* 5:29. doi: 10.3389/fpsyt.2014.00029

Brinsley, J., Smout, M., Girard, D., and Davison, K. (2022). Acute mood and cardiovascular responses to moderate intensity vinyasa yoga, static yin yoga and aerobic

exercise in people with depression and/or anxiety disorders: a 5-arm randomised controlled trial. *Ment. Health Phys. Act.* 22:100450. doi: 10.1016/j.mhpa.2022.100450

Burt, J. S., Davenport, M. P., Welch, J. F., and Davenport, P. W. (2023). fNIRS analysis of rostral prefrontal cortex activity and perception of inspiratory loads. *Respir. Physiol. Neurobiol.* 316:104113. doi: 10.1016/j.resp.2023.104113

Cagas, J. Y., Biddle, S. J., and Vergeer, I. (2023). When an activity is more than just exercise: a scoping review of facilitators and barriers for yoga participation. *Int. Rev. Sport Exerc. Psychol.* 16, 93–154. doi: 10.1080/1750984X.2020.1827448

Cecchini, J. A., Fernández-Losa, J. L., and Pallasá, M. (2016). The accuracy of the motor imagery and the ball reception in children. *Revista Internacional De Medicina Y Ciencias De La Actividad Fisica Y Del Deporte* 62, 297–315. doi: 10.15366/rimcafd2016.62.008

Chen, X.-P., Wang, L.-J., Chang, X.-Q., Wang, K., Wang, H.-F., Ni, M., et al. (2021). Tai chi and Yoga for improving balance on one leg: a neuroimaging and biomechanics study. *Front. Neurol.* 12:746599. doi: 10.3389/fneur.2021.746599

Choo, C. C., Lee, J. J. W., Kuek, J. H. L., Ang, K. K., Yu, J. H., Ho, C. S., et al. (2019). Mindfulness and hemodynamics in asians: a literature review. *Asian J. Psychiatr.* 44, 112–118. doi: 10.1016/j.ajp.2019.07.035

Cope, M., Delpy, D. T., Reynolds, E. O., Wray, S., Wyatt, J., and Van, D. (1988). *Methods of quantitating cerebral near infrared spectroscopy data*. Springer US.

Das, R. R., Sankar, J., and Kabra, S. K. (2021). Role of breathing exercises in asthma—yoga and pranayama. *Indian J. Pediatr.* 89, 174–180. doi: 10.1007/s12098-021-03998-w

Desai, R., Tailor, A., and Bhatt, T. (2015). Effects of yoga on brain waves and structural activation: a review. *Complement. Ther. Clin. Pract.* 21, 112–118. doi: 10.1016/j.ctcp.2015.02.002

Domingues, R. B. (2018). Modern postural yoga as a mental health promoting tool: a systematic review. *Complement. Ther. Clin. Pract.* 31, 248–255. doi: 10.1016/j.ctcp.2018.03.002

Dybvik, H., and Steinert, M. (2021). Real-world fNIRS brain activity measurements during ashtanga vinyasa yoga. *Brain Sci.* 11:742. doi: 10.3390/brainsci11060742

Gao, Q., and Zhang, L. W. (2023). Brief mindfulness meditation intervention improves attentional control of athletes in virtual reality shooting competition: evidence from fNIRS and eye tracking. *Psychol. Sport Exerc.* 69:102477. doi: 10.1016/j.psychsport.2023.102477

Gundel, F., von Spee, J., Schneider, S., Haeussinger, F. B., Hautzinger, M., Erb, M., et al. (2018). Meditation and the brain—neuronal correlates of mindfulness as assessed with near-infrared spectroscopy. *Psych. Res. Neuroimag.* 271, 24–33. doi: 10.1016/j.pscychresns.2017.04.002

Hertrich, I., Dietrich, S., Blum, C., and Ackermann, H. (2021). The role of the dorsolateral prefrontal cortex for speech and language processing. *Front. Hum. Neurosci.* 15:645209. doi: 10.3389/fnhum.2021.645209

Hötting, K., and Röder, B. (2013). Beneficial effects of physical exercise on neuroplasticity and cognition. *Neurosci. Biobehav. Rev.* 37, 2243–2257. doi: 10.1016/j.neubiorev.2013.04.005

Jiang, D., Liu, Z., and Sun, G. (2021). The effect of yoga meditation practice on young Adults' inhibitory control: an fNIRS study. *Front. Hum. Neurosci.* 15:725233. doi: 10.3389/fnhum.2021.725233

Jorrakate, C., Kongsuk, J., Pongduang, C., Sadsee, B., and Chanthorn, P. (2015). Effect of yoga training on one leg standing and functional reach tests in obese individuals with poor postural control. *J. Phys. Ther. Sci.* 27, 59–62. doi: 10.1589/jpts.27.59

Joshanloo, M. (2022). Mental balance in 116 nations: where it is experienced and valued. *Int. J. Environ. Res. Public Health* 19:12457. doi: 10.3390/ijerph191912457

Jurcak, V., Tsuzuki, D., and Dan, I. (2007). 10/20, 10/10, and 10/5 systems revisited: their validity as relative head-surface-based positioning systems. *NeuroImage* 34, 1600–1611. doi: 10.1016/j.neuroimage.2006.09.024

Kabat-Zinn, J. (2021). Meditation is not what you think. *Mindfulness* 12, 784–787. doi: 10.1007/s12671-020-01578-1

Kong, F., Wang, X., Song, Y. Y., and Liu, J. (2016). Brain regions involved in dispositional mindfulness during resting state and their relation with well-being. *Soc. Neurosci.* 11, 331–343. doi: 10.1080/17470919.2015.1092469

Kral, T. R. (2020). *Impact of mindfulness meditation on brain function, connectivity, and structure*. The University of Wisconsin-Madison.

Kupershmidt, S., and Barnable, T. (2019). Definition of a yoga breathing (pranayama) protocol that improves lung function. *Holist. Nurs. Pract.* 33, 197–203. doi: 10.1097/HNP.0000000000000331

Kurth, F., Strohmaier, S., and Luders, E. (2023). Reduced age-related Gray matter loss in the orbitofrontal cortex in long-term meditators. *Brain Sci.* 13:1677. doi: 10.3390/brainsci13121677

Maleki, A., Ravanbakhsh, M., Saadat, M., Bargard, M. S., and Latifi, S. M. (2022). Effect of breathing exercises on respiratory indices and anxiety level in individuals with generalized anxiety disorder: a randomized double-blind clinical trial. *J. Phys. Ther. Sci.* 34, 247–251. doi: 10.1589/jpts.34.247

Mandlik, G. V., Nguyen, B., Ding, D., and Edwards, K. M. (2023). Not all yoga styles are the same: an international survey on characteristics of yoga classes. *J. Integ. Complement. Med.* 29, 321–326. doi: 10.1089/jicm.2022.0712

Marshall, R. S., Basilakos, A., Williams, T., and Love-Myers, K. (2014). Exploring the benefits of unilateral nostril breathing practice post-stroke: attention, language, spatial abilities, depression, and anxiety. *J. Altern. Complement. Med.* 20, 185–194. doi: 10.1089/acm.2013.0019

Ma, X., Yue, Z. Q., Gong, Z. Q., Zhang, H., Duan, N. Y., Shi, Y. T., et al. (2017). The effect of diaphragmatic breathing on attention, negative affect and stress in healthy adults. *Front. Psychol.* 8:874. doi: 10.3389/fpsyg.2017.00874

Miyashiro, S., Yamada, Y., Muta, T., Ishikawa, H., Abe, T., Hori, M., et al. (2021). Activation of the orbitofrontal cortex by both meditation and exercise: a near-infrared spectroscopy study. *PLoS One* 16:e0247685. doi: 10.1371/journal.pone.0247685

Molavi, B., and Dumont, G. A. (2012). Wavelet-based motion artifact removal for functional near-infrared spectroscopy. *Physiol. Meas.* 33, 259–270. doi: 10.1088/0967-3334/33/2/259

Mooneyham, B. W., Mrazek, M. D., Mrazek, A. J., and Schooler, J. W. (2016). Signal or noise: brain network interactions underlying the experience and training of mindfulness. *Ann. N. Y. Acad. Sci.* 1369, 240–256. doi: 10.1111/nyas.13044

Nascimento, S. S., Oliveira, L. R., and DeSantana, J. M. (2018). Correlations between brain changes and pain management after cognitive and meditative therapies: a systematic review of neuroimaging studies. *Complement. Ther. Med.* 39, 137–145. doi: 10.1016/j.ctim.2018.06.006

Okamoto, M., Dan, H., Sakamoto, K., Takeo, K., Shimizu, K., Kohno, S., et al. (2004). Three-dimensional probabilistic anatomical cranio-cerebral correlation via the international 10–20 system oriented for transcranial functional brain mapping. *NeuroImage* 21, 99–111. doi: 10.1016/j.neuroimage.2003.08.026

Pinto, D. P., Moreira, P. V. S., and Menegaldo, L. L. (2022). Postural control adaptations in yoga single-leg support postures: comparison between practitioners and nonpractitioners. *Mot. Control.* 26, 412–429. doi: 10.1123/mc.2021-0088

Prado, E. T., Raso, V., Scharlach, R. C., and Kasse, C. A. (2014). Hatha yoga on body balance. *Int. J. Yoga* 7, 133–137. doi: 10.4103/0973-6131.133893

Selleck, R. A., Giacomini, J., Buchholtz, B. D., Lake, C., Sadeghian, K., and Baldo, B. A. (2018). Modulation of appetitive motivation by prefrontal cortical mu-opioid receptors is dependent upon local dopamine D1 receptor signaling. *Neuropharmacology* 140, 302–309. doi: 10.1016/j.neuropharm.2018.07.033

Semich, A. M. (2012). *Effects of two different hatha yoga interventions on perceived stress and five facets of mindfulness*. [Doctoral dissertation]. California: Northcentral University.

Sheline, Y. I., Barch, D. M., Price, J. L., Rundle, M. M., Vaishnavi, S. N., Snyder, A. Z., et al. (2009). The default mode network and self-referential processes in depression. *Proc. Natl. Acad. Sci.* 106, 1942–1947. doi: 10.1073/pnas.0812686106

Shen, H., Chen, M., and Cui, D. (2020). Biological mechanism study of meditation and its application in mental disorders. *Gen. Psych.* 33:e100214. doi: 10.1136/gpsych-2020-100214

Shen, H., Zhang, L., Li, Y., Zheng, D., Du, L., Xu, F., et al. (2023). Mindfulness-based intervention improves residual negative symptoms and cognitive impairment in schizophrenia: a randomized controlled follow-up study. *Psychol. Med.* 53, 1390–1399. doi: 10.1017/S0033291721002944

Singh, K., Bhargav, H., and Srinivasan, T. M. (2016). Effect of uninostril yoga breathing on brain hemodynamics: A functional near-infrared spectroscopy study. *Int. J. Yoga*, 9:12.

Strangman, G., Culver, J. P., Thompson, J. H., and Boas, D. A. (2002). A quantitative comparison of simultaneous BOLD fMRI and NIRS recordings during functional brain activation. *NeuroImage* 17, 719–731. doi: 10.1006/nimg.2002.1227

Stutz, R., and Schreiber, D. (2017). The effectiveness of occidental breathing therapy methods: a systematic review. *Complement. Med. Res.* 24, 371–379. doi: 10.1159/000464341

Tsuzuki, D., Jurcak, V., Singh, A. K., Okamoto, M., Watanabe, E., and Dan, I. (2007). Virtual spatial registration of stand-alone fNIRS data to MNI space. *NeuroImage* 34, 1506–1518. doi: 10.1016/j.neuroimage.2006.10.043

Vonderlin, R., Biermann, M., Bohus, M., and Lyssenko, L. (2020). Mindfulness-based programs in the workplace: a meta-analysis of randomized controlled trials. *Mindfulness* 11, 1579–1598. doi: 10.1007/s12671-020-01328-3

Wheeler, E. A., Santoro, A. N., and Bembenek, A. F. (2019). Separating the "Limbs" of Yoga: Limited Effects on Stress and Mood. *J. Relig. Health.* 58, 2277–2287. doi: 10.1007/s10943-017-0482-1

Wischnewski, M., Mantell, K. E., and Opitz, A. (2021). Identifying regions in prefrontal cortex related to working memory improvement: a novel meta-analytic method using electric field modeling. *Neurosci. Biobehav. Rev.* 130, 147–161. doi: 10.1016/j.neubiorev.2021.08.017

Yamashita, Y., Maki, A., Ito, Y., Watanabe, E., Mayanagi, Y., and Koizumi, H. (1996). Noninvasive near-infrared topography of human brain activity using intensity modulation spectroscopy. *Opt. Eng.* 35, 1046–1049. doi: 10.1117/1.600721

Yildiz, S., Grinstead, J., Hildebrand, A., Oshinski, J., Rooney, W. D., Lim, M. M., et al. (2022). Immediate impact of yogic breathing on pulsatile cerebrospinal fluid dynamics. *Sci. Rep.* 12:10894. doi: 10.1038/s41598-022-15034-8

Zaccaro, A., Piarulli, A., Melosini, L., Menicucci, D., and Gemignani, A. (2022). Neural correlates of non-ordinary states of consciousness in pranayama practitioners: the role of slow nasal breathing. *Front. Syst. Neurosci.* 16:803904. doi: 10.3389/fnsys.2022.803904

frontiers | Frontiers in Neuroscience

TYPE Systematic Review
PUBLISHED 11 April 2024
DOI 10.3389/fnins.2024.1366747

OPEN ACCESS

EDITED BY
Adriana Ximenes-da-Silva,
Federal University of Alagoas, Brazil

REVIEWED BY
Sidra Tabassum,
University of Texas Health Science Center at Houston, United States
Pankaj Bhatia,
Wayne State University, United States

*CORRESPONDENCE
Georgian Badicu
✉ georgian.badicu@unitbv.ro
Fatma Hilal Yagin
✉ hilal.yagin@inonu.edu.tr
Burak Yagin
✉ burak.yagin@inonu.edu.tr
Fabrício Oliveira Souto
✉ fabricio.souto@ufpe.br

†These authors have contributed equally to this work

RECEIVED 07 January 2024
ACCEPTED 19 March 2024
PUBLISHED 11 April 2024

CITATION
Ramos TL, de Sousa Fernandes MS, da Silva Fidélis DE, Jurema Santos GC, Albuquerque RB, Ferreira DJS, de Souza RF, Badicu G, Yagin FH, Yagin B, Alwhaibi RM, Souto FO and Lagranha CJ (2024) The impact of enriched environments on cerebral oxidative balance in rodents: a systematic review of environmental variability effects. *Front. Neurosci.* 18:1366747. doi: 10.3389/fnins.2024.1366747

The impact of enriched environments on cerebral oxidative balance in rodents: a systematic review of environmental variability effects

Tiago Lacerda Ramos[1], Matheus Santos de Sousa Fernandes[1,2], Débora Eduarda da Silva Fidélis[1], Gabriela Carvalho Jurema Santos[3], Renata B. Albuquerque[1,2], Diorginis José Soares Ferreira[4], Raphael Fabrício de Souza[5], Georgian Badicu[6]*, Fatma Hilal Yagin[7]*, Burak Yagin[7]*, Reem M. Alwhaibi[8], Fabrício Oliveira Souto[1,2]*† and Claúdia Jacques Lagranha[9†]

[1]Programa de Pós-Graduação em Biologia Aplicada à Saúde, Centro de Biociências, Universidade Federal de Pernambuco, Recife, Pernambuco, Brazil, [2]Instituto Keizo Asami, Universidade Federal de Pernambuco, Recife, Pernambuco, Brazil, [3]Programa de Pós-Graduação em Nutrição, Universidade Federal de Pernambuco, Recife, Pernambuco, Brazil, [4]Physical Education Department/Federal University of São Francisco Valley, Petrolina, Pernambuco, Brazil, [5]Department of Physical Education, Federal University of Sergipe, São Cristovão, Sergipe, Brazil, [6]Department of Physical Education and Special Motricity, Transilvania University of Braşov, Braşov, Romania, [7]Department of Biostatistics and Medical Informatics, Faculty of Medicine, Inonu University, Malatya, Türkiye, [8]Department of Rehabilitation Sciences, College of Health and Rehabilitation Sciences, Princess Nourah Bint Abdulrahman University, Riyadh, Saudi Arabia, [9]Programa de Pós-Graduação em Nutrição Atividade Física e Plasticidade Fenotípica, Centro Acadêmico de Vitória, Vitória de Santo Antão, Pernambuco, Brazil

Introduction: The present review aimed to systematically summarize the impacts of environmental enrichment (EE) on cerebral oxidative balance in rodents exposed to normal and unfavorable environmental conditions.

Methods: In this systematic review, four databases were used: PubMed (830 articles), Scopus (126 articles), Embase (127 articles), and Science Direct (794 articles). Eligibility criteria were applied based on the Population, Intervention, Comparison, Outcomes, and Study (PICOS) strategy to reduce the risk of bias. The searches were carried out by two independent researchers; in case of disagreement, a third participant was requested. After the selection and inclusion of articles, data related to sample characteristics and the EE protocol (time of exposure to EE, number of animals, and size of the environment) were extracted, as well as data related to brain tissues and biomarkers of oxidative balance, including carbonyls, malondialdehyde, nitrotyrosine, oxygen-reactive species, and glutathione (reduced/oxidized).

Results: A total of 1,877 articles were found in the four databases, of which 16 studies were included in this systematic review. The results showed that different EE protocols were able to produce a global increase in antioxidant capacity, both enzymatic and non-enzymatic, which are the main factors for the neuroprotective effects in the central nervous system (CNS) subjected to unfavorable conditions. Furthermore, it was possible to notice a slowdown in neural dysfunction associated with oxidative damage, especially in the prefrontal structure in mice.

Discussion: In conclusion, EE protocols were determined to be valid tools for improving oxidative balance in the CNS. The global decrease in oxidative stress biomarkers indicates refinement in reactive oxygen species detoxification, triggering an improvement in the antioxidant network.

KEYWORDS

enriched environment, oxidative stress, brain, central nervous system, biochemistry, antioxidants

1 Introduction

It is well known that vulnerability to oxidative damage varies among organs, with the brain being one of the most susceptible to oxidative stress (OS) (Halliwell, 2006). Characterized by the imbalance between the levels of pro-oxidant and antioxidant, OS is commonly related to the pathogenesis of several diseases, including Alzheimer's, Parkinson's, schizophrenia, and stroke (Chen and Zhong, 2014; Orellana-Urzúa et al., 2020; Ermakov et al., 2021; Balietti and Conti, 2022).

Seeking strategies to minimize OS and even combat pathologies-associated, non-pharmacological strategies have been suggested to attenuate cellular damage induced by OS in different organisms (Wronka et al., 2022; Sharma and Mehdi, 2023) by changing the lifestyle as well as the consumption of specific foods and vitamins (Gomes et al., 2017; Sharma and Mehdi, 2023). Thus, it is postulated that a rich environment can boost mental and physical health and, therefore, attenuate OS by reducing the production of pro-oxidative compounds, generally termed reactive oxygen species (ROS), while increasing their scavenger through antioxidant systems, assembled by enzymatic and non-enzymatic compounds (Fernandes et al., 2022).

The EE paradigm emerged in 1947 through Donald Hebb, who studied animal behavior and realized that the variability of the environment was related to neurological and behavioral improvements. The EE consists of an environment (cage) assembled by inanimate objects varying in shapes and textures, increased social interaction, higher voluntary physical activity, and continuous exposure to learning activities, enhancing both cognitive function and sensory motor aspects. Furthermore, EE upregulates processes linked to neuroplasticity such as neurogenesis, synaptogenesis, and neurotrophin production, culminating in a protective effect against neurodegeneration (Olson et al., 2006; Kempermann, 2019).

Although some mechanisms of EE intervention have been elucidated, there are still several gaps in the literature. Due to the variability of protocols in relation to the number of objects, number of animals, and cage dimensions (width, depth, and length), it is important to clarify the impacts of this variability on OS biomarkers and antioxidant defenses in rodent tissues. Therefore, this study aimed to systematically summarize the impacts of EE on cerebral oxidative balance in rodents.

2 Methods

The review followed the Preferred Reporting Items for Systematic Reviews and Meta-Analysis (PRISMA) guidelines.

2.1 Study selection and eligibility

Eligibility criteria were previously used to minimize the risk of bias. The inclusion and exclusion criteria followed the Population, Intervention, Comparison, Outcomes, and Study (PICOS) (Table 1). There were no restrictions on language or publication date. The following inclusion criteria were used: (a) rodent studies, (b) evaluation of oxidative balance parameters, (c) absence of a control group or comparator, and (d) Studies with any other animal model and biological organism were not used, reviews, letters to editors, duplicates and the presence of data used in different studies were excluded.

2.2 Information sources and search strategy

The search strategy was carried out during the period from April to May 2023. The databases used were PubMed (Medline), Scopus, and Embase. The search strategies used were PubMed (Medline): [(Environmental Enrichment) OR (Enriched Environment)] AND ((((((Oxidative Stress) OR (Stress, Oxidative)) OR (Oxidative Damage)) OR (Oxidative Damages)) OR (Oxidative Injury)) OR (Oxidative Injuries)). In the Embase, Scopus, and Science Direct databases, the following search equation was used: (("Environmental Enrichment") OR ("Enriched Environment")) AND ((((((("Oxidative Stress") OR ("Stress, Oxidative")) OR ("Oxidative Damage")) OR ("Oxidative Damages")) OR ("Oxidative Injury")) OR ("Oxidative Injuries")).

2.3 Selection and data collection process

The screening of studies was performed by reading the title, abstract, and full text. The selection of studies was performed by two independent researchers (MSSF and TLR). The discrepancies were resolved by a third rater. Data were extracted by two independent researchers. The discrepancies were resolved by a third author (FOS).

2.4 Items

To answer the hypothesis of this systematic review, different data were extracted. Initially, we collected the following information: author, year, species, sex, and age. In addition, data were collected on the structure of the environmental enrichment (EE) protocol, including the number of animals per cage, housing dimensions (length, width, and depth or height), and the time of exposure to the EE. Next, data on

TABLE 1 PICOS strategy.

	Inclusion criteria	Exclusion criteria
Population	Rodents	Human and other organisms
Intervention	Environmental enrichment	Non-environmental enrichment
Control	Non-environmental enrichment	Any other comparison group
Outcomes	Carbonyls, 2′,7′-dichlorofluorescein, malondialdehyde, nitrotyrosine, reactive oxygen species (ROS levels), 4-hydroxynonenal, and superanion. antioxidant outcomes include catalase, ferric reducing antioxidant power, glutathione S-transferase, reduced glutathione, oxidized glutathione; reduced glutathione/oxidized glutathione ratio; glutathione peroxidase; copper/zinc superoxide dismutase, SOD-2 (MnSOD), total radical antioxidant	No oxidati contribution ve Balance parameters
Study design	Animal studies	Reviews; case reports; letters to the editor; comments, etc.

brain tissues and OS biomarkers were evaluated, such as carbonyls, 2′,7′-dichlorofluorescein (DCF), malondialdehyde (MDA/TBARS), nitrotyrosine, ROS levels, 4-hydroxynonenal (4-HNE), and superanion. Antioxidant outcomes include catalase, ferric reducing antioxidant power (FRAP), glutathione S-transferase (GST), reduced glutathione (GSH), oxidized glutathione (GSSG), reduced glutathione (GSH)/oxidized glutathione (GSSG) ratio, glutathione peroxidase (GPx), copper/zinc superoxide dismutase (Cu/Zn SOD), superoxide dismutase (SOD), SOD-2 (MnSOD), and total radical antioxidant.

2.5 Methodological quality assessment

The SYRCLE's strategy was used to assess the methodological quality of the animal studies. The tool consisted of 10 questions that evaluated methodological criteria: (Q1)—Was the allocation sequence adequately generated and applied? (Q2)—Were the groups similar at baseline or were they adjusted for confounders in the analysis? (Q3)—Was the allocation to the different groups adequately concealed? (Q4)—Were the animals randomly housed during the experiment? (Q5)—Were the caregivers and/or investigators blinded by the knowledge of which intervention each animal received during the experiment? (Q6)—Were animals selected at random for outcome assessment? (Q7)—Was the outcome assessor-blinded? (Q8)—Were incomplete outcome data adequately addressed? (Q9)—Are reports of the study free of selective outcome reporting? (Q10)—Was the study free of other problems that could result in a high risk of bias? Questions were answered with options of "Yes," "No," or "Not clear." When the answer was "yes," a score was given; when the answer was "no" or "not clear," no score was given. The overall scores for each article were calculated as a score of 0–10 points, with the quality of each study being classified as high (8–10), moderate (5–7), or low (<5). The two authors independently reviewed all the included studies. Discrepancies between authors were resolved by consensus. The quality outcomes are described in Table 2.

3 Results

3.1 Search results

In an initial search, 1,877 articles were identified [PubMed/Medline (830), Scopus (126), Embase (127), and Science Direct (794)]. Then, 346 duplicates were excluded using the EndNote® software. Then, 424 articles were screened and submitted to the eligibility criteria, and 409 articles were excluded based on title and abstract reading. Twenty studies remained for full-text reading. Four studies were excluded due to the following reasons: Two did not agree with the eligibility criteria, one study did not have a control group, and one study did not perform specific analyses of OS. Finally, 16 studies were included in this systematic review (Figure 1).

3.2 Methodological quality assessment

The results of the methodological quality assessment of the included studies are shown in Table 2. All studies showed adequate and randomized allocation with randomly selected animals. In addition, incomplete results were handled appropriately, free from selective results and bias. As these are studies involving intervention (EE), it is not possible to consider the investigation and analysis of the results blindly. In general, all studies presented satisfactory quality criteria.

3.3 Study characteristics

The studies included in this systematic review were published between the years 2004 and 2022. Initially, we observed that the studies used different species of rodents (rats and mice). Five studies used Sprague Dawley rats (Fernández et al., 2004; Jain et al., 2012; Zhang et al., 2016, 2021; Tapias et al., 2022). Five studies used Wistar rats (Pereira et al., 2009; Cechetti et al., 2012; Prado Lima et al., 2018; Molina et al., 2021; Thamizhoviya and Vanisree, 2021). Two studies used Long-Evans rats (Mármol et al., 2015, 2017). Two studies used Swiss mice (Muhammad et al., 2017; Montes et al., 2019). One study used Kunming mice (Cheng et al., 2014), and one study used TgCRND8 mice (Herring et al., 2010). Regarding gender, 10 included studies used male individuals only (Pereira et al., 2009; Cechetti et al., 2012; Jain et al., 2012; Zhang et al., 2016, 2021; Mármol et al., 2017; Prado Lima et al., 2018; Montes et al., 2019; Thamizhoviya and Vanisree, 2021; Tapias et al., 2022). Five studies used both sexes (Fernández et al., 2004; Cheng et al., 2014; Mármol et al., 2015; Muhammad et al., 2017; Molina et al., 2021). Only one study used the female sex (Herring et al., 2010).

Next, we analyzed the different characteristics of the EE protocols. The number of animals per cage varied in the included studies from 5 to 20 rodents. There was heterogeneity of objects inserted into the cages of the rodents, including ramps, three floors, running wheels, several objects, tunnels, plastic colored toys, shelters, balls, soft materials, varied locomotive substrates, tubes, boxes, bells, a climbing ladder,

TABLE 2 Methodological quality assessment.

Author, year	Q1	Q2	Q3	Q4	Q5	Q6	Q7	Q8	Q9	Q10
Cechetti et al. (2012)	Y	Y	Y	Y	N	Y	N	Y	Y	Y
Cheng et al. (2014)	Y	Y	Y	Y	N	Y	N	Y	Y	Y
Fernández et al. (2004)	Y	Y	Y	Y	N	Y	N	Y	Y	Y
Herring et al. (2010)	Y	U	Y	Y	N	Y	N	Y	Y	Y
Jain et al. (2012)	Y	Y	Y	Y	N	Y	N	Y	Y	Y
Prado Lima et al. (2018)	Y	Y	Y	Y	N	Y	N	Y	Y	Y
Mármol et al. (2015)	Y	Y	Y	Y	N	Y	N	Y	Y	Y
Mármol et al., 2017	Y	Y	Y	Y	N	Y	N	Y	Y	Y
Molina et al. (2021)	Y	Y	Y	Y	N	Y	N	Y	Y	Y
Montes et al. (2019)	Y	Y	Y	Y	N	Y	N	Y	Y	Y
Muhammad et al. (2017)	Y	U	Y	Y	N	Y	N	Y	Y	Y
Pereira et al. (2009)	Y	Y	Y	Y	N	Y	N	Y	Y	Y
Tapias et al. (2022)	Y	Y	Y	Y	N	Y	N	Y	Y	Y
Thamizhoviya and Vanisree (2021)	Y	U	Y	Y	N	Y	N	Y	Y	Y
Zhang et al. (2016)	Y	Y	Y	Y	N	Y	N	Y	Y	Y
Zhang et al. (2021)	Y	Y	Y	Y	N	Y	N	Y	Y	Y

Q1: Was the allocation sequence adequately generated and applied?; Q2: Were the groups similar at baseline or were they adjusted for confounders in the analysis?; Q3: Was the allocation to the different groups adequately concealed?; Q4: Were the animals randomly housed during the experiment?; Q5: Were the caregivers and/or investigators blinded from knowledge of which intervention each animal received during the experiment?; Q6: Were animals selected at random for outcome assessment?; Q7: Was the outcome assessor blinded?; Q8: Were incomplete outcome data adequately addressed?; Q9: Are reports of the study free of selective outcome reporting?; and Q10: Was the study apparently free of other problems that could result in a high risk of bias? Y, Yes; N, No; U, Unclear.

chain, and a screen cover with a color block and running wheel. The size of the cages in the included studies varied in length, width, depth, or height, and was expressed in either centimeters or inches. Additionally, the time of exposure to EE varied across the included studies, ranging from 7 days to 20 weeks.

Different brain areas were observed in the included studies. Twelve studies were conducted on the hippocampus (Fernández et al., 2004; Pereira et al., 2009; Cechetti et al., 2012; Jain et al., 2012; Cheng et al., 2014; Mármol et al., 2015, 2017; Prado Lima et al., 2018; Montes et al., 2019; Molina et al., 2021; Zhang et al., 2021; Tapias et al., 2022). One study evaluated the medial-temporal lobe cortex (MTLC) (Cheng et al., 2014). One study evaluated the total cortex and striatum (Fernández et al., 2004). One study evaluated the cerebral hemisphere (Herring et al., 2010). One study evaluated the cortex (Mármol et al., 2015). Two studies evaluated the prefrontal cortex (Zhang et al., 2016; Montes et al., 2019). One study evaluated the total brain (Mármol et al., 2017). One study evaluated the frontal cortex (Pereira et al., 2009). One study evaluated the forebrain (Thamizhoviya and Vanisree, 2021). Of the selected studies, five did not expose the animals to adverse environmental conditions (Cheng et al., 2014; Mármol et al., 2015, 2017; Muhammad et al., 2017), while 11 carried out the exposure to stimulating changes in the results of oxidative balance. The following exposures were used: chronic cerebral hypoperfusion (Cechetti et al., 2012), Alzheimer-like model (Herring et al., 2010), hypobaric hypoxia (Jain et al., 2012), amyloid beta neurotoxicity (Prado Lima et al., 2018), noise (Molina et al., 2021), toluene (Montes et al., 2019), hypoxia-ischemia (Pereira et al., 2009), traumatic brain injury (Tapias et al., 2022), oxidative damage (Thamizhoviya and Vanisree, 2021), hypoxia (Zhang et al., 2016), and post-stroke condition (Zhang et al., 2021) (Table 3).

3.4 Environmental enrichment on oxidative stress biomarkers in brain areas of rodents exposed to normal and unfavorable environmental conditions

In the included studies, different biomarkers of OS were observed, such as carbonyls, DCF, MDA/TBARS, nitrotyrosine, ROS levels, 4-HNE, and superoxide anion. In the absence of unfavorable external environmental stimuli in the hippocampus, two studies evaluated carbonyl levels, which were significantly reduced after intervention with EE (Mármol et al., 2015, 2017). Furthermore, a reduction in MDA (TBARS) ($n = 4$) and superoxide anion levels was observed in the hippocampus, MTLC, cortex, and total brain (Cheng et al., 2014; Mármol et al., 2015, 2017; Muhammad et al., 2017; Figures 2, 3).

Under adverse conditions, similar results on MDA and carbonyl levels were also observed in the hippocampus, cerebral hemisphere, and forebrain when exposed to chronic cerebral hypoperfusion, Alzheimer-like model, hypobaric hypoxia, oxidative damage, and post-stroke (Herring et al., 2010; Cechetti et al., 2012; Jain et al., 2012; Prado Lima et al., 2018; Thamizhoviya and Vanisree, 2021; Zhang et al., 2021). Five studies evaluated DCF levels, three studies only in the hippocampus (Cechetti et al., 2012; Prado Lima et al., 2018; Molina et al., 2021), one study used the hippocampus and frontal cortex (Pereira et al., 2009), and another analyzed the forebrain only (Thamizhoviya and Vanisree, 2021). In the hippocampus, three studies observed a decrease in DCF after exposure to EE associated with chronic cerebral hypoperfusion, noise, and oxidative damage (Cechetti et al., 2012; Molina et al., 2021; Thamizhoviya and Vanisree, 2021). Two studies showed no significance in DCF levels after EE (Prado Lima et al., 2018; Tapias et al., 2022) (Table 4).

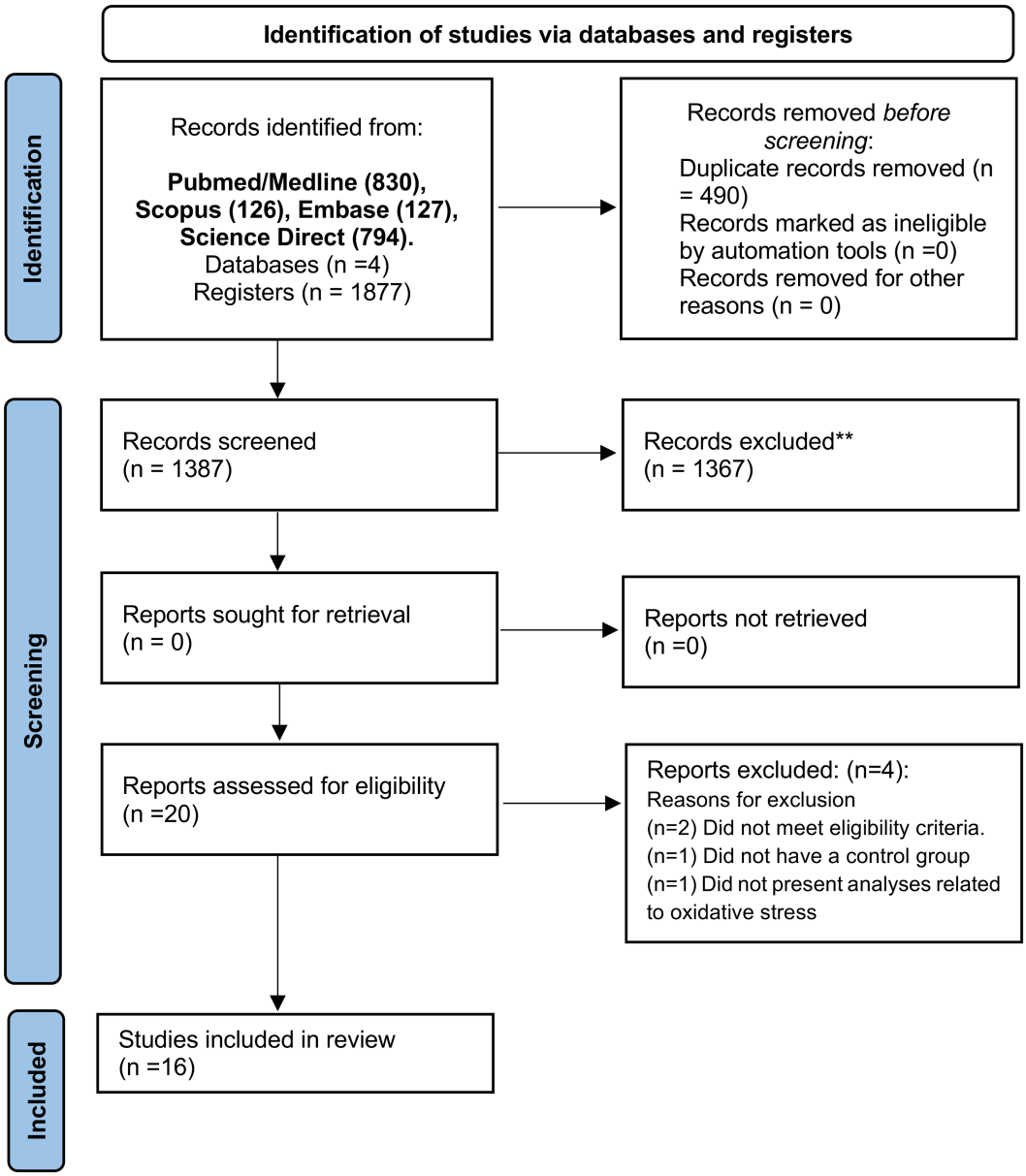

FIGURE 1
PRISMA flow diagram. *Consider, if feasible to do so, reporting the number of records identified from each database or register searched (rather than the total number across all databases/registers). **If automation tools were used, indicate how many records were excluded by a human and how many were excluded by automation tools. From Page et al. (2021). For more information, visit: http://www.prisma-statement.org/.

Two studies evaluated ROS levels, one of them only in the hippocampus (Jain et al., 2012) and the other in the hippocampus and prefrontal cortex, after hypobaric hypoxia and oxidative damage, respectively (Montes et al., 2019). Both studies observed that EE was able to significantly reduce ROS levels. Two studies assessed 4-HNE levels in the hippocampus and prefrontal cortex (Zhang et al., 2016; Tapias et al., 2022). A significant decrease in 4-HNE levels after EE, traumatic brain injury, and hypoxia was observed. Finally, two studies evaluated other compounds related to OS. Nitrotyrosine (Herring et al., 2010) was evaluated in the cerebral hemisphere, and nitrites in the hippocampus and prefrontal (Montes et al., 2019), both of whom observed that EE was able to decrease their levels after the Alzheimer-like model and toluene exposure (Table 5).

3.5 Environmental enrichment and antioxidant response in brain areas of rodents exposed to normal and unfavorable environmental conditions

In 14 included studies, it was observed that there was variability in markers responsible for mediating the antioxidant response, such as catalase, FRAP, GPx (GSH-px), GST, GSH, GSSG, GSH/GSSG ratio, SOD, SOD-1 (Cu/Zn SOD), SOD-2 (MnSOD), and total radical antioxidant. In the absence of environmental damage, two studies observed an increase in catalase enzyme activity in the hippocampus and cortex after EE but not in the total brain (Mármol et al., 2015, 2017). Increases in total antioxidant radical activity were also

TABLE 3 Sample and environmental enrichment protocol description.

Author, Year	Species, sex, and age	Animals per cage	Environmental enrichment protocol and housing dimensions (Length, width, and depth or height)		Exposure time to environmental enrichment
Cechetti et al. (2012)	Wistar rats; Male; age group were not informed	8	Ramps; Three floors; Running Wheels and Several objects	40 cm × 60 cm × 90 cm	12 weeks
Chen and Zhong (2014)	Kunming mice; Female and Male; 3 weeks old	10	Running Wheels; Tunnels; Plastic colored toys; Shelters; Balls;	100 cm × 50 cm × 45 cm	6 weeks
Fernández et al. (2004)	Sprague–Dawley rats; Female and Male; 20 months old	10	Voluntary running; Tunnels; Toys;	0.8 m^2	8 weeks
Herring et al. (2010)	TgCRND8 mice; Female; 5 months old	9	Tunnels; Balls; Soft materials; Varied locomotive substrates;	Not described	20 weeks
Jain et al. (2012)	Sprague–Dawley rats; Male; 3 months old	19	Plastic running wheel; Nesting material and an assortment of differently colored and texture plastic toys (balls, tubes, boxes, and bells).	35 × 9 × 20 in; 9 × 25 in. with two platform (20 × 9 × 15 in)	7 days
Prado Lima et al. (2018)	Wistar rats; Male; 3 weeks old	20	Running wheels; Toys; Balls; Ropes	50 cm × 50 cm × 50 cm	8 weeks
Mármol et al. (2015)	Long-Evans rats; Female and Male; 22 days old	8–16	Toys; Plastic balls; Tubes; Houses; Running wheels	45 cm × 35 cm × 50 cm	8 weeks
Mármol et al. (2017)	Long-Evans rats; Male; 3 weeks old	6	Running Wheel; Toys; and different objects	45 cm × 30 cm × 50 cm	8 weeks
Molina et al. (2021)	Wistar rats; Female and Male; 3 weeks old	3–5	Running Wheels; Tunnels; Ramps; Plastic toys;	40 cm × 25 cm × 16 cm	1–2 weeks
Montes et al. (2019)	Swiss-Webster mice, Male; 35–40 days age	5	Toys and Tunnels; 5 objects of different shapes, sizes, and textures	34 cm × 44 cm × 20 cm	4 weeks
Muhammad et al., 2017	Swiss Albino mice; Female, and Male; 4–5 weeks old	10	Tubes, ramps; stairs, and different toys (hard plastic balls, cubes, cones, and sticks)	66 cm × 46 cm wide × 38 cm	28 days
Pereira et al. (2009)	Wistar rats; Male; 7th postnatal day	7–10	Three floors; Ramps; Running Wheel and Several Objects with different shapes and textures	40 cm × 60 cm × 90 cm	9 weeks
Tapias et al. (2022)	Sprague Dawley rats; Male; 3-month-old	10–12	Toys (e.g., blocks, tubes, balls), nesting materials (e.g., bedding), and *ad libitum* food and water	92 cm × 78 cm × 51 cm	3 weeks
Thamizhoviya and Vanisree (2021)	Wistar Rats; Male; age group were not informed	6	Colorful rearrangeable tunnels; pipes; toys; diverse shapes; running wheel.	120 cm × 75 cm × 75 cm	28 days
Zhang et al. (2016)	Sprague Dawley rats; Male, Postnatal 21 day, and P34.	6	Running Wheel; Environmental complexity for social interaction and environmental novelty.	65 cm × 50 cm × 40 cm	14 days
Zhang et al. (2021)	Sprague Dawley rats; Male; 10 weeks old	12	Had climbing ladder; Chain; Tube of different shapes; Plastic tunnel; and Screen cover with color block and running wheel.	90 cm long × 75 cm wide × 50 cm high	28 days

Cm, Centimeters; m, meters; in, inch; wks, weeks; G, Groups; and P, Postnatal.

10.3389/fnins.2024.1366747

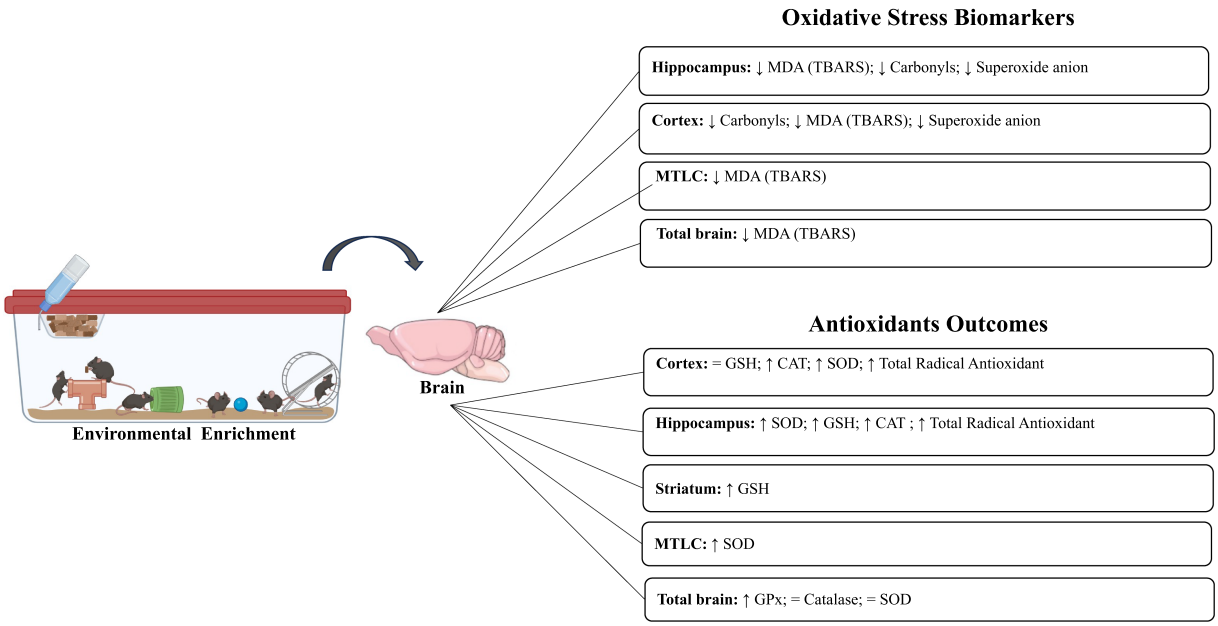

FIGURE 2
Impact of environmental enrichment on oxidative stress and antioxidant outcomes in experimental models subjected to normal environmental conditions.

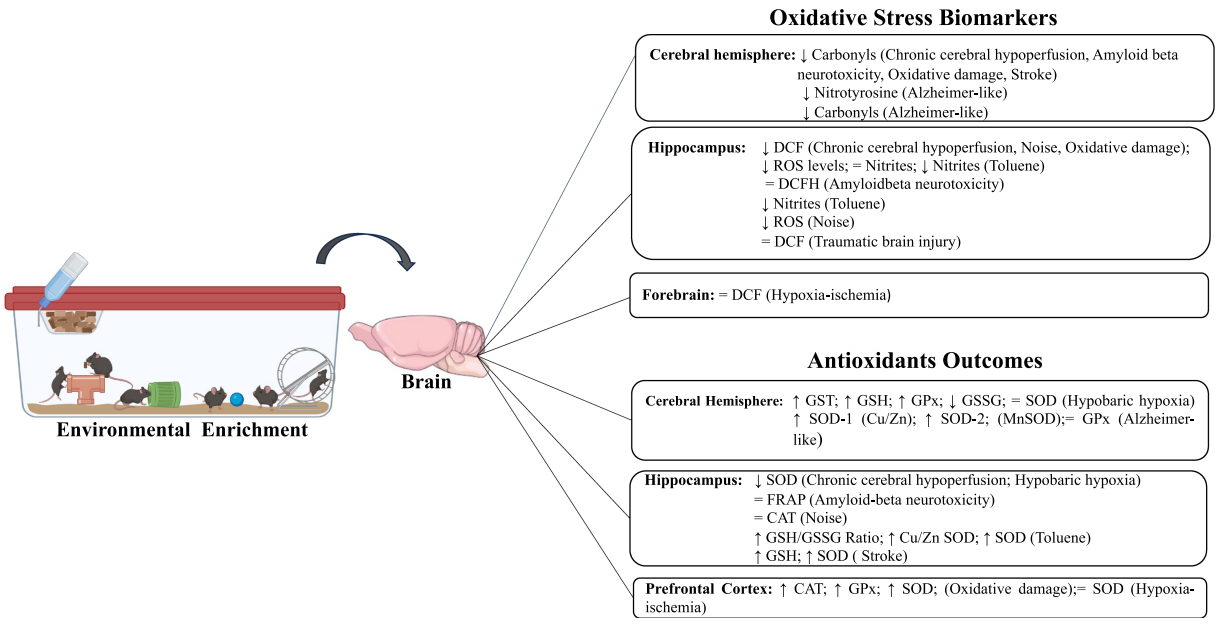

FIGURE 3
Impact of environmental enrichment on oxidative stress and antioxidant outcomes in experimental models subjected to unfavorable environmental conditions.

observed in the same areas (Mármol et al., 2015, 2017). SOD levels were elevated in two studies (hippocampus, MTLC, and cortex; Cheng et al., 2014; Mármol et al., 2015), whereas, in the whole brain, no differences were observed after EE (Muhammad et al., 2017). Similarly, increases in GSH and GPx levels were observed in the hippocampus, striatum, and total brain (Fernández et al., 2004; Muhammad et al., 2017). Only in the total cortex, no differences were observed in GSH (Fernández et al., 2004) (Table 5).

Under adverse conditions, two studies assessed the impact of EE on the activity of catalase levels after exposure to noise and oxidative damage. In the hippocampus, no difference was observed in catalase activity (Molina et al., 2021), whereas in the forebrain, an increase was

TABLE 4 Impacts of environmental enrichment on oxidative stress and antioxidant outcomes in experimental models subjected to normal environmental conditions.

Author, year	Tissue	Oxidative stress biomarkers	Antioxidants outcomes
Cheng et al. (2014)	Hippocampus; MTLC	↓ MDA (TBARS)	↑ SOD
Fernández et al. (2004)	Hippocampus; Total Cortex; Striatum	-	↑ GSH (Hippocampus and Striatum); ↔ GSH (Total Cortex)
Mármol et al. (2015)	Hippocampus; Cortex	↓ Carbonyls; ↓ MDA (TBARS); ↓ Superoxide anion	↑ CAT; ↑ SOD; ↑ Total Radical Antioxidant
Mármol et al. (2017)	Hippocampus	↓ Carbonyls; ↓ MDA (TBARS); ↓ Superoxide anion	↑ CAT; ↑ Total Radical Antioxidant
Muhammad et al. (2017)	Total brain	↓ MDA (TBARS)	↑ GPx; ↔ Catalase; = SOD

Cu/Zn SOD, Copper/zinc superoxide dismutase; CAT, Catalase; DCF, 2′,7′-Dichlorofluorescein; FRAP, Ferric reducing antioxidant power; GST, Glutathione S-transferase, GPx, Glutathione peroxidase; GSH, Reduced glutathione; GSSG, Oxidized glutathione; GSH/GSSG ratio, Reduced glutathione/oxidized glutathione; MDA, Malondialdehyde; MTLC, Medial-temporal lobe cortex; ROS levels, Reactive oxygen species; SOD, Superoxide dismutase; SOD-1, Superoxide dismutase-1; SOD-2, Superoxide dismutase-2. ↔: No significant difference ($p > 0.05$). ↓ Significant decrease; ↑ Significant increase.

observed after EE (Thamizhoviya and Vanisree, 2021). Only one included study evaluated FRAP levels and found no significant difference in the hippocampus after amyloid beta neurotoxicity associated with EE (Prado Lima et al., 2018).

Three included studies evaluated GPx activity after an Alzheimer-like model, hypobaric hypoxia, and oxidative damage. One study evaluated the cerebral hemisphere and found no significant differences after EE (Herring et al., 2010). However, in the forebrain, an increase in GPx activity was observed after EE (Thamizhoviya and Vanisree, 2021). Similarly, in the hippocampus, a significant increase in GPx activity was also observed after intervention with EE (Jain et al., 2012). GST activity was evaluated in only one included study, and it demonstrated a significant increase in the hippocampus after hypobaric hypoxia and EE (Jain et al., 2012).

Two included studies assessed GSH levels in conditions of hypobaric hypoxia and stroke. These studies observed a significant increase in GSH levels only in the hippocampus after EE (Jain et al., 2012; Zhang et al., 2021). Only one study, in the hippocampus evaluated the levels of GSSG, in which it identified a significant decrease after exposure to EE and hypobaric hypoxia (Jain et al., 2012). One included study evaluated the GSH/GSSG ratio in two brain areas, the hippocampus and prefrontal cortex. After EE, there was an increase in both tissues after toluene exposure (Montes et al., 2019).

Seven included studies evaluated SOD activity after unfavorable environmental exposure. Three studies evaluated SOD in the hippocampus only, in which there was heterogeneity of responses produced by EE. One of the studies showed a significant increase (Zhang et al., 2021), another a significant decrease (Cechetti et al., 2012), and one included study did not observe a significant difference (Jain et al., 2012). In these studies, different environmental conditions were observed (chronic cerebral hypoperfusion, hypoxia-ischemia, and stroke). One study evaluated SOD-1 (Cu/ZnSOD) and SOD-2 (MnSOD) activities in the cerebral hemisphere, and the authors observed a significant increase after EE and Alzheimer-like models (Herring et al., 2010). In the forebrain, an increase in SOD activity was identified after the intervention with EE and oxidative damage (Thamizhoviya and Vanisree, 2021). Another included study observed the same response in the hippocampus and prefrontal cortex on SOD activity (Montes et al., 2019). To see summarized resumes, check Figures 2, 3.

4 Discussion

Environmental enrichment is known as an experimental approach for brain improvement based on social stimulation via sensory, motor, social, and/or cognitive nested mechanisms (Kempermann, 2019). Relying on the molecular, physiological, and social aspects, EE affects many domains of brain function by modulating from gene expression to global phenotypes. Thus, in this systematic review, we investigated the brain oxidative balance, as one of the molecular outcomes of EE in rodents exposed or not to brain-related impairments.

Since the EE paradigm arose, it has been described as having effects on behavior, especially learning and memory capacity (Balietti and Conti, 2022). Notably, synaptic plasticity-related memory drives our attention to the hippocampus, which represents the major structure evaluated in the studies selected here. Lying in the medial temporal lobe of the brain, the hippocampus acts actively in mammal neurogenesis, wherein the oxidative balance fluctuates throughout life, especially within the differentiation of neural and/or astroglia lineage; thus, the ability to deal with ROS-related transient stress is crucial to the central nervous system (CNS) health (Huang et al., 2015).

In healthy animals, EE, regardless of type and duration, downregulates OS biomarkers in the CNS, mainly in the hippocampus (Cheng et al., 2014). It is critical for growing animals, that these control OS, especially where the brain developmental process is still prominent and requires a tuning environment for neural development (Morgane et al., 2002). Noteworthy, CAT was the major antioxidant enzyme upregulated in healthy animals exposed to EE, providing a greater ability to deal with H2O2, which, due to its molecular properties, has an increased membrane permeability and can act as a neuromodulator in pathways with different lifetimes (Rice, 2011).

Although EE promoted a neuroprotector effect by reducing oxidative damage, only two studies evaluated both ROS production and removal, we are unable to determine what/how compounds from each arm of the oxidative balance were modulated by EE. Besides, it seems that as the animals get older, their antioxidant enzymes become less responsive to EE protocols, reinforcing the importance of diet-related antioxidant compounds. Compelled by the effects of EE on the CNS of healthy animals, our review further discusses the application of EE as a tool against harmful insults in the CNS. In adverse conditions, EE also demonstrated a positive effect on the oxidative balance. The studies summarized here suggest an overall increase in the antioxidant capacity, both enzymatic and non-enzymatic, which are the main factors for the neuroprotective effects in the CNS under unfavorable conditions.

The endogenous antioxidant enzymes, such as cytosolic and mitochondrial superoxide dismutase as well as glutathione peroxidase,

TABLE 5 Impacts of environmental enrichment on oxidative stress and antioxidant outcomes in experimental models subjected to unfavorable environmental conditions.

Author, year	Tissue	Unfavorable environmental condition	Oxidative stress biomarkers	Antioxidants outcomes
Cechetti et al. (2012)	Hippocampus	Chronic cerebral hypoperfusion	↓ DCF; ↓ MDA (TBARS)	↓ SOD
Herring et al. (2010)	Cerebral hemisphere	Alzheimer-like	↓ Carbonyls; ↓ Nitrotyrosine	↑SOD-1 (Cu/Zn SOD); ↑SOD-2 (MnSOD); ↔ GPx
Jain et al. (2012)	Hippocampus	Hypobaric hypoxia	↓ MDA (TBARS); ↓ ROS levels	↑ GST; ↑ GSH; ↑ GPx; ↓ GSSG; ↔ SOD
Prado Lima et al. (2018)	Hippocampus	Amyloid beta neurotoxicity	= DCFH; ↓ MDA (TBARS)	↔ FRAP
Molina et al. (2021)	Hippocampus	Noise	↓ DCF ↓ ROS	↔ CAT
Montes et al. (2019)	Hippocampus; Prefrontal Cortex	Toluene	↓ Nitrites; ↓ ROS levels (Hippocampus) = Nitrites; ↓ ROS levels (Prefrontal Cortex)	↑ GSH/GSSG Ratio; ↑ Cu/Zn SOD; ↑SOD
Pereira et al. (2009)	Hippocampus; Prefrontal Cortex	Hypoxia-ischemia	= DCF	↔ SOD
Tapias et al. (2022)	Hippocampus	Traumatic brain injury	Ipsilateral: ↓ 4 HNE Contralateral: = DCF	-
Thamizhoviya and Vanisree (2021)	Forebrain	Oxidative damage	↓ DCF; ↓ MDA (TBARS); ↓ ROS levels	↑ CAT; ↑ GPx; ↑ SOD
Zhang et al. (2016)	Prefrontal cortex	Hypoxia	↓ 4 HNE	-
Zhang et al. (2021)	Hippocampus	Stroke	↓ MDA (TBARS)	↑ GSH; ↑ SOD

Cu/Zn SOD, Copper/zinc superoxide dismutase; CAT, Catalase; DCF: 2′,7′-Dichlorofluorescein; FRAP, Ferric reducing antioxidant power; GST, Glutathione S-transferase; GPx, Glutathione peroxidase; GSH, Reduced glutathione; GSSG, Oxidized glutathione; GSH/GSSG, Ratio reduced glutathione/oxidized glutathione; MDA, Malondialdehyde; MTLC, Medial-temporal lobe cortex; ROS levels, Reactive oxygen species; SOD, Superoxide dismutase; SOD-1, Superoxide dismutase-1; SOD-2, Superoxide dismutase-2. ↔: No significant difference ($p > 0.05$).↓ Significant decrease; ↑ Significant increase.

might decelerate oxidative damage-associated neural dysfunction, especially in the prefrontal structure. It is important to point out that, among the harmful conditions included in this review, only in acute stress (immobilization) was EE able to ameliorate all oxidative parameters evaluated, including the enzymes cited above. We believe that this phenomenon correlates with the hormesis effect, as an acute stressful event transiently increases ROS production, triggering a compensatory response in the antioxidant defense, as largely described in exercise training protocols (Ji et al., 2006; Radak et al., 2008).

Furthermore, like SOD, other antioxidant compounds might be differently distributed across the CNS, which may explain why similar EE protocols have been followed by converse outcomes. In any case, it is important to highlight that the augmented dismutation of superoxide anion led by EE represents a stronger antioxidant network, crucial in the encounter of several hypoxic conditions and some neurodegenerative disorders (Lindenau et al., 2000).

This is the first systematic review that addresses the impacts of EE protocols on cerebral oxidative balance in rodents exposed to favorable and unfavorable environmental conditions, including models of chronic cerebral hypoperfusion, Alzheimer's disease, hypobaric hypoxia, amyloid beta neurotoxicity, ischemia-hypoxia, brain damage due to traumatic situations, hypoxia, stroke, oxidative damage, and exposure to toluene. The proposal to address these different exposure conditions to environmental conditions demonstrates the effectiveness of EE in significantly reducing markers linked to the production of OS, such as superoxide anion, DCF, MDA, carbonyls, 4-HNE, and ROS levels in brain regions important for the functioning of the body. Furthermore, its ability to significantly increase components of enzymatic (SOD, CAT, and GST), as well as non-enzymatic (GPx, GSH, GSSG, and REDOX state [GSH/GSSG ratio]) antioxidant defenses.

Among the studies selected here, just three explore the possible mechanisms involved in the EE-related oxidative balance improvements, wherein both pro-oxidant and antioxidant compounds have been modulated. Zhang et al. (2016) proposes that the neuroprotective effects of EE against oxidative damage rely on NADPH oxidase-related ROS reduction, wherein its reduced expression and activity downregulate the overall ROS production (Bedard and Krause, 2007). Along with the pro-oxidant reduction, EE boosts antioxidant defenses by upregulating the nuclear factor erythroid 2-related factor 2 (Nrf2) pathway (Zhang et al., 2021), which modulates GSH levels as well as the expression of SOD, Heme oxygenase 1 (HO1), and NADP(H) quinone oxidoreductase 1 (NQO1), a FAD-dependent protein with cytoprotective and antioxidant functions (Dinkova-Kostova and Talalay, 2010). Additionally, the decrease in OS can modulate itself through the mitogen-activated protein kinase (MAPK) family, diminishing the transduction of stress-activated protein kinases (SAPK)/Jun amino-terminal kinases (JNK), which reduces inflammatory signals, such as prostaglandin E2 receptor (Herring et al., 2010; Davies and Tournier, 2012).

In summary, the direct or indirect modulation of the oxidative balance contributes to protection against cellular oxidative damage, which is related to the pathophysiology of several chronic degenerative diseases, including different types of cancer, cardiovascular diseases,

and especially neurodegenerative diseases. In this sense, the use of non-pharmacological tools, such as the EE approach, emerges as a viable and low-cost alternative for preventive containment of these damages, and their application may be considered translationally in studies with humans. Finally, the structure of each EE protocol must be considered in terms of its structure, size of the space (centimeters, millimeters, and meters, height, length, and width), duration in weeks or months, quantity and types of objectives (plastics and/or wood), and cleaning conditions to guarantee a greater standardization capacity, thus being able to better understand its effects.

5 Limitations and strengths

Although the EE paradigm has been extensively described, the variability of set-ups makes direct comparisons among the studies difficult, limiting our further discussion. In addition, the "clutter" cages make tracking animals throughout the objects, as in physical exercise protocols, tough. Still, regardless of those changing settings, the overall positive outcomes, along with the non-invasive and relatively simple procedure, are advantages of the EE approach.

In any case, studies have suggested basic parameters that must be included in any EE protocol, such as: (I) bigger cage size; (II) increased social interaction; (III) hide-out boxes; (IV) climbing objects; (V) toys that provide somatosensory stimulus in different categories; (VI) augmented physical activity; and (VII) changes in the EE layout. Detailed information can be found elsewhere (Ismail et al., 2021; Love et al., 2022).

6 Conclusion

In conclusion, our systematic review demonstrated that EE is a valid tool for the improvement of the oxidative balance in the CNS, wherein the hippocampus has been the main structure studied and affected. The overall decrease in OS biomarkers indicates a refinement in ROS detoxification, which is differently modulated by the health status of the rodents. Healthy animals have a higher capacity to deal with peroxides, while injured animals reinforce their superoxide detoxification, triggering an improvement in the antioxidant network. From the extensive analysis conducted in our systematic review, it is evident that EE serves as a valuable intervention for enhancing oxidative balance within the CNS, with a predominant focus on the hippocampus. This comprehensive scrutiny revealed a noteworthy reduction in biomarkers associated with OS across various brain areas. Notably, the efficacy of EE varied based on the health status of the rodents, displaying a dual effect: augmenting peroxide management in healthy subjects and bolstering the detoxification of superoxide in injured animals. This modulation ultimately contributes to an enhanced antioxidant network, showcasing the nuanced and adaptive nature of EE's impact on oxidative balance within the CNS.

Data availability statement

The original contributions presented in the study are included in the article/supplementary material, further inquiries can be directed to the corresponding authors.

Author contributions

TR: Conceptualization, Data curation, Investigation, Methodology, Writing – original draft, Writing – review & editing. MS: Conceptualization, Data curation, Investigation, Methodology, Writing – original draft, Writing – review & editing. DS: Data curation, Methodology, Writing – original draft, Writing – review & editing. GJ: Data curation, Methodology, Writing – original draft, Writing – review & editing. RBA: Conceptualization, Data curation, Methodology, Writing – original draft, Writing – review & editing. DF: Data curation, Investigation, Methodology, Writing – original draft, Writing – review & editing. RS: Data curation, Methodology, Writing – original draft, Writing – review & editing. GB: Methodology, Project administration, Resources, Supervision, Writing – original draft, Writing – review & editing. FY: Methodology, Project administration, Resources, Supervision, Writing – original draft, Writing – review & editing, Investigation. BY: Methodology, Resources, Supervision, Writing – original draft, Writing – review & editing. RMA: Methodology, Resources, Supervision, Writing – original draft, Writing – review & editing. FS: Data curation, Investigation, Methodology, Writing – original draft, Writing – review & editing. CL: Conceptualization, Investigation, Methodology, Project administration, Supervision, Writing – original draft, Writing – review & editing.

Funding

The authors declare that financial support was received for the research, authorship, and/or publication of this article. This work was supported by the Princess Nourah bint Abdulrahman University Researchers Supporting Initiative (Project Number: PNURSP2024R117) and Princess Nourah bint Abdulrahman University, Riyadh, Saudi Arabia.

Acknowledgments

We thank all authors for their fundamental contribution to the preparation of this study. The authors appreciate the support from CAPES and UFPE.

Conflict of interest

The authors declare that the research was conducted in the absence of any commercial or financial relationships that could be construed as a potential conflict of interest.

Publisher's note

References

Balietti, M., and Conti, F. (2022). Environmental enrichment and the aging brain: is it time for standardization? *Neurosci. Biobehav. Rev.* 139:104728. doi: 10.1016/j.neubiorev.2022.104728

Bedard, K., and Krause, K. H. (2007). The NOX family of ROS-generating NADPH oxidases: physiology and pathophysiology. *Physiol. Rev.* 87, 245–313. doi: 10.1152/physrev.00044.2005

Cechetti, F., Worm, P. V., Lovatel, G., Moysés, F., Siqueira, I. R., and Netto, C. A. (2012). Environmental enrichment prevents behavioral deficits and oxidative stress caused by chronic cerebral hypoperfusion in the rat. *Life Sci.* 91, 29–36. doi: 10.1016/j.lfs.2012.05.013

Chen, Z., and Zhong, C. (2014). Oxidative stress in Alzheimer's disease. *Neurosci. Bull.* 30, 271–281. doi: 10.1007/s12264-013-1423-y

Cheng, L., Wang, S.-H., Jia, N., Xie, M., and Liao, X.-M. (2014). Environmental stimulation influence the cognition of developing mice by inducing changes in oxidative and apoptosis status. *Brain and Development* 36, 51–56. doi: 10.1016/j.braindev.2012.11.015

Davies, C., and Tournier, C. (2012). Exploring the function of the JNK (c-Jun N-terminal kinase) signalling pathway in physiological and pathological processes to design novel therapeutic strategies. *Biochem. Soc. Trans.* 40, 85–89. doi: 10.1042/BST20110641

Dinkova-Kostova, A. T., and Talalay, P. (2010). NAD(P)H:quinone acceptor oxidoreductase 1 (NQO1), a multifunctional antioxidant enzyme and exceptionally versatile cytoprotector. *Arch. Biochem. Biophys.* 501, 116–123. doi: 10.1016/j.abb.2010.03.019

Ermakov, E. A., Dmitrieva, E. M., Parshukova, D. A., Kazantseva, D. V., Vasilieva, A. R., and Smirnova, L. P. (2021). Oxidative stress-related mechanisms in schizophrenia pathogenesis and new treatment perspectives. *Oxidative Med. Cell. Longev.* 2021:8881770. doi: 10.1155/2021/8881770

Fernandes, M. S., Pedroza, A. A., de Andrade Silva, S. C., de Lemos, M. D. T., Bernardo, E. M., Pereira, A. R., et al. (2022). Undernutrition during development modulates endoplasmic reticulum stress genes in the hippocampus of juvenile rats: involvement of oxidative stress. *Brain Res.* 1797:148098. doi: 10.1016/j.brainres.2022.148098

Fernández, C. I., Collazo, J., Bauza, Y., Castellanos, M. R., and López, O. (2004). Environmental enrichment-behavior-oxidative stress interactions in the aged rat: issues for a therapeutic approach in human aging. *Ann. N. Y. Acad. Sci.* 1019, 53–57. doi: 10.1196/annals.1297.012

Gomes, M. J., Martinez, P. F., Pagan, L. U., Damatto, R. L., Cezar, M. D. M., Lima, A. R. R., et al. (2017). Skeletal muscle aging: influence of oxidative stress and physical exercise. *Oncotarget* 8, 20428–20440. doi: 10.18632/oncotarget.14670

Halliwell, B. (2006). Oxidative stress and neurodegeneration: where are we now? *J. Neurochem.* 97, 1634–1658. doi: 10.1111/j.1471-4159.2006.03907.x

Herring, A., Blome, M., Ambree, O., Sachser, N., Paulus, W., and Keyvani, K. (2010). Reduction of cerebral oxidative stress following environmental enrichment in mice with Alzheimer-like pathology. *Brain Pathol.* 20, 166–175. doi: 10.1111/j.1750-3639.2008.00257.x

Huang, T. T., Leu, D., and Zou, Y. (2015). Oxidative stress and redox regulation on hippocampal-dependent cognitive functions. *Arch. Biochem. Biophys.* 576, 2–7. doi: 10.1016/j.abb.2015.03.014

Ismail, T. R., Yap, C. G., Naidu, R., and Pamidi, N. (2021). Enrichment protocol for rat models. *Curr Protoc* 1:e152. doi: 10.1002/cpz1.152

Jain, V., Baitharu, I., Barhwal, K., Prasad, D., Singh, S. B., and Ilavazhagan, G. (2012). Enriched environment prevents hypobaric hypoxia induced neurodegeneration and is independent of antioxidant signaling. *Cell. Mol. Neurobiol.* 32, 599–611. doi: 10.1007/s10571-012-9807-5

Ji, L. L., Gomez-Cabrera, M. C., and Vina, J. (2006). Exercise and hormesis: activation of cellular antioxidant signaling pathway. *Ann. N. Y. Acad. Sci.* 1067, 425–435. doi: 10.1196/annals.1354.061

Kempermann, G. (2019). Environmental enrichment, new neurons and the neurobiology of individuality. *Nat. Rev. Neurosci.* 20, 235–245. doi: 10.1038/s41583-019-0120-x

Lindenau, J., Noack, H., Possel, H., Asayama, K., and Wolf, G. (2000). Cellular distribution of superoxide dismutases in the rat CNS. *Glia* 29, 25–34. doi: 10.1002/(SICI)1098-1136(20000101)29:1<25::AID-GLIA3>3.0.CO;2-G

Love, C. J., Gubert, C., Renoir, T., and Hannan, A. J. (2022). Environmental enrichment and exercise housing protocols for mice. *STAR Protoc.* 3:101689. doi: 10.1016/j.xpro.2022.101689

Mármol, F., Rodríguez, C. A., Sánchez, J., and Chamizo, V. D. (2015). Anti-oxidative effects produced by environmental enrichment in the hippocampus and cerebral cortex of male and female rats. *Brain Res.* 1613, 120–129. doi: 10.1016/j.brainres.2015.04.007

Mármol, F., Sánchez, J., Torres, M. N., and Chamizo, V. D. (2017). Environmental enrichment in the absence of wheel running produces beneficial behavioural and anti-oxidative effects in rats. *Behav. Process.* 144, 66–71. doi: 10.1016/j.beproc.2017.09.009

Molina, S. J., Buján, G. E., and Guelman, L. R. (2021). Noise-induced hippocampal oxidative imbalance and aminoacidergic neurotransmitters alterations in developing male rats: influence of enriched environment during adolescence. *Dev. Neurobiol.* 81, 164–188. doi: 10.1002/dneu.22806

Montes, S., Yee-Rios, Y., and Páez-Martínez, N. (2019). Environmental enrichment restores oxidative balance in animals chronically exposed to toluene: comparison with melatonin. *Brain Res. Bull.* 144, 58–67. doi: 10.1016/j.brainresbull.2018.11.007

Morgane, P. J., Mokler, D. J., and Galler, J. R. (2002). Effects of prenatal protein malnutrition on the hippocampal formation. *Neurosci. Biobehav. Rev.* 26, 471–483. doi: 10.1016/S0149-7634(02)00012-X

Muhammad, M. S., Magaji, R. A., Mohammed, A., Isa, A. S., and Magaji, M. G. (2017). Effect of resveratrol and environmental enrichment on biomarkers of oxidative stress in young healthy mice. *Metab. Brain Dis.* 32, 163–170. doi: 10.1007/s11011-016-9891-1

Olson, A. K., Eadie, B. D., Ernst, C., and Christie, B. R. (2006). Environmental enrichment and voluntary exercise massively increase neurogenesis in the adult hippocampus via dissociable pathways. *Hippocampus* 16, 250–260. doi: 10.1002/hipo.20157

Orellana-Urzúa, S., Rojas, I., Líbano, L., and Rodrigo, R. (2020). Pathophysiology of ischemic stroke: role of oxidative stress. *Curr. Pharm. Des.* 26, 4246–4260. doi: 10.2174/1381612826666200708133912

Page, M. J., McKenzie, J. E., Bossuyt, P. M., Boutron, I., Hoffmann, T. C., Mulrow, C. D., et al. (2021). The PRISMA 2020 statement: an updated guideline for reporting systematic reviews. *BMJ* 372:n71. doi: 10.1136/bmj.n71

Pereira, L. O., Nabinger, P. M., Strapasson, A. C., Nardin, P., Gonçalves, C. A., Siqueira, I. R., et al. (2009). Long-term effects of environmental stimulation following hypoxia-ischemia on the oxidative state and BDNF levels in rat hippocampus and frontal cortex. *Brain Res.* 1247, 188–195. doi: 10.1016/j.brainres.2008.10.017

Prado Lima, M. G., Schimidt, H. L., Garcia, A., Daré, L. R., Carpes, F. P., Izquierdo, I., et al. (2018). Environmental enrichment and exercise are better than social enrichment to reduce memory deficits in amyloid beta neurotoxicity. *Proc. Natl. Acad. Sci. USA* 115, E2403–E2409. doi: 10.1073/pnas.1718435115

Radak, Z., Chung, H. Y., Koltai, E., Taylor, A. W., and Goto, S. (2008). Exercise, oxidative stress and hormesis. *Ageing Res. Rev.* 7, 34–42. doi: 10.1016/j.arr.2007.04.004

Rice, M. E. (2011). H2O2: a dynamic neuromodulator. *Neuroscientist* 17, 389–406. doi: 10.1177/1073858411404531

Sharma, V., and Mehdi, M. M. (2023). Oxidative stress, inflammation and hormesis: the role of dietary and lifestyle modifications on aging. *Neurochem. Int.* 164:105490. doi: 10.1016/j.neuint.2023.105490

Tapias, V., Moschonas, E. H., Bondi, C. O., Vozzella, V. J., Cooper, I. N., Cheng, J. P., et al. (2022). Environmental enrichment improves traumatic brain injury-induced behavioral phenotype and associated neurodegenerative process. *Exp. Neurol.* 357:114204. doi: 10.1016/j.expneurol.2022.114204

Thamizhoviya, G., and Vanisree, A. J. (2021). Enriched environment enhances the myelin regulatory factor by mTOR signaling and protects the myelin membrane against oxidative damage in rats exposed to chronic immobilization stress. *Neurochem. Res.* 46, 3314–3324. doi: 10.1007/s11064-021-03433-8

Wronka, M., Krzemińska, J., Młynarska, E., Rysz, J., and Franczyk, B. (2022). The influence of lifestyle and treatment on oxidative stress and inflammation in diabetes. *Int. J. Mol. Sci.* 23:1–19. doi: 10.3390/ijms232415743

Zhang, M., Wu, J., Huo, L., Luo, L., Song, X., Fan, F., et al. (2016). Environmental enrichment prevent the juvenile hypoxia-induced developmental loss of Parvalbumin-Immunoreactive cells in the prefrontal cortex and neurobehavioral alterations through inhibition of NADPH Oxidase-2-derived oxidative stress. *Mol. Neurobiol.* 53, 7341–7350. doi: 10.1007/s12035-015-9656-6

Zhang, X., Yuan, M., Yang, S., Chen, X., Wu, J., Wen, M., et al. (2021). Enriched environment improves post-stroke cognitive impairment and inhibits neuroinflammation and oxidative stress by activating Nrf2-ARE pathway. *Int. J. Neurosci.* 131, 641–649. doi: 10.1080/00207454.2020.1797722

frontiers | Frontiers in Nutrition

TYPE Original Research
PUBLISHED 18 July 2024
DOI 10.3389/fnut.2024.1387802

OPEN ACCESS

EDITED BY
Adriana Ximenes-da-Silva,
Federal University of Alagoas, Brazil

REVIEWED BY
Lanni Rocha,
Federal University of Alagoas, Brazil
Gary Landreth,
Indiana University, United States

*CORRESPONDENCE
Ling Liu
✉ neurologyliuling@163.com

RECEIVED 18 February 2024
ACCEPTED 01 July 2024
PUBLISHED 18 July 2024

CITATION
Zhang L, Yang S, Liu X, Wang C, Tan G, Wang X and Liu L (2024) Association between dietary niacin intake and risk of Parkinson's disease in US adults: cross-sectional analysis of survey data from NHANES 2005–2018.
Front. Nutr. 11:1387802.
doi: 10.3389/fnut.2024.1387802

Association between dietary niacin intake and risk of Parkinson's disease in US adults: cross-sectional analysis of survey data from NHANES 2005–2018

Ling Zhang[1,2], Shaojie Yang[2], Xiaoyan Liu[1,3], Chunxia Wang[1,4], Ge Tan[5], Xueping Wang[6] and Ling Liu[1]*

[1]Department of Neurology, West China Hospital of Sichuan University, Chengdu, China, [2]Department of Neurology, Chengdu Eighth People's Hospital (Geriatric Hospital of Chengdu Medical College), Chengdu, China, [3]Department of Neurology, The First People's Hospital of Longquanyi District, Chengdu, China, [4]Department of Neurology, 363 Hospital, Chengdu, China, [5]Mental Health Center, West China Hospital of Sichuan University, Chengdu, China, [6]Department of Neurology, The First Hospital of Lanzhou University, Lanzhou, Gansu, China

Parkinson's disease (PD) is one of the most common neurodegenerative diseases and involves various pathogenic mechanisms, including oxidative stress and neuroinflammation. Niacin, an important cofactor in mitochondrial energy metabolism, may play a key role in the pathogenesis of PD. An in-depth exploration of the relationship between niacin and mitochondrial energy metabolism may provide new targets for the treatment of PD. The present study was designed to examine the association between dietary niacin intake and the risk of PD in US adults. Data from adults aged 40 years and older collected during cycles of the United States (US) National Health and Nutrition Examination Survey (NHANES) from 2005 to 2018 were used. A multiple logistic regression model was used to analyze the relationship between dietary niacin intake and the risk of PD. Further linear tests using restricted cubic splines (RCS) were performed to explore the shape of the dose–response relationship. Subgroup stratification and interaction analyses were conducted according to years of education, marital status, smoking, and hypertension to evaluate the stability of the association between different subgroups. A total of 20,211 participants were included in this study, of which 192 were diagnosed with PD. In the fully adjusted multiple logistic regression model, dietary niacin intake was negatively associated with the risk of PD (OR: 0.77, 95%CI: 0.6–0.99; $p = 0.042$). In the RCS linear test, the occurrence of PD was negatively correlated with dietary niacin intake (nonlinearity: $p = 0.232$). In stratified analyses, dietary niacin intake was more strongly associated with PD and acted as an important protective factor in patients with fewer years of education (OR: 0.35, 95%CI: 0.13–0.93), married or cohabitating (OR: 0.71, 95%CI: 0.5–0.99), taking dietary supplements (OR: 0.6, 95%CI: 0.37 0.97), non-smokers (OR: 0.57, 95%CI: 0.39–0.85), those with hypertension (OR: 0.63, 95%CI: 0.63–0.95), coronary artery disease (OR: 0.77, 95%CI: 0.6–1), and stroke (OR: 0.75, 95%CI: 0.88–0.98), but the interaction was not statistically significant in all subgroups. Dietary niacin intake was inversely associated with PD risk in US adults, with a 23% reduction in risk for each 10 mg increase in niacin intake.

KEYWORDS

Parkinson's disease, niacin, vitamin B3, National Health and Nutrition, NHANES

1 Introduction

Parkinson's disease (PD) is one of the most common neurodegenerative disorders, and is primarily caused by the loss of dopamine-producing neurons in the substantia nigra (1, 2). It affects over 6 million people worldwide and is a leading cause of neurofunctional impairments (3, 4). The pathogenic mechanisms of PD involve multiple aspects, with mitochondrial dysfunction, oxidative stress, and neuroinflammation as the crucial core mechanisms (5–8). Currently, no cure for PD (9) exists, and understanding its pathogenic mechanisms and identifying new drug targets for treatment and prevention is of paramount importance.

Niacin, also known as vitamin B3, is a precursor to nicotinamide adenine dinucleotide (NAD) and nicotinamide adenine dinucleotide phosphate (NADP) (10), possesses anti-inflammatory properties, enhances mitochondrial function by supplying NAD (7, 11), and serves as an essential cofactor in mitochondrial energy metabolism (12). Lack of niacin in the diet may disrupt mitochondrial respiration and reduce oxidative phosphorylation (13). Some studies have suggested that niacin is beneficial in the treatment of PD by alleviating inflammation through an NIARC1-related mechanism and increasing dopamine synthesis in the striatum by supplying NADPH to the mitochondria (14). Research has explored niacin treatment for patients with PD, suggesting a potential role in symptom alleviation and disease progression delay (15–17). However; to date, no studies have been conducted in the general population to investigate the association between niacin and the risk of PD. Therefore, this study aims to evaluate the relationship between dietary niacin intake and the risk of PD in American adults using data from the National Health and Nutrition Examination Survey (NHANES). The specific objective is to determine whether higher dietary niacin intake is negatively associated with the risk of PD.

In a large cross-sectional study of American adults aged 40 and above conducted from 2005 to 2018, we hypothesize that higher dietary niacin intake may be associated with a lower risk of PD. We hope this study will provide stronger evidence for the role of niacin in PD prevention.

2 Materials and methods

2.1 Data source

This cross-sectional observational study utilized data from the NHANES website. The NHANES is a multistage, large, stratified, and nationally representative study of the US population that provides detailed information about study design, interviews, and demographics, etc. (18–20). The present study was reviewed and approved by the National Institute of Public Health Research Ethics Committee. Written informed consent was obtained from the participants' legal guardians or close family members (21).[1] To address potential sources of bias, the NHANES database implemented standardized procedures during data collection, and data collectors received comprehensive training to ensure consistency and accuracy, thereby reducing information bias. Individuals aged 40 and above who completed the interviews participated in our study. We excluded pregnant individuals and those with missing dietary niacin intake and covariate data.

2.2 Diagnosis of PD

Consistent with previous literature (22–24), participants were considered to have PD when using "anti-Parkinson's agents" based on answers to questions about prescribed medications. Owing to the limitations of drug and code inclusion in the NHANES, patients must be treated with Parkinson's drugs to be classified as having PD, whereas others are classified as non-PD.

2.3 Dietary niacin intake

Dietary intake data were collected by trained dietary interviewers using the NHANES Computer-Assisted Dietary Interview (CADI) system. Each Mobile Examination Center (MEC) dietary interview room follows a set of standardized measurement guidelines, which are agreed upon by experts during regular workshops and specifically designed for the current NHANES setting. These guidelines assist respondents in accurately reporting the quantity and portion size of consumed foods. The NHANES Dietary Interview Procedures Manual provides a comprehensive overview of the dietary interview methodology (25).

The database employs the multiple-pass recall method to gather food information, offering two dietary niacin intake recalls, both reflecting intake within a 24 h period. The first recall is conducted at the NHANES MEC, and the second recall is completed via telephone interview on days 3–10 following the first recall (24). To ensure data accuracy, the average of the two dietary niacin intake recalls was used as the final intake value. Niacin in this study refers to dietary niacin and excludes niacin supplements.

2.4 Covariates assessment

The covariates in this study were based on previous literature (20, 26), and a variety of possible covariates were evaluated including age, sex, race, marital status, family income, education level, body mass index (BMI), smoking status, dietary supplements, calorie consumption, carbohydrate consumption, protein consumption, and fat consumption. Chronic comorbidities included diabetes, hypertension, coronary heart disease, and stroke. Marital status was defined as living alone or with a partner. Educational levels were divided into three groups based on the 9-year and 12-year boundaries. Races were classified as Mexican American, non-Hispanic black, non-Hispanic white, and other. Sixty-five years old is commonly regarded as the dividing line between middle age and old age. In this study, participants were divided into middle-aged and elderly groups based on this cutoff point. According to a US government report, family income was classified as low, middle, and high based on a poverty income ratio (PIR) of 1.3 and 3.5 (25). Smoking status was determined based on questionnaire responses, following definitions

1 https://www.cdc.gov/nchs/nhanes/index.htm accessed on 20 November 2023.

from previous literature (27, 28). Individuals who have smoked more than 100 cigarettes in their lifetime were categorized accordingly: those who smoked fewer than 100 cigarettes were classified as non-smokers; current smokers were individuals who currently smoke and have smoked more than 100 cigarettes in their lifetime; former smokers were individuals who have smoked more than 100 cigarettes in the past but have since quit. Chronic comorbidities were obtained through questionnaires, which inquired whether participants had been diagnosed with these diseases by a doctor. We selected four chronic conditions with a high prevalence rate (diabetes, stroke, hypertension, and coronary heart disease) as the chronic comorbidities for this study. BMI was calculated by dividing weight by the square of height, and participants were categorized into normal weight and overweight groups based on the standard proposed by the World Health Organization, with 25 kg/m^2 as the cutoff point. The participants' total dietary calories, fat, protein, and carbohydrate values were obtained through dietary recall. Information on dietary supplements was also obtained through dietary recall from questionnaires regarding whether the participants had taken dietary supplements in the past month.

2.5 Statistical analyses

In this study, the Kolmogorov–Smirnov test was used to determine whether continuous variables were normally distributed. The mean value (standard deviation) was used to represent normally distributed variables and the median (interquartile distance) was used to represent skewed variables. Categorical variables were expressed as percentages. One-way analysis of variance (ANOVA) was used for normal distributions, the Kruskal-Wallis test for skewed distributions, and the Chi-square test was used for categorical variables. Odds ratios (OR) and 95% confidence intervals (95%CI) between dietary niacin intake and PD were calculated using logistic regression models. Due to dimensional problems, when this analysis was performed using niacin as a continuous variable, we divided its value by 10 in units of 10 mg per unit. Model 1 was adjusted for uncontrollable sociodemographic characteristics including age, sex, and race. Model 2 was adjusted for all sociodemographic characteristics and all covariates other than chronic comorbidities including age, sex, race, education level, marital status, family income, BMI, smoking status, calorie consumption, protein consumption, carbohydrate consumption, fat consumption, and dietary supplements. Model 3 was adjusted comprehensively to include chronic comorbidities (hypertension, coronary heart disease, stroke, and diabetes) based on Model 2.

We used a restricted cubic spline (RCS) test to determine the shape of the dose–response relationship between dietary niacin intake and the incidence of PD. Four nodes of dietary niacin level distribution (at the 5th, 35th, 65th, and 95th percentiles) were used to build a smooth curve-fitting plot according to all covariables included in Model 3. Subgroup analyses of sex, age, race, marital status, education, smoking status, family income, BMI, dietary supplements, hypertension, coronary heart disease, stroke, and diabetes were performed using logistic regression models. Interactions between subgroups were tested using the likelihood ratio test (P for interaction). To assess the robustness of the results, we excluded participants with extreme energy consumption, specifically those with a daily energy consumption of <500 or >5,000 kcal, for a sensitivity analyses.

As the sample size of this study was completely dependent on the NHANES database, no statistical performance estimation was performed in advance. The study excluded all missing data, so there is no data missing. In this study, R open-source software version 4.0.4 and Free Statistics software (29) version 1.9 were used for statistical analyses. We conducted a descriptive study of all participants, and a p-value of less than 0.05 was considered significant for two-tailed testing.

3 Results

3.1 Study population

This study screened data from 70,488 participants in seven cycles of NHANES surveys from 2005 to 2018. We excluded 43,945 individuals under the age of 40, 21 pregnant participants, 3,008 with missing niacin intake data, and 3,303 with missing covariate data. Ultimately, the study included 20,211 participants with complete data, among whom 192 had Parkinson's disease. The exclusion and inclusion process is illustrated in Figure 1.

3.2 Demographic characteristics

Table 1 presents the baseline characteristics of all participants grouped according to the presence or absence of PD. A total of 192 patients (0.9%) had PD. The participants' mean age ± SD was 59.5 ± 12.3 years, 10,308 (51%) were women, most of them were non-Hispanic white (9,432, 46.7%), and 50.8% had more than 12 years of education. The minimum daily niacin intake over a 24 h period was 0.002 mg, the maximum intake was 179.1 mg, and the average intake was 23.6 ± 11.7 mg. Individuals with PD may have exhibited the following characteristics: older age, non-Hispanic white ethnicity, lower household income, greater use of dietary supplements, combined hypertension, lower protein consumption, and lower niacin intake. Sex, education, marital status, BMI, smoking status, diabetes, coronary heart disease, total calories, carbohydrates, and fat consumption did not differ in the classification of PD.

3.3 Relationship between dietary niacin intake and PD risk

The univariate analysis demonstrated that age, race, family income, hypertension, protein consumption, and dietary supplements were associated with the risk of PD (Table 2). The results of multivariate logistic proportional risk regression analysis of the relationship between dietary niacin intake and the risk of PD are shown in Table 3. In models without adjustment for covariates, we found a significant independent inverse association between dietary niacin and the risk of PD (OR: 0.83, 95%CI: 0.72–0.95; $p = 0.009$). After adjusting for uncontrollable demographic characteristics variables (gender, age, and race) in Model 1, the inverse association between dietary niacin and the risk of developing PD did not change (OR: 0.84, 95%CI: 0.72–0.98; $p = 0.027$), and the difference was still statistically significant. In Model 2, the inverse association between dietary niacin and PD risk remained after adjustment for all

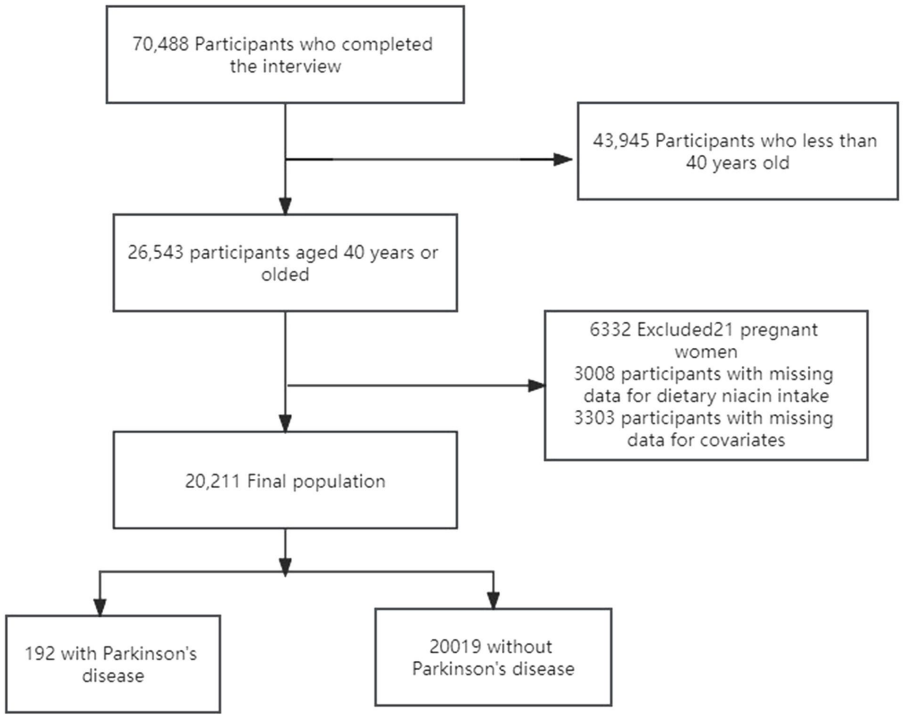

FIGURE 1
The study's flow diagram.

demographic characteristics and smoking, BMI, energy consumption, protein consumption, carbohydrate consumption, and fat consumption (OR: 0.77, 95%CI: 0.6–0.99; $p = 0.04$). On the basis of Model 2, chronic comorbidities (diabetes, hypertension, coronary heart disease, and stroke) were added to Model 3 as a comprehensive adjustment of covariates, and the adjusted results showed that the inverse association between dietary niacin and PD risk remained stable. For every 10 mg/day increase in dietary niacin intake, the risk of PD was reduced by 23% (OR: 0.77, 95%CI: 0.6–0.99; $p = 0.042$). The RCS for the association between dietary niacin intake and the risk of PD is shown in Figure 2. Dietary niacin intake was inversely associated with PD risk when all confounding covariates were considered (nonlinearity, $p = 0.232$).

3.4 Subgroup analyses

To determine whether the association between dietary niacin intake and the risk of PD was consistent across subgroups, we performed stratification and interaction analyses. When stratified by sex, age, race, marital status, education, smoking status, family income, BMI, and dietary supplements, hypertension, coronary heart disease, stroke, and diabetes, as shown in Figure 3, dietary niacin intake was more strongly associated with the risk of PD in those with fewer years of schooling (OR: 0.35, 95%CI: 0.13–0.93), married or cohabiting (OR: 0.71, 95%CI: 0.5–0.99), those taking dietary supplements (OR: 0.6, 95%CI: 0.37–0.97), non-smokers (OR: 0.57, 95%CI: 0.39–0.85), those with hypertension (OR: 0.63, 95%CI: 0.63–0.95), coronary heart disease (OR: 0.77, 95%CI: 0.6–1), and stroke (OR: 0.75, 95%CI: 0.88–0.98). Therefore, dietary niacin intake was an important protective factor for people with fewer years of education, married or cohabitating, taking dietary supplements, non-smokers, and those with hypertension, coronary heart disease, and stroke. When testing for interactions between subgroups using likelihood ratio tests, we found no statistically significant interactions in any subgroup.

3.5 Sensitivity analyses

After excluding the individuals with extreme energy consumption, 20,022 individuals left, and the association between dietary niacin intake and the risk of PD remained stable. In the fully adjusted model, the OR value for dietary niacin intake and PD risk was 0.77 (95%CI, 0.6–0.99, $p = 0.042$) (Table 4).

4 Discussion

Based on NHANES data from 2005 to 2018, we investigated the relationship between dietary niacin intake and Parkinson's disease (PD) among adults aged 40 and above in the United States. We found that PD patients had lower dietary niacin intake, and there was an association between niacin intake levels and PD risk. Both univariate and multivariate logistic regression analyses showed a negative correlation between dietary niacin intake and PD risk. Subgroup analyses revealed that dietary niacin intake was an important protective factor for individuals with shorter educational duration, married or cohabitating status, dietary supplement use, non-smoking status, as well as those with hypertension, coronary heart disease, and

TABLE 1 Population characteristics by categories of PD.

Characteristic	Total (*n* = 20,211)	No PD (*n* = 20,019)	PD (*n* = 192)	*p*-value
Sex, *n* (%)				0.991
Male	9,903 (49.0)	9,809 (49)	94 (49)	
Female	10,308 (51.0)	10,210 (51)	98 (51)	
Age (year), Mean (SD)	59.5 ± 12.3	59.5 ± 12.2	66.1 ± 12.2	<0.001
Race/ethnicity, *n* (%)				<0.001
Non-Hispanic white	9,432 (46.7)	9,304 (46.5)	128 (66.7)	
Non-Hispanic black	4,356 (21.6)	4,328 (21.6)	28 (14.6)	
Mexican American	2,763 (13.7)	2,747 (13.7)	16 (8.3)	
Others	3,660 (18.1)	3,640 (18.2)	20 (10.4)	
Education level (year), *n* (%)				0.553
<9	2,430 (12.0)	2,405 (12)	25 (13)	
9–12	7,517 (37.2)	7,440 (37.2)	77 (40.1)	
>12	10,264 (50.8)	10,174 (50.8)	90 (46.9)	
Marital status, *n* (%)				0.409
Married or living with a partner	12,581 (62.2)	12,467 (62.3)	114 (59.4)	
Living alone	7,630 (37.8)	7,552 (37.7)	78 (40.6)	
Family income, *n* (%)				0.003
Low	5,832 (28.9)	5,759 (28.8)	73 (38)	
Medium	7,722 (38.2)	7,647 (38.2)	75 (39.1)	
High	6,657 (32.9)	6,613 (33)	44 (22.9)	
Dietary supplements taken, *n* (%)	11,584 (57.3)	11,456 (57.2)	128 (66.7)	0.008
Smoking status, *n* (%)				0.981
Never	10,341 (51.2)	10,242 (51.2)	99 (51.6)	
Current	6,129 (30.3)	6,072 (30.3)	57 (29.7)	
Former	3,741 (18.5)	3,705 (18.5)	36 (18.8)	
Body mass index (kg/m^2), *n* (%)				0.65
<25	5,083 (25.1)	5,032 (25.1)	51 (26.6)	
≥25	15,128 (74.9)	14,987 (74.9)	141 (73.4)	
Hypertension, *n* (%)	8,040 (39.8)	7,932 (39.6)	108 (56.2)	<0.001
Diabetes, *n* (%)	3,747 (18.5)	3,704 (18.5)	43 (22.4)	0.167

(Continued)

10.3389/fnut.2024.1387802

TABLE 1 (Continued)

Characteristic	Total (n = 20,211)	No PD (n = 20,019)	PD (n = 192)	p-value
Coronary heart disease, n (%)	1,222 (6.0)	1,204 (6)	18 (9.4)	0.052
Stroke, n (%)	1,108 (5.5)	1,087 (5.4)	21 (10.9)	<0.001
Calorie consumption (kcal/d), Mean ± SD	1955.0 ± 798.0	1955.4 ± 798.3	1917.7 ± 766.7	0.515
Protein consumption (g/d), Mean ± SD	77.1 ± 34.0	77.2 ± 34.0	71.9 ± 29.7	0.031
Carbohydrate consumption (g/d), Mean ± SD	236.3 ± 101.5	236.2 ± 101.5	239.7 ± 101.7	0.643
Fat consumption (g/d), Median (IQR)	68.4 (48.6, 94.0)	68.4 (48.6, 94.0)	67.8 (48.4, 89.7)	0.736
niacin consumption (mg/d), Mean ± SD	23.6 ± 11.7	23.6 ± 11.7	21.4 ± 8.7	0.009

Fat consumption expressed as median (IQR) and rest continuous variables are expressed as mean ± SD.

stroke. Additionally, restricted cubic spline (RCS) analysis indicated no nonlinear association between dietary niacin intake and PD.

Ender et al. (30) found that patients with PD may have chronic vitamin B3 deficiencies. Vascellari et al. (31) also found a decrease in B vitamins (B3 and B5) when studying the gut microbiota of patients with PD. Motawi et al. (32) evaluated the therapeutic effect of niacin on mouse models of PD through behavioral, biochemical, genetic, and histopathological observations, and found that food supplements containing niacin were effective in the treatment of PD. A randomized, double-blind trial in the United Kingdom showed that niacin supplementation might maintain or improve quality of life in people with PD and slow progression of the disease (16). Similarly, a randomized, double-blind controlled trial of U.S. military veterans showed that supplementation with low-dose niacin as adjunct therapy in patients with PD reduced neuroinflammation and improved motor function (15). The aforementioned studies all suggest the therapeutic significance of niacin for patients with PD. However, it is worth noting that there is currently a lack of large-scale clinical studies investigating the relationship between dietary niacin and Parkinson's disease (PD) in the general population. To our knowledge, this study is the first to evaluate the association between dietary niacin intake and the risk of developing PD in US adults. This study included a general population sample from the United States, which was nationally representative. Our results suggest that higher dietary niacin intake may be associated with a reduced risk of PD in the US population, consistent with previous research findings. Earlier research also found that PD patients experienced controlled motor symptoms after taking high doses of niacin (500–2,000 mg/day), but they also encountered nightmares and rashes (33). In our study, the maximum daily dietary intake of niacin was 179.1 mg/day, so no safety issues related to excessive niacin intake were observed.

What is special about this study is the inclusion of total energy consumption, fat consumption, carbohydrate consumption, and protein consumption as covariates. Qu et al. (34) conducted a systematic review using the Embase and PubMed databases, concluding that high total energy consumption is associated with an increased risk of PD, and dietary fat consumption influences the risk of PD. Palavra et al. (35) found that PD patients reported higher total carbohydrate consumption. Kacprzyk et al. (36) searched four databases (Cochrane, PubMed, Embase, and Web of Science) and included 49 studies in their systematic review, analyzing the prevalence of malnutrition in PD patients, concluding that the prevalence or risk of malnutrition in the PD group is significant. Based on these studies, considering that total energy consumption, fat consumption, carbohydrate consumption, and protein consumption may all be related to the risk of PD, these factors were included as covariates in the study. The results showed that after comprehensive adjustment for total energy consumption, fat consumption, carbohydrate consumption, and protein consumption, the inverse relationship between dietary niacin intake and PD risk remained stable.

Based on previous studies, it is suggested that niacin is involved in the pathophysiological processes of PD via multiple mechanisms. First, chronic oxidative stress leads to oxidative damage to neuronal cell lipids, proteins, and DNA, resulting in the degeneration of substantia nigra dopaminergic neurons (37, 38). Degeneration and loss of dopaminergic neurons are the primary factors that contribute to PD progression (5, 39, 40). Experimental studies in various PD

TABLE 2 Association of covariates and PD risk.

Variables	OR (95%CI)	*p*-value	Variables	OR (95%CI)	*p*-value
Sex, *n* (%)			Body mass index (kg/m^2), *n* (%)		
Male	1 (reference)		<25	1 (reference)	
Female	1 (0.75–1.33)	0.991	≥25	0.93 (0.67–1.28)	0.65
Age (years)			Hypertension, *n* (%)		
40–65	1 (reference)		No	1 (reference)	
>65	2.55 (1.91–3.4)	<0.001	Yes	1.96 (1.47–2.61)	<0.001
Race/ethnicity, *n* (%)			Diabetes, *n* (%)		
Non-Hispanic white	1 (reference)		No	1 (reference)	
Non-Hispanic black	0.47 (0.31–0.71)	<0.001	Yes	1.27 (0.9–1.79)	0.168
Mexican American	0.42 (0.25–0.71)	0.001	Coronary heart disease, *n* (%)		
Others	0.4 (0.25 ~ 0.64)	<0.001	No	1 (reference)	
Education level (year), *n* (%)			Yes	1.62 (0.99–2.64)	0.054
<9	1 (reference)		Stroke, *n* (%)		
9–12	1 (0.63–1.57)	0.985	No	1 (reference)	
>12	0.85 (0.55–1.33)	0.478	Yes	2.14 (1.35–3.38)	0.001
Marital status, *n* (%)			Calorie consumption (kcal/d), Median (IQR)	1 (1–1)	0.515
Married or living with a partner	1 (reference)		Protein consumption (g/d), Median (IQR)	0.99 (0.99–1)	0.03
Living alone	1.13 (0.85–1.51)	0.41	Carbohydrate consumption (g/d), Median (IQR)	1 (1–1)	0.643
Family income, *n* (%)			Fat consumption (g/d), Median (IQR)	1 (1–1)	0.802
Low	1 (reference)		Niacin consumption (per 10 mg/d), Median (IQR)	0.83 (0.72–0.95)	0.009
Medium	0.77 (0.56–1.07)	0.121	Dietary supplements taken, *n* (%)	1.49 (1.11–2.02)	0.009
High	0.52 (0.36–0.76)	0.001			
Smoking status, *n* (%)					
Never	1 (reference)				
Current	0.97 (0.7–1.35)	0.861			
Former	1.01 (0.69–1.47)	0.979			

models have shown that niacin can improve oxidative stress associated with PD. Zhou et al. found that intraperitoneal injections of NADPH in an 1-methyl-4-phenyl-5-tetrahydropyridine (MPTP) animal model elevated glutathione levels and reduced the production of reactive oxygen species (ROS) (41). Qin et al. confirmed that exogenous NADPH possesses antioxidant activity both *in vivo* and in primary neuronal cultures (42, 43). In an animal model, Motawi et al. discovered that niacin decreased malondialdehyde and increased glutathione levels, thus reducing oxidative stress (32). Ganji et al. confirmed that niacin could increase NADP levels, inhibit the generation of ROS, and reduce glutathione levels, thereby reducing oxidative stress in endothelial cells (44).

Second, mitochondrial dysfunction has also been implicated in the pathogenesis of PD. Disruptions in mitochondrial dynamics (fission, fusion, transport, autophagy, etc.), complex I inhibition of the electron transport chain (ETC), and bioenergetic defects have all been confirmed to be associated with the pathogenesis of PD (45). The absence of niacin, an important cofactor in mitochondrial oxidative phosphorylation, is directly associated with mitochondrial dysfunction (12, 13).

In addition, a large number of studies have confirmed the link between neuroinflammation and PD. In patients with PD, inflammatory mediators such as TNF, IL-1β, IL-6, and IFNγ have been found in the cerebrospinal fluid and pathological findings of the dense part of the substantia nigra (46, 47). The niacin anti-inflammatory mechanism is mediated through the receptor GPR109A. Macrophages polarize from the M1 (pro-inflammatory) to the M2 (anti-inflammatory) phenotype through GPR109A (48).

Neuroinflammation can be reduced by targeting GPR109A, thereby reducing the incidence of PD (7). Evidence shows that exogenous NADPH inhibits oxidative stress and glial cell-mediated neuroinflammation (41). In the MPTP model, the niacin metabolite NADPH effectively reduced MPP+-induced reactive oxygen species (ROS), p38 phosphorylation, and excessive production of cyclooxygenase-2 (COX2) inflammatory proteins, and inhibited glia-mediated neuroinflammation (41). Wakade et al. showed that in patients with PD, supplementation with low doses of niacin promoted anti-inflammatory processes and inhibited inflammation (48).

In summary, niacin may alter the pathology of PD through various neuroprotective mechanisms, including the reduction of

TABLE 3 The logistic regression of dietary niacin intake associated with PD risk.

Variable	*n*.total	*n*.event_%	Niacin (per 10 mg/d)	
			OR (95%CI)	*p*-value
Unadjusted	20,211	192 (0.9)	0.83 (0.72–0.95)	0.009
Model 1	20,211	192 (0.9)	0.84 (0.72–0.98)	0.027
Model 2	20,211	192 (0.9)	0.77 (0.6–0.99)	0.040
Model 3	20,211	192 (0.9)	0.77 (0.6–0.99)	0.042

Model 1: adjusted for RIAGENDR, age, and race.
Model 2: adjusted for RIAGENDR, age, race, edu, marital, PIR, supp, smoke, energy, protein, carbohydrate, fat, and BMI.
Model 3: adjusted for RIAGENDR, age, race, edu, marital, PIR, supp, smoke, energy, protein, carbohydrate, fat, BMI, hypertension, DM, CHD, and stroke.
CI, confidence interval; OR, odds ratios.

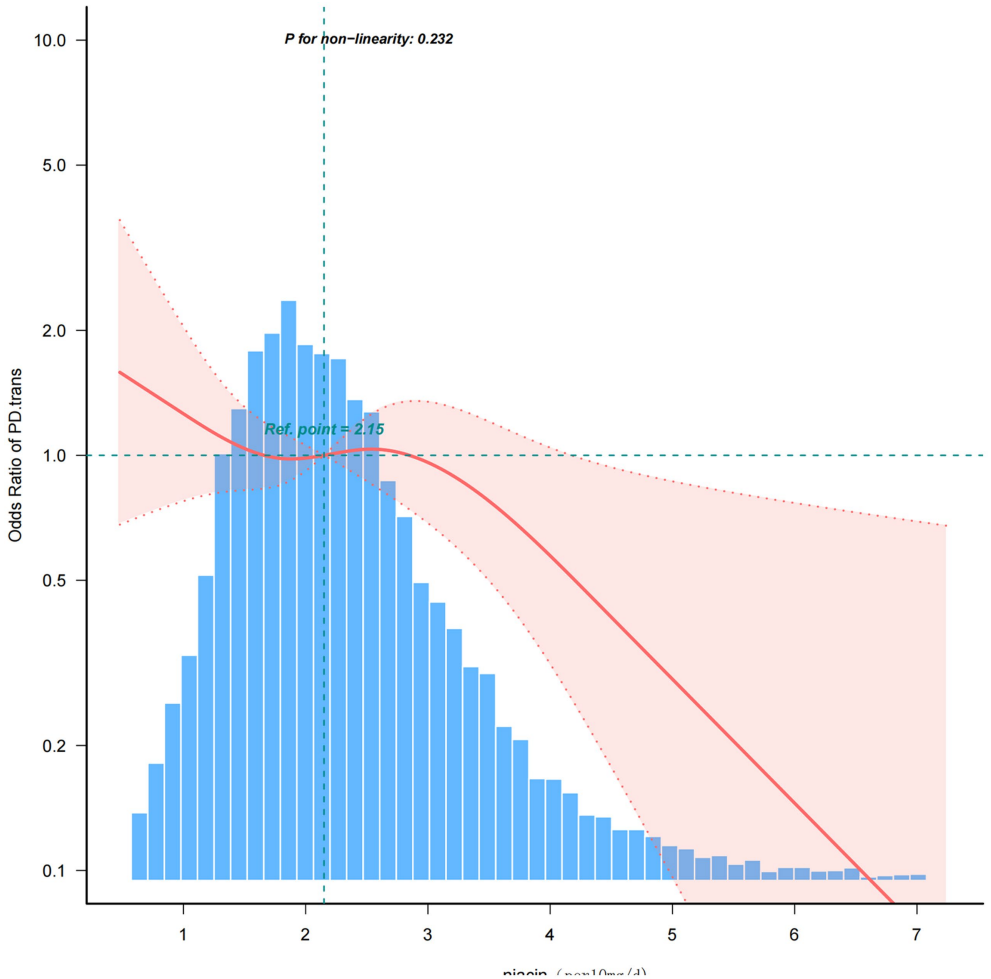

FIGURE 2
Association between dietary niacin intake and PD odds ratio. The solid and dashed lines represent the predicted value and the 95% confidence interval. They adjusted for age, sex, race, marital status, family income, education level, smoking status, body mass index, stroke, hypertension, coronary heart disease, diabetes, energy consumption, carbohydrate consumption, fat consumption, protein consumption, and whether they took dietary supplements. Only 99.5% of the data is displayed.

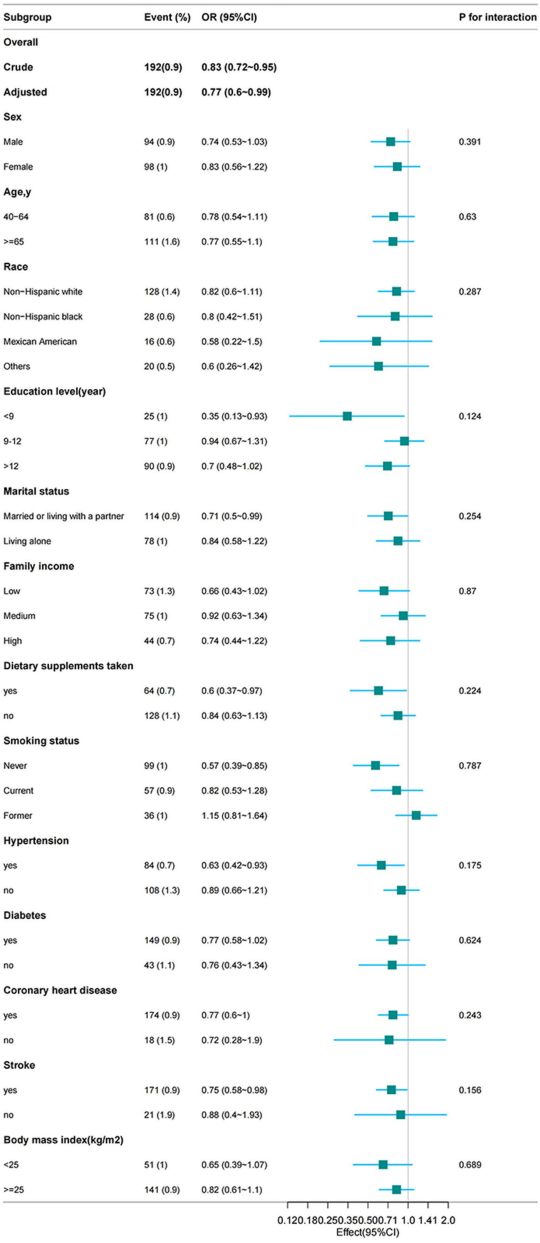

FIGURE 3
From the basic characteristics, the relationship between dietary niacin intake and PD is not only stratified components itself, each stratification factor was adjusted for all other variables (age, sex, marital status, ethnic group, education level, household income, smoking status, hypertension, diabetes, stroke, coronary heart disease, body mass index, energy expenditure, protein expenditure, carbohydrate expenditure, fat expenditure, dietary supplement use).

TABLE 4 Association between dietary niacin intake and PD risk in participants with extreme energy consumption was not included.

Variable	*n*.total	*n*.event_%	Niacin (per 10 mg/d)	
			OR (95%CI)	*p*-value
Unadjusted	20,022	190 (0.9)	0.82 (0.71–0.95)	0.009
Model 1	20,022	190 (0.9)	0.83 (0.71–0.98)	0.026
Model 2	20,022	190 (0.9)	0.77 (0.6–0.99)	0.041
Model 3	20,022	190 (0.9)	0.77 (0.6–0.99)	0.042

Model 1: adjusted for RIAGENDR, age, and race.
Model 2: adjusted for RIAGENDR, age, race, edu, marital, PIR, supp, smoke, energy, protein, carbohydrate, fat, and BMI.
Model 3: adjusted for RIAGENDR, age, race, edu, marital, PIR, supp, smoke, energy, protein, carbohydrate, fat, BMI, hypertension, DM, CHD, and stroke.
CI, confidence interval; OR, odds ratios.

oxidative stress, improvement of mitochondrial function, and amelioration of neuroinflammation.

This study had some limitations. First, owing to the limitations of the cross-sectional survey, we cannot infer causality from the results (49); therefore, further longitudinal research is necessary. Second, the NHANES uses anti-Parkinson drugs to define PD patients with PD, and cannot exclude sample inclusion for confounding reasons. In addition, in this study, we found that the confidence intervals for our conclusions were wide (0.6–0.99), suggesting that our sample size might be insufficient or the data variability might be high, thus necessitating cautious interpretation of these results. Future research requires larger sample sizes to obtain more precise estimates. Despite these uncertainties, our findings may still have practical significance in certain contexts, requiring careful consideration and balance in specific applications. Future research should aim to increase sample size and improve data quality to reduce the width of the confidence intervals, thereby providing more reliable evidence. Finally, there may be other confounding factors, such as physical activity, in the relationship between dietary niacin and PD. These additional factors should be considered in future studies to corroborate the findings of this research.

Since the NHANES dataset is nationally representative, our results can be generalized to the entire adult population of the United States to some extent. However, there may be differences for populations in other countries or regions due to variations in dietary habits, lifestyle, and genetic factors. Therefore, we recommend conducting similar studies in other regions to verify the external validity of these findings. Considering the limitations of this study, further research with larger sample sizes is needed to validate our results.

5 Conclusion

An inverse association between dietary niacin intake and the risk for PD was found in a large cross-sectional study of US adults aged 40 and older. For every 10 mg increase in dietary niacin intake, the risk of PD was reduced by 23%.

Author contributions

LZ: Writing – original draft, Writing – review & editing, Data curation, Investigation, Methodology, Project administration, Resources, Software. SY: Formal analysis, Supervision, Validation, Writing – review & editing. XL: Data curation, Validation, Visualization, Writing – review & editing. CW: Data curation, Validation, Writing – review & editing. GT: Funding acquisition, Methodology, Writing – review & editing. XW: Formal analysis, Funding acquisition, Writing – review & editing. LL: Conceptualization, Methodology, Writing – review & editing.

Funding

The author(s) declare that financial support was received for the research, authorship, and/or publication of this article. This research was funded by the Science & Technology Department of Sichuan Province (Grant No. 2022NSFSC1361) and the Health Commission of Sichuan Province (Grant No. 21PJ032), was supported by two projects of Natural Science Foundation of Gansu Province (grant number was 23JRRA1596 and 20JR10RA671).

Acknowledgments

We are grateful to Fangzhou Liu and Yingchun Xu of the Department of Neurology, West China Hospital, Sichuan University for their support in literature review, writing and typesetting. We gratefully thank Huanxian Liu of the Department of Neurology, Chinese PLA General Hospital for his contribution to the statistical support, study design consultations.

Conflict of interest

The authors declare that the research was conducted in the absence of any commercial or financial relationships that could be construed as a potential conflict of interest.

Publisher's note

References

1. Kalia LV, Lang AE. Parkinson's disease. *Lancet*. (2015) 386:896–912. doi: 10.1016/S0140-6736(14)61393-3

2. Simon DK, Tanner CM, Brundin P. Parkinson disease epidemiology, pathology, genetics, and pathophysiology. *Clin Geriatr Med*. (2020) 36:1–12. doi: 10.1016/J.Cger.2019.08.002

3. Tolosa E, Garrido A, Scholz SW, Poewe W. Challenges in the diagnosis of Parkinson's disease. *Lancet Neurol*. (2021) 20:385–97. doi: 10.1016/S1474-4422(21)00030-2

4. GBD 2016 Neurology Collaborators. Global, regional, and national burden of neurological disorders, 1990-2016: a systematic analysis for the global burden of disease study 2016. *Lancet Neurol*. (2019) 18:459–80. doi: 10.1016/S1474-4422(18)30499-X

5. Rocha EM, De Miranda B, Sanders LH. Alpha-synuclein: pathology, mitochondrial dysfunction and neuroinflammation in Parkinson's disease. *Neurobiol Dis*. (2018) 109:249–57. doi: 10.1016/J.Nbd.2017.04.004

6. Chen C, Turnbull DM, AK R. Mitochondrial dysfunction in Parkinson's disease-cause or consequence. *Biology*. (2019) 8:38. doi: 10.3390/Biology8020038

7. Giri B, Belanger K, Seamon M, Bradley E, Purohit S, Chong R, et al. Niacin ameliorates neuro-inflammation in Parkinson's disease via GPR109A. *Int J Mol Sci*. (2019) 20:4559. doi: 10.3390/Ijms20184559

8. Dexter DT, Jenner P. Parkinson disease: from pathology to molecular disease mechanisms. *Free Radic Biol Med*. (2013) 62:132–44. doi: 10.1016/J.Freeradbiomed.2013.01.018

9. GBD 2016 Parkinson's Disease Collaborators. Global, regional, and national burden of Parkinson's disease, 1990-2016: a systematic analysis for the global burden of disease study 2016. *Lancet Neurol*. (2018) 17:939–53. doi: 10.1016/S1474-4422(18)30295-3

10. Afzal M, Kuipers OP, Shafeeq S. Niacin-mediated gene expression and role of NiaR as a transcriptional repressor of niaX, nadC, and pnuC in *Streptococcus Pneumoniae*. *Front Cell Infect Microbiol*. (2017) 7:70. doi: 10.3389/Fcimb.2017.00070

11. Hellenbrand W, Boeing H, Bp R, Seidler A, Vieregge P, Nischan P, et al. Diet and Parkinson's disease. II: a possible role for the past intake of specific nutrients. Results from a self-administered food-frequency questionnaire in a case-control study. *Neurology*. (1996) 47:644–50. doi: 10.1212/Wnl.47.3.644

12. Kirkland JB, Meyer-Ficca ML. Niacin. *Adv Food Nutr Res*. (2018) 83:83–149. doi: 10.1016/Bs.Afnr.2017.11.003

13. Pirinen E, Auranen M, Na K, Brilhante V, Urho N, Pessia A, et al. Niacin cures systemic NAD(+) deficiency and improves muscle performance in adult-onset mitochondrial myopathy. *Cell Metab*. (2020) 31:1078–1090.E5. doi: 10.1016/J.Cmet.2020.04.008

14. Bjørklund G, Dadar M, Anderson G, Chirumbolo S, Maes M. Preventive treatments to slow substantia nigra damage and Parkinson's disease progression: a critical perspective review. *Pharmacol Res*. (2020) 161:105065. doi: 10.1016/J.Phrs.2020.105065

15. Wakade C, Chong R, Seamon M, Purohit S, Giri B, Morgan JC. Low-dose niacin supplementation improves motor function in us veterans with Parkinson's disease: a single-center, randomized, placebo-controlled trial. *Biomedicines*. (2021) 9:1881. doi: 10.3390/Biomedicines9121881

16. Chong R, Wakade C, Seamon M, Giri B, Morgan J, Purohit S. Niacin enhancement for Parkinson's disease: an effectiveness trial. *Front Aging Neurosci*. (2021) 13:667032. doi: 10.3389/Fnagi.2021.667032

17. Berven H, Kverneng S, Sheard E, Søgnen M, Af Geijerstam SA, Haugarvoll K, et al. NR-SAFE: a randomized, double-blind safety trial of high dose nicotinamide riboside in Parkinson's disease. *Nat Commun*. (2023) 14:7793. doi: 10.1038/S41467-023-43514-6

18. Gong R, Pu X, Cheng Z, Ding J, Chen Z, Wang Y. The association between serum cadmium and diabetes in the general population: a cross-sectional study from NHANES (1999-2020). *Front Nutr*. (2022) 9:966500. doi: 10.3389/Fnut.2022.966500

19. Liu H, Tan X, Liu Z, Ma X, Zheng Y, Zhu B, et al. Association between diet-related inflammation and COPD: findings from NHANES III. *Front Nutr*. (2021) 8:732099. doi: 10.3389/fnut.2021.732099

20. Zeng Z, Cen Y, Wang L, Luo X. Association between dietary inflammatory index and Parkinson's disease from national health and nutrition examination survey (2003-2018): a cross-sectional study. *Front Neurosci*. (2023) 17:1203979. doi: 10.3389/fnins.2023.1203979

21. Fan Y, Zhao L, Deng Z, Li M, Huang Z, Zhu M, et al. Non-linear association between Mediterranean diet and depressive symptom in U.S. adults: a cross-sectional study. *Front Psych*. (2022) 13:936283. doi: 10.3389/fpsyt.2022.936283

22. Wu Y, Song J, Zhang Q, Yan S, Sun X, Yi W, et al. Association between organophosphorus pesticide exposure and depression risk in adults: a cross-sectional study with NHANES data. *Environ Pollut*. (2023) 316:120445. doi: 10.1016/J.Envpol.2022.120445

23. Zhao J, Li F, Wu Q, Cheng Y, Liang G, Wang X, et al. Association between trichlorophenols and neurodegenerative diseases: a cross-sectional study from NHANES 2003-2010. *Chemosphere*. (2022) 307:135743. doi: 10.1016/J.Chemosphere.2022.135743

24. Zeng Z, Cen Y, Xiong L, Hong G, Luo Y, Luo X. Dietary copper intake and risk of Parkinson's disease: a cross-sectional study. *Biol Trace Elem Res*. (2023) 202:955–64. doi: 10.1007/s12011-023-03750-9

25. Liu H, Wang L, Chen C, Dong Z, Yu S. Association between dietary niacin intake and migraine among American adults: national health and nutrition examination survey. *Nutrients*. (2022) 14:3052. doi: 10.3390/Nu14153052

26. Fernandez RD, Bezerra G, Krejcová LV, Gomes DL. Correlations between nutritional status and quality of life of people with Parkinson's disease. *Nutrients*. (2023) 15:3272. doi: 10.3390/Nu15143272

27. Liu L, Shen Q, Bao Y, Xu F, Zhang D, Huang H, et al. Association between dietary intake and risk of Parkinson's disease: cross-sectional analysis of survey data from NHANES 2007-2016. *Front Nutr*. (2023) 10:1278128. doi: 10.3389/Fnut.2023.1278128

28. Xiao Y, Xiao Z. Association between serum klotho and kidney stones in us middle-aged and older individuals with diabetes mellitus: results from 2007 to 2016 national health and nutrition survey. *Am J Nephrol*. (2023) 54:224–33. doi: 10.1159/000531045

29. Ruan Z, Lu T, Chen Y, Yuan M, Yu H, Liu R, et al. Association between psoriasis and nonalcoholic fatty liver disease among outpatient US adults. *JAMA Dermatol*. (2022) 158:745–53. doi: 10.1001/Jamadermatol.2022.1609

30. Bender DA, Earl CJ, Lees AJ. Niacin depletion in Parkinsonian patients treated with L-dopa, benserazide and carbidopa. *Clin Sci*. (1979) 56:89–93. doi: 10.1042/Cs0560089

31. Vascellari S, Palmas V, Melis M, Pisanu S, Cusano R, Uva P, et al. Gut microbiota and metabolome alterations associated with Parkinson's disease. *Msystems*. (2020) 5:e00561-20. doi: 10.1128/Msystems.00561-20

32. Motawi TK, Sadik N, Hamed MA, Ali SA, Khalil W, Ahmed YR. Potential therapeutic effects of antagonizing adenosine A(2A) receptor, curcumin and niacin in rotenone-induced Parkinson's disease mice model. *Mol Cell Biochem*. (2020) 465:89–102. doi: 10.1007/S11010-019-03670-0

33. Alisky JM. Niacin improved rigidity and bradykinesia in a Parkinson's disease patient but also caused unacceptable nightmares and skin rash--a case report. *Nutr Neurosci*. (2005) 8:327–9. doi: 10.1080/10284150500484638

34. Qu Y, Chen X, Xu M, Sun Q. Relationship between high dietary fat intake and Parkinson's disease risk: a meta-analysis. *Neural Regen Res*. (2019) 14:2156–63. doi: 10.4103/1673-5374.262599

35. Palavra NC, Lubomski M, Flood VM, Davis RL, Sue CM. Increased added sugar consumption is common in Parkinson's disease. *Front Nutr*. (2021) 8:628845. doi: 10.3389/Fnut.2021.628845

36. Kacprzyk KW, Milewska M, Zarnowska A, Panczyk M, Rokicka G, Szostak-Wegierek D. Prevalence of malnutrition in patients with Parkinson's disease: a systematic review. *Nutrients*. (2022) 14:5194. doi: 10.3390/Nu14235194

37. De La Fuente M, Miquel J. An update of the oxidation-inflammation theory of aging: the involvement of the immune system in oxi-inflamm-aging. *Curr Pharm Des*. (2009) 15:3003–26. doi: 10.2174/138161209789058110

38. Vida C, Kobayashi H, Garrido A, Martínez De Toda I, Carro E, Molina JA, et al. Lymphoproliferation impairment and oxidative stress in blood cells from early Parkinson's disease patients. *Int J Mol Sci*. (2019) 20:771. doi: 10.3390/Ijms20030771

39. Ghodsi H, Rahimi HR, Aghili SM, Saberi A, Shoeibi A. Evaluation of curcumin as add-on therapy in patients with Parkinson's disease: a pilot randomized, triple-blind, placebo-controlled trial. *Clin Neurol Neurosurg*. (2022) 218:107300. doi: 10.1016/J.Clineuro.2022.107300

40. Dionísio PA, Amaral JD, Rodrigues C. Oxidative stress and regulated cell death in Parkinson's disease. *Ageing Res Rev*. (2021) 67:101263. doi: 10.1016/J.Arr.2021.101263

41. Zhou Y, Wu J, Sheng R, Li M, Wang Y, Han R, et al. Reduced nicotinamide adenine dinucleotide phosphate inhibits MPTP-induced neuroinflammation and neurotoxicity. *Neuroscience*. (2018) 391:140–53. doi: 10.1016/J.Neuroscience.2018.08.032

42. Li M, Zhou ZP, Sun M, Cao L, Chen J, Qin YY, et al. Reduced nicotinamide adenine dinucleotide phosphate, a pentose phosphate pathway product, might be a novel drug candidate for ischemic stroke. *Stroke*. (2016) 47:187–95. doi: 10.1161/Strokeaha.115.009687

43. Qin YY, Li M, Feng X, Wang J, Cao L, Shen XK, et al. Combined NADPH and the NOX inhibitor apocynin provides greater anti-inflammatory and neuroprotective effects in a mouse model of stroke. *Free Radic Biol Med*. (2017) 104:333–45. doi: 10.1016/J.Freeradbiomed.2017.01.034

44. Ganji SH, Qin S, Zhang L, Kamanna VS, Kashyap ML. Niacin inhibits vascular oxidative stress, redox-sensitive genes, and monocyte adhesion to human aortic endothelial cells. *Atherosclerosis*. (2009) 202:68–75. doi: 10.1016/J.Atherosclerosis.2008.04.044

45. Winklhofer KF, Haass C. Mitochondrial dysfunction in Parkinson's disease. *Biochim Biophys Acta*. (1802) 2010:29–44. doi: 10.1016/J.Bbadis.2009.08.013

46. Frank-Cannon TC, Alto LT, Mcalpine FE, Tansey MG. Does neuroinflammation fan the flame in neurodegenerative diseases. *Mol Neurodegener*. (2009) 4:47. doi: 10.1186/1750-1326-4-47

47. Gerhard A, Pavese N, Hotton G, Turkheimer F, Es M, Hammers A, et al. In vivo imaging of microglial activation with [11C](R)-PK11195 pet in idiopathic Parkinson's disease. *Neurobiol Dis*. (2006) 21:404–12. doi: 10.1016/J.Nbd.2005.08.002

48. Wakade C, Giri B, Malik A, Khodadadi H, JC M, RK C, et al. Niacin modulates macrophage polarization in Parkinson's disease. *J Neuroimmunol*. (2018) 320:76–9. doi: 10.1016/J.Jneuroim.2018.05.002

49. Wang X, Cheng Z. Cross-sectional studies: strengths, weaknesses, and recommendations. *Chest*. (2020) 158:S65–71. doi: 10.1016/J.Chest.2020.03.012

frontiers | Frontiers in Nutrition

TYPE Original Research
PUBLISHED 27 August 2024
DOI 10.3389/fnut.2024.1430722

OPEN ACCESS

EDITED BY
Daniel C. Anthony,
University of Oxford, United Kingdom

REVIEWED BY
William B. Grant,
Sunlight Nutrition and Health Research Center, United States
Gerd Faxén Irving,
Karolinska Institutet (KI), Sweden

*CORRESPONDENCE
Jiang Chuan Dong
✉ dongjiangchuan2023@163.com

†These authors share first authorship

RECEIVED 10 May 2024
ACCEPTED 13 August 2024
PUBLISHED 27 August 2024

CITATION
Pan Y, Tang XY, Yang J, Feng ZQ, Yuan Y, Jiang Y, Hu GM and Dong JC (2024) Cognitive frailty in relation to vitamin B12 and 25-hydroxyvitamin D in an elderly population: a cross-sectional study from NHANES. *Front. Nutr.* 11:1430722. doi: 10.3389/fnut.2024.1430722

Cognitive frailty in relation to vitamin B12 and 25-hydroxyvitamin D in an elderly population: a cross-sectional study from NHANES

Yu Pan[1†], Xue Yin Tang[1†], Juan Yang[2†], Zhu Qing Feng[1], Yan Yuan[1], Yi Jiang[1], Gui Ming Hu[1] and Jiang Chuan Dong[3*]

[1]Department of Geriatrics, The Second Affiliated Hospital of Chongqing Medical University, Chongqing, China, [2]Department of Integrated of Chinese and Western Medicine, The First Affiliated Hospital of Chongqing Medical University, Chongqing, China, [3]Department of Integrated of Chinese and Western Medicine, The Second Affiliated Hospital of Chongqing Medical University, Chongqing, China

Background: Nutritional support has been identified as a potential intervention for cognitive frailty; however, the association between 25-hydroxyvitamin D [25-(OH)D], vitamin B12, and cognitive frailty remains ambiguous.

Methods: This study utilized data from two cycles (2011–2012, 2013–2014) of the National Health and Nutrition Examination Survey (NHANES) to investigate this relationship. The researchers constructed a 41-item frailty index encompassing diverse aspects of physical functioning, psychological evaluation, and medical conditions, and evaluated each participant individually. The study utilized Spearman's rank correlation coefficient and univariate ordered logistic regression to assess the relationships between variables and cognitive frailty. Recursive feature elimination and cross-validation methods were employed to identify the most influential variables for building and optimizing multivariate ordered logistic regression models. Subgroup analyses and interaction tests were further conducted to validate the identified correlations.

Results: The findings of this study confirm a negative linear correlation between 25-(OH)D levels and cognitive frailty in older adults. Specifically, a one-unit increase in 25-(OH)D levels was associated with a 12% reduction in the risk of cognitive frailty. The result was further supported by subgroup analyses and interaction tests.

Conclusion: The existence of a negatively correlated linear association between 25-(OH)D levels and cognitive frailty in older adults is plausible, but further rigorously designed longitudinal studies are necessary to validate this relationship.

KEYWORDS

cognitive frailty, 25-hydroxyvitamin D, vitamin B12, cross-sectional study, NHANES

1 Introduction

Frailty is a prevalent clinical syndrome among older adults, marked by susceptibility and diminished capacity for normal physiological functions when faced with acute stress (1). The most commonly recognized manifestation of frailty is a specific physical phenotype outlined by Fried, which encompasses the complex interplay of physiological

functioning in older individuals, including unintentional weight loss, weakness, poor endurance, and energy, slowness of movement, low grip strength, reduced levels of physical activity (2). However, it is now widely acknowledged that this assessment of physical frailty may not fully capture the complexity of frailty, particularly cognitive functioning (3). Recent research has incorporated cognitive functioning into frailty assessments, leading to the emergence of cognitive frailty as a distinct clinical entity characterized by the simultaneous presence of physical frailty and cognitive impairment that has not yet progressed to dementia (4, 5). It is unequivocal that cognitive impairment is closely associated with frailty in a clinical context. Epidemiological studies have demonstrated that frailty is linked to a heightened likelihood of cognitive decline in the future, whereas cognitive impairment may elevate the risk of developing frailty (6, 7). A particular study delved into the causal connection between frailty and cognitive impairment, as well as examined the interplay between these two conditions, thereby enhancing the understanding of cognitive frailty (8). For instance, a research study examining elderly Chinese males found that individuals with cognitive impairment were at a higher risk of developing physical frailty after 4 years compared to those without cognitive impairment (9). Nevertheless, another multicenter study involving community-dwelling older adults in Chicago revealed that older adults with physical frailty were more susceptible to cognitive impairment, which subsequently led to an escalation in somatic frailty (10).

While cognitive frailty has not advanced to dementia, the transition from cognitive decline to dementia is a continuous and irreversible process for which there is currently no effective treatment. Current interventions primarily aim to mitigate the risk of cognitive decline by addressing potential risk factors (11). Although certain factors may be beyond modification, others such as excessive alcohol consumption, smoking, obesity, lack of physical activity, and dietary or nutritional deficiencies can be controlled to decrease the occurrence of cognitive deficits or impede their advancement (11, 12). Therefore, nutritional supplementation may offer a potential avenue for both preventing and treating cognitive frailty (13, 14).

25-hydroxyvitamin D [25-(OH)D] and vitamin B12 are essential organic compounds that are crucial for the proper functioning of the body's physiology and are involved in key metabolic pathways that support fundamental cellular processes (15). Nevertheless, due to their limited endogenous synthesis in the elderly population, regular dietary supplementation of vitamin B12 and 25-(OH)D is necessary (16). Regrettably, the potential impact of these vitamins on cognitive frailty remains unrecognized, as previous research has primarily examined their potential to enhance cognitive function without considering potential somatic frailty effects.

To address this research deficiency, a 41-item Frailty Index (FI) scale was developed in accordance with established standard procedures for FI construction, encompassing various dimensions of psychological and physical health (17). Subsequently, utilizing publicly available datasets, a combination of conventional statistical techniques and machine learning algorithms was employed to explore the associations between cognitive frailty and levels of vitamin B12 and 25-(OH)D, with the overarching aim of offering a nutritional perspective for the management of cognitive frailty.

2 Methods

2.1 Study design

The National Health and Nutrition Examination Survey (NHANES) is a research program aimed at evaluating the health and nutritional wellbeing of individuals residing in the United States. Utilizing a blend of questionnaires and physical assessments, the program focuses on particular demographic groups or health-related concerns. The NHANES study methodology received approval from the Ethics Review Board of the National Center for Health Statistics at the U.S. Centers for Disease Control and Prevention, with all participants providing written informed consent before participation in the survey.

This study incorporated data from two NHANES survey cycles (2011–2012, 2013–2014). A total of 19,931 participants were initially enrolled, with exclusions made for individuals with missing relevant data or those under the age of 65. Ultimately, 2,089 participants met the inclusion criteria for the study (Figure 1).

2.2 Frailty assessment

Employing established criteria and methodologies for constructing the Frailty Index (FI) and utilizing data from the NHANES (17), this study developed a 41-item assessment scale to evaluate an individual's frailty status. The scale was designed to comprehensively evaluate various aspects of health, illness, physical functioning, and mental health in order to determine the level of frailty in each participant. By applying the FI scale and referencing existing research, the study further classified frailty into three categories: absence of frailty ($FI \geq 0.12$), pre-frailty ($0.12 < FI < 0.25$), and frailty ($FI \leq 0.25$) (17, 18). The item composition and scoring criteria of the FI scale are detailed in Appendix 1.

2.3 Cognitive frailty

Currently, there is no gold standard for identifying low cognitive performance on the Consortium to Establish a Registry for Alzheimer's Disease (CERAD), Animal Fluency Test (AFT), and the Digit Symbol Substitution Test (DSST). Consequently, we employed the 25th percentile of scores, or the lowest quartile, as the threshold, aligning with the methodological approach used in existing research (19). Furthermore, given that all study participants fell within the 65–80 age range, scores were stratified by age groups (65–72 years, 73–80 years) to address the known impact of age on cognitive functioning (20). The CERAD test established cutoff values of 22 and 18 for low cognitive performance across the two age groups, while the AFT and DSST had cutoff values of 13, 11, and 34, 28, respectively. Participants were categorized into either the low cognitive performance group, with scores falling below the

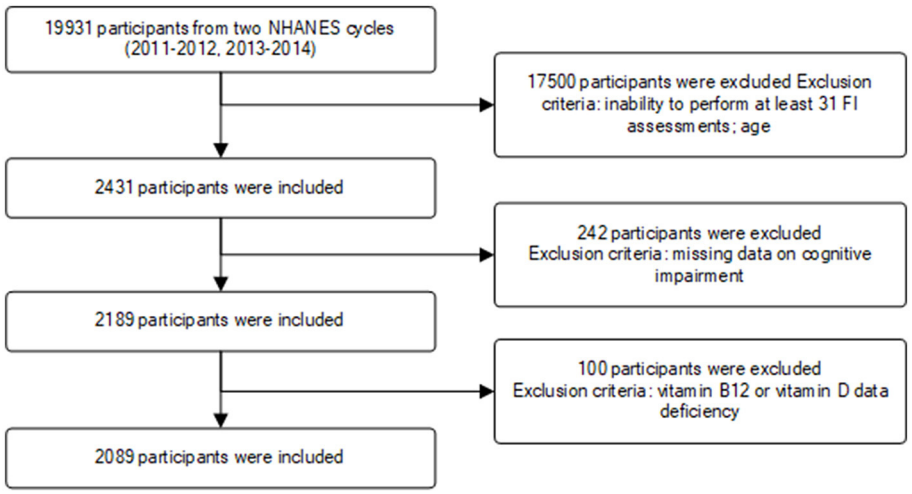

FIGURE 1
The participants' selection process.

specified cutoff values, or the normal cognitive performance group based on their performance in each dimension.

Furthermore, given the bidirectional negative relationship between cognitive impairment and somatic frailty, wherein cognitive impairment significantly heightens the likelihood of somatic frailty and vice versa, individuals with either somatic frailty or cognitive impairment not yet advanced to cognitive frailty were classified as pre-cognitive frail in this study. Cognitive frailty was then categorized as non-cognitive frail, pre-cognitive frail, and cognitive frail.

2.4 25-(OH)D and vitamin B12

According to current guidelines, total serum 25-hydroxy-25-(OH)D (25-(OH)D) is recommended as a suitable biomarker for evaluating 25-(OH)D status, enabling the identification of potential deficiencies or excessive levels of the 25-(OH)D (21). A total serum 25-(OH)D level below 20 ng/mL (<50 nmol/L) may indicate deficiency, while levels between 20–29 ng/mL (50–72.5 nmol/L) are considered insufficient in the absence of evident clinical symptoms (22, 23). Participants with concentrations >30 ng/ml (50 nmol/L) were considered as normal 25-(OH)D status.

Furthermore, the study population was stratified based on distinct serum B12 categories: (1) deficiency, characterized by serum B12 levels < 140 pmol/L; (2) insufficiency, with serum B12 levels ranging from 140 to 300 pmol/L; (3) normal levels, falling within the range of 300 to 700 pmol/L; and (4) elevation, denoted by serum B12 concentrations exceeding 700 pmol/L (24).

2.5 Ethics statement

Studies involving human subjects were reviewed and approved by protocols used by NHANES, approved by the Research Ethics Review Board of the National Center for Health Statistics, and written informed consent was provided by all participants, with information available on the official NHANES website (https://wwwn.cdc.gov/nchs/nhanes/index.htm). Data from the NHANES survey are publicly available, and all participants provided written informed consent to participate in the NHANES study. All patient information in the database used for this study was anonymized, and all participants were aware of and consented to the data collection activities. No further ethical approval or informed consent was required for this study.

2.6 Statistical analysis

This study employed a hybrid approach involving statistical analysis and machine learning methodologies to thoroughly examine the association between 25-(OH)D, vitamin B12, and cognitive frailty. Initially, the study characterized the dataset through descriptive statistics and subsequently investigated the correlation between 25-(OH)D, vitamin B12, and cognitive frailty utilizing Spearman's rank correlation coefficient (25). Furthermore, chi-square tests were utilized to investigate the relationships between various categorical variables and cognitive frailty. Subsequently, the impact of relevant variables on the likelihood of cognitive frailty was thoroughly examined through univariate ordered logistic regression. To address potential issues of covariance among variables, the study employed the variable inflation factor (VIF) for identification and selected key variables using recursive feature elimination and cross-validation (RFECV) (26). In sensitivity analyses, vitamins implicated in cognitive frailty were transformed into categorical variables to further elucidate the relationship between their levels and cognitive frailty, as well as their statistical significance. Subgroup analyses were conducted to explore the interaction between these vitamins and demographic characteristics. Moreover, random forest modeling was utilized to evaluate the significance of each variable, identifying key biomarkers that significantly impacted cognitive frailty. This

TABLE 1 Variables and baseline characteristics of the participants.

Variables		Total	Non-cognitive frail	Pre-cognitive frail	Cognitive frail	*P*-value	Spearman correlation coefficient
Age		73 ± 5	72 ± 5	73 ± 5	74 ± 5	<0.001	0.19
Total cholesterol (mg/dL)		187 ± 40	192 ± 40	188 ± 41	177 ± 39	<0.001	−0.14
WBC (10^9/L)		7.0 ± 1.9	6.7 ± 1.9	7.0 ± 2.0	7.2 ± 1.9	<0.001	0.11
Hemoglobin (g/dL)		14 ± 1.4	14 ± 1.2	14 ± 1.4	13 ± 1.5	<0.001	−0.20
MCV (fL)		91 ± 5.4	91 ± 4.7	91 ± 5.6	90 ± 5.7	0.03	−0.05
HCT (%)		40 ± 4	41 ± 3.6	40 ± 3.9	39 ± 4.4	<0.001	−0.18
PLT (10^9/L)		218 ± 56	219 ± 52	217 ± 56	221 ± 61	0.9	0.002
BUN (mg/dL)		17 ± 7	16 ± 5.8	17 ± 6.8	19 ± 8.3	<0.001	0.11
Glucose, serum (mg/dL)		112 ± 37	105 ± 28	113 ± 37	121 ± 46	<0.001	0.14
Creatinine, serum (mg/dL)		1 ± 0.4	1 ± 0.3	1 ± 0.4	1 ± 0.5	<0.001	0.15
Glycosylated hemoglobin (%)		6 ± 1	5.8 ± 0.7	6 ± 0.9	6 ± 1	<0.001	0.19
Uric acid (mg/dL)		5.8 ± 1.4	5.6 ± 1.3	5.7 ± 1.4	6 ± 1.5	<0.001	0.08
Vitamin B12 (pmol/L)		540 ± 675	540 ± 516	548 ± 888	528 ± 465	0.3	−0.03
25-(OH)D (nmol/L)		79 ± 32	83 ± 32	78 ± 30	75 ± 33	<0.001	−0.09
Erythrocyte folate (nmol/L)		1,427 ± 684	1,428 ± 629	1,434 ± 691	1,412 ± 745	0.07	−0.04
Gender						0.3	
	Male	1,016 (49%)	365 (50%)	405 (50%)	246 (46%)		
	Female	1,061(51%)	372 (50%)	400 (50%)	289 (54%)		
Race						<0.001	
	Asian	169 (8.1%)	72 (9.8%)	69 (8.6%)	28 (5.2%)		
	African-American	423 (20%)	112 (15%)	170 (21%)	141 (26%)		
	The White race	1,113 (54%)	471 (64%)	407 (51%)	235 (44%)		
	Latino/Hispanic	339 (16%)	72 (9.8%)	145 (18%)	122 (23%)		
	Other race	33 (1.6%)	10 (1.4%)	14 (1.7%)	9 (1.7%)		
Education						<0.001	
	Primary education and below	591 (28%)	91 (12%)	221 (28%)	79 (52%)		
	Secondary education	482 (23%)	167 (23%)	194 (24%)	121 (23%)		
	Higher education	1,002 (48%)	479 (65%)	388 (48%)	135 (25%)		
Marital status						<0.001	
	Unmarried	90 (4.3%)	28 (3.8%)	39 (4.9%)	23 (4.3%)		
	Married	1,162 (56%)	474 (64%)	445 (55%)	243 (46%)		
	Widowed	525 (25%)	130 (18%)	204 (25%)	191 (36%)		
	Divorced	299 (14%)	105 (14%)	117 (15%)	77 (14%)		

Gender, race, education, and marital status were expressed as percentages. *P* values for categorical variables were calculated using the chi-square test. *P* values for continuous variables were calculated using Spearman's rank correlation coefficient method. Mean ± standard deviation: age, total cholesterol (mg/dL), WBC (10^9/L), hemoglobin (g/dL), mean corpuscular volume (MCV) (fL), hematocrit (HCT) (%), PLT (10^9/L), urea nitrogen (BUN) (mg/dL), serum glucose (mg/dL), serum creatinine (mg/dL), glycosylated hemoglobin (%), uric acid (mg/dL), vitamin B12 (pmol/L), 25-(OH)D (nmol/L), erythrocyte folate (nmol/L). WBC, white blood cell count; MCV, mean corpuscular volume; HCT, hematocrit; PLT, platelet count; BUN, urea nitrogen.

comprehensive analytical approach, utilizing multiple levels and techniques, enhances comprehension of the impact of vitamins on cognitive health in elderly individuals and establishes a robust scientific foundation for the formulation of prevention and intervention strategies aimed at addressing cognitive frailty.

3 Results

3.1 Participant characteristics

This study included a total of 2089 individuals, all aged between 65 and 80 years, aligning with the criteria set forth by the World Health Organization and the United Nations for defining older adults. The mean age of the sample was 73 years (SD = 5), with females comprising 51% (n = 1,061) of the participants. A majority of the subjects were married (56%) and the subject population was predominantly the White race (54%). Education levels varied significantly within the sample, with nearly half (48%) having received higher education (Table 1). The results of the chi-square test indicated significant correlations between ethnicity, education, and marital status with cognitive frailty, while gender was not. Analysis of blood test results revealed correlations between most variables and cognitive frailty, with the exceptions of platelet and red blood cell folate. Calculations showed that Spearman rank correlation coefficients, which range from −1 to +1, where +1 indicates a perfect positive correlation, −1 indicates a perfect negative correlation, and 0 indicates no correlation (25). Noteworthy findings include positive correlations between uric acid, glycosylated hemoglobin, blood glucose, blood creatinine, blood urea nitrogen (BUN), and leukocytes with cognitive frailty, while negative correlations were observed between total cholesterol, hemoglobin, mean corpuscular volume (MCV), and hematocrit (HCT) with cognitive frailty. Additionally, 25-(OH)D exhibited a negative association with cognitive frailty, while vitamin B12 did not show such a relationship. Consequently, subsequent analyses were focused solely on the relationship between 25-(OH)D and cognitive frailty.

3.2 Univariate ordered logistic regression

Univariate ordered logistic regression analyses were performed to independently evaluate potential relationships between each variable. The findings of the univariate ordered logistic regression analysis for cognitive frailty are presented in Table 2. Notably, a significant correlation was observed between cognitive frailty and 25-(OH)D levels among older individuals ($P < 0.001$), while no such correlation was found with other vitamins such as vitamin B12 and folic acid. In addition, the majority of blood test-related variables exhibited independent associations with cognitive frailty, which warrants further investigation.

Among the categorical variables, one group was designated as the reference. The findings indicated that gender, marital status, White race, and unrepresented races did not demonstrate a statistically significant correlation with cognitive frailty. Conversely, individuals who were widowed, African-American, and Latino/Hispanic were potentially more susceptible to cognitive frailty progression.

TABLE 2 Univariate ordered logistic regression analysis for cognitive frailty.

Variables	Coefficient	OR (95% CI)	*P*-value
Age	0.07	1.07 (1.05, 1.08)	<**0.001**
Total cholesterol	−0.006	0.994 (0.992, 0.996)	<**0.001**
WBC	0.09	1.09 (1.05, 1.14)	<**0.001**
MCV	−0.02	0.978 (0.963, 0.992)	**0.003**
PLT	<0.001	1.0 (0.999, 1.0)	**0.6**
BUN	0.04	1.0 (1.0, 1.1)	**<0.001**
Glucose, serum	0.008	1.0 (1.0, 1.0)	**<0.001**
Creatinine, serum	0.8	2.3 (1.8, 2.8)	**<0.001**
Glycosylated hemoglobin	0.4	1.5 (1.4, 1.6)	**<0.001**
Uric acid	0.1	1.1 (1.1, 1.2)	**<0.001**
HCT	−0.09	0.92 (0.90, 0.93)	**<0.001**
Hemoglobin	−0.3	0.8 (0.7, 0.8)	**<0.001**
Vitamin B12	−0.00001	1.0 (1.0, 1.0)	**0.08**
25-(OH)D	−0.006	0.994 (0.992, 0.997)	**<0.001**
Erythrocyte folate	−0.00002	1.0 (1.0, 1.0)	**0.7**
Gender			
Male		***Reference***	
Female	0.09	1.1 (0.9, 1.3)	**0.3**
Education			
Primary education and below		***Reference***	
Secondary education	−1.0	0.4 (0.3, 0.4)	<**0.001**
Higher education	−1.7	0.2 (0.2, 0.2)	<**0.001**
Marital status			
Married		***Reference***	
Unmarried	0.4	1.4 (1.0, 2.1)	**0.08**
Divorced	0.3	1.3 (1.0, 1.6)	**0.04**
Widowed	0.8	2.1 (1.8, 2.6)	<**0.001**
Race			
Asian		***Reference***	
African-American	0.8	2.2 (1.6, 3.0)	**<0.001**
The White race	0.1	1.1 (0.8, 1.5)	**0.5**
Latino/Hispanic	1.0	2.6 (1.9, 3.7)	**<0.001**
Other race	0.6	1.7 (0.9, 3.4)	**0.1**

Results of univariate ordered logistic regression analysis.

3.3 Linear relationship

The findings from the univariate ordered logistic regression analysis and Spearman's rank correlation coefficients indicate a positive linear association between 25-(OH)D levels and cognitive

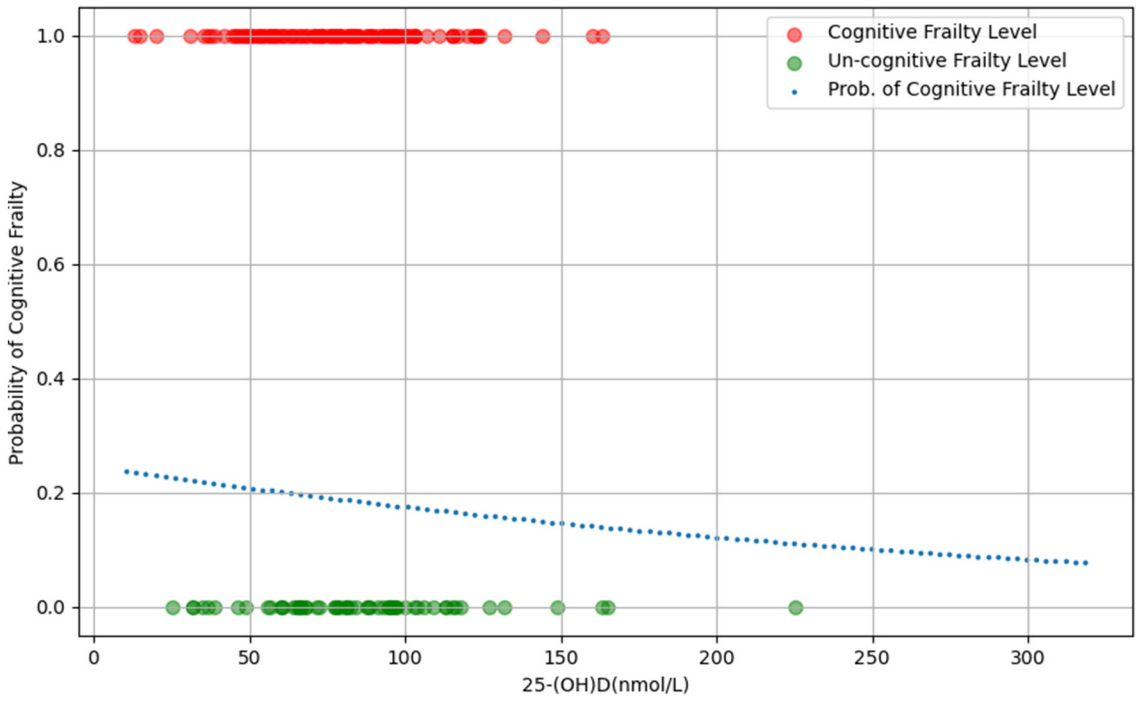

FIGURE 2
The scatter plot of the relationship between 25-(OH)D levels and probability of cognitive frailty.

frailty in the elderly, suggesting that higher levels of 25-(OH)D are associated with a reduced likelihood of cognitive frailty (Figure 2).

3.4 Multivariable adjusted regression models

Before conducting multivariate ordered logistic regression analyses, VIF was utilized to identify and address potential covariance issues among the variables. HCT (VIF>10) was excluded to prevent any potential interference as a covariate (Supplementary Table 1). Following this, the most impactful feature variables were chosen using the RFECV technique to enhance the model's performance. This process resulted in the exclusion of two variables, uric acid and BUN. Table 3 presents the findings of the multivariate logistic regression analysis examining the association between 25-(OH)D levels, other pertinent variables, and cognitive frailty. Following comprehensive adjustment for uric acid, BUN, and HCT variables, a statistically significant inverse relationship between 25-(OH)D levels and cognitive frailty was observed, aligning with the outcomes of univariate ordered logistic regression. Subsequent calculations indicated that a one-unit increase in 25-(OH)D levels corresponded to a 12% decrease in the likelihood of experiencing cognitive frailty.

Following the construction of the multivariate logistic regression model, the receiver operating characteristic curve (ROC) was generated for validation (Figure 3). The findings indicated that the area under the curve (AUC) value of the ROC curve for the multivariate logistic regression model was 0.72, indicating the significant clinical relevance of 25-(OH)D in the diagnosis, treatment, and prognosis assessment of cognitive impairment. This information holds importance in informing clinical decision-making and enhancing personalized treatment approaches.

3.5 Subgroup and sensitive analysis

The potential for reverse causality poses a significant risk in cross-sectional studies. To mitigate this bias, subgroup analyses and interaction tests were conducted to assess variations in the relationship between 25-(OH)D levels and cognitive frailty across different demographic variables such as sex, age group (65–72 and 73–80 years), education, race, and marital status (27). The findings revealed no significant interactions among the subgroups, except the 65–72 age group where a notable interaction was observed between 25-(OH)D levels and the risk of cognitive frailty (Table 4).

This outcome reinforces the applicability of population-based results across various subgroups, underscoring their coherence and dependability. Subsequently, we conducted sensitivity analyses to validate the robustness of the results. By categorizing 25-(OH)D into three groups - deficient, insufficient, and normal - and reevaluating the data, we found results consistent with the analysis in Supplementary Table 2, affirming an inverse relationship between 25-(OH)D levels and cognitive frailty.

TABLE 3 Multivariable regression models.

Variables	Model I			Model II		
	Coefficient	OR	*P*-value	Coefficient	OR	*P*-value
25-(OH)D	−0.1	0.9 (0.8, 1.0)	0.05	−0.1	0.9 (0.8, 1.0)	0.03
Erythrocyte folate	−0.1	1.0 (0.8, 1.0)	0.4	−0.05	1.0 (0.9, 1.1)	0.4
Age	0.4	1.5 (1.4, 1.7)	<0.001	0.4	1.5 (1.3, 1.7)	0.00
Total cholesterol	−0.2	0.8 (0.7, 0.9)	0.001	−0.2	0.8 (0.7, 0.9)	0.001
WBC	0.1	1.1 (1.0, 1.3)	0.04	0.1	1.1 (1.0, 1.3)	0.04
MCV	0.007	1.0 (0.9, 1.1)	0.9	−0.002	1.0 (0.9, 1.1)	0.99
PLT	0.009	1.0 (0.9, 1.1)	0.9	0.01	1.0 (0.9, 1.1)	0.9
BUN	−0.04	1.0 (0.8, 1.1)	0.6			
Glucose, serum	0.06	1.1 (0.9, 1.2)	0.4	0.06	1.1 (0.9, 1.2)	0.4
Creatinine, serum	0.1	1.1 (1.0, 1.3)	0.2	0.1	1.1 (1.0, 1.2)	0.1
Glycosylated hemoglobin	0.2	1.3 (1.1, 1.5)	0.003	0.2	1.3 (1.1, 1.5)	0.003
Uric acid	0.1	1.1 (0.9, 1.2)	0.5			
Hemoglobin	−0.1	0.9 (0.8, 1.0)	0.08	−0.1	0.9 (0.8, 1.0)	0.1
Female	0.1	1.2 (0.9, 1.5)	0.3	0.1	1.1 (0.9, 1.5)	0.4
Secondary education	−0.9	0.4 (0.3, 0.5)	<0.001	−0.9	0.4 (0.3, 0.5)	<0.001
Higher education	−1.4	0.2 (0.2, 0.3)	<0.001	−1.5	0.2 (0.2, 0.3)	<0.001
Unmarried	0.2	1.2 (0.7, 2.0)	0.6	0.2	1.2 (0.7, 1.9)	0.6
Divorced	0.1	1.2 (0.8, 1.6)	0.4	0.2	1.2 (0.8, 1.6)	0.4
Widowed	0.2	1.2 (0.9, 1.6)	0.1	0.2	1.2 (1.0, 1.6)	0.1
African-American	0.4	1.5 (0.9, 2.4)	0.09	0.4	1.5 (1.0, 2.4)	0.07
The White race	−0.2	0.9 (0.6, 1.3)	0.5	−0.2	0.9 (0.6, 1.3)	0.5
Latino/Hispanic	0.5	1.7 (1.1, 2.7)	0.02	0.5	1.7 (1.1, 2.6)	0.03
Other race	−0.2	0.8 (0.3, 2.2)	0.7	−0.2	0.8 (0.3, 2.3)	0.7

Results: OR (95%CI) *P*-value/Outcome: Cognitive frailty; Model I adjusted for: Variables except HCT. Model II adjusted for: Variables except HCT, uric acid, and BUN.

3.6 Importance of variables

In the developmental and validation stages of the study, all variables were inputted into a random forest machine learning algorithm utilizing a 10-fold cross-validation methodology to determine relative importance rankings (Figure 4). In this process, we initially load and clean the data. Subsequently, the variables are preprocessed by categorizing them into continuous and categorical types. Following this, the data is partitioned into training and test sets. Feature selection is then conducted using recursive feature elimination and cross-validation (RFECV) within the framework of a logistic regression model. RFECV assesses the importance of each feature and iteratively eliminates the least significant ones. Finally, the selected features and the cross-validation scores from each stage of the recursive feature elimination process are documented, and the identified features are preserved. This methodology enables RFECV to autonomously determine the most significant features, thereby streamlining the model and enhancing its predictive accuracy.

This was done to gain insight into the impact of these variables on cognitive frailty and to support future research and the development or modification of interventions. Furthermore, given that these variables encompass the socio-demographic data of the participants as well as all pertinent laboratory data, the results may be subject to some degree of uncertainty due to the lack of adjustment for potential confounding factors.

4 Discussion

The co-occurrence of physical frailty and cognitive impairment, known as cognitive frailty, has been linked to increased susceptibility to negative health consequences such as mortality, disability, hospitalization, and the onset of dementia (28). The etiology of cognitive frailty remains unclear, however, various risk factors such as sociodemographic factors, social status, nutritional status, physical and cognitive activity, and physiological functioning have been identified as strongly correlated with cognitive frailty. These findings have prompted the development of exercise rehabilitation and nutritional therapy as primary therapeutic interventions (4, 28). Prior research has established a strong correlation between 25-(OH)D, vitamin B12, and frailty.

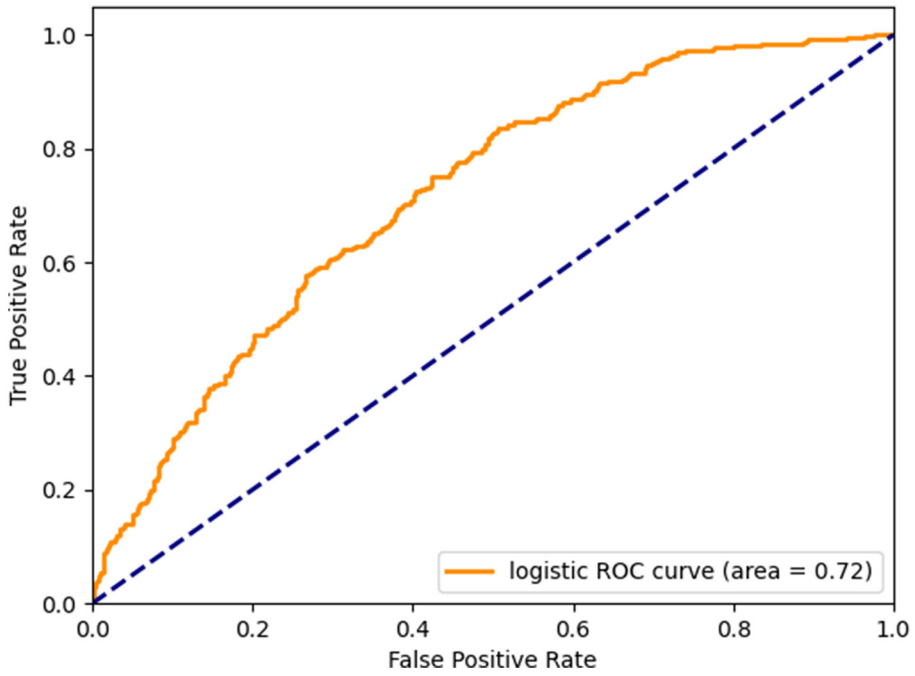

FIGURE 3
Micro-mean Receiver Operating Characteristic curves plotted according to multivariate logistic regression.

Nevertheless, the specific relationship between 25-(OH)D, vitamin B12, and subtypes of frailty, particularly cognitive frailty, remains inadequately understood. This study employs data from the NHANES to investigate the potential protective effects of 25-(OH)D and vitamin B12 in mitigating cognitive frailty among elderly individuals. The findings suggest that 25-(OH)D may play a significant role in protecting older adults against cognitive frailty, whereas vitamin B12 is not.

Several theories may explain our findings. Specifically, 25-(OH)D may enhance cognitive function through mechanisms including neuroprotection, modulation of oxidative stress, regulation of calcium homeostasis, and inhibiting inflammatory processes (29). For instance, in a cross-sectional study involving 2273 older adults, it was observed that individuals with serum 25-(OH)D levels exceeding 20 ng/mL exhibited elevated cognitive scores and a reduced likelihood of cognitive impairment. Conversely, those with serum 25-(OH)D levels equal to or below 20 ng/mL demonstrated a 1.6-fold increased risk of cognitive impairment compared to those with levels exceeding 20 ng/mL (30). Additionally, 25-(OH)D has been shown to modulate cognitive function development through its interaction with the 25-(OH)D receptor (VDR), a nuclear hormone receptor present in the central nervous system and widely distributed among various neurons and glial cells (31). Studies have further demonstrated a notable resemblance in the distribution of VDR between humans and rodents, particularly in regions such as the hippocampus, cerebral cortex, and limbic system, which underscores the significance of 25-(OH)D in the modulation of cognitive functions, including learning and memory (32, 33).

In addition, vitamin B12 (cobalamin), plays an important role in the normal functioning of the brain and nervous system through its association with the cellular metabolism of carbohydrates, proteins, and lipids, and as a cofactor in myelin formation and the normal physiology of the nervous system. Vitamin B12 deficiency has been linked to a range of severe neuropsychiatric symptoms, including depressive symptoms, suicidal behavior, mania, psychosis, and cognitive decline (34, 35). Research has demonstrated a notable correlation between brain size and vitamin B12 levels in individuals aged 61–87 years, with low cobalamin levels increasing the likelihood of cognitive decline, dementia, and Alzheimer's disease, as well as a 5-fold increase in the rate of brain atrophy (36). Additionally, a prospective case-control study found that vitamin B12 supplementation led to significant improvements in frontal lobe function among patients experiencing cognitive decline (37). While previous studies have indicated a potential link between cognitive frailty and vitamin B12 levels, our research indicates that vitamin B12 is not a standalone risk factor for cognitive frailty. This is similar to the findings of a rigorous meta-analysis that investigated the impact of vitamin B12 on cognitive function, depressive symptoms, and fatigue in individuals without advanced neurological conditions. The ongoing debate regarding the association between vitamin B12 and cognitive frailty notwithstanding, the aforementioned results and underlying pathophysiological mechanisms provide a rational explanation and substantiate the assertion that 25-(OH)D exerts a protective influence on the progression of cognitive frailty. These findings hold potential implications for clinical practice aimed at enhancing the outcomes of individuals with cognitive impairment. Furthermore, subgroup and interaction analyses have bolstered the validity and reliability of our findings.

Furthermore, the potential effects of lipids warrant attention. As shown in Figure 4, total cholesterol (TC) exhibited a particularly

TABLE 4 Subgroup analysis and interaction results.

Variables		Coefficient	OR	*P* interaction
Education				**0.7**
	Primary education and below		***Reference***	
	Secondary education	0.001	1.0 (0.8, 1.3)	0.99
	Higher education	0.09	1.1 (0.8, 1.4)	0.5
Marital status				**0.1**
	Married		***Reference***	
	Unmarried	0.1	1.1 (0.7, 1.9)	0.6
	Divorced	0.3	1.3 (1.0, 1.8)	0.08
	Widowed	−0.1	0.9 (0.7, 1.1)	0.3
Race				**0.2**
	Asian		***Reference***	
	African-American	0.2	1.3 (0.8, 2.0)	0.3
	The White race	−0.05	1.0 (0.6, 1.4)	0.8
	Latino/Hispanic	0.2	1.3 (0.8, 2.0)	0.4
	Other race	−0.4	0.7 (0.3, 2.0)	0.5
Age				**0.05**
	Age (73–80)		***Reference***	
	Age (65–72)	−0.2	0.8 (0.7, 1.0)	0.05
Gender				**0.8**
	Male		***Reference***	
	Female	−0.03	1.0 (0.8, 1.2)	0.8

strong association with frailty among all the variables examined. TC encompasses various components, including high-density lipoprotein-cholesterol, low-density lipoprotein-cholesterol, and free cholesterol, which collectively reflect the body's overall lipoprotein levels. Although TC and LDL-C levels often exhibit a parallel relationship, it is crucial to prioritize LDL-C as the primary metric when assessing frailty, particularly in the context of potential cardiovascular disease implications. Despite data limitations precluding the inclusion of HDL-C and LDL-C in the study, this limitation was partially mitigated by considering hyperlipidemia and cardiovascular disease when evaluating frail conditions. Future prospective studies should account for the potential impact of dynamic changes in LDL-C levels on the degree of frailty. Another noteworthy finding is that, although our study did not identify vitamin B12 as an independent risk factor for cognitive frailty in the elderly population, there is reliable evidence indicating that the cholesterol-vitamin B12 nutritional pattern is associated with mild cognitive impairment (MCI) and exhibits beneficial effects on MCI (38). Despite the underlying pathological mechanisms remaining poorly understood, the conclusion that the cholesterol-vitamin B12 nutritional pattern can influence cognitive impairment is highly informative for our research team in the design of further study.

The above outcomes suggest that regular dietary supplementation with TC and vitamin B12, including the consumption of meat, eggs, and dairy products, appears to be crucial for the elderly population. However, the implementation of this strategy remains contentious. A comprehensive health study conducted in Singapore revealed that higher red meat consumption during midlife is correlated with an elevated risk of cognitive impairment in later years (39). Conversely, substituting red meat with poultry or fresh fish/shellfish was associated with a decreased risk of cognitive decline. A prospective study focusing on the oldest segment of the Chinese population indicated that higher meat consumption was associated with a reduced likelihood of cognitive impairment (40). These inconsistent findings highlight the necessity of considering local conditions when examining the intricate relationship between meat consumption and cognitive function. Future research should be meticulously designed to account for the potential influence of local environmental factors and prevailing dietary patterns.

This study demonstrates certain strengths and innovations in comparison to prior research. Firstly, the study is grounded in a real population study conducted in the United States, encompassing 2,089 older adults aged 65 and above, thereby constituting a cross-sectional study with a substantial sample size. Secondly, the concept of pre-cognitive frailty in the elderly population was introduced to enhance the identification of older adults at risk of developing cognitive frailty. Furthermore, Spearman's rank correlation coefficient was utilized to establish the correlation between variables and cognitive frailty. Subsequently, multivariable logistic regression models combined with RFECV

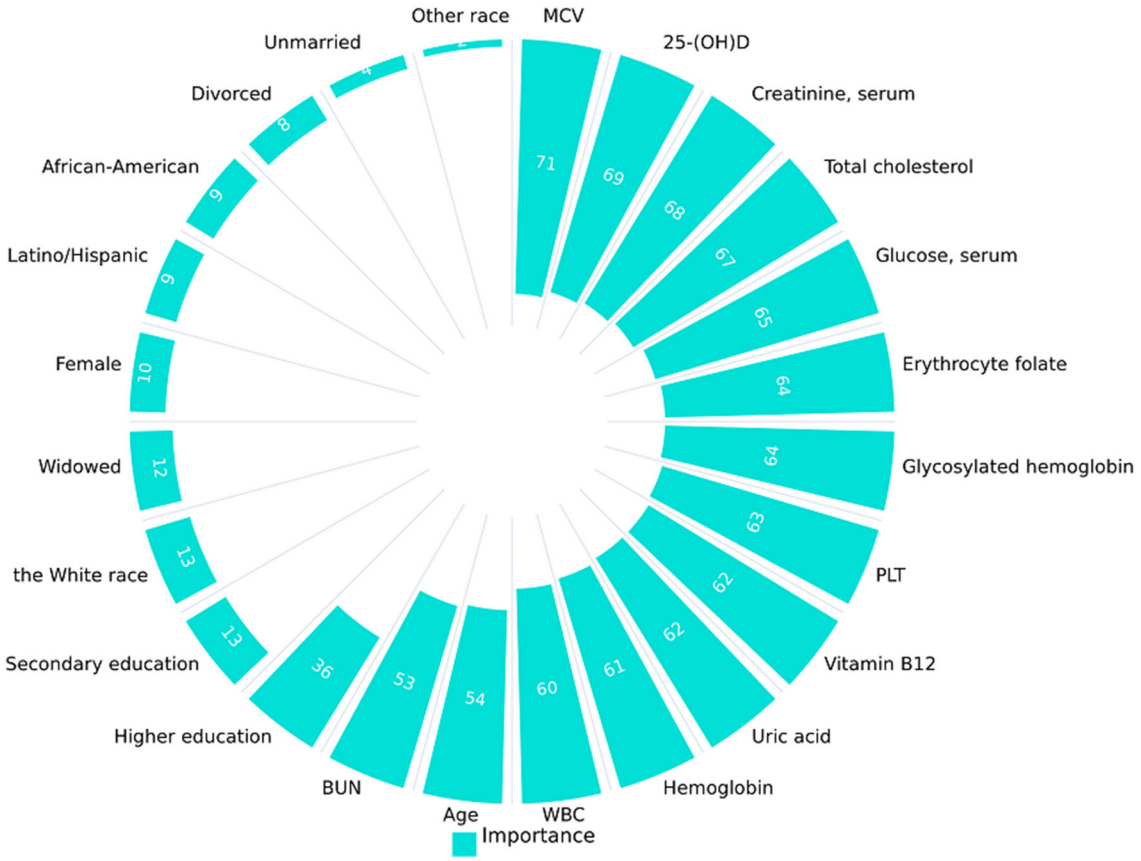

FIGURE 4
Variable importance ranking.

were employed to identify the most significant variables for enhancing model performance. Subgroup analyses and interaction tests were then conducted to validate the findings and broaden their generalizability.

5 Limitations

While our study yielded promising and dependable findings, it is important to acknowledge several limitations. The inherent design of cross-sectional studies presents challenges in establishing causality. To enhance the robustness of our conclusions, future research should consider incorporating prospective cohort studies. Furthermore, future studies should explore the longitudinal correlation between 25-(OH)D levels and individual frailty status to support the advancement of personalized intervention strategies. Furthermore, this study exclusively utilized population-based survey data from the United States, thereby prompting inquiries into the applicability of our results to other nations and geographic areas. Additionally, it is pertinent to acknowledge that elderly individuals frequently experience chronic illnesses such as chronic liver disease and chronic kidney disease. While our investigation encompassed hypertension, diabetes, stroke, and heart disease in the evaluation of frailty, certain disease biomarkers were not taken into account and incorporated. Moreover, diet, particularly the consumption of animal-derived foods, exerts a substantial influence on vitamin levels. Future research should meticulously examine the potential impacts of various dietary patterns, with special attention to those characterized by a high prevalence of vegetarian and meat-based foods, on vitamin status.

6 Conclusion

In summary, the findings of this cross-sectional study utilizing data from the NHANES database indicate a significant inverse relationship between 25-(OH)D levels and cognitive frailty. Specifically, a one-unit increase in 25-(OH)D levels was associated with a 12% decrease in the risk of cognitive frailty. Acknowledging the existence of this adverse correlation holds significant practical implications for the prevention of cognitive frailty. Monitoring 25-(OH)D levels and administering appropriate 25-(OH)D supplementation to patients experiencing cognitive frailty also bears important clinical implications.

Data availability statement

Publicly available datasets were analyzed in this study. This data can be found here: the two cycles (2011–2012, 2013–2014) from National Health and Nutrition Examination Survey (NHANES) (https://wwwn.cdc.gov/nchs/nhanes/index.htm).

Ethics statement

The studies involving humans were approved by the Research Ethics Review Board of the National Center for Health Statistics. The studies were conducted in accordance with the local legislation and institutional requirements. The human samples used in this study were acquired from studies involving human subjects were reviewed and approved by protocols used by NHANES, approved by the Research Ethics Review Board of the National Center for Health Statistics, and written informed consent was provided by all participants, with information available on the official NHANES website (https://wwwn.cdc.gov/nchs/nhanes/index.htm). Written informed consent for participation was not required from the participants or the participants' legal guardians/next of kin in accordance with the national legislation and institutional requirements.

Author contributions

YP: Conceptualization, Data curation, Formal analysis, Investigation, Software, Visualization, Writing – original draft. XT: Data curation, Formal analysis, Investigation, Validation, Writing – review & editing. JY: Data curation, Formal analysis, Investigation, Software, Validation, Writing – review & editing. ZF: Software, Validation, Visualization, Writing – review & editing. YY: Data curation, Formal analysis, Software, Visualization, Writing – review & editing. YJ: Data curation, Supervision, Validation, Writing – review & editing. GH: Data curation, Software, Validation, Writing – review & editing. JD: Conceptualization, Funding acquisition, Project administration, Resources, Supervision, Writing – review & editing.

Funding

The author(s) declare financial support was received for the research, authorship, and/or publication of this article. This work was supported by the 2021 Future Medical Innovation Team Support Program of Chongqing Medical University (Project No. W0070), 2024 Chongqing Municipal Health Commission, Chongqing Municipal Bureau of Science and Technology jointly funded project (2024ZYYB002), and Chongqing Natural Science Foundation (Project No. CSTB2022NSCQ-MSX0125).

Acknowledgments

The authors appreciate all the researchers, staff, and involved patients of NHANES databases.

Conflict of interest

The authors declare that the research was conducted in the absence of any commercial or financial relationships that could be construed as a potential conflict of interest.

Publisher's note

Supplementary material

The Supplementary Material for this article can be found online at: https://www.frontiersin.org/articles/10.3389/fnut.2024.1430722/full#supplementary-material

References

1. Hoogendijk EO, Afilalo J, Ensrud KE, Kowal P, Onder G, Fried LP. Frailty: implications for clinical practice and public health. *Lancet.* (2019) 394:1365–75. doi: 10.1016/S0140-6736(19)31786-6

2. Fried LP, Tangen CM, Walston J, Newman AB, Hirsch C, Gottdiener J, et al. Frailty in older adults: evidence for a phenotype. *J Gerontol A, Biol Sci Med Sci.* (2001) 56:M146–56. doi: 10.1093/gerona/56.3.M146

3. Gobbens RJ, Luijkx KG, Wijnen-Sponselee MT, Schols JM. Towards an integral conceptual model of frailty. *J Nutr Health Aging.* (2010) 14:175–81. doi: 10.1007/s12603-010-0045-6

4. Shimada H, Makizako H, Tsutsumimoto K, Doi T, Lee S, Suzuki T. Cognitive frailty and incidence of dementia in older persons. *J Prev Alzheimer's Dis.* (2018) 5:42–8. doi: 10.14283/jpad.2017.29

5. Ijaz N, Jamil Y, Brown CHt, Krishnaswami A, Orkaby A, Stimmel MB, et al. Role of cognitive frailty in older adults with cardiovascular disease. *J Am Heart Assoc.* (2024) 13:e033594. doi: 10.1161/JAHA.123.033594

6. Panza F, Lozupone M, Solfrizzi V, Sardone R, Dibello V, Di Lena L, et al. Different cognitive frailty models and health- and cognitive-related outcomes in older age: from epidemiology to prevention. *J Alzheimer's Dis.* (2018) 62:993–1012. doi: 10.3233/JAD-170963

7. Solfrizzi V, Scafato E, Frisardi V, Seripa D, Logroscino G, Maggi S, et al. Frailty syndrome and the risk of vascular dementia: the Italian longitudinal study on aging. *Alzheimer's Dement.* (2013) 9:113–22. doi: 10.1016/j.jalz.2011.09.223

8. Godin J, Armstrong JJ, Rockwood K, Andrew MK. Dynamics of frailty and cognition after age 50: why it matters that cognitive decline is mostly seen in old age. *J Alzheimer's Dis.* (2017) 58:231–42. doi: 10.3233/JAD-161280

9. Yu R, Morley JE, Kwok T, Leung J, Cheung O, Woo J. The effects of combinations of cognitive impairment and pre-frailty on adverse outcomes from a prospective community-based cohort study of older Chinese people. *Front Med.* (2018) 5:50. doi: 10.3389/fmed.2018.00050

10. Boyle PA, Buchman AS, Wilson RS, Leurgans SE, Bennett DA. Physical frailty is associated with incident mild cognitive impairment in community-based older persons. *J Am Geriatr Soc.* (2010) 58:248–55. doi: 10.1111/j.1532-5415.2009.02671.x

11. WHO Guidelines Approved by the Guidelines Review Committee. *Risk Reduction of Cognitive Decline and Dementia: WHO Guidelines.* Geneva: World Health Organization (2019).

12. Livingston G, Sommerlad A, Orgeta V, Costafreda SG, Huntley J, Ames D, et al. Dementia prevention, intervention, and care. *Lancet (London, England).* (2017) 390:2673–734. doi: 10.1016/S0140-6736(17)31363-6

13. Morris MC. Nutrition and risk of dementia: overview and methodological issues. *Ann N Y Acad Sci.* (2016) 1367:31–7. doi: 10.1111/nyas.13047

14. Gil Martínez V, Avedillo Salas A, Santander Ballestín S. Vitamin supplementation and dementia: a systematic review. *Nutrients.* (2022) 14:1033. doi: 10.3390/nu14051033

15. Tardy AL, Pouteau E, Marquez D, Yilmaz C, Scholey A. Vitamins and minerals for energy, fatigue and cognition: a narrative review of the biochemical and clinical evidence. *Nutrients.* (2020) 12:228. doi: 10.3390/nu12010228

16. Del Mondo A, Smerilli A, Sané E, Sansone C, Brunet C. Challenging microalgal vitamins for human health. *Microb Cell Fact.* (2020) 19:201. doi: 10.1186/s12934-020-01459-1

17. Searle SD, Mitnitski A, Gahbauer EA, Gill TM, Rockwood K. A standard procedure for creating a frailty index. *BMC Geriatr.* (2008) 8:24. doi: 10.1186/1471-2318-8-24

18. Fan J, Yu C, Guo Y, Bian Z, Sun Z, Yang L, et al. Frailty index and all-cause and cause-specific mortality in Chinese adults: a prospective cohort study. *Lancet Public Health.* (2020) 5:e650–e60. doi: 10.1016/S2468-2667(20)30113-4

19. Chen SP, Bhattacharya J, Pershing S. Association of vision loss with cognition in older adults. *JAMA Ophthalmol.* (2017) 135:963–70. doi: 10.1001/jamaophthalmol.2017.2838

20. Li S, Sun W, Zhang D. Association of zinc, iron, copper, and selenium intakes with low cognitive performance in older adults: a cross-sectional study from national health and nutrition examination survey (NHANES). *J Alzheimer's Dis.* (2019) 72:1145–57. doi: 10.3233/JAD-190263

21. Herrmann M, Farrell CL, Pusceddu I, Fabregat-Cabello N, Cavalier E. Assessment of 25-(OH)D status - a changing landscape. *Clin Chem Lab Med.* (2017) 55:3–26. doi: 10.1515/cclm-2016-0264

22. Pfotenhauer KM, Shubrook JH. 25-(OH)D deficiency, its role in health and disease, and current supplementation recommendations. *J Am Osteopath Assoc.* (2017) 117:301–5. doi: 10.7556/jaoa.2017.055

23. Landel V, Annweiler C, Millet P, Morello M, Féron F. 25-(OH)D, cognition and Alzheimer's disease: the therapeutic benefit is in the D-tails. *J Alzheimer's disease: JAD.* (2016) 53:419–44. doi: 10.3233/JAD-150943

24. Wolffenbuttel BHR, Heiner-Fokkema MR, Green R, Gans ROB. Relationship between serum B12 concentrations and mortality: experience in NHANES. *BMC Med.* (2020) 18:307. doi: 10.1186/s12916-020-01771-y

25. Sedgwick P. Spearman's rank correlation coefficient. *BMJ.* (2018) 362:k4131. doi: 10.1136/bmj.k4131

26. Wu J, Zheng D, Wu Z, Song H, Zhang X. Prediction of buckwheat maturity in UAV-RGB images based on recursive feature elimination cross-validation: a case study in Jinzhong, Northern China. *Plants.* (2022) 11:3257. doi: 10.3390/plants11233257

27. Brookes ST, Whitely E, Egger M, Smith GD, Mulheran PA, Peters TJ. Subgroup analyses in randomized trials: risks of subgroup-specific analyses: power and sample size for the interaction test. *J Clin Epidemiol.* (2004) 57:229–36. doi: 10.1016/j.jclinepi.2003.08.009

28. Sugimoto T, Arai H, Sakurai T. An update on cognitive frailty: Its definition, impact, associated factors and underlying mechanisms, and interventions. *Geriatr Gerontol Int.* (2022) 22:99–109. doi: 10.1111/ggi.14322

29. Bivona G, Gambino CM, Iacolino G, Ciaccio M. 25-(OH)D and the nervous system. *Neurol Res.* (2019) 41:827–35. doi: 10.1080/01616412.2019.1622872

30. Annweiler C, Milea D, Whitson HE, Cheng CY, Wong TY, Ikram MK, et al. 25-(OH)D insufficiency and cognitive impairment in Asians: a multi-ethnic population-based study and meta-analysis. *J Intern Med.* (2016) 280:300–11. doi: 10.1111/joim.12491

31. Gáll Z, Székely O. Role of 25-(OH)D in cognitive dysfunction: new molecular concepts and discrepancies between animal and human findings. *Nutrients.* (2021) 13:3672. doi: 10.3390/nu13113672

32. Cui X, Gooch H, Petty A, McGrath JJ, Eyles D. 25-(OH)D and the brain: genomic and non-genomic actions. *Mol Cell Endocrinol.* (2017) 453:131–43. doi: 10.1016/j.mce.2017.05.035

33. Eyles DW, Smith S, Kinobe R, Hewison M, McGrath JJ. Distribution of the 25-(OH)D receptor and 1 alpha-hydroxylase in human brain. *J Chem Neuroanat.* (2005) 29:21–30. doi: 10.1016/j.jchemneu.2004.08.006

34. Moore E, Mander A, Ames D, Carne R, Sanders K, Watters D. Cognitive impairment and vitamin B12: a review. *Int Psychogeriatr.* (2012) 24:541–56. doi: 10.1017/S1041610211002511

35. Mikkelsen K, Stojanovska L, Tangalakis K, Bosevski M, Apostolopoulos V. Cognitive decline: a vitamin B perspective. *Maturitas.* (2016) 93:108–13. doi: 10.1016/j.maturitas.2016.08.001

36. Vogiatzoglou A, Refsum H, Johnston C, Smith SM, Bradley KM, de Jager C, et al. Vitamin B12 status and rate of brain volume loss in community-dwelling elderly. *Neurology.* (2008) 71:826–32. doi: 10.1212/01.wnl.0000325581.26991.f2

37. Zhou L, Bai X, Huang J, Tan Y, Yang Q. Vitamin B12 supplementation improves cognitive function in middle aged and elderly patients with cognitive impairment. *Nutr Hospital.* (2023) 40:724–31. doi: 10.20960/nh.04394

38. Wang L, Liu K, Zhang X, Wang Y, Liu W, Wang T, et al. The effect and mechanism of cholesterol and vitamin b(12) on multi-domain cognitive function: a prospective study on Chinese middle-aged and older adults. *Front Aging Neurosci.* (2021) 13:707958. doi: 10.3389/fnagi.2021.707958

39. Jiang YW, Sheng LT, Pan XF, Feng L, Yuan JM, Pan A, et al. Meat consumption in midlife and risk of cognitive impairment in old age: the Singapore Chinese health study. *Eur J Nutr.* (2020) 59:1729–38. doi: 10.1007/s00394-019-02031-3

40. An R, Liu G, Khan N, Yan H, Wang Y. Dietary habits and cognitive impairment risk among oldest-old Chinese. *J Gerontol B, Psychol Sci Soc Sci.* (2019) 74:474–83. doi: 10.1093/geronb/gbw170

frontiers | Frontiers in Nutrition

TYPE Original Research
PUBLISHED 13 September 2024
DOI 10.3389/fnut.2024.1397776

OPEN ACCESS

EDITED BY
Rubem C. A. Guedes,
Federal University of Pernambuco, Brazil

REVIEWED BY
Linshuoshuo Lyu,
Vanderbilt University Medical Center, United States
Fulan Hu,
Shenzhen University Health Science Centre, China

*CORRESPONDENCE
Zhuangbin Liao
✉ bin644933454@163.com

†These authors share first authorship

RECEIVED 08 March 2024
ACCEPTED 26 August 2024
PUBLISHED 13 September 2024

CITATION
Lin H, Yin Y, Li J, Liu S, Long X and Liao Z (2024) Exploring the causal links between cigarette smoking, alcohol consumption, and aneurysmal subarachnoid hemorrhage: a two-sample Mendelian randomization analysis. *Front. Nutr.* 11:1397776. doi: 10.3389/fnut.2024.1397776

Exploring the causal links between cigarette smoking, alcohol consumption, and aneurysmal subarachnoid hemorrhage: a two-sample Mendelian randomization analysis

Heng Lin†, Yanqing Yin†, Jie Li, Siwei Liu, Xiaoao Long and Zhuangbin Liao*

Department of Cerebrovascular Surgery, Affiliated Hospital of Guangdong Medical University, Zhanjiang, China

Background: Aneurysmal subarachnoid hemorrhage (aSAH) represents a critical health concern characterized by elevated mortality and morbidity rates. Although both genetic predisposition and lifestyle choices influence aSAH susceptibility, understanding the causative associations between cigarette smoking, alcohol consumption, and aSAH risk remains imperative. Mendelian randomization (MR) offers a robust methodological framework for dissecting these associations, leveraging genetic variants as instrumental variables.

Objective: In this study, a two-sample Mendelian randomization (TSMR) approach was employed to elucidate the causal connections between genetically determined cigarette smoking, alcohol consumption, and aSAH risk.

Methods: Genetic instruments associated with cigarette smoking and alcohol consumption were sourced from the genome-wide association study (GWAS) and Sequencing Consortium of Alcohol and Nicotine use (GSCAN). Using a genome-wide association study (GWAS) dataset that encompassed aSAH cases and controls of European ancestry, TSMR, which utilized the inverse variance weighting (IVW) method, was employed to estimate the causal effects. Rigorous criteria were applied for selecting instrumental variables to ensure a robust Mendelian randomization analysis.

Results: A significant causal association was found between genetically determined cigarette smoking and an increased risk of aSAH, with a 1-standard deviation (SD) increase in cigarette use genetically linked to a 96% relative risk elevation [OR-IVW = 1.96, 95% confidence interval (CI) = 1.28–3.01, p = 0.0021]. However, genetically determined alcohol consumption did not exhibit a statistically significant association with aSAH risk (OR-IVW = 1.22, 95% CI = 0.61–2.45, p = 0.578).

Conclusion: The Mendelian randomization analysis revealed a causal nexus between cigarette smoking and an increased risk of aSAH, advocating for targeted smoking cessation interventions within genetically predisposed cohorts. The results regarding the relationship between alcohol consumption and aSAH were affected by insufficient statistical power. A prudent interpretation of the findings highlights the limitations of Mendelian randomization in

elucidating intricate genetic epidemiological relationships. Ongoing research involving larger cohort sizes and advanced methodological approaches is essential for comprehending the genetic underpinnings of aSAH.

KEYWORDS

cigarette smoking, alcohol consumption, aneurysmal subarachnoid hemorrhage, Mendelian randomization investigation, lifestyle behaviors

Introduction

Aneurysmal subarachnoid hemorrhage (aSAH) is a severe form of stroke resulting from the rupture of an intracranial aneurysm (1). Approximately one-third of patients face mortality, while another one-third require assistance for performing daily activities. Despite advancements in aSAH care and treatment strategies, this life-threatening event still exhibits significant mortality and morbidity rates. Various studies have explored factors predicting the prognosis of aSAH (2). While genetic factors are indicated by familial dominance, lifestyle factors are considered responsible for the majority of aSAH cases (3). Smoking, a highly detrimental behavior, and exposure to cigarette smoking (CSE) are major risk factors for cerebrovascular injury, including atherosclerosis, which is a pivotal process in cerebral aneurysm (CA) formation. Smoking contributes to approximately 18% of deaths in the United States (4). It is a well-established risk factor for the development and rupture of cerebral aneurysm. Despite an improved prognosis with aggressive treatments, subarachnoid hemorrhage often leads to death or severe disability, particularly in individuals under the age of 65. Smoking is the foremost preventable cause of subarachnoid hemorrhage (SAH); this is supported by numerous studies (5, 6) that demonstrated a strong dose–response relationship. The mechanisms that link smoking to the formation and rupture of cerebral aneurysm, as well as the reversibility of this risk, remain unclear. In addition, alcohol use has been identified as a potential risk factor for aSAH (7). However, previous research findings have been inconsistent, often stemming from smaller case–control or cohort studies (8) that lack comprehensive quantitative data on alcohol consumption and abstinence. Furthermore, certain studies have been confined to specific patient subgroups based on age, gender, or occupation (3) and have focused solely on recent alcohol consumption within 24 h before the onset of the disease or exclusively on deceased patients. Observational studies have reported a positive association between smoking, alcohol consumption, and aSAH risk, acknowledging the limitations of traditional statistical methods which include potential confounders and reverse causality (9).

To overcome the inherent limitations of conventional observational studies, such as susceptibility to confounding and reverse causation, and to robustly investigate whether cigarette smoking or alcohol consumption serves as an etiological factor in aneurysmal subarachnoid hemorrhage (aSAH), we strategically employed a two-sample Mendelian randomization (TSMR) approach (10). TSMR offers a methodological advantage by leveraging genetic variants associated with exposures (cigarette smoking and alcohol consumption) as instrumental variables, thereby minimizing biases and providing insights into causal relationships. Unlike observational studies, TSMR leverages the random assortment of alleles at conception, aligning with Mendel's second law, to help overcome confounding issues prevalent in observational research. This approach, akin to randomized controlled trials, strengthened the internal validity of our investigation and enhanced the reliability of the causal inference regarding the impact of lifestyle factors on aSAH risk (11, 12). This analysis estimated the association between single nucleotide polymorphisms (SNPs) linked to cigarette smoking, alcohol consumption, and the risk of aSAH, using two independent and publicly available genome-wide association study (GWAS) datasets (13, 14).

Methods

Data source

Data on genetic variants linked to cigarette smoking were retrieved from the GWAS and Sequencing Consortium of Alcohol and Nicotine use (GSCAN) (Table 1) (13) (Accessed on 08 January from https://conservancy.umn.edu/handle/11299/241912). The files provided summary statistics for associations with each phenotype: alcohol consumption measured as drinks per week (n = 10,93,137 individuals of European descent, n = 1,232,091, 203 SNPs) and smoking initiation (n = 10,93,139 individuals of European ancestry, n = 941,280, 71 SNPs). Our investigation examined the outcomes of a genome-wide association study (GWAS) (Table 1) (14) on aSAH, involving individuals of European ancestry. The outcome data included individual-level genotypes from 23 distinct cohorts (accessed on 08 January from https://cd.hugeamp.org/downloads.html), which were categorized into 9 European ancestry strata based on the genotyping platform and country. Each stratum underwent a separate analysis using a logistic mixed model. The combined dataset consisted of 7,495 cases and 71,934 controls, with 4,471,083 SNPs meeting the quality control (QC) thresholds. It is essential to emphasize that all the individuals analyzed were of European ancestry.

Statistical analysis

In this study, genetic variants were used as instrumental variables (IVs) to estimate the causal effect of cigarette smoking

TABLE 1 The details pf GWASs included in Mendelian randomization.

GWAS	Phenotype	Used as	Participants	Ancestry
Bakker et al. (14)	aSAH	Outcome	5,140 cases/71,952 controls	European
Saunders et al. (13)	Drink per week	Exposure	1,093,137	European
Saunders et al. (13)	Smoking initiation	Exposure	1,093,139	European

on aSAH risk. These IVs were selected based on the assumptions that they (1) predicted exposures (cigarettes and alcohol), (2) were independent of confounders (e.g., BMI), and (3) did not influence the results through pathways other than weekly alcohol consumption and smoking initiation (15). Initially, SNPs associated with exposures at genome-wide significance ($p < 5e\text{-}6$) were considered (S1 and S2). After excluding the SNPs in linkage disequilibrium (LD) ($r^2 < 0.001$; distance $< 10{,}000$ kb), independent SNPs were retained (S3 and S4). Subsequently, the remaining SNPs were cross-referenced with the aSAH GWAS database, resulting in the removal of SNPs not present in the aSAH database, which yielded a final dataset of SNPs. Finally, we obtained merged SNPs as IVs in TSMR.

In the TSMR study, we employed the inverse variance weighting (IVW) method as the primary analysis to assess the causal effect between cigarette use, alcohol consumption, and aSAH. IVW uses the Wald ratio method to calculate the exposure–outcome effect corresponding to each SNP and then conducts a weighted linear regression analysis with a forced intercept of zero. IVW achieves higher estimation accuracy and testing power when three basic assumptions are met (16).

The pleiotropy of the selected SNPs was also evaluated through the Mendelian Randomization Pleiotropy RESidual Sum and Outlier (MR-PRESSO) test. The MR-PRESSO detects outliers through a global test, computes corrected estimates for horizontal multivariate validity after outlier removal (if the p-value of the global test is <0.05), and assesses differences between the original and updated estimates through a distortion test (17). In addition, heterogeneity between the variance-specific estimates was tested using Cochran's Q statistic in an inverse variance-weighted model. The Cochran's Q test was performed on the remaining SNPs using the R software package to identify data heterogeneity.

As a sensitivity analysis, we performed a leave-one-out analysis and assessed the combined effect values of the remaining SNPs in conjunction with the IVW. If the combined effect was consistent with the results of the main effects analysis, it indicated that no individual SNP had a disproportionate effect on the MR analysis.

In our study, we employed the Bonferroni (18) correction for correcting multiple exposures and addressing the issue of inflated type I error rates associated with conducting multiple hypothesis tests. The Bonferroni correction is a widely accepted approach that controls the familywise error rate by adjusting the significance threshold based on the number of tests performed. Given the complexity of our investigation, which involved multiple exposures (cigarette smoking and alcohol consumption) and their potential impact on aSAH risk, it was crucial to mitigate the risk of false positives.

The Bonferroni correction set at a significance level of 0.025 ($p = 0.05/2 = 0.025$) was deliberate and aimed at ensuring a stringent criterion for statistical significance. By setting a more conservative threshold, we aimed to minimize the likelihood of observing statistically significant results purely by chance. This approach aligned with the cautious interpretation of findings and guarded against potential spurious associations. In the context of the Mendelian randomization analysis, where causal inference was a key objective, a higher level of stringency in significance testing enhanced the reliability of our results.

This methodological decision reflects our commitment to maintaining a balance between sensitivity and specificity in hypothesis testing, thereby enhancing the robustness of our conclusions regarding the causal relationships between genetic determinants of exposures and aSAH risk.

All analyses were conducted in R software (version 4.3.2) using the R packages, TwoSampleMR and MR-PRESSO. The results were presented as the mean effect of increased aSAH per 1-standard deviation (SD) genetic determination along with 95% confidence intervals (CIs); two-sided p-values < 0.05 were considered statistically significant. All analytic procedures are shown in Figure 1.

Results

Validity of instrumental variables

To ensure the credibility of our instrumental variables (IVs) and enhance the strength of our Mendelian randomization analysis, we implemented a strict criterion for the genetic variation. Specifically, we chose a 10,000 kb limit with an r^2 threshold of <0.001 when evaluating linkage disequilibrium (LD) between the single nucleotide polymorphisms (SNPs). This approach aimed to minimize the risk of weak instrumental variables, thereby reinforcing the validity of our instrumental variable selection.

The intentional selection of a 10,000 kb limit focused on the genetic variants in close proximity, ensuring that the chosen SNPs were more likely to be in linkage with each other. This proximity facilitated capturing potential causal relationships between the genetic variants and the exposures of interest (cigarette smoking and alcohol consumption) without introducing excessive noise from distant and less relevant genetic markers.

Simultaneously, the r^2 threshold of <0.001 signified a low threshold for LD, indicating that the selected SNPs were relatively independent of each other. This independence was crucial for meeting the assumptions of Mendelian randomization, where instrumental variables should ideally be associated with exposures but not confounded by other factors influencing the outcome (S5–S8).

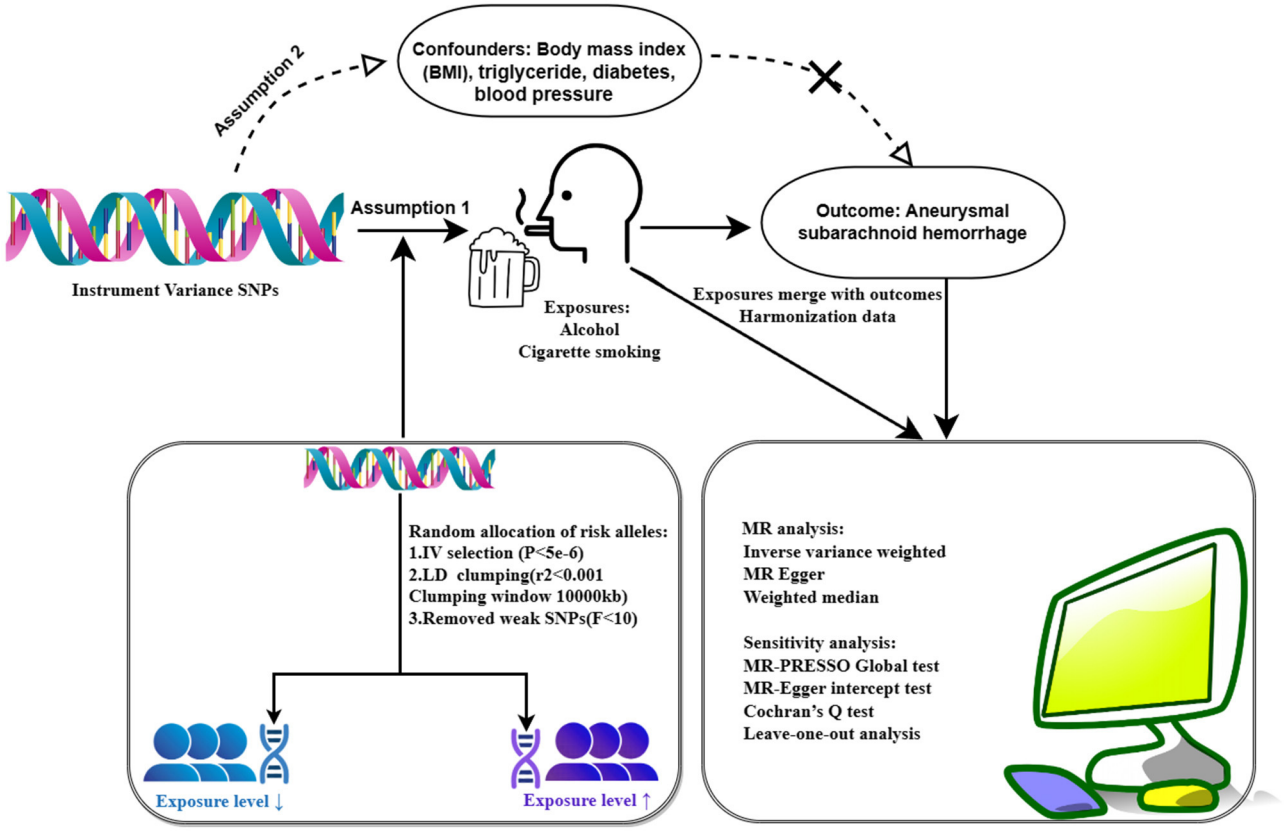

FIGURE 1
Flowchart of two sample Mendelian randomization analysis.

By applying these criteria, we aimed to ensure that the instrumental variables used in our analysis possessed sufficient strength and independence, addressing concerns related to weak instrument bias and enhancing the internal validity of our Mendelian randomization investigation. This process resulted in the inclusion of a total of 123 SNPs (S9: Alcohol: 30 SNPs, S10: Cigarette: 93 SNPs).

After conducting a rigorous instrumental variable screening process, we observed that all F-statistics (19) surpassed the threshold of 10, indicating robust instrumental variable strength and confirming the absence of weak instruments in our analysis. The F-statistic was a crucial metric in the instrumental variable analysis, representing the ratio of the variance explained by the instrumental variable to the unexplained variance. An F-statistic threshold exceeding 10 indicated that the chosen instrumental variables were sufficiently strong predictors of the exposure variable (cigarette smoking and alcohol consumption), ensuring that they contributed substantially to the variation in exposure. This strength was essential for fulfilling the assumptions of Mendelian randomization, where strong instruments enhance the ability to estimate unbiased causal effects. The consistent surpassing of the F-statistic threshold of 10 across all instrumental variables instilled confidence in the reliability and validity of our instrumental variable selection, reinforcing the robustness of our Mendelian randomization analysis.

Mendelian randomization

In our Mendelian randomization investigation, we aimed to uncover the causal relationships between the genetic determinants of cigarette smoking and alcohol consumption and the risk of aneurysmal subarachnoid hemorrhage (aSAH). Overall, our study revealed compelling insights into the potential impact of these lifestyle factors on aSAH risk. Subsequently, we present the results of the inverse variance weighting (IVW) analysis for cigarettes and alcohol, shedding light on their specific associations and magnitudes.

In our two-sample Mendelian randomization (TSMR) study, we selected the inverse variance weighting (IVW) method as the primary analysis method due to its distinct advantages in estimating causal effects and enhancing statistical power. The IVW method utilizes the Wald ratio approach, calculating the exposure–outcome effect corresponding to each single nucleotide polymorphism (SNP) and conducting a weighted linear regression. This method excels in achieving higher estimation accuracy and testing power when the fundamental assumptions of Mendelian randomization are met.

The key advantages of the IVW (17) method lie in its simplicity, efficiency, and reliability. By assigning weights based on the inverse of the variance of each SNP's effect estimate, IVW maximizes the precision of the causal effect estimation. This weighting strategy, combined with a forced intercept of zero, ensures that SNPs with

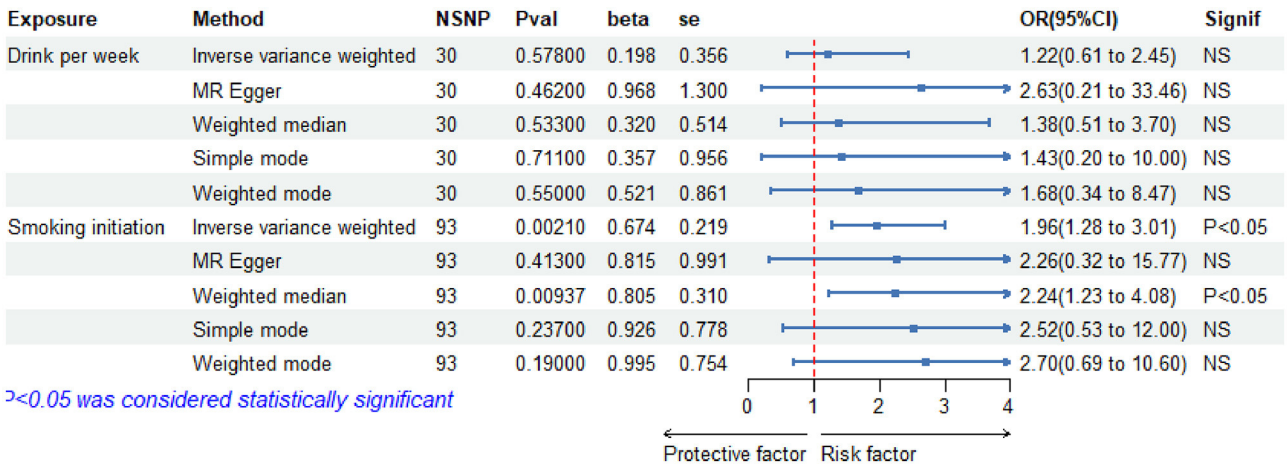

FIGURE 2
Forest plot of five Mendelian randomization estimators of the effect of alcohol and cigarette smoking on a aSAH. OR, odds ratio; CI, confidence under_val; se, standart error.

more precise estimates contribute more to the overall analysis, minimizing the impact of weaker instruments.

Furthermore, the IVW method is known for its statistical efficiency when applied to large-scale genetic data, making it particularly well-suited for our analysis involving a substantial number of SNPs associated with cigarette smoking and alcohol consumption. Its simplicity facilitates straightforward interpretation, which aligns with the clarity required in conveying causal relationships in complex genetic studies.

Figure 2 depicts the MR estimates for the increase in alcohol consumption and cigarette smoking and their impact on aSAH risk. In particular, the IVW results for cigarette smoking indicated a statistically significant increase in the risk of aSAH with increasing cigarette use. Employing the IVW approach, we identified a causal link between cigarette smoking and aSAH risk; a 1-standard deviation (SD) increase in the genetically determined cigarette use was causally associated with an additional 96% relative risk of aSAH ($N = 93$ SNPs; OR-IVW = 1.96; 95% CI = 1.28–3.01; and $p = 0.0021$). Conversely, alcohol consumption did not exhibit a significant association with aSAH risk ($N = 30$ SNPs; OR-IVW: 1.22; 95% CI: 0.61–2.45; and $p = 0.578$).

A Mendelian randomization analysis relies on assumptions. One of these assumptions is that instrumental variables (Genetic locus) must influence the results through exposure factors. To further explore the causal relationship between these assumptions and infer the presence of horizontal pleiotropy, the MR-PRESSO Global Test (Table 2) was conducted. The results indicated no horizontal pleiotropy in the exposure factors and outcome variables (Alcohol: $p = 0.12$ and Cigarette: $p = 0.069$). Figure 3 demonstrates the absence of horizontal pleiotropy between the exposure and outcome data. It further illustrates that as cigarette consumption increased, so did the risk of coronary aSAH.

Considering that the exposure and outcome data in the two-sample Mendelian randomization analysis originated from different samples, the potential population heterogeneity necessitated a heterogeneity test. Table 2 shows no significant

TABLE 2 The MR-PRESSO global test and heterogeneity tests of the instrumental variables.

Exposure	MR-PRESSO global test		Cochran's test		
	RSSobs	*p*-values	Q_df	Q_pval	Q
Drink per week	45.25	0.12	31.00	0.11	40.97
Smoking initiation	26.37	0.69	29.00	0.69	24.83

heterogeneity between alcohol, cigarette, and aSAH (Cochran's Q test result: Q_pval of Alcohol = 0.11 and Q_pval of Cigarette = 0.69). The estimates of the random and fixed effects remained consistent without loss of precision. Figure 4 illustrates a symmetrical distribution of the effect of increased alcohol consumption and cigarette smoking on aSAH risk when a single SNP was used as the IV.

Figure 5 shows that the leave-one-out plot precisely aligned with the right of zero (Figure 5), signifying that the outcome derived from the SNP suggested an elevated risk of developing aSAH with increased cigarette use. As for the lower red line in the chart, it signifies the IVW approach, demonstrating that cigarette use elevated the risk of aSAH.

Discussion

Cigarette smoking

The results of the Mendelian randomization (MR) regarding cigarette smoking revealed a significant causal relationship with an increased risk of aneurysmal subarachnoid hemorrhage (aSAH). A 1-standard deviation (SD) increase in genetically determined cigarette use was associated with an additional 96% relative risk of aSAH. These findings hold substantial implications for public

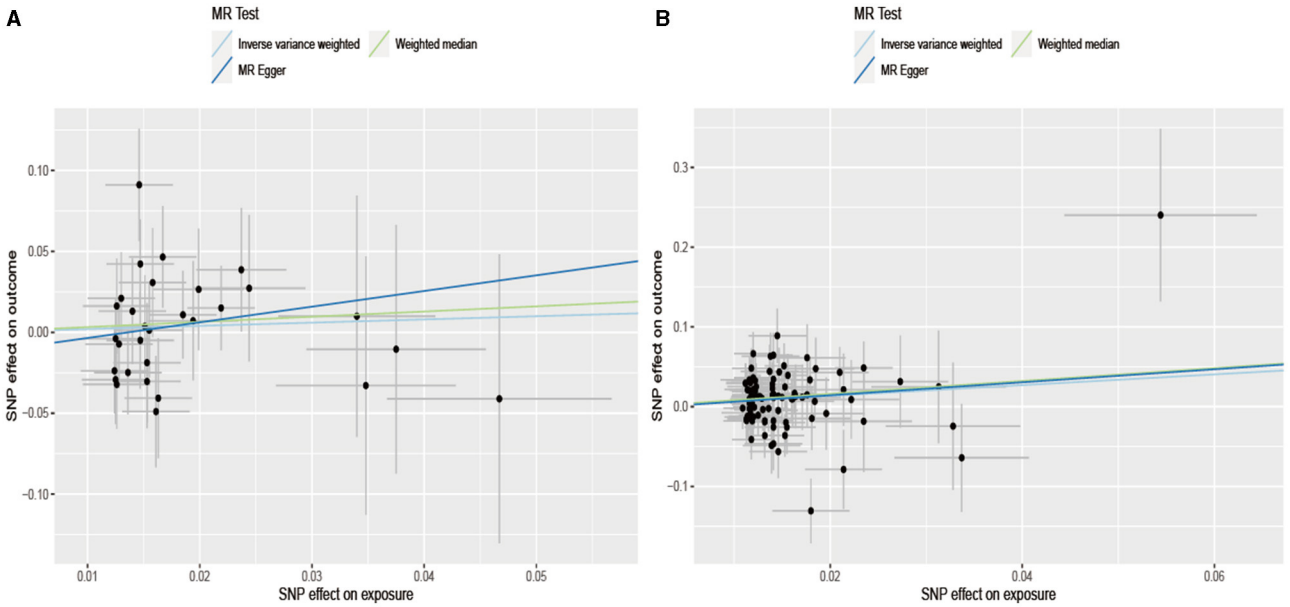

FIGURE 3
Scatterplot of SNPs associated with alcohol/cigarette and aSAH risk. The plot relates the effect sizes of the SNP-alcohol/cigarette association (x-axis, SD units) and the SNP-aSAH association [y axis, log (OR)] to 95% confidence intervals. The regression slopes of the lines correspond to causal estimates using the Mendelian randomization methods (inverse variance weighting method, MR-Egger regression, and weighted median estimator). MR, Mendelian randomization; SNP, single nucleotide polymorphism. **(A)** Drink per week; **(B)** smoking initiation.

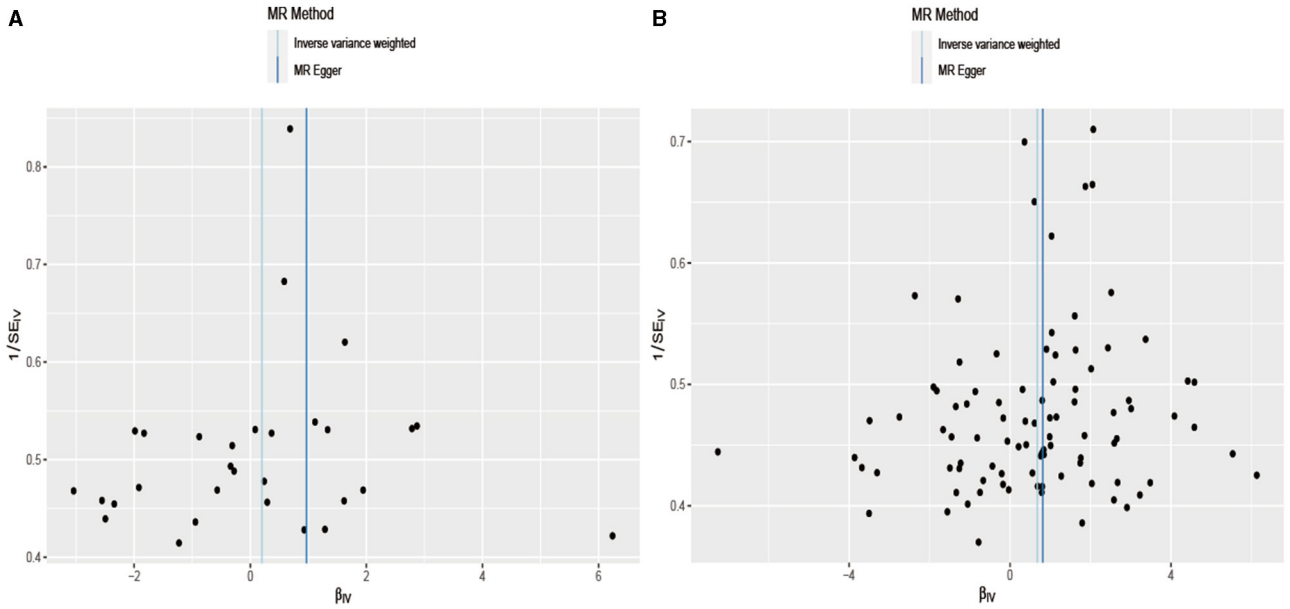

FIGURE 4
In the field of statistical analysis for research validation, a funnel plot is employed to evaluate robustness. Dispersed data points signify the effects estimated through individual SNPs serving as instrumental variables. The vertical lines represent the comprehensive estimates derived from inverse variance weighted estimated and MR-Egger regression, ensuring a through assessment of the data's integrity. **(A)** Drink per week; **(B)** smoking initiation.

health strategies and interventions. Cigarette smoking, a well-established modifiable risk factor, not only contributes to aSAH but also impacts various cardiovascular and cerebrovascular diseases. The causal link identified through the MR analysis suggests that targeted interventions to reduce cigarette smoking could potentially mitigate the risk of aSAH. Public health campaigns, especially focusing on smoking cessation in populations genetically predisposed to higher cigarette use, may significantly reduce the risk of aSAH. The observed dose–response relationship aligned with previous epidemiological evidence, emphasizing the

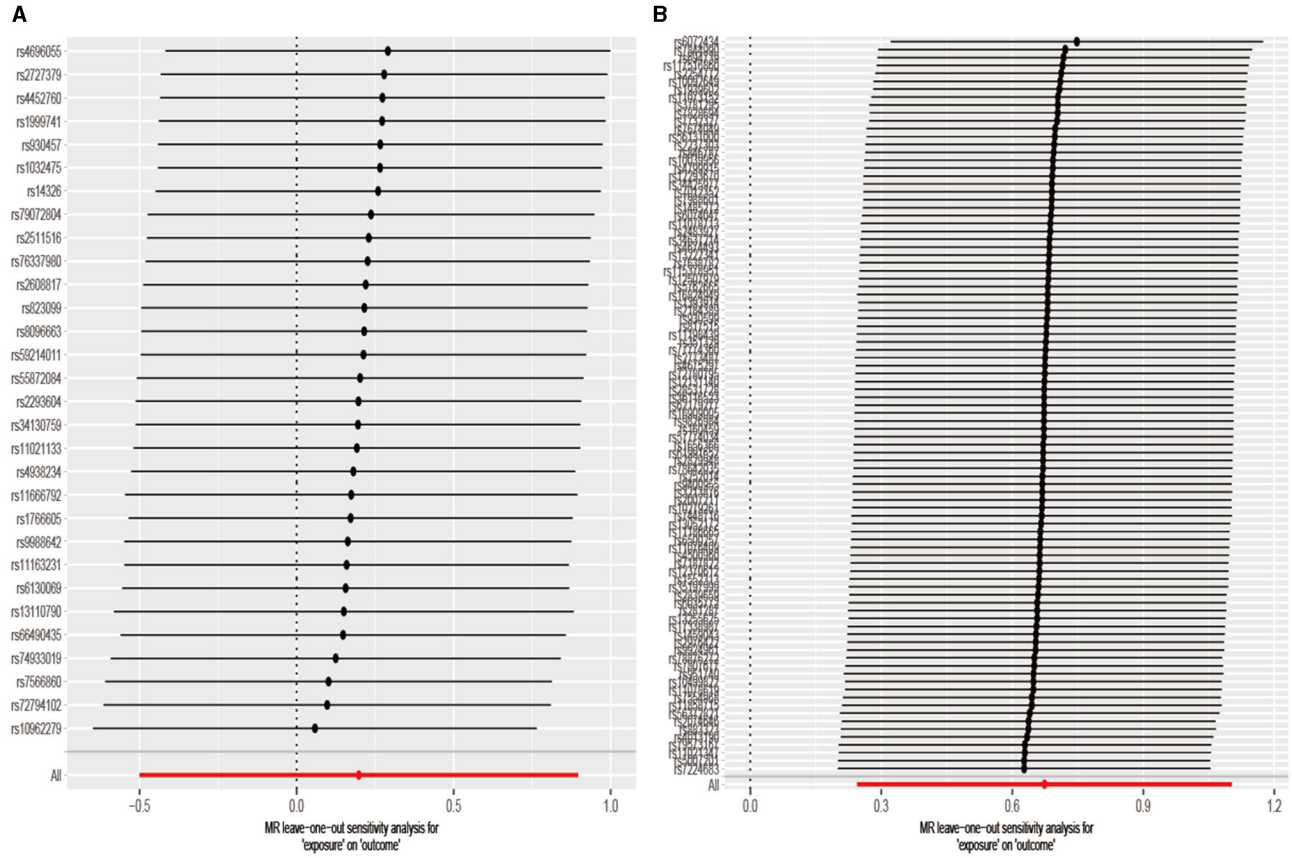

FIGURE 5
The leave-one-out method removes each SNP one by one, and then calculates the meta-effects of the remaining SNPS so as to observe whether the outcome changes significantly after the removal of a specific SNP. If the director of all beta values (>0 or <0) remained consistent, this implied that a positive causal relationship between exposure and outcomes still existed after removing any single SNP. **(A)** Drink per week; **(B)** smoking initiation.

importance of both the prevalence and intensity of smoking in tailoring effective interventions (20, 21). These results, derived from the genotypic data in the general population, are less susceptible to confounding and reverse causation compared to observational studies.

Previous research has demonstrated a dose–response relationship between smoking and SAH, but the mechanisms underlying the increased risk remain unclear. Smoking-induced transient elevations in blood pressure and chronic effects on vessel walls might contribute to aneurysm rupture. The MR results aligned with epidemiological studies, supporting a causal relationship between smoking and aSAH. However, given the complexity of cigarette smoking, the precise mechanisms are not fully understood (22). Animal studies have suggested smoking's impact on hemodynamic stress, hypertension, and vascular fragility, which are all relevant to aSAH risk. Smoking-induced atherosclerosis may affect hemodynamic stress, and a rise in blood pressure and release of enzymes may contribute to vascular fragility. The association persists even after smoking cessation, indicating potential irreversible vascular damage (23–25). Healthcare providers could incorporate genetic information on smoking susceptibility for personalized risk assessments, guiding targeted counseling and interventions. In conclusion, the MR results emphasized cigarette smoking as a causal factor in aSAH, supporting multifaceted interventions for public health.

Alcohol consumption

Contrary to the significant association with cigarette smoking, our two-sample Mendelian randomization (TSMR) study did not reveal a significant causal link between genetically determined alcohol consumption and the risk of aneurysmal subarachnoid hemorrhage (aSAH). Several factors may have contributed to this non-significant association. The impact of alcohol consumption on aSAH risk is complex, being influenced by genetic and environmental factors. The selected genetic variants may not have fully captured these influences, which led to an incomplete representation of the causal relationship. Previous studies have shown significant associations between current and intense alcohol consumption and intracranial aneurysm rupture, but this risk diminishes after cessation (26). Methodological differences in observational studies, population characteristics, and alcohol exposure assessment may contribute to inconsistent findings (27). Mendelian randomization assumes that genetic variants

solely influence the outcome through exposure, but if alternative pathways exist, it may result in a non-significant association. Alcohol flush syndrome, unrelated to alcohol consumption, has been suggested as a potential marker for aSAH risk, indicating the need for further exploration (28).

It is crucial to consider the potential threshold effects or non-linear relationships between alcohol consumption and aSAH risk. The selected genetic variants might have predominantly represented moderate alcohol consumption, while the effects at high or low levels might not have been fully captured. Acknowledging the limitations of the study, including potential population heterogeneity and unaccounted confounders, is essential. In summary, even though the TSMR study did not identify a significant causal association between genetically determined alcohol consumption and aSAH risk, the complexities in alcohol's impact, methodological considerations, and potential limitations should be considered when interpreting the results.

Strengths and weaknesses of the study

The study's strengths include the evaluation of various lifestyle behaviors using data from a large consortium, ensuring a meticulous assessment of aSAH cases. The Mendelian randomization (MR) design mitigates reverse causality and confounding bias (29). Despite potential weak instrumental bias concerns, all exposures in the MR analyses surpassed an F-statistic threshold of 10 in a two-sample setup, minimizing this bias (30). The study employed multiple methods to ensure the robustness of the results, including weighted medians, MR-Egger, and MR-PRESSO, which addressed the issue of multiplicity in the MR analysis (31). Limiting the within-union analyses to individuals of European descent, comparing the cases to the controls at each study center, and adjusting for major components likely mitigated cohort stratification.

However, there were limitations, particularly the statistical power, which impacted the study's robustness. The study exhibited high power for smoking initiation; however, the power for the weaker associations, particularly with alcohol consumption, may have been limited. Future research with larger cohorts is crucial for detecting subtle effects and understanding genetic underpinnings comprehensively. Advancements in genetic research, including the identification of additional variants, may refine instrumental variable selection (32). Integrating multi-omics approaches and emerging genetic databases could offer novel insights into genetic architecture of aSAH. Despite the contributions made through the findings of this study, ongoing research with larger cohorts and advanced methodologies is essential.

Methodological considerations

Mendelian randomization (MR) (33) operates on the principle of utilizing genetic variants (single nucleotide polymorphisms, SNPs) as instrumental variables (IVs) linked to exposures (cigarette smoking and alcohol consumption). This design aligns with Mendel's second law, ensuring random distribution of potential confounders and minimizing confounding bias. The temporal precedence of genetic variants precedes lifestyle behaviors, mitigating reverse causality, which is fundamental for establishing causal relationships. While MR minimizes confounding, it assumes that IVs act exclusively through exposure and are valid instruments. Deviations, such as horizontal pleiotropy, introduce bias. Sensitivity analyses, such as MR-PRESSO and the heterogeneity test address this concern.

Despite its strengths, MR has limitations. Assumptions about IVs' exclusivity and validity rely on the absence of population stratification and pleiotropy. Considering these limitations, caution in interpreting the results is essential. In conclusion, adopting the MR method strengthens causal inference, but it should be interpreted cautiously, recognizing its limitations in advancing the understanding of complex genetic epidemiology relationships.

Data availability statement

The datasets presented in this study can be found in online repositories. The names of the repository/repositories and accession number(s) can be found in the article/Supplementary material.

Ethics statement

The ethical review authority approved the studies included in the published meta-analyses of GWAS study, and participants provided voluntary informed consent. This study solely examined summary-level statistical data that is accessible to the public. Hence, obtaining new approval from an ethical review board was unnecessary. The studies were conducted in accordance with the local legislation and institutional requirements. The participants provided their written informed consent to participate in this study.

Author contributions

HL: Formal analysis, Writing – original draft. YY: Writing – review & editing. JL: Software, Visualization, Writing – original draft. SL: Project administration, Writing – review & editing. XL: Writing – review & editing. ZL: Supervision, Writing – review & editing.

Funding

The author(s) declare that no financial support was received for the research, authorship, and/or publication of this article.

Acknowledgments

The authors would like to thank the ISGC Intracranial Aneurysm working group for their support and the GWAS and Sequencing Consortium of Alcohol and Nicotine use (GSCAN) for providing summary statistics for these analyses.

Conflict of interest

The authors declare that the research was conducted in the absence of any commercial or financial relationships that could be construed as a potential conflict of interest.

Publisher's note

All claims expressed in this article are solely those of the authors and do not necessarily represent those of their affiliated organizations, or those of the publisher, the editors and the reviewers. Any product that may be evaluated in this article, or claim that may be made by its manufacturer, is not guaranteed or endorsed by the publisher.

Supplementary material

The Supplementary Material for this article can be found online at: https://www.frontiersin.org/articles/10.3389/fnut.2024.1397776/full#supplementary-material

References

1. Daou BJ, Koduri S, Thompson BG, Chaudhary N, Pandey AS. Clinical and experimental aspects of aneurysmal subarachnoid hemorrhage. *CNS Neurosci Ther.* (2019) 25:1096–112. doi: 10.1111/cns.13222

2. Claassen J, Park S. Spontaneous subarachnoid haemorrhage. *Lancet.* (2022) 400:846–62. doi: 10.1016/S0140-6736(22)00938-2

3. Sandvei MS, Romundstad PR, Müller TB, Vatten L, Vik A. Risk factors for aneurysmal subarachnoid hemorrhage in a prospective population study: the HUNT study in Norway. *Stroke.* (2009) 40:1958–62. doi: 10.1161/STROKEAHA.108.539544

4. Danaei G, Ding EL, Mozaffarian D, Taylor B, Rehm J, Murray CJ, et al. The preventable causes of death in the United States: comparative risk assessment of dietary, lifestyle, and metabolic risk factors. *PLoS Med.* (2009) 6:e1000058. doi: 10.1371/journal.pmed.1000058

5. Acosta JN, Szejko N, Both CP, Vanent K, Noche RB, Gill TM, et al. Genetically determined smoking behavior and risk of nontraumatic subarachnoid hemorrhage. *Stroke.* (2021) 52:582–7. doi: 10.1161/STROKEAHA.120.031622

6. Lindbohm JV, Kaprio J, Jousilahti P, Salomaa V, Korja M. Sex, smoking, and risk for subarachnoid hemorrhage. *Stroke.* (2016) 47:1975–81. doi: 10.1161/STROKEAHA.116.012957

7. Feigin VL, Rinkel GJ, Lawes CM, Algra A, Bennett DA, van Gijn J, et al. Risk factors for subarachnoid hemorrhage: an updated systematic review of epidemiological studies. *Stroke.* (2005) 36:2773–80. doi: 10.1161/01.STR.0000190838.02954.e8

8. Anderson C, Ni Mhurchu C, Scott D, Bennett D, Jamrozik K, Hankey G, et al. Triggers of subarachnoid hemorrhage: role of physical exertion, smoking, and alcohol in the Australasian Cooperative Research on Subarachnoid Hemorrhage Study (ACROSS). *Stroke.* (2003) 34:1771–6. doi: 10.1161/01.STR.0000077015.90334.A7

9. Carreras-Torres R, Johansson M, Haycock PC, Relton CL, Davey Smith G, Brennan P, et al. Role of obesity in smoking behaviour: Mendelian randomisation study in UK Biobank. *BMJ.* (2018) 361:k1767. doi: 10.1136/bmj.k1767

10. Birney E. Mendelian randomization. *Cold Spring Harb Perspect Med.* (2022) 12:a041302. doi: 10.1101/cshperspect.a041302

11. Zeitoun T, El-Sohemy A. Using Mendelian randomization to study the role of iron in health and disease. *Int J Mol Sci.* (2023) 24:13458. doi: 10.3390/ijms241713458

12. Zeng C, Huang Z, Tao W, Yan L, Tang D, Chen F, et al. Genetically predicted tobacco consumption and risk of intracranial aneurysm: a Mendelian randomization study. *Environ Sci Pollut Res Int.* (2023) 30:12979–87. doi: 10.1007/s11356-022-23074-w

13. Saunders GR, Wang X, Chen F, Jang SK, Liu M, Wang C, et al. Genetic diversity fuels gene discovery for tobacco and alcohol use. *Nature.* (2022) 612:720–4. doi: 10.1038/s41586-022-05477-4

14. Bakker MK, van der Spek RA, van Rheenen W, Morel S, Bourcier R, Hostettler IC, et al. Genome-wide association study of intracranial aneurysms identifies 17 risk loci and genetic overlap with clinical risk factors. *Nat Genet.* (2020) 52:1303–13. doi: 10.1038/s41588-020-00725-7

15. Larsson SC. Mendelian randomization as a tool for causal inference in human nutrition and metabolism. *Curr Opin Lipidol.* (2021) 32:1–8. doi: 10.1097/MOL.0000000000000721

16. Burgess S, Butterworth A, Thompson SG. Mendelian randomization analysis with multiple genetic variants using summarized data. *Genet Epidemiol.* (2013) 37:658–65. doi: 10.1002/gepi.21758

17. Verbanck M, Chen CY, Neale B, Do R. Detection of widespread horizontal pleiotropy in causal relationships inferred from Mendelian randomization between complex traits and diseases. *Nat Genet.* (2018) 50:693–8. doi: 10.1038/s41588-018-0099-7

18. Larsson SC, Traylor M, Malik R, Dichgans M, Burgess S, Markus HS, et al. Modifiable pathways in Alzheimer's disease: Mendelian randomisation analysis. *BMJ.* (2017) 359:j5375. doi: 10.1136/bmj.j5375

19. Levin MG, Judy R, Gill D, Vujkovic M, Verma SS, Bradford Y, et al. Genetics of height and risk of atrial fibrillation: a Mendelian randomization study. *PLoS Med.* (2020) 17:e1003288. doi: 10.1371/journal.pmed.1003288

20. Anderson CS, Feigin V, Bennett D, Lin RB, Hankey G, Jamrozik K, et al. Active and passive smoking and the risk of subarachnoid hemorrhage: an international population-based case-control study. *Stroke.* (2004) 35:633–7. doi: 10.1161/01.STR.0000115751.45473.48

21. Weir BK, Kongable GL, Kassell NF, Schultz JR, Truskowski LL, Sigrest A. Cigarette smoking as a cause of aneurysmal subarachnoid hemorrhage and risk for vasospasm: a report of the Cooperative Aneurysm Study. *J Neurosurg.* (1998) 89:405–11. doi: 10.3171/jns.1998.89.3.0405

22. Shinton R, Beevers G. Meta-analysis of relation between cigarette smoking and stroke. *BMJ.* (1989) 298:789–94. doi: 10.1136/bmj.298.6676.789

23. Handa H, Hashimoto N, Nagata I, Hazama F. Saccular cerebral aneurysms in rats: a newly developed animal model of the disease. *Stroke.* (1983) 14:857–66. doi: 10.1161/01.STR.14.6.857

24. Jungquist G, Hanson BS, Isacsson SO, Janzon L, Steen B, Lindell SE. Risk factors for carotid artery stenosis: an epidemiological study of men aged 69 years. *J Clin Epidemiol.* (1991) 44:347–53. doi: 10.1016/0895-4356(91)90073-I

25. Can A, Castro VM, Ozdemir YH, Dagen S, Yu S, Dligach D, et al. Association of intracranial aneurysm rupture with smoking duration, intensity, and cessation. *Neurology.* (2017) 89:1408–15. doi: 10.1212/WNL.0000000000004419

26. Wiebers DO, Whisnant JP, Huston J, Meissner I, Brown RD, Piepgras DG, et al. Unruptured intracranial aneurysms: natural history, clinical outcome, and risks of surgical and endovascular treatment. *Lancet.* (2003) 362:103–10. doi: 10.1016/S0140-6736(03)13860-3

27. Can A, Castro VM, Ozdemir YH, Dagen S, Dligach D, Finan S, et al. Alcohol consumption and aneurysmal subarachnoid hemorrhage. *Transl Stroke Res.* (2018) 9:13–9. doi: 10.1007/s12975-017-0557-z

28. Chen X, Gui S, Deng D, Dong L, Zhang L, Wei D, et al. Alcohol flushing syndrome is significantly associated with intracranial aneurysm rupture in the Chinese Han population. *Front Neurol.* (2023) 14:1118980. doi: 10.3389/fneur.2023.1118980

29. Lawlor DA, Harbord RM, Sterne JA, Timpson N, Davey Smith G. Mendelian randomization: using genes as instruments for making causal inferences in epidemiology. *Stat Med.* (2008) 27:1133–63. doi: 10.1002/sim.3034

30. Pierce BL, Burgess S. Efficient design for Mendelian randomization studies: subsample and 2-sample instrumental variable estimators. *Am J Epidemiol.* (2013) 178:1177–84. doi: 10.1093/aje/kwt084

31. Burgess S, Davey Smith G, Davies NM, Dudbridge F, Gill D, Glymour MM, et al. Guidelines for performing Mendelian randomization investigations: update for summer 2023. *Wellcome Open Res.* (2023) 4:186. doi: 10.12688/wellcomeopenres.15555.3

32. Lawlor DA, Benfield L, Logue J, Tilling K, Howe LD, Fraser A, et al. Association between general and central adiposity in childhood, and change in these, with cardiovascular risk factors in adolescence: prospective cohort study. *BMJ.* (2010) 341:c6224. doi: 10.1136/bmj.c6224

33. Gage SH, Davey Smith G, Ware JJ, Flint J, Munafò MR, G. = E: What GWAS can tell us about the environment. *PLoS Genet.* (2016) 12:e1005765. doi: 10.1371/journal.pgen.1005765

frontiers | Frontiers in Nutrition

TYPE Original Research
PUBLISHED 18 September 2024
DOI 10.3389/fnut.2024.1410431

OPEN ACCESS

EDITED BY
Adriana Ximenes-da-Silva,
Federal University of Alagoas, Brazil

REVIEWED BY
Yanyao Liu,
The First Affiliated Hospital of Chongqing Medical University, China
Qin Hu,
Shanghai Jiao Tong University, China

*CORRESPONDENCE
Sheng Li
✉ 420648161@qq.com

RECEIVED 01 April 2024
ACCEPTED 03 September 2024
PUBLISHED 18 September 2024

CITATION
Qin L, Cao X, Huang T, Liu Y and Li S (2024) Identification of potential biomarkers of cuproptosis in cerebral ischemia. *Front. Nutr.* 11:1410431. doi: 10.3389/fnut.2024.1410431

Identification of potential biomarkers of cuproptosis in cerebral ischemia

Lihua Qin[1,2], Xi Cao[1], Tengjia Huang[1], Yixin Liu[1] and Sheng Li[2]*

[1]School of Nursing, Hunan University of Chinese Medicine, Changsha, Hunan, China, [2]Key Laboratory of Hunan Province for Prevention and Treatment of Integrated Traditional Chinese and Western Medicine on Cardiocerebral Diseases, Hunan University of Chinese Medicine, Changsha, Hunan, China

Objective: Cerebral ischemia can cause mild damage to local brain nerves due to hypoxia and even lead to irreversible damage due to neuronal cell death. However, the underlying pathogenesis of this phenomenon remains unclear. This study utilized bioinformatics to explore the role of cuproptosis in cerebral ischemic disease and its associated biomarkers.

Method: R software identified the overlap of cerebral ischemia and cuproptosis genes, analyzed Gene Ontology (GO) and Kyoto Encyclopedia of Genes and Genomes (KEGG), and explored hub genes. Expressions and localizations of hub genes in brain tissue, cells, and immune cells were analyzed, along with predictions of protein structures, miRNAs, and transcription factors. A network was constructed depicting hub gene co-expression with miRNAs and interactions with transcription factors. Ferredoxin 1 (*FDX1*) expression was determined using qRT-PCR.

Results: Ten cuproptosis-related genes in cerebral ischemia were identified, with GO analysis revealing involvement in acetyl-CoA synthesis, metabolism, mitochondrial function, and iron–sulfur cluster binding. KEGG highlighted processes like the tricarboxylic acid cycle, pyruvate metabolism, and glycolysis/gluconeogenesis. Using the Human Protein Atlas, eight hub genes associated with cuproptosis were verified in brain tissues, hippocampus, and AF22 cells. Lipoyl(octanoyl) transferase 1 (*LIPT1*), was undetected, while others were found in mitochondria or both nucleus and mitochondria. These genes were differentially expressed in immune cells. *FDX1*, lipoic acid synthetase (*LIAS*), dihydrolipoamide *S*-acetyltransferase (*DLAT*), pyruvate dehydrogenase E1 component subunit alpha 1 (*PDHA1*), *PDHB*, and glutaminase (*GLS*) were predicted to target 111 miRNAs. *PDHA1*, *FDX1*, *LIPT1*, *PDHB*, *LIAS*, *DLAT*, *GLS*, and dihydrolipoamide dehydrogenase (*DLD*) were predicted to interact with 11, 10, 10, 9, 8, 7, 5, and 4 transcription factors, respectively. Finally, FDX1 expression was significantly upregulated in the hippocampus of ovariectomized rats with ischemia.

Conclusion: This study revealed an association between cerebral ischemic disease and cuproptosis, identifying eight potential target genes. These findings offer new insights into potential biomarkers for the diagnosis, treatment, and prognosis of cerebral ischemia, and provide avenues for the exploration of new medical intervention targets.

KEYWORDS

cerebral ischemia, cuproptosis, biomarkers, gene expression, bioinformatics

Background

Cerebral ischemia involves complex pathophysiological processes in cells, such as oxidative stress, calcium overload, mitochondrial damage, and excitatory amino acid toxicity. These processes can activate cell death pathways, including apoptosis, programmed necrosis, autophagy, ferroptosis, and pyroptosis (1, 2). Recently, copper-induced cell death, termed cuproptosis, has been established as a novel form of cell death, differing from other programmed cell death mechanisms. Cuproptosis is induced by the binding of copper ions to thioacylated proteins in the tricarboxylic acid (TCA) cycle. This binding leads to abnormal oligomerization of thioacylated proteins, downregulation of Fe-S cluster protein levels, protein toxicity stress, and ultimately cell death (3).

Previous studies have demonstrated that copper ions are involved in the onset and progression of ischemic stroke (IS) (4, 5). Furthermore, plasma copper levels are positively correlated with the risk of initial IS (6, 7), and elevated plasma copper levels are significantly associated with an increased risk of IS (8). These findings underscore the importance of better understanding the relationship between cerebral ischemia and cuproptosis. However, cuproptosis biomarkers in cerebral ischemia have not been fully characterized. Therefore, this study aimed to investigate the hub genes and biomarkers related to cuproptosis in cerebral ischemia using bioinformatics. Furthermore, the research has not only preliminarily validated through Human Protein Atlas (HPA), but also further experimentally validated in model animals to ensure the accuracy and reliability of the research conclusions.

Methods

Intersection of cerebral ischemia and cuproptosis datasets

Select "Diseases" through keyword search, enter "cerebral ischemia," and click search, cerebral ischemia-related genes were downloaded from the Comparative Toxicogenomics Database (CTD).[1] Ten genes associated with cuproptosis, namely ferredoxin 1 (*FDX1*), lipoyl(octanoyl) transferase 1 (*LIPT1*), lipoic acid synthetase (*LIAS*), dihydrolipoamide dehydrogenase (*DLD*), metal regulatory transcription factor 1 (*MTF1*), dihydrolipoamide S-acetyltransferase (*DLAT*), pyruvate dehydrogenase E1 component subunit alpha 1 (*PDHA1*), *PDHB*, glutaminase (*GLS*), and cyclin-dependent kinase inhibitor 2A (*CDKN2A*), were identified in a previous study by Tsvetkov et al. (3). The genes obtained from both datasets were intersected and visualized using jvenn online tool.[2]

Gene Ontology (GO)/Kyoto Encyclopedia of Genes and Genomes (KEGG) analyses

The GO/KEGG analyses were performed using clusterProfiler (4.4.4) packages in R (4.2.1) software. The ID conversion of the input molecular lists was converted via the org.Hs.eg.db package in the ID conversion library (9). Enrichment analysis and visualization were performed using the ggplot2 (3.3.6), igraph (1.4.1), and ggraph packages (2.1.0) (10).

Hub gene analysis

Protein interactions were analyzed using the STRING Database (Search Tool for the Retrieval of Interacting Genes/Proteins; version 11.0, http://string-db.org) (11). The gene cluster was analyzed using the maximum clique centrality and degree methods (MCODE) plug-in of the Cytoscape software (3.7.2). The full names and descriptions of the hub genes were extracted from Gene Cards.[3]

Expression, localization, and protein structure of hub genes in brain tissues, brain cells, and immune cells

The expression of hub genes was verified using the HPA online database in brain tissues, human neuroepithelial stem cells (AF22 cells), and immune cells.[4] Subcellular localization of hub genes and prediction of their protein structure are shown. Regarding the confidence of the predicted protein structure, deep blue is used to indicate very high confidence (pLDDT >90), light blue is used to indicate high confidence (90 > pLDDT >70), yellow is used to indicate low confidence (70 > pLDDT >50), and orange is used to indicate very low confidence (pLDDT <50) (see Footnote 4).

Co-expression network of hub genes and micro RNAs (miRNAs)

The target miRNAs associated with hub genes related to cuproptosis were predicted using the miRTarBas9.0 database,[5] and two validation methods were selected to verify the predicted target miRNAs. Subsequently, a co-expression network was constructed using Cytoscape software.

Transcription factor (TF)–gene interactions

The TFs of hub genes related to cuproptosis were searched using the NetworkAnalyst database.[6] The JASPAR database[7] was selected as the TF and gene interaction database, and the interaction relationships were visualized using the JASPAR database (see Footnote 7).

1 http://ctdbase.org/
2 https://jvenn.toulouse.inrae.fr/app/index.html
3 http://www.genecards.org
4 https://www.proteinatlas.org/
5 https://mirtarbase.cuhk.edu.cn/~miRTarBase/miRTarBase_2022/php/index.php
6 https://www.networkanalyst.ca/
7 https://www.networkanalyst.ca/NetworkAnalyst/home.xhtml

Quantitative real-time polymerase chain reaction (qRT-PCR)

Previous studies on cerebral ischemia often used male rats to minimize estrogen influence. However, the soaring incidence of IS among postmenopausal women (12), with enlarged infarction and aggravated brain damage in ovariectomized rats (13), poses a critical threat. Our study employed female rats with ovariectomy followed by cerebral ischemia induction for animal experimentation.

According to body weight, 8-week-old female SD rats were randomly divided into sham and model groups, each group with three rats. Rats were adapted to an SPF environment at the Experimental Animal Center of Hunan University of Chinese Medicine for 1 week. Referring to previous literature (14), the ovariectomy was performed and the cerebral ischemia model was prepared, the specific steps are as follows: the rats were fasted for 12 h before surgery and anesthetized with 2% pentobarbital sodium via intraperitoneal injection. The model group rats quickly made approximately 3 cm incisions on both sides of their backs under sterile conditions, and after tightening the fallopian tubes, the ovaries were removed and the incisions were sutured. The back skin of rats in the sham group was cut open, bilateral ovaries were separated, and then directly sutured. After surgery, rats were administered with 160,000 units of penicillin via intraperitoneal injection daily for a total of 3 days. Starting from the 5th day post-surgery, vaginal smears were collected from the rats once daily for a total of 5 days. The success of modeling was determined by the absence of an estrous cycle response during this period. Starting from the 5th day after surgery, vaginal secretion smears from rats were taken for smear testing once a day for a total of 5 days, and the successful modeling was considered as no occurrence of estrous cycle reactions. After the successful ovariectomy model in rats, fasting for 12 h was performed. On the 12th day post-surgery, they were anesthetized by intraperitoneal injection of 2% pentobarbital sodium. A midline incision was made on the neck, blunt dissection was performed, and the right common carotid artery was exposed. The internal and external carotid arteries were separated, and the proximal and distal ends of the external carotid artery were ligated. A monofilament nylon suture was inserted into the internal carotid artery to a depth of (18.5 ± 0.5) mm until slight resistance was felt, and then the suture was fixed. The incision was sutured layer by layer. Neurological function was assessed using the Longa score 24 h after cerebral ischemia, with scores of 1 to 3 indicating a successful model. The skin of the rats in the sham surgery group was cut open, and the right common carotid artery was separated, and sutured.

After successful modeling, the rats were anesthetized via intraperitoneal injection of 2% pentobarbital sodium and sacrificed, and their hippocampal tissue was collected. Total RNA was extracted and synthesized into cDNA using the total RNA Extraction Kit (Jiangsu Cowin Biotech Co., Ltd., CW0581S) and qRT-PCR. The expression of *FDX1* was assessed using the $2^{-\Delta\Delta Ct}$ method (forward: AAGAACCGAGATGGTGAAAC, reverse: AGAGCAAGCCAAAG TCCC, 126 bp).

Statistical analysis

The data calculations and statistical analysis were performed using IBM SPSS Statistics 25.0. Independent sample *t*-test was used for intergroup comparisons ($p < 0.05$).

Results

The flowchart of this study was shown in Figure 1.

GO and KEGG enrichment analyses for cuproptosis genes in cerebral ischemia

Ten genes (*FDX1*, *LIPT1*, *LIAS*, *DLD*, *MTF1*, *DLAT*, *PDHA1*, *PDHB*, *GLS*, and *CDKN2A*) associated with cuproptosis were intersected with genes related to brain ischemia, revealing that all 10 genes were brain ischemia-related genes (refer to Figure 2).

The significance cut-off value for the GO/KEGG analyses was set at a corrected *p*-value (*p*.adj) of <0.05. The results of the identified biological processes (BPs), cellular components (CCs), and molecular functions (MFs) were 81, 6, and 15, respectively. KEGG analysis revealed enrichment in 8 pathways. The top 5 GO and KEGG pathways are presented in Tables 1, 2, as well as Figure 3.

Enriched BPs included acetyl-CoA biosynthetic process from pyruvate, acetyl-CoA metabolic process, acetyl-CoA metabolic process, acetyl-CoA biosynthetic process, acetyl-CoA biosynthetic process, and thioester biosynthetic process. CCs encompassed various complexes, such as mitochondrial matrix, oxidoreductase complex, mitochondrial protein-containing complex, mitochondrial tricarboxylic acid cycle enzyme complex, and tricarboxylic acid cycle enzyme complex. MFs included activities such as oxidoreductase activity, acting on the aldehyde or oxo group of donors, NAD or NADP as acceptor, oxidoreductase activity, acting on the aldehyde or oxo group of donors, iron–sulfur cluster binding, metal cluster binding, and sulfurtransferase activity. Moreover, KEGG analysis revealed involvement in processes such as pyruvate metabolism, citrate cycle (TCA cycle), carbon metabolism, glycolysis/gluconeogenesis, and central carbon metabolism in cancer.

Cuproptosis-related hub gene identification and their expression in the brain

Eight hub genes (*FDX1*, *LIPT1*, *LIAS*, *DLD*, *PDHA1*, *DLAT*, *PDHB*, and *GLS*) were identified as potential core targets of cerebral ischemia (Figure 4A and Table 3). Using the HPA database (see footnote 4), the expression of the hub genes was analyzed in brain tissues, revealing that these genes associated with cuproptosis were expressed in various regions of the human brain, such as the cortex, hippocampus, amygdala, basal ganglia, thalamus, hypothalamus, midbrain, white matter of the spinal cord, and other areas (Figure 4B). Furthermore, these genes were expressed in specific regions within the internal structure of the hippocampus (Figure 4C).

In human neuroepithelial stem cells (AF22 cells) from the HPA database, *PDHA1* exhibited the highest expression, followed by *PDHB*, *DLD*, *GLS*, *DLAT*, and *FDX1*. In contrast, *LIAS* and *LIPT1* exhibited the lowest expression levels (Figure 4D).

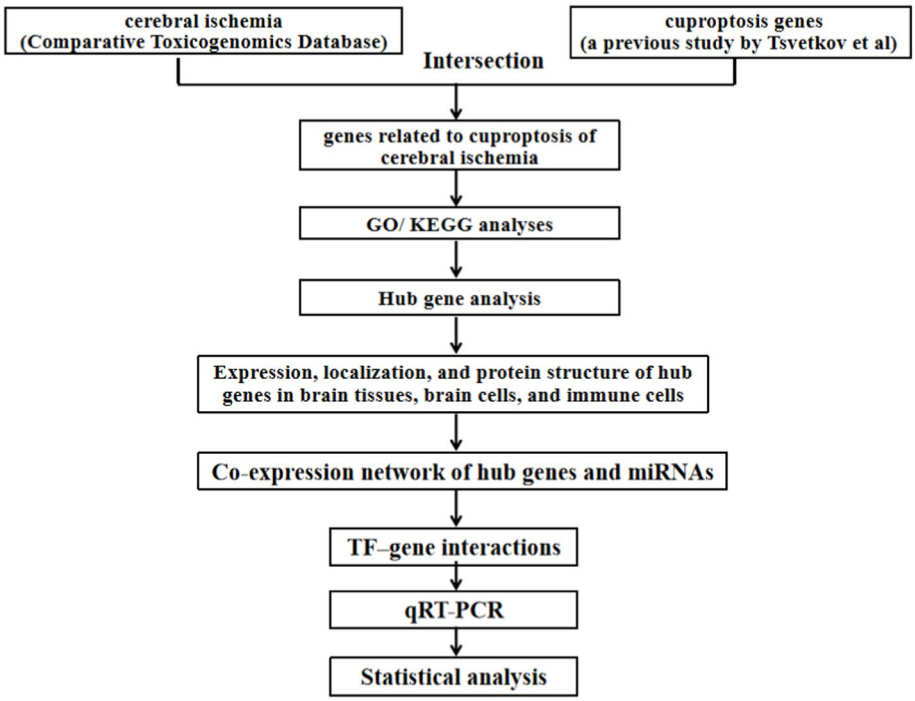

FIGURE 1
Flowchart of this study.

Subcellular localization and structural prediction of cuproptosis-related hub gene

The subcellular localization results indicated that *FDX1*, *DLAT*, *PDHA1*, and *GLS* were detected only in the mitochondria, whereas *LIAS*, *DLD*, and *PDHB* were detected in both the nucleus and mitochondria (Figure 5). The predicted structure diagrams of the hub genes and predicted structures of variant populations are shown in Figures 6A,B, respectively.

Expression of cuproptosis-related hub genes in immune cells

The RNA expression data from the immune cells of the HPA database[8] revealed that *FDX1* exhibited the highest expression in B cells. In contrast, *LIAS*, *LIPT1*, and *GLS* exhibited the highest expression in T cells, *DLAT* and *DLD* in granulocytes, *PDHA1* in monocytes, and *PDHB* in dendritic cells. *FDX1* and *GLS* exhibited the lowest expression levels in peripheral blood mononuclear cells (PBMCs), *LIAS* and *PDHB* in granulocytes, *LIPT1* in dendritic cells, *PDHA1* in T cells, *DLD* in B cells, and *DLAT* in natural killer (NK) cells. Moreover, *FDX*1 and *DLAT* exhibited the lowest expression levels in granulocytes, and *GLS* in monocytes, B cells, NK cells, total PBMC, and dendritic cells (Figure 7A).

8 https://www.proteinatlas.org/humanproteome/immune+cell

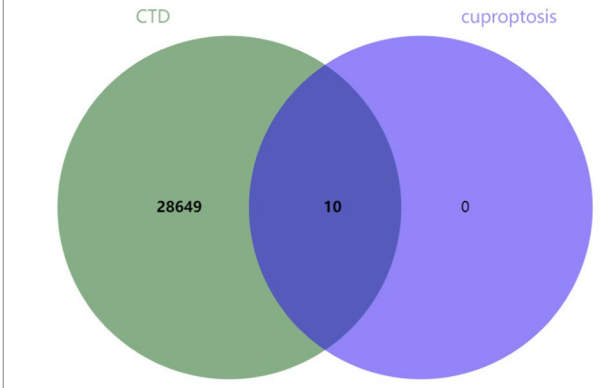

FIGURE 2
Common genes in cerebral ischemia and cuproptosis.

In granulocytes, *FDX1*, *LIAS*, *LIPT1*, *DLD*, and *PDHB* exhibited the highest expression in eosinophils, whereas *PDHA1*, *DLAT*, and *GLS* genes were most highly expressed in basophils (Figure 7B). In monocytes, *FDX1*, *DLAT*, and *DLD* were most highly expressed in non-classical monocytes, *LIPT1* was most highly expressed in classical monocytes, and *LIAS,GLS*, *PDHA1*, *LIAS*, and *PDHB* were most highly expressed in intermediate monocytes (Figure 7C). In T cells, *FDX1*, *DLAT*, and *PDHB* were most highly expressed in T regulatory cells (T-regs), *LIAS* and *LIPT1* in naive CD4 T cells, *DLD* in memory CD8 T cells, and *GLS* and *PDHA1* in mucosal-associated invariant (MAIT) T cells (Figure 7D). In B cells, except for *DLD* and *GLS*, which exhibited the highest expression in naive B cells, the remaining

TABLE 1 Biological process, cellular composition, and molecular function analysis results for genes related to cuproptosis in cerebral ischemia.

Ontology	ID	Description	GeneRatio	BgRatio	*p*-value	*p*.adjust	geneID
BP	GO:0006086	Acetyl-CoA biosynthetic process from pyruvate	4/10	11/18800	1.33e-11	2.53e-09	DLAT/PDHB/DLD/PDHA1
BP	GO:0006085	Acetyl-CoA biosynthetic process	4/10	18/18800	1.23e-10	1.17e-08	DLAT/PDHB/DLD/PDHA1
BP	GO:0006084	Acetyl-CoA metabolic process	4/10	33/18800	1.64e-09	1.04e-07	DLAT/PDHB/DLD/PDHA1
BP	GO:0035384	Thioester biosynthetic process	4/10	45/18800	5.95e-09	2.26e-07	DLAT/PDHB/DLD/PDHA1
BP	GO:0071616	Acyl-CoA biosynthetic process	4/10	45/18800	5.95e-09	2.26e-07	DLAT/PDHB/DLD/PDHA1
CC	GO:0005759	Mitochondrial matrix	8/10	473/19594	4.69e-12	3.75e-11	DLAT/PDHB/GLS/LIPT1/FDX1/DLD/LIAS/PDHA1
CC	GO:1990204	Oxidoreductase complex	4/10	120/19594	2.73e-07	1.09e-06	DLAT/PDHB/DLD/PDHA1
CC	GO:0098798	Mitochondrial protein-containing complex	4/10	281/19594	8.12e-06	2.17e-05	DLAT/PDHB/DLD/PDHA1
CC	GO:0030062	Mitochondrial tricarboxylic acid cycle enzyme complex	1/10	11/19594	0.0056	0.0112	DLD
CC	GO:0045239	Tricarboxylic acid cycle enzyme complex	1/10	16/19594	0.0081	0.0130	DLD
MF	GO:0016620	Oxidoreductase activity, acting on the aldehyde or oxo group of donors, NAD or NADP as acceptor	4/10	38/18410	3.21e-09	1.06e-07	DLAT/PDHB/DLD/PDHA1
MF	GO:0016903	Oxidoreductase activity, acting on the aldehyde or oxo group of donors	4/10	46/18410	7.08e-09	1.17e-07	DLAT/PDHB/DLD/PDHA1
MF	GO:0051536	Iron–sulfur cluster binding	2/10	67/18410	0.0006	0.0048	FDX1/LIAS
MF	GO:0051540	Metal cluster binding	2/10	67/18410	0.0006	0.0048	FDX1/LIAS
MF	GO:0016783	Sulfurtransferase activity	1/10	10/18410	0.0054	0.0269	LIAS

TABLE 2 Kyoto Encyclopedia of Genes and Genomes analysis results for genes related to cuproptosis in cerebral ischemia.

Ontology	ID	Description	GeneRatio	BgRatio	*p*-value	*p*.adjust	geneID
KEGG	hsa00020	Citrate cycle (TCA cycle)	4/8	30/8164	1.03e-08	3.8e-07	DLAT/DLD/DLST/PDHA1/PDHB
KEGG	hsa00620	Pyruvate metabolism	4/8	47/8164	6.64e-08	1.23e-06	DLAT/DLD/DLST/GCSH/PDHA1/PDHB
KEGG	hsa00010	Glycolysis/Gluconeogenesis	4/8	67/8164	2.83e-07	3.49e-06	DLAT/DLD/PDHA1/PDHB
KEGG	hsa01200	Carbon metabolism	4/8	115/8164	2.5e-06	2.32e-05	DLAT/DLD/PDHA1/PDHB
KEGG	hsa05230	Central carbon metabolism in cancer	3/8	70/8164	3.28e-05	0.0002	GLS/PDHA1/PDHB

six genes were most highly expressed in memory B cells (Figure 7E). In dendritic cells (DCs), except for *GLS*, which was most highly expressed in plasmacytoid DCs, and *LIPT1*, which was equally expressed in myeloid DCs and plasmacytoid DCs, all other genes were most highly expressed in myeloid DCs (Figure 7F).

Co-expression network of hub genes and miRNAs

The miRNA targets of the eight cuproptosis-related hub genes were predicted using the miRTarBas9.0 database. Among these genes, six, including *FDX1*, *LIAS*, *DLAT*, *PDHA1*, *PDHB*, and *GLS*, were

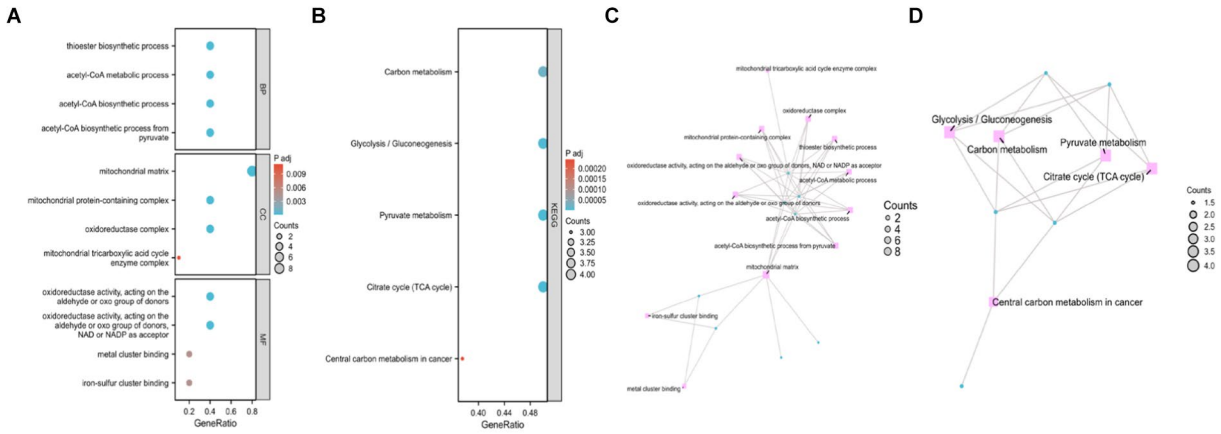

FIGURE 3
Gene Ontology (GO) and Kyoto Encyclopedia of Genes and Genomes (KEGG) enrichment analyses of genes related to cuproptosis in cerebral ischemia. **(A)** Bubble Chart of top four enriched biological process (BP) terms, cellular components (CCs), and molecular function (MF) terms for genes related to cuproptosis on cerebral ischemia. **(B)** Bubble Chart of top five KEGG pathways for genes related to cuproptosis in cerebral ischemia. **(C)** Network diagram of top four enriched BP, (CC), and MF terms for genes related to cuproptosis in cerebral ischemia. **(D)** Network diagram of five KEGG pathways of genes related to cuproptosis in cerebral ischemia.

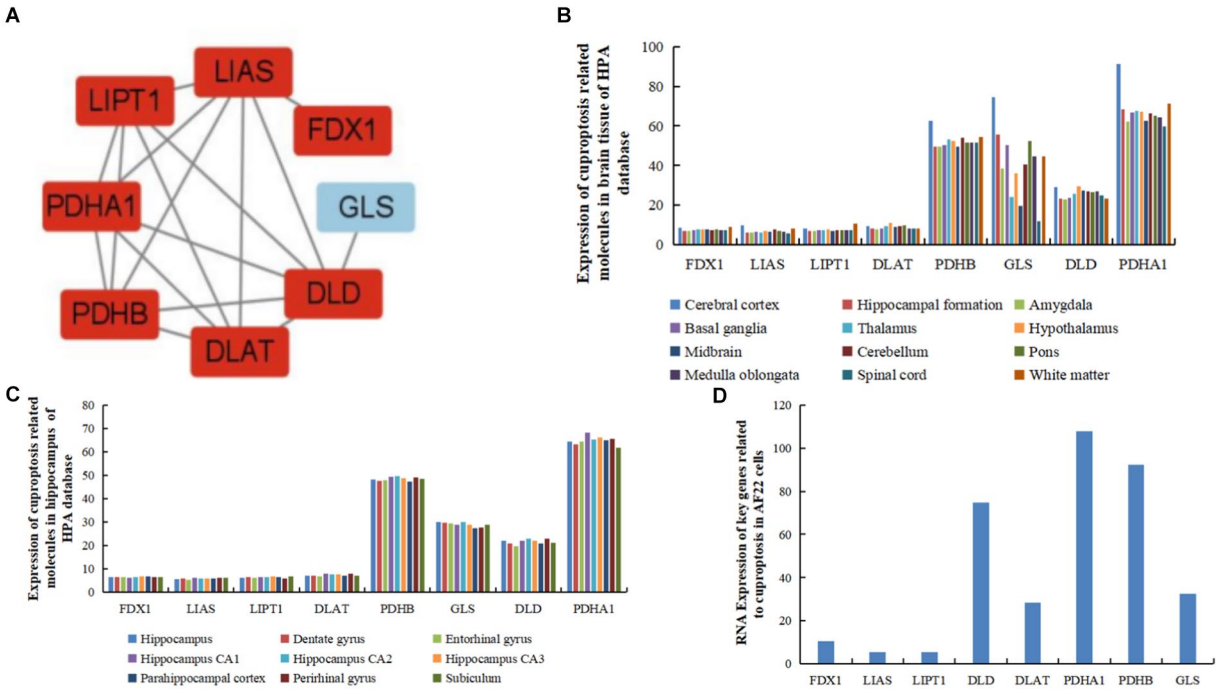

FIGURE 4
Expression of hub genes related to cuproptosis and cerebral ischemia in brain tissues, and human and AF22 cells. **(A)** Hub genes of genes related to cuproptosis in cerebral ischemia identified using MCODE. **(B)** Expression of hub genes related to cuproptosis in brain tissues in the HPA database. **(C)** Expression of hub genes related to cuproptosis in the hippocampus in the HPA database. **(D)** RNA Expression of hub genes related to cuproptosis in human neuroepithelial stem cells (AF22 cells).

predicted to target 111 miRNAs. A co-expression network was then constructed using Cytoscape software, as shown in Figure 8A.

TF–gene interactions

Analysis of TF and gene interactions using the NetworkAnalyst database revealed that *PDHA1*, *FDX1*, *LIPT1*, *PDHB*, *LIAS*, *DLAT*, *GLS*, and *DLD* interact with 11, 10, 10, 9, 8, 7, 5, and 4 TFs, respectively. These interactions are visualized in Figure 8B.

Expression level of *FDX1*

To further validate the aforementioned results, the expression of *FDX1* was determined through qRT-PCR. Compared to that in the

TABLE 3 Details of the hub genes related to cuproptosis in cerebral ischemia.

Gene symbol	Full name	Description
FDX1	Ferredoxin 1	This gene encodes a small iron–sulfur protein that transfers electrons from NADPH through ferredoxin reductase to mitochondrial cytochrome P450, involved in steroid, vitamin D, and bile acid metabolism.
LIAS	Lipoic acid synthetase	The protein encoded by this gene belongs to the biotin and lipoic acid synthetases family. Localized in the mitochondrion, this iron–sulfur enzyme catalyzes the final step in the *de novo* pathway for the biosynthesis of lipoic acid, a potent antioxidant.
LIPT1	Lipoyltransferase 1	The process of transferring lipoic acid to proteins is a two-step process. The first step is the activation of lipoic acid by lipoate-activating enzyme to form lipoyl-AMP. For the second step, the protein encoded by this gene transfers the lipoyl moiety to apoproteins. Alternative splicing results in multiple transcript variants.
DLD	Dihydrolipoamide dehydrogenase	This gene encodes a member of the class-I pyridine nucleotide-disulfide oxidoreductase family. The encoded protein has been identified as a moonlighting protein based on its ability to perform mechanistically distinct functions.
DLAT	Dihydrolipoamide *S*-acetyltransferase	This gene encodes component E2 of the multi-enzyme pyruvate dehydrogenase complex (PDC). PDC resides in the inner mitochondrial membrane and catalyzes the conversion of pyruvate to acetyl coenzyme A.
PDHA1	Pyruvate dehydrogenase E1 subunit alpha 1	The pyruvate dehydrogenase (PDH) complex is a nuclear-encoded mitochondrial multienzyme complex that catalyzes the overall conversion of pyruvate to acetyl-CoA and CO(2), and provides the primary link between glycolysis and the tricarboxylic acid (TCA) cycle.
PDHB	Pyruvate dehydrogenase E1 subunit beta	The pyruvate dehydrogenase (PDH) complex is a nuclear-encoded mitochondrial multienzyme complex that catalyzes the overall conversion of pyruvate to acetyl-CoA and carbon dioxide, and provides the primary link between glycolysis and the tricarboxylic acid (TCA) cycle.
GLS	Glutaminase	This gene encodes the K-type mitochondrial glutaminase. The encoded protein is an phosphate-activated amidohydrolase that catalyzes the hydrolysis of glutamine to glutamate and ammonia.

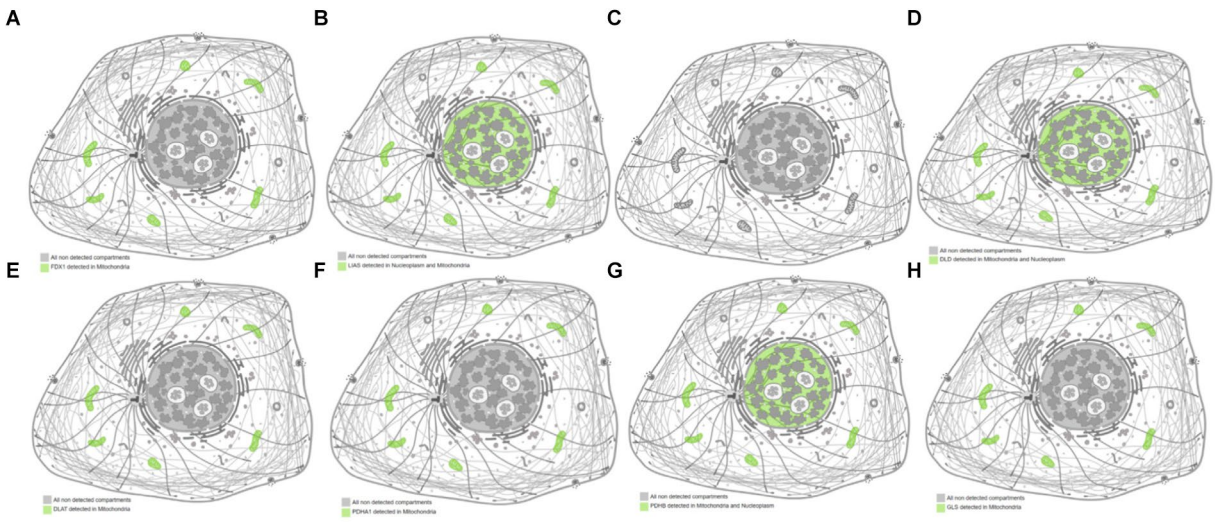

FIGURE 5
Subcellular localization of hub genes related to cuproptosis and cerebral ischemia. **(A)** FDX1; **(B)** LIAS; **(C)** LIPT1; **(D)** DLD; **(E)** DLAT; **(F)** PDHA1; **(G)** PDHB; **(H)** GLS.

sham group (1.68 ± 0.53), *FDX* expression in the hippocampus of ovariectomized rats with ischemia (5.05 ± 0.03) was significantly upregulated ($t = -15.58$, $p = 0.00$), with 95% confidence interval for the difference (−3.84, −2.88).

Discussion

Copper is essential for metal signaling regulation, metal allosteric regulation, mitochondrial respiration, antioxidant defense, and neurotransmitter function, also influencing cell fate through metabolic reprogramming (15, 16). Recent studies have revealed that abnormal accumulation of copper ions in human cells induces a distinct form of cell death, distinct from known regulated cell death mechanisms. Copper ions could still trigger cell death even when known cell death modes such as apoptosis, pyroptosis, ferroptosis, and necrotic apoptosis are blocked, relying on mitochondrial respiration (3).

This study identified *FDX1*, *LIAS*, *LIPT1*, *DLD*, *DLAT*, *PDHA1*, *PDHB*, and *GLS* as eight hub genes associated with cuproptosis in cerebral ischemia. Expression analysis in the HPA database revealed that these hub genes were expressed in the hippocampus, amygdala, basal ganglia, thalamus, hypothalamus, midbrain, spinal cord white

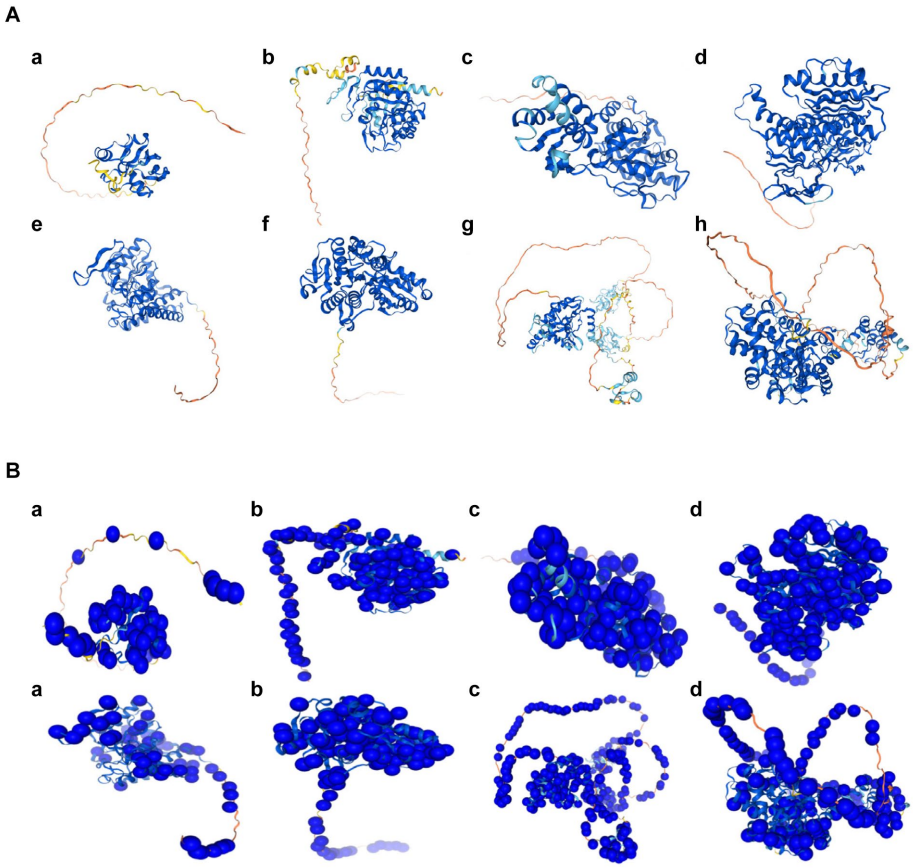

FIGURE 6
The predicted structures of hub genes related to cuproptosis of cerebral ischemia. **(A)** The predicted structure diagrams, colored based on the confidence score per residue (pLDDT); dark blue represents the highest confidence level, and orange represents the lowest confidence level. a, FDX1; b, LIAS; c, LIPT1; d, DLD; e, PDHA1; f, PDHB; g, *DLAT*; h, GLS. **(B)** The predicted structures of the variable populations. a, FDX1; b, LIAS; c, LIPT1; d, DLD; e, PDHA1; f, PDHB; g, DLAT; h, GLS.

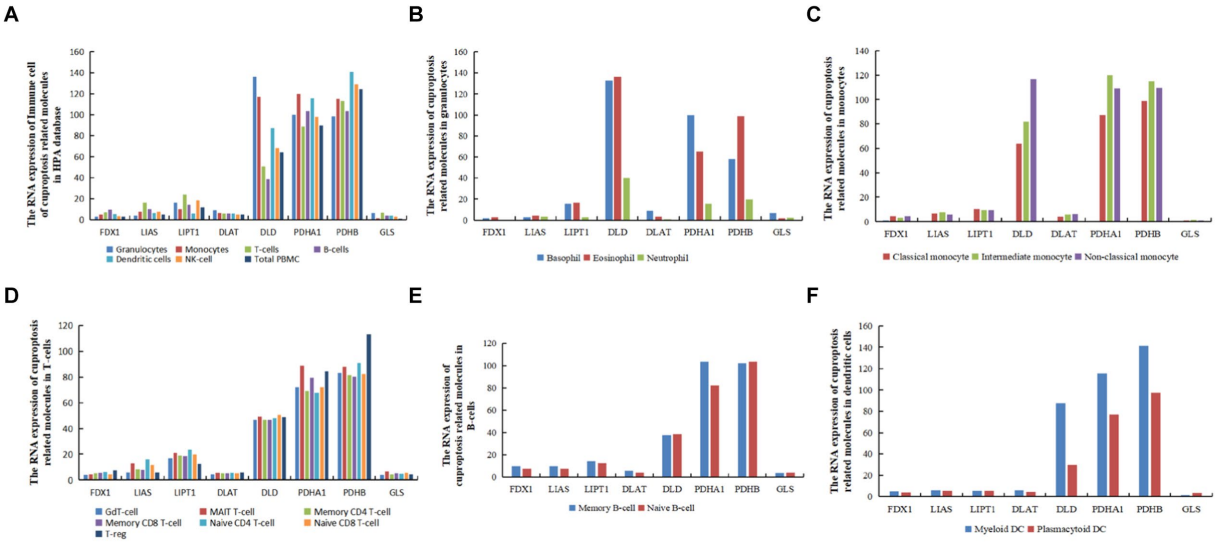

FIGURE 7
The RNA levels of hub genes related to cuproptosis and cerebral ischemia in immune cells in the HPA database (nTPM, transcripts per million). **(A)** The RNA expression of immune cell of cuproptosis related molecules in HPA database. **(B)** The RNA expression of cuproptosis related molecules in granulocytes. **(C)** The RNA expression of cuproptosis related molecules in monocytes. **(D)** The RNA expression of cuproptosis related molecules in T-cells. **(E)** The RNA expression of cuproptosis related molecules in dendritic B-cells. **(F)** The RNA expression of cuproptosis related molecules in dendritic cells.

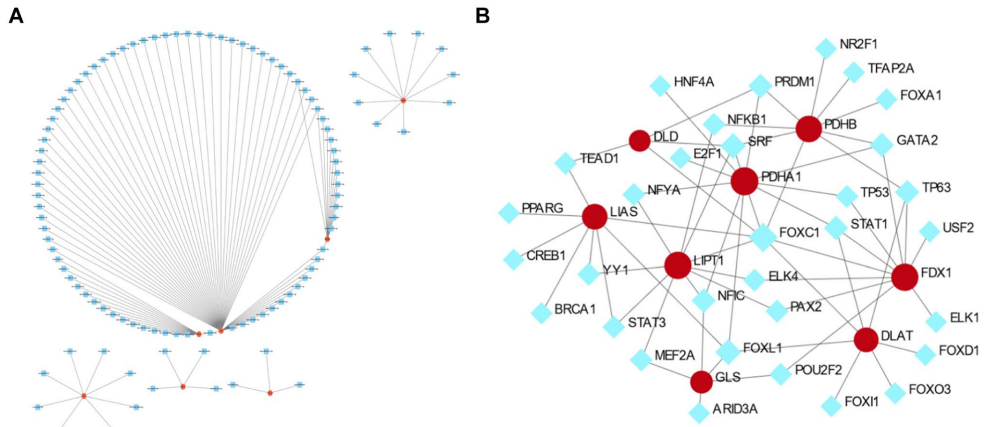

FIGURE 8
The co-expression network of mRNA–microRNA (miRNA) and transcription factor (TF)–mRNA interactions of hub genes related to cuproptosis in cerebral ischemia. **(A)** The co-expression network of mRNA–miRNA of hub genes related to cuproptosis in cerebral ischemia. **(B)** The TF–mRNA interaction of hub genes related to cuproptosis in cerebral ischemia.

matter, as well as in different regions within the internal structure of the hippocampus and immune cells.

FDX1 encodes a small iron–sulfur protein involved in mitochondrial cytochrome reduction, Fe-S cluster biosynthesis, and synthesis of various steroid hormones (17, 18). It serves as a key regulator of cuproptosis (3), primarily localized within the cytosol, endoplasmic reticulum, and nucleus, but its highest activity is observed in the mitochondria (19). The results of this study indicated that its subcellular localization was exclusively in the mitochondria, further elucidating the involvement of specific mitochondrial enzymes in the process of cuproptosis and their relationship with mitochondrial respiration. Moreover, the GO analysis revealed the mitochondrial matrix as the CC, aligning with the subcellular localization predictions and existing literature (19). Previous research demonstrated that *FDX1* knockdown resulted in metabolic alterations, particularly in glucose metabolism, fatty acid oxidation, and amino acid metabolism (7), consistent with the Reactome analysis prediction of the signaling pathway involving the human *FDX1* gene (20). Given that prior literature has conclusively demonstrated and reported FDX1 as a crucial gene in the process of ferroptosis (3), We had prioritized validating the expression of FDX1 through animal experiments in the present study, our research findings indicated an elevated expression level of FDX in the hippocampus of castrated ovariectomized rats with ischemia, which aligns with the previously reported increase of FDX expression in the hippocampus of rats with ischemic injury (21). Overexpression of *FDX1 in vitro* partially reversed the protective effect of dexamethasone (DEX) on rat cerebral infarction, including the DEX-induced significant alleviation of rat cerebral infarction, reduced copper levels, mitochondrial function maintenance, increased GSH levels, and decreased levels of key proteins associated with copper toxicity (21).

The LIAS is primarily expressed in the mitochondria (20), and the present study revealed its localization both in the mitochondria and nucleus. This finding aligns with the CC localization results of the mitochondrial matrix, as shown in the GO analysis. Research indicates that *LIAS* mutations could lead to mitochondrial energy metabolism defects (22). Moreover, LIAS is involved in the synthesis of mitochondria-related metabolic enzymes, the biosynthesis of endogenous fatty acids, energy metabolism, and antioxidant reactions (23, 24). Notably, in the present study, the GO-BP analysis revealed that LIAS participates in complex biosynthetic processes. GO-MF analysis demonstrated the ability of LIAS to bind to iron, sulfur, and metal clusters. FDX1 is a critical upstream regulatory factor for protein thioacylation, which plays a vital role in cells relying on mitochondrial metabolism. FDX1 also acts as a key regulator of steatosis by directly binding to LIAS, thereby exerting a lethal metabolic effect on cancer cells (25). The GO-MF analysis in this study indicated that LIAS can bind to iron–sulfur clusters and metal clusters. Moreover, FDX1 serves as a key regulatory factor for protein lipoylation through direct binding to LIAS and plays a role in metabolic conditioning-induced cell death in cancer cells (25).

LIPT1, an enzyme specific to lipid esters, plays a significant role in copper homeostasis. It is an essential enzyme for activating mitochondrial 2-ketoacid dehydrogenases and is involved in maintaining the oxidative and reductive metabolism of glutamine (26). LIPT1 participates in the biosynthesis and function of lipoic acid and fatty acylation (27, 28). These previous findings align with the results of CC localization in the GO analysis of the present study, indicating mitochondrial matrix as the subcellular localization of LIPT1.

The DLD is an important component of various mitochondrial multienzyme complexes, participating in the composition of complexes such as α-ketoglutarate dehydrogenase, α-ketohexanoate dehydrogenase, and glycine decarboxylase (29). It is also involved in the decarboxylation of pyruvate, converting the product into acetyl-CoA in the TCA cycle (30). The results of this study indicated that DLD was localized in both mitochondria and nuclei. GO-CC analysis results suggested associations with mitochondrial matrix, redox enzyme complex mitochondria, and mitochondrial tricarboxylate cyclase complex. Moreover, KEGG analysis indicated its involvement in pathways such as the TCA cycle and pyruvate metabolism. Research has shown that *DLD* downregulation could affect mitochondrial metabolism, leading to reduced levels of downstream metabolites in the TCA cycle and

inducing melanoma cell death (31). Moreover, DLD is known to promote cell death, such as apoptosis (32), copper poisoning-induced cell death (3), and cuproptosis. *DLD* serves as a key gene in cuproptosis and is a positive regulator, enhancing copper-dependent cell death (30). The present study also identified DLD as one of the hub genes responsible for cuproptosis following cerebral ischemia.

DLAT, a mitochondrial protein involved in glucose metabolism, is located in the inner mitochondrial membrane and plays a role in the conversion of pyruvate to acetyl acetyl-CoA (33). Furthermore, *DLAT* overexpression inhibits the production of acetyl-CoA (34). These findings are consistent with the GO/KEGG analyses results of this study. Notably, DLAT is associated with cuproptosis, as copper promotes the oligomerization of DLAT, thereby increasing the insoluble DLAT, leading to protein toxicity stress and cell death (3). This oligomerization is due to the integration of copper with lipoylated proteins in the TCA cycle (3). Cu-induced neuronal degeneration and oxidative damage have been shown to promote the expression of FDX1, DLAT, and HSP70 while reducing that of Fe-S cluster proteins (35). Noteworthily, proteins such as ATP6V1A, DLAT, and HSP70 are expressed in the hippocampus of patients with temporal lobe epilepsy (36). In contrast, patients with acute myocardial infarction exhibit decreased levels of LIAS, PDHB, LIPT1, DLAT, and GLS, along with increased MTF1 levels. A previous Kaplan–Meier analysis indicated the prognostic value of DLAT in ischemic events (37). The present study also identified DLAT as one of the hub genes responsible for cuproptosis after cerebral ischemia.

PDHA1 serves as a crucial component of the pyruvate dehydrogenase (PDH) complex, an enzyme complex that regulates the TCA cycle (38). PDHA1 plays a crucial role in glucose metabolism, oxidative phosphorylation, and the TCA cycle in the mitochondria (39). The results of this study indicated the involvement of PDHA1 in the biosynthesis of acetyl-CoA from pyruvate, the biosynthesis process of acetyl-CoA, and acetyl-CoA metabolism processes. KEGG analysis results indicated that these processes were related to pathways such as the TCA cycle, pyruvate metabolism, and glycolysis/gluconeogenesis. These results are consistent with previous reports (39). In mice, *PDHA1* knockout resulted in ultrastructural disruptions of hippocampal neurons and lactate accumulation (40), which subsequently caused impaired neuronal function (41), ultimately resulting in hippocampal dysfunction. Moreover, prostate cancer cells and human esophageal squamous cancer cells lacking PDHA1 exhibit impaired normal mitochondrial oxidative phosphorylation and a reliance on glycolysis (42, 43). These previous data are consistent with the results of the present study in terms of the subcellular localization to the mitochondria, and the cellular component annotations in GO/KEGG analyses corroborate the preservation of the CC.

The PDHB catalyzes the conversion of pyruvate to acetyl-CoA, bridging the TCA cycle and glycolytic pathway (44). Its expression is predominantly distributed within the mitochondria (45). Consistently, in the present study, the GO-BP results indicated the involvement of PDHB d in the biosynthesis process of acetyl-CoA from pyruvate, the biosynthesis process of acetyl-CoA, and the metabolism of acetyl-CoA. Moreover, KEGG analysis revealed that PDHB participates in BPs related to the TCA cycle, pyruvate metabolism, and glycolysis pathways. In a previous study, *PDHB* knockdown in primary human muscle inhibited pyruvate metabolism and upregulated Ariadne RBR E3 ubiquitin protein ligase 2 (Arih2) in the cellular catabolic pathway (46). Moreover, *dPDHB* knockout shortened the lifespan of adult flies, leading to rough eye phenotypes and abnormal photoreceptor axon targeting (47). Mutations in *PDHA1* and *PDHB* are associated with coenzyme Q10 levels and mitochondrial homeostasis imbalance, severely affecting the brain (48). Currently, research is primarily focusing on the role of PDHB in cancer, particularly in the cuproptosis pathway associated with non-alcoholic fatty liver disease (NAFLD), where both DLD and PDHB are potential candidate genes for NAFLD diagnosis and treatment options (49). Additionally, five genes related to cuproptosis (*FDX1, LIPT1, PDHA1, PDHB,* and *CDKN2A*) are considered candidate biomarkers or therapeutic targets for osteoarthritis synovitis (50). The present study also reported the involvement of PDHB in the cuproptosis pathway in cerebral ischemia.

The GLS catalyzes the hydrolysis of glutamine to produce glutamic acid (50). It exists in mammals in two isoforms: GLS1 and GLS2. GLS1 is primarily expressed in organs such as the brain, heart, pancreas, and kidneys, while GLS2 is mainly expressed in the liver (51). The subcellular localization of GLS1 is in the mitochondria, while GLS2 is located in the nucleus (51). However, the results of this study indicated that GLS was only localized to the mitochondria. Dysregulated expression or dysfunction of GLS results in the overproduction of glutamate, alterations in the expression of inflammatory factors, and the disruption of metabolic homeostasis, resulting in the activation of microglia (51). Upregulation of *GLS1* expression leads to excessive production of glutamate in microglial cells, increasing extracellular glutamate levels, which in turn cause excitotoxicity and neuronal degeneration (51). Notably, cuproptosis is associated with the TCA cycle and the aggregation of lipoylated proteins in the TCA cycle (3, 51). In rats with cerebral artery occlusion, the expression of GLS1 was substantially upregulated, and the GLS inhibitor CB-839 markedly reduced the expression of pro-inflammatory factors, thereby alleviating neuroinflammation and brain damage (52). The present study also identified GLS as a hub gene associated with copper-induced cell death during cerebral ischemia.

This study presents novel insights into hub genes involved in cuproptosis during cerebral ischemia, validating them through multiple approaches including brain tissue, immune cells, localization, structure, and prediction of miRNAs and TFs. However, some limitations should be noted; for example, currently, only one of the hub genes, *FDX1*, has been validated in animal experiments and the hippocamp of rats, while other hub genes and the expression of brain regions need to be validated in experiments. In addition, there is a lack of clinical research on the hub genes associated with cuproptosis. In the future, we will strive to incorporate a wider range of brain regions and multiple gene targets into our research endeavors, further deepening our understanding of the intricate mechanisms underlying ischemic injury. However, in subsequent studies, we are predicting and understanding the binding interactions between small molecules (ligands) and target proteins related to copper death in cerebral ischemia; Using computer simulation technology, small molecule drug molecules are docked to the surface of proteins to search for possible binding sites for drug molecule docking. This part of the

research work is currently underway, and once progress is made in the next stage, we will share our findings with everyone.

Conclusion

In summary, this study utilized genes related to cerebral ischemic and cuproptosis to identify and validate genes implicated in both cerebral ischemic and cuproptosis. Eight hub genes with the potential to serve as novel markers were identified, holding promise as specific biomarkers for the diagnosis, treatment, and prognosis of cerebral ischemia in clinical applications.

Data availability statement

The datasets presented in this study can be found in online repositories. The names of the repository/repositories and accession number(s) can be found in the article/supplementary material.

Ethics statement

The animal studies were approved by Experimental Animal Ethics Committee of Hunan University of Traditional Chinese Medicine. The studies were conducted in accordance with the local legislation and institutional requirements. Written informed consent was obtained from the owners for the participation of their animals in this study.

Author contributions

LQ: Conceptualization, Formal analysis, Funding acquisition, Writing – original draft. XC: Visualization, Writing – original draft. TH: Data curation, Methodology, Software, Writing – original draft. YL: Formal analysis, Writing – original draft. SL: Supervision, Validation, Writing – review & editing.

Funding

The author(s) declare that financial support was received for the research, authorship, and/or publication of this article. This work was supported by the National Natural Science Foundation of China [Nos. 82374437 and 81904180], Hunan Provincial Natural Science Foundation of China [Nos. 2023JJ50035 and 2024JJ8124], Scientific Research Project of Hunan Provincial Health Commission [No. B202319018677], "Disciplinary Reveal System" project of Hunan University of Chinese Medicine [No. 22JBZ041], Hunan Province Traditional Chinese Medicine Research Plan Project [No. A2024001]. Discipline construction at Hunan University of Chinese Medicine.

Conflict of interest

The authors declare that the research was conducted in the absence of any commercial or financial relationships that could be construed as a potential conflict of interest.

Publisher's note

All claims expressed in this article are solely those of the authors and do not necessarily represent those of their affiliated organizations, or those of the publisher, the editors and the reviewers. Any product that may be evaluated in this article, or claim that may be made by its manufacturer, is not guaranteed or endorsed by the publisher.

References

1. Shi XH, Mang J, Xu ZX. Research progress in cell death modes of cerebral ischemia-reperfusion injury. *J Jilin Univ Med Edit*. (2022) 48:1635–43. doi: 10.13481/j.1671-587X.20220633

2. Hu WX, Xie . Ferroptosis and its roles in cerebral ischemia-reperfusion injury. *Prog Physiol Sci*. (2021) 52:169–75.

3. Tsvetkov P, Coy S, Petrova B, Dreishpoon M, Verma A, Abdusamad M, et al. Copper induces cell death by targeting lipoylated TCA cycle proteinsJ. *Science*. (2022) 375:1254–61. doi: 10.1126/science.abf0529

4. Wu YJ, Sun ZR, Zhang Y. Effect of acupuncture on serum copper and chromium content in rats with acute focal cerebral ischemia. *Inform Tradit Chin Med*. (2004) 6:35–7.

5. Wang TT, Hu LC, Fan H. Cuproptosis and its possible role in neuronal cell death in ischemic stroke. *Chin J of Emerg Med*. (2022) 31:1724–9.

6. Valentine RC. Bacterial ferredoxin. *Bacteriol Rev*. (1964) 28:497–517. doi: 10.1128/br.28.4.497-517.1964

7. Zhang Z, Ma Y, Guo X, du Y, Zhu Q, Wang X, et al. FDX1 can impact the prognosis and mediate the metabolism of lung adenocarcinoma. *Front Pharmacol*. (2021) 12:749134. doi: 10.3389/fphar.2021.749134

8. Xiao Y, Yuan Y, Liu Y, Yu Y, Jia N, Zhou L, et al. Circulating multiple metals and incident stroke in Chinese adults. *Stroke*. (2019) 50:1661–8. doi: 10.1161/STROKEAHA.119.025060

9. Yu G, Wang LG, Han Y, He QY. clusterProfiler: an R package for comparing biological themes among gene clusters. *Omics*. (2012) 16:284–7. doi: 10.1089/omi.2011.0118

10. Csardi G, Tamas N. The igraph software package for complex network research. *Inter J Complex Syst*. (2006) 1695:1–9.

11. Szklarczyk D, Gable AL, Nastou KC, Lyon D, Kirsch R, Pyysalo S, et al. The STRING database in 2021: customizable protein-protein networks, and functional characterization of user-uploaded gene/measurement sets. *Nucleic Acids Res*. (2021) 49:D605–12. doi: 10.1093/nar/gkaa1074

12. Spychala MS, Honarpisheh P, McCullough LD, She J. Sex differences in neuroinflammation and neuroprotection in ischemic stroke. *J Neurosci Res*. (2017) 95:462–71. doi: 10.1002/jnr.23962

13. Qin LH, Liu Y, Huang J, Cheng SW, Liu l, Li S, et al. Effect of Jiawei Naotaifang on cerebral infarction area and level of estrogen of ovariectomized rats with cerebral ischemia and its correlation. *Chin Pharm Bull*. (2018) 34:428–31.

14. Qin LH, Wang GZ, Liu L, Huang J, Liu Y, Yi YQ. Effects of estrogen inhibitor on ATF4/CHOP/Puma pathway in ovariectomized rats with cerebral ischemia and the intervention effect of Jiawei Naotai formula. *Chin J Tradit Chin Med Pharm*. (2020) 35:3594–7.

15. Ruiz LM, Libedinsky A, Elorza AA. Role of copper on mitochondrial function and metabolism. *Front Mol Biosci*. (2021) 8:711227. doi: 10.3389/fmolb.2021.711227

16. Ge EJ, Bush AI, Casini A, Cobine PA, Cross JR, DeNicola GM, et al. Connecting copper and cancer: from transition metal signalling to metalloplasia. *Nat Rev Cancer*. (2022) 22:102–13. doi: 10.1038/s41568-021-00417-2

17. Sheftel AD, Stehling O, Pierik AJ, Elsässer HP, Mühlenhoff U, Webert H, et al. Humans possess two mitochondrial ferredoxins, Fdx1 and Fdx2, with distinct roles in steroidogenesis, heme, and Fe/S cluster biosynthesis. *Proc Natl Acad Sci USA*. (2010) 107:11775–80. doi: 10.1073/pnas.1004250107

18. Strushkevich N, MacKenzie F, Cherkesova T, Grabovec I, Usanov S, Park HW. Structural basis for pregnenolone biosynthesis by the mitochondrial monooxygenase system. *Proc Natl Acad Sci USA*. (2011) 108:10139–43. doi: 10.1073/pnas.1019441108

19. Tang D, Chen X, Kroemer G. Cuproptosis: a copper-triggered modality of mitochondrial cell death. *Cell Res*. (2022) 32:417–8. doi: 10.1038/s41422-022-00653-7

20. Guan YL. Bioinformatics analysis of human ferredoxin 1, the key regulatory gene of Cuproptosis. *J Jiangsu Univ*:1–11. doi: 10.13312/j.issn.1671-7783.y220159

21. Guo Q, Ma M, Yu H, Han Y, Zhang D. Dexmedetomidine enables copper homeostasis in cerebral ischemia/reperfusion via ferredoxin 1. *Ann Med*. (2023) 55:2209735. doi: 10.1080/07853890.2023.2209735

22. Habarou F, Hamel Y, Haack TB, Feichtinger RG, Lebigot E, Marquardt I, et al. Biallelic mutations in LIPT2 cause a mitochondrial lipoylation defect associated with severe neonatal encephalopathy. *Am J Hum Genet*. (2017) 101:283–90. doi: 10.1016/j.ajhg.2017.07.001

23. Lu WF, Cao JJ, Guo YJ, Zhong K, Zha GM, Wang LF, et al. Expression of the porcine lipoic acid synthase (LIAS) gene in *Escherichia coli*. *Genet Mol Res*. (2014) 13:5369–77. doi: 10.4238/2014.July.24.16

24. Yi X, Kim K, Yuan W, Xu L, Kim HS, Homeister JW, et al. Mice with heterozygous deficiency of lipoic acid synthase have an increased sensitivity to lipopolysaccharide-induced tissue injury. *J Leukoc Biol*. (2009) 85:146–53. doi: 10.1189/jlb.0308161

25. Dreishpoon MB, Bick NR, Petrova B, Warui DM, Cameron A, Booker SJ, et al. FDX1 regulates cellular protein lipoylation through direct binding to LIAS. [Epubh ahead of preprint]. (2023). doi: 10.1016/j.jbc.2023.105046

26. Ni M, Solmonson A, Pan C, Yang C, Li D, Notzon A, et al. Functional assessment of Lipoyltransferase-1 deficiency in cells, mice, and humans. *Cell Rep*. (2019) 27:1376–1386.e6. doi: 10.1016/j.celrep.2019.04.005

27. Liu Y, Luo G, Yan Y, Peng J. A pan-cancer analysis of copper homeostasis-related gene lipoyltransferase 1: its potential biological functions and prognosis values. *Front Genet*. (2022) 13:1038174. doi: 10.3389/fgene.2022.1038174

28. Taché V, Bivina L, White S, Gregg J, Deignan J, Boyadjievd SA, et al. Lipoyltransferase 1 gene defect resulting in fatal lactic acidosis in two siblings. *Case Rep Obstet Gynecol*. (2016) 2016:1–4. doi: 10.1155/2016/6520148

29. Duarte IF, Caio J, Moedas MF, Rodrigues LA, Leandro AP, Rivera IA, et al. Dihydrolipoamide dehydrogenase, pyruvate oxidation, and acetylation-dependent mechanisms intersecting drug iatrogenesis. *Cell Mol Life Sci*. (2021) 78:7451–68. doi: 10.1007/s00018-021-03996-3

30. Yang W, Guo Q, Wu H, Tong L, Xiao J, Wang Y, et al. Comprehensive analysis of the cuproptosis-related gene DLD across cancers: a potential prognostic and immunotherapeutic target. *Front Pharmacol*. (2023) 14:1111462. doi: 10.3389/fphar.2023.1111462

31. Yumnam S, Kang MC, Oh SH, Kwon HC, Kim JC, Jung ES, et al. Downregulation of dihydrolipoyl dehydrogenase by UVA suppresses melanoma progression via triggering oxidative stress and altering energy metabolism. *Free Radic Biol Med*. (2021) 162:77–87. doi: 10.1016/j.freeradbiomed.2020.11.037

32. Dayan A, Fleminger G, Ashur-Fabian O. Targeting the Achilles' heel of cancer cells via integrin-mediated delivery of ROS-generating dihydrolipoamide dehydrogenase. *Oncogene*. (2019) 38:5050–61. doi: 10.1038/s41388-019-0775-9

33. Goh WQ, Ow GS, Kuznetsov VA, Chong S, Lim YP. DLAT subunit of the pyruvate dehydrogenase complex is upregulated in gastric cancer-implications in cancer therapy. *Am J Transl Res*. (2015) 7:1140–51.

34. Chen Q, Wang Y, Yang L, Sun L, Wen Y, Huang Y, et al. PM2.5 promotes NSCLC carcinogenesis through translationally and transcriptionally activating DLAT-mediated glycolysis reprograming. *J Exp Clin Cancer Res*. (2022) 41:229. doi: 10.1186/s13046-022-02437-8

35. Zhang Y, Zhou Q, Lu L, Su Y, Shi W, Zhang H, et al. Copper induces cognitive impairment in mice via modulation of Cuproptosis and CREB signaling. *Nutrients*. (2023) 15:972. doi: 10.3390/nu15040972

36. Persike DS, Marques-Carneiro JE, Stein MLL, Yacubian EMT, Centeno R, Canzian M, et al. Altered proteins in the Hippocampus of patients with mesial temporal lobe epilepsy. *Pharmaceuticals*. (2018) 11:95. doi: 10.3390/ph11040095

37. Liu Z, Wang L, Xing Q, Liu X, Hu Y, Li W, et al. Identification of GLS as a cuproptosis-related diagnosis gene in acute myocardial infarction. *Front Cardiovasc Med*. (2022) 9:1016081. doi: 10.3389/fcvm.2022.1016081

38. Deng L, Jiang A, Zeng H, Peng X, Song L. Comprehensive analyses of PDHA1 that serves as a predictive biomarker for immunotherapy response in cancer. *Front Pharmacol*. (2022) 13:947372. doi: 10.3389/fphar.2022.947372

39. Patel MS, Nemeria NS, Furey W, Jordan F. The pyruvate dehydrogenase complexes: structure-based function and regulation. *J Biol Chem*. (2014) 289:16615–23. doi: 10.1074/jbc.R114.563148

40. Chen W, Sun X, Zhan L, Zhou W, Bi T. Conditional knockout of Pdha1 in mouse Hippocampus impairs cognitive function: the possible involvement of lactate. *Front Neurosci*. (2021) 15:767560. doi: 10.3389/fnins.2021.767560

41. Scandella V, Knobloch M. Sensing the environment: extracellular lactate levels control adult neurogenesis. *Cell Stem Cell*. (2019) 25:729–31. doi: 10.1016/j.stem.2019.11.008

42. Zhong Y, Li X, Ji Y, Li X, Li Y, Yu D, et al. Pyruvate dehydrogenase expression is negatively associated with cell stemness and worse clinical outcome in prostate cancers. *Oncotarget*. (2017) 8:13344–56. doi: 10.18632/oncotarget.14527

43. Liu L, Cao J, Zhao J, Li X, Suo Z, Li H. PDHA1 gene knockout in human esophageal squamous Cancer cells resulted in greater Warburg effect and aggressive features in vitro and in vivo. *Onco Targets Ther*. (2019) 12:9899–913. doi: 10.2147/OTT.S226851

44. Li A, Zhang Y, Zhao Z, Wang M, Zan L. Molecular characterization and transcriptional regulation analysis of the bovine PDHB gene. *PLoS One*. (2016) 11:e0157445. doi: 10.1371/journal.pone.0157445

45. Taylor SI, Mukherjee C, Jungas RL. Regulation of pyruvate dehydrogenase in isolated rat liver mitochondria. Effects of octanoate, oxidation-reduction state, and adenosine triphosphate to adenosine diphosphate ratio. *J Biol Chem*. (1975) 250:2028–35. doi: 10.1016/S0021-9258(19)41679-7

46. Jiang X, Ji S, Yuan F, Li T, Cui S, Wang W, et al. Pyruvate dehydrogenase B regulates myogenic differentiation via the FoxP1-Arih2 axis. *J Cachexia Sarcopenia Muscle*. (2023) 14:606–21. doi: 10.1002/jcsm.13166

47. Dung VM, Suong DNA, Okamaoto Y, Hiramatsu Y, Thao DTP, Yoshida H, et al. Neuron-specific knockdown of Drosophila PDHB induces reduction of lifespan, deficient locomotive ability, abnormal morphology of motor neuron terminals and photoreceptor axon targeting. *Exp Cell Res*. (2018) 366:92–102. doi: 10.1016/j.yexcr.2018.02.035

48. Asencio C, Rodríguez-Hernandez MA, Briones P, Montoya J, Cortés A, Emperador S, et al. Severe encephalopathy associated to pyruvate dehydrogenase mutations and unbalanced coenzyme Q10 content. *Eur J Hum Genet*. (2016) 24:367–72. doi: 10.1038/ejhg.2015.112

49. Wu C, Liu X, Zhong L, Zhou Y, Long L, Yi T, et al. Identification of Cuproptosis-related genes in non-alcoholic fatty liver disease. *Oxidative Med Cell Longev*. (2023) 2023:1–18. doi: 10.1155/2023/9245667

50. Chang B, Hu Z, Chen L, Jin Z, Yang Y. Development and validation of cuproptosis-related genes in synovitis during osteoarthritis progress. *Front Immunol*. (2023) 14:1090596. doi: 10.3389/fimmu.2023.1090596

51. Ding L, Xu X, Li C, Wang Y, Xia X, Zheng JC. Glutaminase in microglia: A novel regulator of neuroinflammation. *Brain Behav Immun*. (2021) 92:139–56. doi: 10.1016/j.bbi.2020.11.038

52. Gao G, Li C, Zhu J, Wang Y, Huang Y, Zhao S, et al. Glutaminase 1 regulates Neuroinflammation after cerebral ischemia through enhancing microglial activation and pro-inflammatory exosome release. *Front Immunol*. (2020) 11:161. doi: 10.3389/fimmu.2020.00161

frontiers | Frontiers in Neuroscience

TYPE Original Research
PUBLISHED 09 October 2024
DOI 10.3389/fnins.2024.1469142

OPEN ACCESS

EDITED BY
Rubem C. A. Guedes,
Federal University of Pernambuco, Brazil

REVIEWED BY
Yong Huang,
Southern Medical University, China
Wolfgang Schwarz,
Goethe University Frankfurt, Germany

*CORRESPONDENCE
Min Li
✉ doctorlimin@gzucm.edu.cn
Lihong Li
✉ gzlilihong@163.com

RECEIVED 23 July 2024
ACCEPTED 24 September 2024
PUBLISHED 09 October 2024

CITATION
Hou X, Liang X, Lu Y, Zhang Q, Wang Y, Xu M, Luo Y, Fan T, Zhang Y, Ye T, Zhou K, Shi J, Li M and Li L (2024) Investigation of local stimulation effects of embedding PGLA at Zusanli (ST36) acupoint in rats based on TRPV2 and TRPV4 ion channels.
Front. Neurosci. 18:1469142.
doi: 10.3389/fnins.2024.1469142

Investigation of local stimulation effects of embedding PGLA at Zusanli (ST36) acupoint in rats based on TRPV2 and TRPV4 ion channels

Xunrui Hou[1,2,3], Xin Liang[2,3], Yuwei Lu[2,3], Qian Zhang[4], Yujia Wang[5], Ming Xu[2], Yuheng Luo[2], Tongtao Fan[2], Yiyi Zhang[2], Tingting Ye[3], Kean Zhou[3], Jiahui Shi[3], Min Li[1]* and Lihong Li[2,3]*

[1]Clinical Medical College of Acupuncture Moxibustion and Rehabilitation, Guangzhou University of Chinese Medicine, Guangzhou, China, [2]Affiliated Hospital of Guizhou Medical University, Guiyang, China, [3]Guizhou Medical University, Guiyang, China, [4]The Affiliated TCM Hospital of Guangzhou Medical University, Guangzhou, China, [5]Weihai Hospital of Traditional Chinese Medicine, Affiliated Hospital of Shandong University of Traditional Chinese Medicine, Weihai, China

Introduction: Acupoint Catgut Embedding (ACE) is an extended and developed form of traditional acupuncture that serves as a composite stimulation therapy for various diseases. However, its local stimulation effects on acupoints remain unclear. Acupuncture can activate mechanically sensitive calcium ion channels, TRPV2 and TRPV4, located on various cell membranes, promoting Ca^{2+} influx in acupoint tissues to exert effects. Whether ACE can form mechanical physical stimulation to regulate these channels and the related linkage effect requires validation.

Methods: This study investigates the influence of TRPV2 and TRPV4 ion channels on the local stimulation effects of ACE by embedding PGLA suture at the Zusanli (ST36) acupoint in rats and using TRPV2 and TRPV4 inhibitors. Flow cytometry, immunofluorescence, Western blot, and Real-time quantitative PCR were employed to detect intracellular Ca^{2+} fluorescence intensity, the expression of macrophage (Mac) CD68 and mast cell (MC) tryptase, as well as the protein and mRNA expression of TRPV2 and TRPV4 in acupoint tissues after PGLA embedding.

Results: The results indicate that ACE using PGLA suture significantly increases the mRNA and protein expression of TRPV2 and TRPV4, Ca^{2+} fluorescence intensity, and the expression of Mac CD68 and MC tryptase in acupoint tissues, with these effects diminishing over time. The increasing trends are reduced after using inhibitors, particularly when both inhibitors are used simultaneously. Furthermore, correlation analysis shows that embedding PGLA suture at the ST36 acupoint regulates Mac and MC functions through Ca2+ signaling involving not only TRPV2 and TRPV4 but multiple pathways.

Discussion: These results suggest that embedding PGLA suture at the ST36 acupoint generates mechanical physical stimulation and regulates TRPV2 and TRPV4 ion channels, which couple with Ca^{2+} signaling to form a linkage effect that gradually weakens over time. This provides new reference data for further studies on the stimulation effects and clinical promotion of ACE.

KEYWORDS

Acupoint Catgut Embedding, mechanosensitive TRPV channel, Zusanli (ST36), local stimulation, Ca^{2+} signaling

1 Introduction

Acupoint Catgut Embedding (ACE) originates from the traditional acupuncture theory of "retaining needles," utilizing absorbable sutures to provide continuous stimulation to acupoints for disease prevention and treatment (Guan et al., 2009; Huo et al., 2017). Due to its minimal invasiveness, simple operation, long-lasting stimulation, and low frequency of visits (Guo M. et al., 2022; Zhang X. H. et al., 2023), it has been widely used in clinical practice to treat various systemic diseases (Cheng et al., 2022b). Concurrently, research on the mechanisms of ACE has gradually increased (Wei et al., 2019). However, previous mechanism studies have mainly focused on therapeutic effects or distal acupoint effects (Huo et al., 2017; Teng et al., 2022; Duan et al., 2021), with a need for in-depth research on recognized target points (Huo et al., 2017; Wei et al., 2019). Local acupoints are the initial response sites for acupuncture effects (Chen et al., 2013; Fu et al., 2023) and a common foundation for mechanism research (Li et al., 2015). Although acupoint stimulation effects are involved in various acupuncture methods (Min et al., 2015; Chen T. et al., 2016; Lowe, 2017; Chen et al., 2021), basic research on ACE in this area remains scarce. Therefore, exploring the stimulation effects formed by ACE-induced changes in the local microenvironment of acupoints provides an objective scientific basis for its promotion.

Macrophages (Macs) and mast cells (MCs) in the connective tissue of acupoint areas are generally considered to participate in initiating local stimulation effects (Fu et al., 2023; Jung and Lushniak, 2017). Acupuncture stimulation at acupoints can activate these two immune cells locally, transmitting stimulation signals (Wu et al., 2015; Yan et al., 2020; Yu et al., 2022). Previous research by our team found dynamic changes in the functional state of Macs and MCs in acupoint areas following ACE at the ST36 acupoint in rats. Besides the transient needle stimulation by embedding, the suture material as a foreign body causing a local immune inflammatory response is considered one of the stimulation effects post-ACE (Zhang Q. et al., 2023; Wang et al., 2023). However, as a composite stimulation therapy developed from traditional acupuncture, other local stimulation effects of ACE remain to be further studied (Wei et al., 2019; Xing et al., 2019).

It is known that in the transient receptor potential vanilloid (TRPV) family, TRPV2 and TRPV4 are mechanically sensitive calcium ion (Ca^{2+}) channels (Shibasaki, 2016; Liedtke, 2005). When these channel proteins on different cell membranes perceive mechanical stimulation, the channels are opened, causing transmembrane Ca^{2+} movement into the cells (i.e., Ca^{2+} influx), triggering intracellular signal transduction and cell function activation (Liedtke and Kim, 2005). Recent studies have shown that acupuncture, as a mechanical physical stimulation, can activate TRPV2 and TRPV4 channels at acupoints, promoting Ca^{2+} influx, converting physical stimulation into biological information, and thus exerting acupuncture effects (Huang et al., 2018; Luo et al., 2022). Based on the above, on the one hand, ACE originates from traditional acupuncture and replaces needles with sutures to produce sustained stimulation at acupoints. Whether it can form mechanical physical stimulation in the acupoint area to regulate these two channels needs verification. On the other hand, as a composite stimulation therapy, in addition to causing Macs and MCs to participate in local immune inflammation response, it remains to be further verified whether ACE can couple the functions of these two immune cells through the TRPV2 and TRPV4 mechanosensitive channels on their cell membranes (Link et al., 2010; Chen et al., 2017; Michalick and Kuebler, 2020).

Therefore, this study aims to explore possible local mechanical physical and linkage stimulation effects of ACE by embedding poly(glycolide-co-lactide) (PGLA) sutures (Ke et al., 2020; Jain, 2000), known for their excellent mechanical properties and biocompatibility, at the ST36 acupoint in rats. By intervening with inhibitors of mechanically sensitive TRPV2 and TRPV4 channels, changes in TRPV mRNA and protein expression, intracellular Ca^{2+} fluorescence intensity, CD68 and tryptase expression in MACs and MCs in local tissues of acupoints were dynamically observed. Correlation analysis of the impact of intracellular Ca^{2+} fluorescence intensity on the CD68 and tryptase expression in Macs and MCs in acupoint areas provides new reference data for further studies on the mechanism of ACE stimulation effects and its clinical promotion.

2 Materials and methods

2.1 Experimental animals and grouping

A total of 150 healthy male Sprague–Dawley (SD) rats (170-200 g, 8 weeks old) were purchased from Guangdong Vital River Laboratory Animal Technology Co., Ltd. (production license number: SCXK (Yue) 2022–0063) and housed in the SPF-level animal room of the Clinical Research Center, Affiliated Hospital of Guizhou Medical University. The housing conditions were maintained at a temperature of 22–24°C, humidity of 50–70%, with a 12-h light/dark cycle, and free access to food and water. After a one-week acclimatization period, the 150 rats were randomly divided into five groups (30 rats per group): Blank Control Group (CON), Embedding Group (ACE), Embedding + TRPV2 Inhibitor Group (ACE+T2B), Embedding + TRPV4 Inhibitor Group (ACE+T4B), and Embedding + TRPV (2 + 4) Inhibitor Group (ACE+T(2 + 4)B). Each group was further divided into three subgroups based on time points (1 day, 3 days, 7 days) with 10 rats in each subgroup (Figure 1A). The experimental protocol was approved by the Experimental Animal Ethics Committee of Guizhou Medical University (approval number: 2101330). During the experiment, the handling of animals strictly adhered to the "Guiding Opinions on Treating Experimental Animals Humanely" issued by the Ministry of Science and Technology of the People's Republic of China in 2006. Before interventions, the rats were anesthetized with 3% sodium pentobarbital (P3761, Sigma, USA) administered intraperitoneally at a dose of 0.03 g/kg. The rats were then fixed in a prone position on a rat board with their limbs extended. The hair on

Abbreviations: ACE, Acupoint Catgut Embedding; Ca^{2+}, Calcium ion; PGLA, poly(glycolide-co-lactide); TRPV, Transient receptor potential vanilloid; Mac, Macrophage; MC, Mast cell; mRNA, messenger RNA; SD, Sprague–Dawley; CON, Control; T2B, TRPV2 Inhibitor; T4B, TRPV4 Inhibitor; DMSO, Dimethyl sulfoxide; FCM, Flow Cytometry; IF, Immunofluorescence; CY3, Cyanine 3; DAPI, 4′,6-diamidino-2-phenylindole; WB, Western Blot; BCA, Bicinchoninic Acid; GAPDH, Glyceraldehyde-3-phosphate dehydrogenase; PVDF, Polyvinylidene Fluoride; TBST, Tris-buffered saline with Tween 20; ECL, Enhanced Chemiluminescence; RT-PCR, Real-time fluorescent quantitative polymerase chain reaction; cDNA, Complementary, Deoxyribonucleic Acid; SPSS, Statistical Package for the Social Sciences; ANOVA, Analysis of Variance; PDO, polydioxanone; PDS, polydioxanone suture; PGA, polyglycolic acid; TNF-α, Tumor Necrosis Factor-alpha; IL-1, Interleukin-1; IL-12, Interleukin-12; MMPs, Matrix Metalloproteinases; HA, Histamine; 5-HT, 5-Hydroxytryptamine.

the left hind limb was shaved, and the ST36 acupoint (located approximately 3 mm below the fibular head on the posterolateral side of the knee joint) was identified according to "Common Acupoint Names and Locations for Experimental Animals, Part 2: Rats" (China Association of Acupuncture and Moxibustion, 2021) and marked with a 1 cm × 1 cm square centered on this point (Figure 1B).

2.2 Intervention methods for each group

In the Embedding Group (ACE), rats underwent the ACE procedure at the marked ST36 acupoint on the left side once, and were injected daily with saline containing DMSO (the same amount as the ACE+T(2 + 4)B group). The embedding procedure was based on a method from previous studies by our research group (Wang et al., 2023): after local disinfection of the acupoint marking area, a PGLA suture (specification 2–0, 0.5 mm) (Shanghai Pudong Jinhui Medical Supplies Co., Ltd.) was placed into the cannula of a disposable embedding needle (0.9 mm × 75 mm, Taizhou Minga Medical Equipment Co., Ltd.). The acupoint was fixed with the thumb and forefinger of one hand, while the other hand held the needle, aligning the cannula with the skin at the center of the ST36 acupoint at a 90° angle. The needle was quickly inserted subcutaneously, then advanced slowly to a depth of about 7 mm, slightly twisted (two turns each to the left and right), and the needle core was pushed while withdrawing the needle to embed the suture into the acupoint. After needle withdrawal, the area was pressed with a disinfected cotton swab. Once the rats recovered from anesthesia, they were returned to their housing. In the (ACE+T2B) Group, (ACE+T4B) Group, and (ACE+T(2 + 4)B) Group, the rats underwent the same embedding procedure as described above. Additionally, at the center of the marked ST36 acupoint, they were injected with a mixed solution of

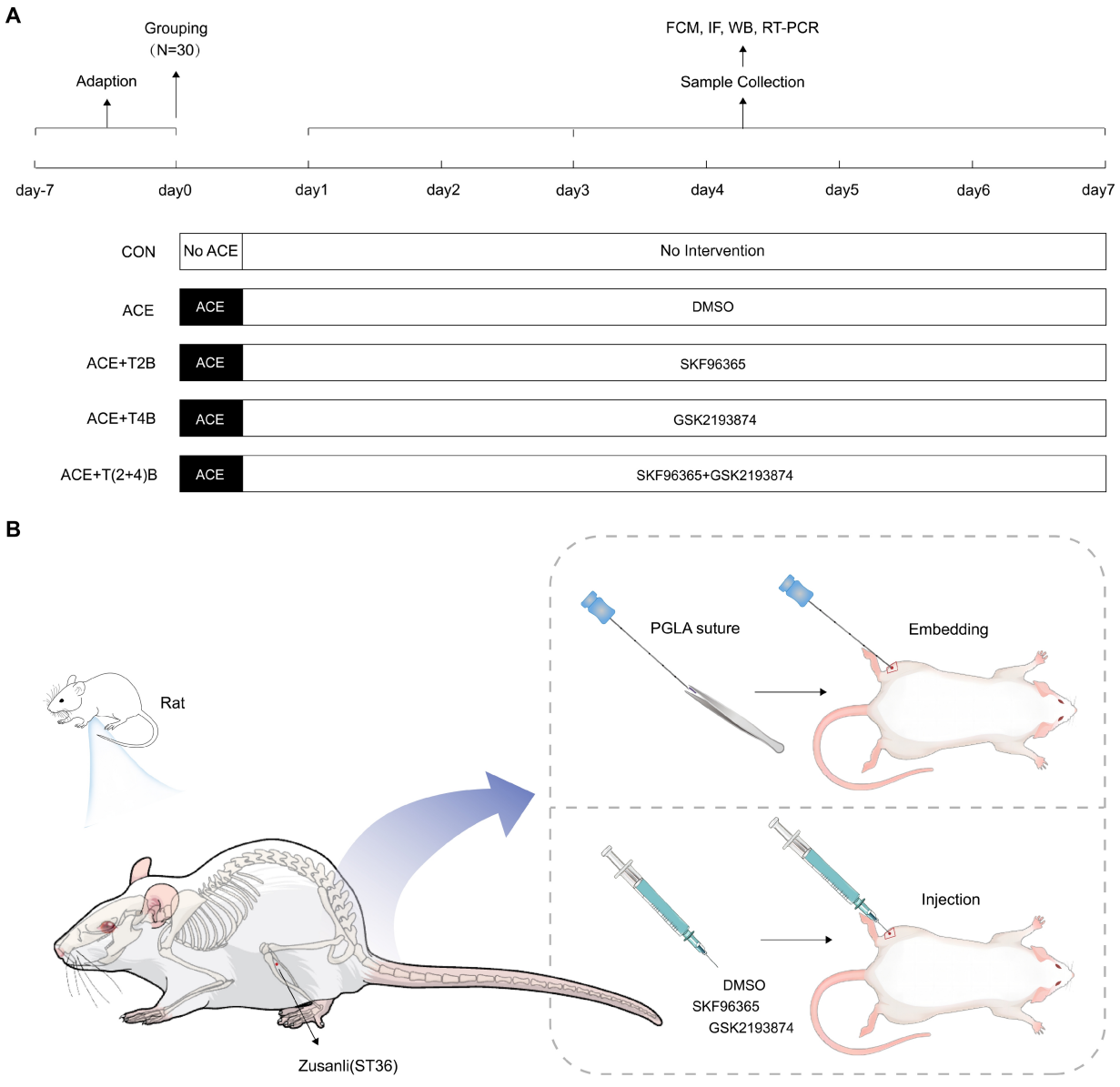

FIGURE 1
Experimental protocol. **(A)** Experimental procedures in this study. **(B)** Location of ST36 acupoint and interventions.

SKF96365 (HY-100001, MCE, USA) (0.5 mg/kg) containing 0.5 mg/mL SKF96365 and 1% DMSO in saline, a mixed solution of GSK2193874 (HY-100720, MCE, USA) (0.5 mg/kg) containing 2.5 mg/mL GSK2193874, 5% DMSO, and 190 mg/mL sulfo-beta-cyclodextrin in saline, and a mixture of the above two solutions, respectively, once daily. In the Blank Control Group, rats received no other interventions besides the same handling and fixation method. All embedding operations and acupoint injections were performed by an experienced acupuncturist. To avoid cross-contamination, a single embedding needle and syringe were used for each rat's acupoint only once. The acupoint area of the rats was observed daily for redness, swelling, or ulceration, and the acupoint area marking was reinforced (Figures 1A,B).

2.3 Tissue sampling

At the corresponding time points (1 day, 3 days, 7 days) post-intervention, tissue samples were collected from the five groups of rats. Following intraperitoneal anesthesia with 3% sodium pentobarbital (0.03 g/kg) and securing the rats on a board (the same fixation method as pre-intervention), tissue blocks (approximately 1 cm × 1 cm × 1 cm) from the marked ST36 acupoint region (including skin, subcutaneous tissue, and some muscle) were excised. Fresh tissue samples from five rats per group were randomly selected; half of each sample was fixed in 4% paraformaldehyde for further analysis, and the other half was used to prepare single-cell suspensions. The remaining five tissue samples were stored in a −80°C freezer for future analysis.

2.4 Observation indicators and detection methods

2.4.1 Flow cytometry

Subcutaneous fat was removed from the acupoint tissue, and the tissue was washed with Tyrode's solution and cut into small pieces. Each gram of tissue was digested with 20 mL of digestion solution (collagenase type I and hyaluronidase, prepared in Hank's solution with 20% fetal bovine serum) and incubated in a 37°C water bath for 4 h. The digested tissue was filtered through a 70 μm mesh sieve and centrifuged at 4°C, and the supernatant was discarded. Cells were washed twice with PBS and collected by centrifugation at 1500 rpm for 5 min. The cells were resuspended in serum-free DMEM medium, and 5 μmol/L Fluo 3-AM working solution (S1056, Shanghai Biyuntian Biotechnology Co., Ltd.) was added to the single-cell suspension. The cells were incubated in the dark at 37°C in a 5% CO_2 incubator for 30 min, washed twice with calcium-free PBS, and resuspended to a final volume of 500 μL. The Ca^{2+} fluorescence intensity in the single-cell suspension was detected using a cytoFLEX flow cytometer (Beckman Coulter, USA).

2.4.2 Immunofluorescence staining

The acupoint tissue fixed in 4% paraformaldehyde was dehydrated through a graded alcohol series, cleared in xylene, infiltrated with paraffin, and embedded. Sections of 4 μm thickness were prepared. The paraffin sections underwent processes including baking, dewaxing, antigen retrieval, and blocking with 10% normal goat serum for 30 min. The sections were incubated overnight at 4°C in a humid chamber with primary antibodies: anti-CD68 (1:200) (97778S, CST, USA) and anti-Mast Cell Tryptase (1:100) (bs-2572R, Bioss, USA). The next day, the primary antibodies were washed off, and the sections were incubated with secondary antibodies conjugated with fluorescent CY3 (goat anti-rabbit IgG, 1:100) (BA1032, Wuhan Boster Biological Technology, Ltd.) at 37°C for 1 h in a humid chamber. After washing off the secondary antibody, nuclei were stained with DAPI (5 min in the dark), excess DAPI was washed off, and the sections were mounted with antifade mounting medium. Images were observed and collected using a fluorescence microscope, with three fields of view per section at 400x magnification. Optical density analysis was performed using Image-Pro Plus 6.0 software, and the average optical density value of the three fields was recorded.

2.4.3 Western blotting

Five cryopreserved acupoint tissue samples (approximately 100 mg each) were taken from each group. The tissue samples were lysed and homogenized with RIPA lysis buffer, then fully lysed on ice for 30 min. The lysate was centrifuged at 12,000 rpm for 5 min at 4°C, and the supernatant was collected. Protein concentration was determined using the BCA method (A G3422, B G3522, GBCBIO Technologies Inc.). The samples were denatured by boiling for 10 min, followed by protein loading, electrophoresis, membrane transfer, and blocking. The membranes were incubated overnight at 4°C with primary antibodies: rabbit polyclonal anti-TRPV2 (1:1,000) (Bs-10297R, Bioss, USA), rabbit polyclonal anti-TRPV4 (1:2,000) (DF8624, Affinity, USA), and rabbit polyclonal anti-GAPDH (1:2,000) (AB-P-R001, Hangzhou Goodhere Biotechnology Co., Ltd). The next day, the PVDF membranes were washed five times with TBST (5 min each), incubated with HRP-labeled goat anti-rabbit IgG secondary antibody (1:10,000) (BA1054, Wuhan Boster Biological Technology, Co. Ltd.) at room temperature for 2 h on a shaker, and washed again five times with TBST (5 min each). ECL reagent was applied, and the membranes were exposed in a dark room. The film was scanned, and gray value analysis was performed using Image-Pro Plus 6.0 software. The relative expression level of the target protein was determined by the ratio of the grayscale value of the target band to the grayscale value of the internal control.

2.4.4 Real-time quantitative PCR

Five cryopreserved acupoint tissue samples (approximately 100 mg each) were taken from each group. Total RNA was extracted using the Trizol method (15596–026, Ambion, USA). The purity and concentration of RNA were calculated. cDNA was synthesized by reverse transcription following the kit instructions (R233-01, Nanjing Vazyme), with reaction conditions set at 50°C for 15 min, 85°C for 5 s, and 4°C for 10 min. PCR amplification was conducted with a reaction system totaling 20 μL, including 4 μL of cDNA, 10 μL of SYBR Green Master Mix, 0.4 μL of forward primer, 0.4 μL of reverse primer, 0.4 μL of 50× ROX Reference Dye 2, and 4.8 μL of H_2O. The amplification conditions were as follows: initial denaturation at 95°C for 10 min, denaturation at 95°C for 15 s, and annealing and extension at 60°C for 60 s, for a total of 40 cycles. Melting curve data was collected under the following conditions: 95°C for 15 s, 60°C for 60 s, and 95°C for 15 s. Using β-actin as an internal control, the relative mRNA expression levels were analyzed by the 2-ΔΔCt method, with each sample analyzed in triplicate. Primer sequences are listed in Table 1.

TABLE 1 Primer sequences.

Gene		Primer Sequence (5′-3′)	Product length/ bp
Rat b-actin	Forward	TGACGTTGACATCCGTAAAGACC	117 bp
	Reverse	GTGCTAGGAGCCAGGGCAGTAA	
Rat TRPV2	Forward	CCGAAAGTTTACTGAGTGGTGTT	217 bp
	Reverse	GCAGGCGAAGTTGAAGAAGAA	
Rat TRPV4	Forward	CAAGTGGCGTAAGTTCGG	131 bp
	Reverse	TGGTACGGTAAGGGTAGGG	

2.5 Statistical analysis

SPSS 23.0 statistical software was used for data analysis, and GraphPad Prism 9.0 was used for statistical charting. Measurement data were expressed as mean ± standard deviation ($\bar{x}\pm s$). Intra-group comparisons (i.e., comparisons within the same experimental group at different time points) and inter-group comparisons (i.e., comparisons across different experimental groups at the same time point) were performed using one-way analysis of variance (one-way ANOVA). When variances were equal, the LSD method was used for pairwise comparisons; when variances were unequal, the Dunnett T3 method was used. A p-value of <0.05 was considered statistically significant. Pearson's correlation coefficient was used for correlation analysis, with a p-value of <0.05 indicating a significant correlation. A correlation coefficient of $0 < r < 1$ indicated a positive correlation, while $-1 < r < 0$ indicated a negative correlation.

3 Results

3.1 Comparison of Ca^{2+} fluorescence intensity in tissue cells of Zusanli (ST36) acupoint area among groups

In this study, flow cytometry was used to detect the Ca^{2+} fluorescence intensity in the acupoint tissue cell suspension to observe changes in the Ca^{2+} concentration in the local tissue cells following the embedding of PGLA suture in the acupoint and the use of TRPV2 and TRPV4 inhibitors. Compared to the CON Group, the Ca^{2+} fluorescence intensity in the tissue cells of the acupoint area in the ACE Group significantly increased at 1 day, 3 days, and 7 days after embedding. However, compared to the ACE Group, the Ca^{2+} fluorescence intensity in the tissue cells of the acupoint area significantly decreased in the (ACE+T2B) Group, (ACE+T4B) Group, and (ACE+T(2 + 4)B) Group at 1 day, 3 days, and 7 days post-embedding. Additionally, compared to the (ACE+T(2 + 4)B) Group, the Ca^{2+} fluorescence intensity in the tissue cells increased in the (ACE+T2B) Group at 1 day, 3 days, and 7 days post-embedding and increased in the (ACE+T4B) Group at 1 day and 3 days post-embedding (Figures 2A,C). The Ca^{2+} fluorescence intensity in the tissue cells of the acupoint area in all intervention groups showed a decreasing trend over time. Compared to 1 day post-embedding, the Ca^{2+} fluorescence intensity in the tissue cells of the acupoint area significantly decreased at 3 days post-embedding in the ACE Group, (ACE+T4B) Group, and (ACE+T(2 + 4)B) Group, and at 7 days post-embedding in the (ACE+T2B) Group (Figures 2B,C). These results indicate that embedding PGLA suture in the acupoint can affect the Ca^{2+} fluorescence intensity in tissue cells by regulating TRPV2 and TRPV4, and the Ca^{2+} fluorescence intensity gradually weakens over time.

3.2 Comparison of positive expression of Mac CD68 and MC tryptase in acupoint tissues among groups

CD68 and tryptase are commonly used markers for Macs and MCs, respectively (Payne and Kam, 2004; Chistiakov et al., 2017). To observe the effect of embedding PGLA suture in acupoints and the use of TRPV2 and TRPV4 inhibitors on the function of these two immune cells, immunofluorescence staining was used to detect the expression of CD68 in Macs and tryptase in MCs in the local tissue of the acupoint area. The results are as follows.

Compared to the blank control group, the expression of CD68 in Macs in the acupoint area of rats in the embedding group significantly increased at 1 day, 3 days, and 7 days after embedding. However, compared to the embedding group, the expression of CD68 in Macs in the acupoint area of rats in the embedding + TRPV4 inhibitor group and the (ACE+T(2 + 4)B) Group significantly decreased at 1 day and 7 days after embedding. The embedding + TRPV2 inhibitor group showed a significant decrease in CD68 expression at 3 days and 7 days after embedding. Furthermore, compared to the (ACE+T(2 + 4)B) Group, the CD68 expression in Macs increased in the embedding + TRPV2 inhibitor group at 1 day, 3 days, and 7 days after embedding, and increased in the (ACE+T4B) Group at 3 days and 7 days after embedding (Figures 3A,C). The expression of CD68 in Macs in the acupoint area of each intervention group showed a decreasing trend over time. Compared to 1 day after embedding, the CD68 expression in Macs in the embedding group, the (ACE+T4B) Group, and the (ACE+T(2 + 4)B) Group significantly decreased at 7 days after embedding, while in the (ACE+T2B) Group, the CD68 expression significantly decreased at 3 days after embedding (Figures 3B,C).

Compared to the blank control group, the expression of tryptase in MCs in the acupoint area of rats in the embedding group significantly increased at 1 day, 3 days, and 7 days after embedding. However, compared to the embedding group, the expression of tryptase in MCs in the (ACE+T(2 + 4)B) Group significantly decreased at 1 day, 3 days, and 7 days after embedding. The expression of tryptase in MCs in the (ACE+T2B) Group and the (ACE+T4B) Group significantly decreased at 3 days and 7 days after embedding. Furthermore, compared to the (ACE+T(2 + 4)B) Group, the expression of tryptase in MCs increased in the (ACE+T2B) Group at 1 day, 3 days, and 7 days after embedding, and increased in the (ACE+T4B) Group at 1 day and 3 days after embedding (Figures 4A,C). The expression of tryptase in MCs in the acupoint area of each intervention group showed a decreasing trend over time. Compared to 1 day after embedding, the expression of tryptase in MCs in the (ACE+T2B) Group, the (ACE+T4B) Group, and the (ACE+T(2 + 4)B) Group significantly decreased at 3 days after embedding, while in the embedding group, the expression of tryptase in MCs significantly decreased at 7 days after embedding (Figures 4B,C).

The above results suggest that embedding PGLA suture in acupoints may influenc the expression of CD68 in Macs and tryptase in MCs through TRPV2 and TRPV4, and the expression levels gradually decrease over time.

10.3389/fnins.2024.1469142

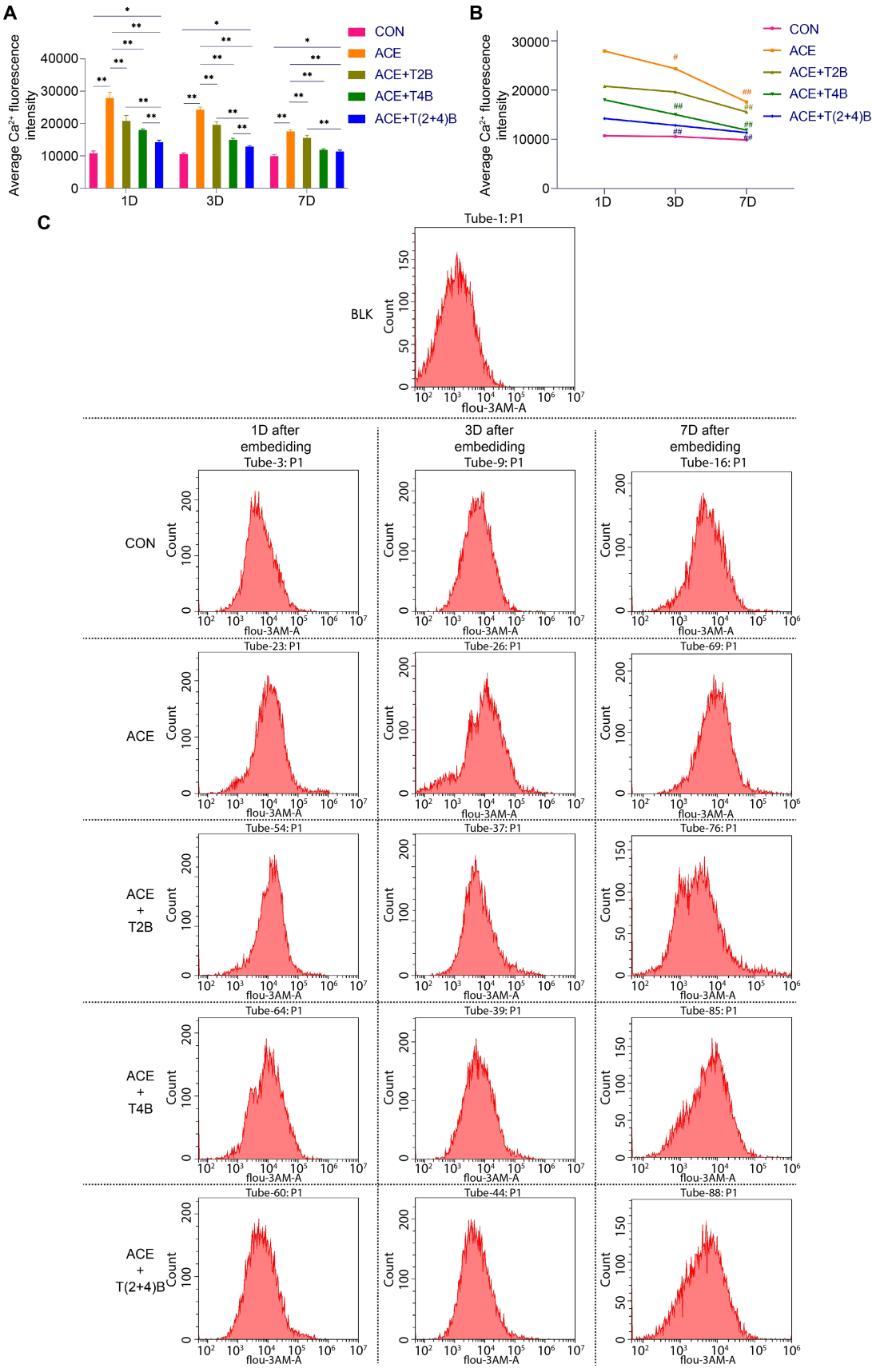

FIGURE 2
Comparison of Ca^{2+} fluorescence intensity in tissue cells of Zusanli (ST36) acupoint area among groups. **(A)**. Inter-group comparison of intracellular Ca^{2+} fluorescence intensity in tissues of acupoint area at the same time point ($n = 5$ per group). **(B)** Intra-group comparison of intracellular Ca^{2+}

(Continued)

FIGURE 2 (Continued)
fluorescence intensity in tissues of acupoint area across different time points ($n = 5$ per group). **(C)** Detection of intracellular Ca^{2+} fluorescence intensity in tissues of acupoint area among groups by flow cytometry. **(A)** Comparison between groups at the same time point, $*p < 0.05$, $**p < 0.01$; **(B)** Comparison of the same group 1 day post-embedding, $\#p < 0.05$, $\#\#p < 0.01$.

3.3 Comparison of TRPV2 and TRPV4 protein expression in acupoint tissues among groups

In this study, Western blots (WB) were used to verify the regulatory effects of PGLA embedding on local TRPV2 and TRPV4 channels by detecting the expression levels of TRPV2 and TRPV4 proteins in acupoint tissues. The results are as follows.

Compared to the blank control group, the expression of TRPV2 protein in the acupoint area of rats in the embedding group significantly increased at 1 day, 3 days, and 7 days after embedding. However, compared to the embedding group, the expression of TRPV2 protein in the acupoint area of rats in the (ACE+T2B) Group and the (ACE+T(2 + 4)B) Group significantly decreased at 1 day, 3 days, and 7 days after embedding. Moreover, compared to the (ACE+T(2 + 4)B) Group at the same time point, the TRPV2 protein expression in the (ACE+T2B) Group increased at 7 days after embedding, with no significant difference at 1 day and 3 days after embedding (Figures 5A,E). The TRPV2 protein expression in the acupoint tissue of each intervention group showed a decreasing trend over time. Compared to 1 day after embedding, the TRPV2 protein expression in the embedding group, the (ACE+T2B) Group, the (ACE+T4B) Group, and the (ACE+T(2 + 4)B) Group significantly decreased at 3 days after embedding (Figures 5B,E).

Compared to the blank control group, the TRPV4 protein expression in the acupoint area of rats in the embedding group significantly increased at 1 day, 3 days, and 7 days after embedding. However, compared to the embedding group, the TRPV4 protein expression in the acupoint area of rats in the (ACE+T4B) Group and the (ACE+T(2 + 4)B) Group significantly decreased at 1 day, 3 days, and 7 days after embedding. Moreover, compared to the (ACE+T(2 + 4)B) Group, TRPV4 protein expression in the (ACE+T4B) Group increased at 1 day after embedding, with no significant difference at 3 days and 7 days after embedding (Figures 5C,E). The TRPV4 protein expression in the acupoint area of each intervention group showed a decreasing trend over time. Compared to 1 day after embedding. The TRPV4 protein expression in the embedding group, the (ACE+T2B) Group, the (ACE+T4B) Group, and the (ACE+T(2 + 4)B) Group significantly decreased at 3 days after embedding (Figures 5D,E).

These results indicate that the stimulation formed by embedding PGLA suture in acupoints can regulate TRPV2 and TRPV4 protein expression, which gradually weakens over time.

3.4 Comparison of TRPV2 and TRPV4 mRNA expression in acupoint tissues among groups

In this study, the expression levels of TRPV2 and TRPV4 mRNA in the tissues of the acupoint area were simultaneously detected using quantitative fluorescence PCR, to validate the results obtained from Western blot (WB) analysis. The results are as follows.

Compared to the blank control group, the expression of TRPV2 mRNA in the acupoint area of rats in the embedding group significantly increased at 1 day, 3 days, and 7 days after embedding. However, compared to the embedding group, the expression of TRPV2 mRNA in the acupoint area of rats in the (ACE+T2B) Group and the (ACE+T(2 + 4)B) Group significantly decreased at 1 day, 3 days, and 7 days after embedding. Moreover, compared to the (ACE+T(2 + 4)B) Group, there was no significant difference in the TRPV2 mRNA expression in the acupoint area of rats in the (ACE+T2B) Group at 1 day, 3 days, and 7 days after embedding (Figure 6A). The expression of TRPV2 mRNA in the acupoint area of each intervention group showed a decreasing trend over time. Compared to 1 day after embedding, the TRPV2 mRNA expression in the embedding group, the (ACE+T2B) Group, the (ACE+T4B) Group, and the (ACE+T(2 + 4)B) Group significantly decreased at 7 days after embedding (Figure 6B).

Compared to the blank control group, the expression of TRPV4 mRNA in the acupoint area of rats in the embedding group significantly increased at 1 day, 3 days, and 7 days after embedding. However, compared to the embedding group, the expression of TRPV4 mRNA in the acupoint area of rats in the (ACE+T4B) Group and the (ACE+T(2 + 4)B) Group significantly decreased at 1 day, 3 days, and 7 days after embedding. Moreover, compared to the (ACE+T(2 + 4)B) Group, the TRPV4 mRNA expression in the acupoint area of rats in the (ACE+T4B) Group increased at 3 days after embedding, with no significant difference at 1 day and 7 days after embedding (Figure 7A). The TRPV4 mRNA expression in the acupoint area of each intervention group showed a decreasing trend over time. Compared to 1 day after embedding, the TRPV4 mRNA expression in the embedding group, the (ACE+T2B) Group, and the (ACE+T4B) Group significantly decreased at 7 days after embedding (see Figure 7B).

These results indicate that the local stimulation formed by embedding PGLA suture in acupoints can regulate TRPV2 and TRPV4 mRNA expression, which gradually weakens over time.

3.5 Correlation analysis of Ca^{2+} fluorescence intensity and expression of Mac CD68 and MC tryptase in acupoint tissues among groups

Pearson correlation analysis was used to compare the correlation between Ca^{2+} fluorescence intensity and the expression of Mac CD68 and MC tryptase in acupoint tissues in the analysis of the overall groups (including the blank control group and the intervention groups) and individual intervention group. The results showed that in the overall analysis, there was a positive correlation between Ca^{2+} fluorescence intensity and the expression of Mac CD68 and MC tryptase in acupoint tissues (Figure 8A). Analysis of the embedding group, the (ACE+T2B) Group, the (ACE+T4B) Group, and the (ACE+T(2 + 4)B) Group showed a positive correlation between Ca^{2+}

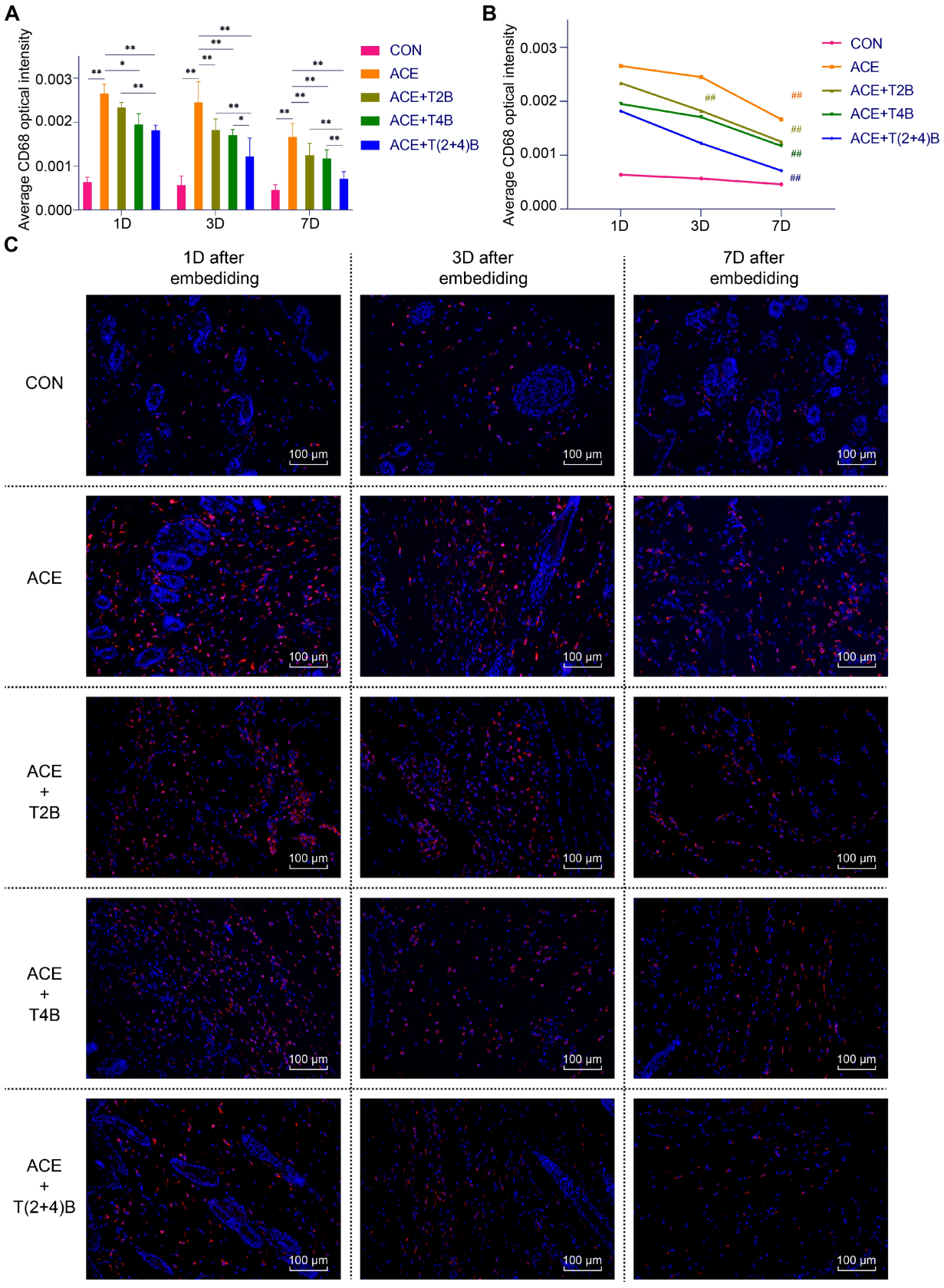

FIGURE 3
Comparison of positive CD68 expression in Macs in acupoint area tissues: inter- and intra-group analysis. **(A)** Inter-group comparison of positive CD68 expression in Macs in tissues of acupoint area at the same time point ($n = 5$ per group). **(B)** Intra-group comparison CD68 expression in Macs in tissues of acupoint area across different time points ($n = 5$ per group). **(C)** Immunofluorescence staining of CD68 expression in Macs in tissues of acupoint

(Continued)

FIGURE 3 (Continued)
area of each group. **(A)** Comparison between groups at the same time point, *$p < 0.05$, **$p < 0.01$. **(B)** Comparison of the same group 1 day after embedding, #$p < 0.05$, ##$p < 0.01$. **(C)** Blue indicates DAPI-stained nuclei, red indicates CD68 positive expression, scale bar = 100 μm.

fluorescence intensity and the expression of Mac CD68 and MC tryptase in acupoint tissues (Figures 8B–E).

4 Discussion

In traditional Chinese medicine theory, the acupoint "Zusanli" (ST36) belongs to the Stomach Meridian of Foot-Yangming. It serves both as the He-Sea point of the Stomach Meridian and the lower He-Sea point of the Stomach Fu organ. Stimulation of this acupoint can harmonize the spleen and stomach, invigorate Qi, and enhance the body's resistance to diseases, making it widely used in the treatment of various ailments throughout history (Shi, 2017; Chen X. L. et al., 2016). Recent meta-analyses have shown that the application of this acupoint has expanded to include treatment for pain, speech disorders, emotional problems, cognitive impairment, gastrointestinal tumors, adverse reactions to radiotherapy, and postoperative ileus (Huang et al., 2022; Zhou et al., 2020; Wu et al., 2020; Li et al., 2022; Wang et al., 2015). Literature reviews indicate that ST36 is the most frequently used acupoint in both clinical acupuncture studies and basic experimental research (Zhu, 2021; Yang et al., 2018). Based on its extensive use and recognition in research, as well as previous findings from our research team showing inflammatory responses in the local acupoint area of both humans and rats after ACE at ST36 (Zhang X. H. et al., 2023; Zhang Q. et al., 2023; Wang et al., 2023; Liang et al., 2019), this acupoint was used in this experimental study. This study selected 1 day, 3 days, and 7 days post PGLA embedding as observation time points. This choice was mainly based on the regulations set forth by the National Standard of the People's Republic of China (GB/T 21709.10–2008), which stipulates that the interval between ACE treatments should be at least 1 week (Guan et al., 2009). Additionally, bibliometric studies have indicated that the most commonly adopted interval in clinical practice is 7 days (Cheng et al., 2022a). Furthermore, observations made by the research team using MRI in clinical studies revealed that local stimulation effects after PGLA embedding change significantly within 1 week, typically appearing within 1 day and lasting for 3 to 7 days (Liang et al., 2016). Therefore, this study employed the aforementioned three time points for observation.

Compared to traditional acupuncture, ACE not only involves transient needling but also provides continuous stimulation of the acupoint due to the embedded threads (Wu et al., 2019), which is crucial. Clinically used threads include catgut, polydioxanone (PDO), polydioxanone suture (PDS), chitosan, polyglycolic acid (PGA), and poly(glycolide-co-lactide) (PGLA) (Cheng et al., 2022a). Catgut has long been the dominant material for ACE, but its propensity to cause allergic reactions and related adverse effects due to its foreign protein nature has limited its use, leading to a gradual replacement by newer materials (Ma et al., 2019). Threads like PDS and chitosan are less commonly used in ACE research due to their later emergence, longer degradation times, unclear degradation mechanisms, and higher costs (Ke et al., 2020; Cheng et al., 2022a; Du and Zhang, 2019). Among these materials, PGA and PGLA are derived from natural plants and do not contain animal-derived proteins, offering good biocompatibility. They degrade through hydrolysis in body fluids into carbon dioxide and water, which are excreted from the body (Bajaj and Singhal, 2011; Makadia and Siegel, 2011). Compared to PGA, PGLA has better biodegradability, and foundational research has further proven that PGLA sutures, due to their superior mechanical and hydrophilic properties, are more suitable for use as embedding materials in acupuncture (Jain, 2000; Xu, 2018).

Acupuncture, as an external mechanical and physical stimulus, can activate two types of mechanosensitive TRPV channels expressed on different cell membranes, causing Ca^{2+} influx and signal transduction (Liedtke and Kim, 2005; Luo et al., 2022). ACE, derived from the traditional acupuncture technique of "needle retention," induces local immune-inflammatory responses at the acupoint due to the foreign body nature of the suture (Zhang X. H. et al., 2023; Zhang Q. et al., 2023; Wang et al., 2023). To verify the mechanical and physical stimulation formed by suture implantation at the acupoint, this study used the inhibitors SKF96365 (Guo Y. Y. et al., 2022) and GSK2193874 (Lawhorn et al., 2021) of the mechanosensitive channels TRPV2 and TRPV4. The results showed that, after embedding PGLA suture, the local tissues of the ST36 acupoint in rats showed an increase in the expression of mRNA and protein in TRPV2 and TRPV4, as well as an increase in intracellular Ca^{2+} fluorescence intensity, both of which decreased over time. When the inhibitors were used, the mRNA and protein expression of TRPV2 and TRPV4 in the local tissues, as well as intracellular Ca^{2+} fluorescence intensity, decreased correspondingly, especially when both inhibitors were used together, resulting in a further reduction in intracellular Ca^{2+} fluorescence intensity compared to using a single inhibitor. These results suggest that the stimulation generated by ACE at the acupoint can modulate the expression of the two mechanosensitive TRPVs (TRPV2 and TRPV4), affecting Ca^{2+} influx in tissue cells, and the stimulation gradually weakens over time. Studies have shown that absorbable sutures gradually soften and are absorbed over time after surgical suturing and embedding at acupoints, leading to a decline in their mechanical properties (Müller et al., 2016; Liang et al., 2019). In light of these findings, the results of this study indicates that the mechanical and physical stimulation at the acupoint post-PGLA embedding may result from the compression and friction of the suture against the local tissue, which diminishes as the suture softens and absorbs within the body.

Macs and MCs are important immune-inflammatory cells in the body, playing crucial roles in regulating inflammatory responses, immune surveillance, and tissue repair (Essandoh et al., 2016; Velez et al., 2018; Xu and Shi, 2012; Ribatti, 2013). They are widely recognized as key participants in initiating the local stimulation effects of acupuncture points (Fu et al., 2023; Dou et al., 2022). In immune-inflammatory responses triggered by foreign bodies, the involvement of these cells differs: Macs primarily clear foreign bodies through phagocytosis and decomposition, whereas MCs mainly trigger inflammatory responses by releasing inflammatory mediators (Velez

10.3389/fnins.2024.1469142

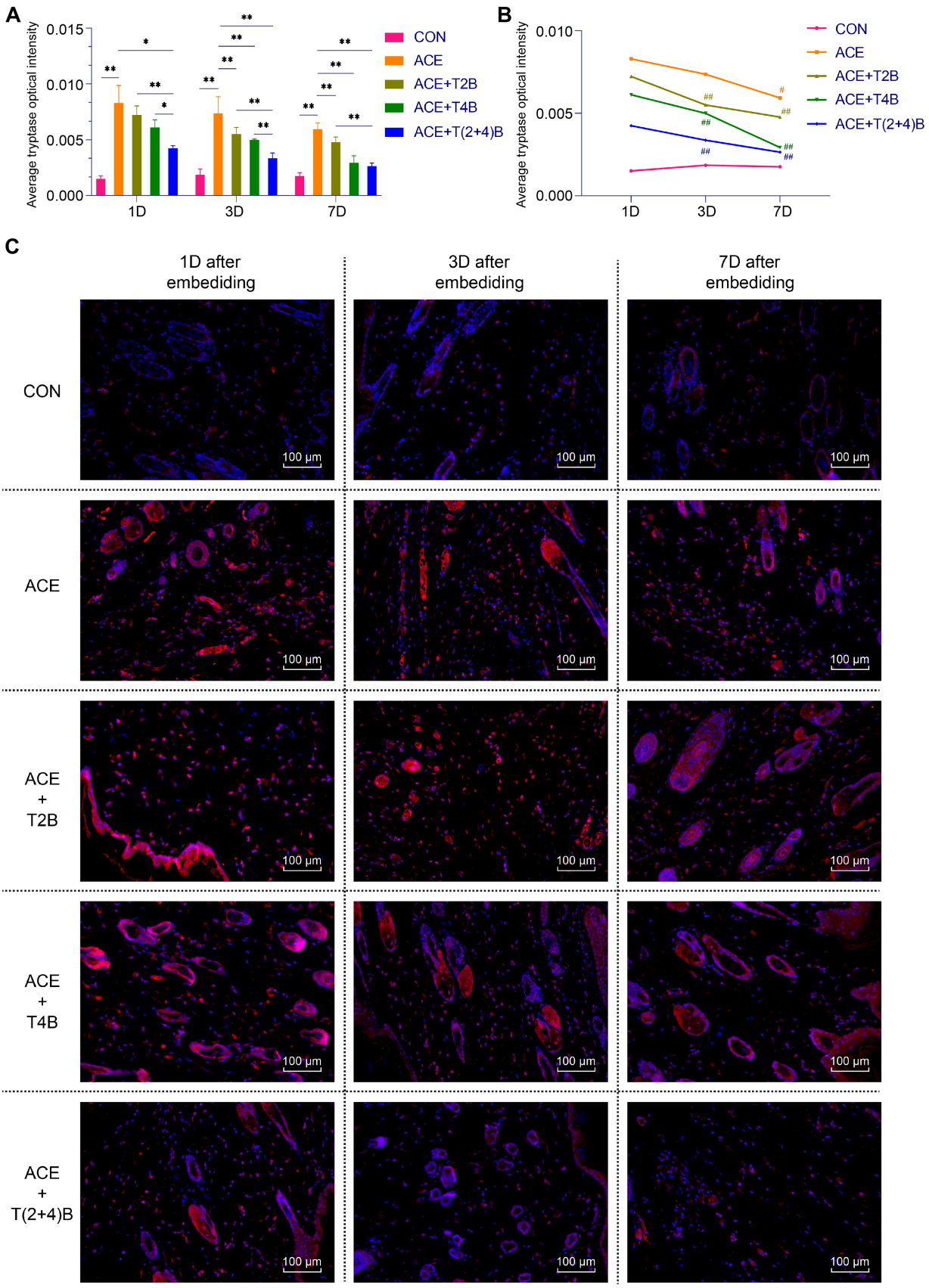

FIGURE 4
Comparison of positive tryptase expression in MCs in acupoint area tissues: inter- and intra-group analysis. **(A)** Inter-group comparison of positive tryptase expression in MCs in in tissues of acupoint area at the same time point ($n = 5$ per group). **(B)** Intra-group comparison of positive tryptase expression in MCs in tissues of acupoint area across different time points ($n = 5$ per group). **(C)** Immunofluorescence staining of tryptase expression in

(Continued)

FIGURE 4 (Continued)
MCs in tissues of acupoint area of each group. **(A)** Comparison between groups at the same time point, $*p < 0.05$, $**p < 0.01$. **(B)** Comparison of the same group 1 day after embedding, $\#p < 0.05$, $\#\#p < 0.01$. **(C)** Blue indicates DAPI-stained nuclei, red indicates tryptase positive expression, scale bar = 100 μm.

et al., 2018; Franz et al., 2011). CD68 is a highly glycosylated glycoprotein. Although it is also expressed in other cells, such as synovial cells and neutrophils (Kunisch et al., 2004; Wu et al., 2022), its high expression in Macs makes it a widely used marker for identifying Macs. CD68 can reflect the number and functional activity of Macs in various physiological and pathological processes (Ramprasad et al., 1996; Chistiakov et al., 2017; Seminerio et al., 2018). Our previous study has found that in the ST36 acupoint area of rats, the expression of Mac CD68 in local tissues dynamically changes over time after embedding catgut (Zhang Q. et al., 2023). In this study, embedding PGLA in the same acupoint resulted in elevated CD68 expression in Macs, which gradually weakened over time. Tryptase, a serine protease mainly derived from MCs and released extracellularly upon mast cell degranulation, is the most specific biomarker of mast cell functional activation (Payne and Kam, 2004). Prior research suggests that the degranulation rate of local MCs in the ST36 acupoint of rats moderately changes over time after PGLA embedding (Wang et al., 2023). Correspondingly, in this study, the expression of MC tryptase increased following PGLA embedding in the same acupoint of rats and then showed a gradual decrease over time. The comprehensive results of this experiment reveal that after embedding PGLA in the ST36 acupoint of rats, the expression of CD68 in Macs and tryptase in MCs in the local tissues changes, suggesting that embedding PGLA suture can alter the functions of Macs and MCs in the acupoint area, which gradually diminishes over time. Additionally, in this study, after embedding PGLA in the ST36 acupoint of rats and subsequently injecting TRPV2 and TRPV4 inhibitors, the expression of Mac CD68 and MC tryptase in the acupoint tissue decreased. Notably, when both TRPV2 and TRPV4 inhibitors were used together, the decreasing trend was more significant compared to using a single inhibitor. As previously mentioned, the mechanosensitive TRPV2 and TRPV4 channels (Shibasaki, 2016; Liedtke and Kim, 2005) are expressed on the membranes of both Macs and MCs (Huang et al., 2018; Link et al., 2010; Michalick and Kuebler, 2020; Chen et al., 2017), and CD68 and tryptase are important markers for identifying Macs and MCs, respectively (Chistiakov et al., 2017; Payne and Kam, 2004). Therefore, these changes in research results indicate that the stimulation generated by embedding PGLA suture in the ST36 acupoint can influence the functions of MCs and Macs by modulating mechanosensitive TRPV channels, with the stimulation effects gradually weakening over time.

Ca^{2+} plays an important role as a messenger in signal transduction in tissue cells, a process known as Ca^{2+} signaling, which is a biochemical process (Bootman and Bultynck, 2020). During macrophage functional activation, an increase in intracellular Ca^{2+} concentration can activate a series of downstream signals, promoting phagocytosis (Zhu et al., 2017) and the release of inflammatory factors, cytokines, and enzymes such as tumor necrosis factor-α (TNF-α), interleukin-1 (IL-1), interleukin-12 (IL-12), lysosomal enzymes, and matrix metalloproteinases (MMPs) (Kusmartsev et al., 2016; Liu et al., 2016; Chen et al., 2015; Huang et al., 2012), thereby influencing their participation in immune-inflammatory responses. In mast cell degranulation, in addition to Ca^{2+} release from the endoplasmic reticulum, the opening of ion channels on the cell membrane allows Ca^{2+} influx, which serves as a key signal, leading to increased intracellular Ca^{2+} concentration, which promotes cell functional activation and degranulation, as well as the release of bioactive mediators such as tryptase, histamine (HA), and serotonin (5-hydroxytryptamine, 5-HT) (Ma and Beaven, 2011; Tsvilovskyy et al., 2018; Wernersson and Pejler, 2014), thereby mediating immune-inflammatory responses. Thus, changes in intracellular Ca^{2+} concentration, or Ca^{2+} signaling, affect the functions of both Macs and MCs. In this experimental study, the overall correlation analysis suggests that the fluorescence intensity of intracellular Ca^{2+} in acupoint tissues correlates positively with the expression of CD68 in Macs and tryptase in MCs, indicating that changes in intracellular Ca^{2+} concentration affect the functional changes of these two immune cells. Correlation analysis in the embedding group showed that after embedding PGLA in the ST36 acupoint of rats, the fluorescence intensity of intracellular Ca^{2+} in local acupoint tissue cells was positively correlated with the expression of CD68 in Macs and tryptase in MCs. This implies that PGLA embedding influences the functional changes of these two immune cells by regulating intracellular Ca^{2+} concentration in local tissue cells. The regulatory pathway, as verified in this experiment, includes mechanosensitive TRPV channels. However, given that ACE is a complex stimulation therapy, the activation mechanisms of MCs and Macs are intricate (Gilfillan and Tkaczyk, 2006; Tatemoto et al., 2018; Gordon and Martinez, 2010). In addition, in the study results, correlation analysis of the (ACE+T2B) Group, (ACE+T4B) Group, and (ACE+T(2 + 4)B) Group showed that after using the two inhibitors, the correlation coefficient between the fluorescence intensity of intracellular Ca^{2+} in local acupoint tissue cells and the expression of Mac CD68 and MC tryptase did not significantly decrease after embedding PGLA suture, and the fluorescence intensity of intracellular Ca^{2+} in acupoint tissue cells in the embedding + TRPV (2 + 4) group was still higher than that in the blank control group. These results suggest that the regulation of the functions of these two immune cells by Ca^{2+} signaling after embedding PGLA suture in the acupoint is not limited to the two mechanosensitive TRPV channels but involves multiple pathways. Therefore, we propose that embedding PGLA suture in the ST36 acupoint of rats may induce the functional changes of MCs and Macs through Ca^{2+} signaling, which includes coupled participation of the mechanosensitive TRPV channels.

5 Conclusion

In summary, embedding PGLA suture in the ST36 acupoint may locally regulate the expression of TRPV2 and TRPV4 through mechanical and physical stimulation, leading to increased intracellular Ca^{2+} concentration in tissue cells. This, in turn couples with Ca^{2+} signaling to affect the functions of MCs and Macs, forming a physico-chemical-immune linkage effect that gradually weakens over time. The findings of this study not only provide new scientific evidence for

10.3389/fnins.2024.1469142

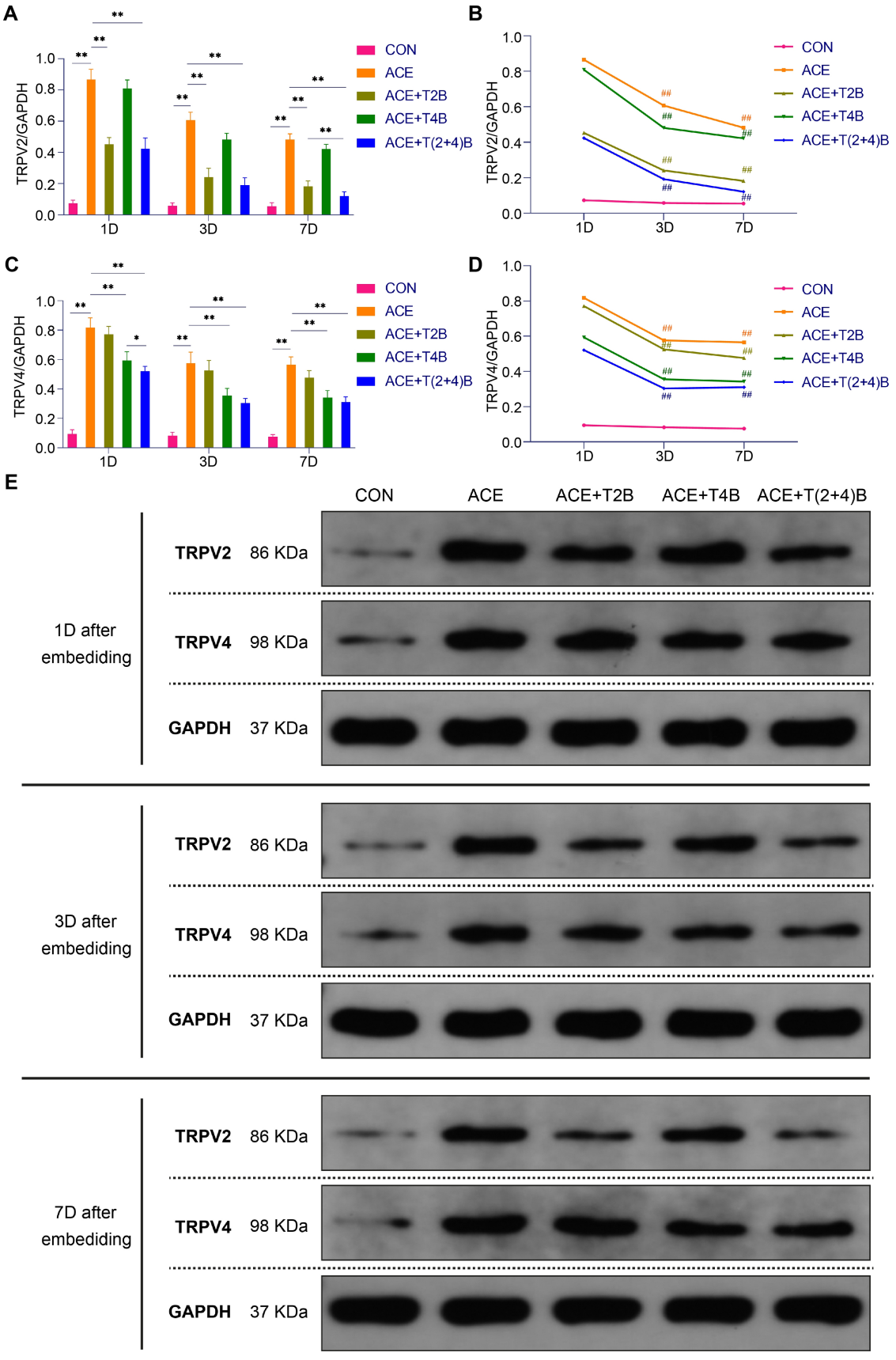

FIGURE 5
Comparison of TRPV2 and TRPV4 Protein Expression in Acupoint Tissues among Groups. **(A)** Inter-group comparison of TRPV2 protein expression in tissues of acupoint area at the same time point ($n = 5$ per group). **(B)** Intra-group comparison of TRPV2 protein expression in tissues of acupoint area

(Continued)

FIGURE 5 (Continued)
across different time points ($n = 5$ per group). **(C)** Inter-group comparison of TRPV4 protein expression in tissues of acupoint area at the same time point ($n = 5$ per group). **(D)** Intra-group comparison of TRPV4 protein expression in tissues of acupoint area across different time points ($n = 5$ per group). **(E)** TRPV2 and TRPV4 protein expression in tissues of acupoint area of each group of rats. **(A)** Comparison between groups at the same time point, $*p < 0.05$, $**p < 0.01$; **(B)** Comparison of the same group 1 day after embedding, $\#p < 0.05$, $\#\#p < 0.01$. **(C)** Comparison between groups at the same time point, $*p < 0.05$, $**p < 0.01$. **(D)** Comparison of the same group 1 day after embedding, $\#p < 0.05$, $\#\#p < 0.01$.

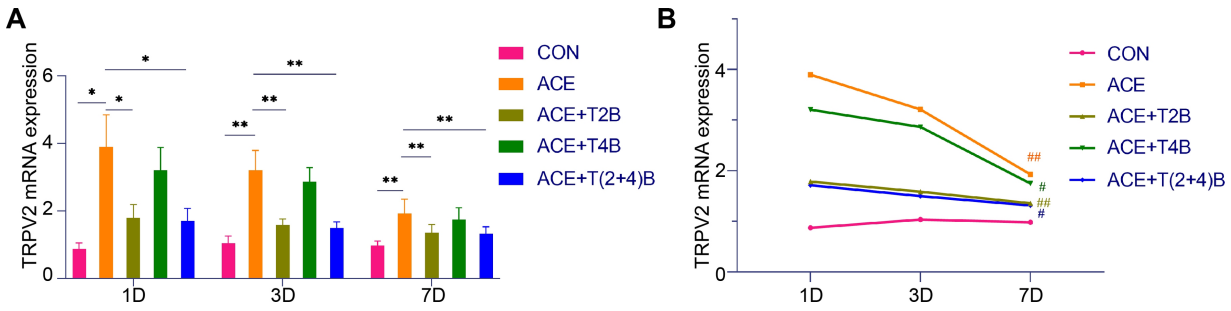

FIGURE 6
Comparison of TRPV2 mRNA Expression in Acupoint Tissues: inter- and intra-group analysis. **(A)** Inter-group comparison of TRPV2 mRNA expression in tissues of acupoint area at the same time point ($n = 5$ per group). **(B)** Intra-group comparison of TRPV2 mRNA expression in tissues of acupoint area across different time points ($n = 5$ per group). **(A)** Comparison between groups at the same time point, $*p < 0.05$, $**p < 0.01$. **(B)** Comparison of the same group 1 day after embedding, $\#p < 0.05$, $\#\#p < 0.01$.

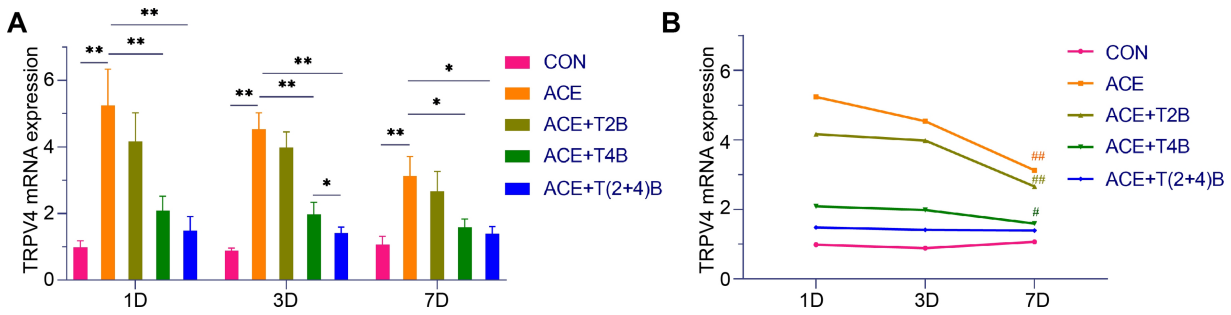

FIGURE 7
Comparison of TRPV4 mRNA Expression in Acupoint Tissues: inter- and intra-group analysis. **(A)** Inter-group comparison of TRPV4 mRNA expression in tissues of acupoint area at the same time point ($n = 5$ per group). **(B)** Intra-group comparison of TRPV4 mRNA expression in tissues of acupoint area across different time points ($n = 5$ per group). **(A)** Comparison between groups at the same time point, $*p < 0.05$, $**p < 0.01$; **(B)** Comparison of the same group 1 day after embedding, $\#p < 0.05$, $\#\#p < 0.01$.

the local stimulation effects of ACE under normal physiological conditions but also offer important reference points for future exploration of ACE's role in pathological states involving TRPV2, TRPV4, MCs, and Macs, as well as its distal effects.

However, WB and qPCR results from the experiment suggest that the two inhibitors used may have interactive inhibitory effects on TRPV2 and TRPV4 ion channels, and future research may consider using specific TRPV gene knockout rats for related studies. Additionally, besides TRPV2 and TRPV4, TRPV1 is also expressed in MCs and Macs (Freichel et al., 2012; Zhang et al., 2012; Vašek et al., 2024). TRPV1 is sensitive to mechanical stimulation under specific conditions such as inflammation, tissue injury, and nerve damage (McGaraughty et al., 2008; Vilceanu et al., 2010; Brenneis et al., 2013). Therefore, whether ACE has a stimulatory effect on TRPV1 is also worth further investigation. Moreover, it remains to be verified whether ACE affects other tissue cells at the acupoint (such as neurons, fibroblasts, and endothelial cells) and their factor release through TRPV ion channels (Wu et al., 2015; Fu et al., 2023), and thus creates a cross-tissue effect, which is significant for exploring the potential distal effects of ACE. Research indicates that acupuncture effects are closely related to purinergic signaling, particularly the release of adenosine (ATP, ADP) by MCs triggered by Ca^{2+} influx, which plays a crucial role in acupuncture analgesia (Burnstock, 2009; Müller et al., 2016; Wang et al., 2022). As a complex stimulation therapy developed from acupuncture, whether ACE, in addition to regulating mechanical sensitivity TRPV at the acupoint, can mediate through purinergic signaling to induce Ca^{2+} influx and affect cell function still needs further exploration. Therefore, future studies could delve deeper into the mechanisms of ACE in these aspects.

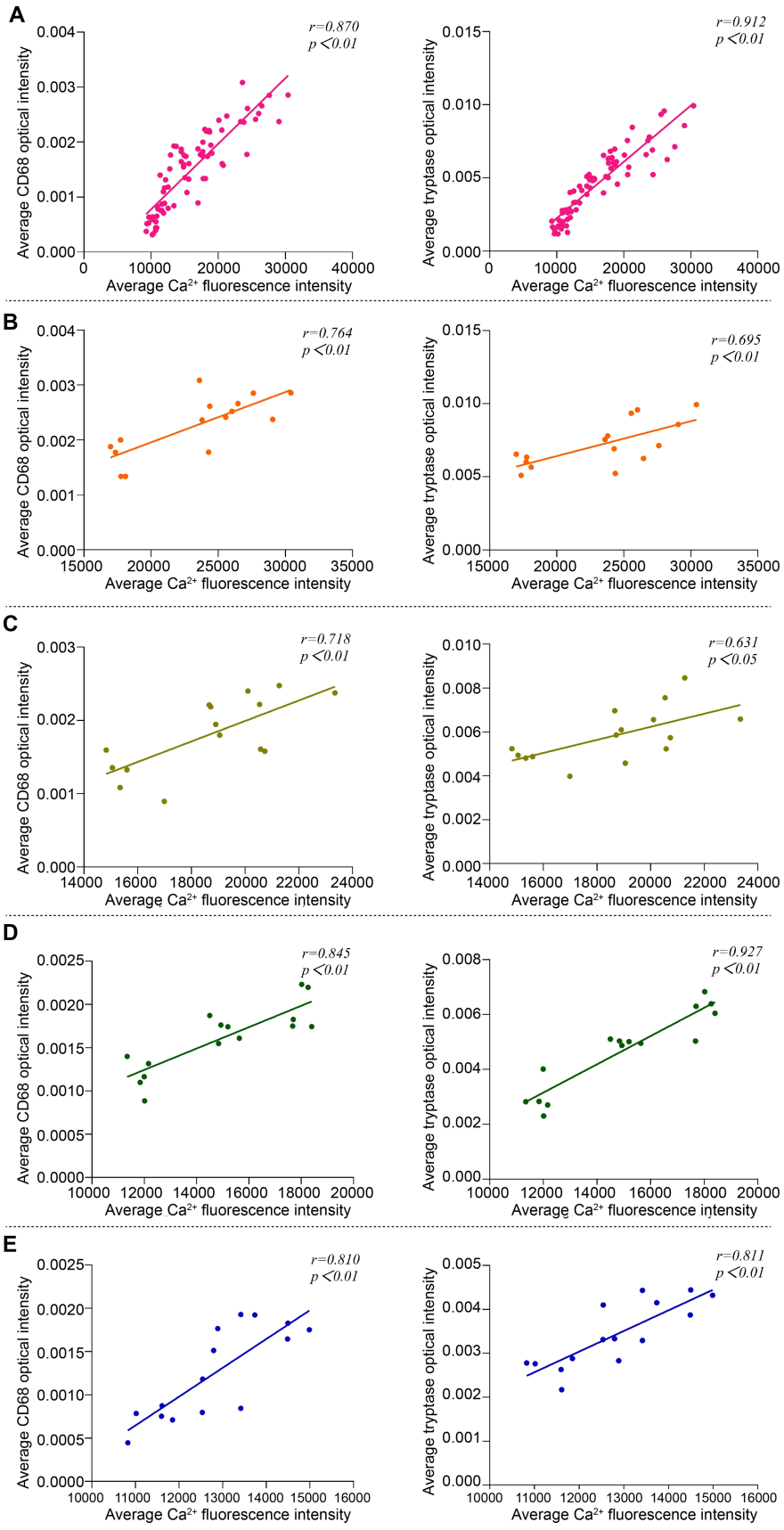

FIGURE 8
Correlation analysis between Ca^{2+} fluorescence intensity and the expression of Mac CD68 and MC tryptase in acupoint tissues in the overall groups (including the blank control group and the intervention groups) and each intervention group. **(A)** Overall Analysis. **(B)** Embedding group. **(C)** (ACE+T2B) Group. **(D)** (ACE+T4B) Group. **(E)** (ACE+T(2 + 4)B) Group.

Data availability statement

The raw data supporting the conclusions of this article will be made available by the authors, without undue reservation.

Ethics statement

The animal study was approved by the Experimental Animal Ethics Committee of Guizhou Medical University (approval number: 2101330). The study was conducted in accordance with the local legislation and institutional requirements.

Author contributions

XH: Conceptualization, Funding acquisition, Methodology, Investigation, Writing – original draft. XL: Funding acquisition, Writing – review & editing, Conceptualization, Methodology. YLu: Writing – review & editing, Data curation, Formal analysis. QZ: Data curation, Formal analysis, Writing – review & editing. YW: Writing – review & editing, Data curation, Formal analysis. MX: Writing – review & editing. YLuo: Writing – review & editing. TF: Writing – review & editing. YZ: Writing – review & editing. TY: Writing – review & editing, Investigation. KZ: Writing – review & editing, Investigation. JS: Investigation, Writing – review & editing. ML: Writing – review & editing, Project administration, Supervision. LL: Writing – review & editing, Project administration, Supervision.

Funding

The author(s) declare that financial support was received for the research, authorship, and/or publication of this article. This work was supported by Guizhou Provincial Science and Technology Plan Project (Qian Ke He Ji Chu-ZK[2022] General 421), National Natural Science Foundation of China (81960894) and Guizhou Medical University National Natural Science Foundation Incubation Project (20NSP021).

Acknowledgments

All authors would like to thank Dr. Pinhao Li (Department of Pathology, Affiliated Hospital of Guizhou Medical University) for his professional guidance on index detection. We also acknowledge the support of the Clinical Research Center, Affiliated Hospital of Guizhou Medical University for providing the necessary laboratory facilities and equipment. Furthermore, We would like to thank KetengEdit (www.ketengedit.com) for its linguistic assistance during the preparation of this manuscript.

Conflict of interest

The authors declare that the research was conducted in the absence of any commercial or financial relationships that could be construed as a potential conflict of interest.

Publisher's note

References

Bajaj, I., and Singhal, R. (2011). Poly (glutamic acid)-an emerging biopolymer of commercial interest. *Bioresour. Technol.* 102, 5551–5561. doi: 10.1016/j.biortech.2011.02.047

Bootman, M. D., and Bultynck, G. (2020). Fundamentals of cellular calcium signaling: a primer. *Perspect. Biol.* 12:802. doi: 10.1101/cshperspect.a038802

Brenneis, C., Kistner, K., Puopolo, M., Segal, D., Roberson, D., Sisignano, M., et al. (2013). Phenotyping the function of trpv1-expressing sensory neurons by targeted axonal silencing. *J. Neurosci.* 33, 315–326. doi: 10.1523/JNEUROSCI.2804-12.2013

Burnstock, G. (2009). Acupuncture: a novel hypothesis for the involvement of purinergic signalling. *Med. Hypotheses* 73, 470–472. doi: 10.1016/j.mehy.2009.05.031

Chen, R., Ji, G., Ma, T., Huang, X., Ren, H., and Xi, L. (2015). Role of intracellular free calcium in killing penicillium marneffei within human macrophages. *Microb. Pathog.* 83-84, 29–34. doi: 10.1016/j.micpath.2015.05.001

Chen, T., Liu, N., Liu, J., Zhang, X., Huang, Z., Zang, Y., et al. (2016). Gua sha, a press-stroke treatment of the skin, boosts the immune response to intradermal vaccination. *PeerJ* 4:e2451. doi: 10.7717/peerj.2451

Chen, Y., Moore, C. D., Zhang, J. Y., Hall, R. R., MacLeod, A. S., and Liedtke, W. (2017). Trpv4 moves toward center-fold in rosacea pathogenesis. *J. Invest. Dermatol.* 137, 801–804. doi: 10.1016/j.jid.2016.12.013

Chen, L., Wang, X., Zhang, X., Wan, H., Su, Y., He, W., et al. (2021). Electroacupuncture and moxibustion-like stimulation relieves inflammatory muscle pain by activating local distinct layer somatosensory afferent fibers. *Front. Neurosci.* 15:695152. doi: 10.3389/fnins.2021.695152

Chen, X. L., Yue, Z. H., Liu, L., Wang, Y., Li, P., Wen, Q. Q., et al. (2016). Ancient and modern applications and research of Zusanli acupoint. *J. Acupunct. Moxibust. Clin.* 32, 80–83. doi: 10.19917/j.cnki.1005-0779.2016.07.028

Chen, B., Zhao, X., Li, M. Y., and Guo, Y. (2013). Progress of researches and comments on promoters initiating effects of acupuncture stimulation of acupoints. *Acupunct. Res.* 38, 511–514. doi: 10.13702/j.1000-0607.2013.06.016

Cheng, L., Liang, X., Hou, X. R., Nie, H. F., Lu, Y. W., Li, L. H., et al. (2022a). Clinical literature metric study on key elements of acupoint embedding in recent 10 years. *Acupunct. Res.* 47, 830–836. doi: 10.13702/j.1000-0607.20210892

Cheng, L., Liang, X., Hou, X. R., Nie, H. F., Zhou, M. D., Li, L. H., et al. (2022b). Clinical research status of acupoint thread embedding in recent decade based on bibliometric analysis. *Chin. J. Clin. Res.* 14, 12–16. doi: 10.3969/j.issn.1674-7860.2022.21.004

China Association of Acupuncture and Moxibustion (2021). Part 2: common Acupoint names and locations for experimental animals: rats. *Acupunct. Res.* 46:351.

Chistiakov, D. A., Killingsworth, M. C., Myasoedova, V. A., Orekhov, A. N., and Bobryshev, Y. V. (2017). Cd68/macrosialin: not just a histochemical marker. *Lab. Investig.* 97, 4–13. doi: 10.1038/labinvest.2016.116

Dou, B. M., Xu, Z. F., Lu, Z. Q., Li, N. C., and Yao, K. F. (2022). Acupoints are "transducers" of coupling response to acupuncture physicochemical information. *Chin. Acupunct. Moxibust.* 42, 1321–1326. doi: 10.13703/j.0255-2930.20220216-k0005

Du, H. M., and Zhang, W. (2019). Progress in application of acupoint embedding threads. *J. Tradit. Chin. Med. Update* 25, 121–124. doi: 10.13862/j.cnki.cn43-1446/r.2019.04.035

Duan, L., Qiu, W., Bai, G., Qiao, Y., Su, S., Lo, P. C., et al. (2021). Metabolomics analysis on mice with depression ameliorated by acupoint catgut embedding. *Front. Psych.* 12:703516. doi: 10.3389/fpsyt.2021.703516

Essandoh, K., Li, Y., Huo, J., and Fan, G. C. (2016). Mirna-mediated macrophage polarization and its potential role in the regulation of inflammatory response. *Shock* 46, 122–131. doi: 10.1097/SHK.0000000000000604

Franz, S., Rammelt, S., Scharnweber, D., and Simon, J. C. (2011). Immune responses to implants - a review of the implications for the design of immunomodulatory biomaterials. *Biomaterials* 32, 6692–6709. doi: 10.1016/j.biomaterials.2011.05.078

Freichel, M., Almering, J., and Tsvilovskyy, V. (2012). The role of trp proteins in mast cells. *Front. Immunol.* 3:150. doi: 10.3389/fimmu.2012.00150

Fu, J. J., Lin, X. W., Dou, B. M., Li, Y. W., Fan, Z. Z., Liu, Q., et al. (2023). Role of acupoint connective tissue in the initiation of acupuncture effect mechanism research. *World Chin. Med.* 18, 2988–2992. doi: 10.3969/j.issn.1673-7202.2023.20.024

Gilfillan, A. M., and Tkaczyk, C. (2006). Integrated signalling pathways for mast-cell activation. *Nat. Rev. Immunol.* 6, 218–230. doi: 10.1038/nri1782

Gordon, S., and Martinez, F. O. (2010). Alternative activation of macrophages: mechanism and functions. *Immunity* 32, 593–604. doi: 10.1016/j.immuni.2010.05.007

Guan, L., Zuo, F., Song, Q., and Shi, X. (2009). Standardization research on acupoint thread embedding technique: establishment of national standard "specifications for acupuncture and Moxibustion techniques part 10: Acupoint thread embedding". *Chin. Acupunct. Moxibust.* 29, 401–405. doi: 10.13703/j0255-2930.2009.05.01

Guo, Y. Y., Gao, Y., Hu, Y. R., Zhao, Y., Jiang, D., Wang, Y., et al. (2022). The transient receptor potential vanilloid 2 (trpv2) channel facilitates virus infection through the ca(2+) -lrmda axis in myeloid cells. *Adv. Sci.* 9:e2202857. doi: 10.1002/advs.202202857

Guo, M., le, X., Qin-yu, W., Ye, M., Sheng-qiang, Z., Yao, X., et al. (2022). Effectiveness and safety of Acupoint catgut embedding for the treatment of Poststroke constipation: a systematic review and Meta-analysis. *eCAM* 2022, 1–10. doi: 10.1155/2022/8080297

Huang, W. C., Sala-Newby, G. B., Susana, A., Johnson, J. L., and Newby, A. C. (2012). Classical macrophage activation up-regulates several matrix metalloproteinases through mitogen activated protein kinases and nuclear factor-κb. *PLoS One* 7:e42507. doi: 10.1371/journal.pone.0042507

Huang, M., Wang, X., Xing, B., Yang, H., Sa, Z., Zhang, D., et al. (2018). Critical roles of trpv2 channels, histamine h1 and adenosine a1 receptors in the initiation of acupoint signals for acupuncture analgesia. *Sci. Rep.* 8:6523. doi: 10.1038/s41598-018-24654-y

Huang, H., Yue, X., Huang, X., Long, W., Kang, S., Rao, Y., et al. (2022). Brain activities responding to acupuncture at st36 (zusanli) in healthy subjects: a systematic review and meta-analysis of task-based fmri studies. *Front. Neurol.* 13:930753. doi: 10.3389/fneur.2022.930753

Huo, J., Zhao, J. Q., Yuan, Y., and Wang, J. J. (2017). Research status of the mechanism of acupoint thread embedding therapy. *Chin. Acupunct. Moxibust.* 37, 1251–1254. doi: 10.13703/j.0255-2930.2017.11.031

Jain, R. A. (2000). The manufacturing techniques of various drug loaded biodegradable poly(lactide-co-glycolide) (plga) devices. *Biomaterials* 21, 2475–2490. doi: 10.1016/s0142-9612(00)00115-0

Jung, P., and Lushniak, B. D. (2017). Preventive medicine's identity crisis. *Am. J. Prev. Med.* 52, e85–e89. doi: 10.1016/j.amepre.2016.10.037

Ke, C., Shan, S. T., Xie, Z. R., Tang, L., Deng, Z. C., Zhang, W., et al. (2020). Application development of acupoint embedding threads and needles. *J. Tradit. Chin. Med.* 35, 5644–5647.

Kunisch, E., Fuhrmann, R., Roth, A., Winter, R., Lungershausen, W., and Kinne, R. W. (2004). Macrophage specificity of three anti-cd68 monoclonal antibodies (kp1, ebm11, and pgm1) widely used for immunohistochemistry and flow cytometry. *Ann. Rheum. Dis.* 63, 774–784. doi: 10.1136/ard.2003.013029

Kusmartsev, S., Dominguez-Gutierrez, P. R., Canales, B. K., Bird, V. G., Vieweg, J., and Khan, S. R. (2016). Calcium oxalate stone fragment and crystal phagocytosis by human macrophages. *J. Urol.* 195, 1143–1151. doi: 10.1016/j.juro.2015.11.048

Lawhorn, B. G., Brnardic, E. J., and Behm, D. J. (2021). Trpv4 antagonists: a patent review (2015-2020). *Expert Opin. Ther. Pat.* 31, 773–784. doi: 10.1080/13543776.2021.1903432

Li, F., He, T., Xu, Q., Lin, L. T., Li, H., Liu, Y., et al. (2015). What is the acupoint? A preliminary review of acupoints. *Pain Med.* 16, 1905–1915. doi: 10.1111/pme.12761

Li, G., Shi, Y., Zhang, L., Yang, C., Wan, T., Lv, H., et al. (2022). Efficacy of acupuncture in animal models of vascular dementia: a systematic review and network meta-analysis. *Front. Aging Neurosci.* 14:952181. doi: 10.3389/fnagi.2022.952181

Liang, X., Nie, H. F., and Hou, X. R. (2016). Temporal observation of the stimulation effects of embedded sutures at acupoints on normal human body after minimally invasive implantation. *Chin. Acupunct. Moxibust.* 36, 607–611. doi: 10.13703/j.0255-2930.2016.06.014

Liang, X., Nie, H. F., Hou, X. R., Lu, Y. W., Li, L. H., Zhou, M. D., et al. (2019). Temporal observation of acupuncture effect of PGLA thread embedding in "Zusanli" acupoint of normal human body. *Chin. Acupunct. Moxibust.* 39, 391–395. doi: 10.13703/j.0255-2930.2019.04.012

Liedtke, W. (2005). Trpv4 plays an evolutionary conserved role in the transduction of osmotic and mechanical stimuli in live animals. *J. Physiol.* 567, 53–58. doi: 10.1113/jphysiol.2005.088963

Liedtke, W., and Kim, C. (2005). Functionality of the trpv subfamily of trp ion channels: add mechano-trp and osmo-trp to the lexicon! *Cell. Mol. Life Sci.* 62, 2985–3001. doi: 10.1007/s00018-005-5181-5

Link, T. M., Park, U., Vonakis, B. M., Raben, D. M., Soloski, M. J., and Caterina, M. J. (2010). Trpv2 has a pivotal role in macrophage particle binding and phagocytosis. *Nat. Immunol.* 11, 232–239. doi: 10.1038/ni.1842

Liu, X., Wang, N., Zhu, Y., Yang, Y., Chen, X., Fan, S., et al. (2016). Inhibition of extracellular calcium influx results in enhanced il-12 production in lps-treated murine macrophages by downregulation of the camkkβ-ampk-sirt1 signaling pathway. *Mediat. Inflamm.* 2016:6152713. doi: 10.1155/2016/6152713

Lowe, D. T. (2017). Cupping therapy: an analysis of the effects of suction on skin and the possible influence on human health. *Complement. Ther. Clin. Pract.* 29, 162–168. doi: 10.1016/j.ctcp.2017.09.008

Luo, D., Liu, L., Zhang, H. M., Zhou, Y. D., Zhou, M. F., Li, J. X., et al. (2022). Relationship between acupuncture and transient receptor potential vanilloid: current and future directions. *Front. Mol. Neurosci.* 15:817738. doi: 10.3389/fnmol.2022.817738

Ma, H. T., and Beaven, M. A. (2011). Regulators of ca(2+) signaling in mast cells: potential targets for treatment of mast cell-related diseases? *Adv. Exp. Med. Biol.* 716, 62–90. doi: 10.1007/978-1-4419-9533-9_5

Ma, Z. B., Liu, A. G., Zhu, T. T., Yang, C. D., and Yan, X. K. (2019). Overview of adverse reactions and treatment methods of acupoint thread embedding therapy. *J. Tradit. Chin. Med.* 34, 4214–4216.

Makadia, H. K., and Siegel, S. J. (2011). Poly lactic-co-glycolic acid (plga) as biodegradable controlled drug delivery carrier. *Polymers* 3, 1377–1397. doi: 10.3390/polym3031377

McGaraughty, S., Chu, K. L., Brown, B. S., Zhu, C. Z., Zhong, C., Joshi, S. K., et al. (2008). Contributions of central and peripheral trpv1 receptors to mechanically evoked and spontaneous firing of spinal neurons in inflamed rats. *J. Neurophysiol.* 100, 3158–3166. doi: 10.1152/jn.90768.2008

Michalick, L., and Kuebler, W. M. (2020). Trpv4-a missing link between mechanosensation and immunity. *Front. Immunol.* 11:413. doi: 10.3389/fimmu.2020.00413

Min, S., Lee, H., Kim, S. Y., Park, J. Y., Chae, Y., Lee, H., et al. (2015). Local changes in microcirculation and the analgesic effects of acupuncture: a laser doppler perfusion imaging study. *J. Altern. Complement. Med.* 21, 46–52. doi: 10.1089/acm.2013.0442

Müller, D. A., Snedeker, J. G., and Meyer, D. C. (2016). Two-month longitudinal study of mechanical properties of absorbable sutures used in orthopedic surgery. *J. Orthop. Surg. Res.* 11:111. doi: 10.1186/s13018-016-0451-5

Payne, V., and Kam, P. C. (2004). Mast cell tryptase: a review of its physiology and clinical significance. *Anaesthesia* 59, 695–703. doi: 10.1111/j.1365-2044.2004.03757.x

Ramprasad, M. P., Terpstra, V., Kondratenko, N., Quehenberger, O., and Steinberg, D. (1996). Cell surface expression of mouse macrosialin and human cd68 and their role as macrophage receptors for oxidized low density lipoprotein. *Proc. Natl. Acad. Sci. USA* 93, 14833–14838. doi: 10.1073/pnas.93.25.14833

Ribatti, D. (2013). Mast cells and macrophages exert beneficial and detrimental effects on tumor progression and angiogenesis. *Immunol. Lett.* 152, 83–88. doi: 10.1016/j.imlet.2013.05.003

Seminerio, I., Kindt, N., Descamps, G., Bellier, J., Lechien, J. R., Mat, Q., et al. (2018). High infiltration of cd68+ macrophages is associated with poor prognoses of head and neck squamous cell carcinoma patients and is influenced by human papillomavirus. *Oncotarget* 9, 11046–11059. doi: 10.18632/oncotarget.24306

Shi, X. M. (2017). Acupuncture and Moxibustion. Beijing: China Traditional Chinese Medicine Press.

Shibasaki, K. (2016). Physiological significance of trpv2 as a mechanosensor, thermosensor and lipid sensor. *J. Physiol. Sci.* 66, 359–365. doi: 10.1007/s12576-016-0434-7

Tatemoto, K., Nozaki, Y., Tsuda, R., Kaneko, S., Tomura, K., Furuno, M., et al. (2018). Endogenous protein and enzyme fragments induce immunoglobulin e-independent activation of mast cells via a g protein-coupled receptor, mrgprx2. *Scand. J. Immunol.* 87:e12655. doi: 10.1111/sji.12655

Teng, F., Ma, X., Cui, J., Zhu, X., Tang, W., Wang, W., et al. (2022). Acupoint catgut-embedding therapy inhibits nf-κb/cox-2 pathway in an ovalbumin-induced mouse model of allergic asthma. *Biomed. Res. Int.* 2022:1764104. doi: 10.1155/2022/1764104

Tsvilovskyy, V., Solís-López, A., Schumacher, D., Medert, R., Roers, A., Kriebs, U., et al. (2018). Deletion of orai2 augments endogenous crac currents and degranulation in mast cells leading to enhanced anaphylaxis. *Cell Calcium* 71, 24–33. doi: 10.1016/j.ceca.2017.11.004

Vašek, D., Fikarová, N., Marková, V. N., Honc, O., Pacáková, L., Porubská, B., et al. (2024). Lipopolysaccharide pretreatment increases the sensitivity of the trpv1 channel and promotes an anti-inflammatory phenotype of capsaicin-activated macrophages. *J. Inflamm. Lond.* 21:17. doi: 10.1186/s12950-024-00391-0

Velez, T. E., Bryce, P. J., and Hulse, K. E. (2018). Mast cell interactions and crosstalk in regulating allergic inflammation. *Curr Allergy Asthma Rep* 18:30. doi: 10.1007/s11882-018-0786-6

Vilceanu, D., Honore, P., Hogan, Q. H., and Stucky, C. L. (2010). Spinal nerve ligation in mouse upregulates trpv1 heat function in injured ib4-positive nociceptors. *J. Pain* 11, 588–599. doi: 10.1016/j.jpain.2009.09.018

Wang, M., Gao, Y. H., Xu, J., Chi, Y., Wei, X. B., Lewith, G., et al. (2015). Zusanli (st36) acupoint injection for preventing postoperative ileus: a systematic review and meta-analysis of randomized clinical trials. *Complement. Ther. Med.* 23, 469–483. doi: 10.1016/j.ctim.2015.03.013

Wang, Y. J., Li, L. H., Hou, X. R., Nie, H. F., Liang, X., Zhang, Q., et al. (2023). Effects of catgut and PGLA embedding on skin MCs, substance P and histamine in "Zusanli" acupoint area of healthy rats. *Chin. Acupunct. Moxibus.* 43, 944–950. doi: 10.13703/j.0255-2930.20220703-k0002

Wang, L. N., Wang, X. Z., Li, Y. J., Li, B. R., Huang, M., Wang, X. Y., et al. (2022). Activation of subcutaneous mast cells in acupuncture points triggers analgesia. *Cells* 11:809. doi: 10.3390/cells11050809

Wei, Y. T., Cao, C. X., Li, X. J., and Yan, X. K. (2019). Research progress on molecular biology mechanisms of acupoint thread embedding therapy. *J. Tradit. Chin. Med.* 34, 3633–3636.

Wernersson, S., and Pejler, G. (2014). Mast cell secretory granules: armed for battle. *Nat. Rev. Immunol.* 14, 478–494. doi: 10.1038/nri3690

Wu, X. Y., Chen, G. Z., Li, Y. T., and Xu, Y. X. (2019). Key issues and countermeasures of acupoint thread implantation therapy. *Chin. Acupunct. Moxibust.* 39, 81–85. doi: 10.13703/j.0255-2930.2019.01.019

Wu, Y. H., Nian, F., Li, Y., Xie, M., and Chen, W. (2020). Meta-analysis of the influence of stimulating Zusanli acupoint on human immune function. *Contemp. Med.* 26, 108–111. doi: 10.3969/j.issn.1009-4393.2020.02.045

Wu, X. R., Peng, H. X., He, M., Zhong, R., Liu, J., Wen, Y. K., et al. (2022). Macrophages-based immune-related risk score model for relapse prediction in stage i-iii non-small cell lung cancer assessed by multiplex immunofluorescence. *Transl. Lung Cancer Res.* 11, 523–542. doi: 10.21037/tlcr-21-916

Wu, M. L., Xu, D. S., Bai, W. Z., Cui, J. J., Shu, H. M., He, W., et al. (2015). Local cutaneous nerve terminal and mast cell responses to manual acupuncture in acupoint LI4 area of the rats. *J. Chem. Neuroanat.* 68, 14–21. doi: 10.1016/j.jchemneu.2015.06.002

Xing, B. F., Hong, M., Zhou, X., Zhang, K. Y., Diao, S. P., Guo, Y. M., et al. (2019). Short-term and long-term efficacy analysis of PGLA acupoint embedding therapy for shoulder-hand syndrome in the early stage after stroke. *Acupunct. Res.* 44, 762–765. doi: 10.13702/j.1000-0607.180805

Xu, X. X. (2018). Preparation and research of woven structure implant materials for acupuncture and moxibustion: Donghua University.

Xu, J. M., and Shi, G. P. (2012). Emerging role of mast cells and macrophages in cardiovascular and metabolic diseases. *Endocr. Rev.* 33, 71–108. doi: 10.1210/er.2011-0013

Yan, M., Wang, R., Liu, S., Chen, Y., Lin, P., Li, T., et al. (2020). The mechanism of electroacupuncture at zusanli promotes macrophage polarization during the fibrotic process in contused skeletal muscle. *Eur. Surg. Res.* 60, 196–207. doi: 10.1159/000503130

Yang, T., Zhao, S. M., Zhao, X., Guo, Y., Chen, Z. L., and Guo, Y. M. (2018). Bibliometric study on the use of rat acupoints in acupuncture basic experiments in recent six years. *Hebei Tradit. Chin. Med.* 40, 1248–1251. doi: 10.3969/j.issn.1002-2619.2018.08.029

Yu, W. L., Park, J. Y., Park, H. J., and Kim, S. N. (2022). Changes of local microenvironment and systemic immunity after acupuncture stimulation during inflammation: a literature review of animal studies. *Front. Neurol.* 13:1086195. doi: 10.3389/fneur.2022.1086195

Zhang, Q., Li, L. H., Hou, X. R., Liang, X., Lu, Y. W., Nie, H. F., et al. (2023). Effect of catgut implantation on macrophage CD68, tumor necrosis factor-α and interleukin-1β in "Zusanli" (ST 36) region of rats. *Zhen Ci Ma Zui* 48, 681–685. doi: 10.13702/j.1000-0607.20220177

Zhang, X. H., Qifu, L. I., Rong, Y. I., Chonghui, X., Yuhao, J., Jiangqiong, M., et al. (2023). Effect of catgut embedding at acupoints versus non-acupoints in abdominal obesity: a randomized clinical trial. *J. Tradit. Chin. Med.* 43, 780–786. doi: 10.19852/j.cnki.jtcm.20230608.002

Zhang, D., Spielmann, A., Wang, L., Ding, G., Huang, F., Gu, Q., et al. (2012). Mast-cell degranulation induced by physical stimuli involves the activation of transient-receptor-potential channel trpv2. *Physiol. Res.* 61, 113–124. doi: 10.33549/physiolres.932053

Zhou, L., Wang, Y., Qiao, J., Wang, Q. M., and Luo, X. (2020). Acupuncture for improving cognitive impairment after stroke: a meta-analysis of randomized controlled trials. *Front. Psychol.* 11:549265. doi: 10.3389/fpsyg.2020.549265

Zhu, B. (2021). On acupoints and acupoint specificity. *Chin. Acupunct. Moxibust.* 41, 943–950. doi: 10.13703/j.0255-2930.20210701-k0002

Zhu, Y., Fan, S., Wang, N., Chen, X., Yang, Y., Lu, Y., et al. (2017). Nadph oxidase 2 inhibitor diphenyleneiodonium enhances ros-independent bacterial phagocytosis in murine macrophages via activation of the calcium-mediated p38 mapk signaling pathway. Am. J. Transl. Res. 9, 3422–3432

frontiers | Frontiers in Nutrition

TYPE Original Research
PUBLISHED 03 February 2025
DOI 10.3389/fnut.2025.1440373

OPEN ACCESS

EDITED BY
Rubem C. A. Guedes,
Federal University of Pernambuco, Brazil

REVIEWED BY
Qixiang Lin,
Emory University, United States
Celia Garau,
University of the Balearic Islands, Spain
Lukasz Bijoch,
Polish Academy of Sciences, Poland

*CORRESPONDENCE
Judith R. A. van Rooij
judith.vanrooij@uantwerpen.be
Marleen Verhoye
marleen.verhoye@uantwerpen.be

RECEIVED 29 May 2024
ACCEPTED 13 January 2025
PUBLISHED 03 February 2025

CITATION
van Rooij JRA, van den Berg M, Vasilkovska T, Van Audekerke J, Kosten L, Bertoglio D, Adhikari MH and Verhoye M (2025) Short-term caloric restriction or resveratrol supplementation alters large-scale brain network connectivity in male and female rats. *Front. Nutr.* 12:1440373. doi: 10.3389/fnut.2025.1440373

Short-term caloric restriction or resveratrol supplementation alters large-scale brain network connectivity in male and female rats

Judith R. A. van Rooij[1,2]*, Monica van den Berg[1,2], Tamara Vasilkovska[1], Johan Van Audekerke[1,2], Lauren Kosten[1], Daniele Bertoglio[1,2], Mohit H. Adhikari[1,2] and Marleen Verhoye[1,2]*

[1]Bio-Imaging Lab, Faculty of Pharmaceutical, Biomedical and Veterinary Sciences, University of Antwerp, Antwerp, Belgium, [2]μNEURO Research Centre of Excellence, University of Antwerp, Antwerp, Belgium

Introduction: Dietary interventions such as caloric restriction (CR) exert positive effects on brain health. Unfortunately, poor compliance hinders the success of this approach. A proposed alternative is resveratrol (Rsv), a CR-mimetic known to promote brain health. Direct comparison between the effects of Rsv and CR on brain health is lacking, with limited knowledge on their sex-specific effects. Therefore, we aimed to compare and unravel the sex-specific impact of these dietary interventions on spontaneous brain activity.

Methods: Here, we used resting-state fMRI to investigate functional connectivity (FC) changes in five prominent resting-state brain networks (RSNs) in healthy 4 month old male and female F344 rats supplemented to either 40% CR or daily Rsv supplementation (10 mg/kg, oral) for the duration of 1 month.

Results: Our results demonstrated a decreased body weight (BW) in CR rats, as well as an increase in body weight in male Rsv supplemented rats, compared to female Rsv supplemented rats, whereas this difference between sexes was not observed in the control or CR groups. Furthermore, we found that both CR or Rsv supplementation induce a female-specific decrease of FC between the subcortical network and hippocampal network, and between the subcortical network and lateral cortical network. Moreover, Rsv supplementation lowered FC within the hippocampal network and between the hippocampal and the default mode like network, the lateral cortical network and the sensory network—an effect not observed for the CR rats.

Discussion: Our findings reveal that both CR and Rsv induce a similar female-specific decrease of FC in RSNs associated with memory and emotion, all the while CR and Rsv induce dissimilar changes in body weight and other within- and between-RSN FC measures. Altogether, this study provides insight into the effects and comparability of short-term CR and Rsv supplementation on brain connectivity within- and between-RSNs in both male and female F344 rats, providing a FC reference for future research of dietary effects.

KEYWORDS

caloric restriction, resveratrol, resting-state functional MRI, resting-state networks, functional connectivity

1 Introduction

Due to the constant exponential growth of the elderly population world-wide, the search for preventative strategies to preserve cognitive function and promote healthy aging have become increasingly important (1). Lifestyle modifications, including regular exercise and dietary adjustments, are known to play a crucial role in this endeavor. One proposed dietary adjustment is caloric restriction (CR) (2), defined as a significant reduction of energy intake without the risk of malnutrition. Through a variety of pathways, short- and long-term CR has been shown to positively influence brain health by reducing neuroinflammation (3) and oxidative stress (4), while simultaneously enhancing neurovascular function (5). In animal models of aging and age-related neurodegenerative diseases, CR has been shown to prevent neuronal degradation (6, 7), enhance neurogenesis in the hippocampus (8), as well as prevent against the age-related decline in motor coordination (9) and learning (7). These findings collectively highlight the potential of CR as a promising approach to maintain and improve brain health.

Despite the proven positive effect of CR on brain health, poor compliance to drastic, life-long CR hinders its success as a therapeutic approach (10). In light of this challenge, CR-mimetics have emerged as a potential alternative strategy. CR-mimetics aim to activate the same pathways and mechanisms and are therefore hypothesized to mimic the beneficial effects of CR on brain health without the life-long commitment to reduced caloric intake (11, 12). One of the most extensively studied CR-mimetics is resveratrol (Rsv), a polyphenol and phytoalexin, present in high concentrations in, for example, blue berries and red grapes. Rsv has shown to exert positive effects on neuroinflammation (13) and oxidative stress (14). The hypothesis of Rsv serving a similar function as CR is further solidified through reported findings from studies in animal models of aging and age-related neurodegenerative diseases (15). Here, Rsv is reported to preserve cognitive function (16) and neurovascular coupling (17) in aging mice, and exert neuroprotective effects in neurodegenerative diseases such as Alzheimer's (18) and Parkinson's Disease (19) through similar pathways as reported for CR. These findings further support the hypothesis that Rsv may serve as a viable alternative to CR in promoting brain health and potentially delaying the onset of aging and age-related neurodegenerative diseases.

Resting-state functional MRI (rsfMRI), a non-invasive neuroimaging method, has proven itself as a powerful tool to assess brain function (20). With rsfMRI, one measures the blood-oxygenation level dependent (BOLD)-contrast, indirectly reflecting fluctuations in neuronal activity via neurovascular coupling while the brain is at rest. The correlation between the BOLD signal time series of brain regions is expressed as functional connectivity (FC), where regions that exhibit highly correlated BOLD signals form the resting-state networks (RSNs) (21). The most prominent RSN in humans is the default mode network (DMN), typically anticorrelated to the frontoparietal network (FPN) (22). Changes in FC as a result of CR and Rsv have been reported in regions belonging to the hippocampal network (Hipp), FPN and the DMN (23–26), emphasizing the potential of rsfMRI to assess changes in brain function as a result of dietary interventions.

While these findings confirm that CR or Rsv supplementation alters brain connectivity, there is a lack of research directly comparing the effects of these dietary interventions. Moreover, even though both CR and Rsv supplementation have been hypothesized to exert effects on brain function in a sex-dependent manner (27, 28), research on the possible sex-specific effects that both dietary interventions can exert on brain connectivity, is sparce. Clinical trials assessing dietary effects are subject to challenges due to low patient adherence, high susceptibility to confounding variables, high patient dropout rates and limited follow-up periods (29). The use of animal models can overcome these challenges, aiding to provide critical insight into the sex-specific effects of CR or Rsv on brain connectivity. RsfMRI is well established in rodents, showing similar findings compared to humans regarding RSNs. Rodent analogs of the human DMN and FPN, along with other major RSNs, have been identified as the default mode-like network (DMLN), the lateral cortical network (LCN), the hippocampal (Hipp), the sensory (Sens) and subcortical (SubC) network (30). In this study, we hypothesized that CR or Rsv supplementation induces changes in connectivity within and between these RSNs in a sex-specific manner. Therefore, we aimed to characterize and compare the sex-specific effects of short-term CR and Rsv supplementation on brain connectivity, using rsfMRI to assess FC changes within and between the five prominent rodent RSNs as a result of dietary intervention.

2 Materials and methods

2.1 Animals

F344 rats (RRID: RGD_60994, Charles River, Italy) used within this study were bred in-house. A total of 42 male and female F344 rats (n = 21/sex) were single-housed at 3 months of age for the duration of the experiment, and kept under controlled environmental conditions [12-h light/dark cycle, (22 ± 2)°C, 40–60% humidity]. Water was provided at libitum. All procedures were in accordance with the guidelines approved by the European Ethics Committee (decree 2010/63/EU), and were approved by the Committee on Animal Care and Use at the University of Antwerp, Belgium (ECD: 2021-59).

2.2 Dietary treatment paradigm

Three-month-old rats were randomly divided into 3 groups (Figure 1), receiving dietary intervention and Rsv supplementation for the duration of 4 weeks, until the age of 4 months. The first group served as controls. The second group received daily Rsv (10 mg/kg, oral, High Potency Trans-Resveratrol 600, Doctor's Best®, California, United States) supplementation. The third group was exposed to a gradual weekly decrease in caloric uptake by 40%. To allow adaptation to restricted feeding, the animals were fed 1 week with 15% CR, a

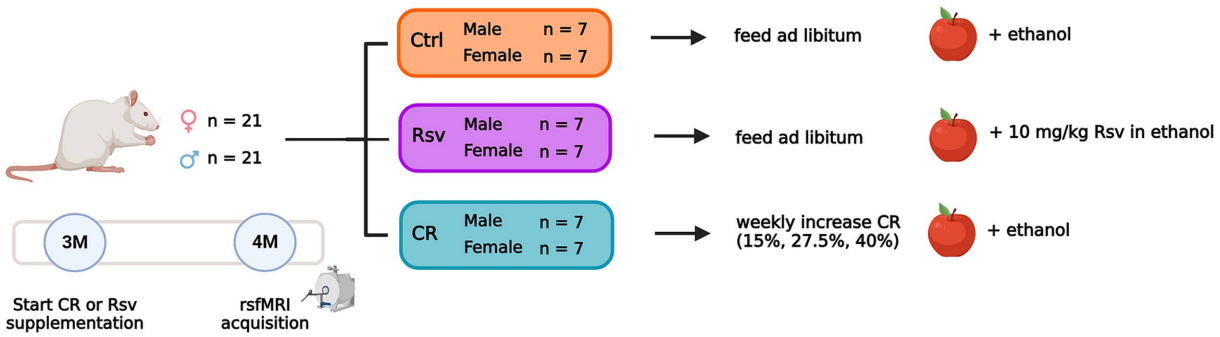

FIGURE 1
Overview of the experimental dietary treatment paradigm and study design. Number of animals per sex and group are given. Dietary intervention and supplementation of the apple chips starts at 3 months of age (3M). RsfMRI data are acquired at 4 months of age (4M). The apple represents the supplementation of Rsv or its vehicle using dried apple chips. Created with Biorender.com.

second week with 27.5% CR and 40% CR thereafter. Food fortified with vitamins and minerals was provided to avoid malnutrition (Rat/Mouse Fortified, Ssniff®, Germany). CR of 15, 27.5, and 40% was calculated based on averaged food intake of Ctrl (male/female $n = 3/3$) and Rsv (male/female $n = 3/2$) rats, adjusted for age and sex. Control and Rsv supplemented rats were provided standard chow (Ssniff®, Germany) ad libitum. Rsv solubilized in 99.8% ethanol (Thermo Fisher Scientific), was applied to dried apple chips (JR Farm, Germany) and supplemented daily to the rats in the Rsv group. To minimize the difference between conditions, all CR and control rats were supplemented with a daily dose of dried apple chips with vehicle only (99.8% ethanol). This volume of ethanol was determined through averaging the daily Rsv volumes, adjusted for age and sex.

Subjects were weighed prior to the start of the dietary intervention and each week afterwards for the duration of the experiment. The percentage body weight (BW) change respective to the starting weight was calculated for each subject.

2.3 RsfMRI acquisition

RsfMRI data of the rats were acquired at 4 months of age, after 1 month of CR or Rsv supplementation. Rats were anesthesia using an isoflurane-medetomidine protocol: an established anesthesia protocol for rsfMRI in rodents (31–34). Anesthesia was induced using 5% isoflurane (IsoFlo®, Zoetis, United States), administered with a gaseous mixture of 200 mL/min O_2 and 400 mL/min N_2. For further animal handling and positioning, the isoflurane level was reduced to 3%. After positioning, a subcutaneous bolus injection of medetomidine (0.05 mg/kg, Domitor®, Vetoquinol, France) was administered. Continuous subcutaneous infusion of medetomidine (0.1 mg/kg/h) started 15 min after bolus administration, with the isoflurane level being lowered to 0.4%, to be maintained throughout the whole MRI session. Physiological parameters (breathing rate, heart rate, O_2 saturation and body temperature) of the animal were closely monitored during the entire procedure (MR-compatible Small Animal Monitoring, Gating, and heating system, SA Instruments). Body temperature was maintained at 37 (± 0.5) °C using a feedback-controlled warm air circuitry (MR-compatible Small Animal Heating System, SA Instruments Inc., United States).

MRI data were acquired on a 7 T Pharmascan MR scanner (Bruker®, Germany) with a volume resonator coil for radiofrequency excitation and a 2 × 2 channel receiver head radiofrequency coil for signal detection. To ensure uniform slice positioning between subjects, multi-slice T2-weighted (T2w) TurboRARE images were acquired in three directions (echo time (TE): 33 ms, repetition time (TR): 1800 ms, RARE factor: 8, field of view (FOV): (35 × 35) mm^2, matrix: [256 × 256]). Whole-brain rsfMRI data were acquired 40 min after the bolus of medetomidine using a single shot gradient echo, echo-planar imaging (EPI) sequence (TE: 18 ms, TR: 600 ms, FOV (30 × 30) mm^2, matrix [96 × 96], 12 coronal slices of 1 mm, slice gap: 0.1 mm, 1000 repetitions), for a total of 10 min. An anatomical 3D image was acquired for registration purposes, with a T2w-TurboRARE sequence (TR: 1,800 ms, TE: 36 ms, RARE factor: 16, FOV: (35 × 35 × 16) mm^3, acquisition matrix: [256 × 256 × 32], reconstruction matrix: [256 × 256 × 64]). At the end of the scan session, a subcutaneous injection of 0.1 mg/kg atipamezole (Antisedan®, Pfizer, Germany) was administered to counteract the effects of the medetomidine anesthesia and the animals were allowed to recover under a heating lamp. All animals recovered within 15–20 min after the end of the scan session.

2.4 rsfMRI image preprocessing

All preprocessing steps were performed with MATLAB R2020a (Mathworks, Natick, MA) and ANTs (Advanced Normalization Tools). The rsfMRI data were padded using an in-house MATLAB script. Debiasing, realignment, normalization, co-registration and smoothing of the data was performed using SPM 12 software (Statistical Parametric Mapping). First, subject-specific 3Ds were debiased after which a study specific 3D-template was created from a subset of animals (male/female: Ctrl $n = 2/2$, Rsv $n = 2/2$, CR $n = 2/3$) in ANTs. All individual 3Ds were normalized to the study-specific 3D template using a global 12-parameter affine transformation followed by a non-linear deformation protocol. The rsfMRI EPI images were realigned to the first EPI image using a 6-parameter rigid body spatial transformation estimated using a least-squares approach. RsfMRI data were co-registered to the animal's respective 3D image using a global 12-parameter affine transformation with mutual information used as similarity metric and normalized to the study-specific template using

the combined transformation parameters. RsfMRI data were smoothed in-plane using a Gaussian kernel with full width at half maximum of twice the voxel size and filtered (0.01–0.2 Hz) with a Butterworth band-pass filter. Finally, quadratic detrending was performed on the filtered images. During the entire process, a total of five subjects [Ctrl (male/female $n = 2/1$), CR (male $n = 2$)] were removed from further analysis due to poor quality of the data.

2.5 Functional connectivity analysis

Region of interest (ROI)-based FC analysis was performed on the preprocessed rsfMRI data. A neuroanatomical atlas comprised of 71 anatomical parcels (Fischer 344[1]), was warped onto the study-specific template and down-sampled (ANTs) to match the EPI space. Out of the 71 parcels, 43 unilateral gray matter ROIs (for both the left (L) and right (R) hemisphere for each region) were selected, excluding regions sensitive to susceptibility artifacts, transient effects and small size. These selected ROIs represent the five prominent rodent RSNs: the default mode-like network, the hippocampal network (Hipp), the sensory network (Sens), the lateral cortical network (LCN) and the subcortical network (SubC) (Supplementary Table S1). For each subject, Pearson correlation coefficients between the ROI-averaged BOLD signal timeseries of each pair of ROIs were calculated and Fisher z-transformed yielding subject-wise 43 × 43 FC matrices. FC within each network was calculated by averaging across FC values between all ROIs belonging to the network. Similarly, between-network FC was calculated by averaging across FC values between all pairs of ROIs belonging to both networks.

2.6 Statistics

The ROI-based and network-based FC matrices were subjected to an one-sample *t*-test (FDR corrected, Benjamini-Hochberg procedure, $p < 0.05$), within group (per sex and treatment). All data was tested for normality using the Shapiro–Wilk test determining the goodness of a normal fit. All data was normally distributed. The BW at week 0, the percentile change in BW at 4 weeks of treatment and the outcomes of the network-based FC were analyzed using a two-way ANOVA (treatment, sex, treatment*sex). In case of a significant treatment*sex interaction, post-hoc tests were performed using Student's *t*-test with FDR correction (Benjamini-Hochberg procedure, $p < 0.05$). When no significant treatment*sex interaction was present, the interaction was removed and the model was recalculated using only the main effects (treatment and sex). In case of a significant treatment effect, post-hoc tests were performed on all groups using a Tukey HSD test. Outlier detection was performed using a principal component analysis, per sex and treatment. Subjects with a Hotelling T2 statistics index higher than the 95% confidence interval were marked as outliers. Subjects with more than 8 out of 15 within- and between-network FC values marked as outliers were excluded. Statistical analyzes were performed using JMP Pro 17 (SAS Institute Inc.) and MATLAB R2020a (Mathworks, Natick, MA). Graphical representation of the data was created using GraphPad Prism (version 9.4.1. for Windows, GraphPad Software, San Diego, California United States) and Adobe Illustrator (Adobe Inc.).

1 https://www.nearlab.xyz/fischer344atlas

3 Results

3.1 Caloric restriction reduces body weight in both male and female rats

In order to test the randomness of the treatment groups prior to dietary intervention, we tested for the effects of treatment and sex on body weight at week 0. No significant effects were found for treatment ($p = 0.4324$) or the interaction treatment*sex ($p = 0.6471$), but, as expected, we did find a significant sex effect ($p < 0.0001$) on BW, where males had a significantly higher weight compared to females (Figure 2A).

Next, we aimed to determine the effect of short-term dietary intervention on BW, by evaluating the percentile change in BW over the course of treatment, from the start of the intervention (Figure 2B). Over the course of the intervention, we observed a positive percentage change of BW in both Ctrl and Rsv rats indicative of weight gain, while observing a negative percentage BW change in the CR rats, indicative of weight loss. Statistical analysis of the percent change in BW at week 4 demonstrated a significant treatment*sex interaction effect ($p = 0.031$). Post-hoc analysis revealed that after 4 weeks the percentage BW change was significantly different in CR female rats [(mean ± SD) %, (−9.18 ± 1.41)%] when compared to female Ctrl [(6.94 ± 2.98)%, $p < 0.0001$] and female Rsv [(7.92 ± 1.44)%, $p < 0.0001$] rats. Similarly, we observed a significant difference in male CR rats (−11.51 ± 3.73)% compared to male Ctrl [(9.95 ± 1.67)%, $p < 0.0001$] and male Rsv [(10.33 ± 1.71)%, $p < 0.0001$] rats. Moreover, male Rsv supplemented rats had a higher percentage increase in BW compared to the female Rsv supplemented rats ($p = 0.009$). This sex-difference was not observed in the Ctrl ($p = 0.1084$) or CR ($p = 0.0739$) groups.

3.2 Dietary interventions alter ROI- and network-based resting-state FC

Next, we investigated the effect of dietary intervention on brain connectivity. To evaluate these effects on FC between ROIs and within and between networks, we first calculated average ROI-based FC matrices between the 43 predefined ROIs, per sex and treatment (Figure 3A), providing insight into the distribution of FC across the groups. Our analysis revealed that within group, FC of regions associated with the DMLN, Hipp, Sens and LCN were statistically significant and thus robustly represented in each of the groups. ROI-based FC, mainly within the SubC [caudate putamen (CPu), medial septum (MS), thalamus (Thal), hypothalamus (Hyp) and nucleus Accumbens (nAcc)], were often not statistically significant in the males, irrespective of treatment. The total number of significant connections was higher in females when compared to males in each group. An additional graphical representation of the ROI-based FC matrices was generated (Supplementary Figure S1), showing strong inter-hemispheric FC within the DMLN and LCN, and intra-hemispheric FC between DMLN, Hipp and Sens. These observations were primarily noted for the Ctrl and CR groups and to a lesser extent in the Rsv supplemented group.

Next, we grouped the ROIs based on their anatomical location and known implications into five RSNs (Figure 3B) and calculated,

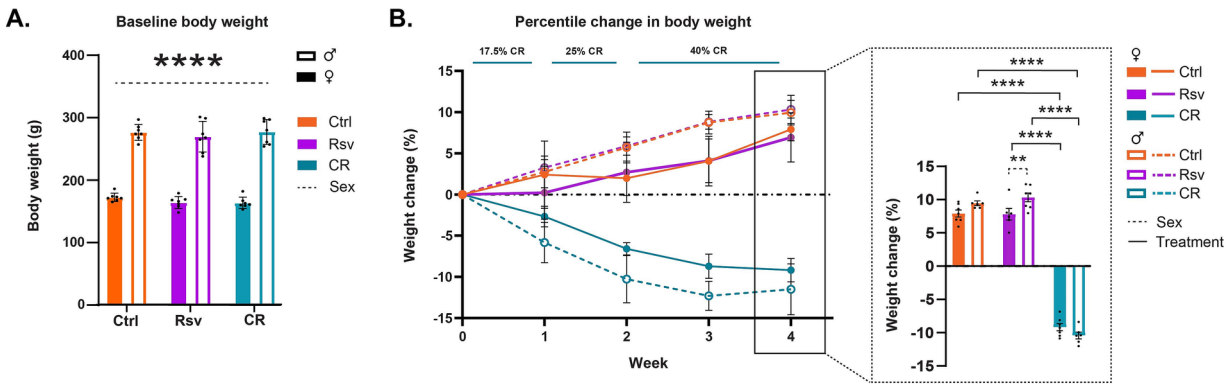

FIGURE 2
Effects of dietary intervention on body weight (BW). **(A)** Mean ± SD BW in grams (g) at baseline, prior to the start of the dietary interventions (week 0). The colors of the bars are indicative of the group each subject was assigned to [control (Ctrl), resveratrol (Rsv), caloric restricted (CR)]. Solid bars represent females and open bars represent the males. Dots represent individual subject data points. **(B)** Percentage change in BW (mean ± SD) with respect to baseline, over the course of the 4 week treatment, Ctrl, Rsv and CR group. Bar graph (insert) shows the percentage change in BW (mean ± SD) at week 4. Asterisks indicate the levels of statistical significance: $^{**}p < 0.01$, $^{****}p < 0.0001$.

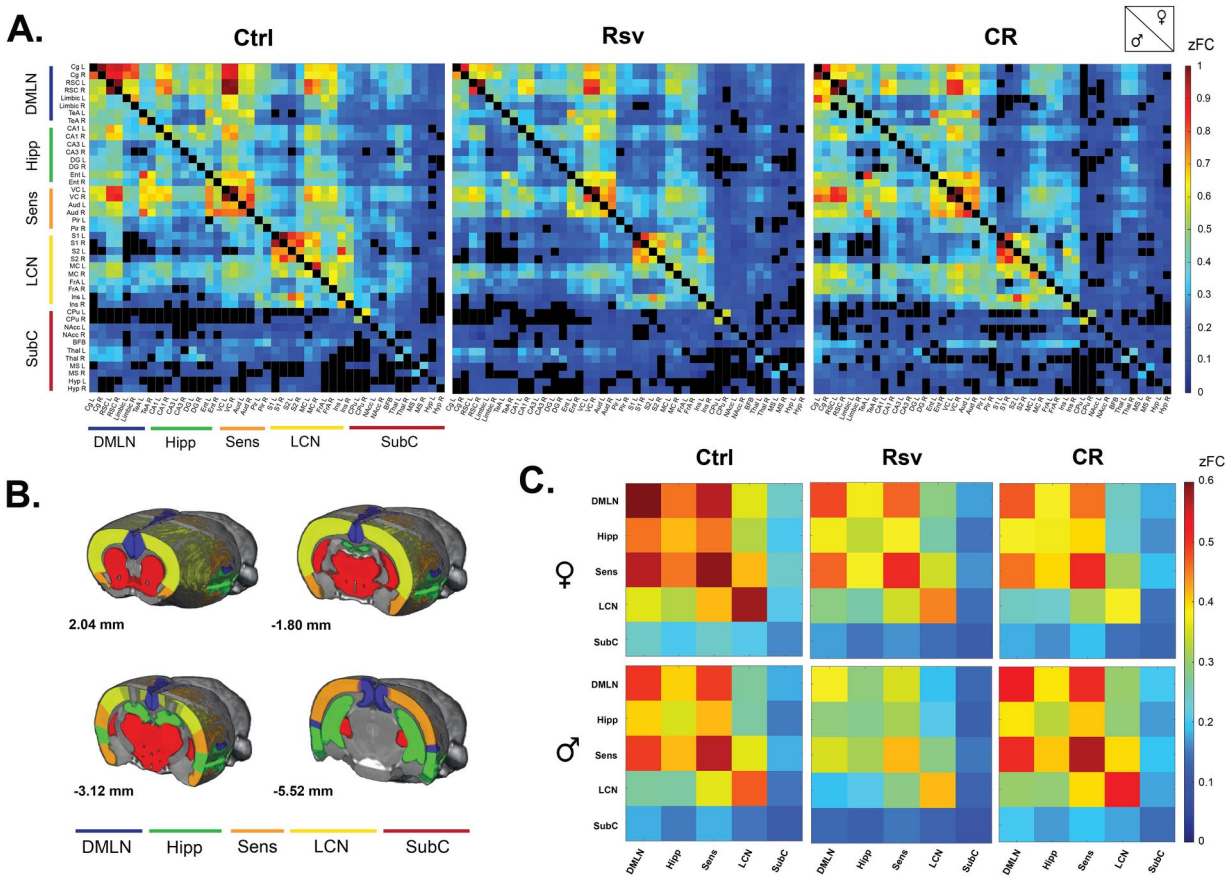

FIGURE 3
Functional connectivity (FC) in male and female Ctrl, Rsv supplemented and CR rats. **(A)** ROI-based FC matrices displaying the mean FC between ROI pairs for males (lower half) and females (upper half) per treatment group (Ctrl = control, CR = caloric restriction, Rsv = resveratrol, zFC = z-scored functional connectivity). The 43 regions of interest with left (L) and right (R) hemispheric location are plotted on the x and y axes (Supplementary Table S1). Non-significant connections ($p > 0.05$, one-sample t-test, FDR corrected per group) are blacked out. **(B)** Anatomical representation of the RSNs used in the network-based FC analysis. Annotated per image are the anatomical Bregma depths. **(C)** Mean network-based FC in females (top row) and males (bottom row) per treatment group. Colors indicate the strength of FC. Off-diagonal connections represent between-network FC, whereas the diagonals represent within network FC: DMLN (default mode-like network), Hipp (hippocampal network), Sens (sensory network), LCN (lateral cortical network), SubC (subcortical network). All within- and between-network FC values were significantly different from 0 as determined with a one-sample t-test (FDR corrected, Benjamini-Hochberg procedure, $p < 0.05$).

similar to the ROI-based FC matrices, average network-based FC matrices per sex and treatment (Figure 3C). Despite the earlier mentioned lack of significance in regions associated with the SubC, all between- and within-network FC measures were significantly higher than zero within each group [$p < 0.05$, one-sample t-test, FDR corrected (Supplementary Tables S2, S3)].

To visualize the effects of dietary intervention on ROI-based and network-based FC, we calculated the mean difference between the treatment groups per sex, highlighting the global changes in FC as a result of dietary intervention (Figures 4A,B).

3.3 Hippocampal and subcortical within- and between-network FC is different between sexes and altered by dietary intervention

To further investigate if FC is altered due to dietary intervention within- and between-RSNs, data was subjected to statistical analysis (two-way ANOVA). We observed a significant interaction effect of treatment*sex in the Hipp-SubC ($p = 0.0250$), SubC-DMLN ($p = 0.0116$) and SubC ($p = 0.0215$) (Figure 5A). Hipp-SubC FC was higher in female Ctrl rats when compared to male Ctrl rats ($p = 0.0229$), female Rsv rats ($p = 0.0038$) and female CR rats ($p = 0.019$). Similarly, in the SubC-DMLN, FC was higher in female Ctrl rats compared to male Ctrl rats ($p = 0.0364$), female Rsv rats ($p = 0.0364$) and female CR rats ($p = 0.0083$) and in addition we observed a difference between male CR and male Rsv rats ($p = 0.0495$). Finally, we also observed this interaction effect in the SubC, where FC was higher in female Ctrl rats compared to male Ctrl rats ($p = 0.0225$), female Rsv rats ($p = 0.0225$), and female CR rats ($p = 0.0225$).

Moreover, we found a significant treatment effect demonstrating lower FC in the Rsv group, compared to the Ctrl group in the Hipp network ($p = 0.0036$), Hipp-DMLN ($p = 0.0030$), Hipp-LCN ($p = 0.0474$), Hipp-Sens ($p = 0.0055$), SubC-LCN ($p = 0.0339$), and SubC-Sens ($p = 0.0076$). Post-hoc analysis (Figure 5B) consistently revealed a lower FC in the Rsv group, when compared to the Ctrl group [Hipp network ($p = 0.0025$), Hipp-DMLN ($p = 0.0020$), Hipp-LCN ($p = 0.0375$), Hipp-Sens ($p = 0.0043$), SubC-LCN

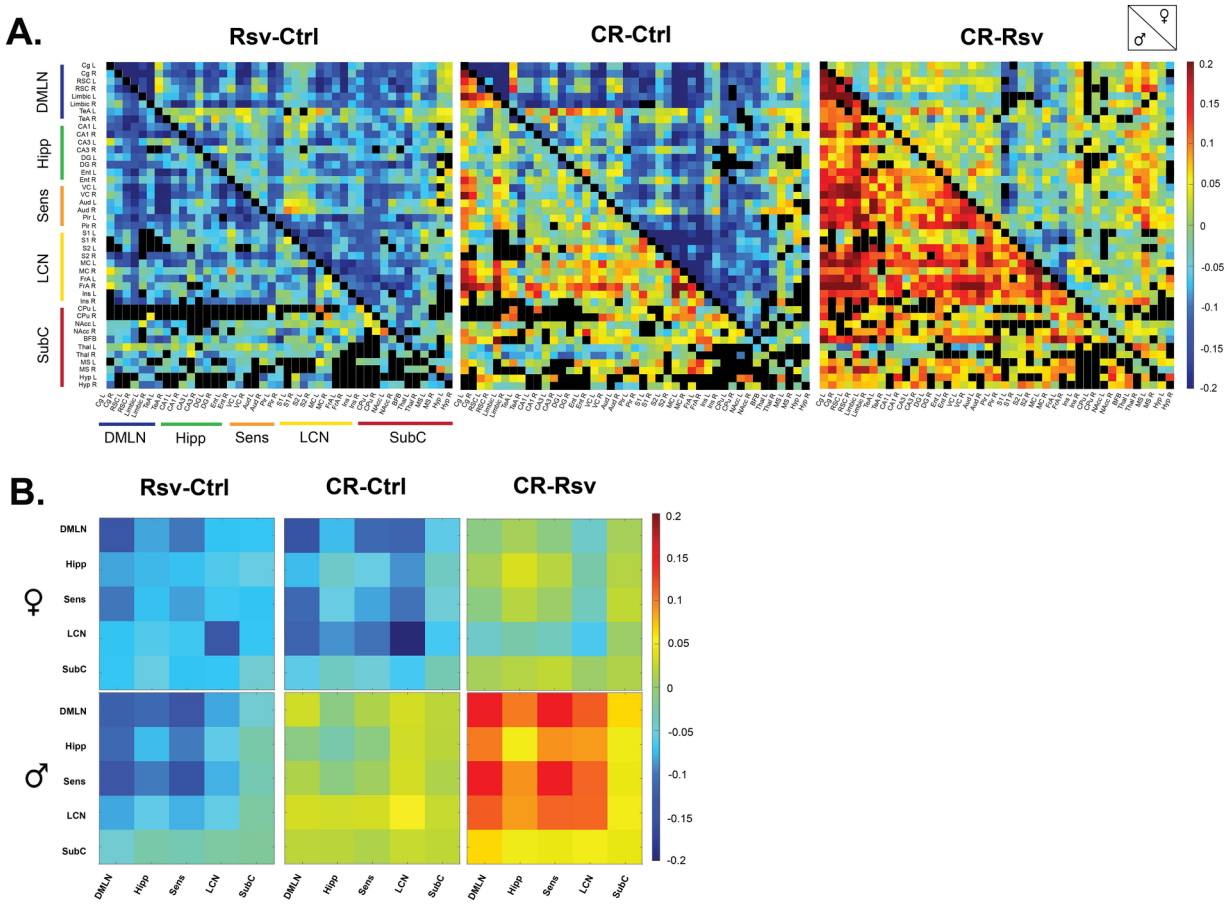

FIGURE 4
Mean difference in FC in male and female Ctrl, Rsv supplemented and CR rats. **(A)** ROI-based FC matrices displaying the mean difference in FC between ROI pairs for males (lower half) and females (upper half) between the treatment groups (Ctrl = control, CR = caloric restriction, Rsv = resveratrol). Non-significant connections (calculated on the mean FC, $p > 0.05$, one-sample t-test, FDR corrected per group) are blacked out. **(B)** Mean difference in network-based FC in females (top row) and males (bottom row) between treatment groups. In both panel A and B, positive (red-color) and negative (blue-color) values indicate, respectively, higher and lower connectivity in the first group relative to the second group. Diagonal and off-diagonal elements represent differences in within- and between-network FC respectively: DMLN (default mode-like network), Hipp (hippocampal network), Sens (sensory network), LCN (lateral cortical network), SubC (subcortical network).

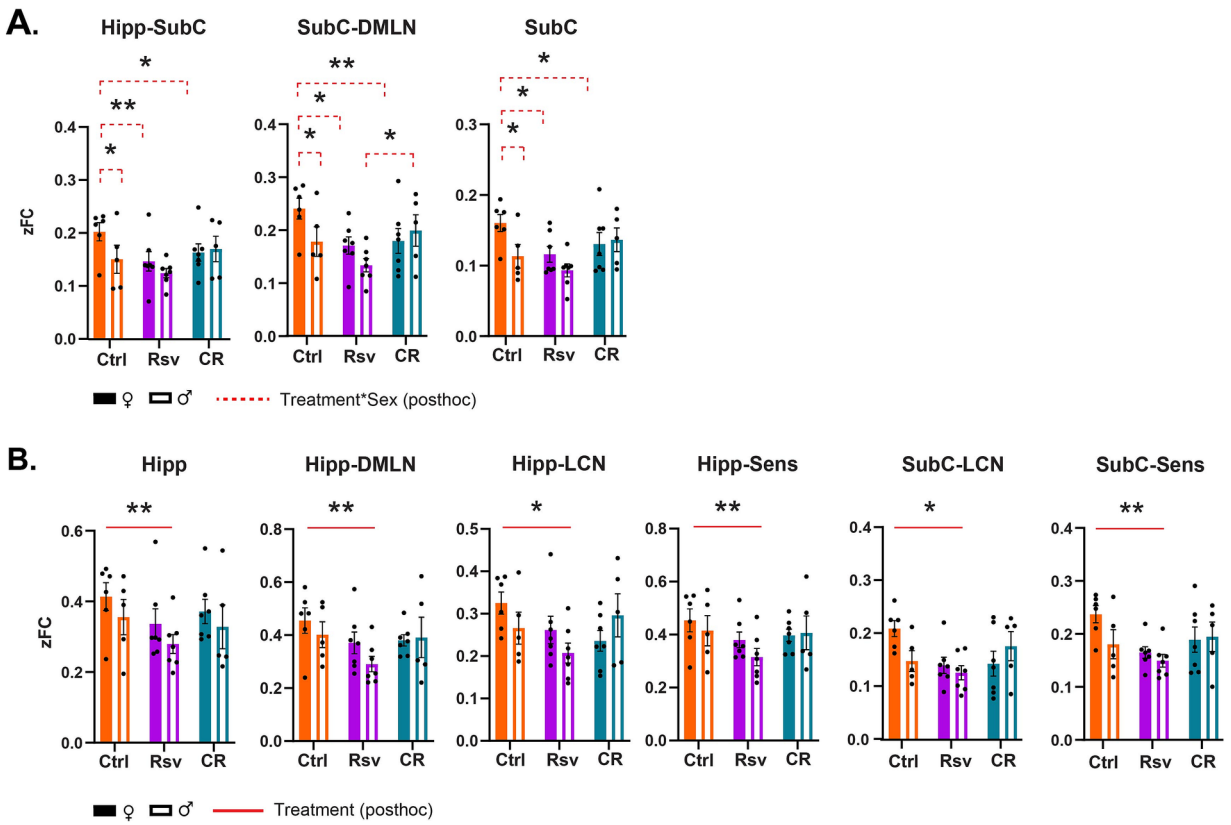

FIGURE 5
Resting-state network (RSN) connectivity alterations in male and female Ctrl, Rsv supplemented and CR rats. Network-based FC demonstrating significant interaction **(A)** or treatment **(B)** effects. Bar graphs show the group-level FC within (e.g., Hipp) or between (e.g., Hipp-Sens) FC. Solid bars represent females and open bars representing the males. Group means ± SEM are presented together with the individual subject data points (dots). Significant interaction effects of treatment*sex (FDR corrected, Benjamini-Hochberg procedure, $p < 0.05$) are noted by the red dotted line. Significant treatment effects (*post-hoc* Tukey HSD, $p < 0.05$) are annotated by the red solid line. Asterisks indicate the levels of statistical significance: *$p < 0.05$, **$p < 0.01$, ***$p < 0.001$, ****$p < 0.0001$.

($p = 0.0266$) and SubC-Sens ($p = 0.0062$)]—an effect we did not observe in the CR group (Supplementary Tables S4–S6).

4 Discussion

To our knowledge, this is the first study to characterize and compare RSN FC in both male and female F344 rats subjected to short-term CR or Rsv supplementation, comparing not only the effects of CR and Rsv on RSN FC, but also highlighting their sex-specific effects. Our results demonstrated decreased BW in CR rats, as well as increased in BW in male Rsv supplemented rats, compared to female Rsv supplemented rats, whereas this difference between sexes was not observed in the Ctrl or CR groups. Furthermore, we found that both CR or Rsv supplementation induced a female-specific decrease of FC between SubC-Hipp, Sub-DMLN, and SubC. Moreover, Rsv supplementation lowered FC within the Hipp network and between Hipp-DMLN, Hipp-LCN, and Hipp-Sens, as well as between the SubC-LCN and SubC-Sens—an effect not observed for the CR rats.

The core mechanism of CR bases itself on the reduction in energy expenditure, in which the slowing of the metabolic rate is hypothesized to improve metabolic health and extend lifespan. The selective use of energy is reflected in the reduction of biomass and thus BW. As energy for activity and basic function maintenance cannot change, limited energy resources are allocated to biomass resulting in weight loss (35). This weight loss has been reported in a plethora of preclinical (36) and clinical (37, 38) studies and is in line with our own findings, as we observe a significant decrease in BW in our male and female CR rats.

Along with the loss of biomass, energy expenditure declines until eventually the energy intake matches the new lower BW. This adaptive process allows for the maintenance of important body functions including metabolic homeostasis, breathing, heart rate, and most importantly, activity of the central nervous system (37). By this principle, RSN FC should remain mostly unaltered, as energy expenditure allocated to neuronal activity is maintained throughout CR. In a mixed-sex human cohort, whole-brain RSN FC analysis has shown to not be altered as a result of dietary intervention through a hypocaloric Mediterranean diet (39). Female-only human cohorts that have been submitted to this hypocaloric Mediterranean diet or CR, revealed a decrease of FC in regions associated with food reward (40), memory consolidation (23), self-perception and emotional functions (41). These processes are known to be modulated by hormones, with fluctuations in FC coinciding with the female menstrual cycle (42–44). This sex-related decrease in FC supports our own findings, as our results similarly show lower FC in CR

females when compared to Ctrl females, between the Hipp-SubC, SubC-DMLN and within the SubC, which are networks involved with learning, memory and emotion, suggesting an underlying sex-specific mechanism of CR (45) on RSN FC. However, to our knowledge, the effects of CR on FC have not been explored in male-only cohorts. Consequently, we cannot conclusively determine if these observations are indeed sex-specific. Further exploration of the sex-specific mechanisms of CR on brain activity is therefore detrimental to understand and optimize its therapeutic potential, tailoring interventions to individual needs.

CR-mimetics are compounds that are able to increase life- and/or health-span and ameliorate age-associated diseases in model organisms, in a CR-like manner (12). Rsv as a proposed CR-mimetic has been implicated with some controversy, with conflicting reports regarding the aforementioned criteria. Rsv supplementation studies in humans do not yield overwhelmingly positive data regarding aging-related benefits (46), even though Rsv has been reported to address age- and disease-related underlying mechanisms such as systemic inflammation and oxidative stress (47, 48). Studies in model organisms using CR or Rsv on age- and obesity-related biomarkers have found small, non-existent, and even opposing effects of Rsv compared to CR mechanisms (11, 49). One of the obesity-related biomarkers in which contradicting results have been reported is BW (50). A handful of preclinical trials in rats and mice supplemented daily with Rsv (5–24 mg/kg, oral, 30–45 days), have shown unaltered (51, 52) or reduced BW (53). In this study we did not observe a significant effect of Rsv supplementation (10 mg/kg, oral) on the percentage change of BW when compared to Ctrl. However, we did observe a higher percentage increase of BW for male Rsv supplemented rats relative to their starting weight, when compared to Rsv supplemented females. This difference of percentage change in BW between males and females is absent in the Ctrl and CR group. To our knowledge, there is currently no literature to support or contradict our observation of this sex-specific effect of Rsv regarding BW. Therefore, further investigation into this aspect and the effect of Rsv on BW in different sexes is warranted.

Supporting the narrative that Rsv is a CR-mimetic, we observed a female-specific decrease in the Hipp-SubC and SubC-LCN connectivity as a result of Rsv supplementation, similar to the decrease observed in female CR rats when compared to Ctrl. However, unlike CR, we observed a treatment effect of Rsv, decreasing FC within the Hipp and between the Hipp, the SubC, and other RSNs compared to Ctrl rats. Despite limited literature on the effects of Rsv on FC, published works in humans manage to directly contradict our reported lowering of FC because of Rsv supplementation. They report increased FC between the hippocampus and other regions including the right and lateral angular cortex, anterior cingulate cortex, precuneus and lateral occipital cortex, speculated to be linked to improved memory retention and attenuated hippocampal atrophy (25, 26). One possible explanation for the observed differential effects of Rsv on FC lies within the experimental design, more specifically, the dosage of Rsv. In both the mentioned human trials as well as our study, Rsv was supplemented orally daily, for the duration of a month. However, their Rsv dosage was 200 mg/kg: 20 times more compared to our daily dosage (10 mg/kg). Rsv is known to exert a hormesis dose-dependent effect (54, 55), with this effect referring to the biphasic response of a cell or organism to a compound. Often, a stimulating effect can be observed at low doses (often associated with beneficial effects), while an inhibitory effect is exerted at high doses (often toxic) (56, 57). The biphasic effect of Rsv has been shown in a plethora of (pre)clinical studies, with a multitude of them reporting differential outcomes depending on the supplied Rsv dosage (58–61). As Rsv demonstrates hormesis in various biological models, further work is required to understand its dose-relationship in context of its exerted effects, highlighting the importance of carefully considering dosage when designing studies involving Rsv supplementation and interpreting their outcomes.

The BOLD signal, used in this study as an indirect measure of neuronal activity, is based on neurovascular coupling, making it heavily dependent on changes in cerebral blood flow (CBF), cerebral blood volume (CBV) and the rate of oxygen consumption in response to changes in neuronal activity (62, 63). Unarguably, it is clear that vascular and neuronal signals both contribute to the BOLD signal (64) and while changes in BOLD are caused by neuronal activation through neurovascular coupling, they can also arise from other physiological processes that affect blood oxygenation or volume (65). CR and Rsv are both known to influence the vasculature by modulating vasodilation and CBF, through the increase of endothelial nitric oxide (NO) production (66, 67). NO plays a big role in cellular oxygen supply and demand, through regulation of the vascular tone and blood flow, as well as modulating mitochondrial oxygen consumption (68). With the increased production of endothelial NO, CR has been shown to decrease arterial blood pressure (69), improve endothelium-dependent vasodilation (70) and increase CBF (20). Similarly, Rsv supplementation leads to a more efficient endothelium-dependent vasodilation (71) and consequently, an improved CBF (72). Considering these vascular effects, it is possible they contribute to changes in the BOLD signal, which should be considered when interpreting BOLD outcomes in the context of interventions like CR and Rsv supplementation. Future work is encouraged to unravel the vascular contribution to the BOLD signal in the context of these interventions.

Sex differences in RSNs have been thoroughly investigated in humans and have shown to be confounded by environmental and sociocultural factors (73). However, sex-differences are often driven by biological factors such as hormones (e.g., estrogen) that are known to exert region-specific effects in the brain, making them potential contributors to the wide range of differences in FC observed (74, 75). Studies often show greater FC in (sub)cortical regions in females compared to males (76) and in addition, females generally show greater between-network FC whereas men have greater within-network FC (77). RsfMRI studies in rats have revealed sex-differences in brain connectivity patterns, with females exhibiting stronger hypothalamus connectivity, while males show more prominent striatum-related connectivity (78). These cumulative findings highlight the importance of taking sex into consideration as a factor when interpreting rsfMRI results in rodents, providing valuable insights into the large-scale functional organization of the brain across sexes.

As with the majority of studies, the design of the current study is subject to limitations. First, the rsfMRI scans in this study were performed in isoflurane- and medetomidine-anesthetized rats. Anesthesia indeed affect neural activity and are likely to have an impact on FC patterns as observed in rsfMRI studies. The combination of isoflurane and medetomidine specifically is known to reduce FC in the subcortical structures such as the hippocampus and (hypo)thalamus. However, studies have shown that FC under these anesthetics shows a very similar FC pattern as is observed in

awake rats (79). Moreover, the combination of isoflurane and medetomidine has shown its own advantages, allowing visualization of interactions in cortical and sub-cortical structures, and the interaction between cortical, striatal and thalamic components (80, 81) and is therefore proposed as the most suitable anesthetic alternative to awake imaging for rsfMRI analysis in rats (31). Secondly, rats were supplemented Rsv daily using dried apple chips to assure oral consumption. Unfortunately, most studies have shown that the oral bioavailability of resveratrol is low (<1%) (82). Consequently, this may be the reason for discrepancies between *in vivo* and *in vitro* studies regarding Rsv efficacy and mechanisms of action (83). The limited bioavailability is often accredited to several factors including poor water solubility, limited chemical stability and high metabolism (18). However, as a polyphenol, Rsv exhibits a lipophilic nature, allowing the compound to cross the blood–brain barrier and thus reach neural tissue (84), providing the speculated beneficial effects as observed in *in vivo* studies. Studies have been able to detect very low Rsv concentrations in neuronal tissue (85, 86), or report that the concentration of Rsv was too low to be detected (51), despite all establishing a wide range of beneficial effects of the compound. Thus, the data suggests that even though there is limited bioavailability of the compound, it is able to exert biological effect. It is essential to consider these limitations and explore alternative delivery methods or formulations to enhance bioavailability. Additionally, further research is needed to elucidate the precise mechanisms underlying the observed effects of Rsv to validate its therapeutic potential.

Continued research into the effects of CR and Rsv on FC using advanced neuroimaging techniques like rsfMRI holds promise for advancing our understanding of dietary interventions in the promotion of brain health. Our work provides valuable insights into the effects and comparability of short-term dietary interventions using CR and Rsv supplementation on RSNs and BW in both male and female F344 rats. With this, we established a benchmark of the sex-specific impact of CR or Rsv as a dietary intervention on spontaneous brain activity, providing an FC reference for future research of dietary effects.

Data availability statement

The raw data supporting the conclusions of this article will be made available by the authors, without undue reservation.

Ethics statement

The animal study was approved by Committee on Animal Care and Use at the University of Antwerp, Belgium (ECD: 2021-59). The study was conducted in accordance with the local legislation and institutional requirements.

Author contributions

JR: Conceptualization, Data curation, Formal analysis, Investigation, Project administration, Validation, Visualization, Writing – original draft, Writing – review & editing. MB: Conceptualization, Formal analysis, Project administration, Software, Supervision, Validation, Visualization, Writing – review & editing. TV: Formal analysis, Software, Supervision, Validation, Writing – review & editing. JA: Methodology, Resources, Software, Writing – review & editing. LK: Conceptualization, Investigation, Writing – review & editing. DB: Supervision, Visualization, Writing – review & editing. MA: Methodology, Resources, Software, Supervision, Validation, Visualization, Writing – review & editing. MV: Conceptualization, Methodology, Project administration, Resources, Supervision, Validation, Writing – review & editing.

Funding

The author(s) declare that financial support was received for the research, authorship, and/or publication of this article. This study was supported by the Fund of Scientific Research Flanders (FWO-G045420N) and Stichting Alzheimer Onderzoek (SAO-FRA 2020/027, granted to Georgios A. Keliris). The computational resources and services used in this work were provided by the HPC core facility CalcUA of the University of Antwerp, the VSC (Flemish Supercomputer Center), funded by the Hercules Foundation and the Flemish Government department EWI. Funding for heavy scientific equipment was provided by the Flemish Impulse funding under grant agreement number 42/FA010100/1230 (granted to Annemie Van der Linden).

Acknowledgments

We would like to acknowledge Dr. Georgios A. Keliris for his initial contributions to the project proposal, which lead to the SAO-granted funding.

Conflict of interest

The authors declare that the research was conducted in the absence of any commercial or financial relationships that could be construed as a potential conflict of interest.

Publisher's note

Supplementary material

The Supplementary material for this article can be found online at: https://www.frontiersin.org/articles/10.3389/fnut.2025.1440373/full#supplementary-material

References

1. Pressley JC, Trott C, Tang M, Durkin M, Stern Y. Dementia in community-dwelling elderly patients: a comparison of survey data, medicare claims, cognitive screening, reported symptoms, and activity limitations. *J Clin Epidemiol*. (2003) 56:896–905. doi: 10.1016/S0895-4356(03)00133-1

2. Liu JK. Antiaging agents: safe interventions to slow aging and healthy life span extension. *Nat Prod Bioprospect*. (2022) 12:18. doi: 10.1007/s13659-022-00339-y

3. Fontana L, Ghezzi L, Cross AH, Piccio L. Effects of dietary restriction on neuroinflammation in neurodegenerative diseases. *J Exp Med*. (2021) 218:e20190086. doi: 10.1084/jem.20190086

4. Hyun DH, Emerson SS, Jo DG, Mattson MP, de Cabo R. Calorie restriction up-regulates the plasma membrane redox system in brain cells and suppresses oxidative stress during aging. *Proc Natl Acad Sci USA*. (2006) 103:19908–12. doi: 10.1073/pnas.0608008103

5. Parikh I, Guo J, Chuang KH, Zhong Y, Rempe RG, Hoffman JD, et al. Caloric restriction preserves memory and reduces anxiety of aging mice with early enhancement of neurovascular functions. *Aging*. (2016) 8:2814–26. doi: 10.18632/aging.101094

6. Hadad N, Unnikrishnan A, Jackson JA, Masser DR, Otalora L, Stanford DR, et al. Caloric restriction mitigates age-associated hippocampal differential CG and non-CG methylation. *Neurobiol Aging*. (2018) 67:53–66. doi: 10.1016/j.neurobiolaging.2018.03.009

7. Portero-Tresserra M, Galofré-López N, Pallares E, Gimenez-Montes C, Barcia C, Granero R, et al. Effects of caloric restriction on spatial object recognition memory, hippocampal neuron loss and Neuroinflammation in aged rats. *Nutrients*. (2023) 15:1572. doi: 10.3390/nu15071572

8. Hornsby AKE, Redhead YT, Rees DJ, Ratcliff MSG, Reichenbach A, Wells T, et al. Short-term calorie restriction enhances adult hippocampal neurogenesis and remote fear memory in a Ghsr-dependent manner. *Psychoneuroendocrinology*. (2016) 63:198–207. doi: 10.1016/j.psyneuen.2015.09.023

9. Maswood N, Young J, Tilmont E, Zhang Z, Gash DM, Gerhardt GA, et al. Caloric restriction increases neurotrophic factor levels and attenuates neurochemical and behavioral deficits in a primate model of Parkinson's disease. *Proc Natl Acad Sci USA*. (2004) 101:18171–6. doi: 10.1073/pnas.0405831102

10. Martin CK, Höchsmann C, Dorling JL, Bhapkar M, Pieper CF, Racette SB, et al. Challenges in defining successful adherence to calorie restriction goals in humans: results from CALERIE™ 2. *Exp Gerontol*. (2022) 162:111757. doi: 10.1016/j.exger.2022.111757

11. Chiba T, Tsuchiya T, Komatsu T, Mori R, Hayashi H, Shimokawa I. Development of calorie restriction mimetics as therapeutics for obesity, diabetes, inflammatory and neurodegenerative diseases. *Curr Genomics*. (2010) 11:562–7. doi: 10.2174/138920210793360934

12. Madeo F, Carmona-Gutierrez D, Hofer SJ, Kroemer G. Caloric restriction Mimetics against age-associated disease: targets, mechanisms, and therapeutic potential. *Cell Metab*. (2019) 29:592–610. doi: 10.1016/j.cmet.2019.01.018

13. dos Santos MG, da Luz DB, de Miranda FB, de Aguiar RF, Siebel AM, Arbo BD, et al. Resveratrol and Neuroinflammation: Total-scale analysis of the scientific literature. *Forum Nutr*. (2024) 4:165–80. doi: 10.3390/nutraceuticals4020011

14. Omidian M, Abdolahi M, Daneshzad E, Sedighiyan M, Aghasi M, Abdollahi H, et al. The effects of resveratrol on oxidative stress markers: a systematic review and Meta-analysis of randomized clinical trials. *Endocr Metab Immune*. (2020) 20:718–27. doi: 10.2174/1871530319666191116112950

15. Lam YY, Peterson CM, Ravussin E. Resveratrol vs. calorie restriction: data from rodents to humans. *Exp Gerontol*. (2013) 48:1018–24. doi: 10.1016/j.exger.2013.04.005

16. Oomen CA, Farkas E, Roman V, van der Beek EM, Luiten PG, Meerlo P. Resveratrol preserves cerebrovascular density and cognitive function in aging mice. *Front Aging Neurosci*. (2009) 1:4. doi: 10.3389/neuro.24.004.2009

17. Toth P, Tarantini S, Tucsek Z, Ashpole NM, Sosnowska D, Gautam T, et al. Resveratrol treatment rescues neurovascular coupling in aged mice: role of improved cerebromicrovascular endothelial function and downregulation of NADPH oxidase. *Am J Physiol Heart Circ Physiol*. (2014) 306:H299–308. doi: 10.1152/ajpheart.00744.2013

18. Ahmed T, Javed S, Javed S, Tariq A, Samec D, Tejada S, et al. Resveratrol and Alzheimer's disease: mechanistic insights. *Mol Neurobiol*. (2017) 54:2622–35. doi: 10.1007/s12035-016-9839-9

19. Dos Santos MG, Schimith LE, Andre-Miral C, Muccillo-Baisch AL, Arbo BD, Hort MA. Neuroprotective effects of resveratrol in *in vivo* and *in vitro* experimental models of Parkinson's disease: a systematic review. *Neurotox Res*. (2022) 40:319–45. doi: 10.1007/s12640-021-00450-x

20. Lin AL, Parikh I, Hoffman JD, Ma D. Neuroimaging biomarkers of caloric restriction on Brain metabolic and vascular functions. *Curr Nutr Rep*. (2017) 6:41–8. doi: 10.1007/s13668-017-0187-9

21. Bajic D, Craig MM, Mongerson CRL, Borsook D, Becerra L. Identifying rodent resting-state Brain networks with independent component analysis. *Front Neurosci*. (2017) 11:685. doi: 10.3389/fnins.2017.00685

22. Fox MD, Snyder AZ, Vincent JL, Corbetta M, Van Essen DC, Raichle ME. The human brain is intrinsically organized into dynamic, anticorrelated functional networks. *Proc Natl Acad Sci USA*. (2005) 102:9673–8. doi: 10.1073/pnas.0504136102

23. Prehn K, Jumpertz von Schwartzenberg R, Mai K, Zeitz U, Witte AV, Hampel D, et al. Caloric restriction in older adults-differential effects of weight loss and reduced weight on Brain structure and function. *Cereb Cortex*. (2017) 27:1765–78. doi: 10.1093/cercor/bhw008

24. Huhn S, Beyer F, Zhang R, Lampe L, Grothe J, Kratzsch J, et al. Effects of resveratrol on memory performance, hippocampus connectivity and microstructure in older adults - a randomized controlled trial. *NeuroImage*. (2018) 174:177–90. doi: 10.1016/j.neuroimage.2018.03.023

25. Witte AV, Kerti L, Margulies DS, Floel A. Effects of resveratrol on memory performance, hippocampal functional connectivity, and glucose metabolism in healthy older adults. *J Neurosci*. (2014) 34:7862–70. doi: 10.1523/JNEUROSCI.0385-14.2014

26. Kobe T, Witte AV, Schnelle A, Tesky VA, Pantel J, Schuchardt JP, et al. Impact of resveratrol on glucose control, hippocampal structure and connectivity, and memory performance in patients with mild cognitive impairment. *Front Neurosci*. (2017) 11:105. doi: 10.3389/fnins.2017.00105

27. Juybari KB, Sepehri G, Meymandi MS, Vakili Shahrbabaki SS, Moslemizadeh A, Saeedi N, et al. Sex dependent alterations of resveratrol on social behaviors and nociceptive reactivity in VPA-induced autistic-like model in rats. *Neurotoxicol Teratol*. (2020) 81:106905. doi: 10.1016/j.ntt.2020.106905

28. Baer SB, Dorn AD, Osborne DM. Sex differences in response to obesity and caloric restriction on cognition and hippocampal measures of autophagic-lysosomal transcripts and signaling pathways. *BMC Neuroscience*. (2024) 25:1. doi: 10.1186/s12868-023-00840-1

29. Mirmiran P, Bahadoran Z, Gaeini Z. Common limitations and challenges of dietary clinical trials for translation into clinical practices. *Int J Endocrinol Metab*. (2021) 19:e108170. doi: 10.5812/ijem.108170

30. Xu N, LaGrow TJ, Anumba N, Lee A, Zhang X, Yousefi B, et al. Functional connectivity of the Brain across rodents and humans. *Front Neurosci*. (2022) 16:816331. doi: 10.3389/fnins.2022.816331

31. Grandjean J, Desrosiers-Gregoire G, Anckaerts C, Angeles-Valdez D, Ayad F, Barriere DA, et al. A consensus protocol for functional connectivity analysis in the rat brain. *Nat Neurosci*. (2023) 26:673–81. doi: 10.1038/s41593-023-01286-8

32. van den Berg M, Adhikari MH, Verschuuren M, Pintelon I, Vasilkovska T, Van Audekerke J, et al. Altered basal forebrain function during whole-brain network activity at pre- and early-plaque stages of Alzheimer's disease in TgF344-AD rats. *Alzheimers Res Ther*. (2022) 14:148. doi: 10.1186/s13195-022-01089-2

33. Vasilkovska T, Adhikari MH, Van Audekerke J, Salajeghe S, Pustina D, Cachope R, et al. Resting-state fMRI reveals longitudinal alterations in brain network connectivity in the zQ175DN mouse model of Huntington's disease. *Neurobiol Dis*. (2023) 181:106095. doi: 10.1016/j.nbd.2023.106095

34. De Waegenaere S, van den Berg M, Keliris GA, Adhikari MH, Verhoye M. Early altered directionality of resting brain network state transitions in the TgF344-AD rat model of Alzheimer's disease. *Front Hum Neurosci*. (2024) 18:1379923. doi: 10.3389/fnhum.2024.1379923

35. Hou C, Bolt KM, Bergman A. A general model for ontogenetic growth under food restriction. *Proc R Soc B Biol Sci*. (2011) 278:2881–90. doi: 10.1098/rspb.2011.0047

36. Taormina G, Mirisola MG. Calorie restriction in mammals and simple model organisms. *Biomed Res Int*. (2014) 2014:308690:1–10. doi: 10.1155/2014/308690

37. Most J, Redman LM. Impact of calorie restriction on energy metabolism in humans. *Exp Gerontol*. (2020) 133:110875. doi: 10.1016/j.exger.2020.110875

38. Trepanowski JF, Canale RE, Marshall KE, Kabir MM, Bloomer RJ. Impact of caloric and dietary restriction regimens on markers of health and longevity in humans and animals: a summary of available findings. *Nutr J*. (2011) 10:107. doi: 10.1186/1475-2891-10-107

39. Gaynor AM, Varangis E, Song S, Gazes Y, Noofoory D, Babukutty RS, et al. Diet moderates the effect of resting state functional connectivity on cognitive function. *Sci Rep*. (2022) 12:16080. doi: 10.1038/s41598-022-20047-4

40. Jakobsdottir S, van Nieuwpoort IC, van Bunderen CC, de Ruiter MB, Twisk JW, Deijen JB, et al. Acute and short-term effects of caloric restriction on metabolic profile and brain activation in obese, postmenopausal women. *Int J Obes*. (2016) 40:1671–8. doi: 10.1038/ijo.2016.103

41. Garcia-Casares N, Bernal-Lopez MR, Roe-Vellve N, Gutierrez-Bedmar M, Fernandez-Garcia JC, Garcia-Arnes JA, et al. Brain functional connectivity is modified by a hypocaloric Mediterranean diet and physical activity in obese women. *Nutrients*. (2017) 9:685. doi: 10.3390/nu9070685

42. Lisofsky N, Martensson J, Eckert A, Lindenberger U, Gallinat J, Kuhn S. Hippocampal volume and functional connectivity changes during the female menstrual cycle. *NeuroImage*. (2015) 118:154–62. doi: 10.1016/j.neuroimage.2015.06.012

43. Hidalgo-Lopez E, Mueller K, Harris T, Aichhorn M, Sacher J, Pletzer B. Human menstrual cycle variation in subcortical functional brain connectivity: a multimodal

analysis approach. *Brain Struct Funct*. (2020) 225:591–605. doi: 10.1007/s00429-019-02019-z

44. Hjelmervik H, Hausmann M, Osnes B, Westerhausen R, Specht K. Resting states are resting traits - an fMRI study of sex differences and menstrual cycle effects in resting state cognitive control networks. *PLoS One*. (2014) 9:e103492. doi: 10.1371/journal.pone.0103492

45. Suchacki KJ, Thomas BJ, Ikushima YM, Chen KC, Fyfe C, Tavares AAS, et al. The effects of caloric restriction on adipose tissue and metabolic health are sex- and age-dependent. *eLife*. (2023) 12:12. doi: 10.7554/eLife.88080

46. Bhullar KS, Hubbard BP. Lifespan and healthspan extension by resveratrol. *Biochim Biophys Acta*. (2015) 1852:1209–18. doi: 10.1016/j.bbadis.2015.01.012

47. Ramirez-Garza SL, Laveriano-Santos EP, Marhuenda-Munoz M, Storniolo CE, Tresserra-Rimbau A, Vallverdu-Queralt A, et al. Health effects of resveratrol: results from human intervention trials. *Nutrients*. (2018) 10:1892. doi: 10.3390/nu10121892

48. Chung JH, Manganiello V, Dyck JRB. Resveratrol as a calorie restriction mimetic: therapeutic implications. *Trends Cell Biol*. (2012) 22:546–54. doi: 10.1016/j.tcb.2012.07.004

49. Pallauf K, Günther I, Kühn G, Chin D, de Pascual-Teresa S, Rimbach G. The potential of resveratrol to act as a caloric restriction mimetic appears to be limited: insights from studies in mice. *Adv Nutr*. (2021) 12:995–1005. doi: 10.1093/advances/nmaa148

50. Hillsley A, Chin V, Li A, McLachlan CS. Resveratrol for weight loss in obesity: an assessment of randomized control trial designs in ClinicalTrials.gov. *Nutrients*. (2022) 14:1424. doi: 10.3390/nu14071424

51. Karuppagounder SS, Pinto JT, Xu H, Chen HL, Beal MF, Gibson GE. Dietary supplementation with resveratrol reduces plaque pathology in a transgenic model of Alzheimer's disease. *Neurochem Int*. (2009) 54:111–8. doi: 10.1016/j.neuint.2008.10.008

52. Raskovic A, Cucuz V, Torovic L, Tomas A, Gojkovic-Bukarica L, Cebovic T, et al. Resveratrol supplementation improves metabolic control in rats with induced hyperlipidemia and type 2 diabetes. *Saudi Pharm J*. (2019) 27:1036–43. doi: 10.1016/j.jsps.2019.08.006

53. Sharma R, Sharma NK, Thungapathra M. Resveratrol regulates body weight in healthy and ovariectomized rats. *Nutr Metab*. (2017) 14:30. doi: 10.1186/s12986-017-0183-5

54. Calabrese EJ, Mattson MP, Calabrese V. Resveratrol commonly displays hormesis: occurrence and biomedical significance. *Hum Exp Toxicol*. (2010) 29:980–1015. doi: 10.1177/0960327110383625

55. Shaito A, Posadino AM, Younes N, Hasan H, Halabi S, Alhababi D, et al. Potential adverse effects of resveratrol: a literature review. *Int J Mol Sci*. (2020) 21:2084. doi: 10.3390/ijms21062084

56. Mattson MP. Hormesis defined. *Ageing Res Rev*. (2008) 7:1–7. doi: 10.1016/j.arr.2007.08.007

57. Calabrese EJ, Baldwin LA. Hormesis: the dose-response revolution. *Annu Rev Pharmacol Toxicol*. (2003) 43:175–97. doi: 10.1146/annurev.pharmtox.43.100901.140223

58. Plauth A, Geikowski A, Cichon S, Wowro SJ, Liedgens L, Rousseau M, et al. Hormetic shifting of redox environment by pro-oxidative resveratrol protects cells against stress. *Free Radic Biol Med*. (2016) 99:608–22. doi: 10.1016/j.freeradbiomed.2016.08.006

59. Juhasz B, Mukherjee S, Das DK. Hormetic response of resveratrol against cardioprotection. *Exp Clin Cardiol*. (2010) 15:e134–8.

60. Dey A, Guha P, Chattopadhyay S, Bandyopadhyay SK. Biphasic activity of resveratrol on indomethacin-induced gastric ulcers. *Biochem Biophys Res Commun*. (2009) 381:90–5. doi: 10.1016/j.bbrc.2009.02.027

61. Posadino AM, Giordo R, Cossu A, Nasrallah GK, Shaito A, Abou-Saleh H, et al. Flavin oxidase-induced ROS generation modulates PKC biphasic effect of resveratrol on endothelial cell survival. *Biomol Ther*. (2019) 9:209. doi: 10.3390/biom9060209

62. Drew PJ. Vascular and neural basis of the BOLD signal. *Curr Opin Neurobiol*. (2019) 58:61–9. doi: 10.1016/j.conb.2019.06.004

63. Hillman EMC. Coupling mechanism and significance of the BOLD signal: a status report. *Annu Rev Neurosci*. (2014) 37:161–81. doi: 10.1146/annurev-neuro-071013-014111

64. Tsvetanov KA, Henson RNA, Rowe JB. Separating vascular and neuronal effects of age on fMRI BOLD signals. *Philos Trans R Soc Lond B Biol Sci*. (2021) 376:20190631. doi: 10.1098/rstb.2019.0631

65. Tong Y, Hocke LM, Fan X, Janes AC, Frederick B. Can apparent resting state connectivity arise from systemic fluctuations? *Front Hum Neurosci*. (2015) 9:285. doi: 10.3389/fnhum.2015.00285

66. Al Attar AA, Fahed GI, Hoballah MM, Pedersen S, El-Yazbi AF, Nasser SA, et al. Mechanisms underlying the effects of caloric restriction on hypertension. *Biochem Pharmacol*. (2022) 200:115035. doi: 10.1016/j.bcp.2022.115035

67. Xia N, Forstermann U, Li HG. Resveratrol and endothelial nitric oxide. *Molecules*. (2014) 19:16102–21. doi: 10.3390/molecules191016102

68. Tejero J, Shiva S, Gladwin MT. Sources of vascular nitric oxide and reactive oxygen species and their regulation. *Physiol Rev*. (2019) 99:311–79. doi: 10.1152/physrev.00036.2017

69. Kord-Varkaneh H, Nazary-Vannani A, Mokhtari Z, Salehi-sahlabadi A, Rahmani J, Clark CCT, et al. The influence of fasting and energy restricting diets on blood pressure in humans: a systematic review and Meta-analysis. *High Blood Press Cardiovasc Prev*. (2020) 27:271–80. doi: 10.1007/s40292-020-00391-0

70. Mattagajasingh I, Kim CS, Naqvi A, Yamamori T, Hoffman TA, Jung SB, et al. SIRT1 promotes endothelium-dependent vascular relaxation by activating endothelial nitric oxide synthase. *Proc Natl Acad Sci USA*. (2007) 104:14855–60. doi: 10.1073/pnas.0704329104

71. Breuss JM, Atanasov AG, Uhrin P. Resveratrol and its effects on the vascular system. *Int J Mol Sci*. (2019) 20:1523. doi: 10.3390/ijms20071523

72. Kennedy DO, Wightman EL, Reay JL, Lietz G, Okello EJ, Wilde A, et al. Effects of resveratrol on cerebral blood flow variables and cognitive performance in humans: a double-blind, placebo-controlled, crossover investigation. *Am J Clin Nutr*. (2010) 91:1590–7. doi: 10.3945/ajcn.2009.28641

73. Becker JB, McClellan ML, Reed BG. Sex differences, gender and addiction. *J Neurosci Res*. (2017) 95:136–47. doi: 10.1002/jnr.23963

74. Biswal BB, Mennes M, Zuo XN, Gohel S, Kelly C, Smith SM, et al. Toward discovery science of human brain function. *Proc Natl Acad Sci USA*. (2010) 107:4734–9. doi: 10.1073/pnas.0911855107

75. Alfano V, Cavaliere C, Di Cecca A, Ciccarelli G, Salvatore M, Aiello M, et al. Sex differences in functional brain networks involved in interoception: an fMRI study. *Front Neurosci*. (2023) 17:1130025. doi: 10.3389/fnins.2023.1130025

76. Gong G, Rosa-Neto P, Carbonell F, Chen ZJ, He Y, Evans AC. Age- and gender-related differences in the cortical anatomical network. *J Neurosci*. (2009) 29:15684–93. doi: 10.1523/JNEUROSCI.2308-09.2009

77. Chung YS, Calhoun V, Stevens MC. Adolescent sex differences in cortico-subcortical functional connectivity during response inhibition. *Cogn Affect Behav Neurosci*. (2020) 20:1–18. doi: 10.3758/s13415-019-00718-y

78. Li Q, Zhang N. Sex differences in resting-state functional networks in awake rats. *Brain Struct Funct*. (2023) 228:1411–23. doi: 10.1007/s00429-023-02657-4

79. Paasonen J, Stenroos P, Salo RA, Kiviniemi V, Grohn O. Functional connectivity under six anesthesia protocols and the awake condition in rat brain. *NeuroImage*. (2018) 172:9–20. doi: 10.1016/j.neuroimage.2018.01.014

80. Grandjean J, Schroeter A, Batata I, Rudin M. Optimization of anesthesia protocol for resting-state fMRI in mice based on differential effects of anesthetics on functional connectivity patterns. *NeuroImage*. (2014) 102:838–47. doi: 10.1016/j.neuroimage.2014.08.043

81. Bukhari Q, Schroeter A, Cole DM, Rudin M. Resting state fMRI in mice reveals anesthesia specific signatures of Brain functional networks and their interactions. *Front Neural Circuits*. (2017) 11:11. doi: 10.3389/fncir.2017.00005

82. Walle T. Bioavailability of resveratrol. *Ann N Y Acad Sci*. (2011) 1215:9–15. doi: 10.1111/j.1749-6632.2010.05842.x

83. Kulkarni SS, Canto C. The molecular targets of resveratrol. *Biochim Biophys Acta*. (2015) 1852:1114–23. doi: 10.1016/j.bbadis.2014.10.005

84. Figueira I, Garcia G, Pimpao RC, Terrasso AP, Costa I, Almeida AF, et al. Polyphenols journey through blood-brain barrier towards neuronal protection. *Sci Rep*. (2021) 11:11456. doi: 10.1038/s41598-021-96179-w

85. Asensi M, Medina I, Ortega A, Carretero J, Baño MC, Obrador E, et al. Inhibition of cancer growth by resveratrol is related to its low bioavailability. *Free Radical Biol Med*. (2002) 33:387–98. doi: 10.1016/S0891-5849(02)00911-5

86. Gambini J, Inglés M, Olaso G, Lopez-Grueso R, Bonet-Costa V, Gimeno-Mallench L, et al. Properties of resveratrol: and studies about metabolism, bioavailability, and biological effects in animal models and humans. *Oxidative Med Cell Longev*. (2015) 2015:1–13. doi: 10.1155/2015/837042

frontiers | Frontiers in Neuroscience

TYPE Original Research
PUBLISHED 08 April 2025
DOI 10.3389/fnins.2025.1489407

OPEN ACCESS

EDITED BY
Rubem C. A. Guedes,
Federal University of Pernambuco, Brazil

REVIEWED BY
Cameron S. Metcalf,
The University of Utah, United States
Ernesto Griego,
Albert Einstein College of Medicine,
United States

*CORRESPONDENCE
Leticia Granados-Rojas
✉ lgranados_2000@yahoo.com.mx
Carmen Rubio
✉ macaru4@yahoo.com.mx

RECEIVED 01 September 2024
ACCEPTED 18 February 2025
PUBLISHED 08 April 2025

CITATION
Granados-Rojas L, Hernández-López L, Bahena-Alvarez EL, Juárez-Zepeda TE, Custodio V, Martínez-Galindo JG, Jerónimo-Cruz K, Tapia-Rodríguez M, Vanoye-Carlo A, Duran P and Rubio C (2025) Effects of the ketogenic diet on dentate gyrus and CA3 KCC2 expression in male rats with electrical amygdala kindling-induced seizures.
Front. Neurosci. 19:1489407.
doi: 10.3389/fnins.2025.1489407

Effects of the ketogenic diet on dentate gyrus and CA3 KCC2 expression in male rats with electrical amygdala kindling-induced seizures

Leticia Granados-Rojas[1]*, Leonardo Hernández-López[2], Emmanuel Leonardo Bahena-Alvarez[1], Tarsila Elizabeth Juárez-Zepeda[1], Verónica Custodio[2], Joyce Graciela Martínez-Galindo[3], Karina Jerónimo-Cruz[1], Miguel Tapia-Rodríguez[4], America Vanoye-Carlo[5], Pilar Duran[6] and Carmen Rubio[2]*

[1]Laboratorio de Biomoléculas y Salud Infantil, Instituto Nacional de Pediatría, Mexico City, Mexico, [2]Departamento de Neurofisiología, Instituto Nacional de Neurología y Neurocirugía, Mexico City, Mexico, [3]Laboratorio de Demencias, Instituto Nacional de Neurología y Neurocirugía, Mexico City, Mexico, [4]Unidad de Microscopía, Instituto de Investigaciones Biomédicas, Universidad Nacional Autónoma de México, Mexico City, Mexico, [5]Laboratorio de Oncología Experimental, Instituto Nacional de Pediatría, Mexico City, Mexico, [6]Laboratorio de Biología Animal Experimental, Facultad de Ciencias, Universidad Nacional Autónoma de México, Mexico City, Mexico

Introduction: Ketogenic diet (KD), a high-fat, low-carbohydrate, and adequate protein diet, is a non-pharmacological treatment for refractory epilepsy. However, their mechanism of action is not fully understood. The cation-chloride cotransporter, KCC2, transports chloride out of neurons, thus contributing to the intraneuronal concentration of chloride. Modifications in KCC2 expression by KD feeding could explain the beneficial effect of this diet on epilepsy. This study aimed to determine the impact of KD on KCC2 expression in dentate gyrus layers and Cornu Ammonis 3 (CA3) strata of rats with seizures induced by amygdaloid kindling.

Materials and methods: Male Sprague Dawley rats were fed a normal diet (ND) or KD from postnatal day 24 until the end of the experiment. At 6 weeks after the start of the diets, rats were subjected to an amygdala kindling epilepsy model, sham or remain intact. Glucose and β-hydroxybutyrate concentrations were quantified. The after-discharge duration (ADD), latency, and duration of stages of kindling were evaluated. In addition, KCC2 expression was evaluated using optical density. A Pearson bivariate correlation was used to determine the relationship between KCC2 expression and ADD.

Results: At the end of the experiment, the KD-fed groups showed a reduction in glucose and an increase in β-hydroxybutyrate. KD reduced ADD and increased latency and duration of generalized seizures. In ND-fed animals, kindling reduced KCC2 expression in all three layers of the dentate gyrus; however, in KD-fed animals, no changes were observed. KD treatment increased KCC2 expression in the kindling group. In CA3, the pyramidal and lucidum strata showed an increase of KCC2 in KD-fed groups. Besides, the kindling had lower levels of KCC2 than the sham and intact groups. In all layers of the dentate gyrus and pyramidal and lucidum CA3 strata, the correlation indicated that the higher the KCC2 expression, the shorter the ADD during generalized seizures.

Conclusion: KD reduces ADD in generalized seizures. In addition, KD has a putative neuroprotective effect by preventing the kindling-induced reduction of KCC2 expression in the molecular, granule, and hilar dentate gyrus layers and pyramidal and lucidum CA3 strata. Increased KCC2 expression levels are related to a shorter duration of generalized seizures.

KEYWORDS

ketogenic diet, kindling, KCC2, dentate gyrus, CA3, rat

1 Introduction

Epilepsy is a chronic disease of the central nervous system that affects individuals of all ages with a bimodal distribution. The features of this disease herald a continuous propensity to trigger abnormal, excessive, and synchronized activity in a group of brain cells with epileptic seizures as the end. This disease is considered an important public health problem worldwide (World Health Organization, 2024). According to the International League Against Epilepsy (ILAE), epilepsy is defined by any of the following conditions: (1) at least two unprovoked or reflex seizures that occur 24 or more hours apart; (2) a non-induced or reflex seizure in a person who has a 60% risk of having another seizure over the next 10 years; and (3) diagnosis of an epileptic syndrome (Fisher et al., 2014). Although, in most cases, epilepsy can be successfully treated, not all epileptic patients respond favorably to medical treatments, which can lead to drug resistant epilepsy. Drug resistant epilepsy may be defined as the failure of adequate trials of two tolerated and appropriately chosen and used antiepileptic drug schedules (whether as monotherapies or in combination) to achieve sustained seizure freedom (Kwan et al., 2010). Epilepsy and numerous neurological and neuropsychiatric disorders are known to be caused by the dysfunction of gamma-aminobutyric acid (GABA)-mediated neurotransmission (Cellot and Cherubini, 2014; Lam et al., 2023; Perucca et al., 2023; Juárez-Zepeda et al., 2024). Researchers have extensively used the amygdala electrical kindling model in the study of epilepsy neurobiology. The kindling process is the result of progressive weakening of the inhibitory system (Ryu et al., 2021; Tescarollo et al., 2023).

The strength and polarity of GABA-mediated neurotransmission are determined by the intracellular chloride (Cl^-) ion concentration. In neurons, the Cl^- concentration gradient is mainly regulated by two cotransporters that belong to the cation-chloride cotransporter family; the Na^+-K^+-Cl^- cotransporter 1 (NKCC1) and the K^+-Cl^- 2 (KCC2); which are encoded by Slc12a2 and Slc12a5, respectively (Kaila et al., 2014; Koumangoye et al., 2021; McMoneagle et al., 2024). The intracellular concentration of Cl^- is very important as it determines the postsynaptic responses to the GABA neurotransmitter, the main inhibitory neurotransmitter of the central nervous system (Belperio et al., 2022). KCC2 functions to extract intracellular Cl^- to maintain low levels of this ion in neurons (Duy et al., 2019). This leads to the discharge of hyperpolarizing currents regulated by $GABA_A$ receptors and thus causes a reduction of epileptiform discharges or seizure activity and prompts a GABA inhibitory response to reduce neuronal excitability. In epileptic disorders, alterations in KCC2-regulated Cl^- transport have been identified along with a decreased efficacy of $GABA_A$ receptor-mediated inhibition (Pathak et al., 2007; Lee et al., 2011; Karlócai et al., 2016; Di Cristo et al., 2018). This is attributed to the fact that an intracellular Cl^- accumulation leads to depolarizing currents that are regulated by GABAergic receptors and thus causes epileptiform discharges or seizure activity (Di Cristo et al., 2018). Recent studies have reported KCC2 downregulation in multiple models of epilepsy (Chen et al., 2017; Wan et al., 2018; Wan et al., 2020; Shi et al., 2023) and humans (Aronica et al., 2007; Shimizu-Okabe et al., 2011; Gharaylou et al., 2019). These studies support the importance of KCC2 regulation for neuronal intracellular Cl^- concentration homeostasis and proper functioning of GABA signaling (Pressey et al., 2023).

Patients suffering from refractory epilepsy (20–30% of the total) are effectively treated with various non-pharmacological treatments, such as the ketogenic diet (KD) (Martin-McGill et al., 2026; El-Shafie et al., 2023), which is characterized by a high level of fat, an adequate protein level, and strict carbohydrate restriction. KD has been introduced as a nutrition-based intervention commonly used to treat drug-resistant epilepsy since the 1920s (Wheless, 2008). KD is an adequate strategy to induce a biochemical model of fasting, where cells become less dependent on glucose energy substrate and more dependent on ketone bodies for the body's energy needs (Fedorovich et al., 2018). To achieve this condition, the liver mitochondrial matrix has to metabolize ketone bodies. Recent research has re-established the efficacy of KD in managing epilepsy, as well as in a spectrum of neurological and neuropsychiatric disorders where a dysfunction in GABA-mediated neurotransmission is evident (Dyńka et al., 2022; Juárez-Zepeda et al., 2024).

The mechanism by which KD acts effectively in epilepsy is not clearly understood; however, the fact that KD has beneficial effects in diseases in which the KCC2 cotransporter is affected has led to the proposal that modifications in the expression of the cation-chloride cotransporter KCC2 could be at least in part the mechanism of action of this diet in epilepsy (Wang et al., 2016; Granados-Rojas et al., 2020; Murakami and Tognini, 2022). Although KD, *per se*, is known to increase KCC2 expression in the cerebral cortex (Wang et al., 2016) and dentate gyrus (Granados-Rojas et al., 2020), little is known about regional alterations of KCC2 in the hippocampus of rats fed with KD under an epilepsy model. Therefore, the present study was focused on investigating the effect of KD on the expression of the cation-chloride cotransporter KCC2, as determined by optical densitometry analysis in the dentate gyrus layers and Cornu Ammonis 3 (CA3) strata of amygdaloidal kindling seizure-induced rats.

2 Materials and methods

2.1 Animals and diets

All experimental procedures developed in the research reported in this study followed the guidelines of the Official Mexican Norm (1999)

(NOM-062-ZOO-1999) and are part of project 085–2010, approved by the Research Board of the National Institute of Pediatrics. The project was also approved by the Institutional Committee for the Care and Use of Laboratory Animals (CICUAL). All efforts were made to minimize the number and suffering of the animals used in the experiments.

Male Sprague Dawley rats were bred and kept in constant controlled conditions of temperature (22°C–24°C), light:dark cycle (12:12 h, lights on from 6:00 am to 6:00 pm), and relative humidity (40%) were used. The air filter (3 microns particles) was exchanged 18 times in 1 h. At postnatal day 24, rats from 8 litters were weaned and randomly assigned to two groups as follows: normal diet-fed rats (ND) (2018S sterilized, Envigo Teklad, United States) and KD (TD 96355, Envigo Teklad, United States) (Gómez-Lira et al., 2011; Granados-Rojas et al., 2020). Both groups of animals had free access to water and their respective diets. Diets were started from weaning and were maintained throughout the experiment. Prior to the dietary treatments, the animals were subject to 8-h fasting.

2.2 Measurements of body weight, glucose, and β-hydroxybutyrate

The body weight, blood glucose, and β-hydroxybutyrate levels of each animal were recorded at the beginning and end of treatment. Similar to our previous study (Granados-Rojas et al., 2020), to measure blood glucose and β-hydroxybutyrate levels, a drop of blood was collected from the lateral tail tip vein and placed on glucose or β-hydroxybutyrate test strips (Abbott Laboratories) inserted into a FreeStyle Optium digital monitoring system (Abbott Laboratories glucometer) that indicated glucose or β-hydroxybutyrate concentrations (Wang et al., 2017; Doyen et al., 2024; Meeusen et al., 2024).

2.3 Stereotaxic surgery

After 6 weeks of ND or KD, a portion of the animals was anesthetized with ketamine (100 mg/kg intraperitoneal). Subsequently, the animals were placed in a stereotaxic device (David Kopf) to implant electrodes for stimulation and recording. The electrodes were implanted in the left basolateral nucleus of the amygdala (previous coordinates of 6.2 mm, side of 5 mm, and 1.5 mm in height). For this purpose, the interaural line was used as a reference in accordance with the Paxinos and Watson Atlas of Stereotaxy (Paxinos and Watson, 2007). Another electrode was placed in the sensory motor cortex to register the propagation of electroencephalographic activity. Each electrode was made with isolated stainless steel (0.005-inch diameter) coated with Teflon, except in the ends. A screw was implanted in the skull to serve as a source of reference. The electrodes were attached to a mini-connector and linked to the skull using dental acrylic. The skin was sutured around the mini-connector. The electrode positioning was later verified using histological staining techniques (Taddei et al., 2022).

2.4 Kindling model

After 10 days of postoperative recovery, the rats were placed in a silenced chamber (22.5 cm x 30 cm x 30 cm). The connector was joined to flexible cables connected to the rat with the S88 Grass stimulator and a stellate system digital polygraph. The settings of the polygraph were 50 microvolts of amplification and a filter between 3.5 and 30 Hz. The rats were stimulated daily with a 60 Hz frequency, pulses of duration of 1.0 s, and an intensity of 5 V (Goddard et al., 1969). The following parameters were measured: amygdala after-discharge duration (ADD), average ADD across 10 generalized seizures, latency or number of stimuli required to reach each kindling stage and their duration, and associated behavior according to the parameters described by Racine (1972). Stage 1: Clonus of the facial muscles, one or both eyes closed; stage 2: Oscillatory movements of the head; stage 3: Myoclonic of the forelimbs in movement; stage 4: Myoclonic movements in both extremities; stage 5: Generalized tonic–clonic seizure. Stages 1–3 were considered focal seizures, whereas stages 4 and 5 were considered generalized seizures. Sham-operated animals were implanted with electrodes but did not receive any stimulation. A part of the animal was left intact.

Finally, 6 groups of animals were used in this study:

1) IND: intact (naive) animals fed with a ND, no kindling ($n = 8$).
2) KND: animals fed with an ND with electrical amygdala kindling ($n = 7$).
3) SND: sham animals fed with a ND ($n = 8$).
4) IKD: intact (naive) animals fed with a KD, no kindling ($n = 8$).
5) KKD: animals fed with a KD with electrical amygdala kindling ($n = 8$).
6) SKD: sham animals fed with a KD ($n = 7$).

2.5 Tissue processing and sample collection

All animals were sacrificed 1 day after the last stimulation. At the end of treatment, rats were anesthetized with sodium pentobarbital (50 mg/kg, intraperitoneally) and transcardially perfused with 0.9% NaCl, followed by 4% paraformaldehyde in phosphate buffer, 0.1 M, pH 7.4 (PFA). The brains were then carefully removed, post-fixed in PFA overnight, and serially cryo-protected in 10, 20, and 30% sucrose at 4°C. Afterward, brain blocks containing the dorsal and ventral hippocampus of both the right and left hemispheres were sectioned in the coronal plane at 50 μm thick using a cryostat (Leica, Germany) at −21°C. Serial sections were stored in a cryoprotectant solution (25% glycerol, 25% ethylene glycol, 50% phosphate buffer 0.1 M, pH 7.4) at −20°C in 24-well plates until use. To select the sections from the serial slides per animal, a systematic random procedure consisting of choosing one of every eight sections that resulted in eight series of 12–14 sections of all rat dentate gyrus and CA3 was used. One of the series was immunohistochemically processed to immunodetection of KCC2 in each rat (Granados-Rojas et al., 2020).

2.6 Immunohistochemical staining

To evaluate the expression of the cation-chloride cotransporter KCC2 in the IND, KND, SND, IKD, KKD, and SKD rat groups, an immunohistochemistry protocol was carried out using a secondary biotinylated antibody according to Granados-Rojas et al. (2020). Free-floating brain tissue sections were processed in parallel at room

temperature and in constant motion. Sections were initially subjected to 3 times 10-min washes with Phosphate Buffered Saline (PBS) between the change of each solution and at the end. After initial washing with PBS, sections were subjected to 1% hydrogen peroxide in PBS for 10 min. Tissues were then incubated with 20X ImmunoDNA retriever buffer (Bio SB, United States) at 65°C for 60 min, followed by incubation with the primary rabbit polyclonal antibody anti-KCC2 (1:2000; Merck Millipore, Germany, Cat. # 07–432), diluted in 5% horse serum (Gibco, United States) and 3% Triton X-100 (Merck, Germany) in PBS overnight. The antibody recognizes their total protein. The next day, the sections were washed and incubated with a secondary biotinylated goat anti-rabbit IgG antibody (1:500; Vector Laboratories, United States, Cat. # BA-1000) for 2 h, and subsequently incubated with avidin peroxidase complex (ABC kit; Vectastain; Vector Laboratories, United States, Cat. # Pk-4000) for 1 h. To determine peroxidase activity, a nickel-intensified 3,3′-diaminobenzidine (DAB; Vector Laboratories, United States, Cat. # SK-4100) solution was used for 2 ½ min. Finally, the sections were mounted on poly-L-lysine-coated slides, and entellan (Merck, Germany) was added to the slides. Then, the slides were covered with a glass coverslip. In additional sections, the primary antibody KCC2 as well as the secondary biotinylated antibody were omitted as negative controls to assess nonspecific binding. The same amount of horse serum used to replace the primary or secondary antibody resulted in a lack of any staining. Evaluation of sections was performed in a blind manner, i.e., the researcher was not aware whether the sections were from the IND, KND, SND, IKD, KKD, or SKD rat groups.

2.7 Optical density analysis of KCC2

The determination of KCC2 expression in the dentate gyrus and CA3 was carried out through digital densitometric analysis of acquired image color intensities. All images with identical characteristics of acquisition (objective lens, aperture condenser, light intensity, exposure time, and white balance) were taken with a MBF-CX9000 RGB CCD camera (MBF Bioscience, VT, United States) coupled to a BX-51 microscope (Olympus Corporation, Japan) and Stereoinvestigator software (MBF Bioscience, VT, United States). ImageJ software (v 1.52e, Rasband, 2018) was used to perform densitometric measurements, and the values obtained were expressed as optical density in arbitrary units. For each image, we converted RGB to 8-bit color depth, segmented the layers of interest, and measured the relative intensity of pixels in each region. The analysis was conducted at 20x in selected sections of the whole dentate gyrus and CA3. Each optical density value was normalized using background subtraction (Granados-Rojas et al., 2020). The KCC2 optical density was estimated in the molecular, granule, and hilar dentate gyrus layers, as well as in the oriens, pyramidal, lucidum, and RLM (radiatum and lacunosum-moleculare) CA3 strata. The total expression of the KCC2 cotransporter in each layer or stratum was obtained by considering the dorsal and ventral regions of both the right and left hemispheres.

2.8 Statistical analysis

Data on glucose, β-hydroxybutyrate, and body weight were submitted to separate three-way mixed Analyses of Variance (ANOVAs) that included the within-subject factor: Time (initial vs. final measurement) and the two between-subject factors: Diet (ND vs. KD) and Manipulation (intact, kindling, and sham).

The data from body weight as well as the KCC2 immunoreactivity (KCC2-IR) optical density in all dentate gyrus layers and all CA3 strata were subjected to separate two-way ANOVAs that included the between-subject factors: Diet (ND vs. KD) and Manipulation (intact, kindling, and sham).

For the analyses, the Mauchly's sphericity test was performed. For all parameters with repeated measures, the Mauchly's test indicated no sphericity ($p < 0.05$) in all cases. Therefore, the Greenhouse–Geisser correction method for sphericity was used (Verma, 2015), and the corrected results are those reported.

For all two-way ANOVAs in CA3, the Levene's test showed equality of variances ($p > 0.05$) for all cases. On the contrary, in the dentate gyrus, Levene's test indicated no homoscedasticity in the molecular and granule layers ($p < 0.05$), but in the hilar layer, there was equality of variances ($p > 0.05$). In all cases, the significant interactions, original degrees of freedom, and corrected probability levels are reported in addition to the partial eta squares. Tukey's honest significant difference (HSD) tests were computed as *post hoc* analyses for the main effects found in the CA3 strata, while the different significant interactions were analyzed with the Bonferroni's *post hoc* test.

The ADD averages were calculated for the kindling establishment and for the days corresponding to the generalized seizures. The effects of diet on these two moments were evaluated using a repeated ANOVA measures that included the between-factor Diet (ND vs. KD). *Post hoc* effects were analyzed by means of the Bonferroni's test. The latencies (number of days needed to reach the different stages) and the duration of each Racine's scale stage were analyzed using separate Mann–Whitney U tests.

Additionally, Pearson's bivariate correlation test was performed to analyze whether there was a relationship between the levels of KCC2 expression in the different dentate gyrus layers and CA3 strata with the ADD generalized seizures. This test was performed independently of the group to which the animals belonged.

For all statistical analyses, the significance level was maintained at $p \leq 0.05$. For all parameters, boxplots with individual data points were created, except for ADD. All analyses were performed using SPSS (Statistical Package for the Social Sciences), version 20.

3 Results

3.1 Body weight

KD was well tolerated during the study. Assessment of body weight was performed at the beginning and end of the study. The three-way ANOVA indicated that the interactions that included the factor Diet were not significant ($p > 0.05$); therefore, there were no significant effects of diet on body weight. However, the interaction Time × Manipulation was significant ($F(2, 40) = 7.202$, $p < 0.01$, $\eta^2 = 0.265$). As expected, the Bonferroni's *post hoc* test showed that at the beginning of the study, there were no significant differences in body weight between the three types of manipulation ($p > 0.05$ for all comparisons), indicating equality of initial conditions. However, at the end of the study, the kindling groups of both diets (KND and KKD) presented a significantly lower body weight (11.69%) than the intact groups of both diets (IND and IKD) ($p < 0.001$ for all comparisons) (Figure 1A, #). For all groups, a significant body weight gain was

observed at the end of the experiment when compared with the beginning of the experiment ($p < 0.001$) (Figure 1A, *).

3.2 Glucose

Assessment of glucose was performed at the beginning and end of the study. The three-way ANOVA indicated that the interaction Time × Diet was significant ($F(1, 40) = 11.347$, $p < 0.01$, $\eta^2 = 0.22$). The Bonferroni's *post hoc* analysis showed that in all groups, there was a significant decrease in peripheral blood glucose concentration at the end of the experiment with respect to the beginning ($p < 0.001$) (Figure 1B, *); however, this decrease was greater (34.69%) in the KD-fed groups (IKD, KKD, and SKD) than in the ND-fed groups (IND, KND, and SND) (25.10%). As expected, at the beginning of the experiment, no significant differences were observed between groups ($p > 0.05$). On the contrary, at the end of the experiment, the glucose concentration was significantly different ($p < 0.01$). The KD-fed groups (IKD, KKD, and SKD) presented a significantly lower glucose concentration (11.26%) than the ND-fed groups (IND, KND, and SND) ($p < 0.01$) (Figure 1B, #).

3.3 β-Hydroxybutyrate

To assess the effectiveness of the ketogenic diet, ketone bodies were measured, particularly β-hydroxybutyrate, at the beginning and end of the study. Three-way ANOVA showed that the interaction Time × Diet was significant ($F(1, 40) = 164.47$, $p < 0.001$, $\eta^2 = 0.804$). As expected, the Bonferroni's *post hoc* test indicated that at the beginning of the study, there were no significant differences ($p > 0.5$) between groups, thus showing equal initial conditions. The concentration of β-hydroxybutyrate decreased significantly (41.53%) at the end of the experiment in the ND-fed groups (IND, KND, and SND) compared with the beginning of the experiment ($p < 0.001$) (Figure 1C, *) and increased significantly (111.49%) in the KD-fed groups (IKD, KKD, and SKD) when compared with the beginning of the experiment ($p < 0.001$) (Figure 1C, #). However, at the end of the experiment, the KD-fed groups (IKD, KKD, and SKD) presented a significantly greater β-hydroxybutyrate concentration (269.47%) than the ND-fed groups (IND, KND, and SND) ($p < 0.001$) (Figure 1C, &).

3.4 After-discharge duration

Kindling model results are shown in Figures 2A-D. The repeated measures ANOVA for the kindling establishment and generalized seizures was significant ($F(1, 11) = 16.187$, $p < 0.01$, $\eta^2 = 0.595$). The Bonferroni's *post hoc* test revealed that the KD-fed kindling group (KKD) had a significantly lower ADD than the ND-fed kindling group (KND) ($p < 0.01$) only during generalized seizures (Figure 2B).

3.5 Latency

Analyses using Mann–Whitney U tests showed that latency to reach stage 3 was significantly higher ($U = 8.5$, $p < 0.05$) in the KD-fed kindling group (KKD) than in the ND-fed kindling group (KND) (Figure 2C, *). The latencies of stages 2 and 3 collapsed because they corresponded to the focal seizure conditions. Similarly, latencies of stages 4 and 5 collapsed under generalized seizure conditions. Mann–Whitney U tests indicated no significant differences in focal seizure conditions ($p > 0.05$) but did indicate the existence of significant differences in generalized seizure ($p = 0.05$), with the latency being longer in the KD-fed kindling group (KKD).

3.6 Stage duration

The Mann–Whitney U tests indicated that the duration of stage 4 was significantly longer ($U = 1$, $p < 0.01$) for the KD-fed kindling group (KKD) than for the ND-fed kindling group (KND).

3.7 KCC2-IR optical density

Evaluation of the cation-chloride cotransport KCC2 expression by optical density was carried out in 12–14 sections of each rat (Figure 3A). The cytoarquitecture and diffuse staining patterns of the dentate gyrus (Figures 3B-F,K-M) and CA3 (Figures 3B-C,G-J) remained unchanged in all groups. The lamination of the dentate gyrus and CA3 was preserved properly in both hemispheres. This allowed the identification and delimitation of each of the regions of analysis: the molecular, granule, and hilar dentate gyrus layers, as well as the oriens, pyramidal, lucidum, and RLM CA3 strata (Figures 3B,C). The anatomical boundaries and criteria to define each layer of the dentate gyrus and each CA3 strata were established according to Amaral and Witter (1989), Gulyás et al. (2001), Amaral et al. (2007), and Paxinos and Watson (2007). Thus, in the dentate gyrus (−1.72 to −6.84 mm posterior to Bregma), the granule layer is the compact layer that contains the somas of the granule cells. KCC2 staining was observed around the neuronal somas, i.e., in the plasma membrane, whereas the somas of the granule cells were not dyed (Figure 3E). Below this layer is the molecular layer containing mainly the dendrites of the granule cells in a dark tone. The strongest neuropil staining of the entire hippocampus was observed in this layer (Figure 3D). Above the granular layer lies the hilar layer, where the labeling was weaker and delimited by the upper and lower borders of the dentate gyrus. KCC2 staining was observed around polymorphic cells and in neural processes (Figure 3F).

In CA3 (−1.72 mm to −6.12 mm posterior to Bregma) (Figure 3G), the compact zone of the somas of the pyramidal cells forms the pyramidal stratum, and peripheral KCC2 staining was observed in the somas of these cells, i.e., in the plasma membrane. Below the pyramidal layer is the dark-toned oriens stratum. Diffuse immunostaining was strongest in stratum oriens, which is delimited by the white matter of the alveus. The basal dendrites of the pyramidal cells are located here. Above the pyramidal layer lies the acellular stratum lucidum, which is very clear. The region contains the axons of the granule cells and the proximal apical dendrites of the pyramidal cells. The only field that presents a stratum lucidum is the CA3 field; therefore, it delimits the CA3. Next are the radiata and lacunosum-moleculare strata. Because they are difficult to delimit, they were evaluated together, and contain the medial and distal apical dendrites of the pyramidal cells.

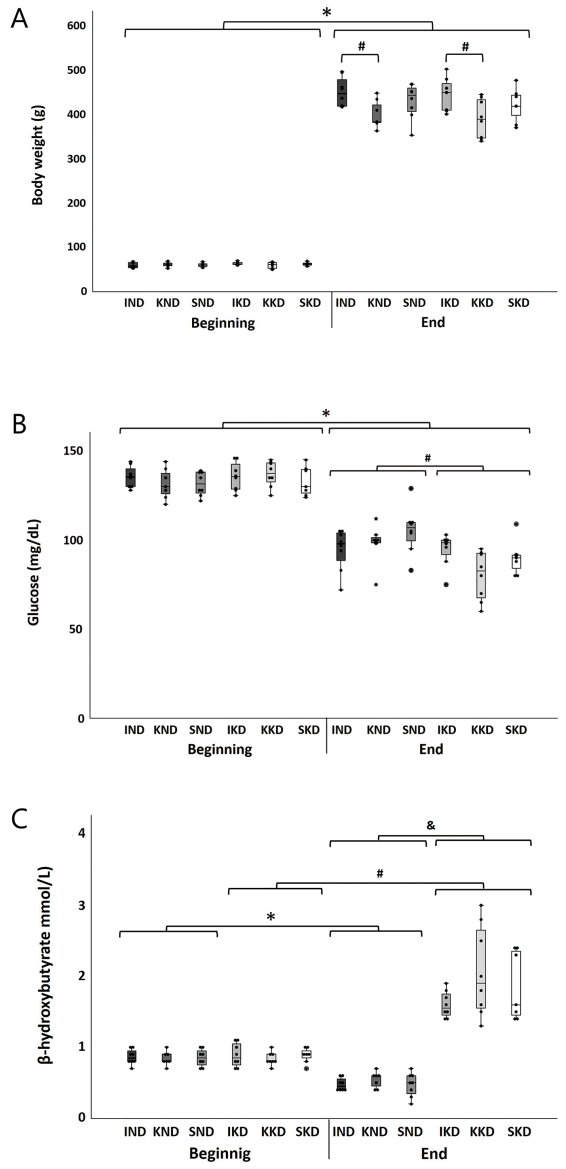

FIGURE 1
Boxplots with individual data points for each group at the beginning and end of the study of body weight **(A)**, glucose **(B)**, and β-hydroxybutyrate **(C)**. The three-way ANOVA and Bonferroni's *post hoc* test indicated a significant body weight increase ($p < 0.001$) at the end of the experiment compared to the beginning for all groups (**A**, *). At the end, body weight was significantly lower ($p < 0.001$) for the kindling groups (KND and KKD) compared to the intact ones (IND and IKD) (**A**, #). Regarding blood glucose concentration, for all groups, there was a significant reduction ($p < 0.001$) at the end of the study regarding the beginning (**B**, *). At the end, the KD-fed groups (IKD, KKD, and SKD) presented significantly lower glucose concentrations ($p < 0.01$) than ND-fed groups (IND, KND, and SND) (**B**, #). For blood β-hydroxybutyrate concentration, at the end of the study, the ND-fed groups (IND, KND, and SND) presented a significant decrease ($p < 0.001$) regarding the beginning (**C**, *), contrary to the KD-fed groups (IKD, KKD, and SKD) that presented a significant elevation ($p < 0.001$) (**C**, #). At the end, the KD-fed groups (IKD, KKD, and SKD) presented significantly higher ($p < 0.001$) β-hydroxybutyrate concentrations than ND-fed groups (IND, KND, and SND) (**C**, &). ND, normal diet; KD, ketogenic diet; IND, ND-fed intact; KND, ND-fed with amygdala kindling; SND, ND-fed sham; IKD, KD-fed intact; KKD, KD-fed with amygdala kindling; SKD, KD-fed sham.

Dentate gyrus: Two-way ANOVA showed that the Diet × Manipulation interaction was significant in the molecular layer ($F(2, 40) = 4.503$, $p < 0.05$, $\eta^2 = 0.184$). The Bonferroni's *post hoc* test indicated that when animals were fed with ND, the kindling group (KND) had presented significantly lower (18.62%) KCC2 expression than the intact group (IND) ($p < 0.001$) (Figure 4A, *) and sham group (SND) (20.30%; $p < 0.001$) (Figure 4A, #). On the contrary, when animals were fed with KD, the kindling group (KKD) was not significantly different from the intact group (IKD) and the sham group (SKD). In the kindling groups, the KD-fed group (KKD) exhibited higher KCC2 expression than the ND-fed group (KND) (26.8%; $p < 0.001$) (Figure 4A, &).

In the granule layer, the Diet × Manipulation interaction was significant ($F(2, 40) = 3.325$, $p < 0.05$, $\eta^2 = 0.143$). In this case, the Bonferroni's *post hoc* test evidenced that when animals were fed with ND, the kindling group (KND) presented significantly lower KCC2 expression than the intact group (IND) (22.15%; $p < 0.001$) (Figure 4B, *) and the sham group (SND) (21.47%; $p < 0.001$) (Figure 4B, #). When the animals were fed with KD, no significant difference was observed between the KKD and SKD groups. However, the KKD group had a significantly lower KCC2 expression than the IKD group (13.03%; $p < 0.01$) (Figure 4B, %), because IKD significantly increased the expression of KCC2, and this was even significantly higher than that in the IND group (19.67%; $p < 0.001$) (Figure 4B, $). The KKD group exhibited a significantly higher KCC2 expression than the KND group (33.70%; $p < 0.001$) (Figure 4B, &).

In the hilar layer, similar to the other layers of the dentate gyrus, the Diet × Manipulation interaction was significant ($F(2, 40) = 10.961$, $p < 0.001$, $\eta^2 = 0.354$). In cases that received ND, the Bonferroni's *post hoc* test indicated that the kindling group (KND) had significantly lower KCC2 expression than the intact group (IND) (18.55%; $p < 0.001$) (Figure 4C, *) and the sham group (SND) (19.6%; $p < 0.001$) (Figure 4C, #). In contrast, when animals were fed with KD, no significant differences were observed in the IKD, KKD, and SKD groups. For the kindling groups, rats fed with a KD diet (KKD) had significantly higher KCC2 expression than those fed with a normal diet (KND) (33.18%; $p < 0.001$) (Figure 4C, &). A similar pattern was observed for the intact groups; the IKD group had significantly higher KCC2 expression than the IND group (15.01%; $p < 0.001$) (Figure 4C, $).

CA3: In the oriens stratum, two-way ANOVA did not reveal significant interactions or main effects on this layer (Figure 5A).

In contrast, in the pyramidal stratum, two-way ANOVA revealed a significant main effect of Diet ($F(1, 40) = 44.58$, $p < 0.001$, $\eta^2 = 0.527$). Tukey's *post hoc* test indicated that the KD-fed groups (IKD, KKD, and SKD) had significantly greater KCC2 expression than the ND-fed groups (IND, KND, and SND) (16.06%, $p < 0.001$) (Figure 5B, *). The factor Manipulation was also significant ($F(2, 40) = 19.06$, $p < 0.001$, $\eta^2 = 0.1488$). The Tukey's *post- hoc* test showed that the kindling groups (KND and KKD) had significantly lower KCC2 expression than the intact groups (IND and IKD) (16.71%, $p < 0.001$) (Figure 5B, &, &′) and the sham groups (SND and SKD) (12.95%; $p < 0.01$) (Figure 5B, #, #′).

In the lucidum stratum, two-way ANOVA showed a significant main effect of Diet ($F(1, 40) = 66.475$, $p < 0.001$, $\eta^2 = 0.624$). The Tukey's *post hoc* test found that the KD-fed groups (IKD, KKD, and SKD) had significantly greater KCC2 expression than the ND-fed groups (IND, KND, and SND) (20%; $p < 0.001$) (Figure 5C, *). For the

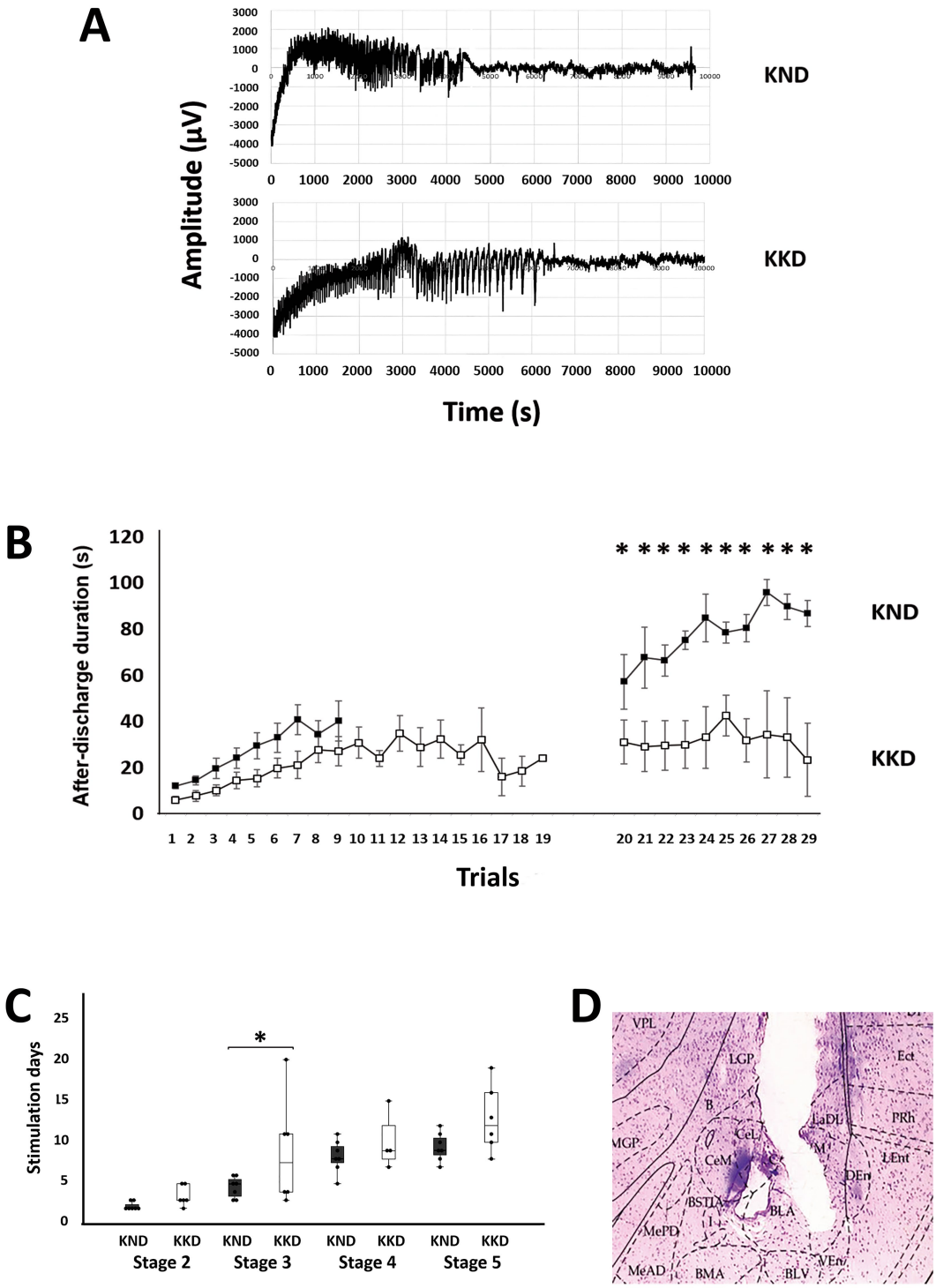

FIGURE 2
Kindling model measurements in the ND-fed group (KND) and the KD-fed group (KKD). **(A)** Representative recordings of after-discharge activity in the amygdala: at the top, the recording from the KND group; at the bottom, the recording from the KKD group. **(B)** Graphs representing the duration of after-discharge activity; values are shown as means ± standard error of the mean. Statistical significance in after-discharge was assessed using a repeated measures ANOVA, followed by Bonferroni's test. On the left, the duration during the first 20 days. On the right, the duration of generalized epileptic activity, with evident differences in the last 10 stimuli ($F = 16.187$, $^*p < 0.01$). Black squares represent the KND group, and white squares represent the KKD group. **(C)** Number of stimuli required to reach each Racine stage. Values are shown as boxplots with individual data points for each group. Analyses using Mann–Whitney U tests showed that the latency to reach stage 3 was significantly higher ($U = 8.5$, $p < 0.05$) for the KKD group than for the KND. **(D)** Microphotograph showing the placement of the electrode in the basolateral nucleus of the amygdala, using a Hematoxylin and Eosin staining technique, 40x. VPL, ventral posterolateral thalamic nucleus; LGP, lateral globus pallidus; Ect, entorhinal cortex; PRh, perirhinal cortex; LEnt, lateral entorhinal cortex; DEn, dorsal endopiriform nucleus; VEn, ventral endopiriform nucleus; LaDL, lateral amygdaloid nucleus, dorsolateral part; BLV, basolateral amygdaloid nucleus, ventral part; BLA, basolateral amygdaloid nucleus, anterior part; CeL, central amygdaloid nucleus, lateral division; B, basal nucleus (Meynert); CeM, central amygdaloid nucleus; medial division; BMA, basomedial amygdaloid nucleus, anterior part; MGP, medial globus pallidus.

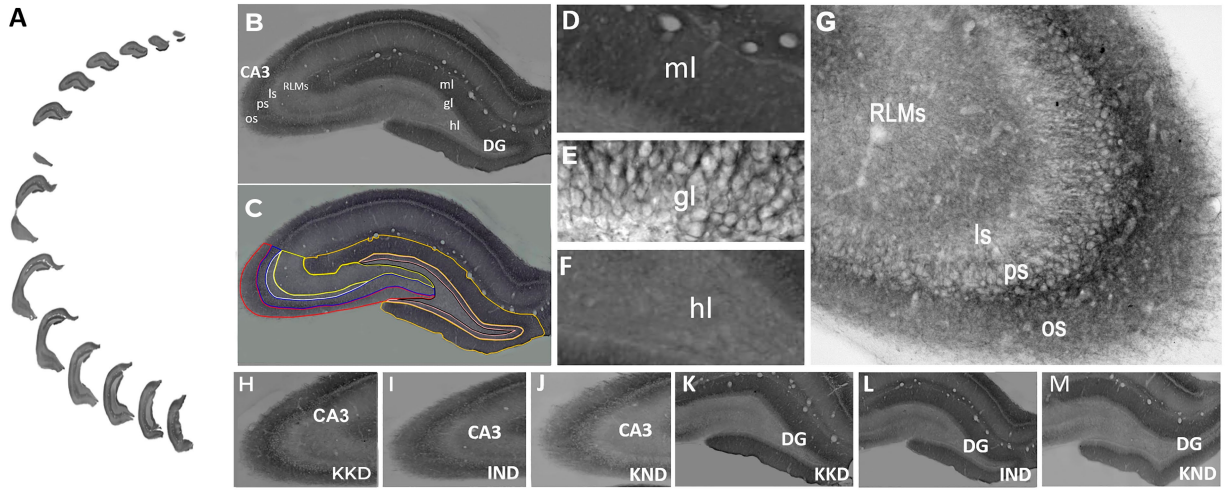

FIGURE 3
KCC2 expression in dentate gyrus and CA3. **(A)** Serial sections of the whole dentate gyrus and CA3 of the right hemisphere. **(B)** Panoramic view of molecular (ml), granule (gl), and hilar (hl) dentate gyrus layers and oriens (os), pyramidal (ps), lucidum (ls), and radiatum and lacunosum-moleculare (RLMs) CA3 strata. **(C)** The regions of interest were delimited with lines of different colors to obtain their optical density. Dentate gyrus layers: molecular (yellow line), granular (pink line), and hilar (black line). CA3 strata: oriens (red line), pyramidal (blue line), lucidum (white line), and RLM (bright yellow line). Higher magnification view of molecular **(D)**, granule **(E)**, and hilar **(F)**, dentate gyrus and oriens, pyramidal, lucidum, and RLM CA3 strata **(G)**. KCC2 immunoreactivity was observed in the plasmalemmal region (perisomal) in the granule cell body in the dentate gyrus **(E)** and in pyramidal cell CA3 **(G)**. CA3 of KD-fed with kindling rat (KKD) **(H)**, ND-fed intact rat (IND) **(I)**, and ND-fed with kindling rat (KND) **(J)**. Dentate gyrus of KKD rat **(K)**, IND rat **(L)**, and KND rat **(M)**. The KCC2 immunoreactivity was lower in the KND group compared to the IND and KKD groups. A-C, H-M, 20x. D-G, 40x.

Manipulation factor ($F(2, 40) = 21.844$, $p < 0.001$, $\eta^2 = 0.522$), it was observed by means of Tukey's *post hoc* test that the kindling groups (KND and KKD) had lower significant KCC2 expression than the intact groups (IND and IKD) (16.38%; $p < 0.001$) (Figure 4C, &, &′) and the sham groups (SND and SKD) (9.59%; $p < 0.001$) (Figure 5C, #, #′). A significant difference was observed between the sham groups (SND and SKD) and intact groups (IND and IKD), with this being higher in the intact groups (7.67%; $p < 0.01$) (Figure 5C, $, $′).

Finally, in the RLM stratum, two-way ANOVA did not reveal significant interactions or main effects on this layer (Figure 5D).

3.8 Pearson's correlation coefficient between KCC2-IR levels and ADD

Pearson's correlation test revealed significant negative correlations in all layers of the dentate gyrus: molecular $r(45) = -0.810$, $p < 0.001$; granule $r(45) = -0.725$, $p < 0.001$; and hilar $r(45) = -0.835$, $p < 0.001$; and in the CA3 strata: pyramidal $r(45) = -0.719$, $p < 0.001$; and lucidum $r(45) = -0.747$, $p < 0.001$. These findings indicate that in these regions, the higher the KCC2 levels, the shorter the ADD in generalized seizures. The correlation in oriens and RLM strata was not significant.

4 Discussion

We demonstrated that KD has an antiepileptic function in amygdala kindling by reducing ADD in generalized seizures. In addition, the present study provides experimental evidence suggesting that KD has a putative neuroprotective effect by preventing the kindling-induced reduction of KCC2 expression in the molecular, granule, and hilar dentate gyrus layers and pyramidal and lucidum CA3 strata. The findings indicate a differential effect of KD on KCC2 expression by region and layer or stratum. The higher the KCC2 expression levels, the shorter the ADD.

Considering the importance of GABA-mediated neurotransmission, regulation of intracellular chloride concentration by cation-chloride cotransporter, specifically KCC2, in epilepsy and the beneficial effects of KD in this disease, the results presented in this study include data on body weight, glucose and β-hydroxybutyrate concentration, as well as ADD, latency and duration of stages in rats fed with a KD under the amygdala kindling model. In addition, we obtained detailed information on the regional expression of KCC2 in different layers of the dentate gyrus and CA3 strata.

In concordance with previous studies, we found that KD-fed rats experienced a significant decrease in glucose concentration (Jiang et al., 2016) and an increase in β-hydroxybutyrate levels (Gómez-Lira et al., 2011; Jiang et al., 2012, 2016; Granados-Rojas et al., 2020). β-hydroxybutyrate concentration was taken as a measure of ketonemia; thus, this result confirmed the efficacy of the diet used in this study to induce ketosis until the end of the experiment (Jiang et al., 2012, 2016; Granados-Rojas et al., 2020; Meeusen et al., 2024). In addition, a decrease in body weight was observed in rats subjected to KD and kindling (Jiang et al., 2012, 2016). This may herald the metabolic effects of KD on epilepsy.

In this study, the KD was started before the establishment of the amygdala kindling model, an experimental paradigm widely used to evaluate the protective effect of the KD. In line with the above, the evaluation of the protective effect of the KD by Jiang et al. (2012) was performed before starting amygdala kindling. In the same manner, Wang et al. (2016) and Jiang et al. (2016) performed the same evaluation even before pentylenetetrazole (PTZ) kindling. Moreover, other authors provided other types of diets, such as caloric restriction, before amygdala kindling (Phillips-Farfán et al., 2015; Rubio-Osornio

10.3389/fnins.2025.1489407

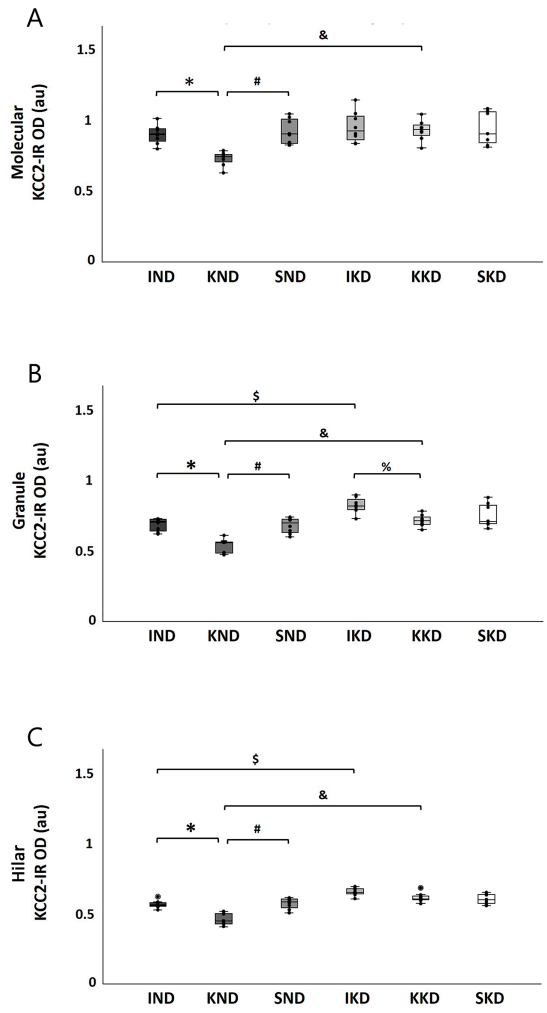

FIGURE 4
Boxplots with individual data points of KCC2 expression [KCC2-immunoreactivity optical density (KCC2-IR OD)] for each group in dentate gyrus layers: molecular **(A)**, granule **(B)**, and hilar **(C)**. The two-way ANOVA and Bonferroni's *post hoc* test indicated that the ND-fed kindling group (KND) has a lower KCC2 expression when compared to the ND-fed intact group (IND) in molecular (**A**, *), granule (**B**, *), and hilar (**C**, *) layers and when compared to the ND-fed sham group (SND) in molecular (**A**, #), granule (**B**, #), and hilar (**C**, #) layers. However, these changes were not observed in the KD-fed groups (IKD, KKD, and SKD). Only in the granule layer had the KD-fed kindling group (KKD) lower KCC2 expression when compared with the KD-fed intact group (IKD) (**B**, %). The IKD group had more KCC2 expression than the IND group in granule (**B**, $) and hilar (**C**, $) layers. KKD has a higher KCC2 expression than the KND group in molecular (**A**, &), granule (**B**, &), and hilar (**C**, &) layers. In all comparisons, $p < 0.001$, except for 4B, % with $p < 0.01$. ND, normal diet; KD, ketogenic diet; SND, ND-fed sham.

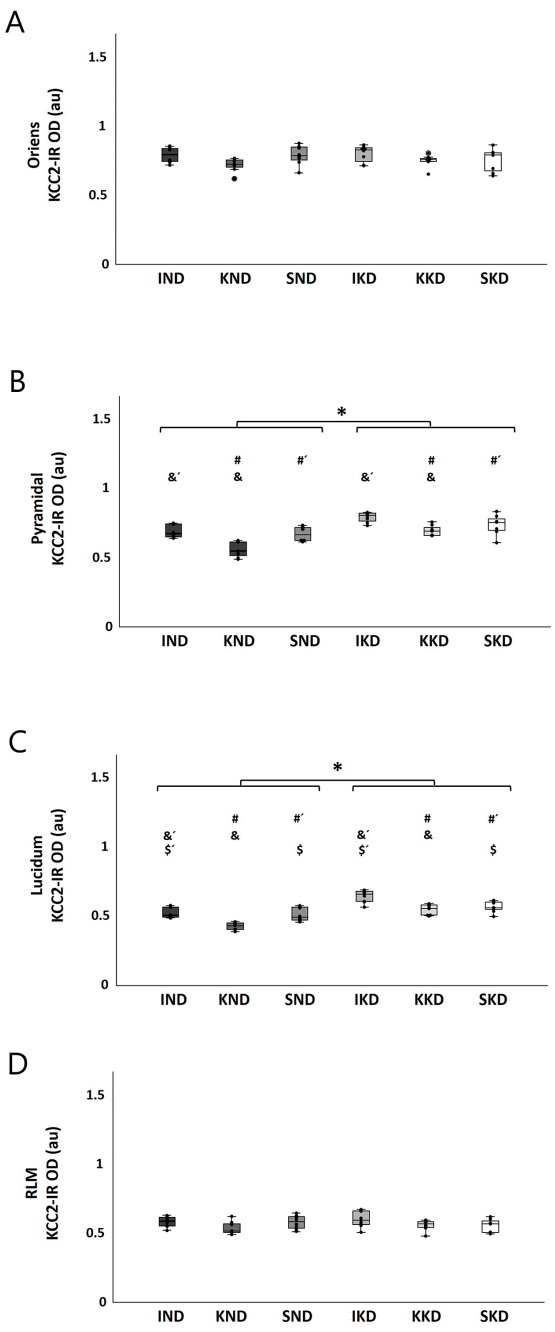

FIGURE 5
Boxplots with individual data points of KCC2 expression [KCC2-immunoreactivity optical density (KCC2-IR OD)] for each group in CA3 strata: oriens **(A)**, pyramidal **(B)**, lucidum **(C)**, and RLM **(D)**. The two-way ANOVA and Tukey's *post hoc* test indicated that there were no significant changes in the oriens **(A)** and RLM strata **(D)**. The KD-fed groups (IKD, KKD, and SKD) had greater KCC2 expression than the ND-fed groups (IND, KND, and SND) in the pyramidal stratum (**B**, *) and the lucidum stratum (**C**, *) ($p < 0.001$). Kindling groups (KND and KKD) had a lower KCC2 expression than the intact groups (IND and IKD) in the pyramidal (**B**, &, &´) and lucidum (**C**, &, &´) strata ($p < 0.001$), and it was also lesser in relation to sham groups (SND and SKD) in pyramidal (**A**, #, #´) and lucidum (**B**, #, #´) strata ($p < 0.01$). A significant difference between sham groups (SND and SKD) and intact groups (IND and IKD) was observed only in the stratum lucidum (**C**, $, $´) ($p < 0.01$). ND, normal diet; KD, ketogenic diet; IND, ND-fed intact; KND, ND-fed with amygdala kindling; SND, ND-fed sham; IKD, KD-fed intact; KKD, KD-fed with amygdala kindling; SKD, KD-fed sham.

et al., 2018). Nonetheless, we propose that future studies are needed to evaluate the impact of KD on KCC2 expression after establishing amygdala kindling. In the study by Hori et al. (1997) in which amygdala kindling was first established and then a KD was provided, no alterations were found in the kindling model, however, the diet used in this study contained zero carbohydrates.

The amygdala kindling model allows researchers to study the neurobiology of epilepsy in rats fed ND and KD diets (Hori et al., 1997; Hu et al., 2011; Jiang et al., 2012). Furthermore, the kindling model used

in this study reflects the generalized tonic–clonic seizures that show a higher incidence in the epileptic population. Focusing on specific kindling outcomes, a significant reduction in ADD was observed in the KD-fed group compared with the ND-fed group (Jiang et al., 2012; Wang et al., 2016; Meeusen et al., 2024). This suggests that KD has a beneficial effect on epileptic activity (Campbell et al., 2015; Murugan and Boison, 2020; Meeusen et al., 2024). In terms of latency, a significant increase in the time taken to reach stage 3 was observed in the KD-fed group compared with the ND-fed group (Jiang et al., 2012; Wang et al., 2016). This may indicate a higher resistance to seizure induction, which could be a positive effect of KD (Qiao et al., 2024). When kindling stages 4 and 5 were combined to analyze the latency corresponding to the generalized seizure condition, an increase in latency was observed in KD-fed animals (Meeusen et al., 2024), indicating that more time is required to establish the generalized seizure condition in KD-fed animals, thus observing the beneficial effect of this diet in this epilepsy model. In the KD-fed group, rats stayed in stage 4 (generalized seizures) for a longer duration than the ND-fed group. The putative neuroprotective effect of KD in the amygdala kindling model was demonstrated by the increase in ADD as well as the latency and duration of generalized seizures. This result coincides with the data reported in other studies (Jiang et al., 2012, 2016; Wang et al., 2016).

The kindling model has been used to study the expression of cation-chloride cotransporter (Rivera et al., 2002; Okabe et al., 2003; Ding et al., 2013; Wang et al., 2016; Tescarollo et al., 2023). Regarding KCC2 expression, a differential effect of KD was observed by cerebral region, since the dentate gyrus was the brain region with the greatest positive changes when compared with CA3. The differential effect of KD was also observed by layer and stratum. The granular layer of the dentate gyrus exhibited the largest changes in KCC2 expression, whereas in CA3, changes were observed only in the pyramidal and lucidum strata. The oriens, radiate, and lacunosum-moleculare strata remained unchanged.

Previous studies have reported that hippocampal kindling reduces KCC2 expression levels in the hippocampus (Rivera et al., 2002), PTZ kindling in the cerebral cortex (Wang et al., 2016), as well as optogenetic kindling in the hippocampus (Tescarollo et al., 2023) in animals fed a normal diet. A similar situation was observed in the present study, where our ND-fed animals that were subjected to kindling showed a reduction of KCC2 expression in the molecular, granular, and hilar layers of the dentate gyrus and pyramidal and lucidum CA3 strata when compared with both intact and sham animals. However, when the KD-fed groups were analyzed, this reduction was not observed in the molecular, granular, and hilar layers of the dentate gyrus. These findings suggest a putative protective effect of KD by preventing the reduction of KCC2 expression induced by kindling in the dentate gyrus layers and cerebral cortex (Wang et al., 2016). Although a reduction in KCC2 expression was observed in the granular layer of KD-fed rats subjected to kindling when compared with the ND-fed rats with kindling, this effect is probably due to the significant increase presented by the latter group. In addition, the KCC2 expression levels of the KD-fed group subjected to kindling did not differ from the ND-fed intact and sham groups.

It must be noted that KD *per se* induces an increase in KCC2 expression levels in the granular and hilar dentate gyrus layers, supporting previous results (Granados-Rojas et al., 2020). KD *per se* also increases KCC2 expression level in the cerebral cortex (Wang et al., 2016). These results indicate that different brain regions increase KCC2 expression in response to KD *per se*.

When KCC2 expression levels were compared among the kindled groups, higher expression was observed in the KD-fed group than in the ND-fed group. This result coincides with that reported by Wang et al. (2016) in the cerebral cortex. In the CA3 region, it was found that kindling reduces KCC2 expression in the pyramidal and lucidum strata compared with the intact and sham groups (Rivera et al., 2002) in both diet groups. The CA3 was the region that exhibited the least changes, indicating that KD possibly exerts its protective action mainly through the dentate gyrus. The sham groups on both diets had less KCC2 expression than the intact groups, suggesting that surgical manipulation reduces KCC2, as was observed in trauma.

In the specific discussion of kindling, it may be noted that KD seems to modulate KCC2 expression differently in the dentate gyrus and CA3 during kindling. In the dentate gyrus, KD appears to preserve KCC2 expression, which could contribute to its anticonvulsant effects observed in kindling ADD and latency. In CA3, the overall decrement in KCC2 expression in the kindling groups on both diets suggests a common response to increased excitability, independent of diet. It is important to note that these results are specific to the kindling model used in this study and that the precise relationship between KD and KCC2 expression may vary in other epilepsy models.

The increase in KCC2 in the dentate gyrus of the KD-fed kindling group compared with the ND-fed kindling group was also reported in a PTZ kindling model (Wang et al., 2016). This finding explains the reduction in ADD during the generalized seizure phase as well as the need for more sessions to reach this phase. The negative correlation observed between KCC2 expression and ADD during generalized seizures suggests a protective effect of diet on KCC2 in the dentate gyrus and CA3 in epilepsy.

In the adult brain, granule cells in the dentate gyrus are strongly inhibited by multiple variants of interneurons. This condition endows the dentate gyrus with the properties of a tightly regulated filter, limiting throughput between the entorhinal cortex and the hippocampus (Pathak et al., 2007). In the dentate gyrus, the granular layer contains the somas of granule cells. The dendrites of these cells are located in the molecular layer that receives efferences from the entorhinal cortex, while the hilar layer contains the axons of granule cells and various types of interneurons. On the other hand, in the CA3 area, the somas of pyramidal cells are found in the pyramidal stratum, while the proximal apical dendrites of these neurons are located in the lucidum stratum, with this being the place where mossy fibers or axons of granule cells arrive to make synapses with thorny excrescence dendrites of pyramidal cells. The prevention of the reduction of KCC2 expression produced by kindling, coupled with the increase in the expression of the same in the molecular, granule and hilar layers of the dentate gyrus, as well as in the pyramidal and lucidum strata of the KD-fed animals subjected to stimulation of the amygdala, suggests that in these layers and strata are where the propagation of excessive or aberrant activity to the circuit is inhibited, which makes the hippocampus less prone to seizures (Bonislawski et al., 2007). Future studies are needed to support this idea. It seems that the main region with the greatest beneficial effects is the dentate gyrus, which is very important since this region is highly epileptogenic (Bonislawski et al., 2007) and is also recognized as the entrance to hippocampal formation. On the other hand, in CA3, which organizes the response that flows to CA1 (the main exit of the hippocampal formation), the strata with the greatest changes were the pyramidal and lucidum.

The preservation of KCC2 expression levels in the dentate gyrus and CA3 in KD-fed animals under amygdala kindling reported in the present study complements previous reports carried out in the cerebral cortex of rats fed with a KD under PTZ kindling (Wang et al., 2016). This indicates that this effect may be general in the brain. This supports the proposal that the beneficial effect of KD on kindling observed in the present and other studies could be due to the increase of KCC2 not only in the cortex but also in the dentate gyrus and CA3. The protective effect of KD has also been observed in preventing neuronal loss in the CA1 area of the hippocampus in amygdaloid kindling (Jiang et al., 2012) and in attenuating spatial and item memory impairment in PTZ-induced seizures (Jiang et al., 2016; Wang et al., 2021).

The KCC2 function is to extract intracellular Cl^- to maintain low levels of Cl^- in neurons (Duy et al., 2019). Low concentrations of this ion in neurons lead to hyperpolarizing currents regulated by the $GABA_A$ receptor. This condition reduces epileptiform discharge or convulsive activity and promotes the inhibitory response of GABA by reducing neuronal excitability. Therefore, the increase and maintenance of KCC2 observed in animals fed with KD could be the mechanism, or one of the mechanisms, of this diet in epilepsy. However, future functional studies are necessary. The causal relationship between KCC2 modulation and the antiepileptic effects of KD should be further investigated.

Several studies have shown that a KD modifies synaptic function, reduces neuronal excitability, and decreases epileptic activity in the hippocampus of rodents. These effects are related to metabolic changes, such as increased ketone bodies, neurotransmitter regulation (GABA/glutamate), modulation of ion channels, and reduction of neuroinflammation. For example, a study by Stafstrom and Rho (2012) highlighted how the KD alters neuronal excitability and neurotransmitter balance and reduces seizure frequency in animal models. Another study by Lang et al. (2016) also demonstrated the role of ketone bodies in modulating synaptic function and enhancing inhibitory neurotransmission. Furthermore, Kasper (2020) found that a KD reduces epileptic activity by regulating ion channels and decreasing neuroinflammation in the hippocampus.

It is well known that there are sex differences in epilepsy. Susceptibility to excitability episodes and the occurrence of epileptic seizures are higher in men than in women (Reddy et al., 2021). Among the proposed molecular mechanisms underlying sex differences in seizure susceptibility are steroid hormones and neuronal chloride homeostasis regulated by the cation-chloride cotransporter NKCC1 and KCC2 (Reddy et al., 2021). We used epileptic male rats because female rats experience significant hormonal fluctuations throughout their estrous cycle. These hormonal fluctuations may influence neuronal activity and seizure susceptibility. On the other hand, there is a sexually dimorphic expression of KCC2, which is higher in females than in males (Galanopoulou and Moshé, 2003; Galanopoulou, 2008). The results obtained in the present study contribute to a better understanding of the effect of KD on epilepsy control; however, it is important to note that observations of KCC2 expression in the dentate gyrus and CA3 might change in epileptic female rats. Future studies are needed to address this issue.

In conclusion, KD has an antiepileptic function in amygdala kindling by reducing ADD in generalized seizures. In addition, KD has a putative neuroprotective effect by preventing the kindling-induced reduction of KCC2 expression in the molecular, granule, and hilar dentate gyrus layers and pyramidal and lucidum CA3 strata. Increased KCC2 expression levels are related to a shorter duration of generalized seizures. These results could explain, at least in part, the beneficial effect of KD in epilepsy.

Data availability statement

The original contributions presented in the study are included in the article/supplementary material, further inquiries can be directed to the corresponding authors.

Ethics statement

The animal study was approved by Research Board of the National Institute of Pediatrics (Protocol 085/2010), registered at the Office for Human Research Protection of the NIH with number IRB00008065. Institutional Committee for the Care and Use of Laboratory Animal. The study was conducted in accordance with the local legislation and institutional requirements.

Author contributions

LG-R: Conceptualization, Data curation, Formal analysis, Funding acquisition, Investigation, Methodology, Project administration, Resources, Software, Supervision, Validation, Visualization, Writing – original draft, Writing – review & editing. LH-L: Formal analysis, Methodology, Supervision, Software, Writing – original draft. EB-A: Data curation, Formal analysis, Methodology, Software, Investigation, Writing – original draft. TJ-Z: Data curation, Formal analysis, Methodology, Software, Writing – original draft. VC: Data curation, Methodology, Software, Writing – original draft. JM-G: Data curation, Formal analysis, Methodology, Writing – original draft. KJ-C: Formal analysis, Methodology, Software, Writing – original draft. MT-R: Methodology, Supervision, Software, Writing – original draft. AV-C: Methodology, Writing – review & editing, Investigation, Supervision. PD: Methodology, Software, Formal analysis, Writing – review & editing. CR: Conceptualization, Data curation, Formal analysis, Funding acquisition, Investigation, Methodology, Project administration, Resources, Software, Supervision, Validation, Visualization, Writing – original draft, Writing – review & editing.

Funding

The author(s) declare financial support was received for the research and/or publication of this article. This study was supported by the Fiscal Resources Program for Research of the National Institute of Pediatrics to the Biomolecules and Infant Health Laboratory and protocol 085/2010. 86784 CONACYT to LG-R.

Conflict of interest

The authors declare that the research was conducted in the absence of any commercial or financial relationships that could be construed as a potential conflict of interest.

Publisher's note

References

Amaral, D. G., Scharfman, H. E., and Lavenex, P. (2007). The dentate gyrus: fundamental neuroanatomical organization (dentate gyrus for dummies). *Prog. Brain Res.* 163, 3–22. doi: 10.1016/S0079-6123(07)63001-5

Amaral, D. G., and Witter, M. P. (1989). The three-dimensional organization of the hippocampal formation: a review of anatomical data. *Neuroscience* 31, 571–591. doi: 10.1016/0306-4522(89)90424-7. PMID: 2687721

Aronica, E., Boer, K., Redeker, S., Spliet, W. G. M., van Rijen, P. C., Troost, D., et al. (2007). Differential expression patterns of chloride transporters, Na^+-K^+-$2Cl^-$-cotransporter and K^+-cl^--cotransporter, in epilepsy-associated malformations of cortical development. *Neuroscience* 145, 185–196. doi: 10.1016/j.neuroscience.2006.11.041

Belperio, G., Corso, C., Duarte, C. B., and Mele, M. (2022). Molecular mechanisms of epilepsy: the role of the chloride transporter KCC2. *J. Mol. Neurosci.* 72, 1500–1515. doi: 10.1007/s12031-022-02041-7

Bonislawski, D. P., Schwarzbach, E., and Cohen, A. S. (2007). Brain injury impairs dentate gyrus inhibitory efficacy. *Neurobiol. Dis.* 25, 163–169. doi: 10.1016/j.nbd.2006.09.002

Campbell, S. L., Robel, S., Cuddapah, V. A., Robert, S., Buckingham, S. C., Kahle, K. T., et al. (2015). GABAergic disinhibition and impaired KCC2 cotransporter activity underlie tumor-associated epilepsy. *Glia* 63, 23–36. doi: 10.1002/glia.22730

Cellot, G., and Cherubini, E. (2014). GABAergic signaling as therapeutic target for autism spectrum disorders. *Front. Pediatr.* 2:70. doi: 10.3389/fped.2014.00070

Chen, L., Wan, L., Wu, Z., Ren, W., Huang, Y., Qian, B., et al. (2017). KCC2 downregulation facilitates epileptic seizures. *Sci. Rep.* 7:156. doi: 10.1038/s41598-017-00196-7

Di Cristo, G., Awad, P. N., Hamidi, S., and Avoli, M. (2018). KCC2, epileptiform synchronization, and epileptic disorders. *Prog. Neurobiol.* 162, 1–16. doi: 10.1016/j.pneurobio.2017.11.002

Ding, Y., Wang, S., Jiang, Y., Yang, Y., Zhang, M., Guo, Y., et al. (2013). Fructose-1, 6-diphosphate protects against epileptogenesis by modifying cation-chloride co-transporters in a model of amygdaloid-kindling temporal epilepticus. *Brain Res.* 1539, 87–94. doi: 10.1016/j.brainres.2013.09.042

Doyen, M., Lambert, C., Roeder, E., Boutley, H., Chen, B., Pierson, J., et al. (2024). Assessment of a one-week ketogenic diet on brain glycolytic metabolism and on the status epilepticus stage of a lithium-pilocarpine rat model. *Sci. Rep.* 14:5063. doi: 10.1038/s41598-024-53824-4

Duy, P. Q., David, W. B., and Kahle, K. T. (2019). Identification of KCC2 mutations in human epilepsy suggests strategies for therapeutic transporter modulation. *Front. Cell. Neurosci.* 13:515. doi: 10.3389/fncel.2019.00515

Dyńka, D., Kowalcze, K., and Paziewska, A. (2022). The role of ketogenic diet in the treatment of neurological diseases. *Nutrients* 14:5003. doi: 10.3390/nu14235003

El-Shafie, A. M., Bahbah, W. A., Abd El Naby, S. A., Omar, Z. A., Basma, E. M., Hegazy, A. A. A., et al. (2023). Impact of two ketogenic diet types in refractory childhood epilepsy. *Pediatr. Res.* 94, 1978–1989. doi: 10.1038/s41390-023-02554-w

Fedorovich, S. V., Voronina, P. P., and Wassem, T. V. (2018). Ketogenic diet versus ketoacidosis: what determines the influence of ketone bodies on neurons? *Neural Regen Res.* 13, 2060–2063. doi: 10.4103/1673-5374.241442

Fisher, R. S., Acevedo, C., Arzimanoglou, A., Bogacz, A., Cross, J. H., Elger, C. E., et al. (2014). ILAE official report: a practical clinical definition of epilepsy. *Epilepsia* 55, 475–482. doi: 10.1111/epi.12550

Galanopoulou, A. S. (2008). Sexually dimorphic expression of KCC2 and GABA function. *Epilepsy Res.* 80, 99–113. doi: 10.1016/j.eplepsyres.2008.04.013

Galanopoulou, A. S., and Moshé, S. L. (2003). Role of sex hormones in the sexually dimorphic expression of KCC2 in rat substantia Nigra. *Exp. Neurol.* 184, 1003–1009. doi: 10.1016/S0014-4886(03)00387-X

Gharaylou, Z., Oghabian, M. A., Azizi, Z., and Hadjighassem, M. (2019). Brain microstructural abnormalities correlate with KCC2 downregulation in refractory epilepsy. *Neuroreport* 30, 409–414. doi: 10.1097/WNR.0000000000001216

Goddard, G. V., McIntyre, D. C., and Leech, C. K. (1969). A permanent change in brain function resulting from daily electrical stimulation. *Exp. Neurol.* 25, 295–330. doi: 10.1016/0014-4886(69)90128-9

Gómez-Lira, G., Mendoza-Torreblanca, J. G., and Granados-Rojas, L. (2011). Ketogenic diet does not change NKCC1 and KCC2 expression in rat hippocampus. *Epilepsy Res.* 96, 166–171. doi: 10.1016/j.eplepsyres.2011.05.017

Granados-Rojas, L., Jerónimo-Cruz, K., Juárez-Zepeda, T. E., Tapia-Rodríguez, M., Tovar, A. R., Rodríguez-Jurado, R., et al. (2020). Ketogenic diet provided during three months increases KCC2 expression but not NKCC1 in the rat dentate gyrus. *Front. Neurosci.* 14:673. doi: 10.3389/fnins.2020.00673

Gulyás, A. I., Sík, A., Payne, J. A., Kaila, K., and Freund, T. F. (2001). The KCl cotransporter, KCC2, is highly expressed in the vicinity of excitatory synapses in the rat hippocampus. *Eur. J. Neurosci.* 13, 2205–2217. doi: 10.1046/j.0953-816x.2001.01600.x

Hori, A., Tandon, P., Holmes, G. L., and Stafstrom, C. E. (1997). Ketogenic diet: effects on expression of kindled seizures and behavior in adult rats. *Epilepsia* 38, 750–758. doi: 10.1111/j.1528-1157.1997.tb01461.x

Hu, X. L., Cheng, X., Fei, J., and Xiong, Z. Q. (2011). Neuron-restrictive silencer factor is not required for the antiepileptic effect of the ketogenic diet. *Epilepsia* 52, 1609–1616. doi: 10.1111/j.1528-1167.2011.03171.x

Jiang, Y., Lu, Y., Jia, M., Wang, X., Zhang, Z., Hou, Q., et al. (2016). Ketogenic diet attenuates spatial and item memory impairment in pentylenetetrazol-kindled rats. *Brain Res.* 1646, 451–458. doi: 10.1016/j.brainres.2016.06.029

Jiang, Y., Yang, Y., Wang, S., Ding, Y., Guo, Y., Zhang, M. M., et al. (2012). Ketogenic diet protects against epileptogenesis as well as neuronal loss in amygdaloid-kindling seizures. *Neurosci. Lett.* 508, 22–26. doi: 10.1016/j.neulet.2011.12.002

Juárez-Zepeda, E., Rubio, C., Molina-Valdespino, D., Marín-Castañeda, L. A., Vanoye-Carlo, A., and Granados-Rojas, L. (2024). "The ketogenic diet in neuropsychiatric disorders" in The ketogenic diet reexamined, myth vs. reality. eds. L. Granados-Rojas and C. Rubio (New York: NOVA), 61–91. doi: 10.52305/KSTQ4025

Kaila, K., Price, T. J., Payne, J. A., Puskarjov, M., and Voipio, J. (2014). Cation-chloride cotransporters in neuronal development, plasticity and disease. *Nat. Rev. Neurosci.* 15, 637–654. doi: 10.1038/nrn3819

Karlócai, M. R., Wittner, L., Tóth, K., Maglóczky, Z., Katarova, Z., Rásonyi, G., et al. (2016). Enhanced expression of potassium-chloride cotransporter KCC2 in human temporal lobe epilepsy. *Brain Struct. Funct.* 221, 3601–3615. doi: 10.1007/s00429-015-1122-8

Kasper, D. (2020). Modulation of ion channels and reduction of neuroinflammation by the ketogenic diet in epilepsy models. *Neurosci. Lett.* 731:135037. doi: 10.1016/j.neulet.2020.135037

Koumangoye, R., Bastarache, L., and Delpire, E. (2021). NKCC1: newly found as a human disease-causing ion transporter. *Function* 2:zqaa028. doi: 10.1093/function/zqaa028

Kwan, P., Arzimanoglou, A., Berg, A. T., Brodie, M. J., Allen Hauser, W., Mathern, G., et al. (2010). Definition of drug resistant epilepsy: consensus proposal by the ad hoc task force of the ILAE commission on therapeutic strategies. *Epilepsia* 51, 1069–1077. doi: 10.1111/j.1528-1167.2009.02397.x

Lam, P., Newland, J., Faull, R. L. M., and Kwakowsky, A. (2023). Cation-chloride cotransporters KCC2 and NKCC1 as therapeutic targets in neurological and neuropsychiatric disorders. *Molecules* 28:1344. doi: 10.3390/molecules28031344

Lang, J., McCune, S. K., and Bhatia, R. (2016). Effects of the ketogenic diet on synaptic function and neurotransmitter regulation. *Epilepsy Res.* 118, 22–28. doi: 10.1016/j.eplepsyres.2015.10.003,

Lee, H. H., Deeb, T. Z., Walker, J. A., Davies, P. A., and Moss, S. J. (2011). NMDA receptor activity downregulates KCC2 resulting in depolarizing $GABA_A$ receptor-mediated currents. *Nat. Neurosci.* 14, 736–743. doi: 10.1038/nn.2806

Martin-McGill, K. J., Bresnahan, R., Levy, R. G., and Cooper, P. N. (2026). Ketogenic diets for drug-resistant epilepsy. *Cochrane Database Syst. Rev.* 6:CD001903. doi: 10.1002/14651858.CD001903.pub5

McMoneagle, E., Zhou, J., Zhang, S., Huang, W., Josiah, S. S., Ding, K., et al. (2024). Neuronal K^+-Cl^- cotransporter KCC2 as a promising drug target for epilepsy treatment. *Acta Pharmacol. Sin.* 45, 1–22. doi: 10.1038/s41401-023-01149-9

Meeusen, H., Kalf, R. S., Broekaart, D. W. M., Silva, J. P., Verkuyl, J. M., van Helvoort, A., et al. (2024). Effective reduction in seizure severity and prevention of a fatty liver by a novel low ratio ketogenic diet composition in the rapid kindling rat model of epileptogenesis. *Exp. Neurol.* 379:114861. doi: 10.1016/j.expneurol.2024.114861

Murakami, M., and Tognini, P. (2022). Molecular mechanisms underlying the bioactive properties of a ketogenic diet. *Nutrients* 14:782. doi: 10.3390/nu14040782

Murugan, M., and Boison, D. (2020). Ketogenic diet, neuroprotection, and antiepileptogenesis. *Epilepsy Res.* 167:106444. doi: 10.1016/j.eplepsyres.2020.106444

Official Mexican Norm. (1999). Technical specifications for the production, care and use of laboratory animals. [NOM-062-ZOO-1999]. Official Journal of the Federation, Mexico. Available online at: https://www.gob.mx/cms/uploads/attachment/file/203498/NOM-062-ZOO-1999_220801.pdf

Okabe, A., Yokokura, M., Toyoda, H., Shimizu-Okabe, C., Ohno, K., Sato, K., et al. (2003). Changes in chloride homeostasis-regulating gene expressions in the rat hippocampus following amygdala kindling. *Brain Res.* 990, 221–226. doi: 10.1016/s0006-8993(03)03528-5

Pathak, H. R., Weissinger, F., Terunuma, M., Carlson, G. C., Hsu, F. C., Moss, S. J., et al. (2007). Disrupted dentate granule cell chloride regulation enhances synaptic excitability during development of temporal lobe epilepsy. *J. Neurosci.* 27, 14012–14022. doi: 10.1523/JNEUROSCI.4390-07.2007

Paxinos, G., and Watson, C. (2007). The rat brain in stereotaxic coordinates. London: Academic Press.

Perucca, E., White, H. S., and Bialer, M. (2023). New GABA-targeting therapies for the treatment of seizures and epilepsy: II. Treatments in clinical development. *CNS Drugs* 37, 781–795. doi: 10.1007/s40263-023-01025-4

Phillips-Farfán, B. V., Rubio Osornio Mdel, C., Custodio Ramírez, V., Paz Tres, C., and Carvajal Aguilera, K. G. (2015). Caloric restriction protects against electrical kindling of the amygdala by inhibiting the mTOR signaling pathway. *Front. Cell. Neurosci.* 9:90. doi: 10.3389/fncel.2015.00090

Pressey, J. C., de Saint-Rome, M., Raveendran, V. A., and Woodin, M. A. (2023). Chloride transporters controlling neuronal excitability. *Physiol. Rev.* 103, 1095–1135. doi: 10.1152/physrev.00025.2021

Qiao, Q., Tian, S., Zhang, Y., Che, L., Li, Q., Qu, Z., et al. (2024). A ketogenic diet may improve cognitive function in rats with temporal lobe epilepsy by regulating endoplasmic reticulum stress and synaptic plasticity. *Mol. Neurobiol.* 61, 2249–2264. doi: 10.1007/s12035-023-03659-3

Racine, J. (1972). Modification of seizure activity by electrical stimulation: II. Motor seizure. *Electroencephalogr. Clin. Neurophysiol.* 32, 281–294. doi: 10.1016/0013-4694(72)90177-0

Rasband, W. S. (2018). ImageJ, U. S. National Institutes of Health, Bethesda, Maryland, USA. Available online at: https://imagej.net/ij/

Reddy, D. S., Thompson, W., and Calderara, G. (2021). Molecular mechanisms of sex differences in epilepsy and seizure susceptibility in chemical, genetic and acquired epileptogenesis. *Neurosci. Lett.* 750:135753. doi: 10.1016/j.neulet.2021.135753

Rivera, C., Li, H., Thomas-Crusells, J., Lahtinen, H., Viitanen, T., Nanobashvili, A., et al. (2002). BDNF-induced TrkB activation down-regulates the K^+-Cl^- cotransporter KCC2 and impairs neuronal Cl^- extrusion. *J. Cell Biol.* 159, 747–752. doi: 10.1083/jcb.200209011

Rubio-Osornio, M. D. C., Custodio-Ramírez, V., Calderón-Gámez, D., Paz-Tres, C., Carvajal-Aguilera, K. G., and Phillips-Farfán, B. V. (2018). Metformin plus caloric restriction show anti-epileptic effects mediated by mTOR pathway inhibition. *Cell. Mol. Neurobiol.* 38, 1425–1438. doi: 10.1007/s10571-018-0611-8

Ryu, B., Nagappan, S., Santos-Valencia, F., Lee, P., Rodriguez, E., Lackie, M., et al. (2021). Chronic loss of inhibition in piriform cortex following brief, daily optogenetic stimulation. *Cell Rep.* 35:109001. doi: 10.1016/j.celrep.2021.109001

Shi, J., Xin, H., Shao, Y., Dai, S., Tan, N., Li, Z., et al. (2023). CRISPR-based KCC2 upregulation attenuates drug-resistant seizure in mouse models of epilepsy. *Ann. Neurol.* 94, 91–105. doi: 10.1002/ana.26656

Shimizu-Okabe, C., Tanaka, M., Matsuda, K., Mihara, T., Okabe, A., Sato, K., et al. (2011). KCC2 was downregulated in small neurons localized in epileptogenic human focal cortical dysplasia. *Epilepsy Res.* 93, 177–184. doi: 10.1016/j.eplepsyres.2010.12.008

Stafstrom, C. E., and Rho, J. M. (2012). The ketogenic diet as an treatment paradigm for diverse neurological disorders. *Front. Pharmacol.* 3:59. doi: 10.3389/fphar.2012.00059

Taddei, E., Rosiles, A., Hernandez, L., Luna, R., and Rubio, C. (2022). Apoptosis in the dentate nucleus following kindling-induced seizures in rats. *CNS Neurol. Disord. Drug Targets* 21, 511–519. doi: 10.2174/1871527320666211201161800

Tescarollo, F. C., Valdivia, D., Chen, S., and Sun, H. (2023). Unilateral optogenetic kindling of hippocampus leads to more severe impairments of the inhibitory signaling in the contralateral hippocampus. *Front. Mol. Neurosci.* 16:1268311. doi: 10.3389/fnmol.2023.1268311

Verma, J. P. (2015). Repeated measures design for empirical researchers. New Jersey: Wiley.

Wan, L., Chen, L., Yu, J., Wang, G., Wu, Z., Qian, B., et al. (2020). Coordinated downregulation of KCC2 and $GABA_A$ receptor contributes to inhibitory dysfunction during seizure induction. *Biochem. Biophys. Res. Commun.* 532, 489–495. doi: 10.1016/j.bbrc.2020.08.082

Wan, L., Ren, L., Chen, L., Wang, G., Liu, X., Wang, B. H., et al. (2018). M-Calpain activation facilitates seizure induced KCC2 down regulation. *Front. Mol. Neurosci.* 11:287. doi: 10.3389/fnmol.2018.00287

Wang, S., Ding, Y., Yan, D. X., Rong, L. Z., Hong, S. C., Jin, B., et al. (2016). Effectiveness of ketogenic diet in pentylenetetrazol-induced and kindling rats as well as its potential mechanisms. *Neurosci. Lett.* 614, 1–6. doi: 10.1016/j.neulet.2015.12.058

Wang, X., Huang, S., Liu, Y., Li, D., Dang, Y., and Yang, L. (2021). Effects of ketogenic diet on cognitive function in pentylenetetrazol-kindled rats. *Epilepsy Res.* 170:106534. doi: 10.1016/j.eplepsyres.2020.106534

Wang, Z., Sun, M., Zhao, X., Jiang, C., Li, Y., and Wang, C. (2017). Study of breath acetone in a rat mode of 126 rats with type 1 diabetes. *J. Anal. Bioanal. Tech.* 8:1. doi: 10.4172/2155-9872.1000344

Wheless, J. W. (2008). History of the ketogenic diet. *Epilepsia* 49, 3–5. doi: 10.1111/j.1528-1167.2008.01821.x

World Health Organization. (2024). Epilepsy. Available online at: https://www.who.int/health-topics/epilepsy#tab=tab_3 (Accessed March 20, 2024).

Frontiers in Neuroscience

Provides a holistic understanding of brain function from genes to behavior

Part of the most cited neuroscience journal series which explores the brain - from the new eras of causation and anatomical neurosciences to neuroeconomics and neuroenergetics.

Discover the latest Research Topics

See more →

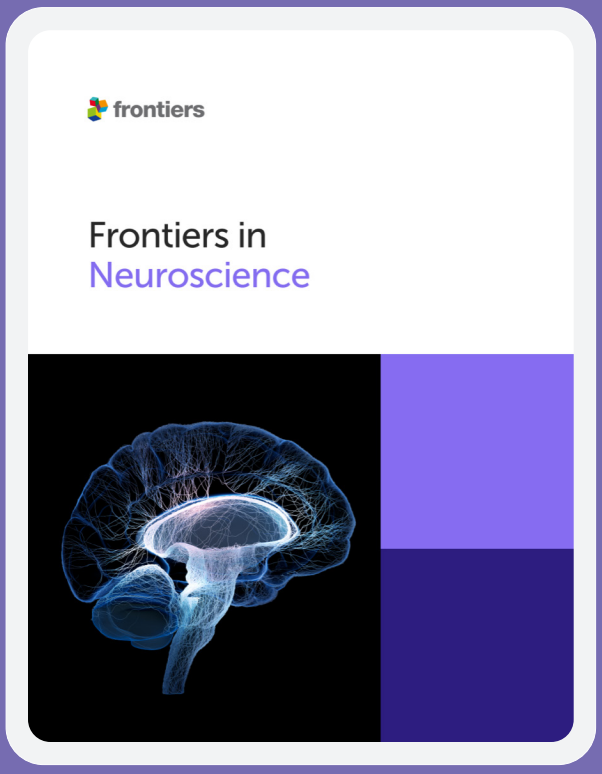

Frontiers

Avenue du Tribunal-Fédéral 34
1005 Lausanne, Switzerland
frontiersin.org

Contact us

+41 (0)21 510 17 00
frontiersin.org/about/contact